frontiers | Research Topics

Challenges of asteroseismology in the era of space missions

Edited by
Javier Pascual Granado, Tiago Campante, Antonio García Hernández and Zhao Guo

Published in
Frontiers in Astronomy and Space Sciences

ISSN 1664-8714
ISBN 978-2-83251-152-7
DOI 10.3389/978-2-83251-152-7

About Frontiers

Frontiers is more than just an open access publisher of scholarly articles: it is a pioneering approach to the world of academia, radically improving the way scholarly research is managed. The grand vision of Frontiers is a world where all people have an equal opportunity to seek, share and generate knowledge. Frontiers provides immediate and permanent online open access to all its publications, but this alone is not enough to realize our grand goals.

Frontiers journal series

The Frontiers journal series is a multi-tier and interdisciplinary set of open-access, online journals, promising a paradigm shift from the current review, selection and dissemination processes in academic publishing. All Frontiers journals are driven by researchers for researchers; therefore, they constitute a service to the scholarly community. At the same time, the *Frontiers journal series* operates on a revolutionary invention, the tiered publishing system, initially addressing specific communities of scholars, and gradually climbing up to broader public understanding, thus serving the interests of the lay society, too.

Dedication to quality

Each Frontiers article is a landmark of the highest quality, thanks to genuinely collaborative interactions between authors and review editors, who include some of the world's best academicians. Research must be certified by peers before entering a stream of knowledge that may eventually reach the public - and shape society; therefore, Frontiers only applies the most rigorous and unbiased reviews. Frontiers revolutionizes research publishing by freely delivering the most outstanding research, evaluated with no bias from both the academic and social point of view. By applying the most advanced information technologies, Frontiers is catapulting scholarly publishing into a new generation.

What are Frontiers Research Topics?

Frontiers Research Topics are very popular trademarks of the *Frontiers journals series*: they are collections of at least ten articles, all centered on a particular subject. With their unique mix of varied contributions from Original Research to Review Articles, Frontiers Research Topics unify the most influential researchers, the latest key findings and historical advances in a hot research area.

Find out more on how to host your own Frontiers Research Topic or contribute to one as an author by contacting the Frontiers editorial office: frontiersin.org/about/contact

Challenges of asteroseismology in the era of space missions

Topic editors

Javier Pascual Granado — Institute of Astrophysics of Andalusia, Spanish National Research Council (CSIC), Spain

Tiago Campante — Instituto de Astrofísica e Ciências do Espaço (IA), Portugal

Antonio García Hernández — University of Granada, Spain

Zhao Guo — University of Cambridge, United Kingdom

Citation

Granado, J. P., Campante, T., Hernández, A. G., Guo, Z., eds. (2023). *Challenges of asteroseismology in the era of space missions*. Lausanne: Frontiers Media SA. doi: 10.3389/978-2-83251-152-7

Table of contents

frontiers | Frontiers in Astronomy and Space Sciences

TYPE Editorial
PUBLISHED 13 December 2022
DOI 10.3389/fspas.2022.1100442

OPEN ACCESS

EDITED AND REVIEWED BY:
Christopher Corbally,
Vatican Observatory, Vatican City

*CORRESPONDENCE
Javier Pascual-Granado,
javier@iaa.es

SPECIALTY SECTION
This article was submitted to Stellar and Solar Physics, a section of the journal Frontiers in Astronomy and Space Sciences

RECEIVED 16 November 2022
ACCEPTED 24 November 2022
PUBLISHED 13 December 2022

CITATION
Pascual-Granado J, Campante T, García Hernández A and Guo Z (2022), Editorial: Challenges of asteroseismology in the era of space missions.
Front. Astron. Space Sci. 9:1100442.
doi: 10.3389/fspas.2022.1100442

Editorial: Challenges of asteroseismology in the era of space missions

Javier Pascual-Granado[1]*, Tiago Campante[2], Antonio García Hernández[3] and Zhao Guo[4]

[1]Institute of Astrophysics of Andalusia (CSIC), Granada, Spain, [2]Instituto de Astrofísica e Ciências do Espaço, Universidade do Porto, Porto, Portugal, [3]Departamento de Física Teórica y del Cosmos, University of Granada, Granada, Spain, [4]Department of Applied Mathematics and Theoretical Physics, University of Cambridge, Cambridge, United Kingdom

KEYWORDS

stars: pulsation, stars: evolution, stellar structure, exoplanets, asteroseismology, data analysis

Editorial on the Research Topic
Challenges of asteroseismology in the era of space missions

New insights into the physics of stellar interiors and evolution are being made possible by asteroseismology. Moreover, asteroseismology is being increasingly applied in studies of Galactic archaeology, exoplanetary systems, and even in tests of fundamental physics. Nevertheless, more data does not always mean a better understanding, and there are long-standing problems that remain unresolved and others that have emerged as a result of the unprecedented quality of the data gathered by space missions like CNES/ESA's CoRoT (Auvergne et al., 2009), as well as NASA's Kepler/K2 (Koch et al., 2010) and TESS (Ricker et al., 2015).

With this Research Topic, our aim was to provide researchers an opportunity to publish works that tackle unresolved problems in asteroseismology from an original perspective, be it of a theoretical or observational nature. A critical point of view is needed to go beyond the limitations of our current understanding of stars and their interiors. The eleven articles published herein fulfill that role, making use of a diverse set of techniques while addressing a heterogeneous mix of subfields.

Fueled by the wealth of high-quality seismic data, the past few years have witnessed an ever-growing effort being devoted to the development of novel techniques for the estimation of fundamental stellar properties (i.e., radius, mass, and age). The focus has been placed on uniform data analysis and stellar modeling strategies, as well as state-of-the-art optimization procedures that make use of individual oscillation frequencies. In Suárez, for example, a new diagnostic diagram—the entropy spectrum (HSpec) — is proposed that makes use of the Shannon entropy to find regular patterns in the oscillation spectra of solar-like and δ Scuti stars.

Such techniques are now making it possible to estimate the precise fundamental properties of large numbers of field stars, for which such information is usually sparse. As a result, asteroseismology is having a profound impact on modern astrophysics, notably on the field of exoplanetary science. In Reda et al., a new approach is put forward that brings together the fields of asteroseismology and space weather in order to better characterize the habitability of exoplanets around solar-like stars. Another interesting application of asteroseismology is its potential use in the detection of dark matter. Ayala reviews this relatively unexplored line of research. Such applications add to the synergetic potential of asteroseismology.

The advent of high-quality, space-based photometry has also enabled the application of sophisticated inversion techniques—hitherto restricted to the field of helioseismology—to asteroseismic data sets. In Buldgen et al., the authors provide a comprehensive review of the topic of seismic inversion of the internal structures of stars, including its limitations and the prospects for future developments in view of current and upcoming space missions.

Precise fundamental stellar properties are a key output of asteroseismology. The analysis of oscillation frequencies of solar-type stars has been extremely successful in this regard. However, this is far from being reached in the case of δ Scuti stars, a class of rapidly-rotating pulsators in the main sequence. Lares-Martiz developed a new method to overcome this issue. The high-quality seismic data currently available allowed for studying small-amplitude peaks in the power spectrum of this type of pulsator. When some of these peaks are identified as resonances of higher-amplitude modes, then the study of their amplitudes and phases makes it possible to relate these quantities to the surface gravity and effective temperature of these stars.

The availability of long time series opens the possibility of carrying out time-frequency analyses. Since pulsation frequencies are not usually stable over time, their study may reveal clues about the physical processes maintaining the oscillations. This is the main motivation behind the brief research report by (Ramón-Ballesta et al.). The authors assess the benefits of the wavelet transform by monitoring the evolution of several pulsation frequencies over time for two δ Scuti stars. Although preliminary, their results show the stability of some pulsation frequencies against others that might be interacting. The development of this technique may shed new light on the excitation mechanism driving the oscillations in this type of pulsator.

Due to the lack of explanation for mode selection in some stars and a large number of pulsation frequencies in the power spectra of others, δ Scuti stars are one of the most challenging types of pulsating stars. FG Virginis is a paradigmatic case, having previously been studied as part of long ground-based, multi-site campaigns during the 1990s and early 2000s, which included multicolor photometry that made mode identification possible. This star has more recently been observed by K2 and TESS in 30- and 2-min cadences, respectively. The unprecedented quality of these data sets provides a great opportunity to shed new light on the interpretation problems characteristic to δ Scuti stars. Guzik et al. compares previous frequency analyses with the ones carried out in their study, finding good agreement regarding the identification of the modes of highest amplitude. However, they also find an increased number of detected modes that make mode identification more challenging. In addition, the presence of low-frequency modes suggests that FG Virginis might be a hybrid δ Scuti/γ Doradus variable star.

High-precision asteroseismology brought with it new questions about pulsating stars. The classical Fourier transform, commonly used to extract mode frequencies from the time-series data, has been at times criticized. Therefore, new ways of dealing with the data are being constantly sought. This is the case in the work by (Garrido et al.). The authors propose a new transform to get the most out of the observations. A new quaternionic Fourier transform is presented and applied to solar data from GOLF/SoHO, unearthing new peaks that could potentially provide insight into the deepest solar interior.

In the age of machine learning and artificial intelligence, it is a natural step to introduce these techniques for the purpose of mode identification and pattern analysis. Especially for rapidly-rotating stars, mode identification is a challenging task and several strategies have been put to the test in the past with mixed success. Mirouh reviews these strategies as well as the new efforts being made, with an emphasis on two promising developments: classification algorithms to automate mode identification and derive patterns for each subclass of acoustic modes, and the adaptation of line-profile variations to rapidly-rotating stars.

Although various types of pulsating stars populate the Hertzsprung–Russell diagram, the asteroseismology of pre-main-sequence stars has not been addressed in detail yet. Pre-main-sequence stars are usually obscured by dust and stellar activity, their pulsation properties thus being difficult to obtain observationally. The relatively short duration of this evolutionary phase makes this problem even worse. Zwintz and Steindl combine observations and theoretical modeling and review the state of the art when it comes to the study of these stars. These young stellar objects hold promise in helping us answer a number of key open questions in stellar evolution, e.g., on angular momentum transport and the formation of magnetic fields.

Intermediate-/high-mass stars are usually rapidly rotating. The effect of rotation is notoriously difficult to be accounted for fully. Although the traditional approximation works well for low-frequency gravity modes, for acoustic modes, the validity of the perturbative approach is quite limited, and the geometric

deformation enforces a two-dimensional modeling of stellar structure and evolution. Reese review the cutting-edge topic of asteroseismic modeling of fast-rotating stars, linking the 2D numerical modeling effort to the direct observables in photometry (amplitude ratios and amplitude-phase diagrams in multiple bands), spectroscopy (line-profile variations), and interferometry.

As a final remark, we would like to point out that the application of open science principles together with a high level of mathematical rigor and (often) an interdisciplinary approach should be pursued in tackling the multiple challenges posed by modern asteroseismology, thus maximizing the scientific potential of future missions such as PLATO (Rauer et al., 2014) and, possibly, HAYDN (Miglio et al., 2021).

Author contributions

All authors listed have made a substantial, direct, and intellectual contribution to the work and approved it for publication.

Funding

JP-G acknowledges funding support from Spanish public funds for research from project PID 2019-107061GB-C63 from the "Programas Estatales de Generación de Conocimiento y Fortalecimiento Científico y Tecnológico del Sistema de I + D + i y de I + D + i Orientada a los Retos de la Sociedad", and from the State Agency for Research through the "Center of Excellence Severo Ochoa" award to the Instituto de Astrofísica de Andalucía (SEV-2017-0709), all from the Spanish Ministry of Science, Innovation and Universities (MCIU). This work was supported by Fundação para a Ciência e a Tecnologia (FCT) through research grants UIDB/04434/2020 and UIDP/04434/2020. TC is supported by FCT in the form of a work contract (CEECIND/00476/2018). This research was supported by STFC through grant ST/T00049X/1. AG acknowledges funding support from Spanish public funds for research under project PID 2019-107061GB-C64 by the Spanish Ministry of Science and Education, and from "European Regional Development Fund/Junta de Andalucía-Consejería de Economía y Conocimiento" under project E-FQM-041-UGR18 by Universidad de Granada.

Acknowledgments

We thank the authors who contributed to this topic with their research. We also thank the reviewers for the constructive comments during the review process, which greatly improved the overall quality of this article collection.

Conflict of interest

The authors declare that the research was conducted in the absence of any commercial or financial relationships that could be construed as a potential conflict of interest.

Publisher's note

References

Auvergne, M., Bodin, P., Boisnard, L., Buey, J. T., Chaintreuil, S., Epstein, G., et al. (2009). The CoRoT satellite in flight: Description and performance. *A&A* 506, 411–424. doi:10.1051/0004-6361/200810860

Koch, D. G., Borucki, W. J., Basri, G., Batalha, N. M., Brown, T. M., Caldwell, D., et al. (2010). *Kepler mission* design, realized photometric performance, and early science. *ApJ.* 713, L79–L86. doi:10.1088/2041-8205/713/2/L79

Miglio, A., Girardi, L., Grundahl, F., Mosser, B., Bastian, N., Bragaglia, A., et al. (2021). Haydn. *Exp. Astron.* 51, 963–1001. doi:10.1007/s10686-021-09711-1

Rauer, H., Catala, C., Aerts, C., Appourchaux, T., Benz, W., Brandeker, A., et al. (2014). The PLATO 2.0 mission. *Exp. Astron.* 38, 249–330. doi:10.1007/s10686-014-9383-4

Ricker, G. R., Winn, J. N., Vanderspek, R., Latham, D. W., Bakos, G. Á., Bean, J. L., et al. (2015). Transiting exoplanet survey satellite. *J. Astron. Telesc. Instrum. Syst.* 1, 014003. doi:10.1117/1.JATIS.1.1.014003

frontiers | Frontiers in Astronomy and Space Sciences

REVIEW
published: 08 June 2022
doi: 10.3389/fspas.2022.914738

The Pre-main Sequence: Challenges and Prospects for Asteroseismology

Konstanze Zwintz and Thomas Steindl*

Institute for Astro- and Particle Physics, University of Innsbruck, Innsbruck, Austria

Stars do not simply pop up on the main sequence. Before the stars arrive on the zero-age main sequence, they form in the collapses of molecular clouds, gain matter through accretion processes, and compress their cores until hydrogen can burn in full equilibrium. Although this evolutionary phase lasts a relatively short time, it is the imprint of these important physical processes that is often ignored by simplified assumptions. While asteroseismology offers a great tool to investigate these physical processes, studying pre-MS oscillations in turn has the potential to further advance the field. Asteroseismology of pre-main sequence stars faces observational and theoretical challenges. The remnants of their birth environment which is often still surrounding the young stars causes variability that can interfere with the signal of pulsations. The lack of long time-base satellite observations in addition limits the applications of the method. Theoretical models of pre-main sequence stars include several assumptions and simplifications that influence the calculation of pulsation frequencies and excitation properties of pulsation modes. Keeping all this in mind, the prospects for pre-main sequence asteroseismology are manifold. An improved understanding of the structure of young stellar objects has the potential to answer some of the open questions of stellar evolution, including angular momentum transport and the formation of magnetic fields. While gyrochronology, for example, struggles to determine the ages of the youngest clusters, pulsations in pre-main sequence stars can function as an independent age indicator yielding higher precision for single stars. The increasing interest of stellar astrophysics in general to investigate the formation and early evolution of stars and planets illustrates the growing importance of pre-main sequence asteroseismology. In this work we discuss its potential for an advancement of our understanding of stellar structure and evolution.

Keywords: early stellar evolution, pre-main sequence, p and g-mode pulsations, stellar structure, accretion physics, angular momentum transport, asteroseismology

OPEN ACCESS

Edited by:
Zhao Guo,
University of Cambridge,
United Kingdom

Reviewed by:
Joyce Ann Guzik,
Los Alamos National Laboratory
(DOE), United States
Paolo Ventura,
Astronomical Observatory of Rome
(INAF), Italy

****Correspondence:***
Konstanze Zwintz
konstanze.zwintz@uibk.ac.at

Specialty section:
This article was submitted to Stellar and Solar Physics, a section of the journal Frontiers in Astronomy and Space Sciences

Received: *07 April 2022*
Accepted: *17 May 2022*
Published: *08 June 2022*

Citation:
Zwintz K and Steindl T (2022) The Pre-main Sequence: Challenges and Prospects for Asteroseismology. Front. Astron. Space Sci. 9:914738. doi: 10.3389/fspas.2022.914738

INTRODUCTION

The study of pre-main sequence stars was initiated in the 1950s when *what appear to be recently formed groups of stars* (Henyey et al., 1955) drew interest from the astronomical community. Henyey et al. (1955) provided the first calculations of stars before their main sequence phase. Their models described the gravitational contraction of radiative stars and the respective evolution of the spectroscopic parameters is still referred to as the 'Henyey track' today. Once it was evident that convection plays a major part in the evolution of stars, Hayashi (1961) delivered improved theoretical models for the pre-main sequence phase, achieving good agreement with the observational data of NGC 2264 (Walker, 1956). Hayashi (1961) discussed the forbidden zone

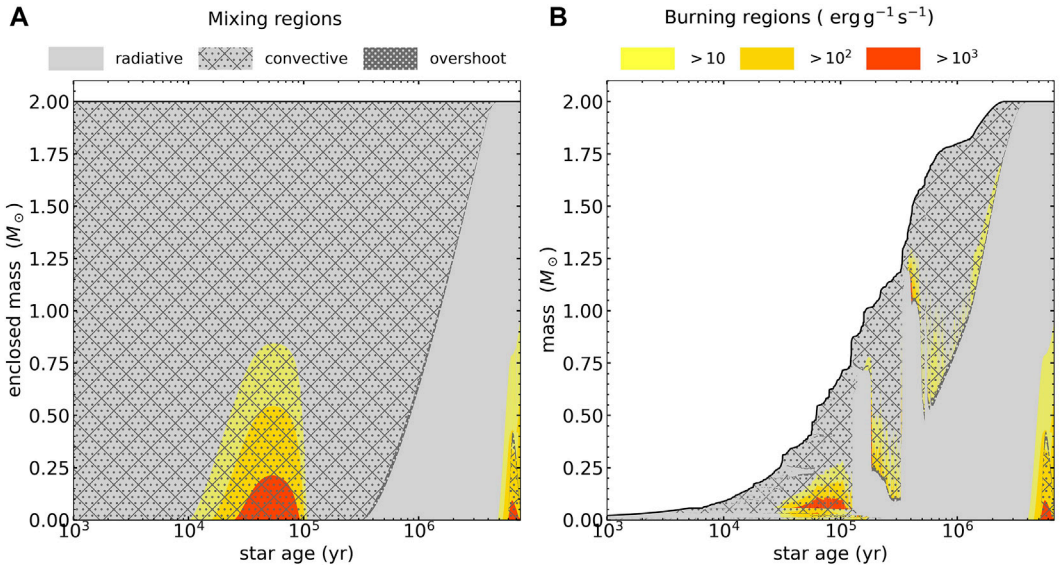

FIGURE 1 | Kippenhahn diagram of the pre-main sequence evolution. **(A)** classical model. **(B)** model including accretion effects (Steindl et al., 2022) with disk-mediated accretion rates from (Elbakyan et al., 2019). The stellar structure is shown between the stellar centre (enclosed mass = 0) and the black line (enclosed mass = stellar mass). Different mixing regions are indicated by textures. Radiative regions are grey, while overshooting and convective regions are hashed according to the legend. Regions of the star producing energy by nuclear reactions are colored according to the energy rate and the legend.

in the Hertzsprung-Russell diagram–an area in which no star can be in the hydrostatic equilibrium as the needed temperature gradient would immediately be brought down by rapid convection–and provided calculation after which stars follow a fully convective 'Hayashi track' before joining the 'Henyey track' on their contraction towards the ZAMS. Because of the forbidden zone in the Hertzsprung-Russell diagram, the models by Hayashi (1961) follow the 'Hayashi track' before joining the 'Henyey track' on their contraction towards the ZAMS. Iben (1965) refined the picture of pre-main sequence evolution (classical pre-main sequence model from here on) by following the C^{12}-depletion in more detail.

Compared to the real star formation process, however, this classical view of the pre-main sequence evolution suffers from a crude approximation: the initial model. While the latter is taken as a huge (~ 55 $R_\odot$ for a 2 $M_\odot$ star) fully convective star at ZAMS mass, real stellar seeds are produced in the collapse of molecular clouds. Such an optically thin cloud collapses under its own gravity. The increase in density and temperature leads to the formation of a first hydrostatic core which will further heat up until molecular hydrogen dissociates at ~ 2000 K. This is a strongly endothermic process and leads to a second collapse, ending in the formation of the second hydrostatic core (see e.g. Larson, 1969). Such a stellar seed with 1–5 $R_\odot$ and 10^{-3} – 10^{-2} $M_\odot$ (Larson, 1969; Bhandare et al., 2018), constitutes the first stage of the pre-main sequence evolution, and continues to accrete material from its surrounding cloud or disk.

The evolution of such accreting protostars was followed by multiple authors including Palla and Stahler (1990), who phrased the word 'birthline' meant as the position in the Hertzsprung-Russell diagram in which the radius of the accreting protostar first coincides with the radius of the classical pre-main sequence models. This created a misconception: a view in which stars evolve along the classical pre-main sequence tracks but are still hidden underneath their dust cloud and become visible when they cross the birthline. This view is a very unphysical picture, as stars evolve along the birthline (or rather their very own track) during their accretion phase. The concept of such a birthline is hence outdated, with state-of-the-art models of the pre-main-sequence providing a very different picture. The latter has been manifested by many authors (e.g., Hartmann and Kenyon, 1996; Hartmann et al., 1997; Wuchterl, 2001; Baraffe et al., 2009; Baraffe and Chabrier, 2010; Hosokawa et al., 2011; Baraffe et al., 2012; Kunitomo et al., 2017; Jensen and Haugbølle, 2018; Elbakyan et al., 2019), but only recently arrived in the field of asteroseismology (Steindl et al., 2021a, 2022; Steindl and Zwintz, 2022).

Introducing accretion effects into the numerical simulations of the pre-main sequence evolution provides an insight into the complicated structure of such young stars. The Kippenhahn diagram in **Figure 1** shows the striking differences between the simplified classical model (1A) and the more realistic simulation including disk-mediated accretion rates (1B). Most notable is the difference in chemical mixing. While the view of fully convective pre-main sequence stars is deeply rooted, state-of-the-art pre-main sequence models show that this is not the case although a large part of the stellar interior can still be affected by convection at different stages of the pre-main sequence evolution.

Naturally, such drastic changes in internal structure are also mirrored by the spectroscopic parameters of the star. **Figure 2** provides the corresponding evolutionary tracks in the Kiel

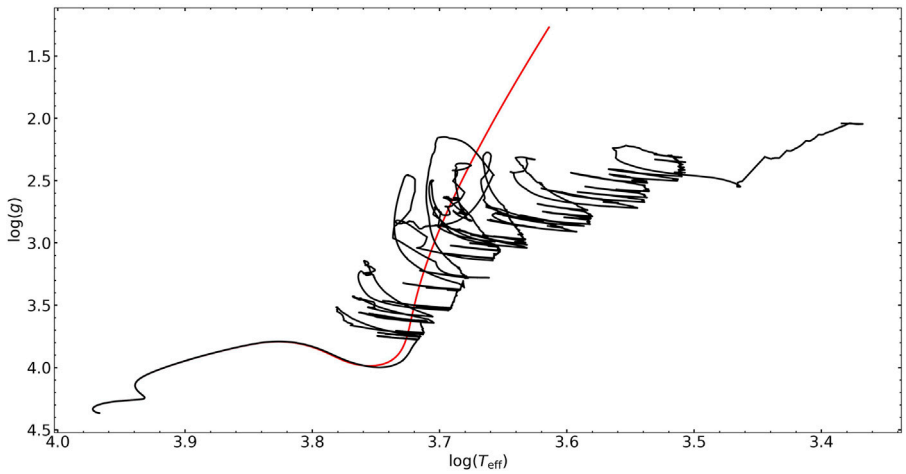

FIGURE 2 | Kiel diagram of the pre-main sequence models shown in **Figure 1**. The classical mode (red) follows the well known Hayashi track before entering the Henyey track and contracting on to the ZAMS. The disk mediated model (black) shows the effect of time-dependent accretion rates. The evolution follows a very chaotic route before entering the Henyey track and converging with the classical model.

diagram (log(g)-log($T_{\rm eff}$)-diagram). It is important to state that the track for the disk-mediated model is unique, that is a different accretion history will lead to significantly changed evolutionary track. In order to provide a realistic picture of pre-main sequence evolution, we have to move on from simplified views (Hayashi-track → Henyey-track → main sequence) and have to accept more complicated evolutionary paths: The spectroscopic parameters and internal structure in the early phases of a stars' lifetime are directly related to the properties of the mass accretion. Only after the disk has dissolved and the star continues to evolve without obtaining new material, will the structure of real stars gradually converge towards the structure that we are used to from the classical models. Even if spectroscopic parameters are rather similar, the internal structure remains different. Most notably is the existence of a temperature inversion towards the centre of the star (see e.g. Figure 8 of Steindl et al., 2021a). An imprint of star formation on the internal structure remains throughout the pre-main sequence phase and at least until the ZAMS; this should provide the opportunity to probe such disk-mediated evolution models with asteroseismology (Steindl et al., 2022).

Astrophysicists of the past have long desired a tool to probe the stellar interior. While direct photometric and spectroscopic methods pierce only the stellar atmosphere, information about the entire star are needed to improve our theory of stellar structure and evolution. Today, such a tool is available. Asteroseismology–the theory of stellar oscillations–provides the opportunity to measure (often) tiny changes in the stellar structure powered by stellar pulsations by means of photometric or spectroscopic methods (overviews about asteroseismology can be found in, e.g., Christensen-Dalsgaard, 1982; Gough, 1987; Unno et al., 1989; Aerts et al., 2010). As the pulsations travel throughout the star, their frequencies hold information about the entire structure hence providing a view deep into the stellar interior. Since its discovery, asteroseismology has allowed many improvements of our understanding of stellar structure throughout the entire Hertzsprung-Russell diagram and all evolutionary stages (e.g., Aerts, 2021).

Especially promising is the research field "Pre-main sequence asteroseismology". Its origin lies in the first discovery of pulsations in young stars by Breger (1972). In his article, he reported that the two members of the young open cluster NGC 2,264–V 588 Mon and V 589 Mon–show δ Scuti-type pulsations. But it took 20 years until the next observational detections were available (e.g., Praderie et al., 1991; Kurtz and Marang, 1995). These observations triggered the search for additional members of this new group of pulsating stars, the pre-main sequence δ Scuti stars, as well as the first theoretical work on pulsational instability in stars before the onset of hydrogen core burning (Marconi and Palla, 1998). Subsequently, more pre-main sequence stars were found to show radial and non-radial oscillations. It soon became obvious that not only δ Scuti type pulsations can be excited in young stars, but also γ Doradus (e.g., Bouabid et al., 2011; Zwintz et al., 2013) and Slowly Pulsating B type variability (e.g., Gruber et al., 2012). A complete overview of the history of pre-main sequence asteroseismology can be found in Zwintz (2019).

A very important milestone in the field of pre-main sequence asteroseismology was the discovery of the presence of non-radial pulsations in pre-main sequence δ Scuti stars and the corresponding theoretical description (Ruoppo et al., 2007; Zwintz et al., 2007). Soon after, the observed pulsation frequencies of a δ Scuti star were used to confirm its pre-main sequence evolutionary stage in combination with theoretical models (Guenther et al., 2007). Pre-main sequence δ Scuti stars have since then proven to be a treasure trove for observational discoveries, with Zwintz et al. (2014) showing a connection between the pulsational properties of pre-main sequence δ Scuti stars and their relative evolutionary stage: the closer the stars are to the onset of hydrogen core burning, the

TABLE 1 | Types of known pre-main sequence pulsators and their properties (as of March 2022).

Pulsation Type	Mass Range	Periods	Known Objects	References
SPB	3.0–7.0 $M_\odot$	0.8–3 d	18	[1], [2]
δ Scuti	1.5–2.5 $M_\odot$	18 min–8 h	> 100	[3]
Tidally perturbed	1.8–1.9 $M_\odot$	48 min–3.3 h	1	[4]
γ Doradus	1.4–1.8 $M_\odot$	0.3–3 d	8	[5], [6]
δ Scuti - γ Doradus hybrids	1.4–2.2 $M_\odot$	18 min–8 h and 0.3–3 d	4	[7]
Solar-like	~ 1$M_\odot$	~1.15 h[a]	1★	[8]
M-stars	~ 0.15$M_\odot$	0.5–5 d	1★	[6]

References: [1] Gruber et al. (2012), [2] Zwintz et al. (2017), [3] multiple papers, e.g., Zwintz (2008); Zwintz et al. (2014); Mellon et al. (2019); Steindl et al. (2021a), [4] Steindl et al. (2021b), [5] Zwintz et al. (2013), [6] Steindl et al. (2021a), [7] Ripepi et al. (2010), [8] Müllner et al. (2021).

[a]*. . . value for* ν_{max}.

★*. . .Only candidate stars detected so far.*

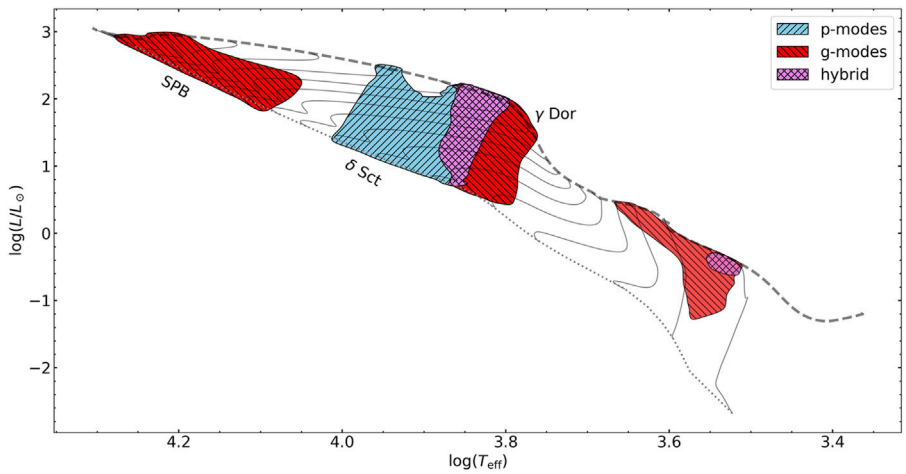

FIGURE 3 | Pre-main sequence instability regions in the Hertzsprung-Russell diagram. The colored areas depict the regions for which stellar pulsations are expected to be excited according to the results of Steindl et al. (2021a). The dashed grey line shows the evolutionary track of an accreting protostar with time-constant accretion rate. The thin grey lines show the subsequent pre-main sequence evolutionary track evolution and the dotted line indicates the ZAMS.

faster they oscillate. Such a direct connection between stellar pulsation frequencies and the relative evolutionary stages has not yet been found for more evolved δ Scuti stars.

More recent milestones include the discovery of a first candidate of solar-like oscillations in pre-main sequence stars by Müllner et al. (2021), after predictions of their existence were already made early on by (Samadi et al., 2005). Furthermore, the case of RS Cha, a pre-main sequence eclipsing binary consisting of two δ Scuti stars, provides the best evidence for the discovery of tidally perturbed pulsations in young stars to date (Steindl et al., 2021b). Pre-main sequence asteroseismology provides the opportunity for many more exciting discoveries. To get there, however, many challenges have to be overcome, in order to uncover the mysteries of this complicated evolutionary stage. The aim of this work is to present these challenges and provide the reader with an outlook on the great prospects this field offers. We review pulsations in young stars in *Introduction* before an in-depth description of the challenges pre-main sequence asteroseismology is faced with, both observational and theoretical, in *Introduction*. An idea for a space mission dedicated to young stars and star forming regions is presented in *Introduction*. *Introduction* concludes this work with a discussion of possible future milestones and how we might be able to achieve them sooner rather than later.

PULSATIONS IN YOUNG STARS

As of March 2022, seven types of pulsations have been discovered theoretically and observationally in pre-main sequence stars. Sorted from most massive to least massive, these are: Slowly Pulsating B (SPB), δ Scuti, tidally perturbed, γ Doradus, δ Scuti–γ Doradus hybrid, solar-like, and M type pulsations. **Table 1** provides an overview of their properties and gives approximate current numbers of known objects, and **Figure 3** illustrates the corresponding instability regions.

Overall, the pre-main sequence pulsators have the same pulsation properties as their counterparts in the main sequence and post-main sequence stages. The difference between the evolutionary stages lies in the pattern of excited

oscillation frequencies (e.g., Suran et al., 2001; Bouabid et al., 2011; Gruber et al., 2012) which is another beautiful illustration of the power of asteroseismology. Below we briefly describe the properties of the known types of pre-main sequence pulsators sorted from most massive to least massive.

SPB type. The pulsations in SPB type stars are excited by the heat-engine (κ) mechamism acting in the ionisation zone of metals (Dziembowski et al., 1993). The pulsation periods lie between about 0.5 and 3 days (Aerts et al., 2010). With masses between ~3 and $7M_{\odot}$, the pre-main sequence evolution of SPB type stars proceeds relatively fast making them statistically less frequent. As a consequence, SPB pulsators before the onset of hydrogen core burning are observationally harder to find. The expected temperature range for pre-main sequence SPB stars is 11,100–18,700 K (Steindl et al., 2021a).

δ Scuti type. The pulsation periods of these intermediate-mass pre-main sequence stars with effective temperatures from 6,300 to 10,300 K (Steindl et al., 2021a) lie between ~18 min and 7 h (Zwintz, 2019). Pre-main sequence δ Scuti stars show p-modes driven by the heat-engine (κ) mechanism in the ionisation zones of hydrogen and helium (Aerts et al., 2010). This is the group of pre-main sequence pulsators that was discovered first. Because of their pulsation periods, pre-main sequence δ Scuti stars could easily be detected with ground-based observations obtained only within a few nights.

Tidally perturbed type. Intermediate-mass δ Scuti type stars can often be found in binary systems. In some cases, the two components of the binary systems interact leading to strong effects on their structure and evolution (e.g., De Marco and Izzard, 2017). If the two components are in a close and eccentric orbit, tidal effects cause self-excited pulsation modes to be perturbed (e.g., Reyniers and Smeyers, 2003b,a). As of March 2022, only one pre-main sequence star, RS Cha, is known to show tidally perturbed oscillations (Steindl et al., 2021b).

γ Doradus type. Pre-main sequence γ Doradus stars have early F spectral types. Their expected range in effective temperature lies between 5,200 and 7,650 K (Steindl et al., 2021a). First theoretical predictions for this type of pulsations in pre-main sequence stars have been conducted by Bouabid et al. (2011) without observational evidence. The first observational detections followed a few years later (Zwintz et al., 2013). The g-mode pulsations of pre-main sequence γ Doradus stars are excited by the convective flux blocking mechanism (Guzik et al., 2000). The pulsation periods are in the range from 0.3 to 3 days (Aerts et al., 2010) and, hence, are quite similar to those in SPB stars. A reliable value for effective temperature is therefore required to identify the type of pulsator as the light curves alone are not sufficient.

δ Scuti–γ Doradus hybrid type. Some pre-main sequence pulsators in the A to F range of spectral types can show both p- and g-modes, hence, δ Scuti and γ Doradus type pulsations. Consequently, this class of objects combines the properties of both classes described above.

Stochastic solar type. Stochastic solar-like p-mode oscillations are predicted to be excited in stars before their arrival on the ZAMS (e.g., Samadi et al., 2005). Pre-main sequence stars in the mass range of our Sun are mostly very active objects with magnetic fields, spots on their surfaces, and partly still accreting material from circumstellar disks. The light curves obtained for such objects often show regular and irregular variability that is not connected to pulsations. To be able to search for stochastic solar-like oscillations in pre-main sequence stars requires a suitable tool that deals with the high activity which introduces a high background signal (Müllner et al., 2021). Only one candidate is known at the moment (Müllner et al., 2021), but the search continues.

K and M type. This is a recently discovered type of pulsation in pre-main sequence stars that has no known counterpart in the main sequence and post-main sequence phases. Steindl et al. (2021a) found a region of instability for K- and M-type stars which was expected from previous works (e.g., Baran et al., 2011) and presented a first candidate pulsator of this class. The driving mechanism for M-dwarfs is expected to be the ϵ-mechanism (e.g., Baran et al., 2011, and references therein) but detailed investigations of the instability regions in Steindl et al. (2021a) have not been performed and are subject of future work.

CHALLENGES

The field of pre-main sequence asteroseismology was met by many challenges throughout its relatively brief history. The initial challenge was taken by Breger (1972) who presented the first evidence for pulsational variability in pre-main sequence stars located in NGC 2264. Since then, due to the advent of space telescopes, the number of known pre-main sequence pulsators has risen above 100. In the last decades, lots of challenges regarding pulsations in such young stars have been identified. Many of these have been partly or fully solved, while others remain open until today. The more we start to understand stellar structure and evolution in detail, the more challenges are continuously being created. This sections aims at discussing the currently most important challenges faced by pre-main sequence asteroseismology.

Observational Challenges

When observations of young stellar objects shall be conducted, several challenges have to be tackled. These are mainly related to the early evolutionary state of the stars.

Activity. Young protostars are formed in molecular clouds. During their first evolutionary stages, they gain mass by accreting matter from their birth environment. Consequently, young stars can be partially or completely embedded in dense gas and dust, magnetic fields influence how the matter is accreted onto the early star, and the angular momentum gained from the birth process lets the young stellar object spin fast in most cases. All these phenomena can be summarized with the description that young stars show different levels of activity which manifest themselves in our observations.

The dense circumstellar material can prevent us completely from viewing the young stars in the optical or generates irregular light variations of up to several magnitudes (e.g., Cody et al., 2014). Slightly less dense material can still be responsible for semi-regular variability (e.g., Alencar et al., 2010). Searching for millimagnitude pulsations in photometric time series of young stars therefore becomes tricky (e.g., Zwintz et al., 2009).

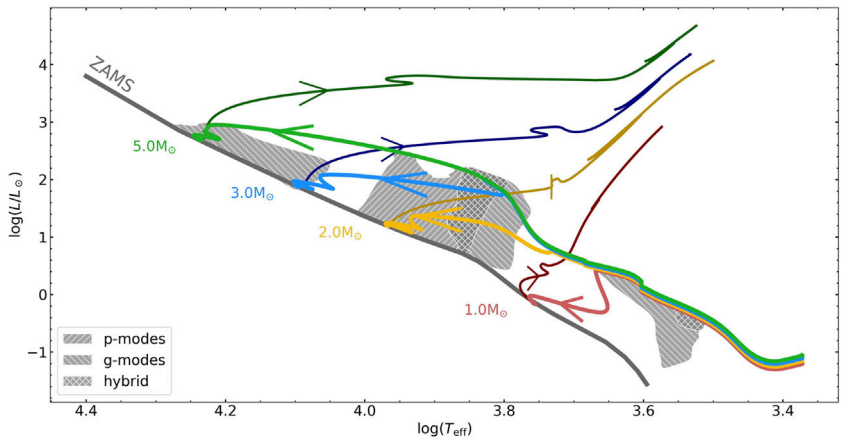

FIGURE 4 | Evolutionary tracks for the protostellar seed until the asymptotic giant branch. The colored lines show the evolution of stars with different masses between 1 and 5 $M_{\odot}$. The pre-main sequence evolution is shown in brighter colors compared to the main- and post-main sequence evolution. Evolutionary tracks are shifted slightly at the beginning of the evolution for better visibility. The zero age main sequence is shown as grey line and the instability regions (i.e., the same as in **Figure 3**) are shown in grey with hashes according to the legend.

The irregular or semi-regular variability originating from the disks has a second challenge for the search and characterization of pulsations: in case the pulsational variability has long periods (i.e., longer than about half a day), the distinction between variability originating from the disk and from the pulsations will be impossible in many cases. The reason is that the irregular variability produces artifacts in the frequency analysis in the low frequency domain where we would also search for the pulsations. Only if the pulsation periods are shorter (i.e., on the order of a few hours and shorter), can they be well distinguished from variability caused by the disk and the artifacts generated during the frequency analysis.

The determination of colors for pre-main sequence stars is also affected by the dense dust that surrounds them: young stars appear much redder than they actually are. Observed colors include the star-disk system and not the star alone. As no general relations for dereddening can be applied for individual young stars with disks (i.e., Herbig Ae/Be stars), the real stellar colors cannot be obtained for embedded objects.

Spectroscopically, the circumstellar matter is visible as very characteristic emission features, for example in the hydrogen lines. Although finding emission lines in the spectra is a good indicator for potentially young stars, in many cases it prevents a reliable calculation of effective temperature and gravitational acceleration which are needed to place the stars into a Kiel diagram.

Evolutionary stage. Taking the atmospheric properties of given stars (i.e., effective temperature, luminosity, and mass) and placing them into a Hertzsprung-Russell diagram does not provide a unique identification of their evolutionary stage which is illustrated in **Figure 4**. Some observational features related to activity have to be used to collect indications for the young evolutionary stage, and the more of these indicators are present, the better. If stars can be attributed to a star forming region or an open cluster as young as–say–ten million years, then this can be considered as excellent evidence for stellar youth. Observational properties such as irregular variability in the photometric time series, infrared and/or ultraviolet excesses, or emission lines in their spectra can point to an early evolutionary stage, but are not unique identifiers because they might also be attributed to quite evolved evolutionary stages. Infrared excesses, for example, can be also found for post-asymptotic giant branch (post-AGB) stars (e.g., Kamath et al., 2014), and circumstellar material is present in the form of Keplerian disks also around classical Be stars (e.g., Rivinius et al., 2013).

Availability of time-series photometry from space. Current and former missions have either not targeted young stellar objects or were quite limited in their observations of the early evolutionary phases of stars and planets.

The currently operational and hugely successful NASA mission TESS (Ricker et al., 2015) can reach down to the galactic plane, but the resulting light curves often suffer from high contamination. The reason is that the CCD pixels are relatively large (i.e., 21 arcseconds per pixel). Consequently, TESS observations avoid to observe deep in the galactic plane.

The NASA mission Kepler (Borucki et al., 2010) observed a single field high above the galactic plane on purpose to avoid star forming regions and any resulting contamination. The Kepler K2 (Gilliland et al., 2010) mission provided some data for young stars and star forming regions in four of 19 campaigns (i.e., campaigns numbers 2, 9, 13, and 15) illustrating the potential of space observations for this research field.

The BRITE-Constellation nano-satellite mission (Weiss et al., 2014) targets only the brightest stars on the sky, limiting the observations of young stars and planets (which are typically fainter by several orders of magnitude) dramatically.

The earlier satellite missions CoRoT (Auvergne et al., 2009) and MOST (Walker et al., 2003) allowed for observations of the youngest objects in the galaxy through dedicated short (i.e., between 10 days and 5–6 weeks) observing runs, for example on the young cluster NGC 2264 (MOST and CoRoT) or on individual young stellar objects such as HD 142666, HD 37806, or TW Hya.

ESA's future mission PLATO (planned launch in 2026; Rauer et al., 2014) is scheduled to observe two selected fields for 2 years each: both fields will not reach down to the galactic plane, hence not be able to target the youngest regions in the Milky Way. Additionally, PLATO's pixel size of 18 μm × 18 μm yields a plate scale of about 26.5 arcseconds per pixel which is even higher than TESS's plate scale. Therefore, observations of star forming regions and young clusters with high object densities will be problematic for PLATO due to high percentages of contamination.

The current maximum time bases for continuous photometric observations of pre-main sequence pulsating stars are ~80 days from Kepler K2 and slightly more than 100 days from TESS (Steindl et al., 2021a). Therefore, pre-main sequence asteroseismology has the challenge to work with way more limited observational material than most of the other fields in asteroseismology.

Theoretical Challenges

Many ingredients are needed to properly describe the earliest phases of stellar evolution since many physical processes are active during that time span. In terms of complexity of the pre-main sequence evolution, the discussion in the introduction only scratches the surface of the challenges we are faced with to create theoretical models of such stars. Stellar rotation, magnetic fields, and star-disk interaction are just a few examples of the physical ingredients, in addition to mass accretion, that need to be kept in mind. All of the above will generally be different for every object. Hence, there might not be a single other phase of stellar evolution in which the spectroscopic parameters and internal structure vary as much on a case by case level as during the pre-main sequence evolution.

Stellar rotation. When stars are born in the collapse of a molecular cloud, they obtain angular momentum. Throughout the accretion phase, in which material from the surrounding disk deposited onto stellar surface, the system is expected to be disk-locked Bouvier et al. (1997). That is, the disk and the star co-rotate until the former is dissolved or its influence on the star becomes minor. The mechanism of disk-locking, however, provides many open questions for the implementation of pre-main sequence models: How long does the disk-locking phase last? What is the distribution of rotation periods and how is it produced? Does the disk lock only the stellar atmosphere or is the whole star co-rotating? If the former, how is the angular momentum distributed in the stellar atmosphere and what is the mechanism of the angular momentum transport? If the latter, what mechanism fixes the rotation rate throughout the star? Some of these questions linger to even later phases of the pre-main sequence stage. After the disk has dissolved, angular momentum throughout the star will evolve according to a not yet fully explained mechanism. Including angular momentum into the current description of stellar evolution models remains an open question with lots of impact on the pulsational characteristics of stars: For gravity mode pulsators, the period spacings are tilted according to the angular momentum of the core while the frequencies of pressure modes are split with respect to the angular velocity and the azimuthal order (Aerts et al., 2010). The Coriolis force in rotating stars gives rise to a new family of pulsation modes, the Rossby modes. The latter have so far not been detected in any pre-main sequence object.

Magnetic fields. As is common in the theory of stellar structure and evolution, many of the theoretical challenges of pre-main sequence asteroseismology are intertwined. Magnetic fields, for example, are expected to play a major role in the rotational evolution of stars. As such, they are expected to dominate the angular momentum transport in radiative zones, albeit not efficient enough to explaining observations (i.e. Fuller et al., 2014). Magnetic braking seems to be the dominant mechanism for angular momentum loss in more evolved stars (i.e. Matt et al., 2015). For pre-main sequence stars, magnetic fields are expected to be an important ingredient for disk-locking (Barnes et al., 2001). As the latter already implies, magnetic fields also carry implications on the mass accretion mechanism and hence the accretion rates themselves (i.e. Bouvier et al., 2007). In addition, magnetic fields directly effect the internal structure of stars including the mode cavities and leave a measurable imprint on the pulsation frequencies (Prat et al., 2019). The interaction between magnetic fields and pulsation can lead to a suppression of the latter, resulting in a change in mode amplitudes (i.e. Lecoanet et al., 2022, and references therein). Magnetic fields with strengths of multiple kG have been found in pre-main sequence stars (Lavail et al., 2017) while their consequences for pre-main sequence asteroseismology have not been explored.

Mass accretion rates. The atmospheric parameters of pre-main sequence stars (Steindl et al., 2021a; Steindl and Zwintz, 2022) as well as their internal structure (see Steindl et al., 2022, and the discussion in the introduction to this article) are dependent on the characteristics of the accretion process. While time-dependent mass accretion rates are, although limited in amount, readily available from 2-dimensional simulations of the disk (e.g. Vorobyov and Basu, 2015; Jensen and Haugbølle, 2018; Elbakyan et al., 2019), many other free parameters need to be set in the calculation of stellar structure models. Most noteworthy, we lack an intrinsic description of the mechanism that describes the energy flow of the accreted material. How much energy is added to the star? How much is radiated away? Where is the energy deposited? At the current stage, we have to manually set many parameters corresponding to different assumptions. For further progress in this field it is inevitable to investigate the detailed physics of the accretion processes in more detail. Additional effects complicate the calculation of the equilibrium stellar structure. The properties of the material transferred from the accretion disk to the star are expected to be dependent on the accretion rate itself. For example, the metallicity should follow the relation $Z_{\rm acc} = \frac{\dot{M}_d}{\dot{M}_{\rm acc}}$ (Kunitomo and Guillot, 2021), where $\dot{M}_d$ is the flux of the gas and $\dot{M}_{\rm acc}$ is the mass accretion rate. Many of the to-date calculated mass accretion histories cannot deliver the needed information of $\dot{M}_d$. However, recent studies provide this information (see e.g. Elbakyan et al., 2020) such that the inclusion of effects from condensing material will be possible in the near future. Most probably, however, the inclusion of these effects will further push the software instrument Modules for Experiments in Stellar Astrophysics (*MESA*) (Paxton et al., 2011, 2013, 2015, 2018, 2019). *MESA* was never designed to perform such calculations and, albeit providing us with an indispensable and

vital tool, repeatedly runs intro convergence issues with strong time-dependent mass accretion rates during the early phases of the pre-main sequence evolution. Strong efforts will need to go into *MESA*-related problems which is a time consuming work. However, we are not concerned that progress in this regard will have to wait long since the core *MESA* team is very helpful in any regards of their community focused tool.

The issue of controlled grid studies. The simple fact that each and every pre-main sequence star has its very own time-dependent accretion rate history and, hence, a very different (and often times chaotic) evolution in the Hertzsprung-Russell diagram (Steindl et al., 2022) complicates the calculation of controlled grids. With the inclusion of disk-mediated accretion rates, the days of (almost) parallel evolutionary tracks are gone which complicates almost every theoretical study. Incorporating assumptions similar to those in the work of Steindl et al. (2021a), namely that each star follows the same accretion track (with constant mass accretion rate) simplifies such studies, but at the cost of completely disregarding the different evolutionary paths. Quasi-random grids, similar to (Steindl and Zwintz, 2022) are in general to be preferred, but the exact values of parameters at a given location in the Hertzsprung-Russell diagram are then not uniquely defined by one evolutionary track. Albeit disk-mediated mass accretion rates are available in a limited amount, the calculation of thousands (as we would wish for in such studies) remain challenging due to the needed computational time.

Pre-main sequence asteroseismology beyond intermediate mass stars. Among known pre-main sequence pulsators, δ Scuti stars significantly outnumber both γ Doradus and SPB stars Steindl et al. (2021a). While it is reasonably simple to verify the pre-main sequence status for δ Scuti and γ Doradus stars, such a verification is much more complicated for the more massive SPB stars. Owing to the fast evolution towards the main sequence, it remains a matter of debate at which mass range will it be still possible to observe stars in their pre-main sequence stage. This, of course, will again be dependent on their evolutionary path from the protostellar stage to the ZAMS. This calls in the need for dedicated calculations with disk-mediated accretion rates that end in higher mass stars (Steindl and Zwintz, 2022). This will not only be helpful in regard to SPB stars, but should provide many insights in asteroseismology of β Cephei stars with even higher mass as well. In the low mass regime, theoretical models suggest an instability region for K- and M-type stars (i.e. Rodríguez-López, 2019; Steindl et al., 2021a) and a first candidate for such pulsation has been presented by Steindl et al. (2021a). According to the theoretical models, many radial orders of g-modes seem to be excited (Steindl et al., 2021a). This instability region needs to be further explored with improved theoretical models for which an important step is to further decrease the mass of the initial stellar seeds which is usually taken to be $\sim 10\,M_{jupiter}$ (Steindl et al., 2021a, 2022; Steindl and Zwintz, 2022).

STRETTO

STRETTO (Early STaRs and planEt evoluTion in Two cOlors) is an innovative project idea that aims to provide a micro-satellite for astronomy from space with the main goal to study early stellar and planetary evolution.

Science goals. STRETTO aims to investigate young stars and planets in star forming regions as well as the youngest open clusters with the goal to address their early evolution. The STRETTO space telescope will be able to study the strength and properties of stellar activity and the amount of rotation present in early stars and their influence on planet formation and evolution. STRETTO will search for signs for the formation of planets and the presence of planets around member stars of young open clusters and star forming regions. The photometric time series obtained by STRETTO will enable studies of the effects of accretion on young stellar objects, of eclipsing binary and multiple systems in their early evolutionary stages, and the interior structures of young stars using asteroseismology. The expected precision of STRETTO will let us investigate the properties of ring systems around exoplanets, other circumplanetary material and the existence of smaller bodies (e.g., exomoons or exocomets) around young stellar objects. Also, the properties of young open clusters and star forming regions as larger-scale objects in our Universe can be investigated with such a mission.

Together with complementary ground-based observations, STRETTO science will allow to improve the input physics for the early phases of stellar and exoplanetary evolution, provide a time-dependent map of rotation and chemical composition from stellar birth to the onset of hydrogen-core burning, determine a complete picture of the angular momentum transport of young stars from the interior to the atmosphere, provide more reliable ages for the youngest stellar and exoplanetary objects, investigate the connection between magnetic fields and variability of stars in their early evolutionary stages, and understand the interaction of the young circumstellar environment with the star, including exoplanets, exomoons, and exocomets.

Instrumental design. STRETTO will carry two 8-cm telescopes each with a 1.5 × 1.5 square degree field of view and a spatial resolution of three to five arcseconds per pixel. Each telescope will have a dedicated filter: one in the optical, the other at infrared wavelengths. From a low-Earth orbit, STRETTO will be able to monitor the young stars and planets for about half a year continuously, providing the necessary long time-bases for the analysis of the objects' different types of variability. STRETTO will be able to take photometric time series measurements of stars in the magnitude range from about 6 to 16 mag (V) in two colors using alternating exposure times in the range from 1 to 60 s. The goal is to utilize a commercially available microsatellite platform (mass: 50–70 kg and power: 60–80W) which shall host two digital camera systems as payloads, one for each passband. A low earth polar orbit in the height range of 600–900 km will be suitable to conduct the scientific observations. The baseline for communication will be one ground station in Europe.

Potential of STRETTO. The scientific potential of monitoring young stars and planets photometrically from space with STRETTO lies in yielding a first clear picture how stars and planets pass through their earliest evolutionary phases.

Status of the project. Presently, a small consortium consisting of researchers and engineers from Austria, Canada, France, the

Netherlands, and Poland is trying to acquire funding for a concept study. If you are interested to learn more about STRETTO and the people involved, please contact the first author of this article.

PROSPECTS AND IMPORTANCE

One might think that our theoretical understanding of stellar evolution is well established with only a minor need for further research. But this is a misconception as there are many physical processes that are either not well-understood (e.g., the impact of accretion on the complete evolution of stars) or not taken into account properly in our theoretical models (e.g., convection, rotation or magnetic fields). The physical effects occurring and defining the earliest evolutionary phases of stars must have an impact on their complete further evolution. It would be physically unlikely that the stars' formation histories do not play a role in their later stages.

One of the biggest questions in this respect is how large the impact of the processes acting in the youngest stellar objects is and how long the pre-main sequence history of stars persists up to later stages. This is one of the questions pre-main sequence asteroseismology can and does address. By adding processes such as accretion to theoretical models of pre-main sequence stars and coupling those to models of pulsational instability lets us investigate the resulting changes in the interior structures of stars.

Pre-main sequence asteroseismology should be able to test the very early evolutionary phases as well. By studying objects with ages of a few million years, we can measure the imprint of the star formation process, thereby shedding light on the many free parameters connected to the accretion physics. The amazing prospect of gathering observational information about the internal structure of stars (rotation rate, chemical mixing profiles, etc.) opens the door to exciting constraints for theoretical models. As of today, the earliest evolutionary phases of stars are often treated as a black box using crude approximations as in the classical model. The resulting stellar structure and atmospheric parameters, however, are used in many different fields to motivate for example the existence of magnetic fields or the evaporation of exoplanet atmospheres. Only dedicated asteroseismic studies of the youngest objects we can possible find, can provide us with the important ingredients to study these processes with the accuracy they deserve.

Chemical composition plays an important role in stellar structure and evolution due to the sensitivity of opacities on the atomic spectra and absorption features of the elements making up the star. Most stars pulsate exactly because of the behaviour of the opacities in relation to perturbations (e.g., the heat engine mechanism). Also, the location of the computed evolutionary tracks for stars at all ages depends on the metallicity, Z (e.g., Montalbán et al., 2004). Presently, we do not understand how the chemical evolution proceeds between stellar birth and the onset of hydrogen core burning upon arrival on the ZAMS. For example, in ~10% of main sequence stars of spectral type B to F chemical peculiarities are found (e.g.; Preston, 1974), but it is unclear when these anomalies are formed. The first few detailed analyses of the atmospheric chemical abundances of pulsating pre-main sequence stars have revealed basically solar or slightly solar chemical composition with two exceptions: 1) stars with masses smaller than ~1.5 $M_{\odot}$ have not burnt the primordial Lithium completely and, hence, show an overabundance compared to the Sun (Zwintz et al., 2013); 2) in the high-resolution spectra of intermediate-mass pre-main sequence pulsators Barium shows a significant overabundance which cannot be fully explained yet (e.g., Zwintz et al., 2013). In the future, high-resolution spectroscopic observations of a statistically large enough sample of pre-main sequence stars should be used to generate a time dependent map of the chemical evolution in the early stages of the lives of stars.

Asteroseismology has successfully revealed the interior chemical structure of stars: it allows measuring the percentage of hydrogen in the cores of main sequence stars (e.g., Moravveji et al., 2015) or detecting chemical gradients in g-mode period spacings (e.g., Miglio et al., 2008; Bouabid et al., 2013). Consequently, pre-main sequence asteroseismology has the potential to probe the interior chemical evolution of stars in the earliest phases of their evolution. Possible topics in this context would be to investigate the influence of the accretion history on the chemical evolution of stars and how long it persists, if observed chemical inhomogeneities on the stellar surfaces extend into the interiors or not, and if stellar pulsations let us deduce, for example, the amount of Deuterium in the earliest stars. But such investigations require an improvement in our theoretical models and dedicated instruments providing the high-accuracy data (both photometrically and spectroscopically) for pre-main sequence stars.

As the excited pulsation frequencies in pre-main sequence stars are different to those in the post-main sequence stages due to the different inner structures (e.g., Suran et al., 2001; Bouabid et al., 2011), it is obvious that stellar pulsations can be used to distinguish the evolutionary stages of stars (Guenther et al., 2007). Even within the pre-main sequence stages, the pulsational properties of stars change following a relation that is not present for the same type of pulsators in later phases: the youngest objects pulsate slower than stars close to the onset of hydrogen core burning (i.e., the ZAMS, Zwintz et al., 2014). Therefore the next logical step is to use the pulsation properties of pre-main sequence stars as an age indicator for stellar astrophysics. In the earliest evolutionary phases, it is difficult to determine precise ages based on our currently available methods. The ages of the youngest open clusters, for example, are typically given with errors of 50–100%. One of the important prospects of pre-main sequence asteroseismology is therefore to provide accurate (relative) ages for young stellar objects - similar to the percentage of hydrogen in the core, X_c, that is determined for the main sequence stages from asteroseismology. This is especially important, as different age indicators that are very useful for the study of older clusters, often fail to improve the accuracy of the age determination of young open clusters. Gyrochronology, for example, can provide fantastic constraints on the age of open clusters, but the usage for pre-main sequence stars is very limited. Measurements of the surface rotation periods of young stars are available, but the only way to reproduce them theoretically is to force a specific distribution of initial rotation

periods. One of the major issues in this regard is the effect of the protostellar disk during the accretion phase. By coupling stellar evolution codes with a designated disk-evolution, we are hopeful to improve the models in this regard. Once we have an accurate picture of the rotation of pre-main sequence stars, we can explore the effects of the stars' rotation on their pulsational properties in much more detail.

Asteroseismology of pre-main sequence stars is needed to address the question why intermediate-mass stars on the main sequence tend to show rigid rotation independent of their core rotation rates (Aerts et al., 2017). Strong coupling between the stellar core and the envelope seems to occur for stars on the main sequence and in later evolutionary phases. With pre-main sequence asteroseismology we will be able to investigate at what earlier point in stellar evolution this strong coupling starts. By measuring nearly-equidistant period spacings we can deduce near-core rotation rates for pre-main sequence g-mode pulsators–as it is already successfully done for stars in later evolutionary stages. First steps in these investigations have been undertaken, but for a complete picture of the angular momentum transport in young stars, longer photometric time-series with highest precision obtained from space are required. The observational material available for pre-main sequence g-mode pulsators now is insufficient to conduct more detailed studies. As a consequence, the idea of the micro-satellite STRETTO (see **Section 4**) dedicated to young star- and planet-forming regions emerged a couple of years ago and will hopefully be realized in the near future.

AUTHOR CONTRIBUTIONS

KZ and TS shared the work on this article and contributed in equal amounts to it.

FUNDING

KZ and TS are funded by the University of Innsbruck and are grateful for the support they are receiving.

ACKNOWLEDGMENTS

We thank Matthew Kenworthy from the University of Leiden (NL), Gregg Wade from the Royal Military College (CAN) and Rainer Kuschnig from the University of Graz (AT) for their collaboration on the satellite project STRETTO. We are grateful to Eduard Vorobyov from the University of Vienna (AT) for the contribution of the time-dependent accretion rates.

REFERENCES

Aerts, C., Christensen-Dalsgaard, J., and Kurtz, D. W. (2010). *Asteroseismology*. Berlin, Germany: Springer.

Aerts, C. (2021). Probing the Interior Physics of Stars through Asteroseismology. *Rev. Mod. Phys.* 93, 015001. doi:10.1103/RevModPhys.93.015001

Aerts, C., Reeth, T. V., and Tkachenko, A. (2017). The Interior Angular Momentum of Core Hydrogen Burning Stars from Gravity-Mode Oscillations. *Astrophysical J. Lett.* 847, L7. doi:10.3847/2041-8213/aa8a62

Alencar, S. H. P., Teixeira, P. S., Guimarães, M. M., McGinnis, P. T., Gameiro, J. F., Bouvier, J., et al. (2010). Accretion Dynamics and Disk Evolution in NGC 2264: a Study Based on CoRoT Photometric Observations. *Astronomy Astrophysics* 519, A88. doi:10.1051/0004-6361/201014184

Auvergne, M., Bodin, P., Boisnard, L., Buey, J. T., Chaintreuil, S., Epstein, G., et al. (2009). The CoRoT Satellite in Flight: Description and Performance. *Astronomy Astrophysics* 506, 411–424. doi:10.1051/0004-6361/200810860

Baraffe, I., and Chabrier, G. (2010). Effect of Episodic Accretion on the Structure and the Lithium Depletion of Low-Mass Stars and Planet-Hosting Stars. *Astronomy Astrophysics* 521, A44. doi:10.1051/0004-6361/201014979

Baraffe, I., Chabrier, G., and Gallardo, J. (2009). Episodic Accretion at Early Stages of Evolution of Low-Mass Stars and Brown Dwarfs: A Solution for the Observed Luminosity Spread in H-R Diagrams? *Astrophysical J. Lett.* 702, L27–L31. doi:10.1088/0004-637X/702/1/L27

Baraffe, I., Vorobyov, E., and Chabrier, G. (2012). Observed Luminosity Spread in Young Clusters and FU Ori Stars: A Unified Picture. *Astrophysical J. Lett.* 756, 118. doi:10.1088/0004-637X/756/2/118

Baran, A. S., Winiarski, M., Krzesiński, J., Fox-Machado, L., Kawaler, S. D., Dróżdz, M., et al. (2011). Mt. Suhora Survey - Searching for Pulsating M Dwarfs. I. *Acta Astron.* 61, 37–58.

Barnes, S., Sofia, S., and Pinsonneault, M. (2001). Disk Locking and the Presence of Slow Rotators Among Solar-Type Stars in Young Star Clusters. *Astrophysical J. Lett.* 548, 1071–1080. doi:10.1086/318988

Bhandare, A., Kuiper, R., Henning, T., Fendt, C., Marleau, G.-D., and Kölligan, A. (2018). First Core Properties: from Low- to High-Mass Star Formation. *Astronomy Astrophysics* 618, A95. doi:10.1051/0004-6361/201832635

Borucki, W. J., Koch, D., Basri, G., Batalha, N., Brown, T., Caldwell, D., et al. (2010). Kepler Planet-Detection Mission: Introduction and First Results. *Science* 327, 977–980. doi:10.1126/science.1185402

Bouabid, M.-P., Dupret, M.-A., Salmon, S., Montalbán, J., Miglio, A., and Noels, A. (2013). Effects of the Coriolis Force on High-Order G Modes in γ Doradus Stars. *MNRAS* 429, 2500–2514. doi:10.1093/mnras/sts517

Bouabid, M.-P., Montalbán, J., Miglio, A., Dupret, M.-A., Grigahcène, A., and Noels, A. (2011). Theoretical Seismic Properties of Pre-main Sequenceγ Doradus Pulsators. *Astronomy Astrophysics* 531, A145. doi:10.1051/0004-6361/201116440

Bouvier, J., Alencar, S. H. P., Harries, T. J., Johns-Krull, C. M., and Romanova, M. M. (2007). "Magnetospheric Accretion in Classical T Tauri Stars," in *Protostars and Planets V*. Editors B. Reipurth, D. Jewitt, and K. Keil, 479.

Bouvier, J., Forestini, M., and Allain, S. (1997). The Angular Momentum Evolution of Low-Mass Stars. *Astronomy Astrophysics* 326, 1023–1043.

Breger, M. (1972). Pre-Main Stars. I. Light Variability, Shells, and Pulsation in NGC 2264. *Astrophysical J. Lett.* 171, 539. doi:10.1086/151308

Christensen-Dalsgaard, J. (1982). Seismological Studies of the Sun and Other Stars. *Adv. Space Res.* 2, 11–19. doi:10.1016/0273-1177(82)90250-2

Cody, A. M., Stauffer, J., Baglin, A., Micela, G., Rebull, L. M., Flaccomio, E., et al. (2014). CSI 2264: Simultaneous Optical and Infrared Light Curves of Young Disk-Bearing Stars in NGC 2264 with CoRoT and Spitzer-Evidence for Multiple Origins of Variability. *Astronomical J.* 147, 82. doi:10.1088/0004-6256/147/4/82

De Marco, O., and Izzard, R. G. (2017). Dawes Review 6: The Impact of Companions on Stellar Evolution. *Publ. Astron. Soc. Aust.* 34, e001. doi:10.1017/pasa.2016.52

Dziembowski, W. A., Moskalik, P., and Pamyatnykh, A. A. (1993). The Opacity Mechanism in B-type Stars - II. Excitation of High-Order G-Modes in Main-Sequence Stars. *Mon. Notices R. Astronomical Soc.* 265, 588–600. doi:10.1093/mnras/265.3.588

Elbakyan, V. G., Johansen, A., Lambrechts, M., Akimkin, V., and Vorobyov, E. I. (2020). Gravitoviscous Protoplanetary Disks with a Dust Component. *Astronomy Astrophysics* 637, A5. doi:10.1051/0004-6361/201937198

Elbakyan, V. G., Vorobyov, E. I., Rab, C., Meyer, D. M.-A., Güdel, M., Hosokawa, T., et al. (2019). Episodic Excursions of Low-Mass Protostars on the

Hertzsprung-Russell Diagram. *MNRAS* 484, 146–160. doi:10.1093/mnras/sty3517

Fuller, J., Lecoanet, D., Cantiello, M., and Brown, B. (2014). Angular Momentum Transport via Internal Gravity Waves in Evolving Stars. *Astrophysical J. Lett.* 796, 17. doi:10.1088/0004-637X/796/1/17

Gilliland, R. L., Brown, T. M., Christensen-Dalsgaard, J., Kjeldsen, H., Aerts, C., Appourchaux, T., et al. (2010). Kepler Asteroseismology Program: Introduction and First Results. *Publ. Astron Soc. Pac* 122, 131–143. doi:10.1086/650399

Gough, D. (1987). Seismological Measurement of Stellar Ages. *Nature* 326, 257–259. doi:10.1038/326257a0

Gruber, D., Saio, H., Kuschnig, R., Fossati, L., Handler, G., Zwintz, K., et al. (2012). New Slowly Pulsating B Stars in the Field of the Young Open Cluster NGC 2244 Discovered by the MOST Photometric Satellite★. *MNRAS* 420, 291–298. doi:10.1111/j.1365-2966.2011.20033.x

Guenther, D. B., Kallinger, T., Zwintz, K., Weiss, W. W., and Tanner, J. (2007). Seismology of Pre-Main-Sequence Stars in NGC 6530. *Astrophysical J. Lett.* 671, 581–591. doi:10.1086/522880

Guzik, J. A., Kaye, A. B., Bradley, P. A., Cox, A. N., and Neuforge, C. (2000). Driving the Gravity-Mode Pulsations in γ Doradus Variables. *Astrophysical J. Lett.* 542, L57–L60. doi:10.1086/312908

Hartmann, L., Cassen, P., and Kenyon, S. J. (1997). Disk Accretion and the Stellar Birthline. *Astrophysical J. Lett.* 475, 770–785. doi:10.1086/303547

Hartmann, L., and Kenyon, S. J. (1996). The FU Orionis Phenomenon. *Annu. Rev. Astron. Astrophys.* 34, 207–240. doi:10.1146/annurev.astro.34.1.207

Hayashi, C. (1961). Stellar Evolution in Early Phases of Gravitational Contraction. *PASJ* 13, 450–452.

Henyey, L. G., Lelevier, R., and Levée, R. D. (1955). The Early Phases of Stellar Evolution. *PASP* 67, 154. doi:10.1086/126791

Hosokawa, T., Offner, S. S. R., and Krumholz, M. R. (2011). On the Reliability of Stellar Ages and Age Spreads Inferred from Pre-main-sequence Evolutionary Models. *Astrophysical J. Lett.* 738, 140. doi:10.1088/0004-637X/738/2/140

Iben, I., Jr. (1965). Stellar Evolution. I. The Approach to the Main Sequence. *Astrophysical J. Lett.* 141, 993. doi:10.1086/148193

Jensen, S. S., and Haugbølle, T. (2018). Explaining the Luminosity Spread in Young Clusters: Proto and Pre-main Sequence Stellar Evolution in a Molecular Cloud Environment. *MNRAS* 474, 1176–1193. doi:10.1093/mnras/stx2844

Kamath, D., Wood, P. R., and Van Winckel, H. (2014). Optically Visible Post-AGB/RGB Stars and Young Stellar Objects in the Small Magellanic Cloud: Candidate Selection, Spectral Energy Distributions and Spectroscopic Examination. *Mon. Notices R. Astronomical Soc.* 439, 2211–2270. doi:10.1093/mnras/stt2033

Kunitomo, M., and Guillot, T. (2021). Imprint of Planet Formation in the Deep Interior of the Sun. *Astronomy Astrophysics* 655, A51. doi:10.1051/0004-6361/202141256

Kunitomo, M., Guillot, T., Takeuchi, T., and Ida, S. (2017). Revisiting the Pre-main-sequence Evolution of Stars. *Astronomy Astrophysics* 599, A49. doi:10.1051/0004-6361/201628260

Kurtz, D. W., and Marang, F. (1995). The Discovery of δ Scuti Pulsational Variability in the Pre-main-sequence Herbig Ae Star, HR 5999, and the Discovery of Rotational Light Variability in the Remarkable He-Weak Bp Star, HR 6000. *MNRAS* 276, 191–198. doi:10.1093/mnras/276.1.191

Larson, R. B. (1969). Numerical Calculations of the Dynamics of a Collapsing Proto-Star*. *Mon. Notices R. Astronomical Soc.* 145, 271–295. doi:10.1093/mnras/145.3.271

Lavail, A., Kochukhov, O., Hussain, G. A. J., Alecian, E., Herczeg, G. J., and Johns-Krull, C. (2017). Magnetic Fields of Intermediate Mass T Tauri Stars. *Astronomy Astrophysics* 608, A77. doi:10.1051/0004-6361/201731889

Lecoanet, D., Bowman, D. M., and Van Reeth, T. (2022). Asteroseismic Inference of the Near-Core Magnetic Field Strength in the Main-Sequence B Star HD 43317. *MNRAS* 512, L16–L20. doi:10.1093/mnrasl/slac013

Marconi, M., and Palla, F. (1998). The Instability Strip for Pre-main-sequence Stars. *Astrophysical J.* 507, L141–L144. doi:10.1086/311704

Matt, S. P., Brun, A. S., Baraffe, I., Bouvier, J., and Chabrier, G. (2015). The Mass-Dependence of Angular Momentum Evolution in Sun-like Stars. *Astrophysical J. Lett.* 799, L23. doi:10.1088/2041-8205/799/2/L23

Mellon, S. N., Mamajek, E. E., Zwintz, K., David, T. J., Stuik, R., J. Talens, G. J., et al. (2019). Discovery of δ Scuti Pulsations in the Young Hybrid Debris Disk Star HD 156623. *Astrophysical J. Lett.* 870, 36. doi:10.3847/1538-4357/aaf008

Miglio, A., Montalbán, J., Noels, A., and Eggenberger, P. (2008). Probing the Properties of Convective Cores through G Modes: High-Order G Modes in SPB and γ Doradus Stars. *Mon. Not. Ras.* 386, 1487–1502. doi:10.1111/j.1365-2966.2008.13112.x

Montalbán, J., D'Antona, F., Kupka, F., and Heiter, U. (2004). Convection in the Atmospheres and Envelopes of Pre-main Sequence Stars. *Astronomy Astrophysics* 416, 1081–1096. doi:10.1051/0004-6361:20031728

Moravveji, E., Aerts, C., Pápics, P. I., Triana, S. A., and Vandoren, B. (2015). Tight Asteroseismic Constraints on Core Overshooting and Diffusive Mixing in the Slowly Rotating Pulsating B8.3V Star KIC 10526294. *Astronomy Astrophysics* 580, A27. doi:10.1051/0004-6361/201425290

Müllner, M., Zwintz, K., Corsaro, E., Steindl, T., Potravnov, I., Guenther, E. W., et al. (2021). Searching for Solar-like Oscillations in Pre-main Sequence Stars Using APOLLO. *Astronomy Astrophysics* 647, A168. doi:10.1051/0004-6361/202039578

Palla, F., and Stahler, S. W. (1990). The Birthline for Intermediate-Mass Stars. *Astrophysical J. Lett.* 360, L47. doi:10.1086/185809

Paxton, B., Bildsten, L., Dotter, A., Herwig, F., Lesaffre, P., and Timmes, F. (2011). Modules for Experiments in Stellar Astrophysics (MESA). *Astrophysical J. Suppl.* 192, 3. doi:10.1088/0067-0049/192/1/3

Paxton, B., Cantiello, M., Arras, P., Bildsten, L., Brown, E. F., Dotter, A., et al. (2013). Modules for Experiments in Stellar Astrophysics (MESA): Planets, Oscillations, Rotation, and Massive Stars. *Astrophysical J. Suppl.* 208, 4. doi:10.1088/0067-0049/208/1/4

Paxton, B., Marchant, P., Schwab, J., Bauer, E. B., Bildsten, L., Cantiello, M., et al. (2015). Modules for Experiments in Stellar Astrophysics (MESA): Binaries, Pulsations, and Explosions. *Astrophysical J. Suppl.* 220, 15. doi:10.1088/0067-0049/220/1/15

Paxton, B., Schwab, J., Bauer, E. B., Bildsten, L., Blinnikov, S., Duffell, P., et al. (2018). Modules for Experiments in Stellar Astrophysics (MESA): Convective Boundaries, Element Diffusion, and Massive Star Explosions. *Astrophysical J. Suppl.* 234, 34. doi:10.3847/1538-4365/aaa5a8

Paxton, B., Smolec, R., Schwab, J., Gautschy, A., Bildsten, L., Cantiello, M., et al. (2019). Modules for Experiments in Stellar Astrophysics (MESA): Pulsating Variable Stars, Rotation, Convective Boundaries, and Energy Conservation. *Astrophysical J. Suppl.* 243, 10. doi:10.3847/1538-4365/ab2241

Praderie, F., Catala, C., Czarny, J., The, P. S., and Tjin A Djie, H. R. E. (1991). Short Term H-Alpha Variations in Two Herbig PMS Stars : HR 5999 and HD 52721. *Astronomy AstrophysicsS* 89, 91.

Prat, V., Mathis, S., Buysschaert, B., Van Beeck, J., Bowman, D. M., Aerts, C., et al. (2019). Period Spacings of Gravity Modes in Rapidly Rotating Magnetic Stars. *Astronomy Astrophysics* 627, A64. doi:10.1051/0004-6361/201935462

Preston, G. W. (1974). The Chemically Peculiar Stars of the Upper Main Sequence. *Annu. Rev. Astron. Astrophys.* 12, 257–277. doi:10.1146/annurev.aa.12.090174.001353

Rauer, H., Catala, C., Aerts, C., Appourchaux, T., Benz, W., Brandeker, A., et al. (2014). The PLATO 2.0 Mission. *Exp. Astron.* 38, 249–330. doi:10.1007/s10686-014-9383-4

Reyniers, K., and Smeyers, P. (2003a). Tidal Perturbations of Linear, Isentropic Oscillations in Components of Circular-Orbit Close Binaries. *Astronomy Astrophysics* 409, 677–688. doi:10.1051/0004-6361:20031098

Reyniers, K., and Smeyers, P. (2003b). Tidal Perturbations of Linear, Isentropic Oscillations in Components of Circular-Orbit Close Binaries. *Astronomy Astrophysics* 404, 1051–1065. doi:10.1051/0004-6361:20030501

Ricker, G. R., Winn, J. N., Vanderspek, R., Latham, D. W., Bakos, G. Á., Bean, J. L., et al. (2015). Transiting Exoplanet Survey Satellite (TESS). *J. Astronomical Telesc. Instrum. Syst.* 1, 014003. doi:10.1117/1.JATIS.1.1.014003

Ripepi, V., Leccia, S., Baglin, A., Ruoppo, A., Bernabei, S., Zwintz, K., et al. (2010). CoRoT Observations of the Young Open Cluster Dolidze 25. *Astrophys. Space Sci.* 328, 119–122. doi:10.1007/s10509-009-0189-1

Rivinius, T., Carciofi, A. C., and Martayan, C. (2013). Classical Be Stars. *Astron Astrophys. Rev.* 21, 69. doi:10.1007/s00159-013-0069-0

Rodríguez-López, C. (2019). The Quest for Pulsating M Dwarf Stars. *Front. Astron. Space Sci.* 6, 76. doi:10.3389/fspas.2019.00076

Ruoppo, A., Marconi, M., Marques, J. P., Monteiro, M. J. P. F. G., Christensen-Dalsgaard, J., Palla, F., et al. (2007). A Theoretical Approach for the Interpretation of Pulsating PMS Intermediate-Mass Stars. *Astronomy Astrophysics* 466, 261–268. doi:10.1051/0004-6361:20066756

Samadi, R., Goupil, M.-J., Alecian, E., Baudin, F., Georgobiani, D., Trampedach, R., et al. (2005). Excitation of Solar-like Oscillations: From PMS to MS Stellar Models. *J. Astrophys. Astron* 26, 171–184. doi:10.1007/BF02702325

Steindl, T., Zwintz, K., Barnes, T. G., Müllner, M., and Vorobyov, E. I. (2021a). Pulsational Instability of Pre-main-sequence Models from Accreting Protostars. *Astronomy Astrophysics* 654, A36. doi:10.1051/0004-6361/202140818

Steindl, T., Zwintz, K., and Bowman, D. M. (2021b). Tidally Perturbed Pulsations in the Pre-main Sequence δ Scuti Binary RS Cha. *Astronomy Astrophysics* 645, A119. doi:10.1051/0004-6361/202039093

Steindl, T., and Zwintz, K. (2022). Pulsational Instability of Pre-main Sequence Models from Accreting Protostars. II. Modelling Echelle Diagrams of δ Scuti Stars without Rotational Splitting. *Astronomy Astrophysics*. in review.

Steindl, T., Zwintz, K., and Vorobyov, E. I. (2022). A Tale from the Past: the Imprint of Star Formation on Stellar Pulsations. in review.

Suran, M., Goupil, M., Baglin, A., Lebreton, Y., and Catala, C. (2001). Comparative Seismology of Pre- and Main Sequence Stars in the Instability Strip. *Astronomy Astrophysics* 372, 233–240. doi:10.1051/0004-6361:20010485

Unno, W., Osaki, Y., Ando, H., Saio, H., and Shibahashi, H. (1989). *Nonradial Oscillations of Stars*. Tokyo: University of Tokyo Press.

Vorobyov, E. I., and Basu, S. (2015). Variable Protostellar Accretion with Episodic Bursts. *Astrophysical J. Lett.* 805, 115. doi:10.1088/0004-637X/805/2/115

Walker, G., Matthews, J., Kuschnig, R., Johnson, R., Rucinski, S., Pazder, J., et al. (2003). TheMOSTAsteroseismology Mission: Ultraprecise Photometry from Space. *Publ. Astron Soc. Pac* 115, 1023–1035. doi:10.1086/377358

Walker, M. F. (1956). Studies of Extremely Young CLUSTERS.I.NGC 2264. *Astrophysical J. Suppl.* 2, 365. doi:10.1086/190026

Weiss, W. W., Rucinski, S. M., Moffat, A. F. J., Schwarzenberg-Czerny, A., Koudelka, O. F., Grant, C. C., et al. (2014). BRITE-constellation: Nanosatellites for Precision Photometry of Bright Stars. *Publ. Astronomical Soc. Pac.* 126, 573–585. doi:10.1086/677236

Wuchterl, G. (2001). "A Dialogue on Dynamical Pre-main Sequence Tracks," in *The Formation of Binary Stars*. Editors H. Zinnecker and R. Mathieu, 200, 492–495. doi:10.1017/s0074180900225588

Zwintz, K. (2008). Comparing the Observational Instability Regions for Pulsating Pre-Main-Sequence and Classical δ Scuti Stars. *Astrophysical J. Lett.* 673, 1088–1092. doi:10.1086/524293

Zwintz, K., Fossati, L., Ryabchikova, T., Guenther, D., Aerts, C., Barnes, T. G., et al. (2014). Echography of Young Stars Reveals Their Evolution. *Science* 345, 550–553. doi:10.1126/science.1253645

Zwintz, K., Fossati, L., Ryabchikova, T., Kaiser, A., Gruberbauer, M., Barnes, T. G., et al. (2013). γ Doradus Pulsation in Two Pre-main Sequence Stars Discovered by CoRoT. *Astronomy Astrophysics* 550, A121. doi:10.1051/0004-6361/201220127

Zwintz, K., Guenther, D. B., and Weiss, W. W. (2007). Nonradial Oscillations on a Pre-Main-Sequence Star. *Astrophysical J. Lett.* 655, 342–344. doi:10.1086/509819

Zwintz, K., Kallinger, T., Guenther, D. B., Gruberbauer, M., Huber, D., Rowe, J., et al. (2009). MOST Photometry of the Enigmatic PMS Pulsator HD 142666. *Astronomy Astrophysics* 494, 1031–1040. doi:10.1051/0004-6361:200811116

Zwintz, K., Moravveji, E., Pápics, P. I., Tkachenko, A., Przybilla, N., Nieva, M.-F., et al. (2017). A Comprehensive Study of Young B Stars in NGC 2264. *Astronomy Astrophysics* 601, A101. doi:10.1051/0004-6361/201630327

Zwintz, K. (2019). The Power of Asteroseismology for Early Stellar Evolution. *Front. Astron. Space Sci.* 6, 68. doi:10.3389/fspas.2019.00068

Conflict of Interest: The authors declare that the research was conducted in the absence of any commercial or financial relationships that could be construed as a potential conflict of interest.

Publisher's Note: All claims expressed in this article are solely those of the authors and do not necessarily represent those of their affiliated organizations, or those of the publisher, the editors and the reviewers. Any product that may be evaluated in this article, or claim that may be made by its manufacturer, is not guaranteed or endorsed by the publisher.

frontiers | Frontiers in Astronomy and Space Sciences

BRIEF RESEARCH REPORT
published: 06 July 2022
doi: 10.3389/fspas.2022.931963

Quaternionic Transform: A new Light on the Solar Power Spectrum

Rafael Garrido[1]*, *Adrián Ayala*[1], *Javier Pascual-Granado*[1], *José Gómez-Torrecillas*[2] and *José Ramón Rodón*[1]

[1]Institute of Astrophysics of Andalusia, Department of Stellar Astrophysics, Granada, Spain, [2]Department of Algebra and IMAG, University of Granada, Granada, Spain

Asteroseismology, that is, the use of the frequency content of a time series caused by variations in brightness or radial velocity of a stellar object, is based on the hypothesis that such a series is harmonic and therefore can be described by a sum of sines and cosines. If this were not the case (e.g., the oscillations of an ellipsoid of revolution) it cannot be guaranteed that the Discrete Fourier transform is the least squares approximation to the time series. This report studies the effect of extending the Fourier kernel to a particular quaternion and exploring the impact when it is applied to the best time series that we have (GOLF/SoHO) from the closest star, our Sun. The results are consistent with a notable improvement in the signal-to-noise ratio in the low frequency range. This opens the possibility of detecting the elusive g modes of the Sun in future works.

Keywords: stellar pulsations, data analysis, solar physics, g-modes, quaternion

OPEN ACCESS

Edited by:
Mario J. P. F. G. Monteiro, University of Porto, Portugal

Reviewed by:
Enrico Maria Nicola Corsaro, Osservatorio Astrofisico di Catania (INAF), Italy
Maria Pia Di Mauro, National Institute of Astrophysics (INAF), Italy

***Correspondence:**
Rafael Garrido
garrido@iaa.es

Specialty section:
This article was submitted to Stellar and Solar Physics, a section of the journal Frontiers in Astronomy and Space Sciences

Received: *29 April 2022*
Accepted: *07 June 2022*
Published: *06 July 2022*

Citation:
Garrido R, Ayala A, Pascual-Granado J, Gómez-Torrecillas J and Rodón JR (2022) Quaternionic Transform: A new Light on the Solar Power Spectrum. Front. Astron. Space Sci. 9:931963. doi: 10.3389/fspas.2022.931963

1 INTRODUCTION

The solar g modes are still a puzzling problem in Asteroseismology (Christensen-Dalsgaard, 2021). After decades of active search, no definitive direct evidence exists of the detection of the gravity driven solar pulsations although they have been indirectly inferred from their period separation in the Sun (García et al., 2007). Also, in red giant stars some authors (Beck et al., 2011; Mosser et al., 2011) could observe the direct interaction between g-modes and p-modes in the form of mixed modes. Fossat et al. (2017) and Fossat and Schmider (2018) proposed that some hints of the solar g modes appear in the splitting of the pressure oscillations due to the rotation of the solar core. However, the uncertainty about the internal rotational velocity of the Sun, hampers the significance of this indirect findings.

In this report, we propose a modification of the usual Fourier transform analysis that takes advantage of a quaternion formulation. This function is chosen intending to: 1) recovering the usual Fourier kernel at solar frequencies (i.e., the 5-min p-modes); 2) improving the signal-to-noise ratio (SNR) all along the frequency spectrum.

As we discuss in **Section 2**, the introduction of a quaternion in the kernel of the transform allow us to perform a rotation in the complex plane $\mathbb{C}^2$ which can be frequency dependent and enhance the SNR at lower frequencies through acting on the complex angles. We also demonstrate that the power spectrum so calculated is a 4-degrees of freedom Chi-square distribution. In **Section 3** we analyze the solar power spectrum obtained from GOLF/SoHO (Domingo et al., 1995; Gabriel et al., 1995, 1997) data using our new transform. Finally, in **Section 4** we discuss the results and prospects for future work.

2 METHOD: FORMULATION OF A NEW TRANSFORM IN FREQUENCY DOMAIN

If ν, t are the frequency and time parameters of a certain frequency domain transform, we call $\theta = \nu t$ the linear phase of the transform. Complex transforms such as Fourier have just one phase but if we extend to a quaternion domain we can introduce a new phase $\hat{\theta}$ corresponding to the complex numbers $\mathbb{C}_i$ while θ is still the original phase corresponding to $\mathbb{C}_j$. The kernel of the new quaternionic transform reads:

$$\mathcal{F}^{ker}_{mod}(\theta) = e^{\mathbf{i}\pi\hat{\theta}} \cdot e^{\mathbf{j}\pi\theta} \tag{1}$$

Expanding the second exponential in trigonometric form:

$$\begin{aligned}\mathcal{F}^{ker}_{mod}(\theta) &= \left[\cos\left(\pi\hat{\theta}\right) + \mathbf{i}\sin\left(\pi\hat{\theta}\right)\right] \cdot e^{\mathbf{j}\pi\theta} \\ &= \cos\left(\pi\hat{\theta}\right) \cdot e^{\mathbf{j}\pi\theta} + \mathbf{i}\sin\left(\pi\hat{\theta}\right) \cdot e^{\mathbf{j}\pi\theta}\end{aligned} \tag{2}$$

This new kernel has two complex components in $\mathbb{C}_j$ that we call $co(\theta)$ and $si(\theta)$ for analogy with trigonometric functions:

$$co(\theta) = \cos\left(\pi\hat{\theta}\right) \cdot e^{\mathbf{j}\pi\theta} \tag{3}$$

$$si(\theta) = \sin\left(\pi\hat{\theta}\right) \cdot e^{\mathbf{j}\pi\theta} \tag{4}$$

$$\mathcal{F}^{ker}_{mod}(\theta) = co(\theta) + \mathbf{i}si(\theta) \tag{5}$$

Note also that **Eq. 5** can be expanded in the quaternion components:

$$\mathcal{F}^{ker}_{mod}(\theta) = Re(co(\theta)) + \mathbf{i}\,Re(si(\theta)) + \mathbf{j}\,Im(co(\theta)) + \mathbf{k}\,Im(si(\theta)) \tag{6}$$

The last equation can be represented in complex matrix representation $\mathbb{C}^{2\times2}$

$$\begin{aligned}&\begin{pmatrix}1 & 0\\ 0 & 1\end{pmatrix}Re(co(\theta)) + \begin{pmatrix}0 & -1\\ 1 & 0\end{pmatrix}Re(si(\theta)) \\ &+\begin{pmatrix}j & 0\\ 0 & -j\end{pmatrix}Im(co(\theta)) + \begin{pmatrix}0 & j\\ j & 0\end{pmatrix}Im(si(\theta))\end{aligned} \tag{7}$$

defining a operator $\mathcal{F}^{ker}_{mod}(\theta)$ on the complex plane $\mathbb{C}^2$

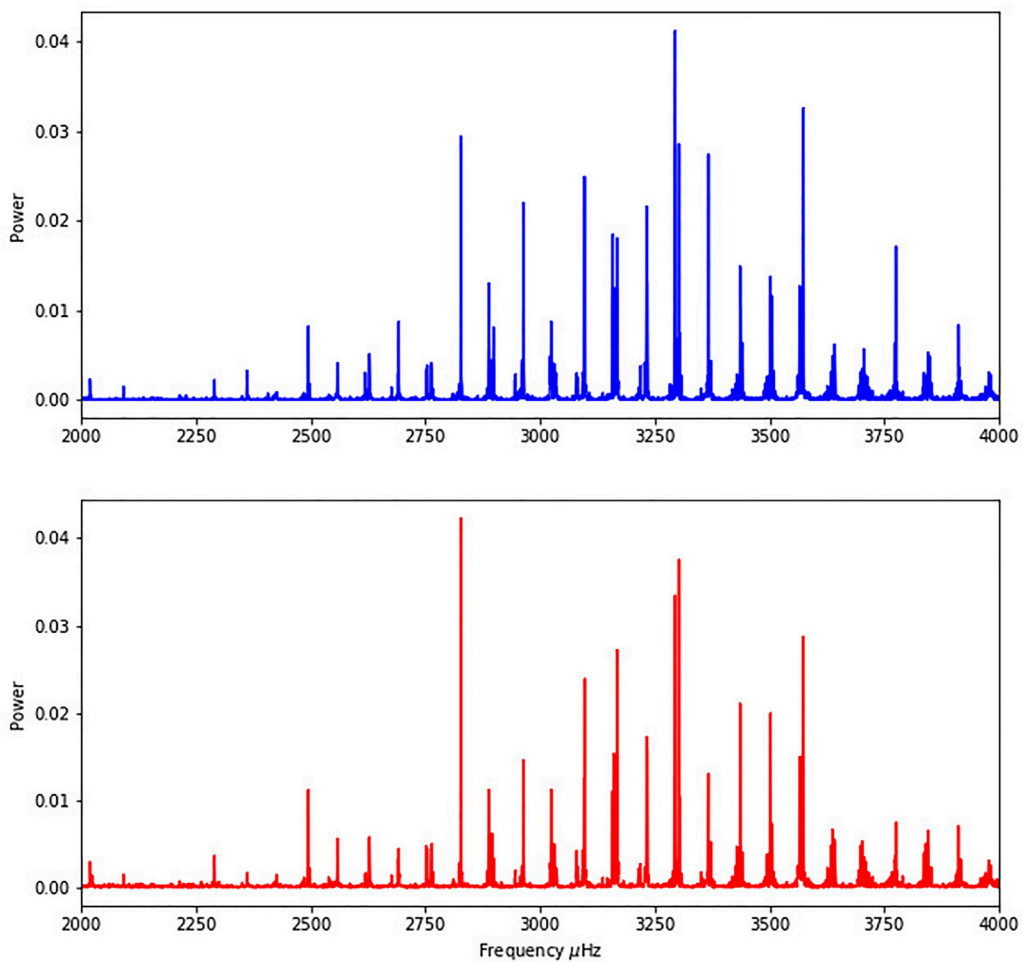

FIGURE 1 | Modified (red) and Classical (blue) Fourier Transforms of the SoHO data obtained during 16 days, at the region between 2,000 and 4,000 μHz. Note that the main differences between both transforms in this range is the higher amplitude in the case of the quaternion Fourier transform, compatible with a better signal-to-noise ratio.

$$\mathcal{F}_{mod}^{ker}(\theta) = \begin{pmatrix} co(\theta) & -\overline{si(\theta)} \\ si(\theta) & \overline{co(\theta)} \end{pmatrix} \tag{8}$$

which is unitary, since.

$$|co(\theta)|^2 = co(\theta)\overline{co(\theta)} = \cos^2(\pi\theta) \tag{9}$$

$$|si(\theta)|^2 = si(\theta)\overline{si(\theta)} = \sin^2(\pi\theta) \tag{10}$$

therefore, $|\mathcal{F}_{mod}^{ker}(\theta)| = 1$.

We observe that **Eq. 8** may be interpreted as a rotation in $\mathbb{C}^2$ of the Fourier kernel $e^{\mathbf{j}\pi\theta}$ with angle $\pi\hat{\theta}$.

In previous equations we made $co(\theta)$, $si(\theta)$ to depend only on θ. Now, the heuristic definition of the new kernel is complete introducing $\hat{\theta}$ as:

$$\hat{\theta} = \sqrt{\theta^2 + 4} \tag{11}$$

This definition is motivated by the limitations of the classical analysis of stellar light curves, that is, high frequencies can be detected in the solar power spectrum but low frequencies cannot. If we left θ instead of $\hat{\theta}$ the new transform would be just a quaternion Fourier transform, with the same limitations as the classical DFT.

We could have also defined $co(\theta)$, $si(\theta)$ through the mapping:

$$f(\theta) = \frac{\theta}{2} + \sqrt{\left(\frac{\theta}{2}\right)^2 + 1} = e^{\sinh^{-1}(\theta/2)} \tag{12}$$

This equation, which derives from the definition of the inverse hyperbolic sine function, will help us to interpret physically the new proposed formulation.

After some mathematical derivations, we can also express $co(\theta)$ and $si(\theta)$ as two functions depending on the variable f instead of θ and $\hat{\theta}$

$$co(f) = \frac{1}{2}\left(e^{2\pi\mathbf{j}f} + e^{2\pi\mathbf{j}/f}\right) \tag{13}$$

$$si(f) = \frac{1}{2\mathbf{j}}\left(e^{2\pi\mathbf{j}f} - e^{2\pi\mathbf{j}/f}\right) \tag{14}$$

therefore.

$$co(f) + \mathbf{j}si(f) = e^{2\pi\mathbf{j}f} \tag{15}$$

$$co(f) - \mathbf{j}si(f) = e^{2\pi\mathbf{j}/f} \tag{16}$$

being these two equations complex numbers instead of quaternions.

We introduce these functions since they allow us to extend the original Fourier transform into quaternions from a sine-cosine decomposition. In this sense, we can recover the tangent function as the ratio $si(\theta)/co(\theta)$ for every value of θ as can be easily see from **Eqs 3**,**4**. Finally, these functions form the basis of a new transform that we can apply to any time series.

This modified kernel allow us to define a new discrete transform $\mathcal{F}_{mod}$ that can be applied to a time series instead of a DFT. Thus, for a certain function $X(t)$ sampled at regular time intervals Δt we have the time series $x(t_i)$ where $t_i = i\Delta t$ for $i = 1 \ldots N$. In order to mitigate spectral leakage at low frequencies, the dataset $x(t_i)$ is usually normalized statistically before applying the transform. Then, we define the modified transform as:

$$\mathcal{F}_{mod}[x(t_i)] = \frac{2}{N}\sum_{i=0}^{N-1} x(t_i) e^{\mathbf{i}\sqrt{\left(\Phi_{ij}/2\right)^2 + 4\pi^2}} e^{\mathbf{j}\Phi_{ij}/2} \tag{17}$$

Here ν_j stands for the discretization of the frequencies ν

$$\nu_j = \frac{j}{N\Delta t} \tag{18}$$

where the angular phase Φ_{ij} is

$$\Phi_{ij} = 2\pi\theta_{ij} = 2\pi \cdot \left[\nu_j t_i \mod 1\right] = 2\pi \cdot \left[ij/N \mod 1\right] \tag{19}$$

As usual we take the modulus of the quaternion transform as defined in **Eq. 17** to obtain a periodogram that estimates the frequency content of the time series.

In the next section we discuss the goodness of our approach with respect to the classical discrete Fourier transform for the case of the solar radial velocities observed by GOLF/SoHO instrument. We will discuss first the underlying statistics of the new transform.

2.1 Statistics

We devote this sub-section to the study of the underlying statistics that the modified DFT produces. We will follow a similar procedure as Scargle (1982) for the a standard DFT where the author proved that the Lomb-Scargle periodogram has a chi-square distribution with two degrees of freedom.

Taking into account the expansion in quaternion components in **Eq. 6** the periodogram corresponding to the modified DFT shown in **Eq. 17** is:

$$\begin{aligned} P_{mod}(\omega_j) = \frac{4}{N^2}\Bigg[& \left(\sum_{i=0}^{N-1} x(t_i) Re(co(\theta))\right)^2 \\ & + \left(\sum_{i=0}^{N-1} x(t_i) Re(si(\theta))\right)^2 \\ & + \left(\sum_{i=0}^{N-1} x(t_i) Im(co(\theta))\right)^2 + \left(\sum_{i=0}^{N-1} x(t_i) Im(si(\theta))\right)^2 \Bigg] \end{aligned}$$

Now with the definitions of $co(\theta)$ and $si(\theta)$ in **Eqs 3**, **4**,

$$\begin{aligned} P_{mod}(\omega_j) = \frac{4}{N^2}\Bigg[& \left(\sum_{i=0}^{N-1} x(t_i)\cos(\pi\hat{\theta})\cos(\pi\theta)\right)^2 \\ & + \left(\sum_{i=0}^{N-1} x(t_i)\sin(\pi\hat{\theta})\cos(\pi\theta)\right)^2 + \left(\sum_{i=0}^{N-1} x(t_i)\cos(\pi\hat{\theta})\sin(\pi\theta)\right)^2 \\ & + \left(\sum_{i=0}^{N-1} x(t_i)\sin(\pi\hat{\theta})\sin(\pi\theta)\right)^2 \Bigg] \end{aligned}$$

Finally, introducing the heuristic formulation of $\hat{\theta}$ and the discretization formula of **Eq. 19**:

$$P_{mod}(\omega_j) = \frac{4}{N^2}\left[\left(\sum_{i=0}^{N-1} x(t_i)\cos\left(\sqrt{(\Phi_{ij}/2)^2 + 4\pi^2}\right)\right.\right.$$
$$\cos(\Phi_{ij}/2)\Big)^2 + \left(\sum_{i=0}^{N-1} x(t_i)\right.$$
$$\sin\left(\sqrt{(\Phi_{ij}/2)^2 + 4\pi^2}\right)\cos(\Phi_{ij}/2)\Big)^2 +$$
$$\left(\sum_{i=0}^{N-1} x(t_i)\cos\left(\sqrt{(\Phi_{ij}/2)^2 + 4\pi^2}\right)\right.$$
$$\sin(\Phi_{ij}/2)\Big)^2 + \left(\sum_{i=0}^{N-1} x(t_i)\sin\right.$$
$$\left.\left.\left(\sqrt{(\Phi_{ij}/2)^2 + 4\pi^2}\right)\sin(\Phi_{ij}/2)\right)^2\right] \tag{20}$$

In the plots, however, we will use the amplitude which is just the square root of $P_{mod}(\omega_j)$. Consider now the case where $x(t_i)$ is an independently and normally distributed noise with zero mean and constant variance σ_0^2. In order to study the distribution of $P_{mod}(\omega_j)$ we define the quantities

$$\begin{aligned} CC(\omega) &= \sum_{i=0}^{N-1} x(t_i)\cos(\pi\hat{\theta}_i)\cos(\pi\theta_i) \\ SC(\omega) &= \sum_{i=0}^{N-1} x(t_i)\sin(\pi\hat{\theta}_i)\cos(\pi\theta_i) \\ CS(\omega) &= \sum_{i=0}^{N-1} x(t_i)\cos(\pi\hat{\theta}_i)\sin(\pi\theta_i) \\ SS(\omega) &= \sum_{i=0}^{N-1} x(t_i)\sin(\pi\hat{\theta}_i)\sin(\pi\theta_i) \end{aligned} \tag{21}$$

which are the content of each parenthesis in **Eq. 20**. Now our modified periodogram can be expressed with these functions as:

$$P_{mod}(\omega_j) = \frac{4}{N^2}\left[CC(\omega_j)^2 + CS(\omega_j)^2 + SC(\omega_j)^2 + SS(\omega_j)^2\right] \tag{22}$$

where CC, CS, SC and SS are linear combinations of independent normal random variables since in **Eq. 21** the sine and cosine functions act as constant coefficients. Since a linear combination of normally distributed random variables is also normal the mean value will be zero for each of these functions. The corresponding variances are:

$$\sigma_{CC}^2 = \sum_k \sum_i \langle x(t_k)x(t_i)\rangle \cos(\pi\hat{\theta}_k)\cos(\pi\theta_k)$$
$$\cos(\pi\hat{\theta}_i)\cos(\pi\theta_i) = N\sigma_0^2 \sum_k \cos^2(\pi\hat{\theta}_k)\cos^2(\pi\theta_k)$$
$$\sigma_{SC}^2 = \sum_k \sum_i \langle x(t_k)x(t_i)\rangle \sin(\pi\hat{\theta}_k)\cos(\pi\theta_k)\sin(\pi\hat{\theta}_i)$$
$$\cos(\pi\theta_i) = N\sigma_0^2 \sum_k \sin^2(\pi\hat{\theta}_k)\cos^2(\pi\theta_k)$$
$$\sigma_{CS}^2 = \sum_k \sum_i \langle x(t_k)x(t_i)\rangle \cos(\pi\hat{\theta}_k)\sin(\pi\theta_k)\cos(\pi\hat{\theta}_i)$$
$$\sin(\pi\theta_i) = N\sigma_0^2 \sum_k \cos^2(\pi\hat{\theta}_k)\sin^2(\pi\theta_k)$$
$$\sigma_{SS}^2 = \sum_k \sum_i \langle x(t_k)x(t_i)\rangle \sin(\pi\hat{\theta}_k)\sin(\pi\theta_k)\sin(\pi\hat{\theta}_i)$$
$$\sin(\pi\theta_i) = N\sigma_0^2 \sum_k \sin^2(\pi\hat{\theta}_k)\sin^2(\pi\theta_k)$$

where we have used the independence of x_i and x_k so the cross-terms vanish.

Now, if the 4 variables have equal variances the distribution of $P_{mod}(\omega_j)$ is a chi-square with 4 degrees of freedom (Papoulis, 1965). If the variances are different we cannot use a chi-square distribution but we have to use the Bessel function instead.

To summarise, we have included in this research report a brief development of the underlying statistics of our heuristic transform since it will have important implications on the analysis of the power spectrum for the detection of pulsation frequencies. In the application we present in the next section we assume that the distribution of $P_{mod}(\omega_j)$ is a chi-square with 4 degrees of freedom. A complete statistical treatment is out of the scope of this note.

3 RESULTS: ANALYSIS OF SOHO DATA

We performed our new analysis on a time series of radial velocities, corresponding to 16 days (with 20 s of sampling time) from the GOLF instrument aboard the SoHO satellite (Gabriel et al., 1995). Although there are much longer observations from SoHO/GOLF, we limited the total duration of our dataset to 16 days as a trade-off between avoiding the influence of rotation and preserving frequency resolution. Following the principles of Open Science we have created a repository[1] with the code and inputs necessary to reproduce the results.

Figure 1 shows the typical solar 5-min p mode spectrum obtained through GOLF/SoHO radial velocity observations. The region from 2 to 4 mHz is almost identical for both the classical and modified DFT. We have verified that the new transform is as computationally expensive in time as the classical DFT.

Figure 2 shows low degree p-modes with a clear improvement using our heuristic modification of Fourier transform. The identification of solar dipole p-modes could be used to study the rotational splitting and constraint the rotational profile in the core Chaplin et al. (2001). In this work we are interested just in introducing the quaternion transform and showing first results.

In **Figure 3** the entire GOLF spectrum is shown in loglog scale to highlight the background. The signature of granulation appears to be similar in both cases.

The total power in the spectrum obtained through the quaternion transform is higher than in a DFT since the higher frequency harmonics are preserved and the lower frequency harmonics are enhanced. While this might contradict Plancherel's theorem, it is inherent to the innovative idea of this work since we are assuming that the observed signal is in some way filtered out and that we can invert the filtering with the quaternion transform. The prove for the conservation of energy must obtained through theoretical models that provide proper constraints to the pulsation energy content, but this is out of the scope of this manuscript.

[1]https://github.com/AsteroSeismologyIAA/QuaternionTransform

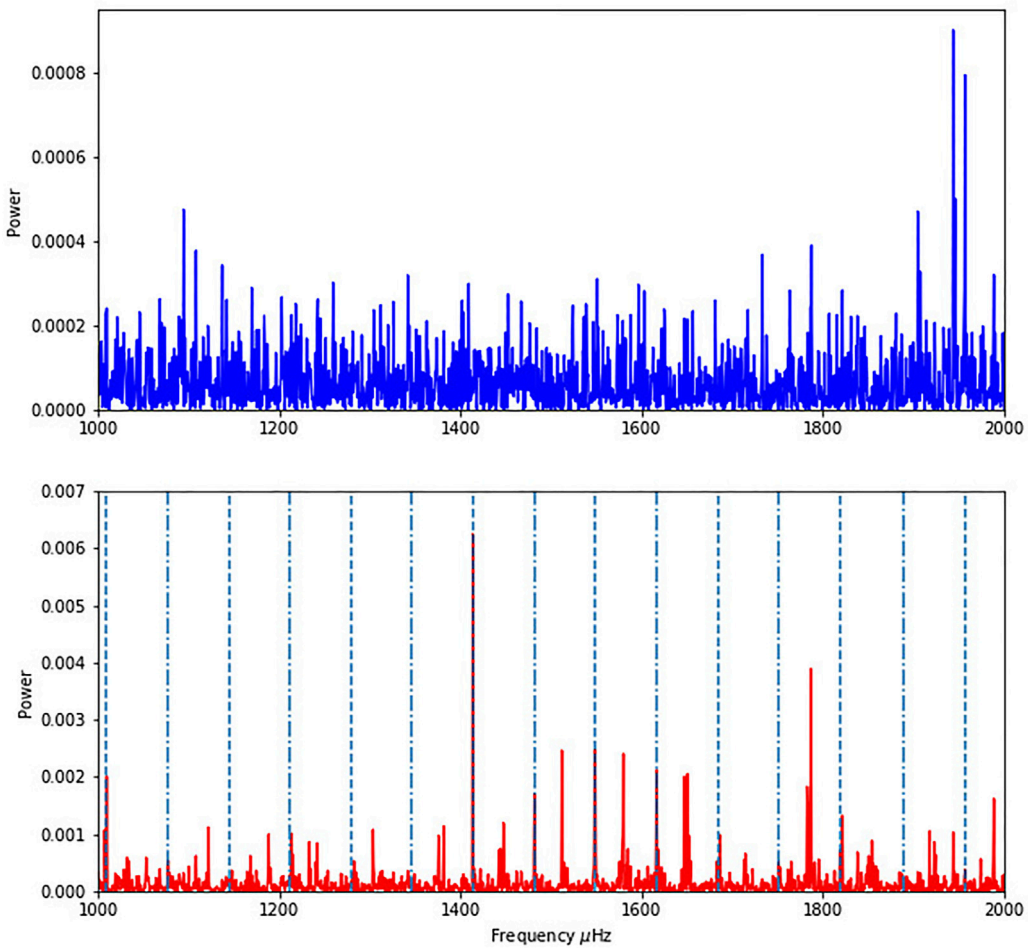

FIGURE 2 | Modified (red) and Classical (blue) Fourier Transforms of the SoHO data obtained during 16 days, at the region between 1,000 and 2,000 μHz. In the red plot we include the l = 0 (dashed) and l = 1 (point-dashed) modes we have identified from the analysis of the new quaternion transform. The Gaussian envelope of the structure visible in the red plot could be a hint of the presence of not identified modes in the common Fourier analysis but further analysis is required to confirm this.

4 DISCUSSION

Now we focus on detection and identification of pulsation modes using the frequency separation in the asymptotic regime taking into account the large separation as defined in Tassoul (1980).

We are going to calculate the successive frequencies for $l = 0$ and $l = 1$ for asymptotic solar p modes from the estimation of large separation in this way:

$$\nu_{n,l}^{calc} = \Delta\nu_0 \cdot (n + l/2 + 1/2) \tag{23}$$

assuming $D_0 = 0$, $\epsilon = 1/2$ and a constant large frequency separation $\Delta\nu_0 = 134.699\ \mu Hz$.

In order to compare with the theoretically calculated frequencies we calculate the modified DFT in a box of $\pm 10\ \mu Hz$ around the expected frequencies from the asymptotic regime. A time span of 44 days is used for this purpose to increase the frequency resolution. Frequencies are estimated in the power spectrum of the modified DFT in a first approximation as the local maxima found in the intervals explored. The formula adopted for the asymptotic regime is given in Tassoul (1980, see Eq.65).

Table 1 shows frequencies calculated from **Eq. 23**, assuming the aforementioned large separation value, in the asymptotic regime of p modes, and the frequencies extracted with the modified DFT. A good agreement between both frequency lists is clear.

In summary, we have introduced in this brief research report a modified Fourier transform which is similar to the classical DFT for high frequencies and consistent with the theoretically predicted large separation frequency for low degree and high order p modes. This shows the consistency of the new transform for the case of the Sun. We could identify l = 0 and l = 1 modes in the 1,000–2,000 μHz region and the identification of other modes require further studies. The analysis here performed is an

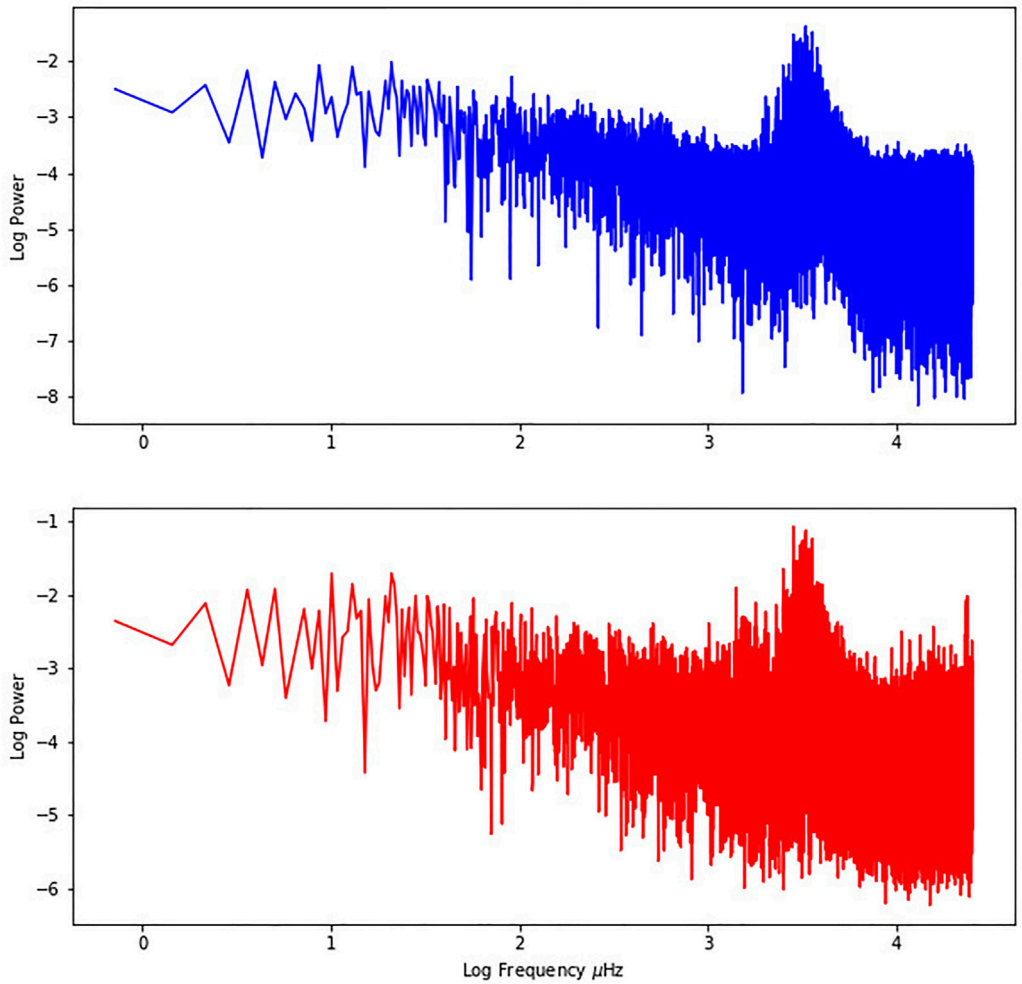

FIGURE 3 | Modified (red) and Classical (blue) Fourier Transforms of the SoHO data obtained during 16 days, from 0 to the Nyquist frequency (i.e., 25 mHz) in loglog scale.

TABLE 1 | Asymptotic behaviour of solar p modes detected with the new transform proposed in this paper. *n* and *l* stands for the radial order and angular degrees of the mode respectively. We show the frequencies detected with the quaternion Fourier transform, $\nu_{n,l}^{obs}$, as well as the frequencies calculated with **Eq. 23**, $\nu_{n,l}^{calc}$.

n	l	$\nu_{n,l}^{obs}$ (μHz)	$\nu_{n,l}^{calc}$ (μHz)
6	0	1,009.8	1,010.2
6	1	1,077.7	1,077.6
7	0	1,145.3	1,144.9
7	1	1,212.3	1,212.3
8	0	1,279.5	1,279.6
8	1	1,346.3	1,347.0
9	0	1,413.6	1,414.3
9	1	1,481.4	1,481.7
10	0	1,548.8	1,549.0
10	1	1,616.2	1,616.4
11	0	1,684.0	1,683.7
11	1	1,751.6	1,751.1
12	0	1,819.7	1,818.4
12	1	1,888.2	1,885.8
13	0	1,956.3	1,953.1

incomplete and rough approximation to the solution but the focus of this brief research report is on the introduction of the new quaternion transform.

DATA AVAILABILITY STATEMENT

The datasets presented in this study can be found in online repositories. The names of the repository/repositories and accession number(s) can be found below: https://www.ias.u-psud.fr/golf/templates/access.html.

AUTHOR CONTRIBUTIONS

RG proposed the original idea and performed most of the calculations. AA did the plots, contributed to the writing of the manuscript, and mathematical developments. JP-G contributed to mathematical discussion and writing of the

manuscript. JG-T introduced the mathematical framework for the second section and contributed to the mathematical rigor to the manuscript. JRR has contributed to the work creating tools for the reproducibility and replicability of the work published in this journal. He has also connected the data and code repository to the Open Science ESCAPE platform. All authors contributed to the revision of the manuscript.

FUNDING

RG, AA, JP-G and JRR acknowledge financial support from the State Agency for Research of the Spanish MCIU through PID2019-107061GB-C63 from the `Programas Estatales de Generaci\'on de Conocimiento y Fortalecimiento Cient\'ifico y Tecnol\'ogico del Sistema de I+D+i y de I+D+i Orientada a los Retos de la Sociedad', and from the State Agency for Research through the "Center of Excellence Severo Ochoa" award to the Instituto de Astrofísica de Andalucía (SEV-2017-0709), all from the Spanish Ministry of Science, Innovation and Universities (MCIU). JG-T is supported by grant PID2019-110525GB-100 from the State Agency for Research and FEDER.\par

ACKNOWLEDGMENTS

RG and JP-G acknowledge Jeff Scargle and Lourdes Verdes Montenegro for fruitful discussions.

REFERENCES

Beck, P. G., Bedding, T. R., Mosser, B., Stello, D., Garcia, R. A., Kallinger, T., et al. (2011). Kepler Detected Gravity-Mode Period Spacings in a Red Giant Star. *Science* 332, 205. doi:10.1126/science.1201939

Chaplin, W. J., Elsworth, Y., Isaak, G. R., Marchenkov, K. I., Miller, B. A., and New, R. (2001). Rigid Rotation of the Solar Core? on the Reliable Extraction of Low-Rotational P-Mode Splittings from Full-Disc Observations of the Sun. *Mon. Notices R. Astronomical Soc.* 327, 1127–1136. doi:10.1046/j.1365-8711.2001.04805.x

Christensen-Dalsgaard, J. (2021). Solar Structure and Evolution. *Living Rev. Sol. Phys.* 18, 2. doi:10.1007/s41116-020-00028-3

Domingo, V., Fleck, B., and Poland, A. I. (1995). The SOHO Mission: an Overview. *Sol. Phys.* 162, 1–37. doi:10.1007/BF00733425

Fossat, E., Boumier, P., Corbard, T., Provost, J., Salabert, D., Schmider, F. X., et al. (2017). Asymptotic G Modes: Evidence for a Rapid Rotation of the Solar Core. *Astronomy Astrophysics* 604, A40. doi:10.1051/0004-6361/201730460

Fossat, E., and Schmider, F. X. (2018). More about Solar G Modes. *Astronomy Astrophysics* 612, L1. doi:10.1051/0004-6361/201832626

Gabriel, A. H., Charra, J., Grec, G., Robillot, J.-M., Cortés, T. R., Turck-Chièze, S., et al. (1997). Performance and Early Results from the GOLF Instrument Flown on the SOHO Mission. *Sol. Phys.* 175, 207–226. doi:10.1023/A:1004911408285 10.1007/978-94-011-5236-5_12

Gabriel, A. H., Grec, G., Charra, J., Robillot, J.-M., Roca Cortés, T., Turck-Chièze, S., et al. (1995). Global Oscillations at Low Frequency from the SOHO Mission (GOLF). *Adv. Space Res.* 162, 61–99. doi:10.1007/978-94-009-0191-9_3

García, R. A., Turck-Chièze, S., Jiménez-Reyes, S. J., Ballot, J., Pallé, P. L., Eff-Darwich, A., et al. (2007). Tracking Solar Gravity Modes: The Dynamics of the Solar Core. *Science* 316, 1591–1593. doi:10.1126/science.1140598

Mosser, B., Barban, C., Montalbán, J., Beck, P. G., Miglio, A., Belkacem, K., et al. (2011). Mixed Modes in Red-Giant Stars Observed with CoRoT. *Astronomy Astrophysics* 532, A86. doi:10.1051/0004-6361/201116825

Papoulis, A. (1965). *Probability, Random Variables and Stochastic Processes*. Tata McGraw-Hill Education.

Scargle, J. D. (1982). Studies in Astronomical Time Series Analysis. II - Statistical Aspects of Spectral Analysis of Unevenly Spaced Data. *Astrophysical J.* 263, 835–853. doi:10.1086/160554

Tassoul, M. (1980). Asymptotic Approximations for Stellar Nonradial Pulsations. *Astrophysical J.* 43, 469–490. doi:10.1086/190678

Conflict of Interest: The authors declare that the research was conducted in the absence of any commercial or financial relationships that could be construed as a potential conflict of interest.

Publisher's Note: All claims expressed in this article are solely those of the authors and do not necessarily represent those of their affiliated organizations, or those of the publisher, the editors and the reviewers. Any product that may be evaluated in this article, or claim that may be made by its manufacturer, is not guaranteed or endorsed by the publisher.

frontiers | Frontiers in Astronomy and Space Sciences

PERSPECTIVE
published: 06 July 2022
doi: 10.3389/fspas.2022.909268

A Synergic Strategy to Characterize the Habitability Conditions of Exoplanets Hosted by Solar-Type Stars

Raffaele Reda[1,2]*, *Maria Pia Di Mauro*[2], *Luca Giovannelli*[1,2], *Tommaso Alberti*[2], *Francesco Berrilli*[1,2] *and Enrico Corsaro*[3]

[1]*Dipartimento di Fisica, Università degli Studi di Roma "Tor Vergata", Roma, Italy,* [2]*INAF-IAPS, Istituto di Astrofisica e Planetologia Spaziali, Roma, Italy,* [3]*INAF-Osservatorio Astrofisico di Catania, Catania, Italy*

We present a new synergic strategy that merges the potential of asteroseismology with solar space weather/climate techniques in order to characterize solar-like stars and their interaction with hosted exoplanets. The method is based on the use of seismic data obtained by the space missions Kepler/K2 and TESS Transiting Exoplanet Survey Satellite, coupled with stellar activity estimates deduced from ground-based campaigns (e.g., Mount Wilson Observatory HK Project). Our investigation allows us to determine not only highly accurate fundamental parameters of the mother star and its orbiting planet, but also to study the stellar magnetic activity and the star-planet interaction: in analogy to the Sun-Earth system, it is possible to infer the mean stellar wind acting on the exoplanet in order to define the conditions of the exoplanetary environment and the erosion of its atmosphere with an impact on the habitability of the planet.

Keywords: exoplanets, solar-type stars, asteroseismology, stellar magnetic activity, habitability, stellar wind, stellar pulsations, star-planet interaction

OPEN ACCESS

Edited by:
Tiago Campante, Instituto de Astrofísica e Ciências do Espaço (IA), Portugal

Reviewed by:
R. Gafeira, University of Coimbra, Portugal

***Correspondence:**
Raffaele Reda
raffaele.reda@roma2.infn.it

Specialty section:
This article was submitted to Stellar and Solar Physics, a section of the journal Frontiers in Astronomy and Space Sciences

Received: *31 March 2022*
Accepted: *03 June 2022*
Published: *06 July 2022*

Citation:
Reda R, Di Mauro MP, Giovannelli L, Alberti T, Berrilli F and Corsaro E (2022) A Synergic Strategy to Characterize the Habitability Conditions of Exoplanets Hosted by Solar-Type Stars. Front. Astron. Space Sci. 9:909268. doi: 10.3389/fspas.2022.909268

1 INTRODUCTION

The high–precision and continuous photometric measurements performed by space missions, such as CoRoT (Baglin et al., 2006), Kepler/K2 (Borucki et al., 2010) and TESS (Ricker et al., 2014), have not only allowed to discover thousands of exoplanets in orbit around solar-like stars, but also to disclose the structural and dynamical properties of many of the detected stars, including their evolutionary state, by applying the methods of asteroseismology. However, stand-alone photometry is a limited tool for the characterization of exoplanetary systems. The combination of different approaches, both theoretical and observational, are needed in order to really progress in this field.

As we have learnt from our Solar system, the main physical parameters of a planet and its equilibrium temperature are not sufficient to characterize the habitability conditions. An accurate knowledge of the fundamental parameters of the host-star is crucial for the interpretation of the detection of an exoplanet, the study of its structure and its evolution. Moreover, a necessary other ingredient for a complete characterization is a detailed assessment of the interaction between host-star and its planets (Airapetian et al., 2020). Indeed, manifestations of stellar activity in the form of coronal mass ejections, energetic particles, stellar flares and winds, as well as an high stellar flux in particular wavelength ranges (e.g., UV, X-ray), can strongly affect the planetary environment. Extreme space weather conditions, such as those created by frequent flares and coronal mass

ejections from active stars and young Sun, may profoundly affect the chemistry and climate of terrestrial type exoplanets (see e.g., Cohen et al., 2015; Dong et al., 2018).

The strategy that we propose here brings together asteroseismic tools and space-weather/space-climate techniques, to characterize host Sun-like stars and the way they influence the environment around exoplanets. In particular, by analyzing the photometric measurements provided by space missions and by making use of asteroseismic techniques, we are able to obtain the main stellar parameters with high precision, allowing to have an accurate characterization of host stars. On the other side, stellar activity measurements from ground-based observatory allow us, by making use of a model that we calibrated on the Sun-Earth system, to estimate the stellar wind pressure acting on exoplanets, and hence to evaluate the effects on their magnetosphere.

The stellar targets to which apply this strategy include main-sequence solar-like stars hosting, possibly rocky, exoplanets, for which both asteroseismic and magnetic activity observations are available. Considering the fact that we wish to extend to other stars the techniques developed for the Sun, it is important to clarify that low mass, intermediate age stars of spectral type G, should represent the best targets for our study. The only limit to the application of the present strategy is represented by the fact that presence of enhanced magnetic activity might be responsible for suppression of solar-like oscillations as already found in several targets (e.g., García et al., 2010; Chaplin et al., 2011; Mathur et al., 2019).

2 STELLAR CHARACTERIZATION WITH ASTEROSEISMOLOGY

During the last decades striking results have been obtained for several hundreds of cool main-sequence, post main-sequence and red-giant stars which exhibit solar-like pulsations, as in the Sun, excited by near-surface turbulent convection. In fact, solar-like pulsations provide the unique opportunity to study in details the internal structure and rotation of the stars and to put very stringent constraints on the fundamental stellar parameters. Accuracy of the order of few % in the determination of the mass and the radius and less than 10% in the age, much higher than with any other method, have been reached by the use of asteroseismic techniques (see e.g., Metcalfe et al., 2010; Mathur et al., 2012) in combination with measurements of chemical composition, position, distance and velocity obtained by large spectroscopic surveys (e.g., GAIA Gaia Collaboration et al., 2016).

Any asteroseismic study starts from the detection and identification of the pulsations properties of a star, deduced by a careful analysis of the oscillation spectrum obtained by photometric observations. Then, by the application of well developed techniques and the use of state-of-the-art stellar structure models built with update evolutionary codes (e.g., Christensen-Dalsgaard, 2008b), it is possible to obtain the stellar fundamental parameters and other details of a star with detected solar-like pulsations.

2.1 Data Analysis

In order to analyze stellar oscillations we require that a power spectral density (PSD) is computed out of the light curve of the star we intend to analyze (e.g., García et al., 2011). Once the PSD is available, the preliminary step is to estimate the overall signal that constitutes each observation. This signal, broadly referred to as background, comprises signal originated from stellar oscillations (which are modeled through a typical Gaussian envelope), granulation activity (often decomposed into multiple components operating at different characteristic timescales, each one reproduced by a Harvey-like profile, Harvey 1985) and possible long-trend variations that could be related to the presence of stellar activity, rotational modulation, and instrumental effects (usually modeled by means of an additional Harvey-like profile). This background fit can be carried out by means of the public Bayesian inference software DIAMONDS (Corsaro and De Ridder, 2014), which has a specific adaptation for dealing with the multiple components that are typically encountered in low- and intermediate-mass stars of spectral types from F to K (Corsaro et al., 2017). Furthermore, one can extract the average (or global) asteroseismic parameters, namely the frequency of maximum oscillation power $\nu_{\max}$ and the large frequency separation $\Delta\nu$, quantities directly linked to fundamental stellar properties. A typical example of this analysis is shown in panel A of **Figure 1** for the solar-type star 16 Cyg A observed by Kepler.

The final step in the data analysis foresees an additional level of detail and it consists in measuring the observational properties of the individual oscillation modes that belong to the region of the oscillation power excess (see panel B of **Figure 1**). This analysis is of particular complexity as it may involve the fitting of a large number of parameters, moreover it can be accomplished only for stars where the PSD has a signal-to-noise ratio that is sufficiently high, along with the available frequency resolution, such that the individual modes can be resolved. In these cases, we make use of the public pipeline FAMED (Corsaro et al., 2020), which can perform an automated analysis of tens of individual mode properties in a reasonable amount of time.

2.2 Asteroseismic Assessment of Stellar Physical Properties

In the context of stellar asteroseismic characterization a key role is played by empirical relations, found by studying oscillation properties of hundreds of stars, that connect observable quantities with stellar physical parameters. In fact, a first estimate of global stellar parameters can be obtained starting from the main properties of the oscillation spectra, such as the large frequency separation ($\Delta\nu$), namely the difference between frequencies of same harmonic degree, and the frequency of maximum oscillation power ($\nu_{\max}$) (Brown et al., 1991; Kjeldsen and Bedding, 1995; Huber et al., 2011). The large frequency separation ($\Delta\nu$), defined as the inverse sound travel time through the stellar radius (Tassoul, 1980), is linearly proportional to the square root of the stellar density (Ulrich, 1986) and hence it is related to the stellar mass and radius. The frequency of maximum oscillation power ($\nu_{\max}$) is expected to scale with the acoustic cutoff frequency ($\nu_{\rm ac}$) (Brown et al., 1991):

$$\nu_{max} \propto \nu_{\rm ac} \propto g\, T_{\rm eff}^{-1/2} \tag{1}$$

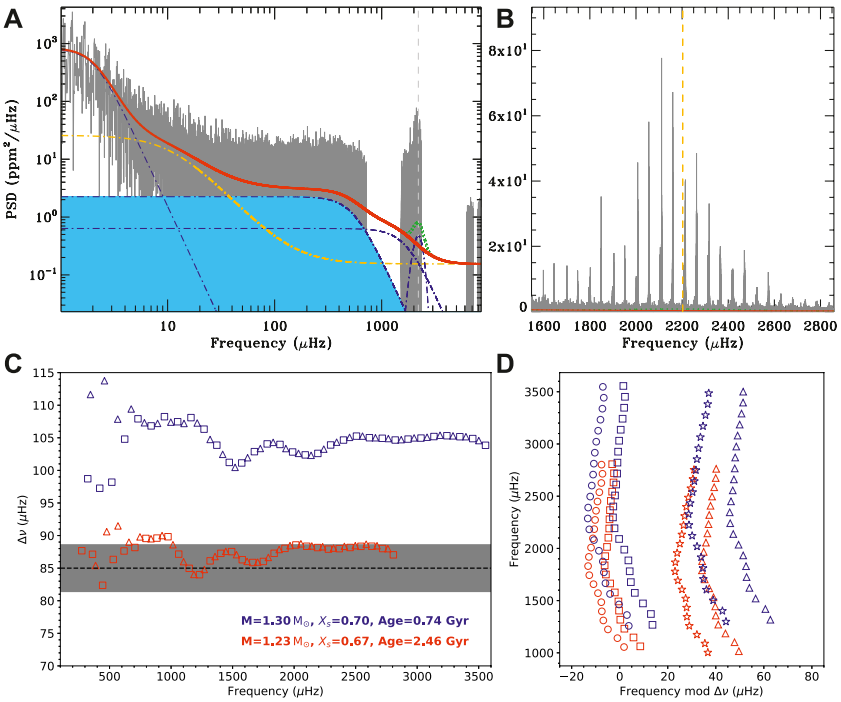

FIGURE 1 | (A): An example of power spectral density (gray) for the solar-like star 16 Cyg A observed by *Kepler*. The solid red curve is a fit to the background as obtained by Corsaro et al. (2020), consisting of three Harvey-like profiles (blue dotted–dashed curves) plus white and colored noise (yellow dotted–dashed line). A global fit to the oscillation power excess is shown by the blue dotted–dashed Gaussian curve and the net effect on the background is visible as a doted green curve. **(B)**: Observed frequency spectrum of 16 Cyg A centered in the frequency range around the frequency of maximum oscillation power (indicated with the yellow dashed line), showing the typical Gaussian-like shape. **(C)**: Large separation $\Delta\nu$ as a function of the frequency for two theoretical models (identified by red and blue colors) of the star GJ 504, chosen to fit the spectroscopic parameters. The dashed line indicates the still uncertain observed value $\Delta\nu$ =(85.0 ± 3.6) μHz, with the confidence interval shown by the gray shaded area. Different symbols are used to distinguish between the modes l =0 (squares) and l =1 (triangles). **(D)**: Échelle diagram for GJ 504 computed for the two models of panel C, with model's average large separation values $\Delta\nu$ =87.8 μHz (blue color model) and $\Delta\nu$ =104.5 μHz (red color model) (Di Mauro et al., 2022). Different symbols are used for modes with different harmonic degrees, squares for l =0, triangles for l =1, circles for l =2 and stars for l =3.

where $T_{\rm eff}$ is the effective temperature of the star and g is its surface gravity. Hence by definition, $\nu_{\rm max}$ is also related to the mass and the radius of the star. A set of powerful scaling-laws, normalized to solar values, can be used to roughly determine the mass and radius of a star once $\Delta\nu$ and $\nu_{\rm max}$ are known, as suggested by Huber et al. (2011):

$$\frac{M}{M_\odot} \simeq \left(\frac{\nu_{max}}{\nu_{max\,\odot}}\right)^3 \left(\frac{\Delta\nu}{\Delta\nu_\odot}\right)^{-4} \left(\frac{T_{\rm eff}}{T_{\rm eff\,\odot}}\right)^{3/2} \quad (2)$$

$$\frac{R}{R_\odot} \simeq \left(\frac{\nu_{max}}{\nu_{max\,\odot}}\right) \left(\frac{\Delta\nu}{\Delta\nu_\odot}\right)^{-2} \left(\frac{T_{\rm eff}}{T_{\rm eff\,\odot}}\right)^{1/2}. \quad (3)$$

A more precise characterization of the stellar structure, and in particular the age, can be obtained looking at individual pulsation frequencies, instead of using the average oscillation properties of the spectra, and comparing them with frequencies obtained by theoretical models built in order to match all the available photometric and spectroscopic parameters of the star under study or by employing more sophisticated techniques, such as inversion methods (Di Mauro, 2016).

Once the planet host has been properly studied, different exoplanetary details can be deduced with a good accuracy (Campante et al., 2018; Lundkvist et al., 2018). Several attempts have been tried to determine, for example, the orbital elements from the parameters of the star, but certainly the estimate of the age is the most important for understanding the history of the planet and its habitability. Generally, the ages of single main-sequence stars are inferred from empirical indicators, such as activity, rotation or from stellar model isochrones that are compared to observed classical parameters. However, the precision and accuracy that can currently be reached with these methods is not good enough (Lebreton and Goupil, 2014), compared to the possibility to use asteroseismic data.

As an example, here we report the case of GJ 504 (HD 115383), a G0-type solar-like star with effective temperature $T_{\rm eff} \simeq 6200$ K and surface gravity log $g = 4.29 \pm 0.07$ dex (D'Orazi et al., 2017). This target appears to be more massive than the Sun ($M = 1.28 \pm 0.07\,M_\odot$), with a radius $R = 1.38 \pm 0.2\,R_\odot$ as predicted by theoretical models (Di Mauro et al., 2022), but its evolutionary stage is still an open question, with consequences for mass estimation of its star's companion named GJ 504b, which could be a Jovian planet or a brown-dwarf. Panel C of **Figure 1** shows the comparison between the average large separation obtained with a very low resolution by the analysis of the photometric TESS data collected in 120-s cadence mode

and the theoretical value as a function of the oscillation frequency for modes $l = 0$ and $l = 1$. Here the theoretical adiabatic oscillation frequencies have been computed by using the ADIPLS package (Christensen-Dalsgaard, 2008a) on theoretical models built in order to match all the observed spectroscopic parameters. Among all the possible models, we show one model which seems compatible with the unconfirmed value of large frequency separation $\Delta\nu = (85.0 \pm 3.6)$ μHz (Di Mauro et al., 2022). It is very interesting to notice that models that match the luminosity deduced from the Gaia Parallax, are characterized by a very young age ≤ 0.7 Gyr, while models which reproduce the provisional large separation (85.0 ± 3.6) μHz show more evolved structures with age above 2 Gyr. It is clear that even just the measurement of the large separation, once confirmed, will definitely help to constrain the debated evolutionary state of this target and of its companion. But this will be achieved only with better conditions of signal to noise ratio (i.e., spectroscopic observations, shorter cadence mode etc, . . .).

A more detailed comparison between theoretical and observational frequencies is usually done by employing a so called échelle diagram, like the ones shown in panel D of **Figure 1**, obtained for two theoretical models of GJ 504 with parameters given in panel C. This diagram shows, for each harmonic degree, vertical ridges of frequencies in which consecutive symbols are equally spaced by the large separations. The distance between two adjacent columns of frequencies represents the small separation. Clearly here, the two theoretical models show a different oscillatory pattern. Please notice that for GJ 504 no individual observational frequencies have been already detected, but a comparison with the theoretical frequencies will have allowed to determine the age with an accuracy of less than 10%. In addition, the échelle diagram shows, for each l, a weak oscillatory signal so that symbols do not form straight columns. The characteristics of such signal are related to the location and thermodynamic properties of discontinuities occurring inside the star. By isolating the oscillatory components from the observed frequencies of oscillations it is possible to determine, for example, the location of the base of the convective envelope. This information is highly important also for testing stellar dynamo theories (Corsaro et al., 2021) and studying the stellar magnetic activity.

3 MAGNETIC ACTIVITY

Characterizing a star does not mean only to determine the main stellar parameters and its spectral type, but it requires also a precise assessment of the activity level, which is a measure of how strong the surface magnetic field is (Schrijver and Zwaan, 2000). In order to quantify the magnetic activity of a star, indices linked to physical quantifies (i.e., physical indices), like the flux in a particular spectral band, are the more appropriate ones. The intensities of emission in the chromospheric H (393.3 nm) and K (396.8 nm) lines of the Ca II represent strong markers of stellar magnetic activity (Hall, 2008) and for this reason many activity indicators are based on them (e.g., $R^{'}_{HK}$, Ca II K index, S-index). The longest and widest observational campaign of the emission in the Ca II H&K lines, for thousand solar-type stars, comes from the HK Project conducted at the Mount Wilson Observatory (MWO) starting from 1966 and operating for almost 40 years. The MWO observations are given in terms of a dimensionless parameter, the S-index, which is defined as the ratio of emission in the H & K lines cores to that in two nearby continuum reference bandpasses (Vaughan et al., 1978; Wilson, 1978). The majority of our knowledge about stellar magnetic activity, the presence of periodic variability (i.e., stellar cycles), as well as how the activity level is related to other stellar properties, come from the analysis of these measurements. For instance, as seen in the Ca II emission, the magnetic activity of main-sequence stars is known to decrease as the inverse square root of the age (Skumanich, 1972). This result constitutes a milestone in the stellar characterization, with a direct impact also from the point of view of habitability conditions around an host star, due to the fact that young stars are typically more active. An example on how information on the magnetic activity cycle can be deduced from the MWO chromospheric emission measurements is depicted in panel A of **Figure 2**, for the star HD 76151, a G3-type solar-like star with effective temperature $T_{\rm eff} \simeq 5790$ K and surface gravity $\log g = 4.49 \pm 0.06$ dex (Marsden et al., 2014). Here we show the Ca II K index, computed from the S-index using the relation by Egeland et al. (2017), which for this star covers a time period of 30 years and allows to see an almost well-defined cycle. Measurements like this one are available, within the MWO dataset, for thousand solar-like stars and constitute a great asset in the stellar characterization, especially for their temporal extension.

4 HOST STAR—PLANET INTERACTION

To date, we have a simplified notion of habitability on extra-solar planets, mainly related to the concept of Habitable Zone (HZ). It is indeed based on the flux of radiation incident on a planet, and is classically defined as the range of distances from the host star in which a planet could potentially maintain liquid water on its surface (Hart, 1979; Kasting et al., 1993; Kopparapu et al., 2013).

Nevertheless, the stellar irradiance is not the only source to consider in the evaluation of the stellar environment from the habitability point of view. The variability of the host star and the extreme events must also be considered, as well as the flux in particular wavelength ranges (e.g., UV) compared to the bolometric one. The increase in UV and X-ray star's flux generated by flares can strongly affect the near stellar environment. This radiation has enough energy to modify the stratospheric ozone cycle of an Earth-like planet, which plays a central role in the thermal structure of high atmosphere (Lovric et al., 2017). Recent studies have assessed the effects of high flaring activity on exoplanets, showing that ozone shield may be comprehensively destroyed, leaving the planet's surface unprotected to extreme radiations that can damage complex organic structures (e.g., Tilley et al., 2019). Looking to more general effects on exoplanet's atmospheres, frequent strong flares on active and young stars are disadvantageous for hosting life,

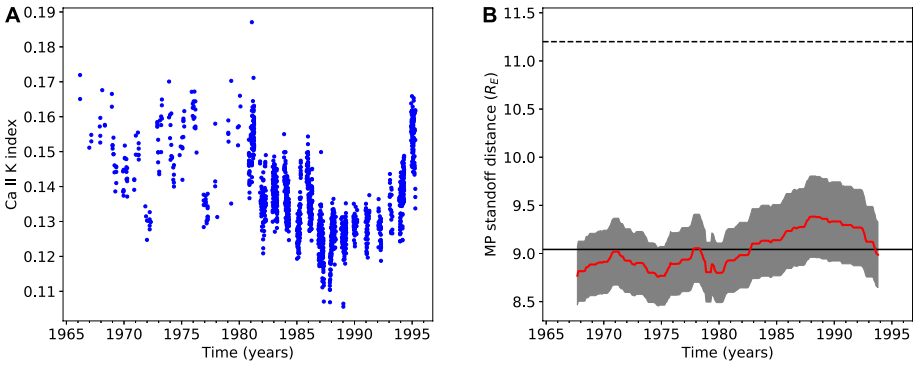

FIGURE 2 | (A): Ca II K index of the star HD 76151 for the time interval 1966–1996, obtained from the MWO S-index measurements. **(B)**: Magnetopause standoff distance (red line, with confidence interval represented by the gray shaded area) of a fictitious Earth-twin planet orbiting at 1 AU around the solar-type star HD 76151. The continuous black line indicates the mean value, while the dashed black line shows the mean Earth value as reference.

because the atmospheric composition of orbiting planets is constantly altered (Vida et al., 2017). In the worst cases of unmagnetized (unprotected) planets, the atmosphere can even be eroded (Roettenbacher and Kane, 2017; Loyd et al., 2020).

When studying the star-planet interaction, a key point is represented by the evaluation of the stellar winds effects on the planetary environment. In magnetized planets, a main outcome of this interaction is represented by the perturbation and compression of the planetary magnetosphere. A direct measurement of the exoplanet magnetic moment is a difficult task. Different methods have been proposed, involving bow-shock observations during transits (Vidotto et al., 2011), radio signature (Hess and Zarka, 2011) or atmospheric escape structure detections (Carolan et al., 2021). All proposed techniques have a bias towards giant planet magnetospheric detection.

Nevertheless, magnetic field in terrestrial exoplanets can be estimated by dynamo models assuming an internal planetary structure model (see e.g., Driscoll and Olson, 2011). In general, it is interesting to estimate the magnetospheric compression of an Earth-twin exoplanet under the effect of host star stellar wind. Such method has been applied to a sample of solar-mass stars by assuming a Parker stellar wind model and using Ca II H&K lines measurements in See et al. (2014). Indeed, the magnetosphere extension can be estimated by the so called magnetopause standoff distance (R_{MP}), defined as the distance from the planet at which the planetary magnetic field pressure balances the stellar wind dynamic pressure. On the Sun-Earth system such interaction results in a day-side average standoff distance of $\sim 11\,R_E$ (Shue et al., 1997), but in general it depends on the solar activity level via the solar wind.

Recently, we calibrate on the Sun-Earth system some relations which allow us to relate the solar activity, by means of the Ca II K index, with the solar wind speed and dynamic pressure (Reda et al., 2021, 2022). We also introduce a model which allows to compute the Earth magnetopause standoff distance simply starting from the above activity index (see Reda et al., 2022 for further details). Because of the use of a physical proxy, as the Ca II K index, such relations are very useful and can be employed to estimate the stellar wind properties in solar-like stars for which similar measurements are available. Panel B of **Figure 2** shows, as example, the magnetopause standoff distance of an hypothetical Earth-twin planet orbiting at 1 AU around the solar-like star HD 76151, computed with our model. Due to the higher level of chromospheric activity of this star compared to the Sun, an Earth-twin planet orbiting around it would have a mean magnetosphere extension of $\sim 9\,R_E$, which would be more compressed than the Earth one because of the stronger stellar wind pressure.

5 DISCUSSION

Although the concept of habitable zone has been in the literature for some time, it is only in the last few years that complementary strategies have allowed a more rigorous definition, in order to understand how long an exoplanet may have been able to maintain habitability, so that life has had the opportunity to originate and to develop. Under the hypothesis that the evolution of life requires sufficient long times in a constant environment, it appears clear that a lasting stability of the atmosphere plays the most crucial role, since the planet should have survived not only to the period of heavy bombardment by asteroids and comets, but also during the host stars' active X-ray, extreme ultraviolet (XUV) and stellar wind exposure (e.g., Wood et al., 2002; Lammer et al., 2003) occurring during the early phases of planetary system formation.

The extreme efficiency of asteroseismology in supporting the exoplanetary program has been demonstrated by several recent works (see e.g., Campante et al., 2018; Lundkvist et al., 2018), but we believe that our synergic strategy has the additional potential of enabling to characterize, not only the main stellar and planetary parameters such as the dimensions, the density and the age, but also to infer the stellar magnetic activity and the interaction between the star and the hosted planets. Knowledge about the magnetic activity level of the host-star and its influence on an orbiting planet will allow for example to get conclusions on the magnetosphere compression which, as known, is directly connected to atmospheric erosion processes induced by stellar

winds, and strictly related to planetary habitability conditions. We believe that this method is clearly advantageous since it only requires asteroseismic and chromospheric activity measurements, already available for a large sample of stars and further new measurements will be available in the next years. This will produce results of particular interest once the incoming data from operating space missions and from ground based campaigns will have been fully exploited and understood.

The outcome will be of relevance especially in the context of the future PLATO (PLAnetary Transits & Oscillations of stars) (Rauer et al., 2014) space mission, whose primary goal is to detect terrestrial exoplanets in the habitable zone of Sun-like stars. Since our model to estimate the mean stellar wind is calibrated on the Sun, the best targets to which to extend our procedure are represented by intermediate age ($\gtrsim$ 2.6 Gyr) G spectral type stars, but we do not exclude the possibility to consider for the future also early K- o late F-type stars. A further requirement is a stellar Rossby number $\gtrsim 1$ which, as recently pointed out by Reinhold et al. (2019), is related to a faculae activity regime, the dominant source of activity in the Sun. In this respect of great help is the calibration from asteroseismology recently made by Corsaro et al. (2021), which allows to determine the Rossby number simply knowing the stellar ($B - V$) color index and the rotation period. At present, we are preparing a catalogue of solar-like targets observed by the Kepler and TESS satellites on which presence of one or more exoplanets has been confirmed. Moreover, for these targets measurements in the Ca II H&K lines have to be available from ground observatories in order to estimate the chromospheric activity and the mean stellar wind acting on the orbiting planets.

DATA AVAILABILITY STATEMENT

The dataset of the HK Project at the Mount Wilson Observatory are available from the National Solar Observatory (NSO) website (https://nso.edu/data/historical-data/mount-wilson-observatory-hk-project/). The TESS asteroseismic data can be found on the TASOC (TESS Asteroseismic Science Operations Center) website (https://tasoc.dk). The Kepler asteroseismic data can be found on the KASOC (Kepler Asteroseismic Science Operations Center) website (https://kasoc.phys.au.dk).

AUTHOR CONTRIBUTIONS

RR assembled the synergic strategy, made the analysis on the magnetic data and the computation of the theoretical adiabatic oscillation frequencies; EC was responsible for the analysis of oscillations data; MPDM provided the theoretical framework to interpret the asteroseismic data; LG and FB took care of the synergies between stellar and solar activity; TA designed the model of star-planet interaction. All authors contributed to manuscript revision, read and approved the submitted version.

FUNDING

Funding for the TESS mission is provided by the NASA Explorer Program.

ACKNOWLEDGMENTS

RR is a PhD student of the PhD course in Astronomy, Astrophysics and Space Science, a joint research program between the University of Rome "Tor Vergata," the Sapienza University of Rome and the National Institute of Astrophysics (INAF). The work presented here is based on data from the HK Project at the Mount Wilson Observatory. This paper includes data collected with the TESS mission, obtained from the MAST data archive at the Space Telescope Science Institute (STScI). The work presented here is also based on NASA Kepler mission. We thank the entire Kepler and TESS teams for the development and operations of these NASA outstanding missions.

REFERENCES

Airapetian, V. S., Barnes, R., Cohen, O., Collinson, G. A., Danchi, W. C., Dong, C. F., et al. (2020). Impact of Space Weather on Climate and Habitability of Terrestrial-type Exoplanets. *Int. J. Astrobiol.* 19, 136–194. doi:10.1017/S1473550419000132

Baglin, A., Auvergne, M., Boisnard, L., Lam-Trong, T., Barge, P., Catala, C., et al. (2006). CoRoT: a High Precision Photometer for Stellar Ecolution and Exoplanet Finding. *36th Cospar Sci. Assem.* 36, 3749.

Borucki, W. J., Koch, D., Basri, G., Batalha, N., Brown, T., Caldwell, D., et al. (2010). Kepler Planet-Detection Mission: Introduction and First Results. *Science* 327, 977–980. doi:10.1126/science.1185402

Brown, T. M., Gilliland, R. L., Noyes, R. W., and Ramsey, L. W. (1991). Detection of Possible P-Mode Oscillations on Procyon. *ApJ* 368, 599. doi:10.1086/169725

Campante, T. L., Barros, S. C. C., Demangeon, O., da Nóbrega, H. J., Kuszlewicz, J. S., Pereira, F., et al. (2018). "Synergy between Asteroseismology and Exoplanet Science: an Outlook," in PHysics of Oscillating STars. Proceedings from the PHOST (PHysics of Oscillating STars) symposium hosted by the Oceanographic Observatory in Banyuls-sur-mer (France) from 2-7 September 2018. This conference honours the life work of Professor Hiromoto Shibahashi. doi:10.5281/zenodo.246321050

Carolan, S., Vidotto, A. A., Hazra, G., Villarreal D'Angelo, C., and Kubyshkina, D. (2021). The Effects of Magnetic Fields on Observational Signatures of Atmospheric Escape in Exoplanets: Double Tail Structures. *Mon. Not. R. Astron. Soc.* 508, 6001–6012. doi:10.1093/mnras/stab2947

Chaplin, W. J., Bedding, T. R., Bonanno, A., Broomhall, A.-M., García, R. A., Hekker, S., et al. (2011). Evidence for the Impact of Stellar Activity on the Detectability of Solar-like Oscillations Observed by Kepler. *ApJ* 732, L5. doi:10.1088/2041-8205/732/1/L5

Christensen-Dalsgaard, J. (2008a). ADIPLS-the Aarhus Adiabatic Oscillation Package. *Astrophys. Space Sci.* 316, 113–120. doi:10.1007/s10509-007-9689-z

Christensen-Dalsgaard, J. (2008b). ASTEC-the Aarhus STellar Evolution Code. *Astrophys. Space Sci.* 316, 13–24. doi:10.1007/s10509-007-9675-5

Cohen, O., Ma, Y., Drake, J. J., Glocer, A., Garraffo, C., Bell, J. M., et al. (2015). The Interaction of Venus-like, M-Dwarf Planets with the Stellar Wind of Their Host Star. *ApJ* 806, 41. doi:10.1088/0004-637x/806/1/41

Corsaro, E., Bonanno, A., Mathur, S., García, R. A., Santos, A. R. G., Breton, S. N., et al. (2021). A Calibration of the Rossby Number from Asteroseismology. *A&A* 652, L2. doi:10.1051/0004-6361/202141395

Corsaro, E., and De Ridder, J. (2014). DIAMONDS: A New Bayesian Nested Sampling Tool. *A&A* 571, A71. doi:10.1051/0004-6361/201424181

Corsaro, E., Mathur, S., García, R. A., Gaulme, P., Pinsonneault, M., Stassun, K., et al. (2017). Metallicity Effect on Stellar Granulation Detected from Oscillating Red Giants in Open Clusters. *A&A* 605, A3. doi:10.1051/0004-6361/201731094

Corsaro, E., McKeever, J. M., and Kuszlewicz, J. S. (2020). Fast and Automated Peak Bagging with DIAMONDS (FAMED). *A&A* 640, A130. doi:10.1051/0004-6361/202037930

Di Mauro, M. P. (2016). "A Review on Asteroseismology," in *Frontier Research in Astrophysics-II (FRAPWS2016)* (Trieste, Italy: PoS) 269, 29. doi:10.22323/1.269.0029

Di Mauro, M. P., Reda, R., Mathur, S., García, R. A., Buzasi, D. L., Corsaro, E., et al. (2022). On the Non-detection of Solar-like Pulsations in the Host Star GJ 504 Observed by TESS. submitted to ApJ

Dong, C., Jin, M., Lingam, M., Airapetian, V. S., Ma, Y., and van der Holst, B. (2018). Atmospheric Escape from the TRAPPIST-1 Planets and Implications for Habitability. *Proc. Natl. Acad. Sci. U.S.A.* 115, 260–265. doi:10.1073/pnas.1708010115

D'Orazi, V., Desidera, S., Gratton, R. G., Lanza, A. F., Messina, S., Andrievsky, S. M., et al. (2017). A Critical Reassessment of the Fundamental Properties of GJ 504: Chemical Composition and Age. *A&A* 598, A19. doi:10.1051/0004-6361/201629283

Driscoll, P., and Olson, P. (2011). Optimal Dynamos in the Cores of Terrestrial Exoplanets: Magnetic Field Generation and Detectability. *Icarus* 213, 12–23. doi:10.1016/j.icarus.2011.02.010

Egeland, R., Soon, W., Baliunas, S., Hall, J. C., Pevtsov, A. A., and Bertello, L. (2017). The Mount Wilson Observatorys-Index of the Sun. *ApJ* 835, 25. doi:10.3847/1538-4357/835/1/25

García, R. A., Hekker, S., Stello, D., Gutiérrez-Soto, J., Handberg, R., Huber, D., et al. (2011). Preparation of Kepler Light Curves for Asteroseismic Analyses. *Mon. Not. R. Astron. Soc.* 414, L6–L10. doi:10.1111/j.1745-3933.2011.01042.x

García, R. A., Mathur, S., Salabert, D., Ballot, J., Régulo, C., Metcalfe, T. S., et al. (2010). CoRoT Reveals a Magnetic Activity Cycle in a Sun-like Star. *Science* 329, 1032. doi:10.1126/science.1191064

Hall, J. C. (2008). Stellar Chromospheric Activity. *Living Rev. Sol. Phys.* 5, 2. doi:10.12942/lrsp-2008-2

Hart, M. H. (1979). Habitable Zones about Main Sequence Stars. *Icarus* 37, 351–357. doi:10.1016/0019-1035(79)90141-6

Harvey, J. (1985). High-resolution Helioseismology. In *Future Missions in Solar, Heliospheric & Space Plasma Physics*, eds. E. Rolfe and B. Battrick. 235 (Noordwijk, Netherlands: ESA Special Publication)

Hess, S. L. G., and Zarka, P. (2011). Modeling the Radio Signature of the Orbital Parameters, Rotation, and Magnetic Field of Exoplanets. *A&A* 531, A29. doi:10.1051/0004-6361/201116510

Huber, D., Bedding, T. R., Stello, D., Hekker, S., Mathur, S., Mosser, B., et al. (2011). Testing Scaling Relations for Solar-like Oscillations from the Main Sequence to Red Giants Usingkeplerdata. *ApJ* 743, 143. doi:10.1088/0004-637X/743/2/143

Kasting, J. F., Whitmire, D. P., and Reynolds, R. T. (1993). Habitable Zones Around Main Sequence Stars. *Icarus* 101, 108–128. doi:10.1006/icar.1993.1010

Kjeldsen, H., and Bedding, T. R. (1995). Amplitudes of Stellar Oscillations: the Implications for Asteroseismology. *Astronomy Astrophysics* 293, 87–106. doi:10.48550/ARXIV.ASTRO-PH/9403015

Kopparapu, R. K., Ramirez, R., Kasting, J. F., Eymet, V., Robinson, T. D., Mahadevan, S., et al. (2013). Habitable Zones Around Main-Sequence Stars: New Estimates. *ApJ* 765, 131. doi:10.1088/0004-637x/765/2/131

Lammer, H., Selsis, F., Ribas, I., Guinan, E. F., Bauer, S. J., and Weiss, W. W. (2003). Atmospheric Loss of Exoplanets Resulting from Stellar X-Ray and Extreme-Ultraviolet Heating. *ApJ* 598, L121–L124. doi:10.1086/380815

Lebreton, Y., and Goupil, M. J. (2014). Asteroseismology for "à la carte" stellar age-dating and weighing. *A&A* 569, A21. doi:10.1051/0004-6361/201423797

Lovric, M., Tosone, F., Pietropaolo, E., Del Moro, D., Giovannelli, L., Cagnazzo, C., et al. (2017). The Dependence of the [FUV-MUV] Colour on Solar Cycle. *J. Space Weather Space Clim.* 7, A6. doi:10.1051/swsc/2017001

Loyd, R. O. P., Shkolnik, E. L., France, K., Wood, B. E., and Youngblood, A. (2020). When "Boring" Stars Flare: The Ultraviolet Activity of GJ 887, a Bright M Star Hosting Newly Discovered Planets. *Res. Notes AAS* 4, 119. doi:10.3847/2515-5172/aba94a

Lundkvist, M. S., Huber, D., Silva Aguirre, V., and Chaplin, W. J. (2018). Using Asteroseismology to Characterise Exoplanet Host Stars. arXiv e-prints , arXiv:1804.02214

Marsden, S. C., Petit, P., Jeffers, S. V., Morin, J., Fares, R., Reiners, A., et al. (2014). A BCool Magnetic Snapshot Survey of Solar-type Stars. *Mon. Not. R. Astron. Soc.* 444, 3517–3536. doi:10.1093/mnras/stu1663

Mathur, S., García, R. A., Bugnet, L., Santos, Â. R. G., Santiago, N., and Beck, P. G. (2019). Revisiting the Impact of Stellar Magnetic Activity on the Detectability of Solar-like Oscillations by Kepler. *Front. Astron. Space Sci.* 6, 46. doi:10.3389/fspas.2019.00046

Mathur, S., Metcalfe, T. S., Woitaszek, M., Bruntt, H., Verner, G. A., Christensen-Dalsgaard, J., et al. (2012). A Uniform Asteroseismic Analysis of 22 Solar-type Stars Observed Bykepler. *ApJ* 749, 152. doi:10.1088/0004-637X/749/2/152

Metcalfe, T. S., Monteiro, M. J. P. F. G., Thompson, M. J., Molenda-Żakowicz, J., Appourchaux, T., Chaplin, W. J., et al. (2010). A Precise Asteroseismic Age and Radius for the Evolved Sun-like Star KIC 11026764. *ApJ* 723, 1583–1598. doi:10.1088/0004-637x/723/2/1583

Gaia CollaborationPrusti, T., de Bruijne, J. H. J., Brown, A. G. A., Vallenari, A., Babusiaux, C., et al. (2016). The Gaia Mission. *Astronomy Astrophysics* 595, A1. doi:10.1051/0004-6361/201629272

Rauer, H., Catala, C., Aerts, C., Appourchaux, T., Benz, W., Brandeker, A., et al. (2014). The PLATO 2.0 Mission. *Exp. Astron.* 38, 249–330. doi:10.1007/s10686-014-9383-4

Reda, R., Giovannelli, L., Alberti, T., Berrilli, F., Bertello, L., Del Moro, D., et al. (2022). The Exoplanetary Magnetosphere Extension in Sun-like Stars Based on the Solar Wind - Solar UV Relation. arXiv e-prints , arXiv:2203.01554

Reda, R., Giovannelli, L., Alberti, T., Berrilli, F., Giobbi, P., and Penza, V. (2021). Correlation of Solar Activity Proxy with Solar Wind Dynamic Pressure in the Last Five Solar Cycles. *Il Nuovo Cimento della Soc. Ital. Fis.* 44 C, 120. doi:10.1393/ncc/i2021-21121-7

Reinhold, T., Bell, K. J., Kuszlewicz, J., Hekker, S., and Shapiro, A. I. (2019). Transition from Spot to Faculae Domination. *A&A* 621, A21. doi:10.1051/0004-6361/201833754

Ricker, G. R., Winn, J. N., Vanderspek, R., Latham, D. W., Bakos, G. Á., Bean, J. L., et al. (2014). "Transiting Exoplanet Survey Satellite (TESS)," in *Space Telescopes and Instrumentation 2014: Optical, Infrared, and Millimeter Wave*. Editors J. Oschmann, M. Jacobus, M. Clampin, G. G. Fazio, and H. A. MacEwen, 914320. 9143 of Society of Photo-Optical Instrumentation Engineers (SPIE) Conference Series. doi:10.1117/12.2063489

Roettenbacher, R. M., and Kane, S. R. (2017). The Stellar Activity of TRAPPIST-1 and Consequences for the Planetary Atmospheres. *ApJ* 851, 77. doi:10.3847/1538-4357/aa991e

Schrijver, C. J., and Zwaan, C. (2000). *Solar and Stellar Magnetic Activity*. Cambridge University Press.

See, V., Jardine, M., Vidotto, A. A., Petit, P., Marsden, S. C., Jeffers, S. V., et al. (2014). The Effects of Stellar Winds on the Magnetospheres and Potential Habitability of Exoplanets. *A&A* 570, A99. doi:10.1051/0004-6361/201424323

Shue, J.-H., Chao, J. K., Fu, H. C., Russell, C. T., Song, P., Khurana, K. K., et al. (1997). A New Functional Form to Study the Solar Wind Control of the Magnetopause Size and Shape. *J. Geophys. Res.* 102, 9497–9511. doi:10.1029/97ja00196

Skumanich, A. (1972). Time Scales for Ca II Emission Decay, Rotational Braking, and Lithium Depletion. *ApJ* 171, 565. doi:10.1086/151310

Tassoul, M. (1980). Asymptotic Approximations for Stellar Nonradial Pulsations. *ApJS* 43, 469–490. doi:10.1086/190678

Tilley, M. A., Segura, A., Meadows, V., Hawley, S., and Davenport, J. (2019). Modeling Repeated M Dwarf Flaring at an Earth-like Planet in the Habitable Zone: Atmospheric Effects for an Unmagnetized Planet. *Astrobiology* 19, 64–86. doi:10.1089/ast.2017.1794

Ulrich, R. K. (1986). Determination of Stellar Ages from Asteroseismology. *ApJ* 306, L37. doi:10.1086/184700

Vaughan, A. H., Preston, G. W., and Wilson, O. C. (1978). Flux Measurements of Ca II H and K Emission. *Publ. Astronomical Soc. Pac.* 90, 267–274. doi:10.1086/130324

Vida, K., Kővári, Z., Pál, A., Oláh, K., and Kriskovics, L. (2017). Frequent Flaring in the TRAPPIST-1 System-Unsuited for Life? *ApJ* 841, 124. doi:10.3847/1538-4357/aa6f05

Vidotto, A. A., Jardine, M., and Helling, C. (2011). Prospects for Detection of Exoplanet Magnetic Fields through Bow-Shock Observations during Transits. *Mon. Not. R. Astron. Soc.* 411, L46–L50. doi:10.1111/j.1745-3933.2010.00991.x

Wilson, O. C. (1978). Chromospheric Variations in Main-Sequence Stars. *ApJ* 226, 379–396. doi:10.1086/156618

Wood, B. E., Müller, H. R., Zank, G. P., and Linsky, J. L. (2002). Measured Mass-Loss Rates of Solar-like Stars as a Function of Age and Activity. *ApJ* 574, 412–425. doi:10.1086/340797

Conflict of Interest: The authors declare that the research was conducted in the absence of any commercial or financial relationships that could be construed as a potential conflict of interest.

The handling editor TC declared a past co-authorship with the authors MM, EC.

Publisher's Note: All claims expressed in this article are solely those of the authors and do not necessarily represent those of their affiliated organizations, or those of the publisher, the editors and the reviewers. Any product that may be evaluated in this article, or claim that may be made by its manufacturer, is not guaranteed or endorsed by the publisher.

frontiers | Frontiers in Astronomy and Space Sciences

TYPE Brief Research Report
PUBLISHED 22 July 2022
DOI 10.3389/fspas.2022.948979

OPEN ACCESS

EDITED BY
Maria Ann Weber,
Delta State University, United States

REVIEWED BY
Joyce Ann Guzik,
Los Alamos National Laboratory (DOE), United States
Ceren Ulusoy,
University of South Africa, South Africa

*CORRESPONDENCE
A. Ramón-Ballesta,
a.ramonballesta@gmail.com

SPECIALTY SECTION
This article was submitted to Stellar and Solar Physics, a section of the journal Frontiers in Astronomy and Space Sciences

RECEIVED 20 May 2022
ACCEPTED 29 June 2022
PUBLISHED 22 July 2022

CITATION
Ramón-Ballesta A, Pascual-Granado J and Garrido R (2022), Time-frequency analysis of HD 174936 and HD 174966 using the synchrosqueezed wavelet transform.
Front. Astron. Space Sci. 9:948979.
doi: 10.3389/fspas.2022.948979

Time-frequency analysis of HD 174936 and HD 174966 using the synchrosqueezed wavelet transform

A. Ramón-Ballesta*, J. Pascual-Granado and R. Garrido

Instituto de Astrofísica de Andalucía (CSIC), Granada, Spain

δ Scuti stars are intermediate-mass pulsators located in the classical Cepheid instability strip with spectral types ranging from A to F. In the last years, some authors found an amplitude and frequency modulation in some of these stars. In our work we have chosen the continuous wavelet transform as the more appropriate tool to perform a time-frequency analysis of the light curves of HD 174936 and HD 174966. We have chosen this tool because, unlike the short time Fourier transform, that uses a fixed windows size, the continuous wavelet transform uses short windows at high frequencies and long windows at low frequencies, making it like an adaptive analysis tool. In order to improve the resolution of the frequencies obtained by the continuous wavelet transform, we have also used the synchrosqueeze algorithm to "focus" the result. Then, we are capable to obtain a measure of the instantaneous frequencies of the signal in a wide range of frequencies. To check our results, we have compared them with the synchrosqueezed continuous wavelet transform of a synthetic signal generated with the frequencies previously obtained by a classical approach. Our results show that some frequencies are stable, at least within the observation run time, although some others show some kind of variation. This is the first time that such variations in the oscillation frequencies of HD 174936 and HD 174966 are reported.

KEYWORDS

stars:Delta Scuti, stars:variable, stars:pulsations, wavelet analysis, wavelet transform, synchrosqueeze, asteroseismology

1 Introduction

The δ Scuti (δ Sct) stars (Baglin et al., 1973; Rodríguez et al., 2000) are intermediate-mass (i.e. between 1.5 and 3 solar masses) pulsators located in the classical Cepheid instability strip, near the main sequence or moving from the main sequence to the giant branch. Their spectral types range from A to F and they are multi-periodic pulsators with frequencies found between 3 d^{-1} and 80 d^{-1} (Aerts et al., 2010; Uytterhoeven et al., 2011). Thus, these stars are very good laboratories to test theories of angular momentum and chemical transport in stellar interiors.

Amplitude modulation in δ Sctstars has been found in recent years (see, e.g., Breger and Pamyatnykh, 2006; Breger et al., 2012; Barceló Forteza et al., 2015). Also, Bowman and Kurtz, (2014); Bowman et al. (2021) found amplitude and frequency modulation in some δ Scuti stars. Amplitude and/or frequency modulation has also been found in other type of stars (see, e.g., a brief compilation in Guzik et al., 2015, and references therein). These authors used a wavelet-based technique, different from the one use in this work, to study amplitude modulations in a sample of different pulsating stars.

In this work we analyse the stability of the oscillation frequencies of the δ Sctstars HD 174936 and HD 174966. We have applied an analysis based on the synchrosqueezed continuous wavelet transform (SSCWT from now on) to the CoRoT (Baglin et al., 2006) light curves of these stars. The curves contain about 27 days of observations for each star with 32 s of sampling. From this data, García Hernández et al. (2009) found 422 oscillation frequencies for HD 174936. The authors did not expect such a high number of frequencies in this star and they also found a flat distribution of lower amplitude peaks. This so-called *grass* has also been found in more stars observed with CoRoT (see, e.g., Poretti et al., 2009) and its origin has been a matter of debate (see Section 1 of de Franciscis et al., 2018, and references therein). They also found a large separation structure of 52 μHz in the frequency spectra. For HD 174966, García Hernández et al. (2013) found 185 frequencies with no *grass* effect. The authors also found a large separation structure of 65 μHz in the frequency spectra of both stars. In a recent study, Ramón-Ballesta et al. (2021) also included these stars in their search for the signature of the rotational splitting in the frequency spectra. They found a rotational splitting value of 26 μHz for HD 174936 and 19 μHz for HD 174966.

As the continuous wavelet transform requires the points to be equally spaced in time, we have previously filled the gaps using the MIARMA method developed by Pascual-Granado et al. (2015). We have compared our results with stationary synthetic time-series generated from the frequencies mentioned before. In particular, we have used the first 160 frequencies to generate the synthetic signal of HD 174936 and the 20 first frequencies to generate the synthetic signal of HD 174966. We needed less frequencies in this last star because the RMS improves much faster than for HD 174936 during the prewhitening cascade. With this article we aim to pave the way for a methodology that can be used in future studies.

This paper is organised as follows: in Section 2 we introduce the wavelet transform as the tool we used for the time-frequency analysis. In section 3 we show our results and discuss them. Finally, in Section 4 we present our conclusions.

2 Methods

The tool we have chosen to do the time-frequency analysis is the continuous wavelet transform (CWT from now on). Unlike the short time Fourier transform, that uses a fixed window size, the CWT uses short temporal windows at high frequencies and long temporal windows at low frequencies, thus making it an adaptive analysis tool. In the same sense, these frequency windows are longer at high frequencies than at low frequencies. This means that the frequency resolution is better at low frequencies and decreases as the frequency rises, as it will be explained in the following paragraphs. These sizes are automatically defined by the CWT algorithm. The CWT relies on the use of a mother wavelet $\psi(t)$, i.e., a wave-like function of finite energy. This function can be scaled and shifted in a way that conserves the energy (Eq. (1)), thus generating daughter wavelets.

$$\psi_{a,b}(t) = a^{-\frac{1}{2}}\psi\left(\frac{t-b}{a}\right) \tag{1}$$

Here, a is the scale factor and b is the translation along the time axis. The choice of the mother wavelet is usually made to match the expected shape of the signal, i.e. a sinusoidal wavelet is used to analyse a sinusoidal signal to ensure the correlation between the wavelet and the signal. In the case of the time-frequency analysis of non-stationary time series generated by natural processes, one of the most used mother wavelets is the Morlet wavelet (see e.g. Percival and Walden, 2000). This wavelet can be expressed as in Eq. (2).

$$\psi_{\sigma}(t) = c_{\sigma}\pi^{-\frac{1}{4}}e^{-\frac{1}{2}t^2}\left(e^{i\sigma t} - \kappa_{\sigma}\right) \tag{2}$$

Here, σ is the parameter that defines the general trade-off between the temporal and the frequency precision, $c_{\sigma} = (1 + e^{-\sigma^2} - 2e^{-\frac{3}{4}\sigma^2})^{-\frac{1}{2}}$ is a normalisation constant and $\kappa_{\sigma} = e^{-\frac{1}{2}\sigma^2}$ is defined by the admissibility condition (i.e. the Fourier transform of the wavelet must vanish at zero frequency) (Mallat, 2009).

The CWT of the signal s can then be defined as in Eq. (3) below. The CWT produces a matrix of power coefficients (see, e.g., Mallat, 2009) that we can represent in a scales versus time diagram. The power of the coefficients is then plotted using a colormap in arbitrary units.

$$\mathrm{CWT}_s(a,b) = \int s(t)\overline{\psi_{a,b}(t)}dt \tag{3}$$

A scale a can be related to a frequency f in several manners. One of the most used definitions of frequency is taking the central frequency of the wavelet as the actual frequency of that particular wavelet. If the signal contains the same frequency, the wavelet and signal will correlate in the CWT, thus providing a measure of the "instantaneous" frequency of the signal at each point. The choice of scales to perform the CWT is dependent on the sampling frequency and the length of the signal. The

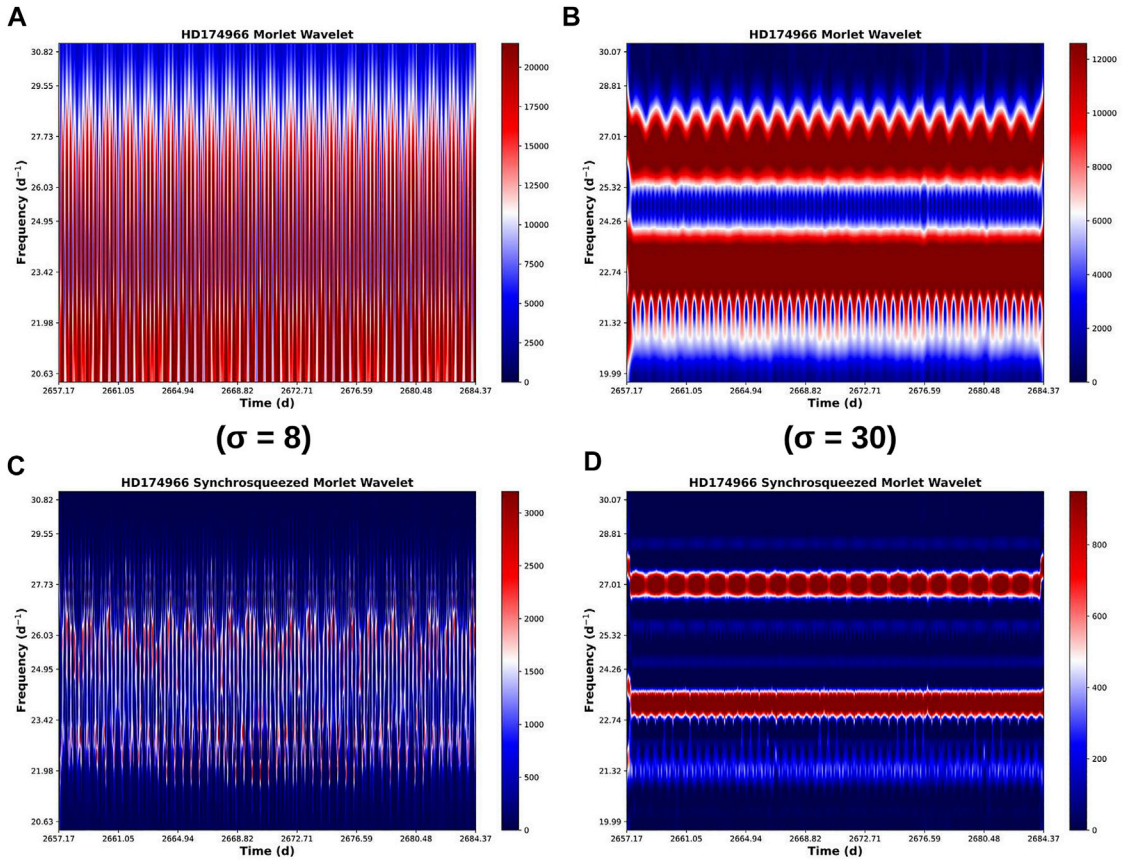

FIGURE 1
Example of a SSCWT analysis of the same region of pulsation frequencies for HD 174966. The plot shows the oscillation frequencies versus time. The colour map shows the power of the wavelet coefficients in arbitrary units. **(A)**: Interference pattern that appears in the CWT when the frequencies are too close to resolve setting σ = 8 in the mother wavelet. The SSCWT in **(C)** is not able to resolve this frequencies either. **(B)**: the same set of frequencies are resolved by setting σ = 30. In this case, the three frequencies at 21.32, 23.24 and 27.01 d^{-1} can be clearly seen. The frequency at 27.01 d^{-1} shows a *wobbling* in the power, probably because the frequencies of the daughter wavelets that scanned that region did not exactly match the frequency of the signal, thus generating the effect. The fact that this *wobbling* also appears in the analysis of the synthetic curve (not shown) is what led us to think that this variation was not a real modulation in amplitude. The light blue bands in **(D)** at about 24.2, 25.3 and 28.7 d^{-1} are artefacts of the synchrosqueezing algorithm, created at the places where there were the edges of the frequency bands in the CWT **(B)**.

sampling frequency defines the maximum frequency (i.e., the Nyquist frequency) the CWT can scan ($f_{max} = f_s/2$) and the length (L) of the signal defines the minimum frequency the CWT is capable of detecting ($f_{min} \propto 1/L$). The relation between scales and frequencies obeys an inverse power law (i.e., $f \propto 1/a$). The frequency resolution is related to the length in the temporal axis of the analysis window at that particular frequency and is translated as the width of the frequency band in the CWT plot. Due to that, the resolution is smaller at lower frequencies (because they require longer temporal windows) than the resolution at high frequencies. Consequently, the frequency bands in the plots will get wider as the frequency increases. Daubechies and Maes, (1996); Daubechies et al. (2011) proposed a "focusing" algorithm that they called synchrosqueezing in order to reduce the width of the frequency bands of the CWT. With this algorithm they reallocate the energy around a central frequency but preserving the time resolution, thus providing a better resolution in the frequency axis. This synchrosqueezed CWT (SSCWT) remains invertible so that the original signal can still be reconstructed and also reduces the background noise in the plots. This algorithm is implemented in Python as the ssqueezepy package (Muradeli, 2020), which we have used in our analysis.

3 Results and discussion

The plots show the frequency in d^{-1} in the vertical axis versus time in d in the horizontal axis. The colour map shows the power of the wavelet coefficients of the CWT and the SSCWT using arbitrary units. As the frequencies used in the synthetic curves are stationary, we expect to find straight bands in all of them. However, unexpected results came across in some

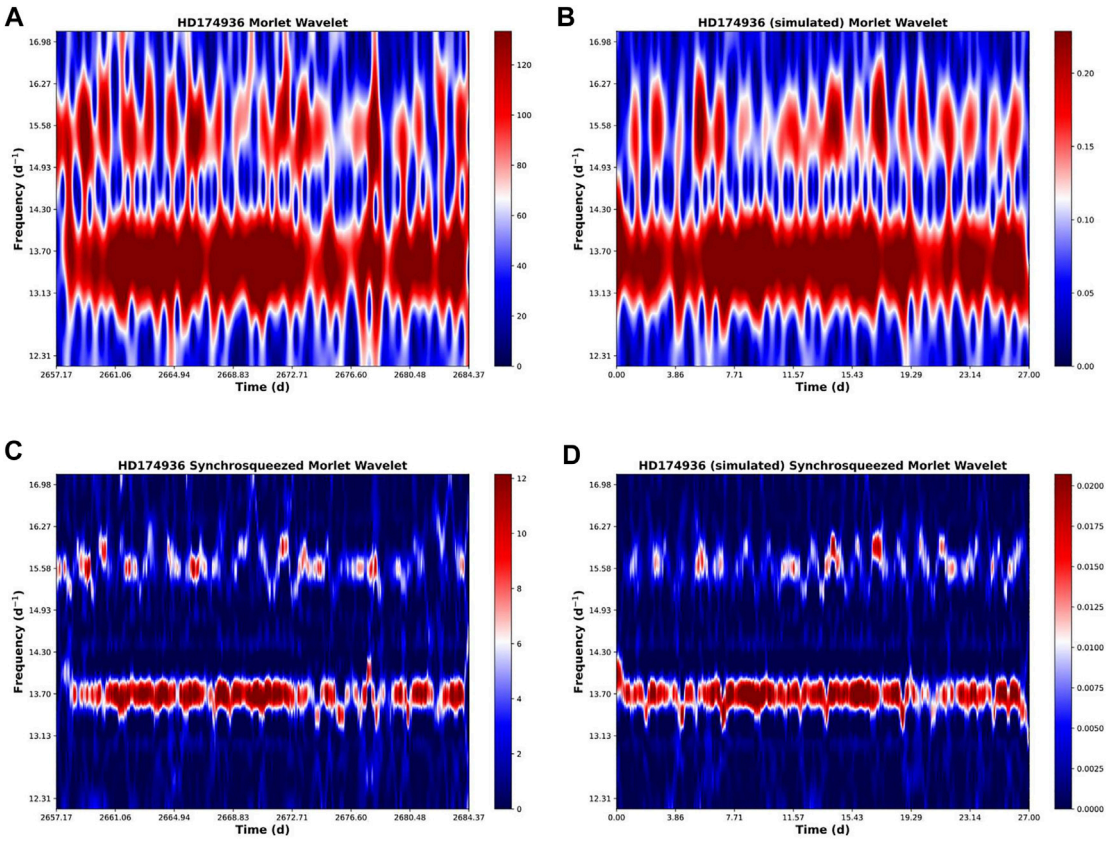

FIGURE 2
Main pulsation frequencies of HD 174936. The similar behaviour of the frequencies at 13.70 and 15.58 d^{-1} found in the analysis of both the real and the synthetic data can be used to confirm that the frequencies found in the light curve are stationary. The CWT of both frequencies shown seem to interact a bit (i.e. the edges of the red bands in panels **(A)** and **(B)**, corresponding to the frequencies at 13.70 and 15.58 d^{-1}, overlap a bit.) That could explain the erratic behaviour of the frequency at 15.58 d^{-1} in the SSCWT in both panels **(C)** and **(D)**. Additionally, there can also be happening the same effect as in the *wobbling* explained in Figure 1.

frequencies. One of the most frequent artefacts occurs when there are two or more frequencies that are too close to each other. In this case, the CWT might not be able to completely separate them, with the coefficients overlapping and thus creating an interference pattern in the SSWCT similar to that of a modulated frequency. Sometimes, these behaviours can be corrected by fine tuning the mother wavelet parameter σ to make the analysis more sensitive to frequency changes at the cost of decreasing the temporal accuracy (i.e., increasing the σ parameter). However, depending on the length of the signal, it is not always possible to reach enough frequency resolution before losing all the information in the temporal axis. An example of this behaviour is shown in Figure 1 where, using the light curve of HD 174936, in the left panels (A and C) a setting of $\sigma = 8$ was used and the interference pattern can be seen in the SSWCT (C). In the right panels (B and C), we increased the parameter to $\sigma = 30$ and the effect has been corrected. It is also worth noting the unavoidable border effect that appears in both ends of the plots. This happens because the CWT takes the beginning and the end of the signal as actual changes of frequency (from 0 to something and from something to 0, respectively). The same effect would happen in the gaps had they not been filled using the MIARMA algorithm. Another artefact that can be seen in panel D of Figure 1 is the appearance of equidistant light blue (almost white) bands around the synchrosqueezed frequency of 27.01 d^{-1}. Comparing with the same frequency in the CWT plot (panel B of Figure 1), we can see that this bands in the SSCWT actually mark the edges of the frequency band in the CWT. This also happens in other frequencies we have analysed (not shown) and therefore we concluded that these light bands are likely a residual of the edge of the CWT bands.

3.1 HD 174936

The frequencies found for the light curve of HD 174936 show a similar behaviour to the frequencies

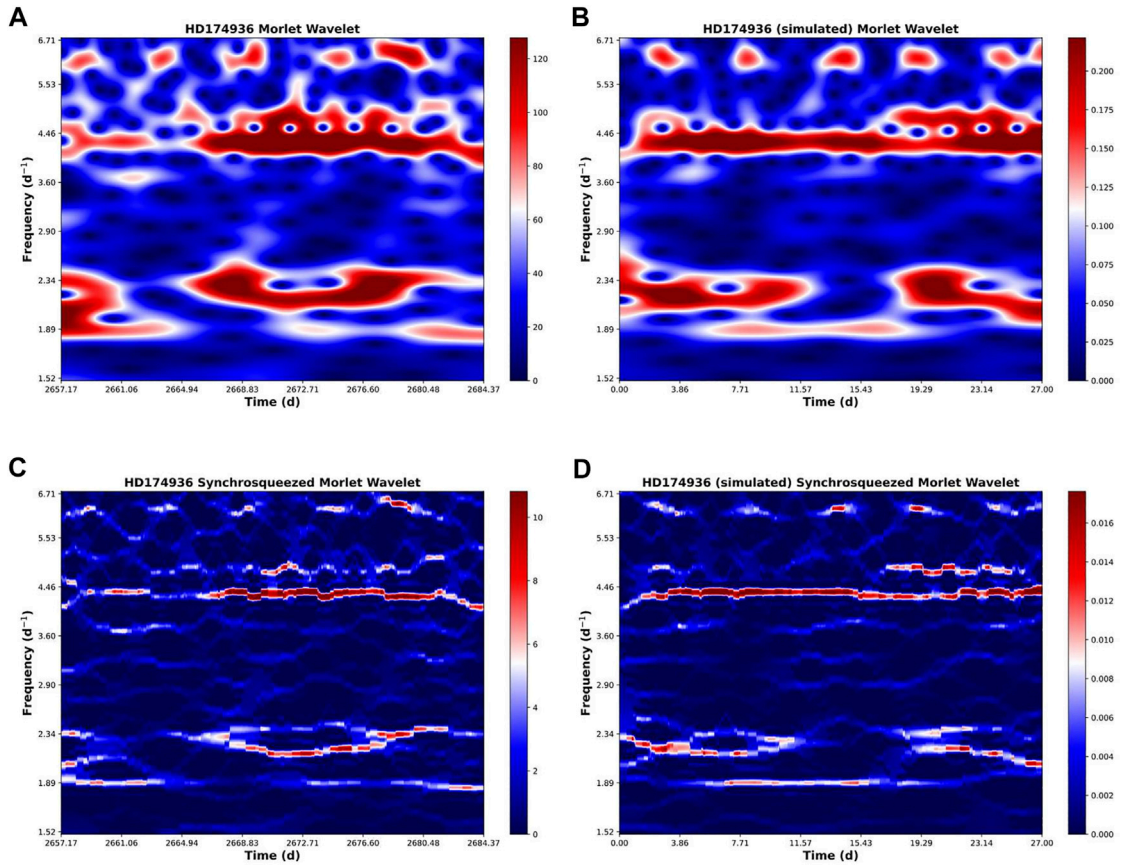

FIGURE 3
Frequencies of HD 174936 between 1.52 d^{-1} and 6.71 d^{-1}. The CWT (panels A and B) of the group of frequencies between 1.89 d^{-1} and 2.34 d^{-1} shows some overlapping in the coefficients (red zones) and this can be hampering the synchrosqueeze algorithm. Hence the apparent instability of these frequencies in the SSWCT (panels C and D). The same could be happening between the frequency at 4.46 d^{-1} and a slightly higher one around 4.8 d^{-1}. In the frequency at 4.46 d^{-1}, the SSWCT of the synthetic curve shows an almost straight and continuous band along the temporal axis whereas in the signal from the star the band seems to be weaker in the first 8-10 days of observation, which could be a sign of an instability of some kind in this frequency.

found in the synthetic signal. An example is given in Figure 2, in which the main pulsation frequency at 13.70 d^{-1} along with another frequency at 15.58 d^{-1} are shown. The upper panels (A and B) display the CWT coefficients, whereas the lower panels (C and D) show the SSCWT result. In the same sense, the left panels (A and C) are for the analysis of the real light curve and the right panels (B and D) for analysis of the synthetic signal. In this case, the CWT (panels A and B) seems unable to completely resolve both frequencies with the red edges of both bands slightly overlapping. This may hamper the synchrosqueezing a bit, which can explain the unexpected changes in the 15.58 d^{-1} frequency.

In Figure 3 a similar overlapping effect can be happening in the different frequencies shown between 1.89 and 2.34 d^{-1}. The same can be happening between the two frequencies at 4.46 and 4.8 d^{-1}. However, in the frequency at 4.46 d^{-1} there is a clear difference between the synthetic (panels B and D) and the real signal (panels A and C). Whereas the analysis of the synthetic curve displays an almost straight band throughout the whole observation time, the frequency in the real observations seems to be weaker during the first eight to 10 days. This could be an indication of an instability of some kind in this particular frequency.

3.2 HD 174966

In HD 174966, Figure 4 shows a frequency at 5.51 d^{-1} and another one at 6.3 d^{-1}. The frequency at 5.51 d^{-1} shows a clearly different behaviour in the light curve of the star (panels A and C in Figure 4) than in the synthetic one (panels B and D). The analysis of the synthetic curve shows a well defined

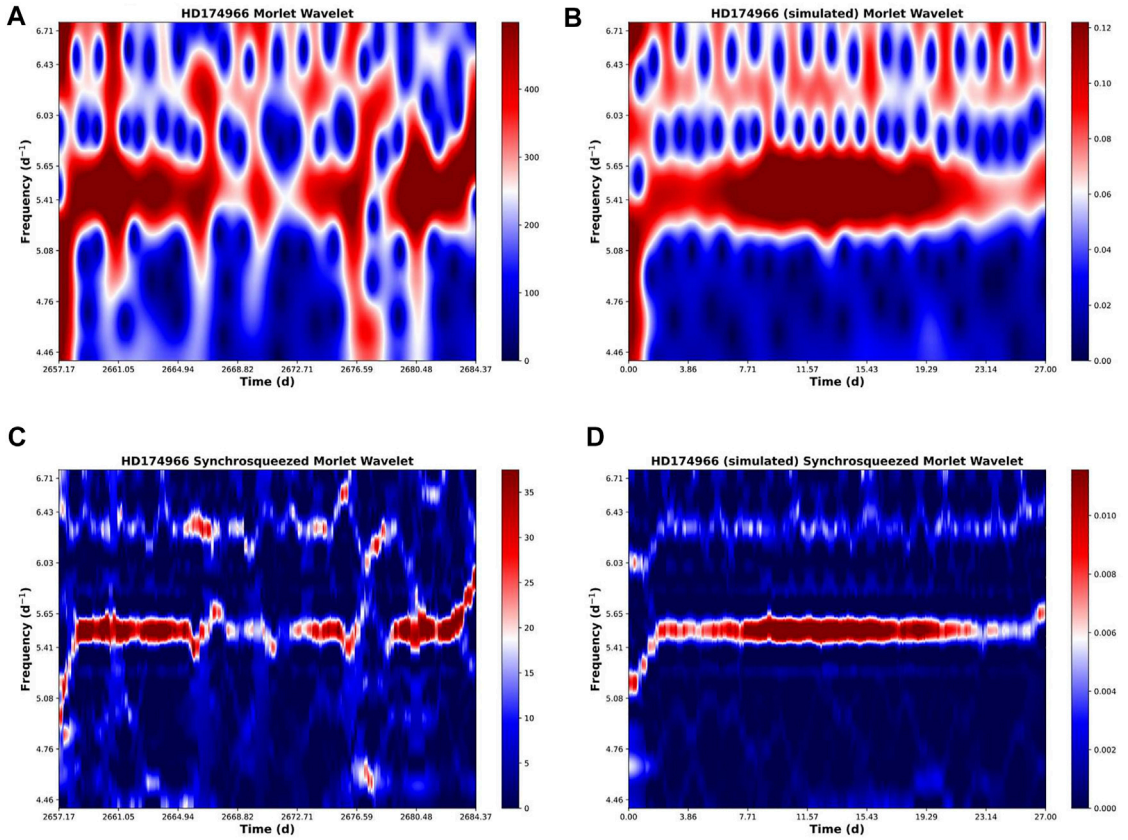

FIGURE 4
Frequencies of HD 174966 between 4.46 d^{-1} and 6.71 d^{-1}. The frequency at 5.51 d^{-1} shows a clearly different behaviour in the signal **(A,C)** compared to the synthetic curve **(B,D)**. The SSWCT of the synthetic curve shows a uniform band, apart from the border effect, whereas the SSWCT of the light curve suffers an interruption at about 2666 *d*, then is resumed at 2672 *d* and then stopped again at 2677 *d* before finally resuming at 2678 *d*. The other frequency at about 6.3 d^{-1} seems to be reacting in an opposite way. This behaviour maybe due to an interaction between these two frequencies but could also be due to a transient of some kind or a magnetic field modulation.

straight band (apart from the border effect), whereas the frequency coming from the analysis of the real signal suffers an interruption at about 2666 *d*, then is resumed at 2672 *d* and stopped again at 2677 *d* before finally resuming at 2678 *d*. The other frequency at about 6.3 d^{-1} seems to be reacting in an opposite way, which might be an indication of an interaction between these two frequencies. We can discard an artefact of the method because of the different behaviour of the synthetic signal. Another possible explanation to this phenomenon could be that this frequency would correspond to a transient of some sort or a magnetic field altering the oscillation mode in a period of few days. A longer observation run of this star would be needed in order to confirm the instability of the pulsation.

The other frequencies found for this star (see e.g. the main pulsation frequencies previously shown in Figure 1) do not show any different behaviour compared to the synthetic signal.

4 Conclusion

We have used the synchrosqueezed continuous wavelet transform to analyse the light curves of HD 174936 and HD 174966 and we have compared the results with the same analysis on synthetic light curves generated for these stars. Most of the frequencies found show a similar behaviour in both real and synthetic cases, although some of them show unexpected variations only in the real light curves. These variations in the light curves of HD 174936 and HD 174966 are here reported for the first time, which shows the high potential of the synchrosqueezed wavelet transform to uncover new physics of δ Sctstars.

The synchrosqueezed wavelet transform shows better results in the low frequency region than in the high frequency region. The continuous wavelet transform is complementary to the synchrosqueezing in order to identify possible artefacts.

Further studies with longer observation runs would be needed in order to confirm our findings.

Data availability statement

Publicly available datasets were analyzed in this study. This data can be found here: CoRoT Data Archive http://idoc-corot.ias.u-psud.fr/sitools/client-user/COROT_N2_PUBLIC_DATA/project-index.html.

Author contributions

RG, JP-G, and AR-B contributed to conception and design of the study. AR-B performed the analyses described in the manuscript and also wrote the first draft of the manuscript. JP-G prepared the data so it could be analysed and also provided the synthetic light curves. All authors contributed to manuscript revision, read, and approved the submitted version.

Funding

AR-B, JP-G, and RG acknowledge funding support from Spanish public funds for research from project ESP 2017-87676-C5-5-R from the "Plan Estatal de Investigación Científica y Técnica y de Innovación", from project PID 2019-107061GB-C63 from the 'Programas Estatales de Generación de Conocimiento y Fortalecimiento Científico y Tecnológico del Sistema de I+D+i y de I+D+i Orientada a los Retos de la Sociedad', and from the State Agency for Research through the "Center of Excellence Severo Ochoa" award to the Instituto de Astrofísica de Andalucía (SEV-2017-0709), all from the Spanish Ministry of Science, Innovation and Universities (MCIU). AR-B also acknowledges funding support from project PRE 2018-084322 from the 'Programa Estatal de Promoción del Talento y su Empleabilidad del Plan Estatal de Investigación Científica y Técnica y de Innovación 2013-2016' of the Spanish MCIU.

Acknowledgments

The authors would like to thank the two reviewers who kindly reviewed the manuscript and provided valuable suggestions and insightful comments.

Conflict of interest

The authors declare that the research was conducted in the absence of any commercial or financial relationships that could be construed as a potential conflict of interest.

Publisher's note

Supplementary material

The Supplementary Material for this article can be found online at: https://www.frontiersin.org/articles/10.3389/fspas.2022.948979/full#supplementary-material

References

Aerts, C., Christensen-Dalsgaard, J., and Kurtz, D. W. (2010). *Asteroseismology*. Dordrecht: Springer.

Baglin, A., Auvergne, M., Barge, P., Deleuil, M., Catala, C., Michel, E., et al. (2006). "Scientific objectives for a minisat: CoRoT," *The CoRoT mission pre-launch status - stellar seismology and planet finding*. Editors M. Fridlund, A. Baglin, J. Lochard, and L. Conroy (1306 of ESA Special Publication), 33.

Baglin, A., Breger, M., Chevalier, C., Hauck, B., Le Contel, J. M., Sareyan, J. P., et al. (1973). Delta Scuti stars. *A and A* 23, 221.

Barceló Forteza, S., Michel, E., Roca Cortés, T., and García, R. A. (2015). Evidence of amplitude modulation due to resonant mode coupling in the δ Scuti star KIC 5892969. A particular or a general case? *Astron. Astrophys.* 579, A133. doi:10.1051/0004-6361/201425507

Bowman, D. M., Hermans, J., Daszyńska-Daszkiewicz, J., Holdsworth, D. L., Tkachenko, A., Murphy, S. J., et al. (2021). KIC 5950759: A high-amplitude δ Sct star with amplitude and frequency modulation near the terminal age main sequence. *Mon. Not. R. Astron. Soc.* 504, 4039–4053. doi:10.1093/mnras/stab1124

Bowman, D. M., and Kurtz, D. W. (2014). Pulsational frequency and amplitude modulation in the δ Sct star KIC 7106205. *Mon. Not. R. Astron. Soc.* 444, 1909–1918. doi:10.1093/mnras/stu1583

Breger, M., Fossati, L., Balona, L., Kurtz, D. W., Robertson, P., Bohlender, D., et al. (2012). Relationship between low and high frequencies in δ Scuti stars: Photometric kepler and spectroscopic analyses of the rapid rotator KIC 8054146. *Astrophys. J.* 759, 62. doi:10.1088/0004-637X/759/1/62

Breger, M., and Pamyatnykh, A. A. (2006). Amplitude variability or close frequencies in pulsating stars - the δ Scuti star FG Vir. *Mon. Not. R. Astron. Soc.* 368, 571–578. doi:10.1111/j.1365-2966.2006.10119.x

Daubechies, I., and Maes, S. (1996). "A nonlinear squeezing of the continuous wavelet transform based on auditory nerve models," in *Wavelets in medicine and biology* (USA: CRC Press), 527–546. 2000 N.W. Corporate Blvd., Boca Raton, FL 33431-9868.

Daubechies, I., Lu, J., and Wu, H.-T. (2011). Synchrosqueezed wavelet transforms: An empirical mode decomposition-like tool. *Appl. Comput. Harmon. Analysis* 30, 243–261. doi:10.1016/j.acha.2010.08.002

de Franciscis, S., Pascual-Granado, J., Suárez, J. C., García Hernández, A., and Garrido, R. (2018). Fractal analysis applied to light curves of δ Scuti stars. *Mon. Not. R. Astron. Soc.* 481, 4637–4649. doi:10.1093/mnras/sty2496

García Hernández, A., Moya, A., Michel, E., Garrido, R., Suárez, J. C., Rodríguez, E., et al. (2009). Asteroseismic analysis of the CoRoT δ Scuti star HD174936. *Astron. Astrophys.* 506, 79–83. doi:10.1051/0004-6361/200911932

García Hernández, A., Moya, A., Michel, E., Suárez, J. C., Poretti, E., Martín-Ruíz, S., et al. (2013). An in-depth study of HD 174966 with CoRoT photometry and HARPS spectroscopy: Large separation as a new observable for δ Scuti stars. *Astron. Astrophys.* 559, A63. doi:10.1051/0004-6361/201220256

Guzik, J. A., Kosak, K., Bradley, P. A., Jackiewicz, J., Uytterhoeven, K., and Kinemuchi, K. (2015). The occurrence of non-pulsating stars in the gamma dor and delta set pulsation instability regions: Results from *Kepler* Quarter 14-17 data. *Astron. Rev.* 29, 1–2. doi:10.1080/21672857.2014.11519738

Mallat, S. (2009). "A wavelet tour of signal processing," in *The sparse way*. Third Edition3rd edn. (Boston: Academic Press). doi:10.1016/B978-0-12-374370-1.X0001-8

Muradeli, J. (2020). ssqueezepy. GitHub. Note. Available at: https://github.com/OverLordGoldDragon/ssqueezepy/.

Pascual-Granado, J., Garrido, R., and Suárez, J. C. (2015). Miarma: A minimal-loss information method for filling gaps in time series. *Astron. Astrophys.* 575, A78. doi:10.1051/0004-6361/201425056

Percival, D. B., and Walden, A. T. (2000). *Wavelet methods for time series analysis*. Cambridge: Cambridge University Press. doi:10.1017/cbo9780511841040

Poretti, E., Michel, E., Garrido, R., Lefèvre, L., Mantegazza, L., Rainer, M., et al. (2009). HD 50844: A new look at δ Scuti stars from CoRoT space photometry. *Astron. Astrophys.* 506, 85–93. doi:10.1051/0004-6361/200912039

Ramón-Ballesta, A., García Hernández, A., Suárez, J. C., Rodón, J. R., Pascual-Granado, J., Garrido, R., et al. (2021). Study of rotational splittings in δ Scuti stars using pattern finding techniques. *Mon. Not. R. Astron. Soc.* 505, 6217–6224. doi:10.1093/mnras/stab1719

Rodríguez, E., López-González, M., and López de Coca, P. (2000). A revised catalogue of delta Sct stars. *Astron. Astrophys. Suppl. Ser.* 144, 469–474. doi:10.1051/aas:2000221

Uytterhoeven, K., Moya, A., Grigahcène, A., Guzik, J., Gutiérrez-Soto, J., Smalley, B., et al. (2011). The Kepler characterization of the variability among A- and F-type stars. I. General overview. *Astron. Astrophys.* 534, A125. doi:10.1051/0004-6361/201117368

frontiers | Frontiers in Astronomy and Space Sciences

REVIEW
published: 22 July 2022
doi: 10.3389/fspas.2022.942373

Inversions of Stellar Structure From Asteroseismic Data

Gaël Buldgen[1]*, *Jérôme Bétrisey*[1], *Ian W. Roxburgh*[2,3], *Sergei V. Vorontsov*[2,4] and *Daniel R. Reese*[5]

[1]*Département d'Astronomie, Université de Genève, Geneva, Switzerland,* [2]*Astronomy Unit, Queen Mary University of London, London, United Kingdom,* [3]*School of Physics and Astronomy, University of Birmingham, Birmingham, United Kingdom,* [4]*Institute of Physics of the Earth, Moscow, Russia,* [5]*LESIA, Observatoire de Paris, Université PSL, CNRS, Sorbonne Université, Université Paris Cité, Meudon, France*

The advent of space-based photometry missions in the early 21st century enabled the application to asteroseismic data of advanced inference techniques until then restricted to the field of helioseismology. The high quality of the observations, the discovery of mixed modes in evolved solar-like oscillators and the need for an improvement in the determination of stellar fundamental parameters such as mass, radius and age led to the development of sophisticated modelling tools, amongst which seismic inversions play a key role. In this review, we will discuss the existing inversion techniques for the internal structure of distant stars adapted from helio-to asteroseismology. We will present results obtained for various Kepler targets, their coupling to other existing modelling techniques as well as the limitations of seismic analyses and the perspectives for future developments of these approaches in the context of the current TESS and the future PLATO mission, as well as the exploitation of the mixed modes observed in post-main sequence solar-like oscillators, for which variational formulations might not provide sufficient accuracy.

Keywords: asteroseismology, stellar physics, inversion techniques, solar-like stars, stellar evolution

OPEN ACCESS

Edited by:
Tiago Campante,
Instituto de Astrofísica e Ciências do Espaço (IA), Portugal

Reviewed by:
Jason Jackiewicz,
New Mexico State University, United States
Frank Pijpers,
University of Amsterdam, Netherlands

***Correspondence:**
Gaël Buldgen
Gael.Buldgen@unige.ch

Specialty section:
This article was submitted to Stellar and Solar Physics, a section of the journal Frontiers in Astronomy and Space Sciences

Received: *12 May 2022*
Accepted: *03 June 2022*
Published: *22 July 2022*

Citation:
Buldgen G, Bétrisey J, Roxburgh IW, Vorontsov SV and Reese DR (2022) Inversions of Stellar Structure From Asteroseismic Data. Front. Astron. Space Sci. 9:942373. doi: 10.3389/fspas.2022.942373

1 INTRODUCTION

In the last 2 decades, asteroseismology has established itself as the golden path to study the internal structure of distant stars. Amongst these, solar-like oscillators have held a special place due to the number of them detected at various masses, chemical composition and evolutionary stages. This revolution was made possible by the recent space-based photometry missions CoRoT (Baglin et al., 2009), *Kepler* (Borucki et al., 2010) and TESS (Ricker et al., 2015). In the near future, the PLATO mission (Rauer et al., 2014) will further extend the dataset, and proposals for future missions have also been laid out, testifying to the scientific success of these missions (e.g., Miglio et al., 2021).

In addition to providing numerous targets to work on, space-based photometry missions also led to a drastic change in data quality compared to previous ground-based observations. While ground-based telescope networks (see Grundahl et al., 2006, for the SONG network) are still very important and can provide high quality data for some close targets (e.g., Bouchy and Carrier, 2001; Bedding et al., 2004; Martić et al., 2004; Kjeldsen et al., 2005; Grundahl et al., 2006), they are no match for nanohertz precision on the observed frequencies of some of the best *Kepler* targets and the large number of stars that can be observed simultaneously by photometric surveys.

This drastic change motivated the use of advanced seismic analyses techniques that were before restricted to the field of helioseismology, where the proximity of the Sun allows the detection of thousands of oscillation modes. Seismic inferences became routinely used and the determination of

fundamental parameters of stars for the purposes of fields such as exoplanetology and Galactic archaeology drove the development of dedicated numerical tools. Large grids of stellar models were also computed for such purposes and coupled to automated seismic modelling pipelines (e.g., Mathur et al., 2012; Gruberbauer et al., 2013; Metcalfe et al., 2015; Bellinger et al., 2016; Rendle et al., 2019; Bazot, 2020; Aguirre Børsen-Koch et al., 2022).

Inference problems are widespread in physics, from the calibration of instrumental responses to the radiative transfer problem in the Earth's atmosphere. They correspond to a specific class of mathematical problems called ill-posed problems, for which specific dedicated techniques have to be developed (see Tarantola, 2005; Pijpers, 2006, for example). These methods require having an appropriate formalism and regularization of the problem, in line with the known or assumed properties of the physical problem under study.

The inversion techniques used in asteroseismology are no exception to this rule. They most often derive from methods developed for helioseismology and for this reason have mostly been applied to solar-like oscillators, for which the underlying hypotheses of the inversion remain valid. It is worth mentioning that most seismic inversion techniques used in helio- and asteroseismology have actually been first applied to inferring the internal rotation of slowly rotating stars, including our Sun (see Thompson et al., 2003, and references therein). Thanks to space-based photometry data, inferences of internal rotation have been made in various cases, from solar-like main-sequence stars (see e.g., Lund et al., 2014; Benomar et al., 2015; Schunker et al., 2016a; Schunker et al., 2016b; Benomar et al., 2018; Bazot et al., 2019), to more massive oscillators (Kurtz et al., 2014; Saio et al., 2015; Hatta et al., 2019; Hatta et al., 2022) and towards later evolutionary stages (see e.g., Deheuvels et al., 2014; Deheuvels et al., 2015; Di Mauro, 2016; Di Mauro et al., 2018; Deheuvels et al., 2020; Fellay et al., 2021) with great successes.

In this short review, we will focus on seismic inversions of the internal structure of stars. We will start by discussing the goals of seismic inversions in **Section 2**. In **Section 3**, we will discuss inversion techniques relying on the calibration of evolutionary models and mention examples of static approaches applied to specific cases in stellar evolution. In **Section 4**, we introduce the variational formalism applied in linear inversions, that will be discussed in **Section 5** for both localized and indicator inversions. Finally, we will discuss non-linear inversions from the use of inner phaseshifts of the oscillations in **Section 6** and conclude in **Section 7**.

2 GOALS OF SEISMIC INVERSION TECHNIQUES AND UNDERLYING HYPOTHESES

The goal of seismic inversion techniques is to provide a model of the internal structure that takes into account all the available observational constraints. This procedure can take various forms that we will discuss in the following sections.

From a mathematical point of view, the inversion procedure consists in solving the system of differential equations describing the stellar structure while taking all the available observational constraints into account. In practice, this already implies assuming a few hypotheses regarding the equilibrium state of the star and the physical processes considered in the description of its internal structure.

The cases on which we focus will be slowly rotating solar-like stars without strong magnetic fields or being subject to tidal interactions capable of breaking the spherical symmetry. While these hypotheses might appear strong, they are in good agreement with observations and can be used for a wide range of targets. Hydrostatic and thermal equilibrium are also considered and the equilibrium equations of stellar structure are written in eulerian form as follows.

$$\frac{\partial m}{\partial r} = 4\pi r^2 \rho, \tag{1}$$

$$\frac{\partial P}{\partial r} = \frac{-Gm\rho}{r^2}, \tag{2}$$

$$\frac{\partial l}{\partial r} = 4\pi r^2 \epsilon, \tag{3}$$

$$\frac{\partial T}{\partial r} = \frac{-GmT\rho}{r^2 P}\nabla, \tag{4}$$

with r the radial position in the spherically symmetric model, m the mass of the sphere of radius r, ρ the local density, T the local temperature, l the local luminosity, P the local pressure,$\nabla = \frac{d\ln T}{d\ln P}$ the temperature gradient, and ϵ the local rate of energy generation. In addition to this system, the equation of state of the stellar material must be defined, namely the relation

$$P = P\left(\rho, T, X_j\right), \tag{5}$$

with X_j the chemical mixture of the stellar plasma. Alongside the determination of the internal structure, the inversion may also provide precise values of the fundamental stellar parameters such as mass, radius and age (when computing evolutionary models). In some specific cases, the full structure equations are solved in a static way, for example when the evolutionary path is unclear or difficult to compute with evolutionary models as for B-type subdwarf stars or white dwarfs for example.

In other cases, the seismic inversion does not aim at determining the full structure. Its goal is rather to determine both the global parameters of the star such as mass and radius, the density profile inside the star, $\rho(r)$ and the first adiabatic exponent profile $\Gamma_1(r) = \frac{\partial \ln \rho}{\partial \ln P}|_S$.

In practice however, Γ_1 deviates only very little from 5/3 in the stellar interior, apart from the ionization regions in the upper convective envelope. It is thus assumed constant or fixed at the value of a given reference structure used for the inversion. This situation is very different from helioseismology, where the quality of the data allows us to distinguish between various equations of state for the solar material based on the inversion of the Γ_1 profile in the convective envelope (See e.g., Elliott, 1996; Elliott and Kosovichev, 1998; Vorontsov et al., 2013, and references therein).

Due to the lower quality of asteroseismic data and the absence of high-degree modes allowing to determine localized corrections

in the upper layers, the equation of state of the stellar material will not be considered an issue[1]. This point will be further discussed in the following sections when presenting the variational formalism used in linear inversion techniques.

In this context, the application of seismic inversions serve as a complement to evolutionary modelling. The inverted quantities can then be compared with those of evolutionary models and potentially constrain missing physical processes. Consequently, seismic inversions constitute an essential approach to improve the accuracy of stellar models and the determination of fundamental stellar parameters such as mass, radius and age.

3 STATIC AND EVOLUTIONARY MODELLING

The inference of the internal structure of a star can take various forms. It may for example result from the adjustment of an evolutionary sequence to an observed target. For stellar systems such as binaries or clusters, simultaneous fitting of all members can even be done so that the modelling is more constraining, sometimes assuming the same chemical composition and age for all members. We hereby provide for the interested reader a few additional references on seismic modelling and asteroseismology of solar-like oscillators Roxburgh (2002); Christensen-Dalsgaard and Houdek (2010); Guzik (2011); Goupil et al. (2011); Chaplin and Miglio (2013); Di Mauro (2016) as well as seismic studies of stellar clusters (Handberg et al., 2017; McKeever et al., 2019) and binaries (see e.g., Bazot et al., 2016; Bazot, 2020; Salmon et al., 2021). In other cases, an inversion can refer to the determination of the internal structure of a given star in a static way, departing from hypotheses regarding its evolutionary history. Such static approaches will sometimes even aim at determining only a key few internal quantities from dedicated formalisms while avoiding simplifying assumptions regarding the internal structure of the star.

Such static approaches constitute powerful tools to further refine stellar evolutionary models and are often referred as "seismic inversion", while the use of evolutionary models is referred to as "forward modelling". This division is only present in the field of asteroseismology and can be misleading when studying inversion techniques used in other fields (See Tarantola, 2005; Pijpers, 2006, for example).

In what follows, we will briefly describe evolutionary and static inferences as applied to asteroseismic data.

3.1 Inferences From Evolutionary Models

The most common approach to determine the internal structure of a star is by coupling an optimization procedure to a stellar evolution code. While this is commonly referred as "forward modelling" in the seismic modelling community, it actually consists in a type of inversion in the mathematical sense of the word.

In this type of inference, the structure of the star is coupled to an assumed evolutionary history. Namely, the evolution of the chemical abundances of the star is simulated by considering the effects of nuclear reactions and transport processes such as microscopic diffusion, macroscopic transport by rotation, convection, accretion and mass-loss.

The main advantage of using evolutionary models resides in the possibility to test the evolutionary scenarios used to model stars and check the validity of the theory of stellar evolution. Moreover, in view of the recent needs of neighbouring fields such as exoplanetology and Galactic archaeology for fundamental stellar parameters such as masses, radii and ages, the use of optimization techniques on large grids of stellar models has now become routine, especially for main-sequence solar-like oscillators. Such modelling approaches have been applied to a wide range of targets from missions such as CoRoT, *Kepler*, and TESS, as well as closer objects such as Alpha Centauri A&B.

In this context, numerous optimization techniques have been adapted to determine optimal stellar parameters. For example, local minimization techniques such as Levenberg-Marquardt algorithms have been applied in the past (e.g., Frandsen et al., 2002; Teixeira et al., 2003; Miglio and Montalbán, 2005). However, due to the problem of local minima, especially with high-quality Kepler data, and the treatment of the uncertainties in such methods, global minimization techniques have been favoured such as Genetic algorithms, Markov Chain Monte Carlo approaches, or even Machine Learning software. Such methods have been applied to either precomputed grids of stellar evolutionary models or by computing the models on the fly to avoid relying on interpolation that could lead to a loss of accuracy. A few examples of such techniques and their associated results can be found in Mathur et al. (2012); Gruberbauer et al. (2013); Metcalfe et al. (2015); Bellinger et al. (2016); Rendle et al. (2019); Bazot (2020); Aguirre Børsen-Koch et al. (2022).

A major drawback of the grid-based approach stems from the limitation to the physical ingredients of the precomputed models. Therefore, any change of abundance scale, opacity table, equation of state, or prescription for the mixing of chemical elements requires the whole grid to be recomputed, which can be time consuming. However, computing the models on the fly is not a viable option for sampling algorithms such as MCMC techniques that require large numbers of walkers to provide a proper distribution of the optimal parameters.

More recently, a hybrid approach was presented (Buldgen et al., 2019a; Bétrisey et al., 2022), where a combination of local and global minimization techniques are used. In the era of high-quality Kepler data, the uncertainties derived from solely propagating the observational error bars are small enough to sometimes be comparable, or smaller, than the changes in the optimal solution observed when varying the physical ingredients of the models. In this context, local minimization techniques offer the flexibility to estimate the change in the solution from a change of the physics, using the optimal solution obtained from an MCMC sampling of the parameter space. A combination of

[1]Constraints on the convective envelope can still be inferred from so-called "acoustic glitches", that can provide estimates of the helium abundance or the position of a sharp transition in temperature gradients at the bottom of the convective zone.

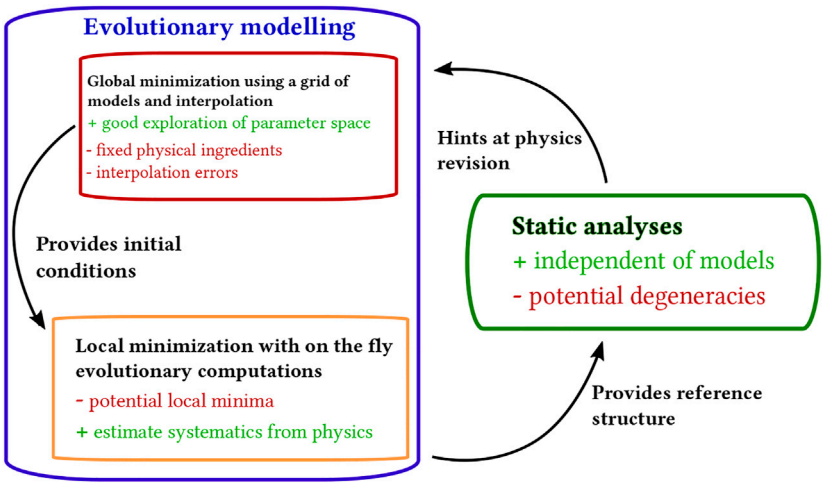

FIGURE 1 | Schematic representation of combinations of evolutionary and static inferences used in stellar modelling. Each box includes the strenghts (green) and weaknesses (red) of the various methods and the arrows represent their relations.

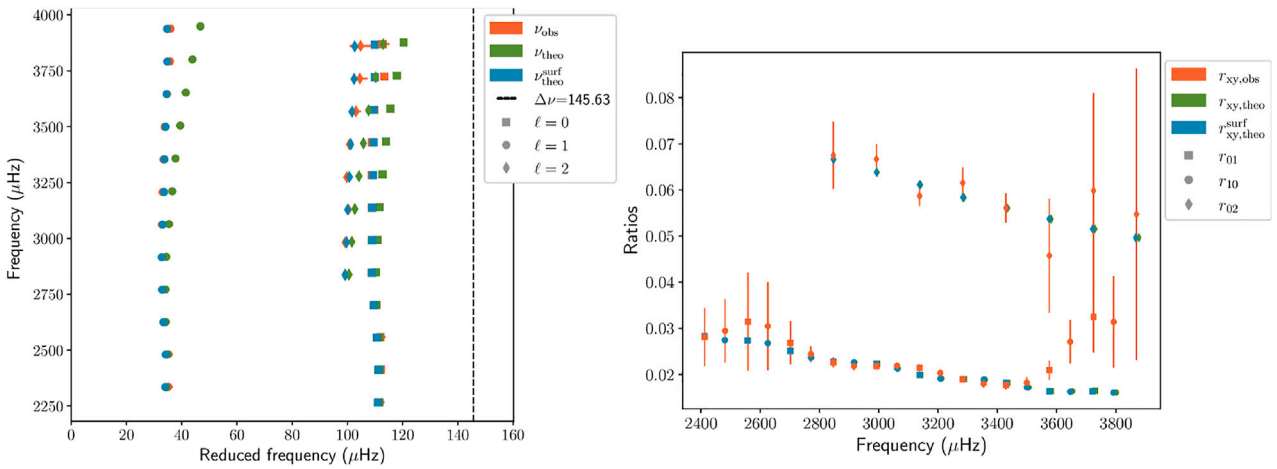

FIGURE 2 | *Left*: Illustration of the effects of surface corrections for the Echelle diagram of Kepler 93, showing the significant effect of the parametric corrections on high frequencies. *Right*: Frequency separation ratios for the data of the left panel, showing their low sensitivity to the empirical surface corrections as the blue and reen symbols are essentially the same.

both is probably a good approach to test the impact of known physical processes on stellar fundamental parameters, while departing from an evolutionary history using static inferences might be optimal to study the presence of unknown physical processes. A schematic illustration of the interplay between the different modelling strategies is provided in **Figure 1**.

Besides the algorithm used to determine the optimal model, the way seismic constraints are combined is also extremely important. One major issue of solar-like oscillations is their sensitivity to surface effects. To mitigate this issue, a first approach is to develop so-called empirical "surface corrections", that are based on solar frequencies (See e.g., Rabello-Soares et al., 1999; Kjeldsen et al., 2008; Ball and Gizon, 2014) and/or on 3D averaged atmospheric models for which adiabatic oscillations are computed (e.g., Sonoi et al., 2015; Ball et al., 2016). More recently, such analyses have been generalized to dipolar mixed modes by Ong and Basu (2020); Ong et al. (2021).

Given the amplitude of the surface effect, a direct fitting of the individual frequencies will be extremely sensitive to the empirical corrections. This is illustrated in the left panel of **Figure 2**, showing the individual frequencies of Kepler 93 and those of the associated optimal stellar model fitting them using the Ball and Gizon (2014) empirical surface correction. The actual amplitude of the surface correction is much larger than the uncertainties on the frequencies themselves, which may lead to strong biases, especially at high frequencies and can result in significant biases in the inferred stellar mass (Jørgensen et al., 2020; Bétrisey et al., 2022).

Another way to circumvent surface effects is to use combinations of frequencies, such as the so-called frequency separation ratios of the large and small frequency separations defined in Roxburgh I. W. and Vorontsov S. V. (2003).

$$r_{01}(n) = \frac{\delta_{01}(n)}{\Delta\nu_1(n)}, \tag{6}$$

$$r_{10}(n) = \frac{\delta_{10}(n)}{\Delta\nu_0(n+1)}, \tag{7}$$

$$r_{02}(n) = \frac{\delta_{02}(n)}{\Delta\nu_1(n)}, \tag{8}$$

with $\Delta\nu_l(n)$ the large separations, $\delta_{ij}(n)$ the small separations, and n the radial order of the mode:

$$\Delta\nu_l(n) = \nu_{n,l} - \nu_{n-1,l}, \tag{9}$$

$$\delta_{01}(n) = \frac{1}{8}\left(\nu_{n-1,0} - 4\nu_{n-1,1} + 6\nu_{n,0} - 4\nu_{n,1} + \nu_{n+1,0}\right), \tag{10}$$

$$\delta_{10}(n) = -\frac{1}{8}\left(\nu_{n-1,1} - 4\nu_{n,0} + 6\nu_{n,1} - 4\nu_{n+1,0} + \nu_{n+1,1}\right), \tag{11}$$

$$\delta_{02}(n) = \nu_{n,0} - \nu_{n-1,2}. \tag{12}$$

As shown in the right panel of **Figure 2**, these ratios are largely independent of the surface layers and thus much more efficient at constraining the internal structure of an observed target. Other techniques of surface-independent model fitting have been developed and presented in Roxburgh (2015). More recently, Farnir et al. (2019) also developed a comprehensive approach to decompose the spectrum of solar-like oscillations in seismic indicators uncorrelated to each other, taking into account both the smooth and the glitch component of the oscillation spectrum.

In general, non-seismic constraints will also be considered when carrying out evolutionary modelling, such as the stellar luminosity, the effective temperature, the surface metallicity or the photospheric radius determined from interferometry (whenever available), or the mass if studying a spectroscopic binary system. While not always available, such non-seismic constraints, especially if determined with high precision, can prove extremely useful in lifting degeneracies between various solutions provided by pure seismic modelling.

3.2 Inferences From Static Models

Static models are depictions of the internal structure of stars without considering their evolutionary history. In a strict sense, the observed oscillation frequencies carry information only on the current state of the star, but there can be multiple paths leading to the current observed properties. Static models are particularly useful to study stars in an evolutionary stage difficult to compute numerically, or for which the evolutionary path is unclear.

Various techniques have been applied in the past to study the internal structure of SdB stars and white dwarfs (Charpinet et al., 2008; Van Grootel et al., 2010; Giammichele et al., 2018; Charpinet et al., 2019; Fontaine et al., 2019), providing constraints on the equation of state of dense stellar matter and the properties of semi-convective mixing in advanced evolutionary phases.

Static seismic models have also been computed for the solar case (See e.g., Basu and Thompson, 1996; Takata and Shibahashi, 1998; Shibahashi et al., 1999; Shibahashi and Tamura, 2006; Buldgen et al., 2020) where the presence of high degree modes allows us to carry out a full scan *via* iterative methods. Some non-standard static models have also been computed by Hatta et al. (2021) for KIC 11145123, a young γ-Doradus δ-Scuti hydrid pulsator. As such, static modelling may also prove useful for modelling non-standard evolutionary products such as results of mergers, stripped cores, ... for which pulsational properties may significantly differ from what their standard evolutionary counterparts would predict (See e.g., Deheuvels et al., 2022).

4 VARIATIONAL EQUATIONS

The most commonly used inversion techniques rely on the so-called variational principle of adiabatic stellar oscillations (See Chandrasekhar, 1964; Clement, 1964; Chandrasekhar and Lebovitz, 1964; Lynden-Bell and Ostriker, 1967), that can be derived from the functional analysis of the adiabatic oscillation equations. It essentially states that at first order, perturbation of the adiabatic eigenfrequencies of gaseous spheres will be related to perturbations of the oscillation operator and link the seismic observables to interior quantities. In other words, small perturbations will follow, to first order, the following equation

$$\frac{\delta\nu^{n,\ell}}{\nu^{n,\ell}} = \frac{<\boldsymbol{\xi}^{n,\ell}, \delta\mathcal{L}\left(\boldsymbol{\xi}^{n,\ell}\right)>}{I^{n,\ell}}, \tag{13}$$

with $\nu^{n,\ell}$ the frequency of the oscillation mode, $\boldsymbol{\xi}^{n,\ell}$ its eigenfunction, $I^{n,\ell}$ the mode inertia (see e.g., Unno et al., 1989, for a general description of non-radial stellar oscillations) and $\delta\mathcal{L}$ the perturbed operator of adiabatic oscillations. The notation $<.>$ denotes the scalar product over the functional space of the solutions of the adiabatic oscillation equations. It is defined as

$$<\mathbf{a}, \mathbf{b}> = \int_V \mathbf{a}\cdot\mathbf{b}\rho dV, \tag{14}$$

with V the volume of the sphere and ρ the local value of the density in the sphere.

Examples of small perturbations in the stellar case include the effects of slow rotation, or minor mismatches between the internal structure of the model and the observed star. The former, that serves as initial condition for the inversion, will often be called "reference model", while the observed star or the target model will often be refereed to as the "target" of the inversion procedure.

It is worth mentioning that while the variational principle is valid for "small perturbations" of an Hermitian operator (as is the general operator describing the full 4^{th} order system of adiabatic stellar oscillations), the domain of validity of the linear approximation is unclear, and likely depends on the oscillation modes and the quality of the reference model. The variational expressions have for example been generalized in the case of mixed oscillation modes by Ong and Basu (2020) and Ong et al. (2021).

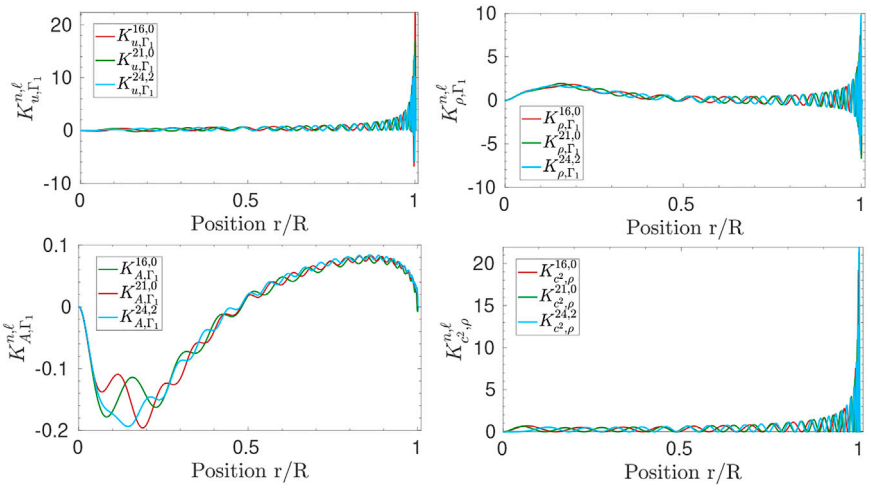

FIGURE 3 | Structural kernels for various structural pairs and for low degree oscillations modes for a representative model of 16CygA from Buldgen et al. (2022). Each panel illustrates a different variable that can be used for variational inversions of the structure of a star as well as the degeneracy in the shape of the kernels for low degree modes.

For the purpose of structure inversions, the equations are reworked to provide a formally simple expression allowing us to derive corrections to the internal structure of a given model (Dziembowski et al., 1990). This expression is

$$\frac{\delta\nu^{n,\ell}}{\nu^{n,\ell}} = \int_0^R K^{n,\ell}_{s_1,s_2}\frac{\delta s_1}{s_1}dr + \int_0^R K^{n,\ell}_{s_2,s_1}\frac{\delta s_2}{s_2}dr + \mathcal{O}(\delta^2), \quad (15)$$

where s_1 and s_2 are structural variables such as density, pressure, sound speed, ... $K^{n,\ell}_{s_j,s_k}$ the structural kernel related to variable s_j in the (s_j, s_k) pair which depends on the structure of the model and the eigenfunction of the oscillation mode. The notation δ defines a difference between the reference model and the observed target of a variable such as the frequency, the density as a function of radius, ... (See Dziembowski et al., 1990, for the associated developments). In **Eq. (15)**, the last term denotes that the formalism is valid to first order, and in some cases, higher order terms can become non-negligible, making the first order approximation inappropriate. Various pairs of structural kernels are illustrated in **Figure 3**, namely for the density, squared adiabatic sound speed, squared isothermal sound speed and Ledoux discriminant. The similarity between the kernels illustrates well the difficulties of asteroseismic inversions who will only have a few available modes to carry out the inversions.

The classical variational expressions are related to the adiabatic sound speed and density profiles. However, these expressions can be easily generalized to any physical quantity appearing in the adiabatic oscillation equations (Elliott, 1996; Basu and Christensen-Dalsgaard, 1997; Kosovichev, 2011; Buldgen et al., 2017b). In addition, assuming a linearized form of the equation of state can also be used to determine "secondary" variables such as temperature or in principle, chemical abundances. In such cases the Γ_1 perturbations are rewritten as

$$\frac{\delta\Gamma_1}{\Gamma_1} = \left.\frac{\partial \ln\Gamma_1}{\partial \ln P}\right|_{\rho,Y,Z}\frac{\delta P}{P} + \left.\frac{\partial \ln\Gamma_1}{\partial \ln \rho}\right|_{P,Y,Z} \frac{\delta\rho}{\rho} + \left.\frac{\partial \ln\Gamma_1}{\partial Y}\right|_{P,\rho,Z}\delta Y + \left.\frac{\partial \ln\Gamma_1}{\partial Z}\right|_{P,\rho,Y}\delta Z, \quad (16)$$

with P, the local pressure, ρ, the local density, Y, the helium mass fraction and Z, the heavy element mass fraction. Other thermodynamic variables can be used in combination with the appropriate Γ_1 derivatives.

In practice however, this expression is not used in asteroseismology to carry out inversions of the chemical composition, but rather to naturally damp the contribution of the second integral in the inversion thanks to the low amplitude of the Γ_1 derivatives with respect to Y. Such "tricks" lead to more stable inversions for which the variational equation almost reduces to an integral expression with one structural variable instead of two. We will come back to this point in **Section 5**.

Lagrangian perturbations can also be considered in **Eq. (15)**. In this case, the perturbations of the structural variables will be considered at fixed mass instead of fixed radius (Christensen-Dalsgaard and Thompson, 1997). Instead of using individual frequency differences, it is also possible to express the variational equations for frequency separation ratios, as was shown in Floranes et al. (2005) and applied in Bétrisey and Buldgen (2022).

One major weakness of the variational expressions using individual frequencies is their strong sensitivity to surface effects. They indeed rely on the adiabatic approximation, which is not valid in the upper layers where the thermal and dynamical timescales are of the same order of magnitude. Moreover, adiabatic oscillation codes often use simplified boundary conditions and the poor modelling of the upper convective layers by the mixing-length theory will lead to inaccuracies of the oscillation frequencies at a significant level with respect to the observational errors. Such sensitivity can however be damped when using frequency separation ratios for the inversion.

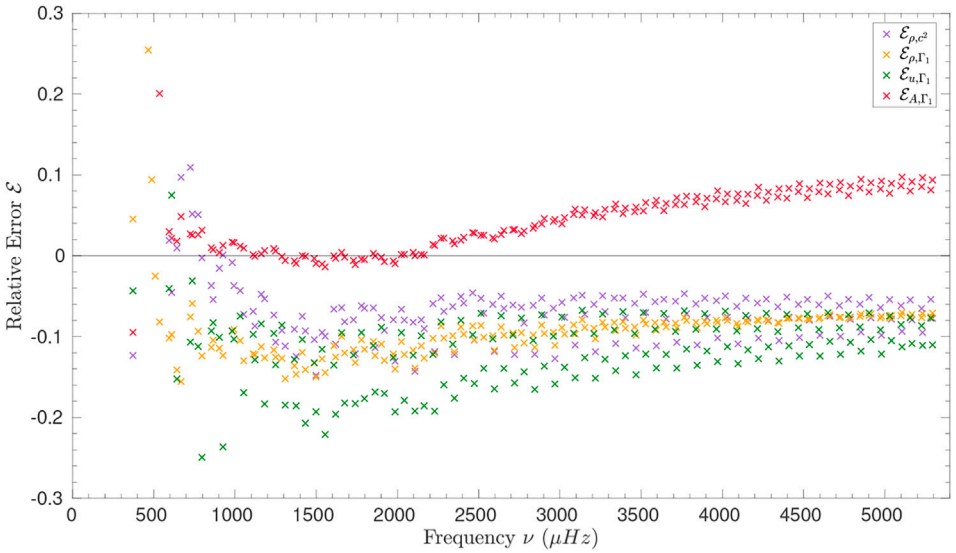

FIGURE 4 | Illustration of the verification of the integral relation between relative frequency differences and relative structure differences for solar models including various transports of the mixing of chemicals, using **Eq. 18**, using models from Buldgen et al. (2017b) and various structural pairs, namely (ρ, c^2) (ρ, Γ_1) (u, Γ_1) and (A, Γ_1).

Indeed, as they directly use frequency differences, the variational equations will suffer to some extent from the same caveats as directly using the individual frequencies as constraints in evolutionary or static modelling. This implies that the variational expression 15 will have to be supplemented by a surface correction term that often takes a polynomial form

$$\mathcal{F}(\nu) = \sum_k c_k(\nu)\nu^k, \tag{17}$$

with ν a given frequency and c_k the surface correction coefficients associated with the power k of the frequency. Existing surface corrections include the classical polynomial approach of degree 7 applied in helioseismology (Rabello-Soares et al., 1999), the two-terms Ball and Gizon (2014) correction and the Sonoi et al. (2015) formula that can also be linearized, or applied to the frequencies beforehand using their empirical relation of the surface correction with effective temperature and surface gravity.

It is therefore important to keep in mind that the validity of the variational relations is limited. It can for example be measured using error functions such as

$$\mathcal{E}^{n,\ell} = \frac{\Lambda^{n,\ell}_{\rm LHS} - \Lambda^{n,\ell}_{\rm RHS}}{\Lambda^{n,\ell}_{\rm LHS}}, \tag{18}$$

with $\Lambda^{n,\ell}_{\rm LHS}$ the relative frequency difference and $\Lambda^{n,\ell}_{\rm RHS}$ the right-hand side of **Eq. (15)**.

As illustrated in **Figure 4**, the accuracy of the variational inversion will vary depending on the oscillation modes considered as well as the structural variables used. Such considerations might be very important when choosing the most adapted variable pair for a given target and set of observed frequencies before carrying out an inversion of the structure.

5 LINEAR INVERSION TECHNIQUES - THE SOLA METHOD

The variational equations provide the basis for the use of linear inversion techniques in helioseismology. Namely, under the hypothesis of the validity of the linear integral relation 15, these equations can be solved to provide corrections to structural variables. The linear approaches provide one step of correction, and are not iterated, unlike the non-linear methods we present in **Section 6**. As mentioned above, the variational equations can be rewritten for a wide range of physical quantities, offering some degree of freedom regarding the target of the inversion.

However, the situation is in practice far more complex. Linear inversion techniques such as the OLA (Backus and Gilbert, 1970), SOLA (Pijpers and Thompson, 1994) or RLS methods (Tikhonov, 1963) have been adapted for inverting helioseismic data (see Christensen-Dalsgaard et al., 1990; Sekii, 1997, for a comparison between OLA and RLS) and (see Reese, 2018, for a review). Inversions of stellar structure using asteroseismic data have so far been limited to the use of the SOLA method[2], which is the one we will describe here.

The philosophy behind the SOLA inversion is to compute linear combinations of the relative frequency differences based the following cost function

$$\begin{aligned}\mathcal{P}(c_i) = &\int_0^R \Big[K_{\rm avg}(r) - \mathcal{T}(r)\Big]dr + \beta\int_0^R K^2_{\rm cross}(r)dr \\ &+\lambda\mathcal{N} + \tan\theta\frac{\sum_i^N (c_i\sigma_i)^2}{<\sigma^2>} + \sum_i^N c_i\sum_k^L a_k\psi_k(\nu_i),\end{aligned} \tag{19}$$

[2]We note however that instances of RLS inversions of the internal rotation of distant stars can be found in Deheuvels et al. (2014); Schunker et al. (2016a).

with $\mathcal{T}$ the target function of the inversion, λ a Lagrange multiplier, $\mathcal{N}$ an additional regularization term (as will be discussed later), c_i the inversion coefficients, θ and β the trade-off parameters, σ_i the uncertainties of the relative frequency differences, $<\sigma^2> = \frac{1}{N}\sum_{i=1}^{N}\sigma_i^2$ and N the number of observed frequencies. The term $\sum_k^L a_k \psi_k(\nu_i)$ is a polynomial expression for the surface correction defined in **Eq. (17)**, with L the number of surface terms in the polynomial definition. In addition to these quantities, we define in **Eq. (19)** two terms, $K_{\rm avg}$ and $K_{\rm cross}$, the averaging and cross-term kernels, defined from the recombination of the structural kernels with the inversion coefficients. They will have the form.

$$K_{\rm avg} = \sum_i^N c_i K^i_{s_1,s_2}, \tag{20}$$

$$K_{\rm cross} = \sum_i^N c_i K^i_{s_2,s_1}, \tag{21}$$

if the target function of the inversion is related to the variable s_1 in the (s_1, s_2) structural pair.

In other words, the SOLA method is based on a trade-off between precision and accuracy. The goal is to compute the best fit to the target function of the inversion while avoiding to amplify too much the observational uncertainties. Looking at **Eq. (20)**, it is straightforward to see that the number of observed frequencies will play a crucial role for the accuracy of the method. The more frequencies are observed, the more structural kernels are available for recombination, and the more accurate the inversion will be.

The situation in asteroseismology is however very far from that of helioseismology. Since the surface of the star is not resolved, geometric cancellation forbids the detection of solar-like oscillations of angular degree higher than 3. This has important consequences for the capabilities of linear inversions, as the datasets for the best *Kepler* targets count at most ≈ 50 to ≈ 60 individual frequencies with low degrees. In such conditions, full scans of the internal structure, as carried out for the Sun, are not achievable.

Most of the time, the linear inversion of the structure will be limited by the number of frequencies and the validity of the linear formalism. An important difference between asteroseismic and helioseismic inversions is that the fundamental parameters, mass, radius and age of the star under study are not known. The solar case thus consists in an ideal environment where the bounds of the integrals in **Eq. (15)** are known, and where the knowledge of the age of the Sun provides a degree of control on the computed models, ensuring the validity of the linear formalism.

This will not be the case in asteroseismology, implying that a workaround has to be found, and some care has to be taken when interpreting the results of linear inversions. In practice, one can include an additional term in the cost function of the inversion related to the minimization of the mean density, as suggested by Roxburgh et al. (1998). In such condtions, one can consider that using dimensional and dimensionless frequencies, denoted ν and $\tilde{\nu}$ would be equivalent and that

$$\frac{\nu_{\rm obs} - \nu_{\rm ref}}{\nu_{\rm ref}} = \frac{\tilde{\nu}_{\rm obs} - \tilde{\nu}_{\rm ref}}{\tilde{\nu}_{\rm ref}}, \tag{22}$$

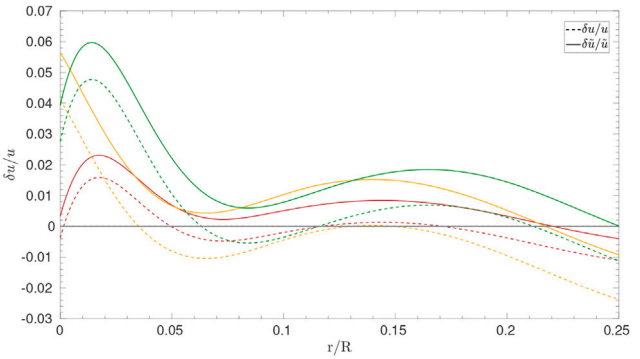

FIGURE 5 | Differences between the dimensional ($\delta u/u$, dashed line) and dimensionless ($\delta\tilde{u}$, plain line) squared isothermal sound speed for models of 16CygA from Farnir et al. (2020). The differences are those computed in Buldgen et al. (2022), **Figure 13A** and are linked to models of 16CygA showing differences in their mean density values between 1 (orange and green lines) and 2% (red lines).

if the mean density is perfectly fitted. This implies that the actual corrections derived by the inversion are for the dimensionless variable and not its dimensional counterpart. Another pragmatic approach to take this scaling effect into account is to carry out inversion for ensembles of models with the same mean density, determined for example from mean density inversions (See **Section 5.3**). This "scaling" effect can become very important when comparing actual differences between models. It also illustrates some degree of degeneracy in seismic inferences, and shows the importance of independent radii estimates from interferometric measurements, or combination of parallaxes and spectroscopic measurements. In practice, any high-quality non-seismic constraints will prove very useful to seismic modelling, and also explains why binary systems are still key testbeds of stellar physics, even in the era of space-based photometry missions (Appourchaux et al., 2015; Metcalfe et al., 2015; Bazot et al., 2016; Farnir et al., 2020; Salmon et al., 2021). **Figure 5** illustrates such differences for two models of the *Kepler* target 16CygA from Farnir et al. (2020). The behaviour of the dimensional and dimensionless relative differences in squared isothermal sound speed can be quite different, showing the importance of understanding what variable is actually constrained by the inversion.

Another limitation of linear inversions is the range of validity of the linear formalism. In practice, calibrations using only non-seismic parameters will not be sufficient to ensure the applicability of the variational formalism to the inverse problem. Thus, as already noted by Thompson and Christensen-Dalsgaard (2002), a preliminary form of seismic modelling must be carried out before the inversion is performed, which implies that seismic data is already used beforehand. From a modelling point of view, this means that the inversion step is not completely independent of the preliminary modelling procedure, and that inversions relying on the variational equations can often be biased. This problem can become more substantial if the amplitification of the observational uncertainties is small, meaning that the

inversion appears artificially precise. In this context, providing a set of reference models large enough is very important to ensure that the precision of the inversion is correctly assessed from the point of view of model-dependencies, non-linearities, and impact of empirical surface corrections.

5.1 Dealing With Surface Effects

The additional surface correction term in **Eq. (17)** leads to various complications in asteroseismic inversions. The additional term in **Eq. (19)** can often have a very significant impact on the inversion results, as it leads to a less favourable trade-off for a method already limited by the low number of observed modes to fit the target function. Determining the actual impact of the surface corrections on inversion results is particularly important, as in some cases they will lead to a larger variation of the inverted result than the uncertainties derived from the SOLA method. This is the case for mean density inversions, which thus require a more careful analysis. Indeed, the precision on the determined mean density will have an impact on the determined stellar mass using evolutionary modelling or the determined planetary mass from a radial velocity curve.

The classical polynomial fit used for helioseismic inversions is not applicable in the context of asteroseismology. It was usually advised to consider a polynomial of order up to 7 to fit the "surface term" (Rabello-Soares et al., 1999), which is not possible with asteroseismic data. Reese et al. (2012) initially attempted to limit the correction to the first order, but tests in hare and hounds exercises showed that this was even less efficient than not considering any correction (Reese et al., 2016).

With the advent of the new empirical corrections of Ball and Gizon (2014) and Sonoi et al. (2015), the surface term could be reduced to two additional terms. In such conditions, the surface term can sometimes be directly included in the fitting of the SOLA cost-function with limited impact on the quality of the fit of the target function of the inversion regarding accuracy, but will actually impact the amplitude of the inversion coefficients and thus the precision of the inversion. However, with very limited datasets, or for some more unstable inversions, the addition of two terms in the cost-function can lead to low quality reproduction of the target.

In such conditions, surface corrections can also be applied following the empirical formula of Sonoi et al. (2015) as a function effective temperature and surface gravity before carrying the inversion, using the corrected frequencies as the observed ones. An analysis of the importance of surface corrections for mean density inversions on red giant stars using averaged 3D atmospheric models and non-adiabatic frequency computations has been carried out in Buldgen et al. (2019b). They showed that applying the surface corrections beforehand could be more efficient than including it in the cost-function, as it did not affect the fit of the target function. A similar observation was made for Kepler 93 by Bétrisey et al. (2022). However, further tests and more thorough analyses have to be carried out for other indicators and datasets before concluding on the best approach to take into account surface effects. In addition, such studies do not necessarily indicate that the surface corrections are ultimately accurate, and an efficient workaround is then to avoid the surface effect dependency in the inversion altogether, as will be discussed in **Section 6**.

5.2 Inversions of Localized Corrections

The original SOLA inversions have been designed for determining local average corrections of the solar rotation profile (Pijpers and Thompson, 1994) from the variational expressions applied in the slowly rotating case. The same approach can be directly applied to structural inversions, with the only major change being that a cross-term contribution appears due to **Eq. (15)** including two integrals compared with the single integral relation of rotation perturbations.

Inversions of localized averages have been extensively performed in helioseismology, as well as comparisons with the RLS technique and applications to various structural pairs. The application of SOLA inversions to asteroseismic data was foreseen quite early, with studies on artificial data already carried out in the 1990s and early 2000s (Gough and Kosovichev, 1993a; Gough and Kosovichev, 1993b; Roxburgh et al., 1998; Basu et al., 2002; Takata and Montgomery, 2002). In most cases, the expected quality of the dataset was actually higher than what was actually brought by the space-based photometry missions, with some artificial datasets going as high as 100 observed frequencies, which unfortunately has not been achieved for any solar-like oscillator observed by *Kepler*.

In the case of localized inversions, the target function of the inversion usually is a Gaussian-like function of the form

$$\mathcal{T} = \alpha r \exp\left(-\left(\frac{r-y}{\Delta} + \frac{\Delta}{2r_0}\right)^2\right), \tag{23}$$

with α a normalisation constant, y the center of the Gaussian target function and $\Delta = \frac{\Delta_A c(y)}{c_A}$ is linked to the width of the Gaussian, Δ_A being a free parameter, and $c(y)$ and c_A the adiabatic sound speed at the maximum of the kernel and at a radius of $0.2R$, respectively.

The regularisation term $\mathcal{N}$ of **Eq. (19)** is then a unimodularity constraint on the averaging kernel of the form

$$\int_0^R K_{\text{avg}} dr = 1, \tag{24}$$

to avoid high amplitudes of the inversion coefficients that can make the procedure unstable.

Applications of the SOLA method in its original form to actual asteroseismic data can be found as early as 2004 (di Mauro, 2004). More recent applications aiming at determining localized corrections to *Kepler* targets can be found in (Bellinger et al., 2017; Bellinger et al., 2019; Kosovichev and Kitiashvili, 2020; Bellinger et al., 2021; Buldgen et al., 2022). Such applications have been limited to the best *Kepler* targets, such as the 16Cyg binary system. Even in such cases, localised kernels can only be obtained in the deep layers, as a result of the availability of only low degree modes. An illustration of Gaussian averaging kernels obtained for 16CygA is illustrated in the right panel of **Figure 6**.

As shown in the left panel of **Figure 6**, such inversions have confirmed the accuracy of the reference evolutionary models for both stars determined from asteroseismic modelling using the

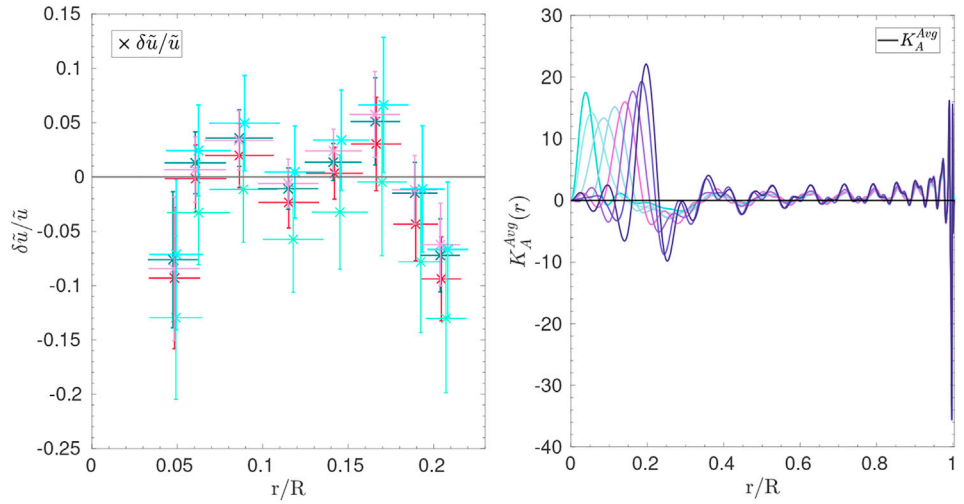

FIGURE 6 | *Left*: relative differences in dimensionless squared isothermal sound speed for 16CygA as a function of normalized radius. Each colour represents a different reference model for the inversion. The set of reference models is that of Buldgen et al. (2022), Table 2. *Right*: averaging kernels for the localized inversion of 16CygA using the (*u*, *Y*) structural pairs [adapted from Buldgen et al. (2022)].

method of Farnir et al. (2020). The fact that the SOLA inversion cannot pinpoint differences between models of solar twins is not really a surprise. Indeed, the effects of varying the transport of chemicals by inhibiting settling of heavy elements to mimick turbulence at the base of the convective envelope, changing the radiative opacity tables, or changing the reference solar abundances is rather small for a given set of parameters such as mass, radius and age. From the analysis of solar models, the differences seen are of the order of 1% at the base of convective envelope and reduce to 0.2% in the deep radiative layers. In these conditions, linear asteroseismic inversions, showing uncertainties of a few percent, might not be able to pintpoint such small differences in structure if the fundamental parameters of a star are well constrained.

This points towards a quite stringent restriction of linear inversions, as they have a sort of "niche" where their application might be useful. In practice, an unsatisfactory agreement between the observed and modelled frequency separation ratios, r_{02} or r_{01}, may indicate that carrying out inversions of the internal structure can be useful, as shown in Bellinger et al. (2019). However, if all frequency separation ratios are well reproduced, linear inversions of the internal structure might only confirm the validity of the evolutionary models and the traces of additional processes such as macroscopic mixing of chemicals might be looked for using frequency glitches (Monteiro and Thompson, 2005; Mazumdar et al., 2012; Mazumdar et al., 2014; Verma et al., 2014; Verma et al., 2017; Verma et al., 2019; Verma and Silva Aguirre, 2019) or depletion of light elements such as Lithium and Beryllium (Deal et al., 2015).

Localised inversions have also been applied to post main-sequence *Kepler* targets such as in Kosovichev and Kitiashvili (2020) and Bellinger et al. (2021). However, the validity of the variational equations in the context of mixed modes still needs to be thoroughly investigated, as shown by Ong and Basu (2020) and Ong et al. (2021), as coupling effects can cause the classical relation to break down for mixed modes, implying that a non-linear formalism, taking properly into account the coupling using the full system of oscillation equations might be required. In this context, non-linear inversions appear the most favourable approach for extracting meaningful constraints from asteroseismic data.

5.3 Inversions of Global Indicators

As a result of the difficulties of carrying out full profile inversions, a compromise was struck by Reese et al. (2012) who decided to focus on global quantities rather than attempt at localizing kernels. The main goal of such "indicator" inversions is to focus on one single quantity at a time using the variational expressions, trying to extract constraints on some well-chosen key quantities instead of detailed profiles. The chosen quantities are determined based on the structural properties under investigation, such as the mean molecular weight gradient in the deep radiative layers, or the profile of an entropy proxy close to the border of a convective zone.

A main difficulty of linear asteroseismic inversions is to find appropriate target functions for SOLA inversions that can be easily fitted with a very limited number of frequencies. Consequently, Reese et al. (2012) focused on a physical quantity well-known to be constrained by solar-like oscillations, the mean density. Buldgen et al. (2015a), Buldgen et al. (2015b), Buldgen et al. (2018) then focused on generalizing the formalism to other physical quantities. The linear inversion of an indicator will be computed as follows

$$\frac{\delta E}{E} = \sum_{i}^{N} c_i \frac{\delta \nu_i}{\nu_i}, \tag{25}$$

with E the indicator, c_i the inversion coefficients determined by the SOLA method and ν_i the individual frequencies.

The indicator is related to structural variables using an integral definition

$$E = \int_0^R f(r)g(s_1)dr, \tag{26}$$

and applying an eulerian linear perturbation to this equation leads to

$$\frac{\delta E}{E} = \int_0^R \frac{s_1 f(r)}{E}\frac{\partial g(s_1)}{\partial s_1}\frac{\delta s_1}{s_1}dr = \int_0^R \mathcal{T}_E \frac{\delta s_1}{s_1}dr, \tag{27}$$

which defines the target function of the indicator $\mathcal{T}_E$ which will be used in **Eq. (19)** for this specific inversion.

An additional term is introduced in the SOLA cost-function, denoted $\mathcal{N}$ in **Eq. (19)**. For the case of indicator inversion, it takes the following form

$$\mathcal{N} = \left[k - \sum_i^N c_i\right], \tag{28}$$

with k an integer that relates the scaling of the indicator with respect to mass. The argument is based on the relation between an indicator and the frequencies, which go as $\sqrt{\frac{GM}{R^3}}$. Since the radius is essentially fixed by the definition of the boundary of the integral variational relation, the scaling ends up being a scaling with mass. The idea is to determine the properties of a homologous transformation that will lead to the correct rescaling of the indicator value.

Essentially, if the indicator goes as $E \propto M^{k/2}$, then a small perturbation of $\delta E/E = \epsilon$ will lead to a small perturbation of the frequencies $\delta\nu/\nu = \epsilon/k$. In these conditions, it can be shown that a homologous transformation with $\sum_i c_i = k$ leads to the correct rescaling of the indicator. Such inversions have been called "unbiased" in Reese et al. (2012). In practice, this term acts as an additional regularization term for the inversion to avoid high amplitudes of the inversion coefficients. As seen above, similar regularization terms are introduced for localized inversions in the form of unimodularity constraints for the kernels.

This additional constraint has also been associated with simple "non-linear" generalizations of the indicator inversions, following the approach of an iterative scaling of the model using homologous relations. This iterative scaling can be shown to provide generalized formulations of **Eq. (25)** which will depend on the value of the additional coefficient in the regularization term.

5.3.1 Mean Density

Mean density inversions were defined in Reese et al. (2012), as a potential application of the SOLA method to refine the determinations of stellar fundamental parameters from asteroseismic data. These inversions have been further tested later on in Buldgen et al. (2015b) for solar like stars, and applied to radial oscillations of post-main sequence stars in Buldgen et al. (2019b). The integral definition of the stellar mean density is

$$\bar{\rho} = \frac{3}{4\pi R^3}\int_0^R 4\pi r^2 \rho dr. \tag{29}$$

Hence, the target function is given by

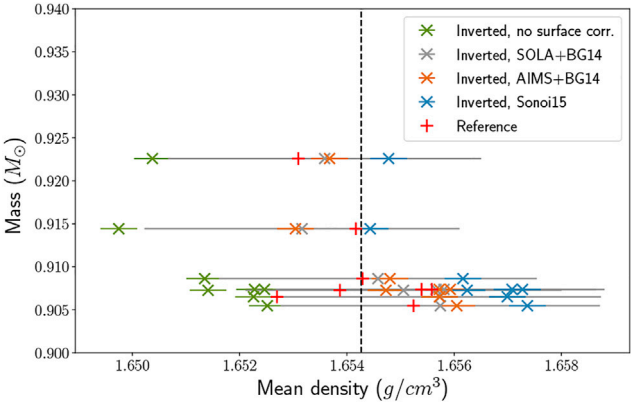

FIGURE 7 | Effect of surface corrections and model-dependency on mean density inversions of Kepler 93 [adapted from Bétrisey et al. (2022)] as a function of mass of the reference model. Red crosses show the reference mean density values, olive green crosses show results without surface corrections, blue and grey crosses show results using the Sonoi et al. (2015) and Ball and Gizon (2014) corrections in the SOLA cost function, whereas brown crosses show results using coefficients extracted from MCMC modelling and applied beforehand.

$$\mathcal{T}_{\bar{\rho}}(r) = \frac{4\pi\rho r^2}{R^3\rho_R}, \tag{30}$$

with $\rho_R = \frac{M}{R^3}$. An illustration of the target function in the case of 16CygA is provided in the bottom right panel of **Figure 8**. This function is usually fitted using structural kernels of the (ρ, Γ_1) structural pair in the variational equation.

Mean density inversions have been applied to a wide variety of targets, mostly on the main sequence. They offer the advantage of providing an accurate determination of the mean density, beyond the capabilities of asymptotic estimates such as the large frequency separation (Vandakurov, 1967) and being less sensitive to surface effects than the latter.

Due to the easily fitted target function, mean density inversions are one of the few that can be applied with a very limited number of observed frequencies (See Reese et al., 2012; Buldgen et al., 2015b), without recalibration of the trade-off parameters. These inversions are thus suitable for an "automated' approach in modelling pipelines. However, they suffer from an overestimated precision of the inversion. As a result of the shape of the target function, the inversion coefficients are not very large and the amplification of the uncertainties is small. While this may seem as an advantage, it also means that the error bars on the determined mean density cannot be directly estimated using the SOLA method. In fact, the spread of results observed when using multiple models and empirical surface corrections is often much larger than the 1σ error bars provided by the SOLA method. This is illustrated in **Figure 7** for Kepler 93. In practice, mean density inversions must then be applied to a given set of models and their precision is closer to 0.2% or 0.3% (See Bétrisey et al., 2022) rather than the claimed 0.1% or less computed from the propagation of the observational uncertainties.

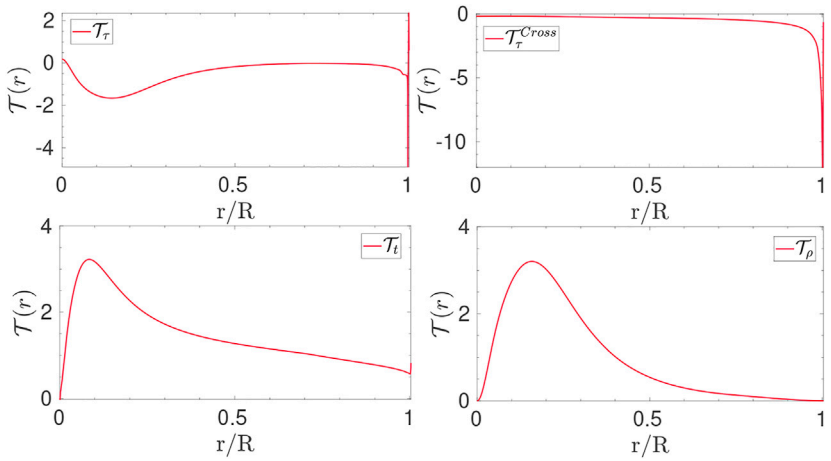

FIGURE 8 | Target functions of various indicators as a function of normalized radius, taken for a model of 16CygA. *Upper left and right*: target functions for the acoustic radius inversion. *Bottom left*: target function for the *t* core condition indicator. *Bottom right*: target function for the mean density.

5.3.2 Acoustic Radius

Acoustic radius inversions were defined in Buldgen et al. (2015b). The acoustic radius of a star is defined as

$$\tau = \int_0^R \frac{dr}{c}, \tag{31}$$

and is related to the large frequency separation in the asymptotic regime as $\Delta\nu = 2/\tau$.

These inversions can be carried out with both the (c^2, ρ) or the (ρ, Γ_1) structural pair. As discussed above, structural pairs involving either Γ_1 or Y as secondary variable should be preferred to minimize naturally the cross-term contribution. Therefore, for the (ρ, Γ_1) structural pair, some manipulations are made using the definition of the squared adiabatic sound speed, c^2, and permutations of integrals to define the target functions of the inversion. In this form, the acoustic radius inversion has a non-zero target function for the cross-term contribution.

The target functions are defined as.

$$\begin{aligned}\mathcal{T}_{\tau,\mathrm{avg}} = &\frac{1}{2c\tau} - \frac{m(r)}{r^2}\rho\left[\int_0^r \frac{1}{2c\tau P}dx\right] \\ &-4\pi r^2\rho\left[\int_r^R\left(\frac{\rho}{x^2}\int_0^x \frac{1}{2c\tau P}dy\right)\right]dx,\end{aligned} \tag{33}$$

$$\mathcal{T}_{\tau,\mathrm{cross}} = \frac{-1}{2c\tau}, \tag{34}$$

with ρ the local density, m the mass contained within the layer of radial position r, P the pressure, c the adiabatic sound speed, and τ the acoustic radius. An illustration of the target functions for 16CygA is illustrated the upper panels of **Figure 8**. Moreover, the supplementary regularization constraints on the inversion coefficients shows that their sum must be equal to −1.

Acoustic radius inversions show a similar behaviour to mean density inversions, as the target functions are easily fitted by the kernels. They can thus be applied to a wide range of targets, but suffer from two main drawbacks. First, just as the mean density inversion, the SOLA method overestimates the precision of the inversion, meaning that the uncertainties derived from the propagation of the observational uncertainties cannot be trusted. Second, as a result of the behaviour of the target function, which results from the definition of the acoustic radius, the inversion is more sensitive to surface effects and thus difficult to apply to observed targets. This high sensitivity prohibits the use of acoustic radius inversions in practice and they have only been applied to the 16Cyg binary system in Buldgen et al. (2016a). While Buldgen et al. (2015b) concluded that the method was robust with respect to surface changes in the models and non-adiabatic effects in the oscillation computations, further investigations are required to determine in more details the robustness of these inversions using more sophisticated tests and comparisons.

5.3.3 Core Condition Indicators

Given the importance of constraining the core conditions of distant stars to determine reliable estimates of their ages, much effort has been devoted to define appropriate core condition indicators. Three of them were defined in recent years, with different observed targets in mind.

The first indicator was defined in Buldgen et al. (2015b) and based on the asymptotic expression of the small frequency separation. The idea was to determine the quantity

$$t = \int_0^R \frac{1}{r}\frac{dc}{dr}dr, \tag{35}$$

using the (c^2, ρ) structural pair. As mentioned above, the use of this structural pair has been shown to lead to higher amplitude of cross-term contributions. The target function for this indicator is defined by

$$\mathcal{T}_t = \frac{\frac{1}{r}\frac{dc}{dr}}{\int_0^R \frac{1}{r}\frac{dc}{dr}dr}. \tag{36}$$

Due to the difficulty of fitting the target function of this indicator, Buldgen et al. (2015b) opted for a modified version of the SOLA method, trying to fit the antiderivative of the target function rather than the target function itself. This leads to a slight modification of the SOLA cost function with the first term being written

$$\int_0^R \left[\int_0^r \mathcal{T}_t(x)dx - \int_0^r K_{\rm avg}(x)dx \right]^2 dr. \tag{37}$$

This approach has been shown by Reese et al. (2012) and Buldgen et al. (2015b) to show reasonably accurate results for both mean density and core condition indicator, at the expense of a lower stability since oscillatory behaviours are allowed around the target function of the inversion. Regarding the additional regularization term, the value of k for the sum of the inversion coefficients is shown to be 1.

An illustration of the target function of the t indicator is provided in the lower left panel of **Figure 8**. Buldgen et al. (2015b) concluded that this indicator would be mostly well-suited for young low mass stars, and published results only include tests on artificial data. It is worth noting that all indicators defined so far, namely $\bar{\rho}$, τ and t have their roots in the asymptotic relations of solar-like oscillations.

A second core condition indicator, denoted t_u, was derived in Buldgen et al. (2015a), to allow us to access to the core conditions of low-mass stars at later stages of core hydrogen burning. The definition of this new quantity is

$$t_u = \int_0^R f(r)\left(\frac{du}{dr}\right)^2 dr, \tag{38}$$

with $u = P/\rho$, the squared isothermal sound speed and $f(r)$ a weight function defined as

$$f(r) = r(r-R)\exp\left(-7\frac{r^2}{R}\right), \tag{39}$$

The target function for this indicator is defined as

$$\mathcal{T}_{t_u} = \frac{-2u}{t_u}\frac{d}{dr}\left(f(r)\frac{du}{dr}\right), \tag{40}$$

and the inversion is carried out using either the (u, Y) or the (u, Γ_1) structural pair. Tests on artificial data showed that both pairs led to a similar accuracy of the inversion. From a numerical point of view, the (u, Y) pair leads to a lower cross-term that is more easily damped, whereas using the (u, Γ_1) pair relies on the low amplitude of the relative differences in Γ_1 between the reference model and the target. An illustration of the target function of the t_u indicator is shown for 16CygA in the right panel of **Figure 9**. The value of k in **Eq. 28** is of 4 for t_u inversions.

The t_u inversion has been applied to a few targets in Buldgen et al. (2016a), Buldgen et al. (2016b), Buldgen et al. (2017a). In the case of 16Cyg, a recent re-study by Buldgen et al. (2022) concluded that the origin of the slight discrepancies were not due to mismatches of the internal structure. As shown in the left panel of **Figure 9** illustrating the results for 16CygB, a main drawback of the t_u inversion is its very high amplification of the observational errors, leading to a reduced significance of the inversion.

The last core condition indicator was defined in Buldgen et al. (2018) and is aimed at applications for stars with convective cores such as F-type solar-like oscillators. The idea is to carry out an inversion related to a proxy of the entropy of the stellar plasma, defined as $S_{5/3} = \frac{P}{\rho^{5/3}}$, which shows a plateau in convective regions. The height of this plateau will be sensitive to the size of the convective core. The definition of the indicator is

$$S_{\rm core} = \int_0^R \frac{g(r)}{S_{5/3}}dr, \tag{41}$$

with

$$\begin{aligned} g(r) = r\Bigg(&\alpha_1 \exp\left(-\alpha_2\left(\frac{r}{R}-\alpha_3\right)^2\right) \\ &+\alpha_4 \exp\left(-\alpha_5\left(\frac{r}{R}-\alpha_6\right)\right)\Bigg) \\ &\tanh\left(\alpha_7\left(1-\frac{r}{R}\right)^4\right), \end{aligned} \tag{42}$$

with $\alpha_1 = 16$, $\alpha_2 = 26$, $\alpha_3 = 0.06$, $\alpha_4 = \alpha_5 = 6.0$, $\alpha_6 = 0.07$, and $\alpha_7 = 50$. The parameter values might be varied depending on the observed star and as discussed in Buldgen et al. (2018). The intricate formulation of the weight is an attempt at extracting at best the information of the entropy plateau of the convective core, while keeping acceptable fits with a limited number of kernels of low degree modes. The target function of the inversion is defined in this case by

$$\mathcal{T}_{S_{\rm core}} = \frac{-g(r)}{S_{\rm core}S_{5/3}}. \tag{43}$$

The value of k in **Eq. 28** is −2/3. The inversion will be carried out using the ($S_{5/3}$, Γ_1) or ($S_{5/3}$, Y) structural pair.

An illustration of the target function for an F-type star model with a convective core is provided in the left panel of **Figure 10**, the extent of the core can be clearly seen from the plateau in the profile of $1/\tilde{S}_{5/3}$, with $\tilde{S}_{5/3} = \frac{GM^{1/3}}{R}S_{5/3}$. This inversion has been applied to artificial data in Buldgen et al. (2018), and to actual observed targets in Buldgen et al. (2017a), Salmon et al. (2021), and Buldgen et al. (2022), showing in some cases significant differences with respect to the reference models.

Detailed studies of F-type stars have not yet been undertaken and require more care as a result of the potential higher impact of surface effects. A generalization of the technique to the use of frequency separation ratios instead of individual frequencies could perhaps alleviate the issue.

5.3.4 Envelope Indicator

In addition to defining core conditions indicators, Buldgen et al. (2018) decided to attempt at providing constraints on the entropy plateau in the convective envelope of solar-like stars. This appproach was partly motivated by results in the solar case (Buldgen et al., 2017c), showing a significant variation of the height of the entropy plateau in the solar convective zone for models built with different opacity tables.

The indicator was defined as follows

$$S_{\rm env} = \int_0^R h(r)S_{5/3}dr. \tag{44}$$

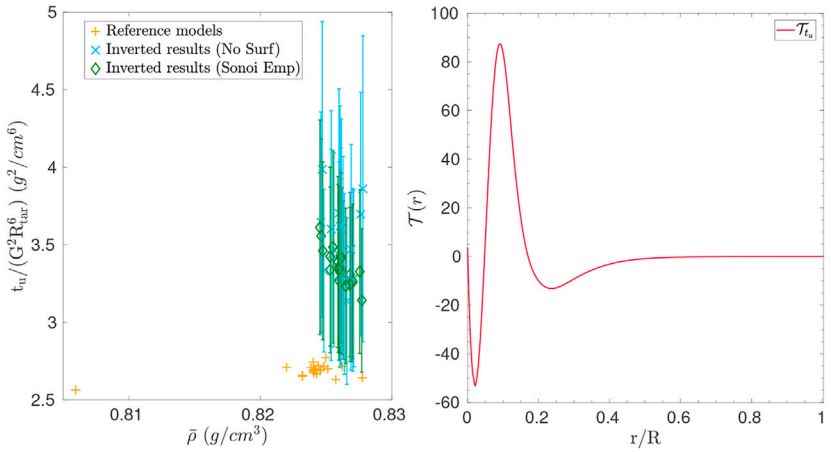

FIGURE 9 | *Left*: t_u inversion results as a function of mean density for 16CygA, using no surface correction (blue) and the Sonoi et al. (2015) correction (green), orange crosses showing the reference values (adapted from Buldgen et al. (2022)). *Right*: target function for the t_u indicator for a model of 16CygA.

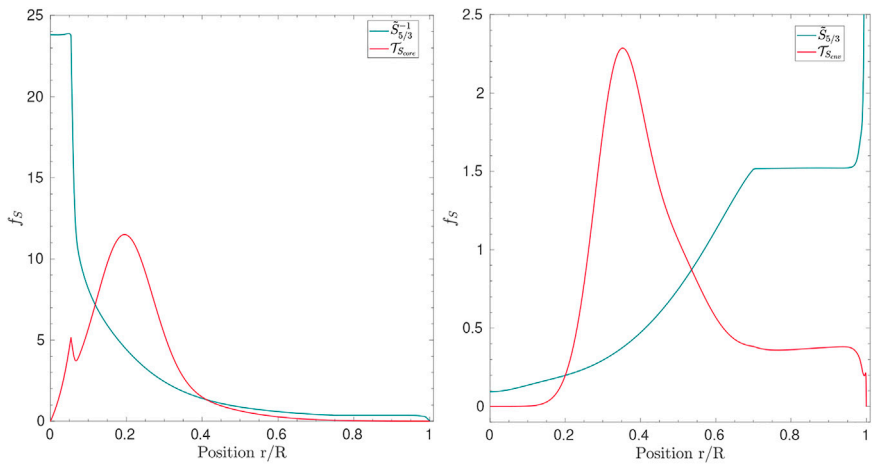

FIGURE 10 | *Left*: target function of the $S_{\rm core}$ indicator and normalized inverse profile of $S_{5/3}$ as a function of normalized radius for a 1.07$M_\odot$ harboring a convective core. *Right*: target function of the $S_{\rm env}$ indicator and normalized profile of $S_{5/3}$ as a function of normalized radius for a solar model [adapted from Buldgen et al. (2018)].

with the weight function $h(r)$ defined as

$$h(r) = \left[\alpha_1 \exp\left(-\alpha_2\left(\frac{r}{R}-\alpha_3\right)^2\right) + \alpha_4 \exp\left(-\alpha_5\left(\frac{r}{R}-\alpha_6\right)^2\right) + \frac{0.78}{1+\left(\exp\left(\left(\frac{R}{r}-\frac{1}{\alpha_7}\right)/\alpha_8\right)\right)}\right] \times r^{\alpha_9}\tanh\left(\alpha_{10}\left(1-\left(\frac{r}{R}\right)^4\right)\right), \tag{45}$$

with $\alpha_1 = 30$, $\alpha_2 = 120$, $\alpha_3 = 0.31$, $\alpha_4 = 7.3$, $\alpha_5 = 26$, $\alpha_6 = 0.33$, $\alpha_7 = 1.7$ $\alpha_8 = 1.2$, $\alpha_9 = 1.5$, and $\alpha_{10} = 50$. The target function of the inversion is given by

$$\mathcal{T}_{\rm env} = \frac{h(r)S_{5/3}}{S_{\rm env}}. \tag{46}$$

With these definitions, the value of k in the additional regularization term is given by 2/3. An illustration of the target function, as well as the normalized variable $\tilde{S}_{5/3} = \frac{GM^{1/3}}{R}S_{5/3}$ is provide in right panel of **Figure 10**.

While the number of parameters in the definition of the weight function is high, only the α_1, α_2 and α_3 values are modified in practice. They drive the peak in the target function that can be used to extract information in intermediate radiative regions or even regions close to the base of the convective envelope. It is however extremely difficult to extract information on the entropy plateau of the convective envelope for asteroseismic targets due to the absence of high and intermediate degree modes. Thus, the corrections derived by the $S_{\rm env}$ indicator will be linked to a

mixture of variations in the deep and intermediate radiative layers.

This indicator has been tested on artificial data, showing promising results, and more recently on 16Cyg, where it did not succeed in providing significant corrections to the models, but rather a confirmation of their quality. This indicator seems to be better suited for low mass stars, for which the convective envelope goes deeper and can be more easily probed with low degree modes using the variational expressions.

6 SURFACE INDEPENDENT NON-LINEAR INVERSIONS

As noted above, linear variational inversions show two main weaknesses. First, the simplified single step correction provided by linear methods may not be sufficient to actually reproduce the data. Iterative approaches (although used for solar models (Antia and Basu, 1994), but have yet to be successfully adapted and applied to asteroseismic data. The adaptation would be quite difficult, especially with the RLS method originally used that usually retains a strong linear trend due to the regularization term. In contrast, damping too much the regularization leads to non-physical oscillatory behaviour of the solution, which is also problematic. Switching from the RLS method to the SOLA method, as done for example in Buldgen et al. (2020) for the Sun, would require additional interpolations and the convergence of the technique would depend heavily on the behaviour of the averaging kernels as well as on the surface correction.

Indeed, the use of individual frequencies leads to a strong impact of surface effects on the inferred values, meaning that the inversion will be intrisically limited by the accuracy of the empirical surface corrections. Using relative differences in frequency separation ratios instead of individual frequencies may partially alleviate the issue, but it might lead to intrinsic non-linearity problems and frequency separation ratios might still be, in some cases, significantly affected by activity effects (Thomas et al., 2021). Another limitation of using frequency separation ratios is that the information of the stellar mean density is lost through the scaling of the ratios by the large frequency separation.

In this context, asteroseismic inversions would ideally need to be able to intrisically and reliably circumvent the surface effects of solar-like oscillations, within an efficient iterative scheme.

In the following Sections, we will present two approaches based on the phase relation of solar-like oscillations that fulfill those two requirements. Another advantage of these methods is that, as they solve the full fourth order system of oscillation equations, the issue of mode coupling arising in the case of mixed modes observed in subgiants and red giants will not affect the results, unlike the variational equations (Ong and Basu, 2020; Ong et al., 2021).

The approach chosen here is based on the fact that if ω is an eigenfrequency of the star, then it must satisfy a phase equation (Vorontsov, 1998; Roxburgh and Vorontsov, 2000) in which the internal structure can be described from inner phaseshifts and the outer layers from outer phaseshifts (see below). In such an approach, the fitting is carried out by reconnecting partial wave solutions in the inner and outer layers at a suitable point. The reconnexion point is chosen such that the oscillation will be almost vertical but still deep enough so that surface effects do not impact the inner solution.

This method allows us to efficiently separate the contribution of the outer layers without the need for additional empirical corrections. As the inner phase shift is independent of the surface layers and is the constraint used to represent the internal structure, the inversion of the inner layers is essentially independent of the surface effects.

The technique will be applied to HD177412A, the more massive component of the binary system HIP 93511, using the dataset derived by Appourchaux et al. (2015) from almost 2 years of continuous Kepler observations.

6.1 Non-Linear Inversion Using Inner Phaseshifts

The inversion technique presented in this Section subtracts the effect of the surface layers and seeks to infer the structure of the inner layers. More specifically, we use as fitting condition that the inner phase shifts of the solution of the oscillation equations of a model, using the observed frequencies, should collapse to a function only of frequency in the outer layers of a star (Vorontsov, 1998; Vorontsov, 2001; Roxburgh I. and Vorontsov S., 2003; Roxburgh, 2015). In other words, we use the fact that the contribution of the outer layers is a function only of frequency (although unknown) for low degree modes. Other surface layer independent fitting procedures could equally be used, e.g., matching the ratio of small to large separations of the model and observations, or matching phase differences (Roxburgh and Vorontsov, 2013; Roxburgh, 2015).

The inner phase shift $\delta_{n,\ell}(\nu)$ is the departure of the solution of the oscillation equations from a harmonic function and is defined by

$$\frac{\omega\psi}{d\psi/dt} = \tan\left(\omega\tau - \ell\pi/2 + \delta\right), \quad \text{where} \quad \psi(t) = \frac{rP'}{(\rho c)^{1/2}}, \quad \omega = 2\pi\nu, \quad (47)$$

calculated at some fractional radius x_f in the outer layers, where $\tau = \int_0^r dr/c$ is the acoustic radius at the radial position r, c the local sound speed and P' the Eulerian pressure perturbation.

This provides a fitting criterion for the inversion of the form

$$\alpha_{n,\ell} \equiv \pi\frac{\nu_{n,\ell}}{\Delta_0} + \delta_{n,\ell} - \pi\left(n + \ell/2\right) = \alpha_0(\nu), \quad (48)$$

where Δ_0 is an estimate of the large frequency separation and $\alpha_0(\nu)$ is an unknown function only of frequency and not of ℓ, depicting the contribution of the surface layers to the eigenfrequency. The outer phase shift, α_0, is a parametrised function of ν, (here we used a sum of N_α Chebyshev polynomials) and the associated coefficients are determined by a best fit to $\alpha_{n\ell}$. The fitting condition is then

$$\chi^2_{df} = \frac{1}{N_\nu - N_\alpha}\sum\left(\frac{\alpha_{n,\ell} - \alpha_0}{\epsilon_{n,\ell}}\right)^2, \quad (49)$$

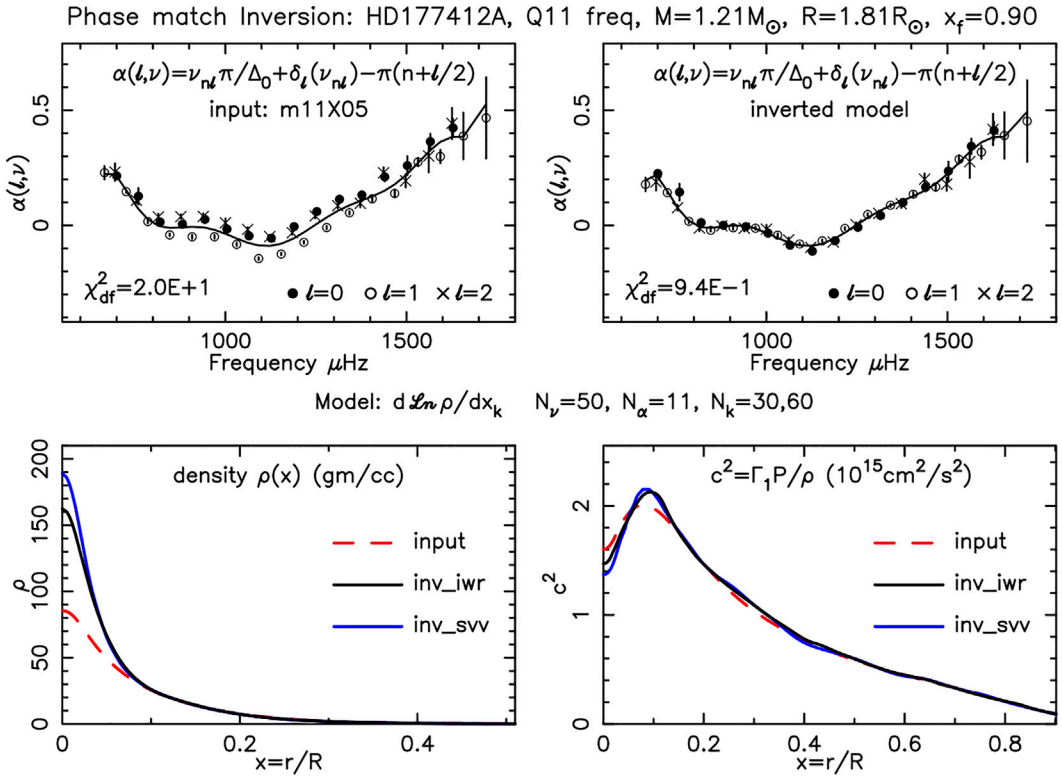

FIGURE 11 | *Upper panels*: Agreement in outer phase shift for the input "LM" model (left) and the inverted model (right). *Lower panels*: Density (left) and squared adiabatic sound speed profiles (right) for inversion result (black) and input model (red) for the so-called "LM" model.

where $\epsilon_{n,\ell}$ is the error in the inner phase shift, $\delta_{n,\ell}$, obtained by propagating the error in the frequencies ($\sigma_{n,\ell}$) through the calculation of the inner phaseshift. N_α is the number of coefficients in the polynomial representation of the outer phase shift α_0. It is worth noting that the value of Δ_0 or the effects of a misidentification of radial order values for the modes has no impact on the method, as they are absorbed in the value of α_0.

6.1.1 Inversion Procedure

The acoustic structure of a model is determined by the profiles of the local density $\rho(r)$, the local pressure $P(r)$ and the first adiabatic exponent $\Gamma_1(r)$. The density profile provides the mass distribution and the pressure follows from hydrostatic support and a pressure surface value, denoted here P_s. The first adiabatic exponent can be taken either from an initial trial model or as given a fixed value of 5/3 since the departure from 5/3 remains very small in the stellar interior (except in massive stars). Errors in the value of the surface pressure are unimportant as they have only a very small effect on the interior solution obtained with the inversion.

The model can be parametrised in many ways. For example one can use the value of the stellar mass and radius, and the local density $\rho(r)$ on a radial mesh or, as we used here, with the values of $d\log\ \rho/dr$ at a set of radial mesh points together with some interpolation and integration algorithm to reconstruct the structure.

The starting point of the inversion is some initial trial (input) model. It can be in principle a very simplified depiction of the structure such as a polytrope, but will be in practice some stellar model calculated with some stellar evolution code. The parameters used in the representation of the model through its inner and outer phaseshifts are iteratively modified to reduce the value of χ^2_{df}, stopping when it reaches 1.0, meaning that the internal structure as seen by the data is correctly reproduced with the parametric profile.

Figure 11 shows the results starting with an input model of HD177412A computed with the Liège evolution code (Scuflaire et al., 2008), denoted here "LM" model. This model has a mass, M, of $1.3M_\odot$, a radius, R, of $1.68R_\odot$ and a central hydrogen abundance, X_c of 0.09. Its initial chemical composition is X_0 = 0.7, Z_0 = 0.02. This model was scaled to $M = 1.25M_\odot$, $R = 1.81R_\odot$, which are the values determined from the seismic scaling relations (Brown et al., 1991; Kjeldsen and Bedding, 1995) and the observed values of $\nu_{\max}$ and Δ. It should be noted that the initial model exhibited a convective core and that the inversion has kept it in the final solution.

Figure 12 shows an inversion starting with an input STAROX model (Roxburgh, 2008) denoted here "IR" with a mass of $1.1M_\odot$, a radius of $1.22R_\odot$, a central hydrogen abundance of 0.05 and an initial chemical composition of X_0 = 0.7, Z_0 = 0.02. This model was also rescaled to the mass and radius values provided by the seismic scaling relations, namely $M = 1.25M_\odot$, $R = 1.81R_\odot$.

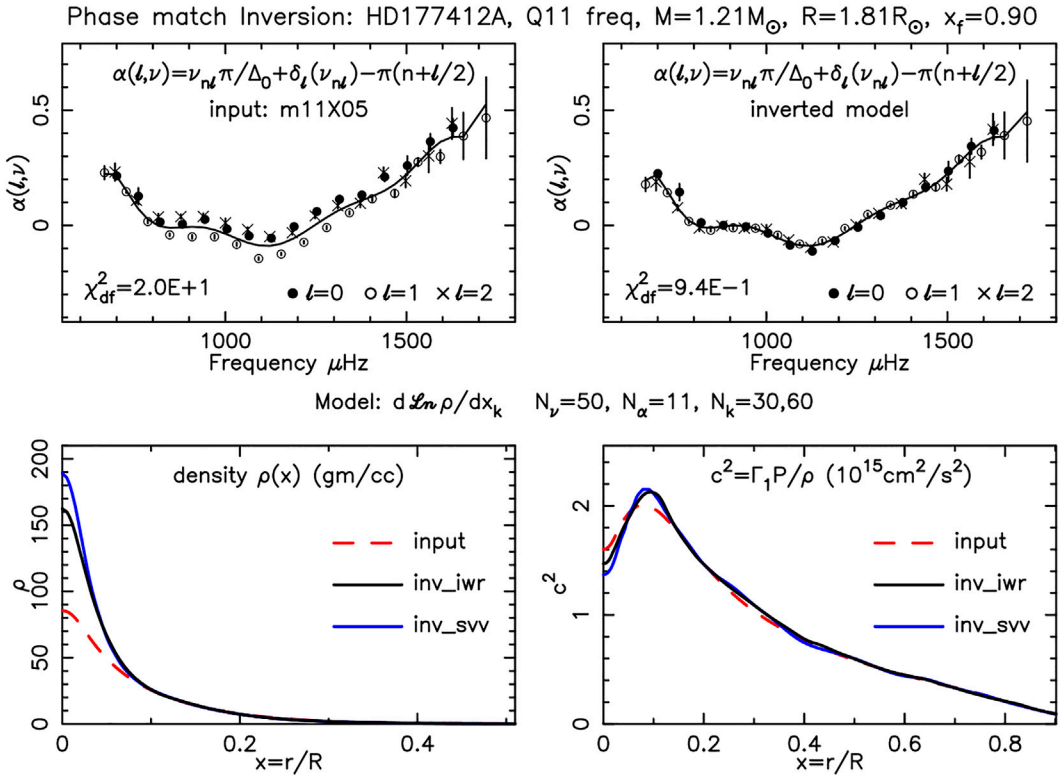

FIGURE 12 | Inversion result (black) and input model (red) for the so-called "IR" model. The profiles resulting from the iterative regularization inversion of **Section 6.2** are shown in blue for comparison.

The models were represented by N_k values of $d\log\ \rho/dr$ on a discrete mesh, and inversions undertaken with different values of N_k between 10 and 180. A downhill simplex method (Nelder and Mead, 1965) was used to search for a minimum in χ^2. The minimisation was made using the downhill simplex method with the adjustable parameters being the density derivatives on the model mesh (but any other model parameters would be suitable). The model was constructed from these model parameters - and the inner phase shift calculated for the model using the observed frequencies as in **Eq. 46** and chi2 as in **Eq. 48**. Various values of the reconnexion point x_f and different Γ_1 profiles (constant or that of the input model) were tested to see the impact on the results.

The results of the inversion using the iterative regularization procedure of **Section 6.2** are also presented in **Figure 12**. In this case, the radius of the model was further adjusted to $1.742R_\odot$ to improve the fit. The solution of both the method illustrated here and that of **Section 6.2** are very similar, if starting from the same input model. However they differ widely from the results using the "LM" model instead of the "IR" one, as the presence of the convective core is not confirmed in the latter case.

6.1.2 Results

As is clear from the figures, different types of inverted models were obtained when starting from different initial conditions: the solution is thus not unique and it appears that some feature of the initial model remain after the inversion. This indicates a degree of degeneracy in the solutions. We can separate two families of solutions:

1. Using the "LM" model as input, the solution of the inversion shows clear signatures of a convective core. However, as shown in **Figure 11** it was already present in the initial model.
2. Using the "IR" model as input, the solution has no convective core but a steep hump in the sound speed typical of the end of main sequence evolution of lower mass stars. Again, this feature was already present in the reference model and the inversion has just enhanced it.

We conclude that seismic inversion alone is unable to distinguish between the solution with or without a convective core. More precise data and higher frequency modes could help lift this degeneracy and distinguish between the two families of solutions. This requires a detailed study of the dependence of the inner phase shifts on the precision of both the model and of the frequencies, and possibly estimates of the limits on the luminosity of the inverted model compared with the observed value.

6.2 Iterative Regularization

The basic approach to make asteroseismic inversions insensitive to the structure of the outermost stellar layers and physics of the oscillations in these layers is here the same as in the previous

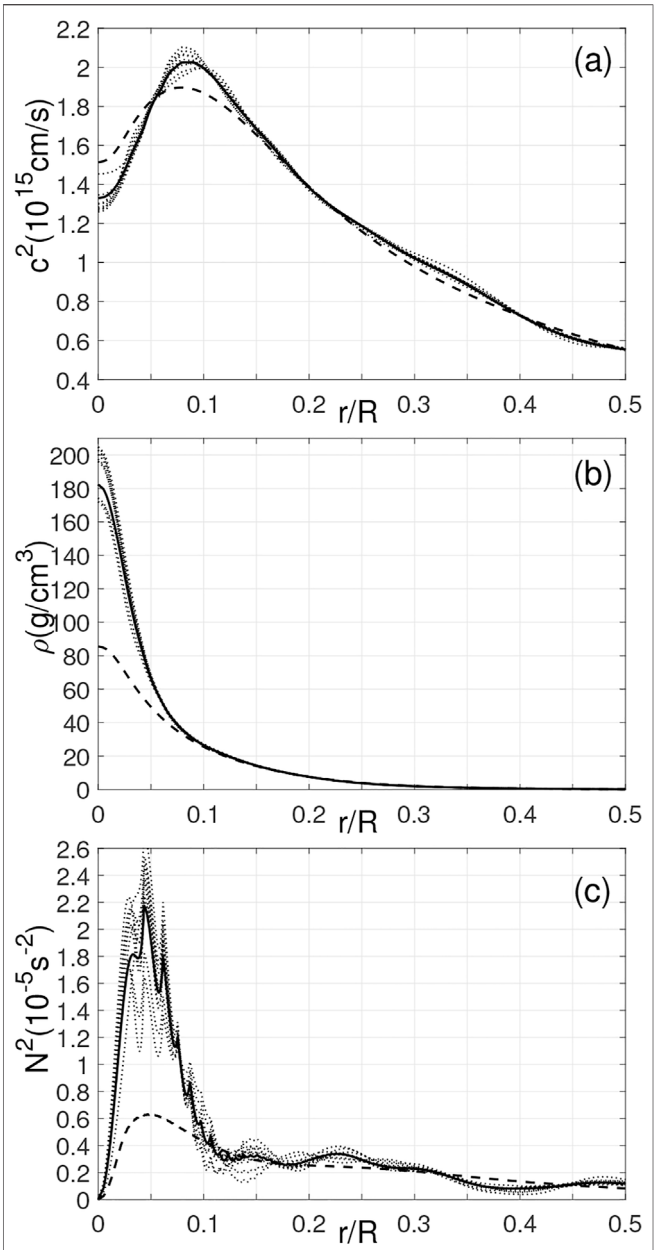

FIGURE 13 | Result of structural inversion for HD177412A: the sound speed **(A)**, density **(B)** and buoyancy frequency **(C)**. Dashed lines show a (re-scaled) model taken as an initial guess; solid lines display the inverted result. Dotted lines are the results obtained when the measured frequencies were added with Gaussian noise, of variance corresponding to the reported uncertainties, in 10 realizations, to address the sensitivity of the inversion to random errors in the input data. The nearly-optimal mean density of the model is 0.293 g/cm^3. The c^2-scale corresponds to a model of the original $M = 1.1M_\odot$ mass but a bigger $R = 1.74R_\odot$ radius.

section. Due to the low values of the sound speed in the subsurface layers, the radial wavenumber of low-degree p-modes is much larger than the horizontal wavenumber. Therefore the radial eigenfunctions are expected to depend on the oscillation frequency ω only, but not on the degree ℓ.

The major difference is in the regularization technique of the inversion. Here, we use a nested iterative algorithm: inner and outer iterations. Inner iterations are performed with a limited number of linearized descents using conjugate gradients; the number of inner iterations plays the role of regularization parameter. The seismic model is taken as a new initial guess, and the optimization process is repeated in the outer iterations. In stellar seismology, the algorithm was tested on artificial data in Roxburgh and Vorontsov (2002), Roxburgh I and Vorontsov S (2003). It was applied to the inversion of observational frequencies of HD177412A (Appourchaux et al., 2015), with the results being described later in this section.

The practical implementation of the technique derives largely from the helioseismic structural inversions of Vorontsov (2001, 2002); Vorontsov et al. (2013). The hydrostatic model is described by cubic B-splines for $m(r)/r^3$ with knots distributed uniformly in r^2, allowing a piecewise-analytic representation of the pressure, density and density-gradient profiles. The number of splines is chosen high enough to reproduce adequately regions of rapid spatial variation (e.g., the base of the convective envelope). In stellar inversions, the radial profile of the adiabatic exponent $\Gamma_1(r)$ is taken from the initial model and remains unchanged.

The seismic model is truncated at some level $r = r_b$ below the photosphere, where wave propagation is close to that of a pure sound wave, but not too deep for waves to remain nearly vertical ($r_b = 0.99R$ in the inversion described below). For each mode in the data set, of frequency $\boldsymbol{\omega}$ and degree $\boldsymbol{\ell}$, we solve the fourth-order system of the adiabatic oscillation equations by a shooting technique in the interval $0 \le r \le r_b$. From the two solutions regular at the center, we form the linear combination statisfying the Laplace equation for gravity perturbations in the envelope. At the truncation boundary $r = r_b$, we match this numerical solution with the wave function ψ_p proportional to the Eulerian pressure perturbation (see Vorontsov et al. (2013)), and measure the "phase propagation time" $T_{\ell n}$ defined as

$$\omega T_{\ell n} = \pi\left(n - n_{\rm int} + \frac{1}{2}\right) + \arctan\left.\frac{d\psi_p/d\tau}{\omega\psi_p}\right|_{r=r_b}, \qquad (50)$$

with n the mode radial order, $n_{\rm int}$ the number of nodes in the Eulerian pressure perturbation below the truncation boundary, and τ the acoustic depth. $T_{\ell n}$ can be interpreted as the wave propagation time between $r = r_b$ and the upper turning point. When the model fits the observational frequencies, the $T_{\ell n}$-values of all the observed modes fit an approximation

$$T_{\ell n} = T_1(\omega), \qquad (51)$$

where $T_1(\omega)$ is a slowly-varying function of frequency. We approximate this function by a polynomial. The degree of the polynomial shall be significantly smaller than the number of modes in the observational data set, but high enough to absorb variations coming from e.g., HeII ionization (which enter $T_1(\omega)$ if this region is not well described by the model). In the results presented below, the polynomial degree is 10.

The mismatch between the model and the data is measured by the merit function M defined as

$$M^2 = \frac{1}{N}\sum_{\ell,n}\left[\frac{T_{\ell n} - T_1(\omega)}{\delta T_{\ell n}}\right]^2, \quad (52)$$

where N is number of modes in the data set, and uncertainties $\delta T_{\ell n}$ are calculated from the uncertainties of the frequencies. Values of M close to 1.0 or below indicate that the model fits the oscillation frequencies adequately.

The relations between small variations of the model parameters and variations of the phase of the wave function ψ_p at the truncation boundary (the last term in **Eq. (49)**), needed for the linearized descents, as well as the relation between this phase variation and variation of frequency, needed for calculating $\delta T_{\ell n}$, stem from the linear perturbation analysis of Vorontsov et al. (2013), Appendix A.

A set of "elementary" model variations is then defined as partial sums of the B-splines describing $m(r)/r^3$ starting from the stellar center (i.e., each elementary variation is defined as a truncated representation of the equilibrium model). They are then normalized such as to ensure nearly equal relative variations of equilibrium density. We thus arrive to an algebraic system

$$A\mathbf{x} = \mathbf{f}_\delta, \quad (53)$$

where the components of the $\mathbf{x}$ vector are the amplitudes of elementary variations, and the mismatch between $T_{\ell n}$ and $T_1(\omega)$ defines the components of $\boldsymbol{f_\delta}$. The equations are then normalized to bring random errors in the right-hand side to unit variance.

The amplitudes of elementary variations are controlled by a set of orthogonal polynomials of a discrete (integer) variable (index i of x_i). A choice of the polynomial set is known to be governed by a choice of the weight function in their orthogonality relation. This function is specified by the Euclidean norms of corresponding columns of matrix A (Strakhov and Vorontsov, 2001). This particular choice of the weight function, which defines the polynomials, ensures that the response of the components of $\mathbf{x}$ to random frequency errors is nearly uniform, at least in the first gradient descents. The upper degree of the polynomial set has to be high enough to allow proper resolution of the inversion (set at 35 in the results below; the exact choice is not important as regularization is performed by limiting the number of iterative descents, not by constraining the functional space of allowed solutions). To ensure better stability of the inversion in the outer layers, the polynomials were additionally apodized with a cosine bell function in the interval between $r = 0.7R$ and $r = 0.9R$ and set to zero above.

An important ingredient of the seismic inversion when the stellar mass M and radius R are not well known is the degeneracy of the oscillation frequencies with respect to an homology rescaling. When represented in dimensionless variables, one particular seismic model describes a two-parametric family of physical models, where the density profile $\rho(r)$ scales as M/R^3, the squared sound speed $c^2(r)$ scales as M/R, the squared buoyancy frequency N^2 and squared oscillation frequencies ω^2 both scale as M/R^3. Thus an initial proxy model represented in dimensionless variables will describe a two-parametric family of physical models which differ in M and R. We bring the measured frequencies to their dimensionless values without imposing the stellar mass and radius: instead, we adjust M/R^3 in this scaling such as to achieve the best performance of the inversion (the best likelihood of the result after convergence). In this way, the inversion provides a best-fit value for M/R^3. The inverted dimentionless model now describes a one-parametric family of physical models, all of which satisfy the input data. Each model in this family can be rescaled to different values of M and R, keeping M/R^3 unchanged. In this re-scaling, which does not change the oscillation frequencies, $\rho(r)$ and $N^2(r)$ remain unchanged, but $c^2(r)$ re-scales in proportion to $M^{2/3}$.

The results obtained with the observational p-mode frequencies of HD177412A and an evolved model of $1.1M_\odot$ star with a central hydrogen abundance of $X_c = 0.05$ (model "IR" of the previous section) taken as an initial guess are shown in **Figure 13**. Descents to an adequate value of the merit function (below 1.0) were performed in 7 inner and 15 outer iterations. The steep decrease in the sound-speed towards the center (panel a of **Figure 13**), together with big density contrast (panel b of **Figure 13**) indicate that the star is at a very late stage of the main-sequence evolution. The resulting steep gradient in the molecular weight is responsible for the sharp variation of the buoyancy frequency (panel c of **Figure 13**). We note that the prominent wiggles in the N^2-curves below $0.1R$ are due to model discretisation (the cubic spline for $m(r)/r^3$ is continuous together with two derivatives, but provides $N^2(r)$ with discontinuities in its gradient).

We do not see any signature of a convective core in the results of this inversion. Comparing with results reported in the previous section, we have to admit that with the amount and quality of frequency measurements available for HD177412A, the seismic inversion alone cannot answer the question of whether or not the star has a convective core. Additional non-seismic constraints have to be invoked to address this question.

7 CONCLUSION

This paper is an attempt at providing a brief review of the available inversion techniques for determining the structure of solar-like oscillators. In general, seismic inversions can also involve the determination of the internal structure of a star from evolutionary computations or static computations, which we briefly discussed in **Section 3**. Most inversions wrongly refer today to the specific class of the linear methods based on the variational integral relations between frequency perturbations and structural corrections. These techniques have originated in helioseismology and are now being applied to the high-quality datasets provided by space-based photometry missions.

These methods still allow us to provide interesting estimates of the corrections to be applied to the internal structure of a given target, but intrinsic limitations such as the linearity of the integral relations and the treatment of surface effects remain major weaknesses of these techniques. In practice, while the era of space-based photometry missions has provided high quality data, it is still far from being enough to enable a full scan of the internal structure of a distant star using, for example, the SOLA method described in **Section 5**. As discussed in this section, the versatility

in the definition of the target function of the SOLA method allows us to compromise between determining global or local estimates of corrections, with global estimates being sometimes more easy to derive from a limited dataset. Another good example of this versatility being shown in Pijpers et al. (2021). Such approaches have been applied with success to the best *Kepler* targets and will remain applicable to both TESS and PLATO data in the future, especially to very precisely estimate the mean density of observed targets from a limited oscillation spectrum. Inversions of indicators as well as localized inversions would remain only applicable for the best targets with very rich oscillation spectra.

Further improvements of the linear methods include the development and application of inversions based on relative frequency separation ratios. Indeed, Deheuvels et al. (2016) and Farnir et al. (2019) have shown that they could be used to constrain the extent of convective cores from solar-like oscillations and such inversions would likely alleviate the issue of the surface-effect dependency.

In addition to discussing linear variational inversion techniques, we also presented surface independent non-linear inversions based on the phase shifts of solar-like oscillations. Such methods have proven to be very efficient at determining the internal structure of solar-like oscillators for both artificial and real *Kepler* datasets while suppressing efficiently the contribution of surface regions.

In practice however, our results confirm that non-seismic data can play a key role in discriminating between various families of inverted models. In this context, GAIA data will certainly be helpful in determining precise luminosity values, provided that accurate spectroscopic parameters are available. Interferometric radii determinations, when available, may also prove extremely helpful in this respect. It is indeed no surprise that the results presented here are for bright components of binary system, which are known to be prime testbeds of the theory of stellar structure and evolution.

An important point to note is that most of the inversions so far have been performed for main-sequence solar-like oscillators exhibiting only pure pressure modes (with the exception of Kosovichev and Kitiashvili (2020) and Bellinger et al. (2021)). The wealth of seismic information contained in mixed oscillation modes thus still remains to be fully exploited. In this aspect, the non-linear inversions presented in **Section 6** are a promising avenue to take directly into account the intrinsic non-linearity of the mixed modes and to provide constraints on the internal stratification of subgiant and red-giant stars. Initial applications of phase matching for mixed modes can be found in Roxburgh (2015) for artificial data and a detailed characterization using evolutionary models of the stratification of a subgiant can be found in Noll et al. (2021), studying its consequence for core overshooting in the main sequence. These works provide benchmark approaches to further constrain the internal structure of evolved stars, for which insights on the core stratification will play a key role in improving our understanding of the missing efficient angular momentum transport at play in these stages.

AUTHOR CONTRIBUTIONS

GB, JB, and DR provided the data for **Sections 2**, **3**, **4** and **5**. IR and SV provided the data for **Section 6**. All authors read the manuscript and contributed to the discussion.

FUNDING

GB and JB acknowledge fundings from the SNF AMBIZIONE grant No 185805 (Seismic inversions and modelling of transport processes in stars).

REFERENCES

Aguirre Børsen-Koch, V., Rørsted, J. L., Justesen, A. B., Stokholm, A., Verma, K., Winther, M. L., et al. (2022). The BAyesian STellar Algorithm (BASTA): a Fitting Tool for Stellar Studies, Asteroseismology, Exoplanets, and Galactic Archaeology. *Mon. Notices R. Astronomical Soc.* 509, 4344–4364. doi:10.1093/mnras/stab2911

Antia, H. M., and Basu, S. (1994). Nonasymptotic Helioseismic Inversion for Solar Structure. *Astronomy Astrophysics Suppl. Ser.* 107, 421–444.

Appourchaux, T., Antia, H. M., Ball, W., Creevey, O., Lebreton, Y., Verma, K., et al. (2015). A Seismic and Gravitationally Bound Double Star Observed by Kepler. Implication for the Presence of a Convective Core. *Astronomy Astrophysics* 582, A25. doi:10.1051/0004-6361/201526610

Backus, G., and Gilbert, F. (1970). Uniqueness in the Inversion of Inaccurate Gross Earth Data. *Phil. Trans. R. Soc. Lond. A* 266, 123–192. doi:10.1098/rsta.1970.0005

Baglin, A., Auvergne, M., Barge, P., Deleuil, M., and Michel, E.CoRoT Exoplanet Science Team (2009). CoRoT: Description of the Mission and Early Results. *Transiting Planets, Proc. Int. Astronomical Union, IAU Symposium* 253, 71–81. eds. F. Pont, D. Sasselov, and M. J. Holman. doi:10.1017/S1743921308026252

Ball, W. H., Beeck, B., Cameron, R. H., and Gizon, L. (2016). MESA Meets MURaM. Surface Effects in Main-Sequence Solar-like Oscillators Computed Using Three-Dimensional Radiation Hydrodynamics Simulations. *Astronomy Astrophysics* 592, A159. doi:10.1051/0004-6361/201628300

Ball, W. H., and Gizon, L. (2014). A New Correction of Stellar Oscillation Frequencies for Near-Surface Effects. *Astronomy Astrophysics* 568, A123. doi:10.1051/0004-6361/201424325

Basu, S., and Christensen-Dalsgaard, J. (1997). Equation of State and Helioseismic Inversions. *Astronomy Astrophysics* 322, L5–L8.

Basu, S., Christensen-Dalsgaard, J., and Thompson, M. J. (2002). "SOLA Inversions for the Core Structure of Solar-type Stars," in *Stellar Structure and Habitable Planet Finding*. Editors B. Battrick, F. Favata, I. W. Roxburgh, and D. Galadi (Córdoba, Spain: ESA Special Publication), 485, 249–252.

Basu, S., and Thompson, M. J. (1996). On Constructing Seismic Models of the Sun. *Astronomy Astrophysics* 305, 631.

Bazot, M., Benomar, O., Christensen-Dalsgaard, J., Gizon, L., Hanasoge, S., Nielsen, M., et al. (2019). Latitudinal Differential Rotation in the Solar Analogues 16 Cygni A and B. *Astronomy Astrophysics* 623, A125. doi:10.1051/0004-6361/201834594

Bazot, M., Christensen-Dalsgaard, J., Gizon, L., and Benomar, O. (2016). On the Uncertain Nature of the Core of α Cen A. *Mon. Not. R. Astron. Soc.* 460, 1254–1269. doi:10.1093/mnras/stw921

Bazot, M. (2020). Uncertainties and Biases in Modelling 16 Cygni A and B. *Astronomy Astrophysics* 635, A26. doi:10.1051/0004-6361/201935565

Bedding, T. R., Kjeldsen, H., Butler, R. P., McCarthy, C., Marcy, G. W., O'Toole, S. J., et al. (2004). Oscillation Frequencies and Mode Lifetimes in α Centauri A. *Astrophysical J.* 614, 380–385. doi:10.1086/423484

Bellinger, E. P., Angelou, G. C., Hekker, S., Basu, S., Ball, W. H., and Guggenberger, E. (2016). Fundamental Parameters of Main-Sequence Stars in an Instant with Machine Learning. *Astrophysical J.* 830, 31. doi:10.3847/0004-637X/830/1/31

Bellinger, E. P., Basu, S., Hekker, S., and Ball, W. H. (2017). Model-independent Measurement of Internal Stellar Structure in 16 Cygni A and B. *Astrophysical J.* 851, 80. doi:10.3847/1538-4357/aa9848

Bellinger, E. P., Basu, S., Hekker, S., Chrisensen-Dalsgaard, J., and Ball, W. H. (2021). Asteroseismic Inference of Central Structure in a Subgiant Star. *APJ* 915 (2), 100. arXiv e-prints, arXiv:2105.04564. doi:10.3847/1538-4357/ac0051

Bellinger, E. P., Basu, S., Hekker, S., and Christensen-Dalsgaard, J. (2019). Testing Stellar Evolution with Asteroseismic Inversions of a Main-Sequence Star Harboring a Small Convective Core. *Astrophysical J.* 885, 143. doi:10.3847/1538-4357/ab4a0d

Benomar, O., Bazot, M., Nielsen, M. B., Gizon, L., Sekii, T., Takata, M., et al. (2018). Asteroseismic Detection of Latitudinal Differential Rotation in 13 Sun-like Stars. *Science* 361, 1231–1234. doi:10.1126/science.aao6571

Benomar, O., Takata, M., Shibahashi, H., Ceillier, T., and García, R. A. (2015). Nearly Uniform Internal Rotation of Solar-like Main-Sequence Stars Revealed by Space-Based Asteroseismology and Spectroscopic Measurements. *Mon. Not. R. Astron. Soc.* 452, 2654–2674. doi:10.1093/mnras/stv1493

Bétrisey, J., and Buldgen, G. (2022). *Probing Stellar Cores from Inversions of Frequency Separation Ratios*. Paris: Astronomy and Astrophysics. *arXiv e-prints* , arXiv:2205.09625.

Bétrisey, J., Pezzotti, C., Buldgen, G., Khan, S., Eggenberger, P., Salmon, S. J. A. J., et al. (2022). Kepler-93: A Testbed for Detailed Seismic Modelling and Orbital Evolution of Super-earths Around Solar-like Stars. *Astronomy Astrophysics* 659, A56. doi:10.1051/0004-6361/202141083

Borucki, W. J., Koch, D., Basri, G., Batalha, N., Brown, T., Caldwell, D., et al. (2010). Kepler Planet-Detection Mission: Introduction and First Results. *Science* 327, 977–980. doi:10.1126/science.1185402

Bouchy, F., and Carrier, F. (2001). P-mode observations on α Cen A. *Astronomy Astrophysics* 374, L5–L8. doi:10.1051/0004-6361:20010792

Brown, T. M., Gilliland, R. L., Noyes, R. W., and Ramsey, L. W. (1991). Detection of Possible P-Mode Oscillations on Procyon. *Astrophysical J.* 368, 599. doi:10.1086/169725

Buldgen, G., Eggenberger, P., Baturin, V. A., Corbard, T., Christensen-Dalsgaard, J., Salmon, S. J. A. J., et al. (2020). Seismic Solar Models from Ledoux Discriminant Inversions. *Astronomy Astrophysics* 642, A36. doi:10.1051/0004-6361/202037980

Buldgen, G., Farnir, M., Eggenberger, P., Bétrisey, J., Pezzotti, C., Pinçon, C., et al. (2022). *Thorough Characterisation of the 16 Cygni System. II. Seismic Inversions of the Internal Structure. aap* 661, A143. *arXiv e-prints* , arXiv:2202.10081. doi:10.1051/0004-6361/202142001

Buldgen, G., Farnir, M., Pezzotti, C., Eggenberger, P., Salmon, S. J. A. J., Montalban, J., et al. (2019a). Revisiting Kepler-444. I. Seismic Modeling and Inversions of Stellar Structure. *Astronomy Astrophysics* 630, A126. doi:10.1051/0004-6361/201936126

Buldgen, G., Reese, D., and Dupret, M.-A. (2017a). Asteroseismic Inversions in the Kepler Era: Application to the Kepler Legacy Sample. *EPJ Web Conf.* 160, 03005. doi:10.1051/epjconf/201716003005

Buldgen, G., Reese, D. R., and Dupret, M. A. (2017b). Analysis of the Linear Approximation of Seismic Inversions for Various Structural Pairs. *Astronomy Astrophysics* 598, A21. doi:10.1051/0004-6361/201629485

Buldgen, G., Reese, D. R., and Dupret, M. A. (2018). Constraining Convective Regions with Asteroseismic Linear Structural Inversions. *Astronomy Astrophysics* 609, A95. doi:10.1051/0004-6361/201730693

Buldgen, G., Reese, D. R., and Dupret, M. A. (2016a). Constraints on the Structure of 16 Cygni A and 16 Cygni B Using Inversion Techniques. *Astronomy Astrophysics* 585, A109. doi:10.1051/0004-6361/201527032

Buldgen, G., Reese, D. R., Dupret, M. A., and Samadi, R. (2015b). Stellar Acoustic Radii, Mean Densities, and Ages from Seismic Inversion Techniques. *Astronomy Astrophysics* 574, A42. doi:10.1051/0004-6361/201424613

Buldgen, G., Reese, D. R., and Dupret, M. A. (2015a). Using Seismic Inversions to Obtain an Indicator of Internal Mixing Processes in Main-Sequence Solar-like Stars. *Astronomy Astrophysics* 583, A62. doi:10.1051/0004-6361/201526390

Buldgen, G., Rendle, B., Sonoi, T., Davies, G. R., Miglio, A., Salmon, S. J. A. J., et al. (2019b). Mean Density Inversions for Red Giants and Red Clump Stars. *Mon. Notices R. Astronomical Soc.* 482, 2305–2319. doi:10.1093/mnras/sty2346

Buldgen, G., Salmon, S. J. A. J., Noels, A., Scuflaire, R., Reese, D. R., Dupret, M.-A., et al. (2017c). Seismic Inversion of the Solar Entropy. A Case for Improving the Standard Solar Model. *Astronomy Astrophysics* 607, A58. doi:10.1051/0004-6361/201731354

Buldgen, G., Salmon, S. J. A. J., Reese, D. R., and Dupret, M. A. (2016b). In-depth Study of 16CygB Using Inversion Techniques. *Astronomy Astrophysics* 596, A73. doi:10.1051/0004-6361/201628773

Chandrasekhar, S. (1964). A General Variational Principle Governing the Radial and the Non-radial Oscillations of Gaseous Masses. *Astrophysical J.* 139, 664. doi:10.1086/147792

Chandrasekhar, S., and Lebovitz, N. R. (1964). Non-Radial Oscillations of Gaseous Masses. *Astrophysical J.* 140, 1517. doi:10.1086/14805610.1086/148056

Chaplin, W. J., and Miglio, A. (2013). Asteroseismology of Solar-type and Red-Giant Stars. *Annu. Rev. Astron. Astrophys.* 51, 353–392. doi:10.1146/annurev-astro-082812-140938

Charpinet, S., Brassard, P., Giammichele, N., and Fontaine, G. (2019). Improved Seismic Model of the Pulsating DB White Dwarf KIC 08626021 Corrected from the Effects of Neutrino Cooling. *Astronomy Astrophysics* 628, L2. doi:10.1051/0004-6361/201935823

Charpinet, S., Van Grootel, V., Reese, D., Fontaine, G., Green, E. M., Brassard, P., et al. (2008). Testing the Forward Modeling Approach in Asteroseismology. II. Structure and Internal Dynamics of the Hot B Subdwarf Component in the Close Eclipsing Binary System PG 1336-018. *Astronomy Astrophysics* 489, 377–394. doi:10.1051/0004-6361:200809907

Christensen-Dalsgaard, J., and Houdek, G. (2010). Prospects for Asteroseismology. *Astrophys. Space Sci.* 328, 51–66. doi:10.1007/s10509-009-0227-z

Christensen-Dalsgaard, J., Schou, J., and Thompson, M. J. (1990). A Comparison of Methods for Inverting Helioseismic Data. *Mon. Notices R. Astronomical Soc.* 242, 353–369. doi:10.1093/mnras/242.3.353

Christensen-Dalsgaard, J., and Thompson, M. J. (1997). On Solar P-Mode Frequency Shifts Caused by Near-Surface Model Changes. *Mon. Notices R. Astronomical Soc.* 284, 527–540. doi:10.1093/mnras/284.3.527

Clement, M. J. (1964). A General Variational Principle Governing the Oscillations of a Rotating Gaseous Mass. *Astrophysical J.* 140, 1045. doi:10.1086/148004

Deal, M., Richard, O., and Vauclair, S. (2015). Accretion of Planetary Matter and the Lithium Problem in the 16 Cygni Stellar System. *Astronomy Astrophysics* 584, A105. doi:10.1051/0004-6361/201526917

Deheuvels, S., Ballot, J., Beck, P. G., Mosser, B., Østensen, R., García, R. A., et al. (2015). Seismic Evidence for a Weak Radial Differential Rotation in Intermediate-Mass Core Helium Burning Stars. *Astronomy Astrophysics* 580, A96. doi:10.1051/0004-6361/201526449

Deheuvels, S., Ballot, J., Eggenberger, P., Spada, F., Noll, A., and den Hartogh, J. W. (2020). Seismic Evidence for Near Solid-Body Rotation in Two Kepler Subgiants and Implications for Angular Momentum Transport. *Astronomy Astrophysics* 641, A117. doi:10.1051/0004-6361/202038578

Deheuvels, S., Ballot, J., Gehan, C., and Mosser, B. (2022). Seismic Signature of Electron Degeneracy in the Core of Red Giants: Hints for Mass Transfer between Close Red-Giant Companions. *Astronomy Astrophysics* 659, A106. doi:10.1051/0004-6361/202142094

Deheuvels, S., Brandão, I., Silva Aguirre, V., Ballot, J., Michel, E., Cunha, M. S., et al. (2016). Measuring the Extent of Convective Cores in Low-Mass Stars Using Kepler Data: toward a Calibration of Core Overshooting. *Astronomy Astrophysics* 589, A93. doi:10.1051/0004-6361/201527967

Deheuvels, S., Doğan, G., Goupil, M. J., Appourchaux, T., Benomar, O., Bruntt, H., et al. (2014). Seismic Constraints on the Radial Dependence of the Internal Rotation Profiles of sixKeplersubgiants and Young Red Giants. *Astronomy Astrophysics* 564, A27. doi:10.1051/0004-6361/201322779

Di Mauro, M. P. (2016). "A Review on Asteroseismology," in *Frontier Research in Astrophysics II (FRAPWS2016)*. Trieste: Proceedings of Science, 29.

di Mauro, M. P. (2004). "Theoretical Aspects of Asteroseismology: Small Steps towards a Golden Future," in *SOHO 14 Helio- and Asteroseismology: Towards a Golden Future*. Editor D. Danesy (New Haven, CT: ESA Special Publication), 559, 186.

Di Mauro, M. P., Ventura, R., Corsaro, E., and Moura, B. L. D. (2018). The Rotational Shear Layer inside the Early Red-Giant Star KIC 4448777. *Astrophysical J.* 862, 9. doi:10.3847/1538-4357/aac7c4

Dziembowski, W. A., Pamyatnykh, A. A., and Sienkiewicz, R. (1990). Solar Model from Helioseismology and the Neutrino Flux Problem. *Mon. Notices R. Astronomical Soc.* 244, 542–550.

Elliott, J. R. (1996). Equation of State in the Solar Convection Zone and the Implications of Helioseismology. *Mon. Notices R. Astronomical Soc.* 280, 1244–1256. doi:10.1093/mnras/280.4.1244

Elliott, J. R., and Kosovichev, A. G. (1998). The Adiabatic Exponent in the Solar Core. *Astrophysical JournalL* 500, L199–L202. doi:10.1086/311417

Farnir, M., Dupret, M.-A., Salmon, S. J. A. J., Noels, A., and Buldgen, G. (2019). Comprehensive Stellar Seismic Analysis. New Method Exploiting the Glitches Information in Solar-like Pulsators. *Astronomy Astrophysics* 622, A98. doi:10.1051/0004-6361/201834044

Farnir, M., Dupret, M. A., Buldgen, G., Salmon, S. J. A. J., Noels, A., Pinçon, C., et al. (2020). Thorough Characterisation of the 16 Cygni System. I. Forward Seismic Modelling with WhoSGlAd. *Astronomy Astrophysics* 644, A37. doi:10.1051/0004-6361/202038522

Fellay, L., Buldgen, G., Eggenberger, P., Khan, S., Salmon, S. J. A. J., Miglio, A., et al. (2021). Asteroseismology of Evolved Stars to Constrain the Internal Transport of Angular Momentum. IV. Internal Rotation of Kepler-56 from an MCMC Analysis of the Rotational Splittings. *Astronomy Astrophysics* 654, A133. doi:10.1051/0004-6361/202140518

Floranes, H. O., Christensen-Dalsgaard, J., and Thompson, M. J. (2005). The Use of Frequency-Separation Ratios for Asteroseismology. *Mon. Notices R. Astronomical Soc.* 356, 671–679. doi:10.1111/j.1365-2966.2004.08487.x

Fontaine, G., Bergeron, P., Brassard, P., Charpinet, S., Randall, S., Van Grootel, V., et al. (2019). Testing Seismic Models of Hot B Subdwarfs with Gaia Data. *Astrophysical J.* 880, 79. doi:10.3847/1538-4357/ab2885

Frandsen, S., Carrier, F., Aerts, C., Stello, D., Maas, T., Burnet, M., et al. (2002). Detection of Solar-like Oscillations in the G7 Giant Star ξ Hya. *Astronomy Astrophysics* 394, L5–L8. doi:10.1051/0004-6361:20021281

Giammichele, N., Charpinet, S., Fontaine, G., Brassard, P., Green, E. M., Van Grootel, V., et al. (2018). A Large Oxygen-Dominated Core from the Seismic Cartography of a Pulsating White Dwarf. *Nature* 554, 73–76.doi:10.1038/nature25136

Gough, D. O., and Kosovichev, A. G. (1993a). Initial Asteroseismic Inversions. *Int. Astron. Union Colloq.* 137, 541–543. eds. W. W. Weiss and A. BaglinAstronomical Society of the Pacific Conference Series. doi:10.1017/s0252921100018388

Gough, D. O., and Kosovichev, A. G. (1993b). "Seismic Analysis of Stellar P-Mode Spectra," in GONG 1992. Seismic Investigation of the Sun and Stars, Boulder, Colorado, August 11–14, 1993. Editor T. M. Brown, 351. Astronomical Society of the Pacific Conference Series.42

Goupil, M. J., Lebreton, Y., Marques, J. P., Samadi, R., and Baudin, F. (2011). Open Issues in Probing Interiors of Solar-like Oscillating Main Sequence Stars 1. From the Sun to Nearly Suns. *J. Phys. Conf. Ser.* 271, 012031. GONG-SoHO 24: A New Era of Seismology of the Sun and Solar-Like Stars. doi:10.1088/1742-6596/271/1/012031

Gruberbauer, M., Guenther, D. B., MacLeod, K., and Kallinger, T. (2013). Bayesian Asteroseismology of 23 Solar-like Kepler Targets. *Mon. Notices R. Astronomical Soc.* 435, 242–254. doi:10.1093/mnras/stt1289

Grundahl, F., Kjeldsen, H., Frandsen, S., Andersen, M., Bedding, T., Arentoft, T., et al. (2006). SONG: Stellar Oscillations Network Group . A Global Network of Small Telescopes for Asteroseismology and Planet Searches. *Mem. della Soc. Astron. Ital.* 77, 458.

Guzik, J. A. (2011). Recent Advances in Modeling Stellar Interiors. *Astrophys. Space Sci.* 336, 95–101. doi:10.1007/s10509-010-0552-2

Handberg, R., Brogaard, K., Miglio, A., Bossini, D., Elsworth, Y., Slumstrup, D., et al. (2017). NGC 6819: Testing the Asteroseismic Mass Scale, Mass Loss and Evidence for Products of Non-standard Evolution. *Mon. Notices R. Astronomical Soc.* 472, 979–997. doi:10.1093/mnras/stx1929

Hatta, Y., Sekii, T., Benomar, O., and Takata, M. (2022). Bayesian Rotation Inversion of KIC 11145123. *Astrophysical J.* 927, 40. doi:10.3847/1538-4357/ac4699

Hatta, Y., Sekii, T., Takata, M., and Benomar, O. (2021). Nonstandard Modeling of a Possible Blue Straggler Star, KIC 11145123. *Astrophysical J.* 923, 244. doi:10.3847/1538-4357/ac23c9

Hatta, Y., Sekii, T., Takata, M., and Kurtz, D. W. (2019). The Two-Dimensional Internal Rotation of KIC 11145123. *Astrophysical J.* 871, 135. doi:10.3847/1538-4357/aaf881

Joel Ong, J. M., Basu, S., and Roxburgh, I. W. (2021). Mixed Modes and Asteroseismic Surface Effects. I. Analytic Treatment. *Astrophysical J.* 920, 8. doi:10.3847/1538-4357/ac12ca

Jørgensen, A. C. S., Montalbán, J., Miglio, A., Rendle, B. M., Davies, G. R., Buldgen, G., et al. (2020). Investigating Surface Correction Relations for RGB Stars. *Mon. Notices R. Astronomical Soc.* 495, 4965–4980. doi:10.1093/mnras/staa1480

Kjeldsen, H., and Bedding, T. R. (1995). Amplitudes of Stellar Oscillations: the Implications for Asteroseismology. *Astronomy Astrophysics* 293, 87–106.

Kjeldsen, H., Bedding, T. R., Butler, R. P., Christensen-Dalsgaard, J., Kiss, L. L., McCarthy, C., et al. (2005). Solar-like Oscillations in α Centauri B. *Astrophysical J.* 635, 1281–1290. doi:10.1086/497530

Kjeldsen, H., Bedding, T. R., and Christensen-Dalsgaard, J. (2008). Correcting Stellar Oscillation Frequencies for Near-Surface Effects. *Astrophysical J.* 683, L175–L178. doi:10.1086/591667

Kosovichev, A. G. (2011). Advances in Global and Local Helioseismology: An Introductory Review. *Lect. Notes Phys.* 832, 3. doi:10.1007/978-3-642-19928-8_1

Kosovichev, A. G., and Kitiashvili, I. N. (2020). Resolving Power of Asteroseismic Inversion of the Kepler Legacy Sample. *Proc. IAU* 15, 107–115. Solar and Stellar Magnetic Fields: Origins and Manifestations, eds. A. Kosovichev, S. Strassmeier, and M. Jardine. doi:10.1017/S1743921320001416

Kurtz, D. W., Saio, H., Takata, M., Shibahashi, H., Murphy, S. J., and Sekii, T. (2014). Asteroseismic Measurement of Surface-To-Core Rotation in a Main-Sequence A Star, KIC 11145123. *Mon. Notices R. Astronomical Soc.* 444, 102–116. doi:10.1093/mnras/stu1329

Lund, M. N., Miesch, M. S., and Christensen-Dalsgaard, J. (2014). Differential Rotation in Main-Sequence Solar-like Stars: Qualitative Inference from Asteroseismic Data. *Astrophysical J.* 790, 121. doi:10.1088/0004-637X/790/2/121

Lynden-Bell, D., and Ostriker, J. P. (1967). On the Stability of Differentially Rotating Bodies. *Mon. Notices R. Astronomical Soc.* 136, 293–310. doi:10.1093/mnras/136.3.293

Martić, M., Lebrun, J. C., Appourchaux, T., and Korzennik, S. G. (2004). p-Mode Frequencies in Solar-like Stars. I. Procyon A. *Astronomy Astrophysic* 418, 295–303. doi:10.1051/0004-6361:20034574

Mathur, S., Metcalfe, T. S., Woitaszek, M., Bruntt, H., Verner, G. A., Christensen-Dalsgaard, J., et al. (2012). A Uniform Asteroseismic Analysis Of 22 Solar-Type Stars Observed Bykepler. *Astrophysical J.* 749, 152. doi:10.1088/0004-637x/749/2/152

Mazumdar, A., Monteiro, M. J. P. F. G., Ballot, J., Antia, H. M., Basu, S., Houdek, G., et al. (2012). Acoustic Glitches in Solar-type Stars fromKepler. *Astron. Nachr.* 333, 1040–1043. doi:10.1002/asna.201211825

Mazumdar, A., Monteiro, M. J. P. F. G., Ballot, J., Antia, H. M., Basu, S., Houdek, G., et al. (2014). Measurement Of Acoustic Glitches In Solar-Type Stars From Oscillation Frequencies Observed Bykepler. *Astrophysical J.* 782, 18. doi:10.1088/0004-637x/782/1/18

McKeever, J. M., Basu, S., and Corsaro, E. (2019). The Helium Abundance of NGC 6791 from Modeling of Stellar Oscillations. *Astrophysical J.* 874, 180. doi:10.3847/1538-4357/ab0c04

Metcalfe, T. S., Creevey, O. L., and Davies, G. R. (2015). Asteroseismic Modeling of 16 Cyg A & B Using the Complete Kepler Data Set. *Astrophysical J.* 811, L37. doi:10.1088/2041-8205/811/2/l371

Miglio, A., Girardi, L., Grundahl, F., Mosser, B., Bastian, N., Bragaglia, A., et al. (2021). Haydn. *Exp. Astron* 51, 963–1001. doi:10.1007/s10686-021-09711-1

Miglio, A., and Montalbán, J. (2005). Constraining Fundamental Stellar Parameters Using Seismology. Application to α Centauri AB. *Astronomy Astrophysics* 441, 615–629. doi:10.1051/0004-6361:20052988

Monteiro, M. J. P. F. G., and Thompson, M. J. (2005). Seismic Analysis of the Second Ionization Region of Helium in the Sun -- I. Sensitivity Study and Methodology. *Mon. Notices R. Astronomical Soc.* 361, 1187–1196. doi:10.1111/j.1365-2966.2005.09246.x

Nelder, J. A., and Mead, R. (1965). A Simplex Method for Function Minimization. *Comput. J.* 7, 308–313. doi:10.1093/comjnl/7.4.308

Noll, A., Deheuvels, S., and Ballot, J. (2021). Probing Core Overshooting Using Subgiant Asteroseismology: The Case of KIC10273246. *Astronomy Astrophysics* 647, A187. doi:10.1051/0004-6361/202040055

Ong, J. M. J., and Basu, S. (2020). Semianalytic Expressions for the Isolation and Coupling of Mixed Modes. *Astrophysical J.* 898, 127. doi:10.3847/1538-4357/ab9ffb

Pijpers, F. (2006). *Methods in Helio- and Asteroseismology*. London, UK: Imperial College Press.

Pijpers, F. P., Di Mauro, M. P., and Ventura, R. (2021). Asteroseismogyrometry of Low-Mass Red Giants. I. The SOLA Inversion Method. *Astronomy Astrophysics* 656, A151. doi:10.1051/0004-6361/202140933

Pijpers, F. P., and Thompson, M. J. (1994). The SOLA Method for Helioseismic Inversion. *ASTRONOMY Astrophysics* 281, 231–240.

Rabello-Soares, M. C., Basu, S., and Christensen-Dalsgaard, J. (1999). On the Choice of Parameters in Solar-Structure Inversion. *Mon. Notices R. Astronomical Soc.* 309, 35–47. doi:10.1046/j.1365-8711.1999.02785.x

Rauer, H., Catala, C., Aerts, C., Appourchaux, T., Benz, W., Brandeker, A., et al. (2014). The PLATO 2.0 Mission. *Exp. Astron.* 38, 249–330. doi:10.1007/s10686-014-9383-4

Reese, D. R., Chaplin, W. J., Davies, G. R., Miglio, A., Antia, H. M., Ball, W. H., et al. (2016). SpaceInn Hare-And-Hounds Exercise: Estimation of Stellar Properties Using Space-Based Asteroseismic Data. *Astronomy Astrophysics* 592, A14. doi:10.1051/0004-6361/201527987

Reese, D. R., Marques, J. P., Goupil, M. J., Thompson, M. J., and Deheuvels, S. (2012). Estimating Stellar Mean Density through Seismic Inversions. *Astronomy Astrophysics* 539, A63. doi:10.1051/0004-6361/201118156

Reese, D. R. (2018). "Stellar Inversion Techniques," in *Asteroseismology and Exoplanets: Listening to the Stars and Searching for New Worlds*. Editors T. L. Campante, N. C. Santos, and M. J. P. F. G. Monteiro. New York City, NY: Springer International Publishing, 49, 75. *Astrophysics and Space Science Proceedings*. doi:10.1007/978-3-319-59315-9_4

Rendle, B. M., Buldgen, G., Miglio, A., Reese, D., Noels, A., Davies, G. R., et al. (2019). Aims- a New Tool for Stellar Parameter Determinations Using Asteroseismic Constraints. *Mon. Notices R. Astronomical Soc.* 484, 771–786. doi:10.1093/mnras/stz031

Ricker, G. R., Winn, J. N., Vanderspek, R., Latham, D. W., Bakos, G. Á., Bean, J. L., et al. (2015). Transiting Exoplanet Survey Satellite (TESS). *J. Astronomical Telesc. Instrum. Syst.* 1, 014003. doi:10.1117/1.JATIS.1.1.014003

Roxburgh, I., and Vorontsov, S. (2003). Diagnostics of the Internal Structure of Stars Using the Differential Response Technique. *Astrophys. Space Sci.* 284, 187–191. doi:10.1007/978-94-017-0799-2_24

Roxburgh, I. W., Audard, N., Basu, S., Christensen-Dalsgaard, J., and Vorontsov, S. V. (1998). "Inversion for the Internal Structure of an Evolved Small-Mass Star Using Modes with L =0-3," in Proceedings of the IAU Symposium 181: Sounding Solar and Stellar Interiors, Nice, September 30–October 3, 1996. Editors J. Provost and F. X. Schmider, 245–246.181

Roxburgh, I. W. (2015). Surface Layer Independent Model Fitting by Phase Matching: Theory and Application to HD 49933 and HD 177153 (Aka Perky). *Astronomy Astrophysics* 574, A45. doi:10.1051/0004-6361/201425289

Roxburgh, I. W. (2008). The STAROX Stellar Evolution Code. *Astrophys. Space Sci.* 316, 75–82. doi:10.1007/s10509-007-9673-7

Roxburgh, I. W. (2002). "The Tools of Asteroseismology," in Proceedings of the First Eddington Workshop on Stellar Structure and Habitable Planet Finding, Córdoba, Spain, June 11–15, 2001. Editors B. Battrick, F. Favata, I. W. Roxburgh, and D. Galadi (ESA Special Publication), 75–85.485

Roxburgh, I. W., and Vorontsov, S. V. (2002). "Inversion for a 0.8 M_{solar} Star Using Differential-Response Technique," in Proceedings of the First Eddington Workshop on Stellar Structure and Habitable Planet Finding, Córdoba, Spain, June 11–15, 2001. Editors B. Battrick, F. Favata, I. W. Roxburgh, and D. Galadi (ESA Special Publication), 337–339.485

Roxburgh, I. W., and Vorontsov, S. V. (2013). On the Use of the Ratio of Small to Large Separations in Asteroseismic Model Fitting. *Astronomy Astrophysics* 560, A2. doi:10.1051/0004-6361/201321333

Roxburgh, I. W., and Vorontsov, S. V. (2000). Semiclassical Approximation for Low-Degree Stellar P Modes - I. The Classical Eigenfrequency Equation. *Mon. Notices R. Astronomical Soc.* 317, 141–150. doi:10.1046/j.1365-8711.2000.03623.x

Roxburgh, I. W., and Vorontsov, S. V. (2003). The Ratio of Small to Large Separations of Acoustic Oscillations as a Diagnostic of the Interior of Solar-like Stars. *Astronomy Astrophysics* 411, 215–220. doi:10.1051/0004-6361:20031318

Saio, H., Kurtz, D. W., Takata, M., Shibahashi, H., Murphy, S. J., Sekii, T., et al. (2015). Asteroseismic Measurement of Slow, Nearly Uniform Surface-To-Core Rotation in the Main-Sequence F Star KIC 9244992. *Mon. Notices R. Astronomical Soc.* 447, 3264–3277. doi:10.1093/mnras/stu2696

Salmon, S. J. A. J., Van Grootel, V., Buldgen, G., Dupret, M.-A., and Eggenberger, P. (2021). Reinvestigating α Centauri AB in Light of Asteroseismic Forward and Inverse Methods. *Astronomy Astrophysics* 646, A7. doi:10.1051/0004-6361/201937174

Schunker, H., Schou, J., and Ball, W. H. (2016a). Asteroseismic Inversions for Radial Differential Rotation of Sun-like Stars: Sensitivity to Uncertainties. *Astronomy Astrophysics* 586, A24. doi:10.1051/0004-6361/201525937

Schunker, H., Schou, J., Ball, W. H., Nielsen, M. B., and Gizon, L. (2016b). Asteroseismic Inversions for Radial Differential Rotation of Sun-like Stars: Ensemble Fits. *Astronomy Astrophysics* 586, A79. doi:10.1051/0004-6361/201527485

Scuflaire, R., Théado, S., Montalbán, J., Miglio, A., Bourge, P.-O., Godart, M., et al. (2008). CLÉS, Code Liégeois D'Évolution Stellaire. *Astrophys. Space Sci.* 316, 83–91. doi:10.1007/s10509-007-9650-1

Sekii, T. (1997). "Internal Solar Rotation," in *Sounding Solar and Stellar Interiors*. Editors J. Provost and F.-X. Schmider. Dordrecht: Kluwer Academic Publishers, 181. ISBN0792348389. doi:10.1007/978-94-011-5163-4_17

Shibahashi, H., Hiremath, K. M., and Takata, M. (1999). Seismic Solar Model: Both of the Radiative Core and the Convective Envelope. *Adv. Space Res.* 24, 177–180. doi:10.1016/S0273-1177(99)00498-6

Shibahashi, H., and Tamura, S. (2006). "A Seismic Solar Model with the Updated Elemental Abundances," in Proceedings of SOHO 18/GONG 2006/HELAS I, Beyond the spherical Sun, Sheffield, UK, August 7–11, 2006. Editors K. Fletcher and M. Thompson (ESA Special Publication), 81.624

Sonoi, T., Samadi, R., Belkacem, K., Ludwig, H. G., Caffau, E., and Mosser, B. (2015). Surface-effect Corrections for Solar-like Oscillations Using 3D Hydrodynamical Simulations. I. Adiabatic Oscillations. *Astronomy Astrophysics* 583, A112. doi:10.1051/0004-6361/201526838

Strakhov, V. N., and Vorontsov, S. V. (2001). "Adaptive Regularization Technique in Linear Inverse Problem," in OHO 10/GONG 2000 Workshop: Helio- and Asteroseismology at the Dawn of the Millennium, Santa Cruz de Tenerife, October 2–6, 2000. Editors A. Wilson and P. L. Pallé (ESA Special Publication), 539–542.464

Takata, M., and Montgomery, M. H. (2002). Seismic Inversions for White Dwarf Stars. *Int. Astron. Union Colloq.* 185, 606–607. Editors C. Aerts, T. R. Bedding, and J. Christensen-DalsgaardAstronomical Society of the Pacific Conference Series. doi:10.1017/s025292110001722x

Takata, M., and Shibahashi, H. (1998). Solar Models Based on Helioseismology and the Solar Neutrino Problem. *Astrophysical J.* 504, 1035–1050. doi:10.1086/306094

Tarantola, A. (2005). *Inverse Problem Theory and Methods for Model Parameter Estimation*. Philadelphia: Society for Industrial and Applied Mathematics.

Teixeira, T. C., Christensen-Dalsgaard, J., Carrier, F., Aerts, C., Frandsen, S., Stello, D., et al. (2003). Giant Vibrations in Dip. *Astrophysics Space Sci.* 284, 233–236. doi:10.1007/978-94-017-0799-2_31

Thomas, A. E. L., Chaplin, W. J., Basu, S., Rendle, B., Davies, G., and Miglio, A. (2021). Impact of Magnetic Activity on Inferred Stellar Properties of Main-Sequence Sun-like Stars. *Mon. Notices R. Astronomical Soc.* 502, 5808–5820. doi:10.1093/mnras/stab354

Thompson, M. J., Christensen-Dalsgaard, J., Miesch, M. S., and Toomre, J. (2003). The Internal Rotation of the Sun. *Annu. Rev. Astron. Astrophys.* 41, 599–643. doi:10.1146/annurev.astro.41.011802.094848

Thompson, M. J., and Christensen-Dalsgaard, J. (2002). "On Inverting Asteroseismic Data," in Proceedings of the First Eddington Workshop on Stellar Structure and Habitable Planet Finding, Córdoba, Spain, June 11–15, 2001. Editors B. Battrick, F. Favata, I. W. Roxburgh, and D. Galadi (ESA Special Publication), 95–101.485

Tikhonov, A. N. (1963). Solution of Incorrectly Formulated Problems and the Regularization Method. *Sov. Math. Dokl.* 4, 1035–1038.

Unno, W., Osaki, Y., Ando, H., Saio, H., and Shibahashi, H. (1989). *Nonradial Oscillations of Stars*. Tokyo: University of Tokyo Press.

Van Grootel, V., Charpinet, S., Fontaine, G., Green, E. M., and Brassard, P. (2010). Structural and Core Parameters of the Hot B Subdwarf KPD 0629-0016 from CoRoT G-Mode Asteroseismology. *Astronomy Astrophysics* 524, A63. doi:10.1051/0004-6361/201015437

Vandakurov, Y. V. (1967). The Frequency Distribution of Stellar Oscillations. *Astron. Zhurnal* 44, 786.

Verma, K., Faria, J. P., Antia, H. M., Basu, S., Mazumdar, A., Monteiro, M. J. P. F. G., et al. (2014). Asteroseismic Estimate of Helium Abundance of a Solar Analog Binary System. *Astrophysical J.* 790, 138. doi:10.1088/0004-637X/790/2/138

Verma, K., Raodeo, K., Antia, H. M., Mazumdar, A., Basu, S., Lund, M. N., et al. (2017). Seismic Measurement of the Locations of the Base of Convection Zone and Helium Ionization Zone for Stars in theKeplerSeismic LEGACY Sample. *Astrophysical J.* 837, 47. doi:10.3847/1538-4357/aa5da7

Verma, K., Raodeo, K., Basu, S., Silva Aguirre, V., Mazumdar, A., Mosumgaard, J. R., et al. (2019). Helium Abundance in a Sample of Cool Stars: Measurements from Asteroseismology. *Mon. Notices R. Astronomical Soc.* 483, 4678–4694. doi:10.1093/mnras/sty3374

Verma, K., and Silva Aguirre, V. (2019). Helium Settling in F Stars: Constraining Turbulent Mixing Using Observed Helium Glitch Signature. *Mon. Notices R. Astronomical Soc.* 489, 1850–1858. doi:10.1093/mnras/stz2272

Vorontsov, S. V. (2002). "Helioseismic Structural Inversion with SOHO MIDI Data," in Proceedings of the SOHO 11 Symposium on From Solar Min to Max: Half a Solar Cycle with SOHO, Davos, March 11–15, 2002. Editor A. Wilson (ESA Special Publication), 107–110.508

Vorontsov, S. V. (2001). "Inversion for the Solar Hydrostatic Structure," in SOHO 10/GONG 2000 Workshop: Helio- and Asteroseismology at the Dawn of the Millennium, Santa Cruz de Tenerife, October 2–6, 2000. Editors A. Wilson and P. L. Pallé (ESA Special Publication), 563–566.464

Vorontsov, S. V. (1998). "Seismic Sounding of the Solar Interior: Differential Response Technique," in Sounding Solar and Stellar Interiors, IAU Symp. 181 (Posters), Nice, September 30–October 3, 1996. Editors P. Janine and S. Francois-Xavier, 135.

Vorontsov, S. V., Baturin, V. A., Ayukov, S. V., and Gryaznov, V. K. (2013). Helioseismic Calibration of the Equation of State and Chemical Composition in the Solar Convective Envelope. *Mon. Notices R. Astronomical Soc.* 430, 1636–1652. doi:10.1093/mnras/sts701

Conflict of Interest: The authors declare that the research was conducted in the absence of any commercial or financial relationships that could be construed as a potential conflict of interest.

Publisher's Note: All claims expressed in this article are solely those of the authors and do not necessarily represent those of their affiliated organizations, or those of the publisher, the editors and the reviewers. Any product that may be evaluated in this article, or claim that may be made by its manufacturer, is not guaranteed or endorsed by the publisher.

frontiers | Frontiers in Astronomy and Space Sciences

TYPE Brief Research Report
PUBLISHED 22 August 2022
DOI 10.3389/fspas.2022.953231

OPEN ACCESS

EDITED BY
Tiago Campante,
Instituto de Astrofísica e Ciências do Espaço (IA), Portugal

REVIEWED BY
Jadwiga Daszynska-Daszkiewicz,
University of Wrocław, Poland
Enrico Maria Nicola Corsaro,
Osservatorio Astrofisico di Catania (INAF), Italy

*CORRESPONDENCE
J. C. Suárez,
jcsuarez@ugr.es

SPECIALTY SECTION
This article was submitted to Stellar and Solar Physics,
a section of the journal
Frontiers in Astronomy and Space Sciences

RECEIVED 26 May 2022
ACCEPTED 29 June 2022
PUBLISHED 22 August 2022

CITATION
Suárez JC (2022), The potential of Shannon entropy to find the large separation of δ Scuti stars: The entropy spectrum.
Front. Astron. Space Sci. 9:953231.
doi: 10.3389/fspas.2022.953231

The potential of Shannon entropy to find the large separation of δ *Scuti* stars: The entropy spectrum

J. C. Suárez*

Física Teórica y del Cosmos Dept, University of Granada, Granada, Spain

This study explores the use of Shannon entropy to find periodic patterns in the oscillation spectra of δ *Scuti* stars. We have developed a new diagnostic tool for detecting potential patterns that scans for minimal entropic states in the well-known échelle diagrams. Here, we describe the basic mathematical grounds of the Shannon entropy and how it can be applied to échelle diagrams through a new diagnostic diagram: the entropy (H) spectrum (HSpec). The method is first validated with the solar-like pulsator HD 49933, for which the large separation was found compatible with values published in the literature. Then we computed the entropy spectrum for two well-studied δ *Scuti* stars: HD 174936 and HD 174966, for which HSpec analysis was able to accurately determine their large separation (or some multiple or submultiple of it). Although these results are promising, the HSpec tool presents several limitations: it has a strong dependence on the probability distribution of the frequencies in the échelle diagram, and on the way it is calculated. We discuss possible solutions to this that rely on 2D probability distributions and conditional entropy.

KEYWORDS

asteroseismology, time series analysis, stellar structure and evolution, information theory, stellar pulsations, *delta Scuti* stars, solar-like oscillations

1 Introduction

The analysis of periodic patterns is crucial for asteroseismology. Up to date, the search for individual mode identification has been found to be an almost unreachable task for most of the variable stars. This has barely progressed even with the availability of ultra-precise data from space. However, some structures in the oscillation power spectrum of pulsating stars provide very useful information about the stellar interiors. This has been especially successful for the Sun and solar-like pulsators (e.g., red giants), whose periodic patterns can be observed without difficulty (see e.g., Aerts et al., 2010; Corsaro et al., 2012). In fact, from main-sequence to read giants solar-like pulsators, the automated mode identification (including mixed modes) is nowadays a reality (details in e.g., Kallinger, 2019; Corsaro et al., 2020; Nielsen et al., 2021) This has led to a revolution in the understanding of their internal structure and evolution with the use of scaling relations

(see e.g., Hekker and Christensen-Dalsgaard, 2016, and references therein), which have been used as a proxy of stellar masses, radii, mean densities, ages, etc. This has allowed us to perform more accurate stellar population studies of the galaxy (Miglio et al., 2016, 2013). On the other hand, for other stars with different pulsation mechanisms, such periodic patterns are not so easy to detect.

Thanks to a great observational effort, Breger et al. (1999) found periodic regularity in the oscillation spectrum of FG Vir, which was proposed as possible large separation-like pattern in the low-frequency regime (around the fundamental radial mode). Later on, in the era of space missions like *MOST* (Walker et al., 2003), *CoRoT* (Baglin et al., 2006), and *Kepler* (Koch et al., 2010), thanks to ultra-precise photometric time series, such patterns in the low-frequency regime of δ *Scuti* stars were again observed (see e.g., García Hernández et al., 2009; Handler, 2009; García Hernández et al., 2013). These patterns were also predicted theoretically (Reese et al., 2008; Ouazzani et al., 2015) and were found to be compatible with a large separation that scales with the mean density of the star ($\Delta\nu$, Suárez et al., 2014). This scaling was then empirically confirmed by García Hernández et al. (2015) using binary systems with a δ *Scuti* component. Then Hernández et al. (2017) used the scaling $\Delta\nu - \rho$ relation to demonstrate that it was possible to accurately determine the surface gravity of those stars when precise measurements of stellar parallaxes are available. This paved the way to perform multivariable correlations analyses in the observed seismic data (Moya et al., 2017) as well as to find the empiric relation between the frequency at maximum power of their oscillation spectra ($\nu_{\max}$) and the effective temperature (Barceló Forteza et al., 2018), or even with surface gravity through the study of the gravity darkening in fast rotators (Barceló Forteza et al., 2020). Interestingly, Mirouh et al. (2019) retrieved a similar $\Delta\nu - \rho$ scaling relation for fast rotating stars using island modes identified using a convolutional neural network. The most recent theoretical relation has been obtained by Rodríguez-Martín et al. (2020) using synthetic spectra of rotating models.

A confident knowledge of the large separation is also valuable because it allows to better search for other interesting patterns, such as the rotational splitting (see e.g., Barceló Forteza et al., 2017; Ramón-Ballesta et al., 2021), the identification of certain radial modes in young δ *Scuti* stars (see Bedding et al., 2020, for more details), or put asteroseismic constraints on the age of open clusters (Pamos Ortega et al., 2022).

Despite all this progress, the detection of periodicities remains critical. In the last decades, methods based on pattern recognition have been applied in the time domain (see e.g., Mosser and Appourchaux, 2009, and references therein) with significant success in solar-like pulsators, red giants, etc. For A–F stars, the discrete Fourier transform (DFT) of the frequency positions (García Hernández et al., 2009) is the most successful method to detect large separations in A–F stars. Some attempts to automatize its use have been developed (see e.g., Paparó et al., 2016); however, all of them still requires some supervision, preventing the implementation in automatic pipelines.

In this work, we tackled the problem of frequency pattern detection with a concept borrowed from Information Theory: the Shannon entropy. This concept has mainly been applied in the realm of information transmission, computer science, etc. In astronomy, Cincotta et al. (1995) and Cincotta et al. (1999) developed the first methods to detect patterns in astronomical time series.

In recent years, Shannon entropy has regained interest in the so-called big data and machine learning fields as a reliable measure of statistical dependence (see e.g., Malakar et al., 2012), as well as a criterion for feature selection in engineering (Tourassi et al., 2001). This work considers the frequency patterns as features in stellar power spectra, and thus we applied the concept of Shannon entropy to detect them with no hypothesis about their statistical distributions. In Section 2, we define the concept of Shannon entropy in the manner we calculated it and the new diagnostic tool based on it, the entropy spectrum (HSpec). The method is then validated against well-known frequency patterns of the solar-like star HD 49993 and applied to the two selected δ *Scuti* stars (Section 3). Finally, in Section 4, we interpret the results as compared with other methods and discuss the limitations of the tool as well as possible solutions to improve its robustness.

2 Methods

The methodology followed in this work relies entirely upon the use of the Shannon entropy, a concept which was introduced for the first time by Claude Shannon in the context of communication theory (see his famous study Shannon, 1948, for details). In the following, for the sake of simplicity the word "entropy" will be used as a shortcut of "Shannon Entropy". It is thus worthy defining it to better understand its importance for the method. The entropy H of a discrete random variable X is defined in terms of its probability distribution $P(X)$, as follows:

$$H(X) = -\sum_{x} P(x)\log P(x). \tag{1}$$

When there is no knowledge about the distribution of probabilities $P(x)$ we need to estimate it. This thus implies that instead of calculating the entropy we will estimate it $\hat{H}(X)$. The better the estimate of the distribution of probabilities is, the closer $\hat{H}(X)$ will be to the actual entropy. In the present work, we use the method of maximum-likelihood (ML) to estimate $\hat{P}(x)$ from the observed counts (see Hausser and Strimmer, 2009, for details). In practice, we computed the following:

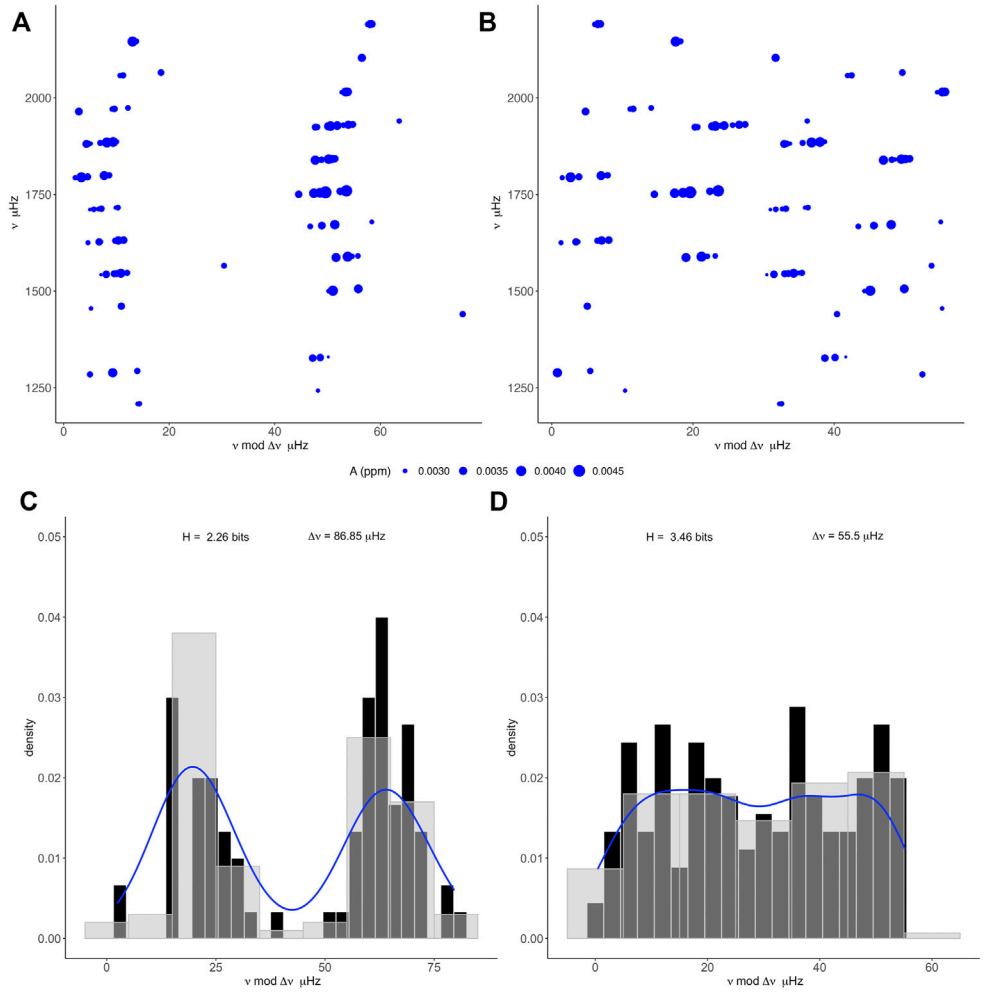

FIGURE 1
Upper panels show the échelle diagrams of the solar-like star HD 49933, the first solar-like star observed by *CoRoT*. These were built using its oscillation frequencies obtained from a pre-whitening process (see Section 3.1). The size of dots indicates the amplitude of the observed modes in ppm. **(A)** shows the classical vertical ridges corresponding to modes ordered by $\Delta\nu$ = 86.85 μHz. **(B)** shows the same diagram for a random value of $\Delta\nu$ = 55.5 μHz. Lower panels, **(C,D)**, are the histograms (density of counts) of the échelle diagrams corresponding to **(A,B)**, respectively. Grey and black represent histograms computed with bandwidths of 10 μHz and 3 μHz, respectively. For illustration the density curve for the latter is also depicted in blue color.

$$\hat{H}(X) = -\sum_{x} \hat{P}(x)\log\hat{P}(x), \tag{2}$$

where

$$\hat{P}(x) = \frac{y_k}{n} \tag{3}$$

is the ML estimate of probability distribution based on the observed counts y_k normalized by the total number of observations.

2.1 The échelle diagrams

We are interested in finding frequency patterns in the oscillation spectra, that is, the set of observed oscillation frequencies of a given pulsating star. For this purpose, we use the following statistical variables:

$$x = \left[\nu_i \bmod \Delta\nu_j\right], \tag{4}$$

$$y = [\nu_i], \tag{5}$$

where $[\nu_i]$ represents the set of observed frequencies and $\Delta\nu_j$ is a given frequency periodicity.

Such a relation between variables is the well-known échelle diagram, widely used in asteroseismology for the visual inspection and determination of large separations (mainly in solar-type stars). When $\Delta\nu_j$ corresponds to the large separation, the oscillation modes appear aligned, with a vertical distance between points of $\Delta\nu_j$ for the same angular degree. The different

ridges represent the modes with different mode degrees, although the identification of the modes is out of the scope of this study.

Figure 1 shows the échelle diagram of HD 49993 for two different spacing: its large separation and a random value. Notice that when vertical ridges come up, most of the modes are vertically aligned, which indicates certain regularity. This is indeed, the way of finding the correct $\Delta\nu$ using échelle diagrams. However, the clarity of the vertical ridges is progressively lost as one moves away from the optimal value, up to some $\Delta\nu_j$ at which points seem to be randomly distributed, and therefore indicates less regularity, or at least, less regularity than the previous case, which is the main point of the present method.

2.2 The entropy of échelle diagrams

The concept of order and disorder are somewhat ambiguous. Instead, let us use the notion of measure of information, as originally proposed by C. Shannon. This measure can also be understood as a kind of uncertainty about the information itself[1]. The measure of information conveys how hard it is to transmit information through a message. Hard means that you need more bits of information to transmit the same information. In this case, the message is carried by the distribution of points in the échelle diagram. In other words, an ordered-like distribution as the one seen in Figure 1A requires less bits of information to be transmitted, as compared with the random-like distribution of Figure 1B. Qualitatively this means that $H_A < H_B$.

In order to quantify the entropy, H, it is necessary to know the distribution of the points $P(X)$ in the échelle diagram (see Eq. 1). The simplest way of obtaining such information is to compute the histogram of the échelle diagram's abscissa, that is, how ν $|\Delta\nu_j|$, for a given $\Delta\nu_j$. This is illustrated in panels C and D of Figure 1, where the distribution of counts (bars) or density (shaded curve) is P(X). As expected, when points are distributed in two regions (lobes of panel A), the uncertainty about the location of points is low (or equivalently, the amount of bits necessary to transmit the information about the distribution of the points is low), $H_A = 1.96$ bits, as compared with a uniform P(X) of panel B, for which is $H_B = 3.46$ bits.

At this point it is important to emphasize that this is an interpretation of entropy in terms of measure of information, hence nothing can be said about the information it may conveys. That is, one can deduce or extract useful information from panels A or B of Figure 1, regardless their measure of information, which is just related with how the distribution of points in the échelle diagrams can be coded. It can also be interpreted as the degree of uncertainty or even as the average unlikelihood of occurrence of the outcomes.

2.3 The Hspec

The main objective of the method is to find the distribution of points in the échelle diagram that minimizes its entropy H. In practice, we proceed according to the following steps:

1. Selection of the interval of the periodicities $\Delta\nu_j$ to be explored and its resolution R. Depending on the previous knowledge about type of pulsation, estimates of periodic patterns, etc., we establish how wide the scan frequency will be. For solar-like pulsations this is quite straightforward since scaling relations can provide an initial guess on $\Delta\nu$, which may help to shorten the interval to explore. However, the scaling relations for δ *Scuti* stars relies the large separation with the mean density of the star (see Rodríguez-Martín et al., 2020, for the most updated relation), calibrated for eclipsing binaries, for which independent measurements of the mean density are available. The resolution, that is, the step in frequency $R = \Delta\nu_j - \Delta\nu_{j-1}$ can be arbitrarily small. However, this can increase the amount of numerical operations needed. The lower limit, in any case, should be twice the observational uncertainties of the oscillation frequencies: $2\ |\epsilon(\nu_j)|$.
2. Choosing the range of observed frequencies to be explored. Although, this step is not strictly required, it is recommended to restrict it (if possible) to the frequency domain where the targeted periodic patterns are expected to be. Complete exploration is also possible, although the - spectra might be noisier or less reliable.
3. Estimation of the number of bins n_b to sample the probability distributions. We selected a given number of bins for the scan of $\Delta\nu_j$.
4. Building the entropy spectrum, HSpec. Échelle diagrams are computed for each the scanned $\Delta\nu_j$ values explored within the selected ranges of frequency and periodicities $[\Delta\nu_{\min}, \Delta\nu\max]$. Then H_j is calculated for each one of those échelle diagrams. The complete set of $(H_j,\ \Delta\nu_j)$ is what I called entropy spectrum.

The absolute minimum of entropy in HSpec is considered the dominant periodicity, which can be interpreted as the large separation or a submultiple of it (see Section 4).

2.4 A first glance to HSpec on a synthetic oscillation spectrum

Notice that the Shannon entropy is sensitive not only to variations in the overall distribution of the points but also in the

1 Note that, here, H does not deal with the information itself, but with its measure.

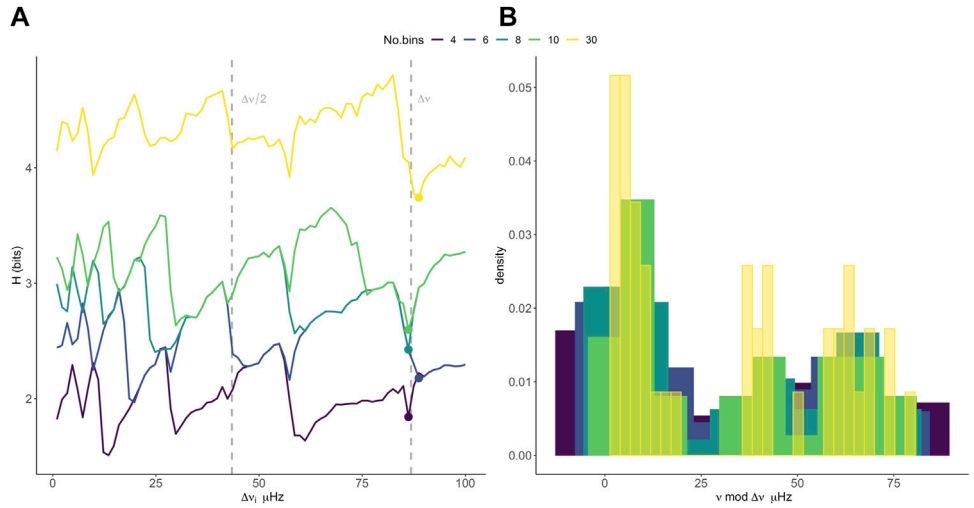

FIGURE 2
Panel **(A)** shows the variation of HSpec with the number of bins for an asteroseismic model of 1.52 $M_{\odot}$. For illustration, the large separation of the model, $\Delta\nu$ = 86.84 μHz, and its half, are shown as vertical dashed lines. Filled dots indicate the location of the local minima that spot the large separation value. **(B)** depicts the histograms from which the probability distributions were extracted to compute the entropy spectra shown in **(A)**.

way the probability distribution is computed, that is, the size and/or number of bins used in the histograms.

A detailed analysis of HSpec for different configuration of parameters lies beyond the scope of this study. Nonetheless, a first glance to synthetic oscillation spectra indicates that HSpec would be more sensitive to the number of bins than any other factor (see Figure 2). The entropy spectra showed in that figure were computed for an asteroseismic model of 1.52 $M_{\odot}$ using the evolutionary code MESA (Paxton et al., 2019) and the adiabatic pulsation code FILOU (Suárez and Goupil, 2008). Standard physics for δ *Scuti* stars were considered with solar metallicity and a moderately fast surface rotation (40% of the break-up frequency). Adiabatic frequencies were corrected for the effect of rotation including near-degeneracy effects (Suárez et al., 2006). The theoretical large separation of $\Delta\nu$ = 86.83 μHz was computed as the median of the large separations obtained for each ℓ within the range n = [2, 10].

The value of the actual large separation is always spotted whatever the number of bins considered. However, these local minima do not always correspond with the absolute minima. In some cases, it is hard to find out which of the peaks would be the right one. For lower $\Delta\nu_i$ values, the analysis is even more difficult since there are significant shifts of the peaks of about 5–20 μHz. Bear in mind that all the modes are considered (from ℓ = 0 to 2), that is, no visibility function was convoluted with the oscillation spectrum. This is therefore the best case, for which there is no lack of modes contributing to $\Delta\nu$. (see Section 4 for more details on the next steps foreseen to improve the method).

3 Results

As the main goal of the HSpec analysis is to find the large separation in δ *Scuti* stars, it is important to validate the method on stars for which the large separation is known and easily detectable, such as solar-type stars.

3.1 The HSpec of the solar-like pulsator HD 49933

For this star, we used the 60 days data from the *CoRoT* initial run (IR) processed with the MIARMA code to fill the gaps due to the satellite duty cycle (in particular the gaps caused by the passage of the satellite through the South Atlantic anomaly (see details in Pascual-Granado et al., 2015). We then obtained the pulsation frequencies of the star using the pre-whitening procedure described in Pascual-Granado et al. (2018), using the code SIGSPEC (Reegen, 2007).

The large separation of HD 49933 was estimated from the light curve by Appourchaux et al. (2008) and later on by Benomar et al. (2009) is $\Delta\nu$ = 85.9 ± 0.15 μHz. In the frequency domain,

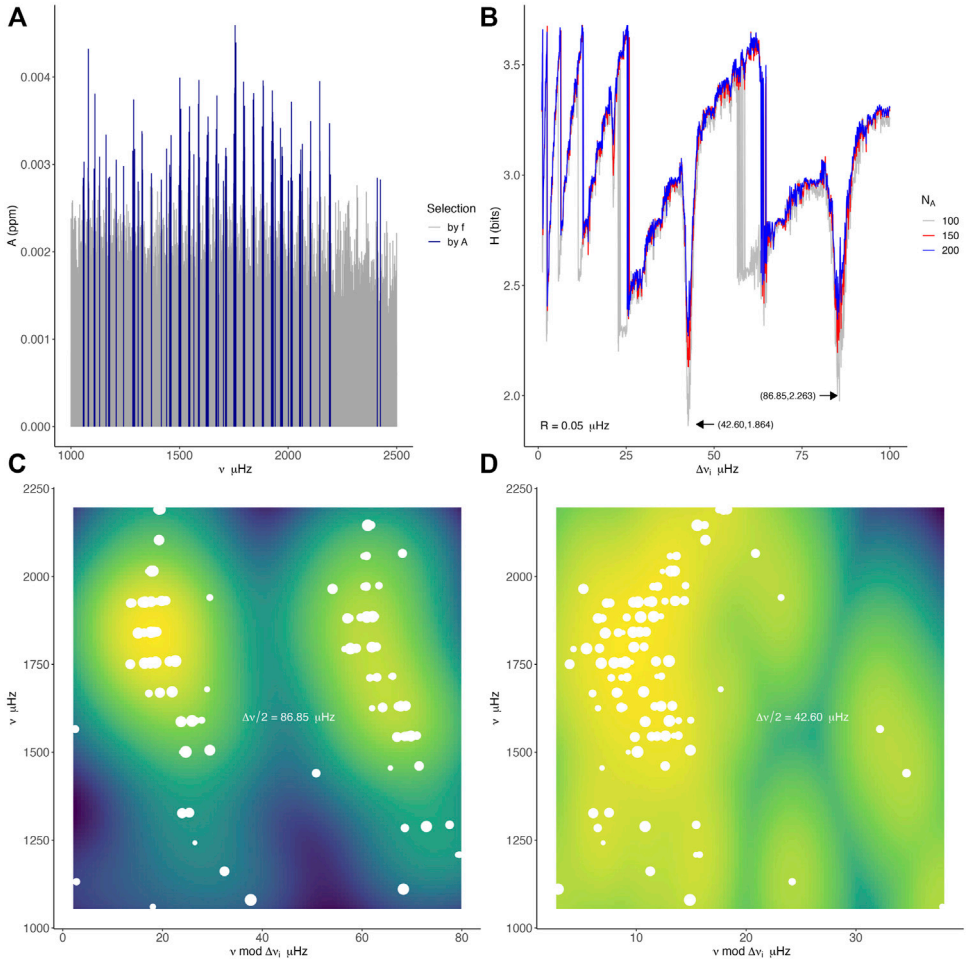

FIGURE 3
Panel **(A)** depicts the oscillation spectrum in the frequency range where p-modes are found (in grey), and a selection of N_A =100 frequencies from that range with the largest amplitude (an explanation of this arbitrary number is given in the discussion section). Panel **(B)** shows the entropy spectrum (HSpec) computed for three different numbers of large amplitude frequencies: N_A = 100, 150, and 200. Notice that the minimum H value is found for the half of the observed large separation whatever N_A. Panels **(C,D)** show the échelle diagram for both the estimated large separation and its half. As for panel 3, the size of white dots is proportional to the amplitude of the modes, and the background is the 2D density of the échelle diagrams..

using échelle diagrams, its value is confirmed (Figure 1A). In addition, in those studies a rotational splitting in the range of 3.5 – 6 μHz is also reported.

Following the procedure explained in the previous section, we built the entropy spectrum for HD 49933 by first selecting the frequency range, and second, by keeping only a set of frequencies with the largest amplitudes. This procedure, similar to the one followed in García Hernández et al. (2009), helps us to obtain better results, assuming that the modes with the highest amplitudes (in general low-degree modes when observed with photometry) are those that mostly contribute to $\Delta\nu$. Figure 3 shows the aforementioned selection (panel A) and the HSpec (panel B) for HD 49993.

As expected, HSpec shows high variability with different entropy minima corresponding to, say, local states of low H. When exploring low $\Delta\nu_i$ values peaks may correspond with échelle diagrams with a too small number of points. From the information theory interpretation, this is equivalent to the presence of a pattern; hence, the actual H value may be similar. Therefore, as happens for the DFT method, the peaks in that range will not be considered in this first study.

It can be seen that the absolute minimum (H = 1.864 bits) within the range of $\Delta\nu$ is reached for $\Delta\nu_i$ = 42.60 μHz, which is half of the large separation found by Benomar et al. (2009). The entropy spectrum was constructed with a resolution of R = 0.05 μHz. If we consider this resolution as the uncertainty of

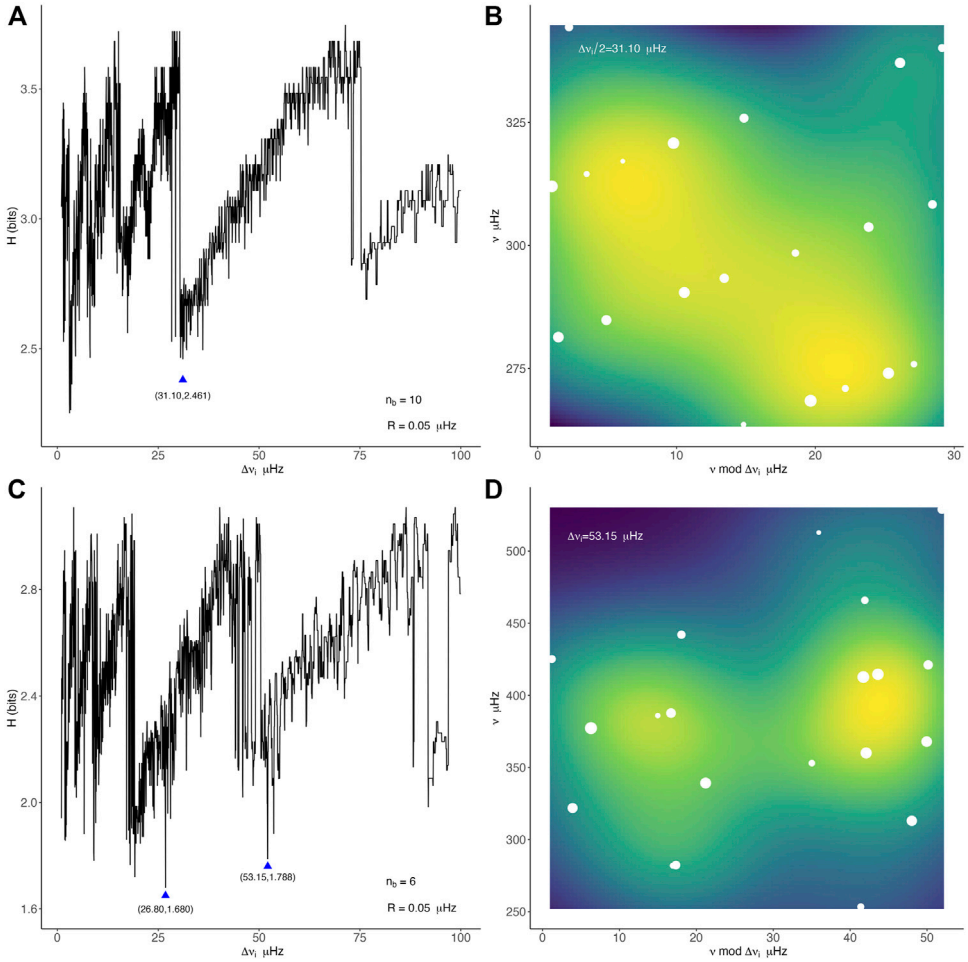

FIGURE 4
Entropy spectrum (HSpec) for HD 174966 **(A)** and HD 174936 **(C)**. Panels **(B,D)** show the resulting échelle diagram (white dots) for the large separation determined by the HSpec in panels **(A,B)**, respectively. The size of dots is proportional to the amplitude of the modes. Background corresponds with the 2D density of the échelle diagrams, which help to visually guess the probability distribution of the points in both vertical and horizontal axes. Notice that for HD 174966, the échelle diagram is built for the half of the large separation, corresponding to the absolute minimum in HSpec.

the estimate, the detected periodicity would thus be $\Delta\nu_i$ = 42.60 ± 0.05 μHz. However, this must be considered with caution, since a comprehensive analysis of the different sources of errors must be done in order to properly estimate the uncertainty of $\Delta\nu$. As an example, the HSpec shows different local minima and even some shifts in $\Delta\nu$ when using a different amount of frequencies of highest amplitude to construct the échelle diagrams for each $\Delta\nu_i$. The depth and width of the peaks and their relation might be good estimators for the uncertainty in the measure when all the error sources are included. They can be modified by, for example, the number of frequencies, number of bins used to construct the probability distribution, method used to estimate entropy, etc. (see Section 2). This however exceeds the scope of this exploratory work. As for the DFT and AC, the HSpec show both the large separation and its submultiples. The presence of an absolute minimum may be used to consider that periodicity as the one to which more modes are contributing due to their visibility.

3.2 The HSpec of the δ *Scuti* stars HD 174936 and HD 174966

These objects are two of the best-known δ *Scuti* stars, for which there is a reliable determination of the large separation using the discrete Fourier transform method. Any method based on statistical estimators has an intrinsic dependence upon the number of realizations (observations). This is the case of the discrete Fourier transform, autocorrelation (AC), and histogram of frequency differences (HFD),

currently used for determining the large separation of δ *Scuti* stars[2].

As for HD 49993, the light curves of both δ *Scuti* stars were observed by the *CoRoT* satellite (Seismo Field). Their oscillation spectra were obtained from the fractal analysis of the pre-whitening process (see De Franciscis et al., 2018; De Franciscis et al., 2019, for more details). That method allowed us to find the harmonic content of the light curve without imposing any statistical criterion about the significance, thereby minimizing the presence of spurious peaks, which is key to avoid any distortion in the échelle diagrams and hence on the computation of HSpec.

As it happens in other statistical methods (DFT, autocorrelation function, etc.), the detection of regularities in these stars is more difficult, due to the complexity of their oscillation spectrum (see Goupil et al., 2005, for an interesting review of the asteroseismology of δ *Scuti stars*). In contrast to the HSpec of HD 49993, the number of bins, resolution, and frequency domain play an important role in the determination of the large separation. This implies to perform several iterations to find the optimum HSpec from which the $\Delta\nu$ and its multiples (and submultiples) were determined.

Figure 4 depicts the HSpec for both stars together with the échelle diagram corresponding to the detected $\Delta\nu$. It is worth noting that the leftmost part of the entropy spectrum is quite similar to the one found for HD 49993, which reinforces the explanation of the peaks as a consequence of the lack points in the échelle diagram. When the number of frequencies is small this configuration may lead to the absolute minimum of entropy. This is the case of HD 174966, for which the second minimum is compatible with the half of the large separation determined by the DFT method $\Delta\nu = 65 \pm 1\ \mu$Hz (García Hernández et al., 2013). The next minima are above 75 μHz, far beyond twice the $\Delta\nu/2$. As discussed before, this may be caused by the way in which the distribution of probability is constructed.

Moreover, the number of bins used for HD 174966 is 10, while only six were sufficient for HD 174936. This is because although the total number of frequencies for both stars is somewhat similar (120 and 177 frequencies for HD 174966 and HD 174936, respectively), the frequency range in which the highest amplitude peaks are found is [250, 350] μHz for HD 174966 and [160, 650] μHz for HD 174936. This implies that échelle diagrams were built with 20 frequencies for HD 174966 and 127 frequencies for HD 174936.

For HD 174936, both the half of the large separation $\Delta\nu/2 = 28.80 \pm 0.05\ \mu$Hz and twice the value (i.e., the large separation) $\Delta\nu = 53.15 \pm 0.05\ \mu$Hz were found, which is compatible with the large separation found using the DFT technique, that is, $\Delta\nu = 52 \pm 10\ \mu$Hz (García Hernández et al., 2009). Notice that, once again the absolute minimum within the range of explored $\Delta\nu_i$ is identified with the half of the large separation, which might be interpreted in terms of the modes' visibility.

In addition, the échelle diagram of HD 174936 frozen at its large separation shows a glimpse of the classical échelle configuration with two vertical ridges composed by the modes with the highest amplitudes. In contrast, this configuration is not visible in the échelle diagram of HD 174966, but a series of inclined fringes with no clear pattern for the modes with the highest amplitudes. A similar distribution of points in the échelle diagram is found for twice $\Delta\nu/2$, even if this is not clearly a minimum in HSpec.

Regarding the values of H, it can be seen that the HSpec of HD 17966 is shifted by about 1 bit on average respect to the HSpec of HD 174936. Since there is no reference value for the entropy, except maybe its average over the HSpec, which allows us to calculate some statistics, there is no way to compare two HSpec by their absolute H values. The hypothesis that seems more plausible to explain such a shift is the amount of frequencies that are actually contributing to the large separation.

4 Discussion

The entropy spectrum analysis was found to be reliable and robust for the solar-like pulsator HD 49993. For this star $\Delta\nu/2$ and $\Delta\nu$ were found the two minima of the HSpec. As happens with other methods mentioned previously, additional information is required to spot $\Delta\nu$ multiples or submultiples, and thereby the actual value of $\Delta\nu$. This has implications on the visibility of the modes which are inherently related with the angle of inclination of the star respect to the observer.

For the two selected δ *Scuti* stars HD 174966 and HD 174936 HSpec was able to accurately determine the periodicities corresponding to either the large separation or its half. However, in contrast to HD 49993, the optimum HSpec was obtained by several iterations with different combinations of frequency ranges, number of bins, and number of frequencies with the highest amplitudes. Although this is an evident limitation of the method, the HSpec looks promising as a tool to determine the large separation of δ *Scuti* stars, even for oscillation spectra containing a few tens of modes.

In order to render the method here presented more robust, it is necessary to minimize both the human supervision and the additional information required to accurately determine the large separation of δ *Scuti* stars. The next steps will thus be focused on improving the treatment of the probability distribution of the échelle diagram points. I envisage to work on two main aspects: 1) the enhancement of the signal through the échelle diagrams, i.e., to implement a modified version of those diagrams that enhance the vertical alignment features in

2 Throughout the study, when referring to large separation in δ *Scuti* stars means the low-order (n = [2, 8–10]) large separation.

the probability distribution, and 2) the incorporation of joint probability distribution that accounts for the relation between *nu* ad ν modulo $\Delta\nu_j$. For 1) there is well-known method widely used for solar-like pulsators, the so-called collapsed échelle diagrams (see e.g., Corsaro et al., 2012, and references therein). These collapsed échelle diagrams take into account the entire observed power spectrum, which may render transitions between entropic states smoother. The background signal would also be present so it might be used somewhat as reference entropy for each star. Another interesting point is that it can be quite fast since no pre-whitening process is necessary, so it might be used in pipelines for asteroseismic analyses. Regarding the joint probability distributions 2), the inclusion of an additional dimension, the distribution of frequencies, might render HSpec method more sensitive to the presence of vertical patterns than any other patterns (for instance tilted ridges or even diagonal fringes).

Data availability statement

The original contributions presented in the study are included in the article further inquiries can be directed to the corresponding author.

Author contributions

JCS is the unique contributor to this work, from conception of the idea to development, test, and manuscript writing.

Funding

This work has been supported by Spanish public funds for research under project "Contribution of the UGR to the PLATO2.0 space mission. Phase C/D-1", funded by MCNI/AEI/PID2019-107061GB-C64.

Acknowledgments

JCS acknowledges support by University of Granada and by Spanish public funds for research under project "Contribution of the UGR to the PLATO2.0 space mission. Phase C/D-1", funded by MCNI/AEI/PID2019-107061GB-C64.

Conflict of interest

The author declares that the research was conducted in the absence of any commercial or financial relationships that could be construed as a potential conflict of interest.

Publisher's note

References

Aerts, C., Christensen-Dalsgaard, J., and Kurtz, D. W. (2010). *Asteroseismology*. Dordretch, Netherlands: Springer. doi:10.1007/978-1-4020-5803-5

Appourchaux, T., Michel, E., Auvergne, M., Baglin, A., Toutain, T., Baudin, F., et al. (2008). CoRoT sounds the stars: p-Mode parameters of sun-like oscillations on HD 49933. *Astron. Astrophys.* 488, 705–714. doi:10.1051/0004-6361:200810297

Baglin, A., Auvergne, M., Barge, P., Deleuil, M., Catala, C., Michel, E., et al. (2006). "Scientific objectives for a minisat: CoRoT," in *ESA special publication*. Editors M. Fridlund, A. Baglin, J. Lochard, and L. Conroy (Noordwijk, Netherlands: ESTEC), 33.

Barceló Forteza, S., Moya, A., Barrado, D., Solano, E., Martín-Ruiz, S., Suárez, J. C., et al. (2020). Unveiling the power spectra of δ Scuti stars with TESS. The temperature, gravity, and frequency scaling relation. *Astron. Astrophys.* 638, A59. doi:10.1051/0004-6361/201937262

Barceló Forteza, S., Roca Cortés, T., García Hernández, A., and García, R. A. (2017). Evidence of chaotic modes in the analysis of four δ Scuti stars. *Astron. Astrophys.* 601, A57. doi:10.1051/0004-6361/201628675

Barceló Forteza, S., Roca Cortés, T., and García, R. A. (2018). The envelope of the power spectra of over a thousand δ Scuti stars. The - $\nu_{\max}$ scaling relation. *Astron. Astrophys.* 614, A46. doi:10.1051/0004-6361/201731803${\bar{T}}_{\spmathit{{eff}}}}$

Bedding, T. R., Murphy, S. J., Hey, D. R., Huber, D., Li, T., Smalley, B., et al. (2020). Very regular high-frequency pulsation modes in young intermediate-mass stars. *Nature* 581, 147–151. doi:10.1038/s41586-020-2226-8

Benomar, O., Baudin, F., Campante, T. L., Chaplin, W. J., García, R. A., Gaulme, P., et al. (2009). A fresh look at the seismic spectrum of HD49933: Analysis of 180 days of CoRoT photometry. *Astron. Astrophys.* 507, L13–L16. doi:10.1051/0004-6361/200913111

Breger, M., Pamyatnykh, A. A., Pikall, H., and Garrido, R. (1999). The δ Scuti star FG virginis IV. Mode identifications and pulsation modelling. *Astronomy Astrophysics* 341, 151–162.

Cincotta, P. M., Helmi, A., Mendez, M., Nunez, J. A., and Vucetich, H. (1999). Astronomical time-series analysis – II. A search for periodicity using the Shannon entropy. *Mon. Notices R. Astronomical Soc.* 302, 582–586. doi:10.1046/j.1365-8711.1999.02128.x

Cincotta, P. M., Mendez, M., and Nunez, J. A. (1995). Astronomical time series analysis. I. A search for periodicity using information entropy. *Astrophys. J.* 449, 231. doi:10.1086/176050

Corsaro, E., McKeever, J. M., and Kuszlewicz, J. S. (2020). Fast and automated peak bagging with DIAMONDS (FAMED). *Astron. Astrophys.* 640, A130. doi:10.1051/0004-6361/202037930

Corsaro, E., Stello, D., Huber, D., Bedding, T. R., Bonanno, A., Brogaard, K., et al. (2012). Asteroseismology of the open clusters ngc6791, ngc6811, and ngc6819 from 19 months of kepler photometry. *Astrophys. J.* 757, 190. doi:10.1088/0004-637X/757/2/190

De Franciscis, S., Pascual-Granado, J., Suárez, J. C., García Hernández, A., and Garrido, R. (2018). Fractal analysis applied to light curves of δ Scuti stars. *Mon. Not. R. Astron. Soc.* 481, 4637–4649. doi:10.1093/mnras/sty2496

De Franciscis, S., Pascual-Granado, J., Suárez, J. C., García Hernandez, A., Garrido, R., Lares-Martiz, M., et al. (2019). A fractal analysis application of the

pre-whitening technique to δ Scuti stars time series. *Mon. Not. R. Astron. Soc.* 487, 4457–4463. doi:10.1093/mnras/stz1571

García Hernández, A., Martín-Ruiz, S., Monteiro, M. J. P. F. G., Suárez, J. C., Reese, D. R., Pascual-Granado, J., et al. (2015). Observational δ ν –$\bar{\rho }$ relation for δ sct stars using eclipsing binaries and space photometry. *Astrophys. J.* 811, L29. doi:10.1088/2041-8205/811/2/l29

García Hernández, A., Moya, A., Michel, E., Garrido, R., Suárez, J. C., Rodríguez, E., et al. (2009). Asteroseismic analysis of the CoRoT δ Scuti star HD 174936. *Astron. Astrophys.* 506, 79–83. doi:10.1051/0004-6361/200911932

García Hernández, A., Moya, A., Michel, E., Suárez, J. C., Poretti, E., Martín-Ruíz, S., et al. (2013). An in-depth study of HD 174966 with CoRoT photometry and HARPS spectroscopy. Large separation as a new observable for δ Scuti stars. *Astron. Astrophys.* 559, A63. doi:10.1051/0004-6361/201220256

Goupil, M. J., Dupret, M. A., Samadi, R., Boehm, T., Alecian, E., Suárez, J. C., et al. (2005). Asteroseismology of δ Scuti stars: Problems and prospects. *J. Astrophys. Astron.* 26, 249–259. doi:10.1007/bf02702333

Handler, G. (2009). "Delta Scuti variables," in Proceedings of the International Conference. AIP Conference Proceedings, Melville, NY Vol. 1170, 403–409.

Hausser, J., and Strimmer, K. (2009). Entropy inference and the james-stein estimator, with application to nonlinear gene association networks. *J. Mach. Learn. Res.* 10, 1469–1484.

Hekker, S., and Christensen-Dalsgaard, J. (2016). Giant star seismology. *Astron. Astrophys. Rev.* 49, 1. doi:10.1007/s00159-017-0101-x

Hernández, A. G., Suárez, J. C., Moya, A., Monteiro, M. J. P. F. G., Guo, Z., Reese, D. R., et al. (2017). Precise surface gravities of δ Scuti stars from asteroseismology. *Mon. Notices R. Astronomical Soc. Lett.* 471, L140–L144. doi:10.1093/mnrasl/slx117

Kallinger, T. (2019). Release note: Massive peak bagging of red giants in the Kepler field. arXiv e-prints , arXiv:1906.09428.

Koch, D. G., Borucki, W. J., Basri, G., Batalha, N. M., Brown, T. M., Caldwell, D., et al. (2010). Kepler mission design, realized photometric performance, and early science. *Astrophys. J.* 713, L79–L86. doi:10.1088/2041-8205/713/2/l79

Malakar, N. K., Knuth, K. H., and Lary, D. J. (2012). Maximum joint entropy and information-based collaboration of automated learning machines. *AIP Conf. Proc.* 1443, 230–237. doi:10.1063/1.3703640

Miglio, A., Chaplin, W. J., Brogaard, K., Lund, M. N., Mosser, B., Davies, G. R., et al. (2016). Detection of solar-like oscillations in relics of the milky way: asteroseismology of K giants in M4 using data from the NASA K2 mission. *Mon. Not. R. Astron. Soc.* 461, 760–765. doi:10.1093/mnras/stw1555

Miglio, A., Chiappini, C., Morel, T., Barbieri, M., Chaplin, W. J., Girardi, L., et al. (2013). Galactic archaeology: Mapping and dating stellar populations with asteroseismology of red-giant stars. *Mon. Not. R. Astron. Soc.* 429, 423–428. doi:10.1093/mnras/sts345

Mirouh, G. M., Angelou, G. C., Reese, D. R., and Costa, G. (2019). Mode classification in fast-rotating stars using a convolutional neural network: Model-based regular patterns in ' Scuti stars. *Mon. Notices R. Astronomical Soc. Lett.* 483, L28–L32. doi:10.1093/mnrasl/sly212

Mosser, B., and Appourchaux, T. (2009). On detecting the large separation in the autocorrelation of stellar oscillation times series. *Astron. Astrophys.* 508, 877–887. doi:10.1051/0004-6361/200912944

Moya, A., Suárez, J. C., García Hernández, A., and Mendoza, M. A. (2017). Semi-empirical seismic relations of A-F stars from CoRoT and Kepler legacy data. *Mon. Not. R. Astron. Soc.* 471, 2491–2497. doi:10.1093/mnras/stx1717

Nielsen, M. B., Davies, G. R., Ball, W. H., Lyttle, A. J., Li, T., Hall, O. J., et al. (2021). PBjam: A Python package for automating asteroseismology of solar-like oscillators. *Astron. J.* 161, 62. doi:10.3847/1538-3881/abcd39

Ouazzani, R.-M., Roxburgh, I. W., and Dupret, M.-A. (2015). Pulsations of rapidly rotating stars. II. Realistic modelling for intermediate-mass stars. *Astron. Astrophys.* 579, A116. doi:10.1051/0004-6361/201525734

Pamos Ortega, D., García Hernández, A., Suárez, J. C., Pascual Granado, J., Barceló Forteza, S., Rodón, J. R., et al. (2022). Determining the seismic age of the young open cluster α Per using δ Scuti stars. *Mon. Not. R. Astron. Soc.* 513, 374–388. doi:10.1093/mnras/stac864

Paparó, M., Benkő, J. M., Hareter, M., and Guzik, J. A. (2016). Unespected series of regular spacing of S δ Scuti stars in the non-asymptotic regime. I. The methodology. *Astrophys. J.* 822, 100. doi:10.3847/0004-637X/822/2/100

Pascual-Granado, J., Garrido, R., and Suárez, J. C. (2015). Miarma: A minimal-loss information method for filling gaps in time series. *Astron. Astrophys.* 575, A78. doi:10.1051/0004-6361/201425056

Pascual-Granado, J., Suárez, J. C., Garrido, R., Moya, A., Hernández, A. G., Rodón, J. R., et al. (2018). Impact of gaps in the asteroseismic characterization of pulsating stars. *Astron. Astrophys.* 614, A40. doi:10.1051/0004-6361/201732431

Paxton, B., Smolec, R., Schwab, J., Gautschy, A., Bildsten, L., Cantiello, M., et al. (2019). Modules for experiments in stellar astrophysics (mesa): Pulsating variable stars, rotation, convective boundaries, and energy conservation. *Astrophys. J. Suppl. Ser.* 243, 10. doi:10.3847/1538-4365/ab2241

Ramón-Ballesta, A., García Hernández, A., Suárez, J. C., Rodón, J. R., Pascual-Granado, J., Garrido, R., et al. (2021). Study of rotational splittings in δ Scuti stars using pattern finding techniques. *Mon. Not. R. Astron. Soc.* 505, 6217–6224. doi:10.1093/mnras/stab1719

Reegen, P. (2007). SigSpec. I. Frequency- and phase-resolved significance in Fourier space. *Astron. Astrophys.* 467, 1353–1371. doi:10.1051/0004-6361:20066597

Reese, D., Lignières, F., and Rieutord, M. (2008). Regular patterns in the acoustic spectrum of rapidly rotating stars. *Astron. Astrophys.* 481, 449–452. doi:10.1051/0004-6361:20078075

Rodríguez-Martín, J. E., García Hernández, A., Suárez, J. C., and Rodón, J. R. (2020). Study of the low-order $\Delta\nu$-ρ^{-} relation for moderately rotating δ Scuti stars and its impact on their characterization. *Mon. Not. R. Astron. Soc.* 498, 1700–1709. doi:10.1093/mnras/staa2378

Shannon, C. E. (1948). A mathematical theory of communication. *Bell Syst. Tech. J.* 27, 379–423. doi:10.1002/j.1538-7305.1948.tb01338.x

Suárez, J. C., and Goupil, M. J. (2008). Filou oscillation code. *Astrophys. Space Sci.* 316, 155–161. doi:10.1007/s10509-007-9568-7

Suárez, J. C., Goupil, M. J., and Morel, P. (2006). Effects of moderately fast shellular rotation on adiabatic oscillations. *Astron. Astrophys.* 449, 673–685. doi:10.1051/0004-6361:20054181

Suárez, J. C., Hernández, A. G., Moya, A., Rodrigo, C., Solano, E., Garrido, R., et al. (2014). Measuring mean densities ofδScuti stars with asteroseismology. *Astron. Astrophys.* 563, A7. doi:10.1051/0004-6361/201322270

Tourassi, G. D., Frederick, E. D., Markey, M. K., and Floyd, C. E. (2001). Application of the mutual information criterion for feature selection in computer-aided diagnosis. *Med. Phys.* 28, 2394–2402. doi:10.1118/1.1418724

Walker, G., Matthews, J., Kuschnig, R., Johnson, R., Rucinski, S., Pazder, J., et al. (2003). *The MOST Asteroseismology Mission: Ultraprecise Photometry from Space*. (Bristol, England: Publications of the Astronomical Society of the Pacific) Vol. 115, 1023–1035.

frontiers | Frontiers in Astronomy and Space Sciences

TYPE Brief Research Report
PUBLISHED 30 August 2022
DOI 10.3389/fspas.2022.948180

OPEN ACCESS

EDITED BY
Javier Pascual Granado,
Institute of Astrophysics of Andalusia (CSIC), Spain

REVIEWED BY
Simon Murphy,
University of Southern Queensland, Australia
Dominic Bowman,
KU Leuven, Belgium

*CORRESPONDENCE
Joyce A. Guzik,
joy@lanl.gov

SPECIALTY SECTION
This article was submitted to Stellar and Solar Physics, a section of the journal Frontiers in Astronomy and Space Sciences

RECEIVED 19 May 2022
ACCEPTED 11 July 2022
PUBLISHED 30 August 2022

CITATION
Guzik JA, Jackiewicz J and Hedlund AM (2022), Revisiting the δ Scuti star FG Virginis using Kepler K2 and TESS data. *Front. Astron. Space Sci.* 9:948180. doi: 10.3389/fspas.2022.948180

Revisiting the δ Scuti star FG Virginis using *Kepler K2* and *TESS* data

Joyce A. Guzik[1]*, Jason Jackiewicz[2] and Anne M. Hedlund[1,2]

[1]Los Alamos National Laboratory, Los Alamos, NM, United States, [2]Department of Astronomy, New Mexico State University, Las Cruces, NM, United States

FG Virginis is a δ Scuti variable star that was the target of several ground-based multisite photometric campaigns from 1992 to 2004. Over 75 pulsation frequencies were detected (Breger et al., Astron. Astrophys., 2005, 435, 955–965), more than for any other δ Sct star before the era of space photometry. FG Vir was observed for 52 days in 30-minute cadence photometry by the NASA *Kepler* spacecraft *K2* mission in 2016, and for 23 days in 2-minute cadence photometry by the NASA *TESS* spacecraft in 2021. We present light curves and amplitude spectra obtained from these space missions. We find around 30 significant frequencies in the *K2* data, and more than 100 significant frequencies in the *TESS* data. There is good correspondence between the first 10 or so highest-amplitude modes found in the *K2* and *TESS* data and those found from the ground-based multisite campaigns, although the amplitude order is slightly different, indicating some stability in mode frequencies and amplitudes spanning 20 years. However, the 9th highest-amplitude mode of Breger et al. has moved down considerably in amplitude rank, while the 35th highest-amplitude mode has moved up to near the top ten as seen in both the *K2* and *TESS* data. We find several low frequencies between 0.3 and 3 cycles per day in the *TESS* data that were not detected using the ground-based data. If low-frequency pulsations are confirmed, FG Vir would be classified as a δ Sct/γ Dor hybrid variable star. We also review stellar model results and some of the challenges for asteroseismology for this well-studied δ Sct star.

KEYWORDS

stars: pulsations, stars: evolution, asteroseismology, stars: FG Vir, NASA Kepler mission, NASA TESS mission, NASA K2 mission, stars: δ Scuti

1 Introduction

The δ Scuti variables lie at the intersection of the classical Cepheid instability strip with the main sequence (Aerts et al., 2010; Kurtz 2022). They have spectral types A through mid F, effective temperatures 6400–8600 K (Uytterhoeven et al., 2011), and masses 1.4–2.7 $M_{\odot}$ (Bowman and Kurtz, 2018). Most are in the main-sequence (core hydrogen burning) or slightly post-main-sequence (burning hydrogen in a shell just outside the hydrogen-exhausted core) evolutionary phases, but they have also been found in the pre-main-sequequence phase (see, e.g., Zwintz and Steindl 2022; Murphy et al.,

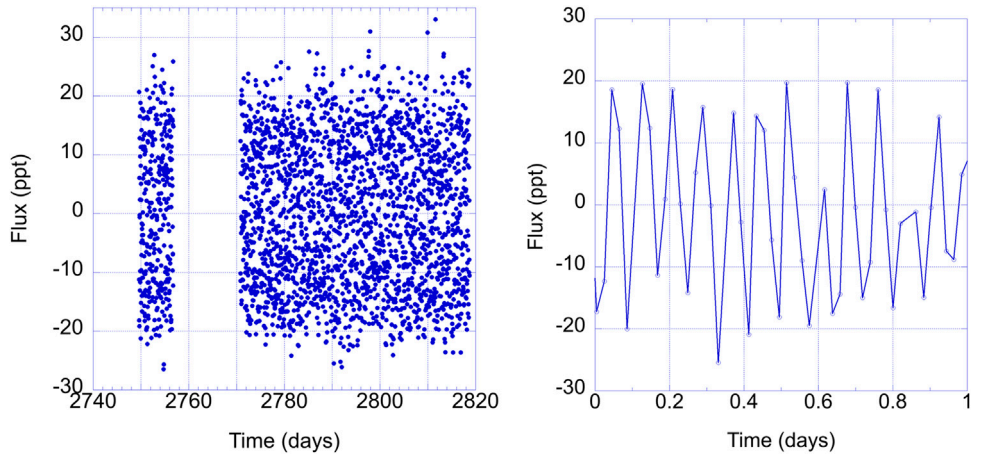

FIGURE 1
Left: FG Vir *K2* 30-min cadence light curve from Campaign 10, showing 52.5 days of data, excluding the gap near the beginning of the data set. Time is measured after barycentric Julian day 2454833.0. Right: Zoom-in on FG Vir *K2* light curve on day 2790.

2021). δ Scuti stars pulsate with frequencies 5–50 c/d (Balona et al., 2015) in one or more radial and non-radial low-order pressure (p) modes, low-order gravity (g) modes, and modes having a mixture of p- and g-type nodes. Their pulsations are driven by the "kappa" opacity-valving effect in the 2nd helium ionization region of the stellar envelope around 50,000 K (Chevalier 1971); in some δ Sct stars the hydrogen ionization region and turbulent pressure may also play a role in pulsation driving (Antoci et al., 2019).

These stars are of interest for asteroseismology, i.e., using the pulsation properties in conjunction with modeling to derive stellar interior structure and to test theories of stellar evolution and pulsation driving (see, e.g., Antoci et al., 2019; Bowman et al., 2021; Daszynska-Daszkiewicz et al., 2021, 2022).

FG Virginis (HD 106384) is a well-studied bright (V = 6.558) δ Scuti star of spectral type A8. FG Vir was the object of ground-based single-site (1982; see Lopez de Coca et al., 1984) and multisite (1992–2004; see Breger et al., 1995, 1996, 1998, 2004, 2005; Breger and Lenz 2019) photometric campaigns. These campaigns resulted in detection of 75+ pulsation frequencies (Breger et al., 2005), more than any other δ Sct star before the era of long time-series space photometric missions such as CoRoT (Poretti et al., 2009), *Kepler* (Borucki et al., 2010; Gilliland et al., 2010; Koch et al., 2010), and *TESS* (Ricker et al., 2015). See also Guzik (2021) and Daszynska-Daszkiewicz et al. (2005, 2021) for more information about δ Sct stars and results from space missions.

FG Vir was observed for 52.5 days in 30-minute cadence photometry by the NASA *Kepler* spacecraft during Campaign 10 (6 July–20 September 2016) of the extended *Kepler* mission (*K2*, Howell et al., 2014) as part of our request to the Guest Observer program (Guzik et al., 2019). FG Vir was observed by the NASA *TESS* spacecraft for 23 days in December 2021. We present a first look at the amplitude spectra derived from these data, and comparisons with the amplitude spectra obtained using the ground-based multisite data. We also review some of the findings from asteroseismology and unanswered questions for this interesting δ Sct star.

2 *Kepler* data analysis and results

FG Vir is EPIC 201132898 in the *K2* Ecliptic Plane Input Catalog (Huber et al., 2016). We retrieved the pre-search data conditioning simple-aperture photometry (PDC_SAP) light-curve data from the Mikulski Archive for Space Telescopes (MAST, https://archive.stsci.edu/), *K2* pipeline data release 37, January 2020. Figure 1 shows the *K2* light curve and a 1-day zoom-in on a portion of the light curve. Figure 2 shows the amplitude spectrum resulting from a Fourier analysis of the light curve and the amplitude spectrum after pre-whitening all frequencies with amplitude >1 ppt. To determine the significant frequencies, the highest-amplitude modes were removed from the light curve successively until only noise remained, a process called pre-whitening. For evenly spaced 29.4244-min cadence data, the Nyquist frequency limit is 24.4695 c/d, so the amplitude spectrum is truncated at this frequency. In reality, the *K2* data are not exactly evenly spaced because of light travel-time corrections due to the spacecraft's orbit around the solar system barycenter (Murphy et al., 2013).

Table 1 lists the 34 frequencies obtained from the pre-whitening analysis in order of signal-to-noise (S/N) ratio, down to S/N = 4.0. Uncertainties on frequencies and amplitudes were calculated using the process derived by

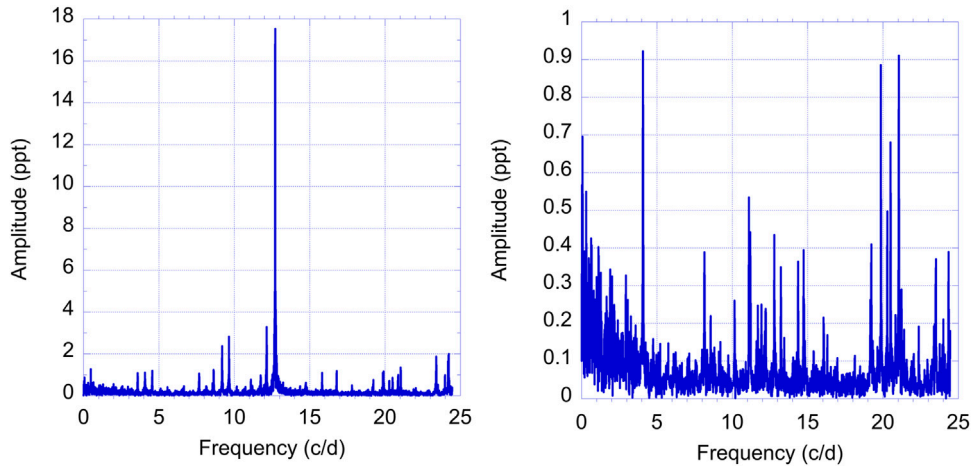

FIGURE 2
Left: FG Vir *K2* amplitude spectrum from 0 to 24.5 c/d. Right: Amplitude spectrum after pre-whitening modes with amplitude >1 ppt.

Montgomery and O'Donoghue (1999). Table 1 also notes associations of these frequencies with those from Breger et al. (2005) obtained using multisite observations. Considering the first 9 modes, all of them are found among the 10 highest-amplitude modes of Breger et al., although the amplitude ordering is slightly different. Breger et al.'s 9th highest-amplitude mode (frequency 19.228 c/d) is only the 14th highest-amplitude using the *K2* data. Many of the remaining frequencies found in the *K2* data can be associated with the Breger et al. frequencies. It is interesting that the 35th highest-amplitude mode in the Breger et al. list (frequency 20.511 c/d) corresponds to the 11th highest in the *K2* data. While Breger et al. (2005) adopted a S/N limit of 4 for a significant detection, this limit may be too low for space-based data (Baran and Koen 2021; Bowman and Michielsen 2021) and so the list may contain some false detections. However, we find frequencies in the *K2* data associated with Breger et al. (2005) frequencies down to a S/N of 4 and lower. Frequencies at 11.69952 and 11.94247 c/d were also found in the *K2* data, corresponding to f33 and f29, respectively, in the Breger et al. list, but these modes have S/N ratio 3.27 and 3.14, respectively, in the *K2* analysis, and were not included in the table.

To compensate for the loss of a second reaction wheel, the *K2* mission used solar radiation pressure to keep the spacecraft pointed in the same direction, and in addition fired thrusters every 5.8849 h (*K2* Handbook, Mighell and Van Cleve 2020). The thruster-firing frequency of 4.0782 c/d and its harmonic at 8.1564 c/d appear in the *K2* frequency list.

We searched for combination frequencies by algorithm with tolerance of 10% of the inverse of the time series length. For the *K2* data with length 69.121 days, the tolerance is 0.001446 c/d. We found no combination frequencies among the list in Table 1.

Table 1 lists nine modes with frequencies 0.3 to ~3 c/d, in the right frequency range to be γ Dor gravity modes (see, e.g., Aerts et al., 2010; Li et al., 2020). Six of of these are among the lowest-amplitude modes, with S/N < 4.5, and are likely to be spurious. However, if low-frequency modes were to be detected, FG Vir would be considered a hybrid δ Sct/γ Dor variable-star candidate.

The multisite data is not evenly spaced, so the 24.4695 c/d *K2* Nyquist limit does not apply, and Breger et al. (2005) find frequencies up to 44.2591 c/d. One *K2* frequency at 14.36915 c/d was found that could be a Nyquist reflection of the 34.5737 f23 mode of the Breger et al. list. We also made use of the *TESS* data with higher Nyquist limit (see below) to verify that only this one frequency in the *K2* list is a Nyquist alias.

3 *TESS* data

The *Kepler* spacecraft was retired in November 2018; the *TESS* spacecraft (Ricker et al., 2015) was launched in April 2018 into a 13.7-day elliptical orbit around Earth, maintained by a 2:1 lunar resonance. *TESS* data for FG Vir is now available at MAST, taken during the 27.4 observing days of sector 46 (December 2–30, 2021). Moreover, data were taken at 2-minute cadence, so the S/N is much larger, and the Nyquist frequency limit is 360 c/d, much higher than for 30-min cadence *K2* data.

FG Vir is TIC 277227048 in the *TESS* Input Catalog (Stassun et al., 2019). Figure 3 (left) shows the *TESS* FG Vir light curve, including data from 22.84 days, excluding the gap of about 5 days in the middle of the data set. Figure 3 (right) shows a 1-day zoom-in on the light curve; small features are resolved in the *TESS* 2-min cadence light curve that were not resolvable in *K2* 30-min cadence light curve.

TABLE 1. FG Vir *K2* frequencies in order of S/N compared with Breger et al. (2005) frequencies. Low frequencies between 0.3 and ~3 c/d are highlighted using red font. The calculated uncertainties in *K2* frequencies and amplitudes, respectively, are 4.22×10^{-4} c/d and 50.1 ppm.

Freq. #	Freq. (c/d)	Amplitude (ppt)	S/N	Notes	Breger et al. freq. (c/d)	Breger et al. freq. #	Breger et al. S/N
f1	12.71617	15.943	171.48		12.7162	f1	442
f2	12.15361	2.805	30.19		12.1541	f2	85
f3	9.65608	2.667	28.90		9.6563	f5	71
f4	9.19909	2.062	22.16		9.1991	f7	53
f5	24.22769	1.868	19.54		24.2280	f3	74
f6	23.40337	1.676	17.95		23.4034	f4	71
f7	24.19443	1.441	15.34		24.1940	f10	29
f8	21.05045	1.188	12.50		21.0515	f6	55
f9	19.86748	0.959	10.26		19.8679	f8	55
f10	4.07820	0.775	9.96	*K2* thruster frequency			
f11	20.51103	0.815	8.52		20.5112	f35	6.6
f12	20.28543	0.630	7.00		20.2878	f11	26
f13	0.31527	0.593	6.53	Low frequency			
f14	19.22828	0.575	6.16		19.2278	f9	30
f15	11.10514	0.557	5.93		11.1034	f20	11
f16	4.09555	0.525	5.79				
f17	0.63921	0.474	5.64	Low frequency			
f18	0.52930	0.538	5.50	Low frequency			
f19	12.79427	0.492	5.28		12.7944	f17	13
f20	14.36915	0.479	4.94	Nyquist reflection	34.5737[a]	f23	9.3
f21	11.21071	0.479	4.88		11.2098	f38	6.4
f22	23.50894	0.442	4.76				
f23	13.23679	0.414	4.53		13.2365	f27	8.3
f24	14.73503	0.412	4.46		14.7354	f49	5.3
f25	1.91184	0.373	4.38	Low frequency			
f26	0.67536	0.411	4.34	Low frequency			
f27	8.15785	0.402	4.31	2x *K2* thruster frequency			
f28	1.29143	0.411	4.30	Low frequency			
f29	1.12657	0.406	4.25	Low frequency			
f30	24.34917	0.384	4.23		24.3485	f18	12
f31	0.49314	0.421	4.13	Low frequency			
f32	4.06518	0.386	4.07				
f33	21.23122	0.371	4.04		21.2323	f16	14
f34	0.47434	0.371	4.03	Low frequency			

[a]Frequency reflected around Nyquist frequency of 24.4695 c/d.

Figure 4 shows the FG Vir amplitude spectrum using *TESS* data, truncated at 50 c/d, and the amplitude spectrum after pre-whitening frequencies with amplitude >1 ppt. Figure 5 shows the K2 and TESS amplitude spectra overlayed. Table 2 lists the first 100 frequencies pre-whitened in order of amplitude, and notes associations with Breger et al. (2005) frequencies. Uncertainties on frequencies and amplitudes were determined using the process derived by Montgomery and O'Donoghue (1999). The highest frequency on this list is 42.1 c/d. The 9 highest-amplitude *TESS* frequencies are among the 10 highest-amplitude Breger et al. (2005) frequencies, although the amplitude order is slightly different. The 9th highest-amplitude frequency in the Breger et al. list is 28th highest in the *TESS* list, while f35 in the Breger et al. list is 11th highest in the *TESS* list, confirming the significant amplitude changes in these modes found using the *K2* data.

The S/N ratio of the 100th frequency in the list is 31, so it is likely that many more significant frequencies remain in the residual. Continued pre-whitening results in 718 additional frequencies with S/N ratio >4. However, we hesitate to claim that all of these frequencies are separate intrinsic frequencies. Handler (2009) points out several reasons why spurious small-amplitude peaks may be found in pre-whitening analyses. These

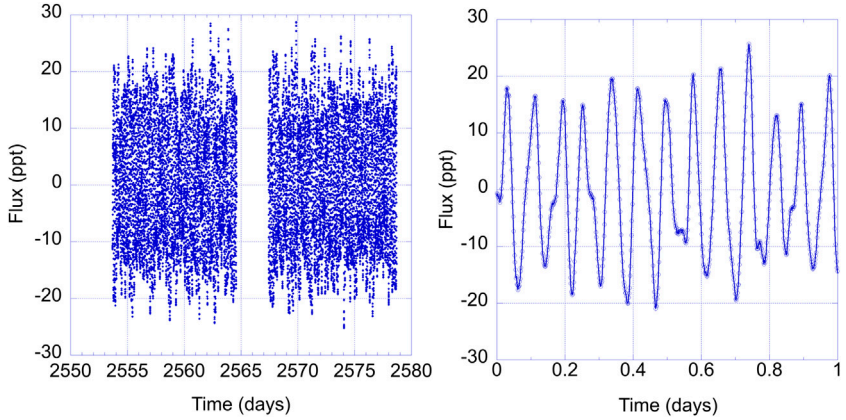

FIGURE 3
Left: FG Vir *TESS* 2-min cadence light curve from sector 46, showing 22.84 days of data, excluding the ~5-day gap in the middle of the data set. Time is measured after barycentric Julian day 2457000. Right: Zoom-in on *TESS* light curve on day 2560. Small features are resolved that were not resolved using *K2* 30-min cadence data.

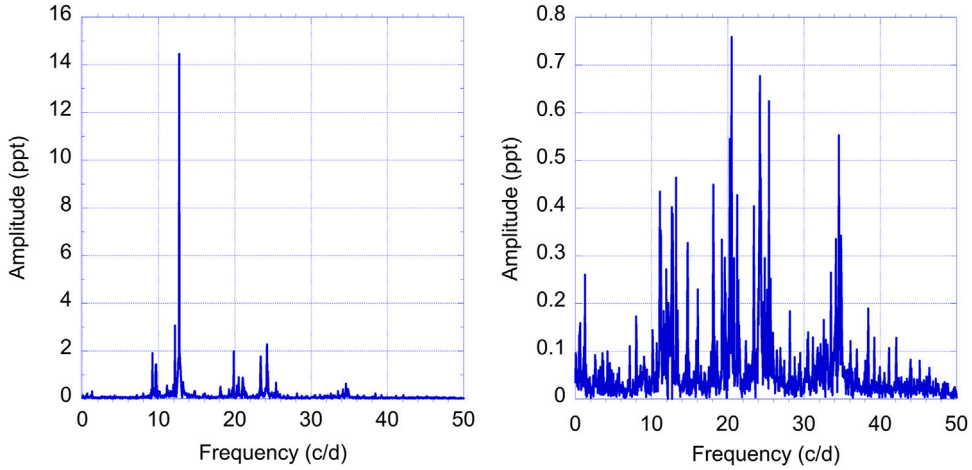

FIGURE 4
Left: FG Vir amplitude spectrum from *TESS* 2-min cadence data. Right: Amplitude spectrum after pre-whitening modes with amplitude >1 ppt.

reasons include short time-series limit, non-sinusoidal light curve shape, amplitude and frequency variations, and modulation from stellar or substellar companions.

Table 2 includes five low frequencies between 0.3 and ~3 c/d, highlighted in red font. These frequencies are more likely to be real, as opposed to the low frequencies in the *K2* data, as their S/N ratio is high. These low frequencies do not coincide with any of the likely spurious low frequencies found in the *K2* data. If confirmed as gravity-mode pulsations, FG Vir would be classified as a δ Sct/γ Dor hybrid. To confirm these frequencies would require ruling out spacecraft artifacts, light curve contamination by nearby or background objects, and rotation (possibly differential) and starspots as the source of the low frequencies. Time-series spectroscopy may be useful, e.g., to distinguish starspots, which may show signatures of chromospheric activity, or to detect line-profile variations on the expected timescales, indicating nonradial pulsations. Perhaps it may be possible to directly image starspots on FG Vir using optical interferometry (see, e.g., Cunha et al., 2007).

We searched for combination frequencies by algorithm with tolerance of 10% of the inverse of the time-series length. For the *TESS* data set with length 25.008 days, this tolerance is 0.003998 c/d. Because of this high tolerance, many combinations were found; however, many of these

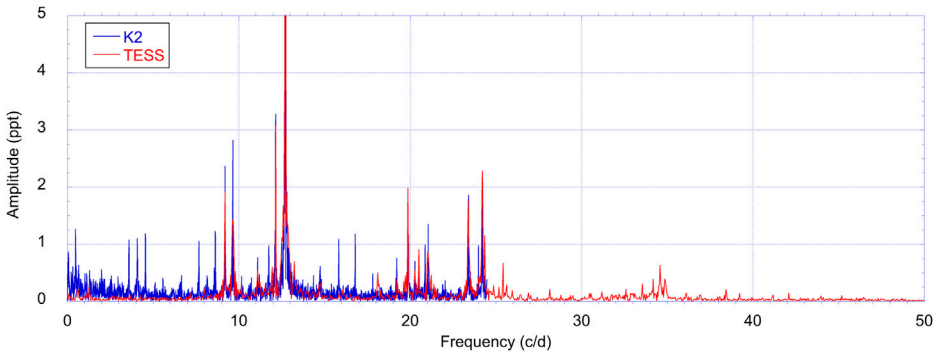

FIGURE 5
FG Vir *K2* and *TESS* amplitude spectra overlayed. The amplitude axis has been truncated at 5 ppt to show the low-amplitude peaks.

combinations involve lower-amplitude modes, and are likely to be fortuitous (see also discussions by Papics 2012; Kurtz et al., 2015). A longer series of *TESS* data would help to sort out intrinsic from combination frequencies.

The *Kepler/K2* photometry has a bandpass of 400–850 nm, while the *TESS* bandpass is redder, 600–1000 nm. Because of FG Vir's late-A spectral type, its mode amplitudes are therefore generally higher using the *K2* data compared to the TESS data. Although the *K2* and *TESS* data time series discussed in this paper are relatively short and non-overlapping, it is possible that phase differences between modes using photometric time-series data taken at different bandpasses could be exploited for mode identification in the same way that techniques using multi-color ground-based data were applied for FG Vir mode identification.

4 Unresolved questions for asteroseismology

As discussed by, e.g., Guzik (2021), there are many inter-related unresolved problems for δ Sct stars that make asteroseismology challenging.

First, there is a mode visibility problem for non-radial oscillations as seen in δ Sct stars. Temperature variations described by spherical harmonic patterns average out over the unresolved stellar disk, making higher degree (ℓ) modes more difficult to see in photometry. Usually, it is expected to detect modes of degree 0 (radial), 1 (dipole), and 2 (quadrupole). Is it possible to measure modes of degree $\ell = 3$ or higher, particularly with the higher precision and longer continuous time series of space-based photometry? Daszynska-Daszkiewicz et al. (2006) conclude that modes of degree $\ell = 3$ and probably much larger ℓ should be visible, even using the FG Vir ground-based data, and that most of the modes discovered for FG Vir below 30 c/d must have $\ell > 2$.

Second is the rotational splitting problem. Stellar rotation splits modes into a multiplet of $2\ell + 1$ frequencies. Rotation also shifts frequencies so that the multiplet members are not equally spaced (Goupil and Dziembowski 2000). Rotation can shift frequencies even for radial ($\ell = 0$) modes (see, e.g., Di Criscienzo et al., 2008) and the $m = 0$ multiplet of non-radial modes (Saio 1981). Rotation also makes a star oblate and changes its mean density, affecting the accuracy of radial mode frequencies predicted using non-rotating models (Murphy et al., 2022). FG Vir's equatorial rotation velocity is 30–80 km/sec (Mantegazza and Poretti 2002; Zima et al., 2006), so we should expect a rotational splitting frequency of around 0.5 c/d for FG Vir stellar radius ~2.2 $R_\odot$. We do not see obvious rotationally split modes in the FG Vir amplitude spectrum.

Third is the mode selection problem. Not all of the modes expected from stellar models for δ Sct stars are seen in the amplitude spectrum (see, e.g., Bedding et al., 2020; Murphy et al., 2021). Also, there are modes observed that are not expected from the best-fit pulsation models.

Then there is the mystery of amplitude and frequency variations found in many types of variable stars including δ Sct stars (see, e.g., Bowman et al., 2016). Amplitudes and frequencies of individual δ Sct modes can be relatively stable over time. It is possible to associate many of the highest-amplitude frequencies in the *K2* (2016) and *TESS* (2021) data sets with frequencies in the Breger et al. (2005) list. However, the order of the mode amplitudes is somewhat different for the first dozen or more modes; some modes appear in the *K2* and *TESS* data that are not in the Breger et al. list, and vice versa; and the Breger et al. f9 mode has moved down in amplitude rank, while the f35 mode increased in rank. Nonlinear mode-coupling effects (see, e.g., Buchler and Regev 1983; Buchler et al., 1997; Dziembowski 1993) are suspected as the cause of these variations.

TABLE 2. 100 highest S/N FG Vir *TESS* frequencies. Low frequencies between 0.3 and ~3 c/d are highlighted using red font. The calculated uncertainties in *TESS* frequencies and amplitudes, respectively, are 3.79×10^{-4} c/d and 9.82 ppm.

Freq. #	Freq. (c/d)	Amplitude (ppt)	S/N	Potential combinations and notes	Breger et al. freq. #
f1	12.7151	13.671	3776.72	—	f1
f2	24.2107	2.663	811.51	—	f3
f3	12.1553	2.468	702.20	—	f2
f4	9.6563	2.295	641.36	—	f5
f5	23.4070	2.029	577.76	—	f4
f6	19.8684	1.961	528.05	—	f8
f7	9.2005	1.793	498.21	—	f7
f8	21.0519	1.369	365.23	—	f6
f9	24.2427	0.996	253.82	—	
f10	24.1747	0.857	227.61	2f9-2f3	
f11	20.5121	0.795	226.58	—	f35
f12	34.5708	0.769	208.61	—	f23
f13	20.2882	0.756	204.74	—	f11
f14	25.4343	0.679	191.88	—	f15 = 2f1
f15	12.6871	0.580	182.56	—	
f16	18.1291	0.611	170.30	—	
f17	34.8826	0.570	168.79	—	
f18	11.0998	0.537	158.94	—	f20
f19	24.3547	0.557	150.51	—	
f20	11.2117	0.535	149.78	—	f38
f21	14.7344	0.534	148.38	3f8-2f2	f49
f22	13.2389	0.484	139.21	—	f27
f23	23.4350	0.363	133.53	—	f24
f24	21.2319	0.439	127.39	—	f16
f25	19.6445	0.414	116.93	—	f65
f26	12.7951	0.411	114.59	—	f17
f27	34.1949	0.393	105.00	—	f54?
f28	19.2286	0.361	101.11	—	f9
f29	11.9434	0.345	92.45	—	f29
f30	20.8320	0.329	91.89	—	f39
f31	33.5352	0.328	90.38	—	
f32	1.2875	0.310	87.64	2f11-2f6, low frequency	
f33	24.8705	0.267	76.71	1f3+1f1	f36 = f1+f2
f34	25.6342	0.273	73.29	3f24-3f15	f68
f35	23.4870	0.251	69.59	2f37-2f4	
f36	12.6072	0.199	69.52	—	
f37	16.0738	0.259	69.43	2f30-2f26	f13
f38	21.3998	0.257	68.96	1f27-1f26	f46
f39	25.1824	0.240	67.81	1f29+1f22	
f40	24.1428	0.288	67.40	—	
f41	19.3246	0.235	64.74	—	f41
f42	12.7511	0.230	64.23	—	
f43	12.1274	0.227	63.85	—	
f44	38.4173	0.220	61.63	1f16+1f13	
f45	28.1412	0.222	61.30	—	f19?
f46	11.6076	0.233	60.52	2f13-3f4	f50

(Continued on following page)

TABLE 2. (*Continued*) 100 highest S/N FG Vir *TESS* frequencies. Low frequencies between 0.3 and ~3 c/d are highlighted using red font. The calculated uncertainties in *TESS* frequencies and amplitudes, respectively, are 3.79×10^{-4} c/d and 9.82 ppm.

Freq. #	Freq. (c/d)	Amplitude (ppt)	S/N	Potential combinations and notes	Breger et al. freq. #
f47	13.4469	0.216	59.77	—	
f48	0.5038	0.210	58.49	2f41-3f1, low frequency	
f49	23.9988	0.216	58.14	—	f58
f50	23.3750	0.208	56.87	—	
f51	7.9889	0.199	56.34	—	f44
f52	34.1189	0.194	55.22	—	f72
f53	10.1721	0.190	54.33	—	f25
f54	24.5426	0.173	51.91	—	
f55	34.7627	0.183	51.33	—	
f56	22.3714	0.176	50.03	1f4+1f1	f42 = f1+f5
f57	12.2313	0.180	49.32	2f32+1f4	
f58	32.5835	0.171	49.03	1f6+1f1	
f59	21.4678	0.166	46.60	—	
f60	18.1650	0.161	46.23	—	
f61	31.2000	0.163	45.60	—	f57
f62	36.1182	0.163	44.93	1f29+1f10	f40 = f1+f4
f63	21.5677	0.155	43.91	2f38-1f24	
f64	33.9990	0.155	43.56	2f50-1f42	
f65	11.7875	0.180	43.42	—	
f66	30.4563	0.159	42.92	—	
f67	0.5918	0.152	41.92	1f49-1f5, low frequency	
f68	39.2170	0.151	41.37	—	f69
f69	11.7115	0.156	41.15	—	
f70	30.5483	0.147	40.86	—	
f71	2.6590	0.143	40.19	Low frequency	
f72	20.0643	0.144	40.18	2f13-1f11	
f73	34.6547	0.145	39.38	—	
f74	20.6681	0.138	39.37	—	
f75	32.1797	0.137	39.27	—	
f76	32.8554	0.143	39.14	—	
f77	11.4876	0.134	38.22	—	f70? = f3-f1
f78	31.7718	0.137	38.00	1f43+1f25	
f79	23.8069	0.134	37.63	2f32+1f24	f48
f80	42.1039	0.133	37.30	2f8	f64 = 2f6
f81	15.8659	0.141	37.02	—	
f82	18.6009	0.135	36.95	—	
f83	14.5424	0.132	36.81	—	
f84	26.9217	0.130	36.41	1f34+1f32	f61?
f85	33.0433	0.131	36.35	—	f74
f86	25.9421	0.124	36.04	—	
f87	24.6666	0.126	34.99	—	
f88	25.3863	0.124	34.32	2f33-1f19	
f89	7.1493	0.121	34.31	3f23-3f8	
f90	41.1922	0.123	34.23	—	
f91	17.8212	0.122	33.98	—	

(Continued on following page)

TABLE 2. (*Continued*) 100 highest S/N FG Vir *TESS* frequencies. Low frequencies between 0.3 and ~3 c/d are highlighted using red font. The calculated uncertainties in *TESS* frequencies and amplitudes, respectively, are 3.79×10^{-4} c/d and 9.82 ppm.

Freq. #	Freq. (c/d)	Amplitude (ppt)	S/N	Potential combinations and notes	Breger et al. freq. #
f92	29.4927	0.122	33.90	—	
f93	16.1058	0.121	33.44	2f33-3f20	f31
f94	11.1317	0.121	33.43	2f14-2f6	
f95	8.8966	0.120	33.01	1f8-1f3	
f96	10.6839	0.121	32.85	—	f79 = f4-f1
f97	3.0588	0.118	32.61	Low frequency	
f98	26.5298	0.115	32.39	—	f71
f99	8.5767	0.117	32.34	—	
f100	4.2424	0.113	31.34	2f29-1f25	

Breger and Pamyatnykh (2006) investigate the problem of closely spaced modes in FG Vir, with separations less than 0.1 c/d, too small to be the result of rotational splitting. Are these separate modes, or are they the result of amplitude variability of a single frequency? Breger and Pamyatnykh (2006) were able to rule out amplitude variability for several of the FG Vir closely spaced modes.

These many complications lead to a mode identification problem. We cannot identify modes by patterns in the amplitude spectrum and match them directly with modes expected from theoretical models. However, methods have been developed to identify the angular degree (ℓ) and azimuthal order (m) of the highest-amplitude modes using multi-color photometry, phase information, line profile variations and radial velocities from spectroscopy (see, e.g., Viskum et al., 1998; Breger et al., 1999, Mantegazza and Poretti 2002, Daszynska-Daszkiewicz et al., 2005; Zima et al., 2006). Some FG Vir modes have been identified using these methods, but mode identification has been somewhat uncertain. For example, Daszynska-Daszkiewicz et al. (2005) identified the angular degrees for twelve FG Vir modes to 80% probability, but there are ambiguities for six of these modes. In early studies of FG Vir, the highest-amplitude mode at 12.7162 c/d was thought to be the radial fundamental mode (e.g., Mantegazza et al., 1994; Breger et al., 1995), but later studies (e.g., Viskum et al., 1998; Mantegazza and Poretti 2002) showed that this mode is most likely an $\ell = 1$ dipole mode, and the radial fundamental mode actually is the 2nd-highest-amplitude mode at 12.1541 c/d.

Attempts have been successful to find patterns of frequency spacings in δ Sct stars (e.g., Breger et al., 2009). The spacings could correspond to the large separations between modes of successive ℓ values, or a rotational splitting spacing, or a combination of these two spacings (see also Paparo et al., 2016a; Paparo et al., 2016b; Suarez et al., 2014; Bedding et al., 2020). Bedding et al. (2020) found very regular patterns of high-frequency modes in a sample of young δ Sct stars observed by *TESS* and *Kepler*, enabling definitive mode identification. Patterns of mode spacings can therefore be useful to identify modes of common ℓ value, determine the stellar mean density, or even to measure the stellar interior rotation rate.

5 FG Vir models

The goal of asteroseismology of FG Vir is to use the observed frequency properties to determine the stellar interior structure and evolution state. Evolution and pulsation models of FG Vir have been calculated over the years to attempt to make use of the observed frequencies. It is helpful to have additional constraints from multi-color photometry, spectroscopy, and stellar model grids to provide a starting point for detailed model explorations. The *TESS* Input Catalog (TIC, Stassun et al., 2019) lists FG Vir properties derived from several sources and methods: effective temperature T_{eff} = 7361 ± 131 K, log surface gravity (log g) = 3.974 ± 0.086, radius R = 2.205 ± 0.082 $R_\odot$, mass M = 1.6 ± 0.282 $M_\odot$, luminosity L = 12.86 ± 0.44 $L_\odot$, and distance 83.02 ± 0.37 pc.

Viskum et al. (1998) use models and frequencies scaled from a 2.2 $M_\odot$ non-rotating evolution model of Christensen-Dalsgaard (1993) to derive a mean stellar density (ρ) = 0.1645 ± 0.005 $\rho_\odot$ for FG Vir. Assuming T_{eff} = 7500 K and metallicity Z = 0.02, they find M = 1.82 ± 0.03 $M_\odot$, L = 14.1 ± 0.9 $L_\odot$, R = 2.227 ± 0.012 $R_\odot$, and log g = 4.002 ± 0.003. Their derived luminosity places FG Vir at a distance of 82 ± 3 pc.

Breger et al. (1999) find a best-fit model to the FG Vir frequencies with M = 1.95 $M_\odot$, T_{eff} = 7492 K, L = 14.92 $L_\odot$, R = 2.301 $R_\odot$, and log g = 4.002. This model has metallicity Z = 0.02, initial helium mass fraction Y = 0.28, and mean density 0.1597 $\rho_\odot$. The model uses artificially modified opacities, has mixing-length parameter α = 1.0, and included core convective overshooting with overshooting distance 0.2 pressure scale heights. The models were evolved without rotation, but

10.3389/fspas.2022.948180

TABLE 3 Unstable low-degree frequencies of 1.82 $M_{\odot}$ FG Vir model.

Mode degree	Freq. (c/d)	Linear growth rate per period	Notes
0	12.1557	2.87E-06	Radial fundamental mode
0	15.7240	3.30E-05	
0	19.4744	1.66E-04	
0	23.2361	5.67E-04	
0	27.0256	1.54E-03	
0	30.8235	3.32E-03	
0	34.6365	4.67E-03	
0	38.5319	3.27E-03	
1	9.4303	5.92E-09	
1	12.4568	3.87E-06	Nearest frequency to highest-amplitude observed mode
1	16.1672	4.23E-05	
1	19.6468	9.23E-05	
1	20.7309	1.61E-04	
1	24.3940	8.35E-04	
1	28.4415	2.24E-03	
1	32.3942	4.19E-03	
1	36.3191	4.57E-03	
1	40.3270	1.55E-03	
2	10.0989	5.41E-08	
2	11.8952	6.09E-07	
2	12.5352	1.72E-06	
2	14.3243	8.09E-06	
2	16.7172	3.68E-05	
2	19.3467	1.17E-04	
2	22.5367	4.33E-04	
2	26.3052	1.32E-03	
2	30.2200	3.06E-03	
2	32.6560	2.60E-04	
2	34.2273	4.55E-03	
2	38.1374	3.61E-03	
3	8.8390	4.69E-09	
3	9.7564	2.42E-09	
3	10.5646	1.52E-07	
3	11.9282	1.25E-06	
3	13.9073	3.88E-06	
3	15.5789	2.23E-05	
3	16.8010	2.97E-06	
3	18.7368	7.41E-05	
3	20.2535	1.23E-04	
3	23.6239	6.51E-04	
3	27.6333	1.87E-03	
3	31.6207	3.86E-03	
3	35.5724	4.76E-03	
3	39.4859	1.51E-03	
3	39.7631	8.63E-04	

rotational splitting was taken into account up to second order in the pulsation frequency comparisons. The best-fit model had rotation velocity 32 km/sec.

Templeton et al. (2001) find a best-fit model for FG Vir with M = 1.9 $M_\odot$, T_{eff} = 7413 K, L = 14.16 $L_\odot$, and age 0.93 Gyr. This model has Z = 0.03 and hydrogen mass fraction Y = 0.28. The model was evolved without rotation, used mixing-length parameter α = 1.92, and includes core convective overshooting with overshooting distance 0.3 pressure scale heights. First-order rotational splitting was taken into account in the pulsation frequency comparisons, assuming rotation velocity 50 km/sec.

Kirbiyik et al. (2004) evolve models with uniform rotation and conservation of angular momentum, and calculate pulsation frequencies including first-order rotational splitting. Their paper does not discuss whether convective overshooting is included. They find best-fit models for FG Vir with M = 1.85 $M_\odot$, T_{eff} = 7540–7560 K, L = 15.06–15.12 $L_\odot$ and rotation rate 32–66 km/s.

Table 3 lists the ℓ = 0, 1, 2, and 3 pulsationally unstable frequencies (positive linear growth rates) for an FG Vir model calculated by Guzik. The frequencies include p modes, modes with mixed p-mode and g-mode character, and a few low-order g modes which have frequencies lower than the radial fundamental mode. These model frequencies were used by Paparo et al. (2016a), Paparo et al. (2016b) to illustrate how frequency spacings could be used to help identify modes in δ Scuti stars. The physics of the models is the same as used in the Guzik et al. (2000) FG Vir models, except for minor opacity table updates. The evolution models have mixing-length parameter α = 1.77, and do not include rotation or core convective overshooting. A model was selected on the 1.82 $M_\odot$, Z = 0.02, Y = 0.28 evolutionary track that has radial fundamental mode frequency near 12.1541 c/d, identified as the FG Vir radial fundamental mode. For this model, L = 13.92 $L_\odot$, T_{eff} = 7419 K, R = 2.26 $R_\odot$, log g = 3.9896, and mean density 0.1577 $\rho_\odot$. The model age is 0.867 Gyr, and core helium mass fraction is 0.708, indicating that about 2/3 of the core hydrogen has been converted to helium.

The calculated model frequencies in Table 3 do not include rotational splitting, which will divide non-radial modes multiplets with 2 ℓ + 1 components, with spacings of around 0.5 c/d, depending on the rotational velocity adopted. Rotation will cause the multiplet members to be unequally spaced in frequency. A total of 98 ℓ = 0, 1, and 2 modes are predicted, taking into account rotational splitting. However, even including rotational splitting, not all of the observed frequencies of Breger et al. (2005) can be matched for FG Vir. Considering in addition the 15 calculated unstable ℓ = 3 modes would increase the total number of predicted modes by another 105, to 203. These predictions assume that FG Vir has an inclination such that all modes of a multiplet are visible. As discussed in Section 4, it is possible that modes of even higher angular degree are visible in photometric data.

Breger and Pamyatnykh (2006) found 18 frequency doublets with frequency spacing < 0.1 c/d in their FG Vir frequency list. They concluded that accidental agreement between frequencies of excited modes can be ruled out because of the large number of doublets. We examined our ℓ = 0–3 frequency list in Table 3 for close frequency spacings. Only three pairs with spacing <0.1 c/d are found if rotational splitting is not taken into account. However, assuming the nonradial modes are split into 2ℓ + 1 multiplets with 0.5 c/d spacing between multiplets, we find 88 close frequency pairs. While this assumption of equally spaced multiplets is not realistic, this example does show that accidental agreements could explain the close spacings if modes of high-enough degree are visible.

We do not include in Table 3 high-order g-mode frequencies. These frequencies are predicted to have negative growth rates in our pulsation analyses because the envelope convection zone is too shallow (temperature at the base 54,000 K) to drive γ Doradus-type gravity modes via the convective blocking mechanism (Guzik et al., 2000). Nevertheless, many δ Sct stars show low-frequency modes in the γ Dor frequency range (Grigahcene et al., 2010; Uytterhoeven et al., 2011; Balona 2014).

The stellar properties derived for FG Vir using asteroseismic data and stellar models are in good agreement with each other. However, none of the models provided an exact fit to all of the observed FG Vir frequencies, and there is much more that could be learned about FG Vir's evolution and interior structure using ground-based data as well as the *K2* and *TESS* data.

The models available in the literature are quite old, having been calculated in 2004 or earlier, before Gaia parallaxes and revised lower solar abundance determinations (e.g., Asplund et al., 2021). FG Vir should be revisited taking into account modern constraints and using updated modeling tools, for example, using the MESA evolution code (see Paxton et al., 2019 and references therein).

It is an interesting question whether FG Vir has a stellar or planetary companion, and whether these objects might affect pulsation properties. FG Vir is listed as a visual binary in the catalog of Liakos and Niarchos (2017), who reference catalogs of Abt (1981) and Mason et al. (2001). However, the properties of the binary companion and orbital period are not given in these catalogs. An angular separation of 0.1 arc sec is given by Mason et al. (2001), but this separation may be a lower limit to the resolution of the observations.

Kervella et al. (2019) use Hipparcos (van Leeuwen 2007) and Gaia Early Data Release 3 (Gaia Collaboration 2016; Gaia Collaboration 2020; Brown et al., 2021a; 2021b) data to discover stellar and substellar companions using proper motion anomalies. For FG Vir they find no low velocity resolved companions, no bound resolved companions, and no common proper motion candidate companions. They find a tangential velocity anomaly of 6.89 m/s with position angle 196.22 deg. Using their assumptions for a potential orbit and assuming FG Vir mass M_1 = 1.85 $M_\odot$, they derive a companion mass M_2 = 2.10 M_{Jup} (3 AU orbit), 1.05 M_{Jup} (5 AU orbit), or 1.31 M_{Jup} (10 AU orbit). Therefore, we conclude that FG Vir does not have a stellar companion that could affect the analysis, but it may have a substellar one.

6 Conclusion

We compare the FG Vir frequencies detected using 52.4 days of 30-min cadence *Kepler K2* photometry with those detected using at least 363 nights (Breger and Lenz 2019) of multisite ground-based network data. More than 75 significant frequencies were measured in the ground-based data (Breger et al., 2005), compared to around 30, depending on S/N limit adopted, using the *K2* data. The *K2* frequency detections were limited to frequencies below the Nyquist frequency limit of ~24.5 c/d for 29.4-min cadence nearly equally spaced data, while frequencies as high as 44.25 c/d were identified using the ground-based data. The ground-based multisite data included multi-color photometry, which turned out to be extremely useful for mode identifications of the highest-amplitude modes.

The *TESS* data appear more promising for further FG Vir discoveries. The time-series length of the *TESS* data was 22.84 days, shorter than for the *K2* series, but the shorter 2-minute cadence increased greatly the S/N, allowing the detection of at least 100 modes with S/N > 31. The 2-minute cadence also increased the Nyquist frequency limit, so that modes up to 45 c/d, as found in the ground-based data, were detected. The *TESS* data should reveal many more modes of even lower amplitude than found in the ground-based data, requiring consideration of modes of angular degree $\ell > 3$ for asteroseismic models. The increased number of detected modes will make mode identification even more challenging.

There is general agreement among the frequencies of the 10 or so highest-amplitude modes between the ground-based, *K2*, and *TESS* data. Two modes of interest are the f9 mode of Breger et al. (2005), which moved down in amplitude rank, and the f35 mode of Breger et al., which moved up in amplitude rank according to both the *K2* and *TESS* data.

The continuity of the *K2* and *TESS* time-series data, and, possibly, the elimination of day/night aliases, enables detection of low-frequency modes. Several modes of significant amplitudes with frequencies between 0.3 and 3 c/d were detected in the TESS data, which may be high-order γ Dor gravity-mode pulsations. If confirmed, FG Vir would be a hybrid δ Sct/γ Dor variable star.

FG Vir models in the literature were calculated before 2005. FG Vir modelling should be revisited using modern codes in light of new constraints for distance and metallicity, making use of the *K2* and *TESS* data.

Data availability statement

Publicly available datasets were analyzed in this study. These data can be found here: https://mast.stsci.edu/portal/Mashup/Clients/Mast/Portal.html.

Author contributions

JG wrote the text of this article, created the figures and tables, and calculated the FG Vir model discussed. JJ performed the analysis of the FG Vir *Kepler* and *TESS* data, including processing light curves, and performing the pre-whitening analysis to identify significant frequencies and combination frequencies. AH contributed by reviewing literature on possible FG Vir binary companions.

Funding

This collaboration was facilitated by a Los Alamos National Laboratory Center for Space and Earth Sciences grant XX8P ASF2. JG acknowledges support from LANL, managed by Triad National Security, LLC for the U.S. DOE's NNSA, Contract #89233218CNA000001.

Acknowledgments

We are grateful for data from the NASA *Kepler* and *TESS* spacecraft, and the opportunities to propose these observations via the *K2* Guest Observer and *TESS* Guest Investigator programs. This research has made use of the SIMBAD database, operated at CDS, Strasbourg, France, and the Mikulski Archive for Space Telescopes (MAST). JG thanks the Society for Astronomical Sciences for the opportunity to present these results at their 2022 Symposium for Telescope Sciences. The authors thank the two reviewers for their many comments and suggestions which greatly improved this paper.

Conflict of interest

The authors declare that the research was conducted in the absence of any commercial or financial relationships that could be construed as a potential conflict of interest.

Publisher's note

References

Abt, H. (1981). Visual multiples. VII. MK classifications. *Astrophys. J. Suppl. Ser.* 45, 437. doi:10.1086/190719

Aerts, C., Christensen-Dalsgaard, J., and Kurtz, D. W. (2010). *Asteroseismology*. New York, New York, United States: Springer Astronomy & Astrophysics Library.

Antoci, V., Cunha, M. S., Bowman, D. M., Murphy, S. J., Kurtz, D. W., Bedding, T. R., et al. (2019). The first view of δ Scuti and γ Doradus stars with the *TESS* mission. *Mon. Not. R. Astron. Soc.* 490, 4040–4059. doi:10.1093/mnras/stz2787

Asplund, M., Amarsi, A. I., and Grevesse, N. (2021). The chemical make-up of the sun: A 2020 vision. *Astron. Astrophys.* 653, A141. doi:10.1051/0004-6361/202140445

Balona, L. A., Daszynska-Daszkiewicz, J., and Pamyatnykh, A. A. (2015). Pulsation frequency distribution in δ Scuti stars. *Mon. Not. R. Astron. Soc.* 452, 3073–3084. doi:10.1093/mnras/stv1513

Balona, L. A. (2014). Low frequencies in Kepler δ Scuti stars. *Mon. Not. R. Astron. Soc.* 437, 1476–1484. doi:10.1093/mnras/stt1981

Baran, A. S., and Koen, C. (2021). A detection threshold in the amplitude spectra calculated from *TESS* time-series data. *Acta Astron.* 71, 113. doi:10.48550/arXiv.2106.09718

Bedding, T., Murphy, S. J., Hey, D. R., Huber, D., Li, T., Smalley, B., et al. (2020). Very regular high-frequency pulsation modes in young intermediate-mass stars. *Nature* 581, 147–151. doi:10.1038/s41586-020-2226-8

Borucki, W. J., Koch, D., Basri, G., Batalha, N., Brown, T., Caldwell, D., et al. (2010). *Kepler* planet-detection mission: Introduction and first results. *Science* 327, 977–980. doi:10.1126/science.1185402

Bowman, D. M., Hermans, J., Daszynska-Daszkiewicz, J., Holdsworth, D. L., Tkachenko, A., Murphy, S. J., et al. (2021). KIC 5950759: A high-amplitude δ Sct star with amplitude and frequency modulation near the terminal age main sequence. *Mon. Not. R. Astron. Soc.* 504, 4039–4053. doi:10.1093/mnras/stab1124

Bowman, D. M., and Kurtz, D. W. (2018). Characterizing the observational properties of δ Sct stars in the era of space photometry from the Kepler mission. *Mon. Notices Royal Astron. Soc.* 476, 3169. doi:10.1093/mnras/sty449

Bowman, D. M., Kurtz, D. W., Breger, M., Murphy, S. J., and Holdsworth, D. L. (2016). Amplitude modulation in δ Sct stars: Statistics from an ensemble study of *Kepler* targets. *Mon. Not. R. Astron. Soc.* 460, 1970–1989. doi:10.1093/mnras/stw1153

Bowman, D. M., and Michielsen, M. (2021). Towards a systematic treatment of observational uncertainties in forward asteroseismic modelling of gravity-mode pulsators. *Astron. Astrophys.* 656, A158. doi:10.1051/0004-6361/202141726

Breger, M., Handler, G., Nather, R. E., Winget, D. E., Kleinman, S. J., Sullivan, D. J., et al. (1995). The δ Scuti star FG Virginis. I. Multiple pulsation frequencies determined with a combined DSN/WET campaign. *A&A* 297, 473.

Breger, M., Handler, G., Serkowitsch, E., Reegen, P., Provencal, J., Wood, M. A., et al. (1996). The δ Scuti star FG Virginis. II. A search for high pulsation frequencies. *A&A* 309, 197.

Breger, M., Lenz, P., Antoci, V., Guggenberger, E., Shobbrook, R. R., Handler, G., et al. (2005). Detection of 75+ pulsation frequencies in the δ Scuti star FG Virginis. *Astron. Astrophys.* 435, 955–965. doi:10.1051/0004-6361:20042480

Breger, M., Lenz, P., and Pamyatnykh, A. A. (2009). Towards mode selection in δ Scuti stars: Regularities in observed and theoretical frequency spectra. *Mon. Not. R. Astron. Soc.* 396, 291–298. doi:10.1111/j.1365-2966.2008.14330.x

Breger, M., and Lenz, P. (2019). Photometric data by the δ Scuti network II. EE cam, FG Vir, 44 tau. *J. Astronomical Data* 25, 1.

Breger, M., and Pamyatnykh, A. A. (2006). Amplitude variability or close frequencies in pulsating stars—The δ Scuti star FG Vir. *Mon. Not. R. Astron. Soc.* 368, 571–578. doi:10.1111/j.1365-2966.2006.10119.x

Breger, M., Pamyatnykh, A. A., Pikall, H., and Garrido, R. (1999). The δ Scuti star FG Vir. IV. Mode identification and pulsation modelling. *A&A* 341, 151.

Breger, M., Rodler, F., Pretorius, M. L., Martin-Ruiz, S., Amado, P. J., Costa, V., et al. (2004). The δ Scuti star FG Vir. V. The 2002 photometric multisite campaign. *Astron. Astrophys.* 419, 695–701. doi:10.1051/0004-6361:20035830

Breger, M., Zima, W., Handler, G., Poretti, E., Shobbrook, R. R., Nitta, A., et al. (1998). The δ Scuti star FG Vir. III. The 1995 multisite campaign and the detection of 24 pulsation frequencies. *A&A* 331, 271.

Brown, A. G. A., Vallenari, A., Prusti, T., de Bruijne, J. H. J., Babusiaux, C., et al. Gaia Collaboration (2021a). Gaia early data release 3. Summary of the contents and survey properties. *A&A* 649, A1. doi:10.48550/arXiv.2012.0153

Brown, A. G. A., Vallenari, A., Prusti, T., de Bruijne, J. H. J., Babusiaux, C., et al. Gaia Collaboration (2021b). Gaia early data release 3. Summary of the contents and survey properties (corrigendum) 2021b. *A&A* 650, C3. doi:10.1051/0004-6361/202039657e

Buchler, J. R., Goupil, M.-J., and Hansen, C. J. (1997). On the role of resonances in nonradial pulsators. *A&A* 321, 159.

Buchler, J. R., and Regev, O. (1983). The effects of nonlinearities on radial and nonradial oscillations. *A&A* 123, 331.

Chevalier, C. (1971). Short-period variables. VIII. Evolution and pulsation of δ-scuti stars. *A&A* 14, 24.

Christensen-Dalsgaard, J. (1993). "Pulsation theory and stellar structure," in Inside the stars, IAU Colloquium 137, ASP Conf. Ser. 40, Austria, April 13–18, 1992.

Cunha, M., Aerts, C., Christensen-Dalsgaard, J., Baglin, A., Bigot, L., Brown, T. M., et al. (2007). Asteroseismology and interferometry. *Astron. Astrophys. Rev.* 14, 217–360. doi:10.1007/s00159-007-0007-0

Daszynska-Daszkiewicz, J., Dziembowski, W. A., Pamyatnykh, A. A., Breger, M., Zima, W., and Houdek, G. (2005). Inferences from pulsational amplitudes and phases for multimodeδSct star FG Vir. *Astron. Astrophys.* 438, 653–660. doi:10.1051/0004-6361:20052902

Daszynska-Daszkiewicz, J., Dziembowski, W. A., and Pamyatnykh, A. A. (2006). On the nature of small amplitude peaks in δ Scuti oscillation spectra. *Mem. S.A.It.* 77, 113.

Daszynska-Daszkiewicz, J., Pamyatnykh, A. A., Walczak, P., Handler, G., Pigulski, A., and Szewczuk, W. (2021). Mode identification and seismic study of δ Scuti, the prototype of a class of pulsating stars. *Mon. Not. R. Astron. Soc.* 505, 88–102. doi:10.1093/mnras/stab1292

Daszynska-Daszkiewicz, J., Walczak, P., Pamyatnykh, A. A., and Szewczuk, W. (2022). Asteroseismology of the double-radial mode δ Scuti star BP Pegasi. *Mon. Not. R. Astron. Soc.* 512, 3551–3565. doi:10.1093/mnras/stac646

Di Criscienzo, M., Ventura, P., D'Antona, F., Marconi, M., Ruoppo, A., and Ripepi, V. (2008). Matching the frequency spectrum of pre-main sequence stars by means of standard and rotating models. *Mon. Not. R. Astron. Soc.* 389, 325–332. doi:10.1111/j.1365-2966.2008.13560.x

Dziembowski, W. (1993). Mode selection and other nonlinear phenomena in stellar oscillations. *Int. Astron. Union Colloq.* 40, 521–534. doi:10.1017/s0252921100018352

Gaia Collaboration (2016). The Gaia mission. *A&A* 595, A1. doi:10.1051/0004-6361/201629272

Gaia Collaboration (2020). VizieR online data catalog: Gaia EDR3, I/350, 2020yCat.1350. *A&A* 649A, 1G. doi:10.5270/esa-1ug

Gilliland, R. L., Brown, T. M., Christensen-Dalsgaard, J., Kjeldsen, H., Aerts, C., Appourchaux, T., et al. (2010). *Kepler* asteroseismology program: Introduction and first results. *PASP* 122, 131–143. doi:10.1086/650399

Goupil, M.-J., and Dziembowski, W. (2000). "Rotational splitting of δ Scuti stars," in ASP Conference Series, Vienna, Austria, 4-7 August.210

Grigahcene, A., Antoci, V., Balona, L., Catanzaro, G., Daszynska-Daszkiewicz, J., Guzik, J. A., et al. (2010). Hybrid γ doradus-δ Scuti pulsators: New insights into the physics of the oscillations from *Kepler* observations. *Astrophys. J.* 713, L192–L197. doi:10.1088/2041-8205/713/2/l192

Guzik, J. A., Garcia, J., and Jackiewicz, J. (2019). Properties of 249 δ Scuti variable star candidates observed during the NASA *K2* mission. *Front. Astron. Space Sci.* 6, 40G. doi:10.3389/fspas.2019.00040

Guzik, J. A., Bradley, P. A., and Templeton, M. R. (2000). "Approaches to asteroseismology of core and shell hydrogen-burning δ Scuti stars," in ASP Conference Series, Vienna, Austria, 4-7 August.210

Guzik, J. A. (2021). Highlights of discoveries for δ Scuti variable stars from the *Kepler* era. *Front. Astron. Space Sci.* 8, 55G. doi:10.3389/fs-pas.2021.653558

Handler, G. (2009). "Delta Scuti variables," in Proceedings of the International Conference "Stellar Pulsation: Challenges for Observation and Theory. Editors J. A. Guzik and P. A. Bradley, 403–409. AIP Conference Proceedings. doi:10.1063/1.32465281170

Howell, S. G., Sobeck, C., Haas, M., Still, M., Barclay, T., Mullally, F., et al. (2014). The *K2* mission: Characterization and early results. *Publ. Astron. Soc. Pac.* 126, 398–408. doi:10.1086/676406

Huber, D., Bryson, S. T., Haas, M. R., Barclay, T., Barentsen, G., Howell, S. B., et al. (2016). The *K2* ecliptic Plane Input catalog (EPIC) and stellar classifications of 138,

600 targets in campaigns 1–8. *Astrophys. J. Suppl. Ser.* 224, 2. doi:10.3847/0067-0049/224/1/2

Kervella, P., Arenou, F., Mignard, F., and Thevenin, F. (2019). Stellar and substellar companions of nearby stars from Gaia DR2: Binarity from proper motion anomaly. *Astron. Astrophys.* 623, 72. doi:10.1051/0004-6361/201834371

Kirbiyik, H., Civelek, R., and Kiziloglu, N. (2004). A new oscillating model suggestion for FG Vir. *Astrophys. Space Sci.* 295, 473–484. doi:10.1007/s10509-005-1085-y

Koch, D. G., Borucki, W. J., Basri, G., Batalha, N. M., Brown, T. M., Caldwell, D., et al. (2010). *Kepler* mission design, realized photometric performance, and early science. *Astrophys. J.* 713, L79–L86. doi:10.1088/2041-8205/713/2/l79

Kurtz, D. W. (2022). "Asteroseismology across the HR diagram," in Annual Reviews of Astronomy and Astrophysics, April 8, 2022.

Kurtz, D. W., Hambleton, K. M., Shibahashi, H., Murphy, S. J., and Prsa, A. (2015). A unifying explanation of complex frequency spectra of γ dor, SPB and Be stars: Combination frequencies and highly non-sinusoidal light curves. *Mon. Not. R. Astron. Soc.* 446, 1223–1233. doi:10.1093/mnras/stu2075

Li, G., Zhao, M., Xie, J., Yao, Y., Mou, L., Zhang, X., et al. (2020). Efficient synthesis of cyclic amidine-based fluorophores *via* 6π-electrocyclic ring closure. *Chem. Sci.* 491, 3586–3591. doi:10.1039/d0sc00798f

Liakos, A., and Niarchos, P. (2017). Catalogue and properties of δ Scuti stars in binaries. *Mon. Not. R. Astron. Soc.* 465, 1181–1200. doi:10.1093/mnras/stw2756

Lopez de Coca, P., Garrido, R., Costa, V., and Rolland, A. (1984). *Narrow band photometry of FG Vir*. Commission 27 of the I.A.U. Budapest, Hungary: International Bulletin on Variable Stars. Number 2465, 27 January.

Mantegazza, L., Poretti, E., and Bossi, M. (1994). Simultaneous intensive photometry and high-resolution spectroscopy of δ Scuti stars. I. Mode typing of HD 106384 = FG Virginis. *A&A* 287, 95.

Mantegazza, L., and Poretti, E. (2002). Line profile variations in the δ Scuti star FG Virginis: A high number of axisymmetric modes. *Astron. Astrophys.* 396, 911–916. doi:10.1051/0004-6361:20021456

Mason, B. D., Wycoff, G. L., Hartkopf, W. I., Douglass, G. G., and Worley, C. E. (2001). The 2001 US naval observatory double star CD-ROM. I. The Washington double star catalog. *Astron. J.* 122, 3466–3471. doi:10.1086/323920

Mighell, K., and Van Cleve, J. (2020). K2, *extending* Kepler's *power to the ecliptic*, K2 *Handbook*. Moffett Field, CA: NASA Ames Research Center. KSCI-19166-003.

Montgomery, M., and O'Donoghue, D. (1999). A derivation of the errors for least squares fitting to time series data. *Delta Scuti Star. Newsl.* 13, 9.

Murphy, S. J., Bedding, T. R., White, T. R., Li李亚光, Y., Hey, D., Reese, D., et al. (2022). Five young δ Scuti stars in the pleiades seen with *Kepler/K2. Mon. Not. R. Astron. Soc.* 511, 5718–5729. doi:10.1093/mnras/stac240

Murphy, S. J., Joyce, M., Bedding, T. R., White, T. R., and Kama, M. (2021). A precise asteroseismic age and metallicity for HD 139614: A pre-main-sequence star with a protoplanetary disc in upper centaurus–lupus. *Mon. Not. R. Astron. Soc.* 502, 1633–1646. doi:10.1093/mnras/stab144

Murphy, S. J., Shibahashi, H., and Kurtz, D. W. (2013). Super-nyquist asteroseismology with the *Kepler* space telescope. *Mon. Not. R. Astron. Soc.* 430, 2986–2998. doi:10.1093/mnras/stt105

Paparo, M., Benko, J. M., Hareter, M., and Guzik, J. A. (2016b). Unexpected series of regular frequency spacing of δ Scuti stars in the non-asymptotic regime. II. Sample-echelle diagrams and rotation. *Astrophys. J. Suppl. Ser.* 224, 41. doi:10.3847/0067-0049/224/2/41

Paparo, M., Benko, J. M., Hareter, M., and Guzik, J. A. (2016a). Unexpected series of regular frequency spacing ofδscuti stars in the non-asymptotic regime. I. The methodology. *Astrophys. J.* 822, 100. doi:10.3847/0004-637x/822/2/100

Papics, P. (2012). The puzzle of combination frequencies found in heat-driven pulsators. *Astron. Nachr.* 333 (10), 1053–1056. doi:10.1002/asna.201211809

Paxton, B., Smolec, R., Schwab, J., Gautschy, A., Bildsten, L., Cantiello, M., et al. (2019). Modules for experiments in stellar Astrophysics (MESA): Pulsating variable stars, rotation, convective boundaries, and energy conservation. *Astrophys. J. Suppl. Ser.* 243, 10. doi:10.3847/1538-4365/ab2241

Poretti, E., Michel, E., Garrido, R., Lefevre, L., Mantegazza, L., Rainer, M., et al. (2009). HD 50844: A new look atδScuti stars from CoRoT space photometry. *Astron. Astrophys.* 506 (1), 85–93. doi:10.1051/0004-6361/200912039

Ricker, G. R., Winn, J. N., Vanderspek, R., Latham, D. W., Bakos, G. A., Bean, J. L., et al. (2015). Transiting exoplanet survey satellite (*TESS*). *J. Astron. Telesc. Instr. Syst.* 1, 014003. doi:10.1117/1.JATIS.1.1.014003

Saio, H. (1981). Rotational and tidal perturbations of nonradial oscillations in a polytropic star. *Astrophys. J.* 244, 299. doi:10.1086/158708

Stassun, K., Oelkers, R. J., Paegert, M., Torres, G., Pepper, J., Lee, N. D., et al. (2019). The revised *TESS* Input catalog and candidate target list. *Astron. J.* 158, 138. doi:10.3847/1538-3881/ab3467

Suarez, J. C., Garcia Hernandez, A., Moya, A., Rodrigo, C., Solano, E., Garrido, R., et al. (2014). Measuring mean densities of Scuti stars with asteroseismology. *Astron. Astrophys.* 563, A7. doi:10.1051/0004-6361/201322270

Templeton, M., Basu, S., and Demarque, P. (2001). Asteroseismology of δ Scuti stars: A parameter study and application to seismology of FG Virginis. *Astrophys. J.* 563, 999–1012. doi:10.1086/324041

Uytterhoeven, K., Moya, A., Grigahcene, A., Guzik, J. A., Gutierrez-Soto, J., Smalley, B., et al. (2011). The *Kepler* characterization of the variability among A- and F-type stars I. General overview. *Astron. Astrophys.* 534, A125. doi:10.1051/0004-6361/201117368

Van Leeuwen, F. (2007). *Hipparcos, the new reduction of the raw DataAstrophysics and space science library*, 350. New York, New York, United States: Springer Science+Business Media B.V. ISBN 978-1-4020-6341-1.

Viskum, M., Kjeldsen, H., Bedding, T. R., and Dall, T. H. (1998). Oscillation mode identifications and models for the δ Scuti star FG Virginis. *A&A* 335, 549.

Zima, W., Wright, D., Bentley, J., Cottrell, P. L., Heiter, U., Mathias, P., et al. (2006). A new method for the spectroscopic identification of stellar non-radial pulsation modes II. Mode identification of the δ Scuti star FG Virginis. *Astron. Astrophys* 455, 235. doi:10.1051/0004-6361:20064877

Zwintz, K., and Steindl, T. (2022). The pre-main sequence: Challenges and prospects for asteroseismology. *Front. Astron. Space Sci.* 9, 914738. doi:10.3389/fspas.2022.914738

frontiers | Frontiers in Astronomy and Space Sciences

TYPE Review
PUBLISHED 21 September 2022
DOI 10.3389/fspas.2022.958502

OPEN ACCESS

EDITED BY
Zhao Guo,
University of Cambridge,
United Kingdom

REVIEWED BY
Alejandro Hugo Córsico,
National University of La Plata, Argentina
Maria Pia Di Mauro,
National Institute of Astrophysics (INAF),
Italy

*CORRESPONDENCE
Adrián Ayala,
aayala@iaa.es

SPECIALTY SECTION
This article was submitted to Stellar and Solar Physics,
a section of the journal
Frontiers in Astronomy and Space Sciences

RECEIVED 31 May 2022
ACCEPTED 02 September 2022
PUBLISHED 21 September 2022

CITATION
Ayala A (2022), Looking into dark matter with asteroseismology.
Front. Astron. Space Sci. 9:958502.
doi: 10.3389/fspas.2022.958502

Looking into dark matter with asteroseismology

Adrián Ayala*

Institute of Astrophysics of Andalusia, Department of Stellar Astrophysics, Granada, Spain

Dark matter remains as an elusive component of modern Cosmology. According to previous research, stellar physics observables can be affected by the presence of hypothetical dark matter particles, which can be produced or accreted into the stars. Stellar pulsations are among the observables affected by dark matter, because the changes of the internal structure of the stars due to dark matter produce variations in the pulsation frequencies. We review the current research in the interplay between astroparticles, precise stellar observations, and accurate asteroseismic models, which can be extremely useful in order to constrain dark matter candidates from asteroseismic observables.

KEYWORDS

dark matter, stellar physics, asteroseismology, solar physics, stellar populations, space missions

1 Introduction

Staying as one of the most puzzling problems in Astrophysics, dark matter has motivated a lot of experiments and theoretical research (Bertone, 2010). The hypothetical existence of dark matter has been supported by the mismatch between our knowledge of Gravity and the dynamics of several systems like galaxy clusters, rotating galaxies, etc. Although this mismatch could be also explained by the Modified Newtonian Dynamics (MOND) hypothesis (Milgrom, 1983), many theoretical models consider that dark matter is composed by exotic weakly interacting particles. This is an appealing possibility, if we attend to some open questions in our description of the Standard Model (Jaeckel and Ringwald, 2010) like, for instance, strong CP violation (Peccei and Quinn, 1977) or some aspects of neutrino physics (Raffelt, 1999), which require invoking new particles, arising from additional terms in the Standard Model (SM) Lagrangian.

In the theoretical frame of Quantum Field Theory, couplings between the new terms of the Lagrangian, accounting for dark matter, and the previous ones can be expected. In particular, these couplings can happen between the new additional terms of the dark matter and the electromagnetic, weak or strong sectors, and they give account of the relatively scarce interactions of dark matter and SM particles. As a consequence of this, it is possible to calculate the rate of decay of dark matter particles into SM ones, or alternatively the rate of production of dark matter from SM components, within several models (Raffelt, 1999). Therefore in principle, experiments and astrophysical observations can constrain the parameter space of many dark matter candidates, on the basis of the phenomenology of the interactions of dark and baryonic matter.

Stellar interiors are suitable environments to expect the production, accretion, and/or annihilation of dark matter (Raffelt and Dearborn, 1987; Córsico et al., 2001; Iocco, 2008; Isern and García-Berro, 2008; Scott et al., 2008; Taoso et al., 2008; Bertone, 2010; Córsico et al., 2012; Vinyoles et al., 2015; Isern et al., 2022), and the star life times are long enough to be affected by continous emission fluxes of dark matter from their interiors. Thus, the observables related to stars and stellar populations can be significantly modified when dark matter is introduced in the stellar models (Scott et al., 2008; Taoso et al., 2008; Casanellas and Lopes, 2011; Ayala et al., 2014). In particular, the observables related to the stellar structure, like the size of the convective and/or radiative regions, could change as a consequence of the energy carried away for the dark matter particles (Martins et al., 2017; Ayala et al., 2020).

As it has been demonstrated (Aerts et al., 2010), the stellar pulsations, studied by Asteroseismology, are critically affected by changes in the stellar structures, like those due to hypothetical dark matter particles. In this review we justify the use and explore the future prospects of Asteroseismology, as a tool to constrain the dark matter. The ongoing and future space missions, and surveys of pulsating stars, open a promising opportunity for Asteroseismology, in order to impose more accurate constraints on several dark matter models, improving the previous asteroseismic bounds derived from main sequence (Cadamuro and Redondo, 2010; Lopes and Silk, 2012; Turck-Chièze and Lopes, 2012; Redondo and Raffelt, 2013; Vinyoles et al., 2015) and evolved stars (Lopes et al., 2019; Ayala et al., 2020), as well as in WDs (Córsico et al., 2019, 2001). In addition, some theoretical predictions about the pulsations of exotic stellar objects, composed of dark matter, could be tested by means of future observations (Panotopoulos and Lopes, 2019; Lopes and Panotopoulos, 2020).

In this paper, we focus on the asteroseismic observables related to the stellar structures and discuss three dark matter candidates: weakly interacting massive particles (WIMPs), asymmetric dark matter (ADM), and weakly interacting slim particles (WISPs) like axions or dark photons. Concerning the latter particles, my collaborators and I have made some valuable contributions, constraining for the first time dark photon properties from the study of the pulsations of the red giant stars. We also recall that the techniques we discuss in this work are general enough to be applied to other particle models, apart from the aforementioned.

This review is organized as follows: in section 2 we explore the role of Asteroseismology in elucidating the internal structure of stars. Section 3 explains the effects of some dark matter candidates on the stellar evolution and structure and the way the asteroseismic observables have been used to constrain these effects. Finally we present a general discussion and prospects of future work in section 4.

2 Asteroseismology and stellar structure

Asteroseismology, the study of stellar pulsations (Christensen-Dalsgaard, 2004; Aerts et al., 2010; Kurtz, 2022), is nowadays a powerful technique. Part of its success is due to space missions devoted to ultra-precise photometry like CoRoT (Baglin et al., 2006), Kepler (Koch et al., 2010) or TESS (Ricker et al., 2015). By means of asteroseismic techniques, stellar parameters are inferred with an uncertainty of up to 2% on the radius, 4% on the mass and 15% on the age for stars showing solar-like oscillations (Silva Aguirre et al., 2017). Moreover, Asteroseismology, enables us to pierce into the stellar interiors, giving a useful information about the extensions of the convective structures inside the stars, which could shade some light on the energy transport mechanism. About this last topic, it is worth mentioning that the period variation of the stellar pulsations have been proposed in order to study the size variation of the internal cavities of the stars, which is related to the convective transport, (Kurtz, 2022). Moreover, the measured change of periods of some white dwarfs has been proposed as a way to look into their radiative cooling mechanisms, constraining also some dark matter properties, like the mass of the axion (Isern and García-Berro, 2008; Isern et al., 2022).

Driven by different mechanisms of pulsation, from the stochastic to the classical cepheids one (Aerts et al., 2010), pulsating stars are spread throughout the Hertzsprung-Russell diagram, the distribution of pulsating stars on the $L/L_{\odot}$ vs. T_{eff} plane. The oscillation modes on solar-like and some giant stars form a clear structure where p modes of consecutive radial orders n and the same spherical degree l are separated by an almost constant frequency distance. As it was shown by previous research (Tassoul, 1990, 1980), the frequency pattern of these modes satisfy:

$$\nu_{nl} = \Delta\nu\left(n + \frac{l}{2} + \tilde{\alpha}\right) + \epsilon_{nl}, \tag{1}$$

where $\tilde{\alpha}$ is a constant of order unity and $\Delta\nu$ is a periodic spacing known as the large separation. The large separation is defined as the inverse of the sound travel from the surface of the star to the core and back again, (Aerts et al., 2010)

$$\Delta\nu = \left(2\int_0^R \frac{dr}{c(r)}\right)^{-1}, \tag{2}$$

where $c(r)$ stands for the sound speed. Alternatively, the large separation can be defined by means of the asymptotic formula:

$$\Delta\nu = \nu_{n+1,l} - \nu_{n,l} \tag{3}$$

The term ϵ_{nl} in Eq. 1 gives rise to the small frequency separation, $\delta\nu_l$, defined as

$$\delta\nu_l = \nu_{nl} - \nu_{n-1l+2} \tag{4}$$

Whereas the large separation is sensitive to the radius, and therefore to the stellar mass at the main sequence, the small frequency separation is related to the core condensation and the stellar age (Aerts et al., 2010).

Finally, we defined the ratio of small separation and large separation as r_{02}

$$r_{02} = \frac{\nu_{n,0} - \nu_{n-1,2}}{\nu_{n,1} - \nu_{n-1,1}} \quad (5)$$

The aforementioned quantities can be obtained from the periodograms of pulsating stars and are sensitive to the structure of stellar cores, in such a way that they can be used to constraint dark matter candidates. Among the previous studies which proposed to use the asteroseismic parameters to bound dark matter, we mention:

- Vinyoles et al. (2015), focused on the sound velocity profile, in the case of the Sun.
- Ayala et al. (2020) and Casanellas and Lopes (2013), about the large separation in evolved and solar-like stars, respectively. Casanellas and Lopes (2013) also regard the small separation in solar-like stars.
- Martins et al. (2017), focused on r_{02} parameter in solar-like stars.
- Córsico et al. (2019) and Isern and García-Berro (2008), which focus on the period variation of white dwarfs.

In the next sections we will review the bounds on dark matter from these observables. In particular we point out that changes in the large separation throughout the red giant branch could be produced by additional energy losses, related to a kind of dark matter candidate: dark photons. Besides the large separation, dark photon could also influence the luminosity of the RGB tip and bump phases, as we have proved **in previous studies** (Ayala et al., 2015; Ayala et al., 2020).

3 Dark matter models and stars. Constraints from asteroseismology

The role of stars as particle physics laboratories, or more specifically, as dark matter probes has attained an increasing interest in the last decades (Raffelt, 1999; Casanellas and Lopes, 2011). The main reasons are the possibility of constraining dark matter on the basis of their hypothetical influence on stellar structure and evolution. In addition, dark matter could drive the formation and evolution of stars (Turck-Chièze and Lopes, 2012) and therefore, to have a complete understanding of stars, it is mandatory to elucidate the hypothetical production or annihilation of dark matter, or the energy transported by it, inside stellar interiors.

Regarding the search of dark matter in stellar interiors, the Sun has been more studied than other stars, due to its proximity. However, with the advent and refinement of space missions and the improvements in photometry, the search of dark matter inside stars has extended to main sequence (Casanellas and Lopes, 2013), red giants (Ayala et al., 2020), and white dwarfs (Isern and García-Berro, 2008; Córsico et al., 2012). The forthcoming missions as HAYDN (Miglio et al., 2021), which aims to provide a large survey of the pulsating stars from both Open and Globular Clusters, or PLATO (Rauer, 2021), devoted to obtain ultra precise light curves of variable stars and planetary transits, will hopefully make possible to analyze more in detail the presence of dark matter in stars.

3.1 Constraints on the dark matter from solar-like and low mass stars

As the closest star, the Sun has been observed with a detail unavailable for other stellar objects. Besides optical, UV, and X-ray observational data, we have information about neutrino fluxes, gravity and acoustic measurements (Turck-Chièze and Lopes, 2012), as well as measurements of the magnetic activity. The study of the solar pulsations is the scope of the discipline called "Helioseismology", which has motivated many observations to obtain precise data of the solar light curves (Domingo et al., 1995; Gabriel et al., 1995; Gabriel et al., 1997).

The Sun, a potential laboratory for discovering new particles, is the first target of IAXO (International Axion Observatory, described in Armengaud et al. (2014)), which is devoted to the detection of axions, a pseudoscalar, low-mass dark matter candidate (Peccei and Quinn, 1977; Wilczek, 1978). According to some models, axions can be produced inside the Sun by means of the Primakoff process (Vinyoles et al., 2015). Besides axions, other hypothetical light dark matter particles called dark or hidden photons (An et al., 2014) could carry away energy from the solar interior (Redondo and Raffelt, 2013).

Vinyoles et al. (2015) propose a global best-fit of solar models, neutrino observations and Helioseismology, in order to constrain axions and dark photons, both emitted from the solar interior. The changes in the sound speed profile can be used to discriminate among several axion and dark photon models at the solar internal regions ($r/R \leq 0.2$). In particular the variations of the sound speed profile depend on the axion coupling to the photon, and are also influenced by the product of dark photon mass and dark photon-photon coupling (or kinetic mixing). From a detailed statistical analysis, considering two different solar compositions, Vinyoles et al. (2015) derive the constraint $g_{a\gamma} < 4.1 \times 10^{-10}\ GeV^{-1}$ for the axion-photon coupling, and $1.8 \times 10^{-12}\ eV$ for the product of dark photon mass and kinetic mixing, both at 3σ confident level.

In addition to the search of light dark matter candidates, the Sun has motivated several studies with the aims of constraining massive particles. For example, some authors looked for signatures of WIMPs (Weakly Interacting Massive Particles,

with masses in the range of GeV) in the solar helioseismic data, as these particles could vary the local luminosity and sound speed in the Sun (Turck-Chièze and Lopes, 2012). The reason is, that even though the massive WIMPS can not be produced by thermal processes of the plasma, they can be accreted into the star cores, providing a certain density of dark matter in the vicinity of the star. Thus the massive WIMPs can annihilate with their antiparticles, releasing energy and changing the stellar evolution predicted by models without dark matter (Casanellas and Lopes, 2011).

A number of massive particle models, consider the existence of an asymmetry in the number of dark matter particles and antiparticles of dark matter. They are referred as ADM (Asymmetric Dark Matter) models in the literature (Gudnason et al., 2006; Lopes and Silk, 2012). An important feature of these theoretical treatments is that annihilation of the accreted particles is not so important or even excluded. Therefore the accretion of dark matter contributes more to the energy transport inside the stars than to the existence of an additional source of energy. As in the case of WIMPs models, most theoretical descriptions of ADM consider either the spin-independent or the spin-dependent interactions with baryonic matter.

The ADM models have been constrained successfully using asteroseismic observations and models of low mass stars (Casanellas and Lopes, 2013; Martins et al., 2017). As a consequence of the ADM energy transport in these stars, the models predict that the central temperature decreases, whereas the central density increases. Figure 1 shows these effects for models of KIC 8006161, a star with a mass of 0.92 $M_{\odot}$, computed by Casanellas and Lopes (2013). The models were performed considering different values of ADM masses and ADM-baryon cross sections. The authors found that these changes of the central conditions of low mass stars could be used to impose constraints on ADM masses and cross sections, more stringent than the previously derived from the Sun (Taoso et al., 2010).

A key point is that this additional energy transport, due to ADM, can reduce and eventually suppress the convective cores that appear in main-sequence stars in the mass interval 1.1 $M_{\odot}$ – 1.3 $M_{\odot}$, as it was also demonstrated by Casanellas and Lopes (2013) (see Figure 2, for the case of the star HD 52265 with a mass of 1.18 $M_{\odot}$).

The bounds derived on ADM by Casanellas and Lopes (2013) rely on the impact that the ADM energy transport has on the small frequency separation: a decrease of the predicted value of this observable, as it was obtained from the models of HD 52265 and KIC 8006161. They also verified this effect with models of the low-mass star α Cen B (0.93 $M_{\odot}$), which they compared with asteroseismic observations of the small separation of this star. On the basis of this analysis, it was

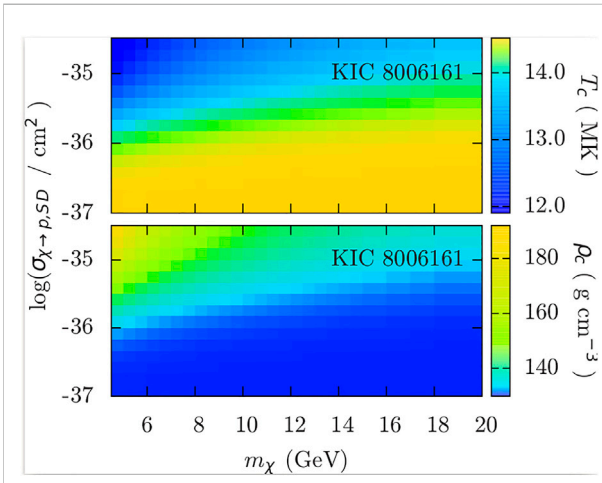

FIGURE 1
Theoretically predicted central temperature (upper panel, in MK), and density (lower panel, in g cm^{-3}), of KIC 8006161 (0.92 $M_{\odot}$). Notice the variations with respect to the asymmetric dark matter masses (m_χ) and baryon-dark matter spin-dependent cross sections (log ($\sigma_{\chi\to p}$)). Taken from Casanellas and Lopes (2013).

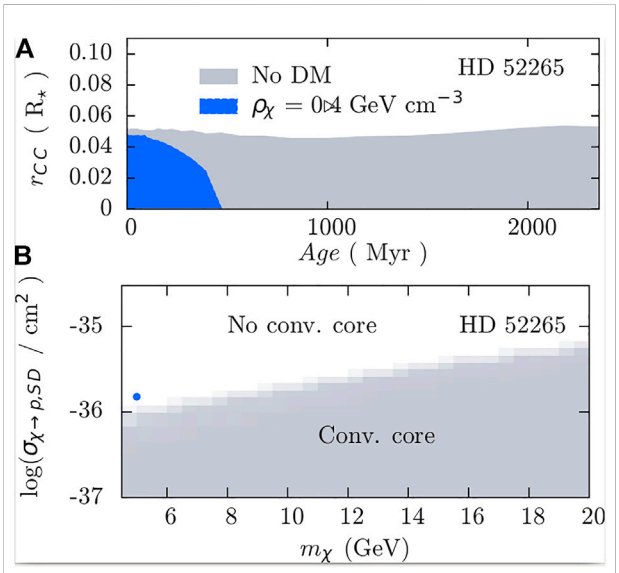

FIGURE 2
Upper **(A)**: convective core radius (r_{cc}) vs. star age, computed for two evolution models of the star HD 52265 (1.18 $M_{\odot}$), one of them without dark matter (grey); the other considering the presence of asymmetric dark matter (ADM) with mass m_χ = 5 *GeV*, cross-section 1.5 × 10^{-36} cm^2, and a density ρ_x = 0.4 GeV cm^{-3} (blue). Notice that the convective core rapidly disappears at the beginning of the main sequence. Lower **(B)**: HD 52265 models, at its estimated age, considering the action of ADM particles. The vertical axis is the logarithm of the spin-dependent baryon-dark matter cross section (log ($\sigma_{\chi\to p}$)), the horizontal axis is the dark matter particle mass (m_χ). Only some values are compatible with the existence of a convective core (notice the transition between the white and the gray shaded area, defining the separation between the regions where the convective core is excluded or not). The blue point corresponds to the ADM model with the conditions of the upper panel. Taken by Casanellas and Lopes (2013).

possible to exclude the values of the ADM cross section $\sigma \geq 3 \times 10^{-36}\ cm^2$, for an ADM mass $m_\chi \simeq 5\ GeV$, at 99% confidence level (see Figure 3).

An interesting additional analysis, also focused on the ADM particles within the spin-dependent interaction models, was performed by Martins et al. (2017), a work which also discusses WIMP models with low annihilation. They derive bounds on ADM by means of the r_{02} parameter defined in Eq 5. The choice of r_{02} is motivated by the fact it is weighted towards the stellar core, and therefore r_{02} is more sensitive to the effects of ADM, which are stronger on this region (Martins et al., 2017). The authors used a careful calibration of the Sun, a less massive star, KIC 7871531 (0.85 $M_\odot$), and KIC 8379927 a star more massive than the Sun (1.12 $M_\odot$). An interesting point is that the simulations of energy transport, due to asymmetric dark matter, show that this process is more important in the less massive KIC 7871531 star than in the Sun. This is because of the lower mass and older age of the former, which implies that the energy transport is a larger fraction of the luminosity and that the star has accumulated ADM for longer. On the other hand, for the more massive star KIC 8379927 the energy transport is more efficient, whereas the accretion of ADM is less important than in the Sun and KIC 7871531, due to KIC 8379927 younger age. These outcomes implies different bounds on the ADM from each star. For instance for a mass of the ADM $m_\chi = 5\ GeV$, r_{02} data exclude a cross section $\sigma \gtrsim 6 \times 10^{-36}$ for the Sun; $\sigma \gtrsim 5 \times 10^{-36}$ for KIC 7871531, and $\sigma \gtrsim 4 \times 10^{-36}$ for KIC 8379927.

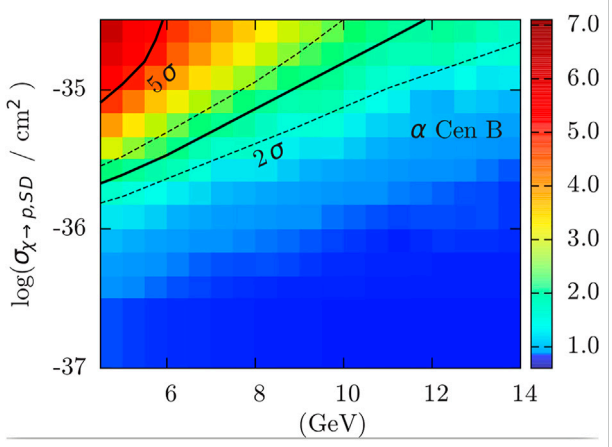

FIGURE 3
Deviations of the observed and simulated (with ADM) small separation values of α Cen B (0.93 $M_\odot$), in units of σ (color map). The deviations are plotted vs. the logarithm of the spin-dependent cross sections ($\log(\sigma_{\chi\to p})$), and masses in GeV, two parameters of the asymmetric dark matter. The solid black line shows the two σ region. The dashed lines around the solid black one indicate the observational errors. Taken by Casanellas and Lopes (2013).

3.2 Constraints on dark matter from evolved stars

In this section we discuss the constraints imposed by Ayala et al. (2020) on dark matter models from red giant branch stars. We focused on the dark photons, which can interact with the electromagnetic sector of the Standard Model, being produced by means of plasmon oscillations in the degenerate cores of red giant stars. These particles could carry away energy from the stellar cores, affecting the luminosities at the RGB bump and tip phases, as we have found before (Ayala et al., 2015).

In a previous work by Khan et al. (2018) the authors looked into the effect of introducing the core overshooting on the pulsation models of RGB stars at the bump, finding an increase of the average large separation. As both processes, core overshooting and dark photon emission, could affect the size of the internal core of the stars, we made the hypothesis that dark photons would increase the large separation too. Therefore, to check this hypothesis, we decided to simulate RGB stars at the bump phase, including the production of dark photons in the models, and to obtain the frequencies of pulsation and the large separation from each simulation. We computed a grid of stellar models with different initial star masses and allowing different values of dark photon masses (m_V) and kinetic mixing (χ). As core overshooting could compete with the effect of dark photons, we also included this in some models of our grid.In order to characterize the frequencies and large separation of a sample of RGB stars at the bump phase, we used a catalogue of seismic data of RGB stars (Albareti et al., 2017) and the previous analysis of Khan et al. (2018). The observational data of the average **large** separation and the corresponding errors are represented by the black line at Figure 4. Our models prediction for large separation are represented by the color and color dashed lines, the latter considering the combined effect of overshooting and dark photon energy losses. We verified the increase of large separation with respect to the increase of the mass and the kinetic mixing of the dark photon, which drive the total amount of energy carried away by this particle (Redondo and Raffelt, 2013; Ayala et al., 2015; Ayala et al., 2020). As both processes, dark photon emission and overshooting, reinforce together on increasing the large separation, we were able to rule out several dark photon models, where even a minimum core overshooting implies a large separation beyond the observational 2σ limits (see Figure 4 and Figure 5). In particular, we excluded the models with mass $900eV$ and χ values 5×10^{-15}, 7×10^{-15}, and 9×10^{-15}; mass $700eV$ and χ values of 7×10^{-15}, and 9×10^{-15}; and mass $500eV$ and χ of 9×10^{-15}.

With this study, we demonstrated that near the so-called RGB bump, dark photons production may be an energy sink for the star significative enough to modify the extension of the convective zones, in a way detectable with modern asteroseismic techniques. A follow-up of this study, taking

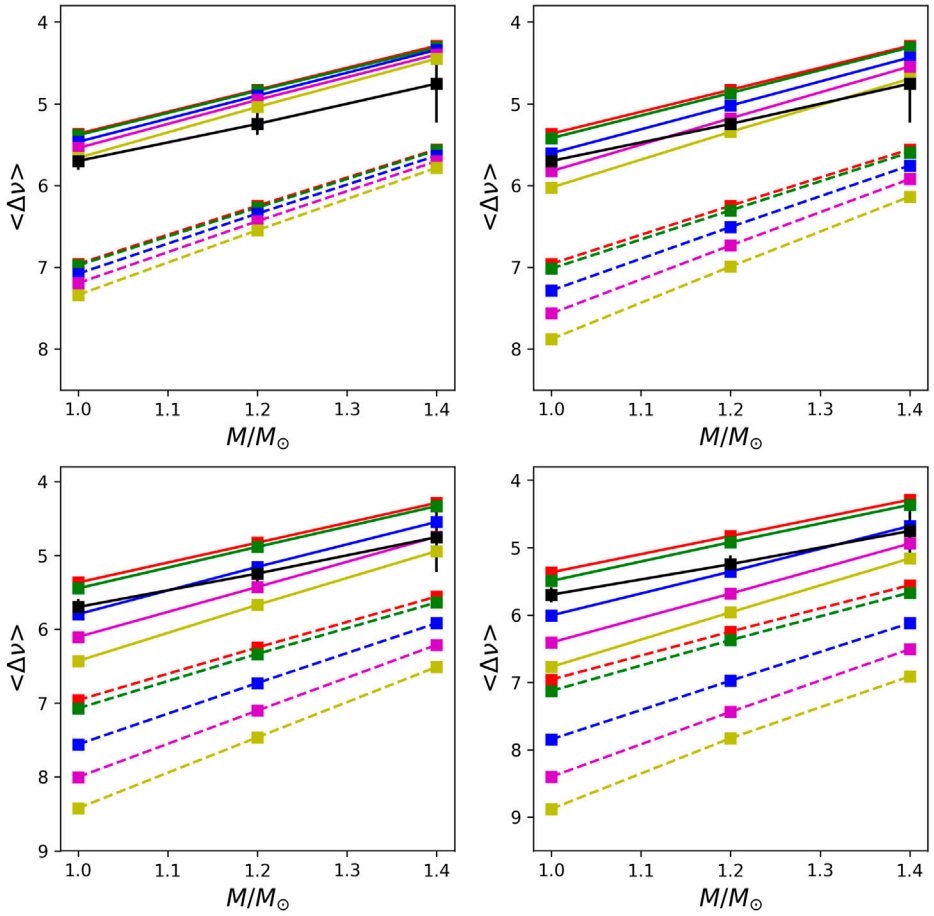

FIGURE 4
Variations of the large separation, $\Delta\nu$, vs. the initial mass $M/M_{\odot}$ for a set of simulations of RGB stars, introducing the production of dark photon models. Black line correspond to the observations of the large separation. The different panels correspond to m_V (dark photon masses) of 300 eV (upper left panel), 500 eV (upper right), 700 eV (lower left) and 900 eV (lower right). For each panel the solid lines correspond to models with kinetic mixing (χ) values of $\chi = 0$ (red), $\chi = 2 \times 10^{-15}$ (green), $\chi = 5 \times 10^{-15}$ (blue), $\chi = 7 \times 10^{-15}$ (magenta), and $\chi = 9 \times 10^{-15}$ (yellow). Dashed lines correspond to stellar models with χ given by the same color code, but considering a moderate core overshooting, $\alpha_{ov} = 0.025$. Taken from Ayala et al. (2020).

into account the observational uncertainties, and where we expect to derive stronger bounds, is in progress.

3.3 Degenerate stars and new hypothetical objects

In case of the degenerate stars, white dwarfs are a good scenario for axion physics. These objects excite g-mode oscillations with a period well measured by several authors (Córsico et al., 2019; Kepler et al., 2021). According to previous research, the period drift of g-modes of some pulsating white dwarfs, that is, the rate of change of the pulsation period, can not be explained by means of the standard cooling mechanism, which invokes mainly photon and neutrino cooling processes. Therefore an excess in the rate of change of the period exists. This is the case of the pulsating WD G117-B15A (Figure 6), a ZZ Ceti object Isern et al. (2022); Córsico et al. (2019). For this white dwarf the discrepancy between the standard theory and the observations has been explained with the inclusion in the models of an additional cooling process, due to axion emission (Isern et al., 2022). If an additional axion cooling is included for G117-B15A, the energy, ϵ_{eff} changes, according to Eq 6.

$$\epsilon_{eff} = \epsilon_{nu} - \epsilon_{\nu} - \epsilon_{a} \tag{6}$$

Where ϵ_{nu}, ϵ_{ν} and ϵ_{a} stand for the nuclear energy, neutrino and axion rates, respectively. ϵ_{nu} vanishes in general in the case of white dwarfs. Therefore, G117-B15A losses energy by means of the combined emission of neutrinos and axions, the latter with a rate proportional to the square of axion-electron coupling, g_{ae}

$$\epsilon_{a} \propto g_{ae}^{2} \tag{7}$$

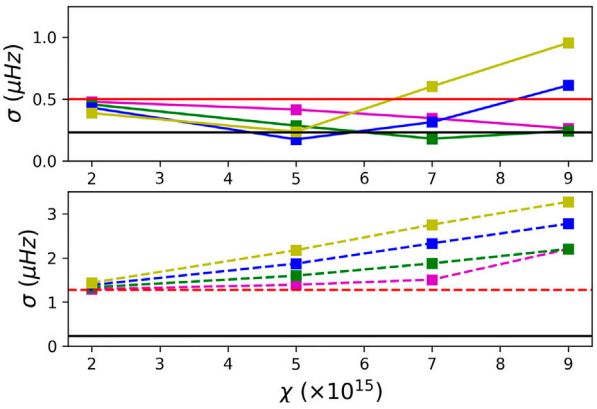

FIGURE 5
χ^2 test values (given by σ (μHz)), of the theoretical large separation, when dark photons are introduced in the models, with respect to the RGB observations. The plot shows the variation of σ (μHz) vs. the dark photon kinetic mixing, χ. We consider dark photons and overshooting. The solid lines with squares represent the scenarios without overshooting, whereas the dashed with squares are the models combining dark photons and overshooting. The red solid line in the upper panel corresponds to models without dark photons nor overshooting, whereas the dashed red line in lower panel represents the overshooting models, without dark photons. The colors indicate dark photon masses of 300 *eV* (magenta), 500 *eV* (green), 700 *eV* (blue) and 900 *eV* (yellow). The observational 2σ errors are indicated by the black solid line.

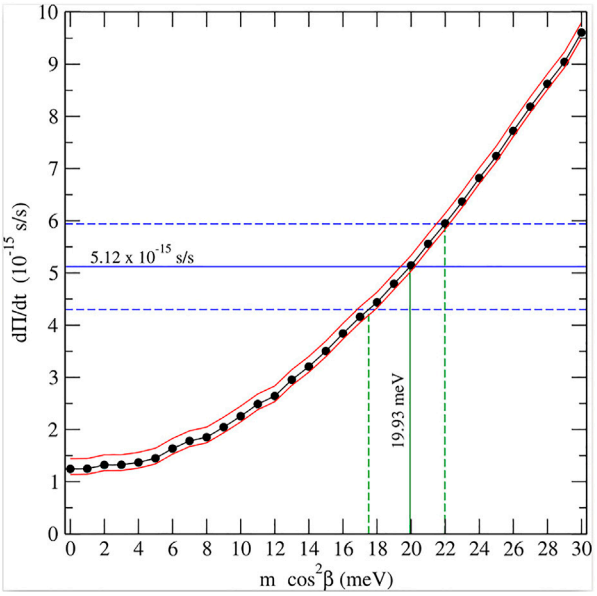

FIGURE 6
Period drift, $d\Pi/dt$ in s/s, vs. $m_a \cos^2\beta$ (in meV) in G117-B15A: a plausible consequence of axion additional cooling (see text for details. Taken from Kepler et al. (2021).

On the other hand, g_{ae} is proportional to the axion mass and the square of the cosine of a certain angle β (Córsico et al., 2019; Isern et al., 2022)

$$g_{ae} = 2.8 \times 10^{-14} m_a \cos^2 \beta \tag{8}$$

The more massive the axion is the larger is the axion emission, which speeds up the cooling process and increases the rate of change of period of the white dwarf. Using this axion cooling model and the period drift of G117-B15A, Isern et al. (1992) obtained an upper limit for the axion-electron coupling ($g_{ae} \leq 2.4 \times 10^{-13}$), as well as for the product $m_a \cos^2\beta$ ($m_a \cos^2\beta \leq 8.7\ meV$). Considering recent measurements of the period change ratio, and excluding the hypothetical effects on the light curve due to magnetic fields or planets, Kepler et al. (2021) give the values $g_{ae} = 5.66 \pm 0.57 \times 10^{-13}$, and $m_a \cos^2\beta = 20 \pm 2\ meV$. These are obtained from the theoretical curve of period drift vs. $m_a \cos^2\beta$, computed using a complete asteroseismic model, and the observational value limits, as it is shown in Fig 6.

Concerning the constraints on dark matter from the Asteroseismology of more exotic objects, it is worth mentioning boson or axion stars (Hung-Hsu Chan et al., 2022). These are puzzling theoretical objects, predicted by some light dark-matter models, where Bose-Einstein condensate of axions is supposed to originate self-gravitant axion spheres, called axion stars. The theoretical non-radial pulsation power spectrum, originated by the tidal distorsion of the axion star due to a neutron star companion has been calculated in a recent paper (Panotopoulos and Lopes, 2019). This spectrum is derived assuming well-known asteroseismic model, compatible with the equation of state of the axion star, and should be characteristic of this kind of object. The spectrum is also potentially detectable, if the axion star interacts with the magnetic field of a companion, for instance a neutron star with a strong magnetic field, which enables the conversion of axions into photons.

4 Discussion and future work

The search of dark matter using Asteroseismology will become more important in next decades. Next generation missions, like PLATO (Martins et al., 2017; Rauer, 2021), or HAYDN (Miglio et al., 2021) will increase the volume of available data and will make possible the systematic study of stellar populations like those of the Globular Clusters. This will be a great opportunity to complement the previous constraints on dark matter from these stars, coming from photometry (Viaux et al., 2013; Ayala et al., 2014). Moreover, the increase of precision of the future asteroseismic surveys could find significative differences between the stars close to the halo of the Milky Way and those laying on the galactic plane, which

could confirm or not the influence of dark matter on the internal processes of the halo stars.

The refinement of asteroseismic observations will impact the accurate description of the stellar interiors. The elucidation of the role played by convection in the overall energy transport of the stars, and the determination of the extensions of the convective structures are two goals of Asteroseismology, which, when fully accomplished, will impose bounds on several dark matter models.

In the next years, the increase of precision in the measurements of solar-like and giant stars pulsations will enable to impose constraints on light **particle dark** matter, which can be produced by thermal resonant processes in stars. These constraints will complement the direct and indirect search of WISPs (Weakly Interacting Slim Particles) like axions or dark photons (Jaeckel and Ringwald, 2010). In summary, Asteroseismology besides stellar models will be fundamental for the study of dark matter in the next decades.

Author contributions

I am the first and only author. The preparation of the manuscript and the figures was done by me. I am also responsible of the selection of the contents and the discussion of this review.

Acknowledgments

I thank professor Ilidio Lopes and Jordi Casanellas for fruitful conversations about the topic of this review. I also acknowledge the support and motivation for writing this paper, given to me from my colleagues of the Variable Stars group at IAA-CSIC. Finally, I thank two referees for several suggestions to improve the original manuscript. The author acknowledges financial support from the State Agency for Research of the Spanish MCIU through the "Center of Excellence Severo Ochoa" award to the Instituto de Astrofísica de Andalucía (SEV-2017-0709).

Conflict of interest

The author declares that the research was conducted in the absence of any commercial or financial relationships that could be construed as a potential conflict of interest.

Publisher's note

References

Aerts, C., Christensen-Dalsgaard, J., and Kurtz, D. W. (2010). *Asteroseismology*.

Albareti, F. D., Prieto, C. A., Almeida, A., Anders, F., Anderson, S., Andrews, B. H., et al. (2017). The 13th data release of the sloan digital sky survey: First spectroscopic data from the sdss-iv survey mapping nearby galaxies at Apache point observatory. *Astrophysical J. Suppl. Ser.* 233, 25.

An, H., Pospelov, M., Pradler, J., and Ritz, A. (2014). *Direct detection constraints on dark photon dark matter. ArXiv e-prints*.

Armengaud, E., Avignone, F. T., Betz, M., Brax, P., Brun, P., Cantatore, G., et al. (2014). Conceptual design of the international axion observatory (IAXO). *J. Instrum.* 9, T05002. doi:10.1088/1748-0221/9/05/T05002

Ayala, A., Domínguez, I., Giannotti, M., Mirizzi, A., and Straniero, O. (2014). Revisiting the bound on axion-photon coupling from globular clusters. *Phys. Rev. Lett.* 113, 191302. doi:10.1103/PhysRevLett.113.191302

Ayala, A., Lopes, I., García Hernández, A., Suárez, J. C., and Muñoz Elorza, Í. (2020). Constraining dark photon properties with Asteroseismology. *Mon. Not. R. Astron. Soc.* 491, 409–416. doi:10.1093/mnras/stz3002

Ayala, A., Straniero, O., Giannotti, M., Mirizzi, A., and Dominguez, I. (2015). "Effects of hidden photons during the red giant branch (RGB) phase," in 11th Patras Workshop on Axions, WIMPs and WISPs, 189–192. doi:10.3204/DESY-PROC-2015-02/ayala_adrian

Baglin, A., Michel, E., and Auvergne, M.COROT Team (2006). "The seismology programme of the CoRoT space mission," in *Proceedings of SOHO 18/GONG 2006/ HELAS I, beyond the spherical Sun. Vol. 624 of ESA special publication*, 34.

Bertone, G. (2010). "Dark matter and stars," in *Particle dark matter : Observations, models and searches*. Editor G. Bertone, 586.

Cadamuro, D., and Redondo, J. (2010). *Hidden photons from the Sun. ArXiv e-prints*.

Casanellas, J., and Lopes, I. (2013). First asteroseismic limits on the. *Astrophys. J.* 765, L21. doi:10.1088/2041-8205/765/1/L21

Casanellas, J., and Lopes, I. (2011). Signatures of dark matter burning in nuclear star clusters. *Astrophys. J.* 733, L51. doi:10.1088/2041-8205/733/2/L51

Christensen-Dalsgaard, J. (2004). Physics of solar-like oscillations. *Sol. Phys.* 220, 137–168. doi:10.1023/B:SOLA.0000031392.43227.7d

Córsico, A. H., Althaus, L. G., Miller Bertolami, M. M., and Kepler, S. O. (2019). Pulsating white dwarfs: New insights. *Astron. Astrophys. Rev.* 27, 7. doi:10.1007/s00159-019-0118-4

Córsico, A. H., Althaus, L. G., Romero, A. D., Mukadam, A. S., García-Berro, E., Isern, J., et al. (2012). An independent limit on the axion mass from the variable white dwarf star R548. *J. Cosmol. Astropart. Phys.* 2012, 010. doi:10.1088/1475-7516/2012/12/010

Córsico, A. H., Benvenuto, O. G., Althaus, L. G., Isern, J., and García-Berro, E. (2001). The potential of the variable DA white dwarf G117-B15A as a tool for fundamental physics. *New Astron.* 6, 197–213. doi:10.1016/S1384-1076(01)00055-0

Domingo, V., Fleck, B., and Poland, A. I. (1995). The SOHO mission: An overview. *Sol. Phys.* 162, 1–37. doi:10.1007/BF00733425

Gabriel, A. H., Charra, J., Grec, G., Robillot, J. M., Roca Cortés, T., Turck-Chièze, S., et al. (1997). Performance and early results from the GOLF instrument flown on the SOHO mission. *Sol. Phys.* 175, 207–226. doi:10.1023/A:1004911408285

Gabriel, A. H., Grec, G., Charra, J., Robillot, J. M., Roca Cortés, T., Turck-Chièze, S., et al. (1995). Global oscillations at low frequency from the SOHO mission (GOLF). *Sol. Phys.* 162, 61–99. doi:10.1007/BF00733427

Gudnason, S. B., Kouvaris, C., and Sannino, F. (2006). Towards working technicolor: Effective theories and dark matter. *Phys. Rev. D.* 73, 115003. doi:10.1103/PhysRevD.73.115003

Hung-Hsu Chan, J., Sibiryakov, S., and Xue, W. (2022). *Condensation and evaporation of boson stars. arXiv e-prints, arXiv:2207.04057*.

Iocco, F. (2008). Dark matter capture and annihilation on the first stars: Preliminary estimates. *Astrophys. J.* 677, L1–L4. doi:10.1086/587959

Isern, J., and García-Berro, E. (2008). White dwarfs as physics laboratories: The axion case. *PATRAS* 79, 545.

Isern, J., Hernanz, M., and Garcia-Berro, E. (1992). Axion cooling of white dwarfs. *Astrophys. J.* 392, L23. doi:10.1086/186416

Isern, J., Torres, S., and Rebassa-Mansergas, A. (2022). White dwarfs as physics laboratories: Lights and shadows. *Front. Astron. Space Sci.* 9, 6. doi:10.3389/fspas.2022.815517

Jaeckel, J., and Ringwald, A. (2010). The low-energy frontier of particle physics. *Annu. Rev. Nucl. Part. Sci.* 60, 405–437. doi:10.1146/annurev.nucl.012809.104433

Kepler, S. O., Winget, D. E., Vanderbosch, Z. P., Castanheira, B. G., Hermes, J. J., Bell, K. J., et al. (2021). The pulsating white dwarf G117-B15A: Still the most stable optical clock known. *Astrophys. J.* 906, 7. doi:10.3847/1538-4357/abc626

Khan, S., Hall, O. J., Miglio, A., Davies, G. R., Mosser, B., Girardi, L., et al. (2018). The red-giant branch bump revisited: Constraints on envelope overshooting in a wide range of masses and metallicities. *Astrophys. J.* 859, 156. doi:10.3847/1538-4357/aabf90

Koch, D., Borucki, W., Jenkins, J., Basri, G., Batalha, N. M., Brown, T. M., et al. (2010). "The kepler mission and early results," in 38th COSPAR Scientific Assembly. vol. 38 of COSPAR Meeting.

Kurtz, D. (2022). *Asteroseismology across the HR diagram*. *arXiv e-prints*, arXiv: 2201.11629.

Lopes, I., and Panotopoulos, G. (2020). Radial oscillations of boson stars made of ultralight repulsive dark matter. *Nucl. Phys. B* 961, 115266. doi:10.1016/j.nuclphysb.2020.115266

Lopes, I., and Silk, J. (2012). Solar constraints on asymmetric dark matter. *Astrophys. J.* 757, 130. doi:10.1088/0004-637X/757/2/130

Lopes, J., Lopes, I., and Silk, J. (2019). Asteroseismology of red clump stars as a probe of the dark matter content of the galaxy central region. *Astrophys. J.* 880, L25. doi:10.3847/2041-8213/ab2fdd

Martins, A., Lopes, I., and Casanellas, J. (2017). Asteroseismic constraints on asymmetric dark matter: Light particles with an effective spin-dependent coupling. *Phys. Rev. D.* 95, 023507. doi:10.1103/PhysRevD.95.023507

Miglio, A., Girardi, L., Grundahl, F., Mosser, B., Bastian, N., Bragaglia, A., et al. (2021). Haydn. *Exp. Astron.* 51, 963–1001. doi:10.1007/s10686-021-09711-1

Milgrom, M. (1983). A modification of the Newtonian dynamics as a possible alternative to the hidden mass hypothesis. *Astrophys. J.* 270, 365–370. doi:10.1086/161130

Panotopoulos, G., and Lopes, I. (2019). Acoustic modes of pulsating axion stars: Nonradial oscillations. *Int. J. Mod. Phys. D.* 28, 1950111. doi:10.1142/S0218271819501116

Peccei, R. D., and Quinn, H. R. (1977). Constraints imposed byCPconservation in the presence of pseudoparticles. *Phys. Rev. D.* 16, 1791–1797. doi:10.1103/PhysRevD.16.1791

Raffelt, G. G., and Dearborn, D. S. P. (1987). Bounds on hadronic axions from stellar evolution. *Phys. Rev. D.* 36, 2211–2225. doi:10.1103/PhysRevD.36.2211

Raffelt, G. G. (1999). "Stars as particle-physics laboratories," in *The Eighth mexican school on particles and fields. Vol. 490 of American Institute of physics conference series*. Editors J. C. D'Olivo, G. López Castro, and M. Mondragón, 125–162. doi:10.1063/1.1301384

Rauer, H. (2021). "PLATO science objectives and PLATO Mission Consortium," in Plato Mission Conference 2021. Presentations and posters of the online PLATO Mission Conference 2021, 104. doi:10.5281/zenodo.5585341

Redondo, J., and Raffelt, G. (2013). Solar constraints on hidden photons re-visited. *J. Cosmol. Astropart. Phys.* 1308, 034. doi:10.1088/1475-7516/2013/08/034

Ricker, G. R., Winn, J. N., Vanderspek, R., Latham, D. W., Bakos, G. Á., Bean, J. L., et al. (2015). Transiting exoplanet survey satellite. *J. Astron. Telesc. Instrum. Syst.* 1, 014003. doi:10.1117/1.JATIS.1.1.014003

Scott, P., Fairbairn, M., and Edsjo, J. (2008). "Impacts of WIMP dark matter upon stellar evolution: Main-sequence stars," in Identification of Dark Matter 2008, Stockholm, Sweden, 73.

Silva Aguirre, V., Lund, M. N., Antia, H. M., Ball, W. H., Basu, S., Christensen-Dalsgaard, J., et al. (2017). Standing on the shoulders of dwarfs: The kepler asteroseismic LEGACY sample. II.Radii, masses, and ages. *Astrophys. J.* 835, 173. doi:10.3847/1538-4357/835/2/173

Taoso, M., Bertone, G., Meynet, G., and Ekström, S. (2008). "WIMPs annihilations in Pop III stars," in Identification of Dark Matter 2008, Stockholm, Sweden, 76.

Taoso, M., Iocco, F., Meynet, G., Bertone, G., and Eggenberger, P. (2010). Effect of low mass dark matter particles on the sun. *Phys. Rev. D.* 82, 083509. doi:10.1103/PhysRevD.82.083509

Tassoul, M. (1980). Asymptotic approximations for stellar nonradial pulsations. *Astrophys. J. Suppl. Ser.* 43, 469–490. doi:10.1086/190678

Tassoul, M. (1990). Second-order asymptotic approximations for stellar nonradial acoustic modes. *Astrophys. J.* 358, 313. doi:10.1086/168988

Turck-Chièze, S., and Lopes, I. (2012). Solar-stellar astrophysics and dark matter. *Res. Astron. Astrophys.* 12, 1107–1138. doi:10.1088/1674-4527/12/8/011

Viaux, N., Catelan, M., Stetson, P. B., Raffelt, G. G., Redondo, J., Valcarce, A. A. R., et al. (2013). Neutrino and axion bounds from the globular cluster M5 (NGC 5904). *Phys. Rev. Lett.* 111, 231301. doi:10.1103/PhysRevLett.111.231301

Vinyoles, N., Serenelli, A., Villante, F. L., Basu, S., Redondo, J., and Isern, J. (2015). New axion and hidden photon constraints from a solar data global fit. *J. Cosmol. Astropart. Phys.* 10, 015. doi:10.1088/1475-7516/2015/10/015

Wilczek, F. (1978). Problem of strong *P* and *T* invariance in the presence of instantons. *Phys. Rev. Lett.* 40, 279–282. doi:10.1103/PhysRevLett.40.279

frontiers | Frontiers in Astronomy and Space Sciences

TYPE Review
PUBLISHED 30 September 2022
DOI 10.3389/fspas.2022.934579

OPEN ACCESS

EDITED BY
Zhao Guo,
University of Cambridge,
United Kingdom

REVIEWED BY
Catherine Lovekin,
Mount Allison University, Canada
Dominic Bowman,
KU Leuven, Belgium

*CORRESPONDENCE
Daniel Roy Reese,
daniel.reese@obspm.fr

SPECIALTY SECTION
This article was submitted to Stellar and Solar Physics,
a section of the journal
Frontiers in Astronomy and Space Sciences

RECEIVED 02 May 2022
ACCEPTED 11 July 2022
PUBLISHED 30 September 2022

CITATION
Reese DR (2022), 2D modelling of pulsating stars with rapid rotation. *Front. Astron. Space Sci.* 9:934579. doi: 10.3389/fspas.2022.934579

2D modelling of pulsating stars with rapid rotation

Daniel Roy Reese*

LESIA, Observatoire de Paris, Université PSL, CNRS, Sorbonne Université, Université Paris Cité, Meudon, France

Rapid stellar rotation is an important phenomenon in stellar physics, particularly for massive and intermediate mass main-sequence stars. This affects all aspects of the star's physics including its structure, evolution, and pulsations, and makes it necessary to use 2D numerical approaches rather than the 1D approaches typically used. In this contribution, we will review 2D numerical methods for modelling and interpreting pulsation modes in rapidly rotating stars. We will start by deriving the pulsation equations, both in an adiabatic and non-adiabatic setting, then provide a description of the 2D numerical implementation. We will then explain approximate implementations of the effects of rotation, namely first, second, and third order perturbative approaches, as well as the traditional approximation. This will then be followed by a description on how to calculate disk-integrated mode visibilities in various photometric bands, and how to apply this to mode identification in rapid rotators. Finally, we will review some of the recent works that interpret the pulsation spectra of various stars as viewed in either a single photometric band or in multiple bands, and including supplementary constraints from interferometry and spectroscopy.

KEYWORDS

stars: pulsation, stars: rotation, stars: interior, stars: evolution, numerical simulations, stars: individual: μ Eridani, β Pictoris, Altair

1 Introduction

Much progress has been made in our understanding of stellar physics thanks to the advent of elaborate 1D numerical simulations of stars. The basic hydrostatic structure, energy transport, and essential stages of stellar evolution are understood. Nonetheless, the shortcomings of 1D spherically symmetric models are becoming increasingly apparent, particularly on a macroscopic scale. Indeed, rotation, convection, and transport processes remain poorly understood and require the use of higher dimensional simulations to be modelled correctly. In particular, rapid stellar rotation causes significant departures from spherical symmetry thanks to centrifugal distortion and gravity darkening, as confirmed by increasingly sophisticated observations such as those coming from interferometry (e.g., Domiciano de Souza et al., 2003; Monnier et al., 2007). Furthermore, it affects the evolution, lifetimes, and chemical yields of such stars (Meynet and Maeder, 2000) through transport processes caused by rotation-related instabilities. As can be seen in Figure 1, based on Royer, (2009), the majority of intermediate and high mass main sequence stars rotate rapidly. Accordingly, in order to describe such stars, it is necessary to use a 2D approach when modelling the structure, evolution, and pulsations of these stars.

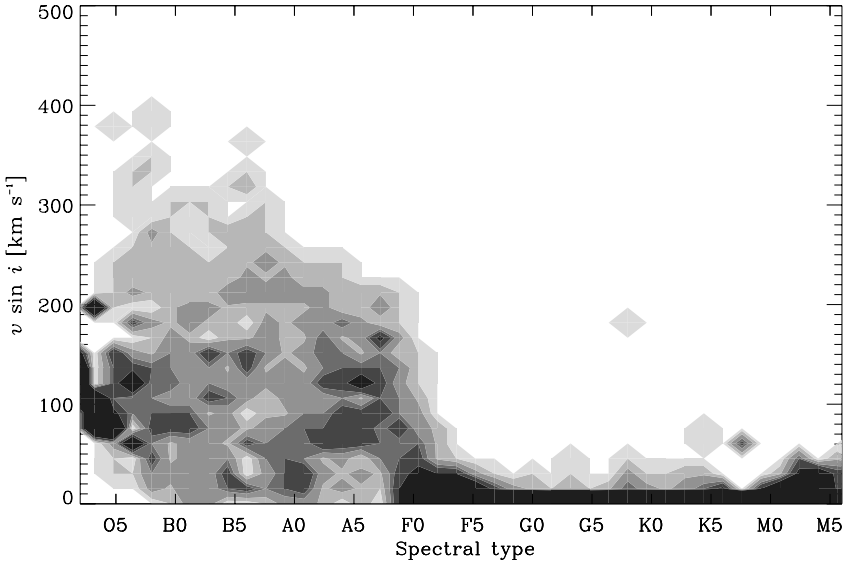

FIGURE 1
Distribution of projected equatorial velocities, $v \sin i$, as a function of stellar spectral type. As can be seen, there is a clear distinction between stars earlier than F0, and later type (solar-like) stars (Credit: F. Royer, based on Royer, 2009).

In the present contribution, we will focus on the 2D modelling and interpretation of stellar pulsations in rapidly rotating stars. Understanding such pulsations is one of the keys to understanding such stars and the effects of rotation, as it is currently the only way to probe their internal structure. However, rotation greatly complicates the pulsation spectra of these stars thus making them more difficult to decipher. In particular, correctly identifying modes, i.e., finding the match between observed and theoretically calculated pulsations, is a long-standing obstacle but also a prerequisite to detailed seismic investigations of such stars. Therefore, various strategies have been devised in order to overcome this obstacle as described below.

This contribution is organised as follows: Section 2 describes how to calculate stellar pulsations in rotating stellar models. More specifically, it briefly addresses rotating stellar models before explaining how to carry out 2D pulsation calculations, both in the adiabatic and non-adiabatic cases. It also describes approximate methods for including the effects of rotation, namely the perturbative approach and the use of the traditional approximation. Section 3 briefly describes some of the impacts of rapid rotation on stellar pulsations and introduces acoustic island modes. Section 4 describes some of the mode observables that may be used to help identify the observed modes, namely mode visibilities, amplitude ratios, and phase differences. Section 5 then provides a few recent examples of mode identification and seismic interpretation of rapidly rotating stars. Finally, Section 6 briefly concludes this paper.

2 Calculating stellar pulsations

2.1 Rotating models

The equations describing stellar pulsations are obtained by perturbing the fluid dynamic equations around an equilibrium model of the star. Accordingly, in order to fully account for the effects of rotation, it is essential to have at one's disposal an equilibrium model that fully takes into account the effects of rotation. In particular the effects of centrifugal acceleration on the hydrostatic equilibrium of the model are crucial for calculating pulsations, even when the adiabatic approximation is being made, i.e., where energy exchanges are neglected during the pulsations. This is expressed *via* the following relation:

$$\vec{v}_0 \cdot \vec{\nabla}\vec{v}_0 = -\frac{\vec{\nabla}P_0}{\rho_0} - \vec{\nabla}\Psi_0 \tag{1}$$

where $\vec{v}$ is the fluid velocity field, ρ the density, P the pressure, Ψ the gravitational potential, and where we have neglected viscosity. The subscript "0" signifies that these are equilibrium quantities as opposed to perturbations resulting from oscillations (see following section). The velocity field is mainly caused by rotation and therefore takes on the expression $\vec{v}_0 = \Omega(s,z)s\vec{e}_\phi$, where $\Omega(s,\ z)$ is the rotation profile. Accordingly, the left-hand side of the above equation takes on the following expression:

$$\vec{v}_0 \cdot \vec{\nabla}\vec{v}_0 = -\Omega^2(s,z)s\vec{e}_s \tag{2}$$

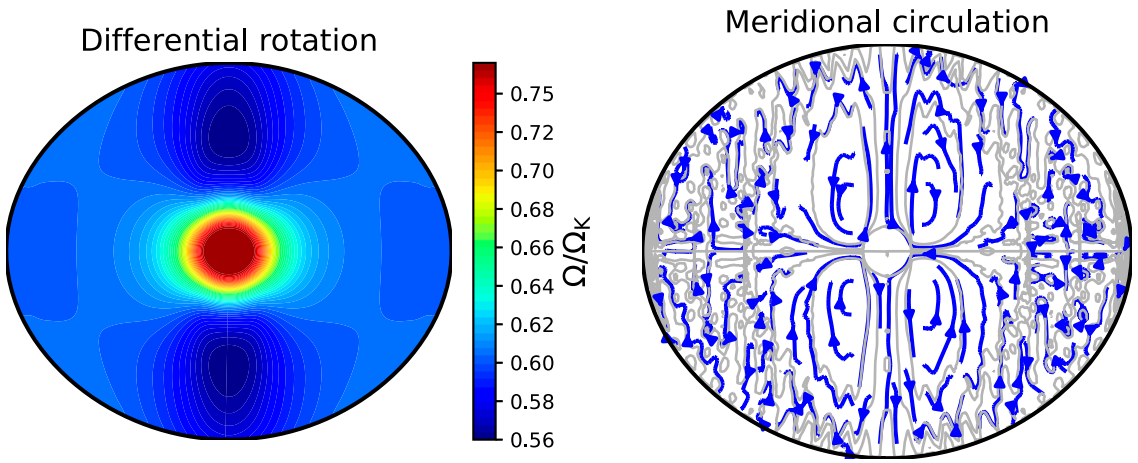

FIGURE 2
Differential rotation **(A)** and meridional circulation **(B)** as a result of baroclinic effects in a 2 M ESTER model rotating at 0.6 Ωk (see also Espinosa and Rieutord 2013, and Rieutord et al., 2016 for similar plots).

where we have used cylindrical coordinates (s, ϕ, z) and their associated unit vectors for convenience. This expression is easily recognised as the centrifugal acceleration.

Various models fully take into account centrifugal deformation such as ROTORC models (Deupree, 1990; Deupree, 1995), Self-Consistent Field (SCF) models (Jackson et al., 2005; MacGregor et al., 2007), or Evolution STEllaire en Rotation (ESTER) models (Espinosa Lara and Rieutord, 2013; Rieutord et al., 2016). Another approach is to deform 1D (i.e., spherically symmetric) models by subsequently introducing the effects of the centrifugal acceleration. This approach was first proposed by Roxburgh, (2006) for arbitrary 2D rotation profiles. More recently, Manchon, (2021) applied a similar strategy for CESTAM models (Marques et al., 2013). The advantage of such an approach is the possibility of using highly sophisticated 1D stellar evolution models which take into account in a 1D formalism the horizontally-averaged effects of rotation (Meynet and Maeder, 2000; Palacios et al., 2003; Maeder, 2009; Marques et al., 2013).

If one wishes to take into account energy exchanges during the pulsations, i.e., carry out fully non-adiabatic pulsation calculations, it is necessary to deal with the energy conservation equation in a self-consistent way in the model itself. Taking these effects into account leads to baroclinic models, i.e., models where lines of constant pressure, density, and temperature do not coincide. Indeed, lines of constant pressure are determined by the hydrostatic equilibrium whereas lines of constant temperature depend on the propagation of energy inside the star, and typically tend to be more spherical. As a result, this leads to baroclinic flows, namely a non-conservative (i.e., non-cylindrical) rotation profile and meridional circulation. To show the link between non-cylindrical rotation and baroclinicity, one can take the curl of Eq. 1:

$$-s\frac{\partial \Omega^2}{\partial z}\vec{e}_\phi = \frac{\vec{\nabla}\rho_0 \times \vec{\nabla}P_0}{\rho_0^2} \tag{3}$$

The right hand side of this equation differs from zero because lines of constant pressure and density do not coincide, and thus leads to a vertical gradient of the rotation profile. Figure 2 illustrates a differential rotation profile and meridional circulation resulting from baroclinic effects[1], obtained in an ESTER model. This in turn causes various instabilities, turbulence, and transport processes. Currently, the only models where the energy equation and baroclinic effects are taken into account in a fully 2D setting are ESTER models. In 1D models such as those from the Geneva code, STAREVOL, or CESTAM, this is achieved in a horizontally-averaged rather than local way based on the assumption of anisotropic turbulence and mixing (Zahn, 1992).

Having briefly described the rotating models at our disposal, we now turn our attention to the pulsation calculations themselves.

2.2 Adiabatic analysis

As a first step, it is simpler to calculate stellar pulsations using the adiabatic approximation, i.e., to neglect energy

1 We note that viscosity must also be taken into account in order to fully determine Ω (Espinosa Lara and Rieutord, 2013).

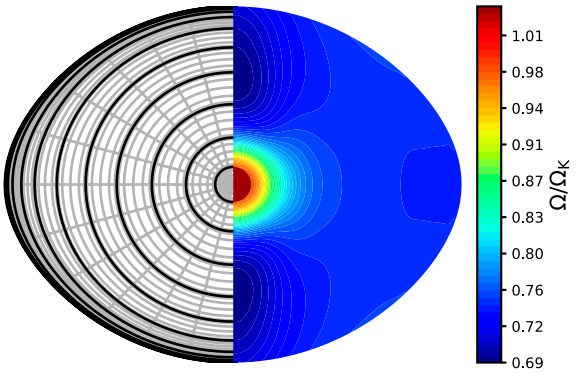

FIGURE 3
Multi-domain coordinate system **(A)** and rotation profile **(B)** in the best fitting model for Altair from Bouchaud et al. (2020) (see also Rieutord et al., 2016 for a similar plot involving a 3 M⊙ rotating model).

exchanges (primarily in the form of heat) during the pulsations. When rotation is present, various effects must be taken into account. Firstly, the centrifugal deformation must be taken into account, typically through the use of surface-fitting spheroidal coordinates in the pulsation equations. Indeed, using such coordinates are necessary in order to maintain accuracy when imposing boundary conditions. Figure 3 illustrates a multi-domain surface-fitting coordinate system in an ESTER model. Secondly, the Coriolis acceleration intervenes in the oscillatory motions. In some cases such as inertial modes, it is the restoring force and thus the reason for their existence. Putting this together leads to the following set of equations in an inertial frame:

$$\frac{\delta\rho}{\rho_0} + \vec{\nabla}\cdot\vec{\xi} = 0 \tag{4}$$

$$\frac{D_0^2\vec{\xi}}{Dt^2} - \vec{\xi}\cdot\vec{\nabla}\left(\vec{v}_0\vec{\nabla}\cdot\vec{v}_0\right) = -\frac{\vec{\nabla}P'}{\rho_0} + \frac{\rho'\vec{g}_{\rm eff}}{\rho_0} - \vec{\nabla}\Psi' \tag{5}$$

$$\frac{\delta p}{P_0} = \Gamma_1\frac{\delta\rho}{\rho_0} \tag{6}$$

$$\Delta\Psi' = 4\pi G\rho' \tag{7}$$

where Eq. 4 corresponds to the continuity equation, Eq. 5 to Euler's momentum equation, Eq. 6 to the adiabatic relation, and Eq. 7 to Poisson's equation. Quantities preceded by δ correspond to Lagrangian perturbations, and quantities with a prime to Eulerian perturbations. The operator $\frac{D_0}{Dt} = \frac{\partial}{\partial t} + \vec{v}_0\cdot\vec{\nabla}$ denotes the Lagrangian time derivative, $\vec{\xi}$ the Lagrangian displacement, $\vec{g}_{\rm eff} = \vec{\nabla}P_0/\rho_0$ the effective gravity (i.e., including both gravity and the centrifugal acceleration), Γ_1 the first adiabatic exponent, and G the gravitational constant. We note that Eq. 5 is obtained by taking the Lagrangian perturbation of Euler's momentum equation (e.g., Lynden-Bell and Ostriker, 1967), and rearranging some of the terms thanks to the hydrostatic equilibrium (Eq. 1).

When studying pulsation modes, one assumes a harmonic time dependence of the form $\exp(i\omega t)$, where ω corresponds to the pulsation frequency. Furthermore, although the star is no longer spherically symmetric because of centrifugal deformation, it is still symmetric around the rotation axis. As a result, pulsation modes have an azimuthal dependence of the form $\exp(im\phi)$, where m is the azimuthal order. This can be used to rewrite the left-hand side of Eq. 5:

$$\begin{aligned}\frac{D_0^2\vec{\xi}}{Dt^2} - \vec{\xi}\cdot\vec{\nabla}\left(\vec{v}_0\vec{\nabla}\cdot\vec{v}_0\right) = &-(\omega+m\Omega)^2\vec{\xi} + 2i(\omega+m\Omega)\vec{\Omega}\times\vec{\xi} \\ &+\vec{\Omega}\times\left(\vec{\Omega}\times\vec{\xi}\right) + \vec{\xi}\cdot\vec{\nabla}\left(s\Omega^2\vec{e}_s\right)\end{aligned} \tag{8}$$

where $\vec{\Omega} = \Omega\vec{e}_z$ is the rotation vector. The above dependencies on t and ϕ lead prograde modes (i.e., modes that travel in the same direction as stellar rotation) to having negative m values and retrograde modes to having positive m values. This could be described as the "retrograde convention". Some authors, notably in helioseismology, prefer the opposite convention (i.e., prograde modes have positive m values—we will call the "prograde convention") and therefore introduce a time dependence of the form $\exp(-i\omega t)$ (while maintaining an azimuthal dependence of the form $\exp(im\phi)$). With such a convention, the occurrences of $(\omega + m\Omega)$ would need to be replaced by $(-\omega + m\Omega)$ in the above expression.

The right-hand side of Eq. 5 can also be re-expressed in terms of the Lagrangian perturbations to pressure and density, thus leading to:

$$\begin{aligned}-\frac{\vec{\nabla}P'}{\rho_0} + \frac{\rho'\vec{g}_{\rm eff}}{\rho_0} - \vec{\nabla}\Psi' = &-\frac{P_0}{\rho_0}\vec{\nabla}\left(\frac{\delta p}{P_0}\right) + \frac{\vec{\nabla}P_0}{\rho_0}\left(\frac{\delta\rho}{\rho_0} - \frac{\delta p}{P_0}\right) \\ &-\vec{\nabla}\Psi + \vec{\nabla}\left(\frac{\vec{\xi}\cdot\vec{\nabla}P_0}{\rho_0}\right) \\ &+\frac{\left(\vec{\xi}\cdot\vec{\nabla}P_0\right)\vec{\nabla}\rho_0 - \left(\vec{\xi}\cdot\vec{\nabla}\rho_0\right)\vec{\nabla}P_0}{\rho_0^2}\end{aligned} \tag{9}$$

The last term in the alternate formulation is particularly interesting as it only appears in baroclinic models. In barotropic models, $\vec{\nabla}P_0$ and $\vec{\nabla}\rho_0$ are parallel thus causing the term to vanish.

Various boundary conditions must be added to the above equations to ensure the solutions are regular in the centre, the Lagrangian pressure perturbations vanish at the surface, and the perturbations to the gravitational potential vanish at infinity. This leads to a generalised eigenvalue problem where the pulsation frequency is the eigenvalue, and the pulsation mode the eigenfunction. This problem must then be solved numerically as described in the next section.

2.2.1 Numerical implementation

Various steps must be carried out before implementing the above equations numerically. The first step is to express them

explicitly in a suitable coordinate system, typically surface-fitting spheroidal coordinates as described above. For instance, the continuity equation expressed in the coordinate system used in Reese et al. (2006) is:

$$\frac{\delta\rho}{\rho_o}+\frac{\zeta^2}{r^2 r_\zeta}\left[\frac{\partial_\zeta\left(\zeta^2\xi^\zeta\right)}{\zeta^2}+\frac{\partial_\theta\left(\sin\theta\xi^\theta\right)}{\zeta\sin\theta}+\frac{\partial_\phi\xi^\phi}{\zeta\sin\theta}\right]=0 \tag{10}$$

where (ζ, θ, ϕ) designates the spheroidal coordinate system, r the distance from the centre, and $r_\zeta = \frac{\partial r}{\partial\zeta}$. Usually, such a coordinate system is non-dimensionalised so that $\zeta = 1$ corresponds to the stellar surface.

The next step is to discretise the equations. This can be subdivided into two parts. The first is the horizontal discretisation. Two options exist: using finite-differences or projecting onto the spherical harmonic basis. Various authors have used finite differences[2] (e.g., Clement, 1998; Espinosa et al., 2004; Lovekin and Deupree, 2008). However, many authors nowadays prefer to project the equations onto the spherical harmonic basis in order to improve the accuracy (this amounts to applying a spectral method based on spherical harmonics). This projection takes place in two steps. First the unknowns are expressed as a sum of spherical harmonics, e.g.:

$$\left(\frac{\delta\rho}{\rho}\right)=\sum_{\ell'=|m|}^{\infty}\left(\frac{\delta\rho}{\rho_o}\right)_m^{\ell'}(\zeta)Y_{\ell'}^m(\theta,\phi) \tag{11}$$

$$\begin{aligned}\vec{\xi}=\sum_{\ell'=|m|}^{\infty}&\left(\xi_{\zeta_m}^{\ell'}(\zeta)\vec{R}_{\ell'}^m(\theta,\phi)+\xi_{\theta_m}^{\ell'}(\zeta)\vec{S}_{\ell'}^m(\theta,\phi)\right.\\&\left.+\xi_{\phi_m}^{\ell'}(\zeta)\vec{T}_{\ell'}^m(\theta,\phi)\right)\end{aligned} \tag{12}$$

where $(\frac{\delta\rho}{\rho_o})_m^{\ell'}(\zeta)$, $\xi_{\zeta_m}^{\ell'}(\zeta)$, $\xi_{\theta_m}^{\ell'}(\zeta)$, and $\xi_{\phi_m}^{\ell'}(\zeta)$ are unknown radial functions, $Y_{\ell'}^m(\theta,\phi)$ the spherical harmonic of harmonic degree ℓ' and azimuthal order m, and $(\vec{R}_{\ell'}^m, \vec{S}_{\ell'}^m, \vec{T}_{\ell'}^m)$ vectorial spherical harmonics[3] given by the following expressions:

$$\vec{R}_{\ell'}^m = Y_{\ell'}^m\vec{a}_\zeta, \tag{13}$$

$$\vec{S}_{\ell'}^m = \frac{\partial Y_{\ell'}^m}{\partial\theta}\vec{a}_\theta+\frac{1}{\sin\theta}\frac{\partial Y_{\ell'}^m}{\partial\phi}\vec{a}_\phi, \tag{14}$$

$$\vec{T}_{\ell'}^m = \frac{1}{\sin\theta}\frac{\partial Y_{\ell'}^m}{\partial\phi}\vec{a}_\theta-\frac{\partial Y_{\ell'}^m}{\partial\theta}\vec{a}_\phi \tag{15}$$

$(\vec{a}_\zeta, \vec{a}_\theta, \vec{a}_\phi)$ being a vector basis suitable for the spheroidal coordinate system. As can be seen, the sums in Eqs 11, 12 are only carried out over the harmonic degree ℓ' and not over m, since the different azimuthal orders are decoupled as a result of the symmetry around the rotation axis (hence the reason why modes are proportional to $\exp(im\phi)$). Furthermore, in practice, the sums are truncated at a maximal harmonic degree, $\ell_{\max}$. Then the equations are projected onto the spherical harmonic basis by calculating the dot product between the equation and the complex conjugate of successive spherical harmonics (or vectorial spherical harmonics in the case Euler's momentum equation), and integrating the result over 4π steradians. For the continuity equation, this would yield:

$$\begin{aligned}0=\left(\frac{\delta\rho}{\rho_o}\right)_m^{\ell}+\sum_{\ell'=|m|}^{\ell_{\max}}&\left[I_{\ell\ell'}^m\left(\frac{\zeta^2}{r^2r_\zeta}\right)\partial_\zeta\xi_{\zeta_m}^{\ell'}+I_{\ell\ell'}^m\left(\frac{2\zeta}{r^2r_\zeta}\right)\xi_{\zeta_m}^{\ell'}\right.\\&\left.-I_{\ell\ell'}^m\left(\frac{\ell'(\ell'+1)\zeta}{r^2r_\zeta}\right)\xi_{\theta_m}^{\ell'}\right]\end{aligned} \tag{16}$$

where the coupling integral operator, $I_{\ell\ell'}^m(\cdot)$, is defined as follows for a generic function $G(\zeta, \theta)$:

$$I_{\ell\ell'}^m(G)(\zeta)=\iint_{4\pi}G(\zeta,\theta)Y_{\ell'}^m(\theta,\phi)\{Y_\ell^m(\theta,\phi)\}^*\mathrm{d}\Omega, \tag{17}$$

in which $\mathrm{d}\Omega$ is a solid angle element, and where we have made use of the following spherical harmonic identity:

$$-\ell'(\ell'+1)Y_{\ell'}^m=\frac{1}{\sin\theta}\frac{\partial}{\partial\theta}\left(\sin\theta\frac{\partial Y_{\ell'}^m}{\partial\theta}\right)+\frac{1}{\sin^2\theta}\frac{\partial^2Y_{\ell'}^m}{\partial\phi^2}, \tag{18}$$

By varying ℓ from $|m|$ to $\ell_{\max}$, i.e., by projecting the continuity equation onto spherical harmonics of successive degrees, and applying the above methodology to the entire system, Eqs 4–7, we end up with a large system of 1D differential equations which depends on the pseudo-radial variable ζ, the solution of which yields the unknown radial functions introduced above. Due to the symmetry with respect to the equatorial plane, only even or odd harmonics intervene in this system (apart from the $\xi_{\phi_m}^{\ell'}$ functions which typically have the opposite parity).

The second part is the radial discretisation, i.e., according to radial variable ζ. Once more, different options exist and are typically chosen to suit the equilibrium model. A number of authors use finite differences (e.g., Clement, 1998; Lovekin and Deupree, 2008; Ouazzani et al., 2012; Reese et al., 2013). We note that the finite difference scheme used in Ouazzani et al. (2012), first introduced by Scuflaire et al. (2008), is very stable and achieves a 4th order accuracy using only two consecutive grid points at a time, thanks to the use of equilibrium quantities and their radial derivatives. Reese et al. (2013) used a different 4th order scheme which is stable to mesh drift, makes use of superconvergence, and does not require the radial derivatives of equilibrium quantities (see Reese, 2013, for a derivation of the scheme). The main advantage of using finite differences is their high flexibility in the choice of the underlying grid which can be essentially arbitrary. Accordingly, grids that are dense near the surface can be used to resolve acoustic modes in that region as well as rapid variations in the Γ_1 profile. Grids with a higher density of points in the central regions of the star will be more suitable for gravity modes.

2 Even in these cases, the solutions are typically projected onto the spherical basis to facilitate comparison with the non-rotating case.

3 We note that these are slightly different than the usual vectorial spherical harmonics due to the use of spheroidal basis vectors in the definition.

The second option for the radial discretisation is using spectral methods, i.e., where the solutions are decomposed over a function basis for which the analytical derivatives are known. Various authors use spectral methods based on Chebyshev polynomials (e.g., Rieutord and Valdettaro, 1997; Lignières et al., 2006). The main advantage of spectral methods is their high accuracy (provided the calculations have converged). However, unlike for finite differences, the choice of grid is imposed by the spectral method. Hence, there is little freedom to increase the grid density in a specific region of the star. To overcome this limitation, one may apply a multi-domain approach. For instance, ESTER models are cut up into a number of concentric spheroidal domains in which a Chebyshev spectral method is applied (e.g., Rieutord et al., 2016). Interface conditions are applied between the domains in order to ensure the continuity of various quantities such as the pressure. Likewise, pulsation calculations using these models also apply a multi-domain spectral approach (Reese et al., 2021). With such an approach, one can set up a thin domain near the surface with a high resolution that captures rapid variations in the model and in the pulsation modes.

Once the problem has been discretised, it takes on the form of an algebraic generalised eigenvalue problem:

$$\mathcal{A}\vec{v} = \omega\mathcal{B}\vec{v} \tag{19}$$

where $\mathcal{A}$ and $\mathcal{B}$ are matrices, $\vec{v}$ the eigenvector (containing all of the variables relevant to the pulsation mode), and ω the associated frequency. Such problems can be solved either using a QR decomposition[4] which searches for all of the eigensolutions (but typically this would be too costly numerically for even a moderate resolution), or an iterative method that searches for a limited number of solutions around target frequencies. Iterative methods include the simple power method or more sophisticated approaches such as the Arnoldi-Chebyshev method which applies a QR decomposition on a reduced matrix representative of the original matrix. However, given that these methods find the eigenvalues with the largest absolute value, a shift-invert strategy must first be applied in order to transform the above eigenvalue problem into an equivalent problem where the largest eigenvalues in the new formulation correspond to those closest to a given target, σ, in the original problem:

$$(\mathcal{A} - \sigma\mathcal{B})^{-1}\mathcal{B}\vec{v} = \mu\vec{v} \tag{20}$$

The original eigenvalues are then deduced from the eigenvalues μ *via* the relation $\omega = \sigma + \frac{1}{\mu}$.

A number of authors have carried out adiabatic oscillation calculations using a 2D approach to fully account for the effects of rapid rotation. Clement studied acoustic and gravity modes in N = 1, 2, and 3 polytropic uniformly rotating models, as well as 15 $M_\odot$ uniformly rotating models, appropriate for β Cep pulsators, using a full 2D finite-difference method (Clement, 1981; Clement, 1998) as well as a method based on the variational principle and involving approximate eigenfunctions (Clement, 1984; Clement, 1986; Clement, 1989). Later on, Espinosa et al. (2004) developed a finite-difference code[5] called OMASS2d in which the system of pulsation equations is reduced to a single equation thanks to a number of approximations (Cowling approximation, neglect of Coriolis force, neglect of Brunt-Väisälä frequency). He used this code to study acoustic pulsation modes in uniform density models and realistic models. Lovekin and Deupree, (2008) used Clement's pulsation code (called NRO for "Nonradial Oscillation code") to study pulsation modes in 10 $M_\odot$ uniformly rotating ZAMS models based on the 2D stellar evolution code ROTORC (Deupree, 1990; Deupree, 1995). They went on to extend this work to 10 $M_\odot$ models with a nonuniform cylindrical rotation profile (Lovekin et al., 2009). Meanwhile, a new 2D approach based on spectral methods was being developed starting with Lignières et al. (2001). This led to the development of the TOP (Two-dimensional Oscillation Program) pulsation code as well as accurate calculations of acoustic pulsation modes in uniformly rotating N = 3 polytropic models, first without (Lignières et al., 2006) then with the Coriolis force (Reese et al., 2006). This allowed Reese et al. (2006) to establish validity domains for third-order perturbative methods. TOP was subsequently extended to models based on the SCF method which have cylindrical differential rotation (Reese et al., 2009) then to models based on the ESTER code with full 2D rotation profiles (Reese et al., 2021). Ballot et al. (2010) used TOP to study gravity modes in polytropic models and to establish the corresponding validity domains. Later on, Ouazzani et al. (2012) developed the ACOR pulsation code and compared its results with those from TOP. In Ouazzani et al. (2015), they then went on to study acoustic and gravity pulsation modes in a 2 $M_\odot$ model with a radial (or shellular) differential rotation, obtained using the centrifugal deformation code from Roxburgh, (2006).

In addition to these works, there are a number of studies focusing on oscillations of rapidly rotating neutron stars. These have made use of polytropic models (e.g., Ipser and Lindblom, 1991; Yoshida and Eriguchi, 1995; Stergioulas et al., 2004) as well as realistic neutron star models (e.g., Yoshida and Eriguchi, 1999; Ferrari, 2005). A key difference when calculating pulsations in polytropic neutron star models is the fact that the polytropic and adiabatic exponents are kept the same, whereas they typically differ for classical stars. Some of the important goals in studying such oscillations include determining the stability of neutron

4 A QR decomposition consists in decomposing a matrix A into a product QR where Q is an orthogonal matrix and R an upper triangle matrix. It serves as the basis for an algorithm which searches for all of the eigenvalues of A.

5 The discretised problem is subsequently projected onto the spherical harmonic basis.

stars with respect to gravitational-wave radiation which may help to limit their rotation rate (e.g., Ipser and Lindblom, 1991; Yoshida and Eriguchi, 1995), and testing the equation of state (e.g., Ferrari, 2005). Some authors have also inspected mode damping due to mass-shedding at near-critical rotation rates, thus requiring the use of time evolution simulations of pulsating neutron stars (e.g., Stergioulas et al., 2004). Such simulations typically yield less accurate pulsation frequencies since these depend on the time span covered by the simulation, but are able to take into account in a straightforward way non-linear effects including amplitude saturation, mode coupling, and pulsation-induced mass-shedding.

2.2.2 Variational principle

Given the complexity of the pulsation calculations in the presence of rapid rotation, it is important to check the accuracy of the calculations. One way of achieving this is by recalculating the frequencies thanks to a variational formula. Such a formula may be obtained by calculating the dot product of Euler's momentum equation and the complex conjugate of the Lagrangian displacement field, $\vec{\xi}^{*}$, integrating over the star's volume, and rearranging the various terms thanks to integration by parts and other manipulations (see, e.g., Appendix B of Reese et al., 2021, for a full derivation). This leads to a second order equation in ω of the form:

$$-\omega^2\langle\vec{\xi},\vec{\xi}\rangle+\omega\langle\vec{\xi},\mathcal{C}\vec{\xi}\rangle+\langle\vec{\xi},\mathcal{L}\vec{\xi}\rangle=0, \tag{21}$$

where $\mathcal{C}$ is an operator associated with the Coriolis force, $\mathcal{L}$ an operator representing a combination of other fluid dynamic terms, and where we have introduced the following dot product:

$$\langle\vec{\xi},\vec{\eta}\rangle=\iiint_V\vec{\xi}^{*}\cdot\vec{\eta}\rho_0 dV, \tag{22}$$

$\vec{\xi}$ and $\vec{\eta}$ being two displacement fields, and $\{.\}^{*}$ denoting the complex conjugate of a quantity. Solving Eq. 21 then leads to an independent estimate of the pulsation frequency which furthermore benefits from the variational principle. Indeed, as was shown in Lynden-Bell and Ostriker, 1967 in a very general case, the fluid dynamic operators are symmetric with respect to the above dot product. One of the consequences of this is that a small variation or error on the displacement field, $\delta\vec{\xi}$, leads to a second order error on the variational frequency thus obtained:

$$\omega_{\mathrm{var}}=\omega+\mathcal{O}\left(\|\delta\vec{\xi}\|^2\right) \tag{23}$$

As a result, this property has been used to check the accuracy with which pulsation modes have been calculated or to increase their accuracy, both in the 1D non-rotating case (e.g., Christensen-Dalsgaard, 1982; Christensen-Dalsgaard and Mullan, 1994), and 2D rapidly rotating case (e.g., Reese et al., 2006; Reese et al., 2021). Some authors have used this as a means of calculating pulsation frequencies by assuming an approximate analytical form for the eigenfunctions (e.g., Clement, 1984; Clement, 1986; Clement, 1989).

2.3 Non-adiabatic calculations

Although adiabatic pulsation calculations have the advantage of being simpler yet sufficiently realistic to provide accurate pulsation frequencies, they also have various disadvantages compared to non-adiabatic calculations. Indeed, it is only possible to calculate damping or growth rates and to predict which modes are unstable with non-adiabatic calculations. Furthermore, accurate perturbations of the effective temperature, which are essential for correctly calculating mode visibilities and associated amplitude ratios, may only be obtained in a non-adiabatic context.

In order to carry out non-adiabatic calculations, one must replace the adiabatic relation by a perturbed version of the energy equation:

$$\begin{aligned}i(\omega+m\Omega)\rho_0 T_0\delta S=\epsilon_0\rho_0\left(\frac{\delta\epsilon}{\epsilon_0}+\frac{\delta\rho}{\rho_0}\right)-\vec{\nabla}\cdot\delta\vec{F}+\vec{\xi}\cdot\vec{\nabla}\left(\vec{\nabla}\cdot\vec{F}_0\right)\\-\vec{\nabla}\cdot\left[\left(\vec{\xi}\cdot\vec{\nabla}\right)\vec{F}_0\right]\end{aligned} \tag{24}$$

where T corresponds to temperature, S to entropy, ϵ to energy generated *via* nuclear reactions, and $\vec{F}$ the energy flux. The energy flux may be decomposed into a radiative, $\vec{F}^{\mathrm{R}}$, and convective flux, $\vec{F}^{\mathrm{C}}$. The perturbed radiative energy flux may be obtained by perturbing the radiative transfer equation:

$$\begin{aligned}\delta\vec{F}^{\mathrm{R}}=&\left[4\frac{\delta T}{T_0}-\frac{\delta\kappa}{\kappa_0}-\frac{\delta\rho}{\rho_0}\right]\vec{F}_0^{\mathrm{R}}\\&-\frac{4acT_0^3}{3\kappa_0\rho_0}\left[T_0\vec{\nabla}\left(\frac{\delta T}{T_0}\right)+\vec{\xi}\cdot\vec{\nabla}\left(\vec{\nabla}T_0\right)-\vec{\nabla}\left(\vec{\xi}\cdot\vec{\nabla}T_0\right)\right]\end{aligned}$$

where κ is the opacity and $a=\frac{4\sigma}{c_l}$ the radiation constant, σ being the Stefan-Boltzmann constant and c_l the speed of light. The perturbed convective flux is usually neglected in what is generally known as the frozen convection approximation. To these equations must be added perturbed equations of state and of opacity.

There are relatively few works on non-adiabatic pulsation calculations in rapidly rotating stars using a fully 2D approach. Lee and Baraffe, (1995) devised a first approach involving a perturbative modelling of the centrifugal distortion and a two-term expansion of the pulsation modes over the spherical harmonic basis. This has been followed by various works using a larger number of spherical harmonics when calculating the pulsation modes (e.g., Lee, 2001). In a particularly interesting study, Lee, (2008) compares this approach with an approach based on the traditional approximation (Section 2.5) and finds that in full 2D calculations low frequency retrograde modes tend be

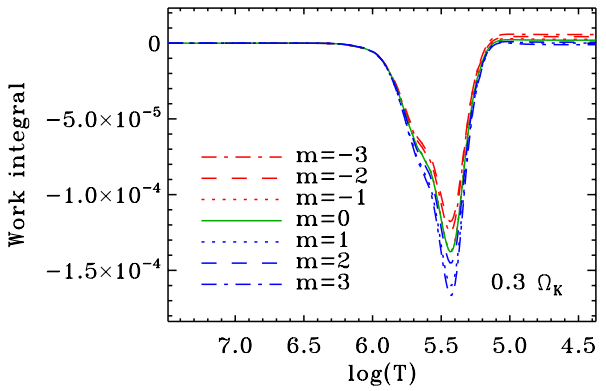

FIGURE 4
Work integrals for a set of modes from the same multiplet, in a 9 $M_\odot$ ESTER model rotating at 0.3 Ω_K. Integration has already been carried out along the horizontal directions, only leaving the radial direction as shown in this plot. The left of the plot corresponds to the centre of the star, whereas the right corresponds to its surface. Only the most retrograde mode ($m = 3$) is damped, i.e., its work integral is negative at the surface (taken from Reese et al., 2017a).

damped, in contrast with what is obtained using the traditional approximation. More recently, Savonije, (2007) studied the non-adiabatic tidal response of a 20 $M_\odot$ stellar model using a 2D finite difference scheme. The effects of the Coriolis force were included whereas those of the centrifugal force were neglected. Finally, Reese et al. (2017a) devised a non-adiabatic version of the TOP code, applicable to 2D models from the ESTER code. This approach has the advantage of using models in which the energy equation is satisfied in a 2D context. It also takes into account the baroclinic structure of the model and differential rotation.

2.3.1 Work integral

As was done above in the adiabatic case, one can once more calculate the dot product of Euler's momentum equation with $\vec{\xi}^*$, integrate over the volume, and rearrange the various terms. This leads to an equation that is analogous to Eq. 21, except that the terms involved are now complex. This equation can be separated into a real and imaginary part. The real part once more provides an independent formula for the frequency. However, it does not benefit from the variational principle since the non-adiabatic terms in the fluid operators are not symmetric with respect to the dot product defined in Eq. 22. The imaginary part provides an integral expression for the damping/excitation rate and corresponds to what is commonly known as the work integral:

$$\tau = \frac{W}{2\left(A\omega + C\right)} \tag{25}$$

where τ is the excitation rate, and where

$$A = \iiint_V \rho_0 \xi^2 \mathrm{dV}, \tag{26}$$

$$C = \iiint_V \rho_0 \left[m\Omega\xi^2 - i\vec{\Omega} \cdot \left(\vec{\xi} \times \vec{\xi}^* \right) \right] \mathrm{dV}, \tag{27}$$

$$W = -\iiint_V \Im\left\{ \frac{\delta P \delta \rho^*}{\rho_0} \right\} \mathrm{dV} \tag{28}$$

where $\Im(\cdot)$ corresponds to the imaginary part of a given complex quantity. As can be seen from the above expression, excitation or damping occurs when there is a phase shift between the Lagrangian pressure and density perturbations, as can be expected from the thermodynamic identity $\delta W = -PdV$.

The work integral is useful for pinpointing what parts contribute to mode excitation or damping. In particular, by looking at what temperatures excitation occurs, it is possible to narrow down which chemical elements are responsible for the underlying κ-mechanism. Figure 4 shows various work integrals for a multiplet of modes in a 9 $M_\odot$ ESTER model rotating at 0.3 Ω_K. As can be seen in this plot, only the most retrograde mode ($m = 3$) is damped and the other modes are excited. As the rotation rate increases in the model, all of the modes in this multiplet are progressively damped starting with the retrograde modes first. Inasmuch as this multiplet is representative of pulsation modes in β Cep stars, one can expect to see more prograde modes excited than retrograde modes, as seems to be confirmed by observations (e.g., Balona, 2000).

2.4 Perturbative analysis and its limits

An alternate approach for calculating the effects of rotation on stellar pulsations is to apply a perturbative approach. In this approach, the rotation rate, or more specifically the ratio of the rotation rate to the Keplerian break-up velocity $\epsilon = \Omega/\Omega_K$ where $\Omega_K = \sqrt{GM/R_{eq}^3}$ and R_{eq} is the equatorial radius, is treated as a small parameter and the pulsation modes and frequencies are expanded into a series expression in terms of this parameter. The advantage of this approach is that the successive terms at each order are solutions to 1D problems thus reducing the numerical cost. Furthermore, it establishes a clear link between the solutions in the non-rotating case, which are thus the zeroth order solutions, and the solutions in the rotating case, thereby naturally extending the mode labelling, i.e., quantum numbers, from the former to the latter. As described in Mirouh (this volume—see also Mirouh et al., 2019), mode labelling is far from trivial when considering pulsations modes calculated using a 2D approach.

Historically, perturbative methods have been applied to first, second, and third order. Frequencies thus take on the following expression:

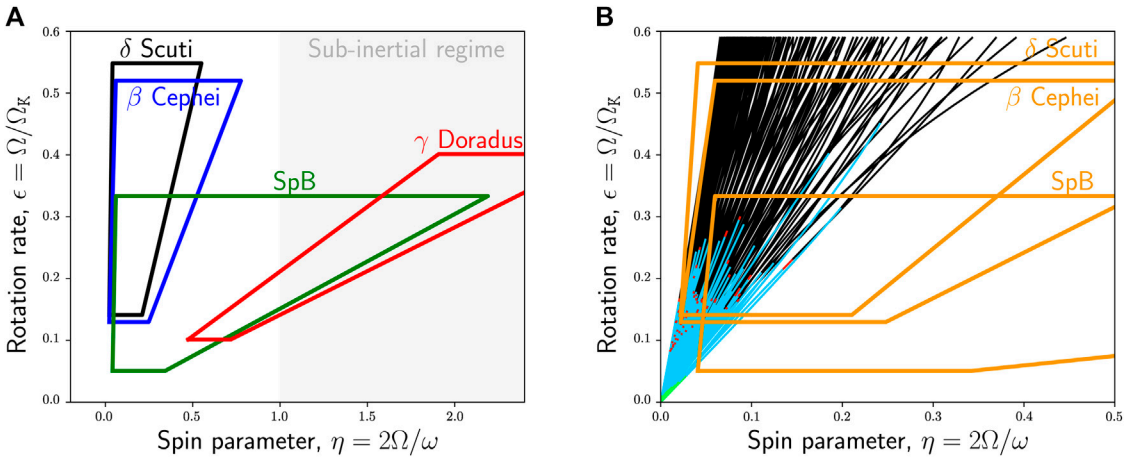

FIGURE 5
(A, B) Domains covered by various classes of pulsating stars in a μ-ε diagram. Panel **(A)** also shows the region corresponding to the sub-inertial regime (see Section 3.1). Panel **(B)** is a zoom of panel **(A)** and shows validity domains of perturbative methods of various orders using error bars of 0.1 μHz for acoustic pulsation modes superimposed on the domains of the different classes of pulsating stars. The various curves correspond to individual pulsation modes for a range of rotation rates: the green, cyan, and red sections correspond to the portions where first, second, and third order perturbative methods are valid. The black sections show where full 2D calculations are needed. (adapted from Goupil and Talon, 2002 and Reese, 2006).

$$\omega = \omega_0 - m(1-C)\Omega + \left(D_1 + m^2 D_2\right)\Omega^2 + m\left(T_1 + m^2 T_2\right)\Omega^3 + \mathcal{O}\left(\Omega^4\right) \tag{29}$$

where the various coefficients C, D_1, D_2, T_1 and T_2 come from the different order methods, and ω_0 corresponds to the pulsation frequency in the non-rotating case. In general, due to the symmetry of the pulsation equations with respect to the $\phi = 0$ meridional plane, the coefficients of even powers of Ω are even functions of m, and those of odd powers are odd functions (Reese et al., 2006).

Ledoux (1951) came up with a first order integral expression of the effects of rotation which takes into account both mode advection by rotation and the effects of the Coriolis force. The latter is typically represented by a mode-dependent coefficient, C, known as the Ledoux constant. This expression, initially derived for a uniform rotation profile, was subsequently generalised to profiles that depend on the radial coordinate alone (e.g., Gough, 1981; Christensen-Dalsgaard et al., 1990), and on the radial coordinate and colatitude (e.g., Schou et al., 1994). It has been used to probe rotation profiles of slowly rotating stars starting with the Sun (e.g., Schou et al., 1998; Thompson et al., 2003; Hatta et al., 2019).

To go to higher rotation rates, second order methods have been derived (e.g., Saio, 1981; Gough and Thompson, 1990; Goode and Thompson, 1992). Compared to first order methods, this approach has the added difficulty of including first order effects of the centrifugal deformation of the model (which scales as $(\Omega/\Omega_K)^2$) as well as first order perturbed eigenfunctions (as opposed to just the perturbed frequency, see e.g., Saio, 1981). Such an approach leads to departures from uniform rotational splittings, even for uniform rotation profiles. Another phenomenon which intervenes is the effects of avoided crossings, also known as near-degeneracies. As shown in Suárez et al. (2010), such effects start to play an important role on the pulsation frequencies.

Only few authors have ventured to third order methods (Soufi et al., 1998; Karami, 2008). To achieve such high orders, these methods include the first order rotation effects into the zeroth order solution, and third order effects into the second order solution. This avoids having to calculate eigenfunction perturbations for successive powers of ϵ. Furthermore, it was necessary to introduce a second small parameter, namely $\mu = \frac{2\Omega}{\omega}$ the ratio of the Coriolis to the pulsation frequency. This parameter is indicative of the impact of Coriolis force on pulsations and is particularly relevant to low frequency modes such as gravity and inertial modes. In contrast, the former parameter, $\epsilon = \Omega/\Omega_K$, is characteristic of the amount of centrifugal deformation of the star and is thus relevant to acoustic modes. Figure 5 (adapted from Goupil and Talon, 2002) shows the μ-ϵ domains associated with various classes of pulsating stars. As can be seen, large values[6] of ϵ and μ are reached by these classes of

6 We note that Soufi et al., 1998; Karami, 2008 actually used the small parameter Ω/ω. However, we prefer keeping the extra 2 factor in the numerator as it leads to a more straightforward physical interpretation and corresponds to the spin parameter commonly used when applying the traditional approximation.
We note that $\epsilon = 0.4$ leads to equatorial radius 8% larger than the polar radius in a Roche model, that $\epsilon = 1$ roughly corresponds to the critical break-up rotation rate beyond which the star decretes matter at the equator, and that modes with $\mu \geq 0.5$ are in the sub-inertial regime thus leading to forbidden regions (Section 3).

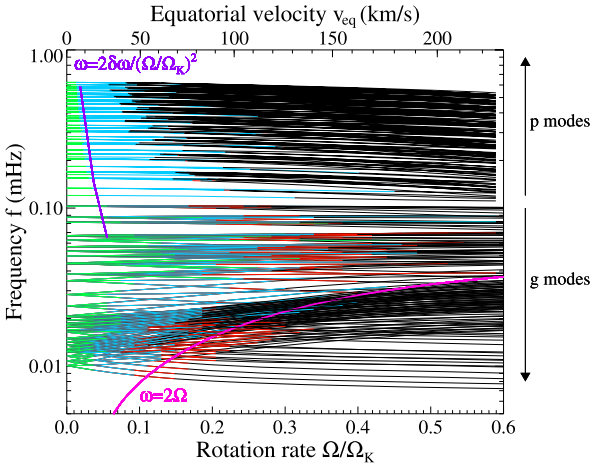

FIGURE 6
Validity domains for perturbative methods of various orders. Green, cyan, and red curves correspond to the domain where first, second, and third order methods reproduce full 2D calculations to within an error bar of $\delta\omega = 0.1\,\mu$Hz. The purple line labelled $\omega = 2\Omega$ delimits sub-inertial gravito-inertial modes (below) from the super-inertial modes (above). The blue line shows the expected frequency threshold that comes from neglecting centrifugal deformation (see text for details). (Material from: Ballot et al., 2013).

stars, thus raising the question as to the validity of perturbative methods for these stars.

In order to answer this question, Reese et al. (2006) carried out full 2D calculations of acoustic pulsation modes in rapidly rotating polytropic models. They then fitted polynomial functions to the frequencies thus obtained in order to mimic perturbative calculations. This enabled them to come up with validity domains for perturbative methods of various orders. A similar analysis was carried out by Burke et al. (2011) using realistic models from the ASTEC code (Christensen-Dalsgaard, 2008) and including a perturbative description of their centrifugal deformation. Ballot et al. (2010) subsequently applied a similar method to gravity modes in polytropic models, thus extending the validity domains to low frequencies. Figure 6 shows such validity domains for a polytropic model of a typical A-type star. The error bars used to define these domains are $0.1\,\mu$Hz (which corresponds to 116 days of observation, as based on the Rayleigh criterion).

It is interesting to note that at high frequencies, the validity domains of perturbative methods shrink. This is because the wavelength of acoustic pulsation modes is smaller at these frequencies, and thus these modes are more sensitive to the centrifugal deformation. In first order perturbative methods, the centrifugal deformation is neglected entirely, thus leading to a relative error on the pulsation frequency, $\delta\omega/\omega$, that scales as the flattening of the star, $(R_{eq} - R_{pol})/R_{eq} \simeq \frac{1}{2}\Omega/\Omega_K$, where R_{eq} and R_{pol} are the equatorial and polar radii, respectively. If we use an error bar of $\delta\omega = 0.1\,\mu$Hz, this leads to the blue curve shown in Figure 6.

Likewise, at low frequencies, the validity domains of perturbative methods become smaller. This is due to the increasing influence of the Coriolis force on the pulsations, as can be seen by the ratio between the pulsation and rotation periods. Also shown in this plot is the curve $\omega = 2\Omega$, which marks the separation between sub- and super-inertial modes. As can be seen, it correlates nicely with the validity domains for gravito-inertial modes.

2.5 Traditional approximation

Another approximate approach to calculating stellar pulsations in the presence of rapid rotation is to apply what is known as the traditional approximation. In this approach, the horizontal component of the rotation vector, $-\Omega \sin\theta \vec{e}_\theta$, is neglected. If furthermore, the centrifugal distortion is neglected, and the Cowling[7] and adiabatic approximations are made, then the pulsation equations become separable in r and θ. Specifically, the horizontal parts of the pulsation modes are no longer described by spherical harmonics but by Hough functions, which are the solutions to the eigenvalue problem known as Laplace's tidal equation. The associated eigenvalues correspond to the horizontal wavenumber.

The traditional approximation was first introduced in the context of stellar pulsations by Berthomieu et al. (1978), thus enabling them to obtain asymptotic expressions for the frequencies of gravity modes in rotating stars. Since then, other authors have also applied the traditional approximation (e.g., Lee and Saio, 1987; Savonije et al., 1995; Bildsten et al., 1996; Townsend, 1997; Bouabid et al., 2013). Townsend, (2003b) carried out an extensive asymptotic analysis of the behaviour of Hough functions and provided a classification of gravito-inertial modes. Ballot et al. (2012) showed that the period spacings of gravito-inertial modes predicted by the traditional approximation are a close match to those from full 2D calculations, apart from some cases where the centrifugal deformation causes a slight mismatch.

Savonije et al. (1995) showed how to generalise the traditional approximation to non-adiabatic calculations. This approach was subsequently used by Townsend, (2003a) when calculating the disk-integrated visibilities of pulsation modes and by Townsend, (2005) and Bouabid et al. (2013) when studying the instability domains of slowly pulsating B stars and γ Doradus stars. Lee, (2008) compared non-adiabatic

7 In the Cowling approximation, the perturbations to the gravitational potential are neglected (Cowling, 1941).

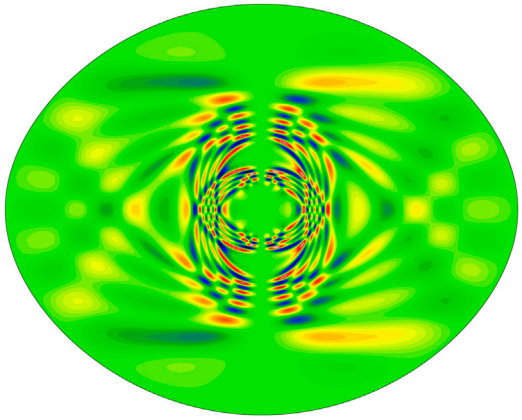

FIGURE 7
Meridional cross-section of a rosette mode in an SCF model rotating at 70 % of the critical rotation rate (Credit: Resse (2013), reproduced with permission © ESO).

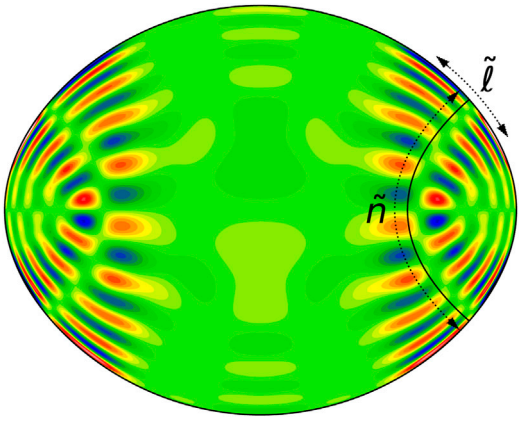

FIGURE 8
Meridional cross-section of an acoustic island pulsation mode in a 2 $M_\odot$ ESTER model rotating at 0.7 Ω_K. The underlying periodic orbit is indicated by the solid black line. The quantum numbers $\tilde{n}$ and $\tilde{\ell}$ correspond to the number of nodes in the directions that are indicated on the plot.

calculations based on the traditional approximation with those based on full 2D calculations. He showed that retrograde g-modes are unstable when applying the traditional approximation, but stable when applying a 2D approach. Mode coupling and centrifugal deformation play a role in stabilising these modes.

3 Impact of rapid rotation on stellar pulsations

Having described how to calculate pulsation modes in the presence of rapid rotation, we now briefly look at some of its effects on stellar pulsations. For a more complete review of these effects, in particular on mode frequencies, geometry, and classification, we refer to the review by Mirouh (this volume).

3.1 General effects

One of the first impacts of rotation on pulsation frequencies is to lift the degeneracy between modes with the same radial order, n, and harmonic degree, ℓ, but different azimuthal orders, m. Hence, a frequency multiplet composed of $2\ell + 1$ frequencies appears where there was only a single frequency. This is a simple consequence of first order perturbative effects (Eq. 29). For rotation profiles that do not depend on θ, the frequencies in a multiplet are evenly spaced (to first order). Such a spacing is known as the rotational splitting. As the rotation rate increases, the multiplets become uneven as was already pointed out in Section 2.4. They also start to overlap thus leading to a complex spectrum. Progressively, a new frequency organisation emerges.

At this point, it is useful to distinguish between acoustic modes, which typically have high frequencies, and gravity modes at low frequencies. At rapid rotation rates, acoustic modes subdivide into several classes of pulsation modes each with its own frequency organisation and characteristic mode geometry, as was shown by Lignières and Georgeot, 2008 and Lignières and Georgeot, 2009 using ray dynamics. These include acoustic island modes, chaotic modes, and whispering gallery modes. Probably, the most important of these different classes when it comes to interpreting observed pulsations are acoustic island modes, as described below.

In the rotating case, gravity modes subdivide between modes in the super-inertial regime ($\omega > 2\Omega$) and those in the sub-inertial regime ($\omega < 2\Omega$). Those in the super-inertial regime keep a mode geometry which is similar to that of their non-rotating counterparts. A notable exception are the "rosette" modes discovered by Ballot et al. (2012). These have a non-separable geometric structure and cannot be described correctly using the traditional approximation (see Figure 7). Modes in the sub-inertial regime are affected by forbidden regions which appear around the poles. Indeed, above and below the critical latitudes[8] $\pm\Theta_c$, where $\Theta_c = \arcsin[\omega/(2\Omega)]$, gravito-inertial waves are evanescent and are thus confined to the equatorial region (e.g., Dintrans and Rieutord, 2000; Townsend, 2003b). If centrifugal deformation is taken into account, this boundary takes on a more complex shape (Ballot et al., 2010). Furthermore, the period spacings of gravity modes go from being uniform in

8 We use the notation Θ to distinguish the latitude (the angle from the equator) from the colatitude θ (the angle from the north pole).

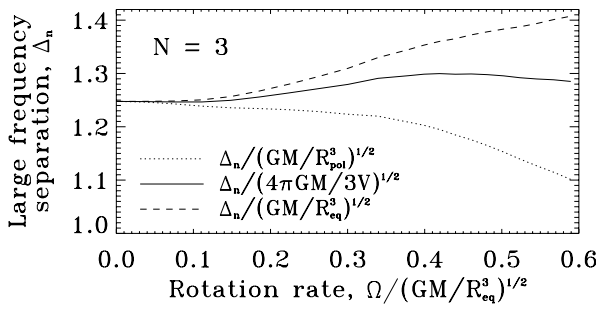

FIGURE 9
Large frequency separation, Δ_n, as a function of rotation rate in rotating polytropic models. As can be seen, Δ_n scales with volume rather than the cube of the equatorial or polar radii (Credit: Reese et al. (2008), reproduced with permission © ESO).

the non-rotating case to following well-defined functions which depend on the pulsation period, harmonic degree, ℓ, and azimuthal order, m. This result was first predicted thanks to the traditional approximation before being confirmed by 2D pulsation calculations (Ballot et al., 2012; Ouazzani et al., 2017).

Finally, we note the emergence of inertial modes at low frequencies, for which the Coriolis acceleration acts as the restoring force. These can be subdivided into modes with a singular structure in the ideal inviscid limit as they focus around wave attractors (e.g., Rieutord and Valdettaro, 1997; Dintrans et al., 1999; Baruteau and Rieutord, 2013; Mirouh et al., 2016), thus potentially playing an important role in tidal dissipation (e.g., Ogilvie, 2009; Rieutord and Valdettaro, 2010), and modes with a more regular structure such as r-modes (e.g., Papaloizou and Pringle, 1978; Saio, 1982; Rieutord, 2001; Lee, 2006). Recently, Ouazzani et al. (2020) studied mixed modes which take on an inertial characteristic in the convective core and a gravito-inertial behaviour above. These lead to kinks in the period separation relation described above and have been observed in some stars (Saio et al., 2021).

3.2 Acoustic island modes

Among the different types of acoustic modes, island modes are particularly important. Indeed, these are the rotating counterparts to low degree modes and are thus typically the most visible of the acoustic modes. Accordingly, they are likely candidates to explain some of the pulsations observed in rapidly rotating stars. As shown in Figure 8, these modes focus around periodic ray orbits that start at mid-latitudes and go around the equator.

Various authors have studied their pulsation spectra starting with Lignières et al. (2006). In Reese et al. (2009), the following empirical formula was obtained (after taking into account into account the fact that the frequencies depend on $m/\sqrt{\tilde{n}}$ rather than m):

$$\omega_{\tilde{n},\tilde{\ell},m} = \tilde{n}\Delta_{\tilde{n}} + D_{\tilde{m}}\left(\tilde{\ell}\right)\sqrt{\frac{m^2}{\tilde{n}} + \mu\left(\tilde{\ell}\right)^2} - m\Omega + \tilde{\alpha}\left(\tilde{\ell}\right). \quad (30)$$

where $\tilde{n}$, and $\tilde{\ell}$ are quantum numbers specific to island modes (Figure 8). Reese et al. (2008) and Mirouh et al. (2019) showed that the pseudo-large separation[9], $\Delta_{\tilde{n}}$, that intervenes in this formula roughly scales with the mean density of the star (Figure 9). This theoretical prediction was subsequently confirmed thanks to δ Scuti stars in binary systems (García Hernández et al., 2015). Lignières and Georgeot, (2008) and Lignières and Georgeot, (2009) showed that the large separation (or twice the pseudo-large separation) is the inverse of the time it takes for an acoustic wave to travel along the underlying ray orbit from one end to the other (Figure 8).

4 Mode observables

Before reviewing some of the recent works on interpreting pulsations of rapidly rotating stars, it is important to describe various mode observables, namely mode visibilities, amplitude ratios, phase differences, and line profile variations. Indeed, one of the long-standing obstacles to detailed seismic investigations of rapidly rotating stars is mode identification, i.e., finding the correspondence between observed pulsations and theoretical modes, as is particularly well illustrated, for instance, in Figure 5 of Deupree (2011). Finding observational constraints, such as those based on the above observables, become particularly crucial in narrowing down plausible mode identifications.

4.1 Mode visibilities

Mode visibilities correspond to disk-integrated luminosity variations for some given normalisation of the mode amplitude. If multiplied by the intrinsic mode amplitudes, these provide the observed pulsation amplitudes. However, predicting the intrinsic mode amplitudes is a formidable and unsolved problem as the pulsations of such stars are typically excited by the κ mechanism and are thus subject to non-linear saturation effects as well as mode coupling, all of this, in a centrifugally deformed stellar structure. Some of these effects have been explored in various theoretical works (e.g., Dziembowski, 1982; Dziembowski and Krolikowska, 1985; Dziembowski et al., 1988; Gastine and Dintrans, 2008) but a full comprehensive theory is currently out of reach. Hence, mode visibilities only give an idea of what

9 The pseudo-large separation, $\Delta_{\tilde{n}}$, corresponds to half the large separation, Δ_n, from the non-rotating case due to the relationship between the pseudo-radial order, $\tilde{n}$, and the radial order, n, of pulsation modes in non-rotating stars.

modes are most visible and the least affected by disk cancellation effects, but should by no means be used in a quantitative comparison with observed mode amplitudes.

In order to calculate mode visibilities, we first need to express the disk-integrated energy radiated by a star in some given direction:

$$E = \frac{1}{d^2}\iint_{Vis.\,Surf.} I\left(\mu, g_{\rm eff}, T_{\rm eff}\right)\vec{e}_{\rm obs.}\cdot\overrightarrow{\rm dS} \tag{31}$$

where d is the distance to the observer, I the specific radiation intensity, $\mu = \vec{e}_{\rm obs.}\cdot\vec{n}$ where $\vec{e}_{\rm obs.}$ is the unit vector in the direction of the observer and $\vec{n}$ the outward normal to the surface, $g_{\rm eff}$ the effective gravity (including the centrifugal acceleration), $T_{\rm eff}$ the effective temperature, and "Vis. Surf." the part of the stellar surface that is visible to the observer. We note that the shape of the boundary between the visible and hidden side of the star is not trivial when the star is deformed by the centrifugal force. It can only be determined by calculating whether the orientation of each surface element is towards or away from the observer. This expression then needs to be perturbed to account for the variations caused by a pulsation.

$$\begin{aligned}\Delta E(t) = \frac{1}{d^2}\Re\Bigg\{&\iint_{Vis.\,Surf.}\delta I\left(\mu, g_{\rm eff}, T_{\rm eff}, t\right)\vec{e}_{\rm obs.}\cdot\overrightarrow{\rm dS}\\ &+\iint_{Vis.\,Surf.} I\left(\mu, g_{\rm eff}, T_{\rm eff}\right)\vec{e}_{\rm obs.}\cdot\delta\left(\overrightarrow{\rm dS}\right)\Bigg\}\end{aligned} \tag{32}$$

where we have neglected the perturbation to the visible surface since it turns out to be of second order compared to the other terms. The variations of the specific radiation intensity can be expanded as follows:

$$\delta I = I\left(\frac{\partial \ln I}{\partial \ln T_{\rm eff}}\frac{\delta T_{\rm eff}}{T_{\rm eff}} + \frac{\partial \ln I}{\partial \ln g_{\rm eff}}\frac{\delta g_{\rm eff}}{g_{\rm eff}}\right) + \frac{\partial I}{\partial \mu}\delta\mu \tag{33}$$

These expressions show that pulsations cause light variations in multiple ways. They cause local variations of effective temperature and gravity which in turn affect I. They also cause geometric variations of the surface which affect the size and orientation of surface elements, as well as I *via* limb darkening effects.

The various terms related to pulsation modes are calculated as follows. The Lagrangian variations of effective temperature, $\delta T_{\rm eff}/T_{\rm eff}$, are deduced from full non-adiabatic calculations. If the pulsation modes have been calculated using the adiabatic approximation, $\delta T_{\rm eff}/T_{\rm eff}$ may be approximated by the local temperature variations, $\delta T/T$ (a rather drastic approximation according to Dupret et al., 2003), which in turn are deduced from the Lagrangian pressure perturbations. Some authors (e.g., Watson, 1988; Garrido et al., 1990; Heynderickx et al., 1994) include an ad-hoc parameter to account for non-adiabatic effects. The Lagrangian variations in effective gravity are fairly complex to derive as they include the variations in the gravitational field caused by perturbations to the distribution of matter as well as variations related to the fact that the surface is displaced in this field, and finally the acceleration of the surface itself. This leads to the following expression (Reese et al., 2013):

$$\begin{aligned}\delta\vec{g}_{\rm eff} = &-\vec{\nabla}\Psi - \vec{\xi}\cdot\vec{\nabla}\left(\vec{\nabla}\Psi_0\right) + (\omega + m\Omega)^2\vec{\xi}\\ &-2i(\omega + m\Omega)\vec{\Omega}\times\vec{\xi} - \vec{\Omega}\times\left(\vec{\Omega}\times\vec{\xi}\right).\end{aligned} \tag{34}$$

Finally, the geometric terms may be deduced from the Lagrangian displacement. The perturbations to the surface elements is given by:

$$\delta\left(\overrightarrow{\rm dS}\right) = \left(\partial_\theta\vec{\xi}\times\partial_\phi\vec{r} + \partial_\theta\vec{r}\times\partial_\phi\vec{\xi}\right){\rm d}\theta{\rm d}\phi \tag{35}$$

and those of μ by:

$$\delta\mu = \vec{e}_{\rm obs.}\cdot\left\{\frac{\delta\overrightarrow{\rm dS}}{\|\overrightarrow{\rm dS}\|} - \left(\vec{n}\cdot\frac{\delta\overrightarrow{\rm dS}}{\|\overrightarrow{\rm dS}\|}\right)\vec{n}\right\} \tag{36}$$

Figure 10 illustrates the different terms that intervene in mode visibility calculations for a particular pulsation mode.

4.2 Amplitude ratios and phase differences

Besides calculating mode visibilities, one can also calculate amplitude ratios and phase differences using essentially the same set of equations as above. The main difference is that the intensity I should be multiplied by the instrument's and filter's transmission curves, prior to calculating the integrals. Repeating this procedure for different filters provides pulsation amplitudes and phases in different photometric bands. One can then calculate the amplitude ratios and phase differences between these bands. Unlike mode visibilities, these do not depend on the intrinsic mode amplitudes since these factor out. Furthermore, in the non-rotating stars, amplitude ratios and phase differences do not depend on the azimuthal order, m, or the inclination of the star. Hence, amplitude ratios and phase differences only depend on the geometric properties of the modes, and as such, may be used to constrain mode identification, and more particularly the harmonic degree, ℓ, in non-rotating stars.

Historically, Dziembowski, (1977) is among the first to have obtained an expression for pulsation-induced light variations in non-rotating stars. Subsequent expressions were derived by including further effects such as perturbations to limb darkening and the surface normal, culminating in the work by Heynderickx et al. (1994). At this point, non-adiabatic effects were only approximated *via* an ad-hoc parameter and the effects of rotation were not included. Later on, fully non-adiabatic calculations were included thus improving mode identification in non-rotating or slowly rotating stars (Dupret et al., 2002; Dupret et al., 2003).

Then, Daszyńska-Daszkiewicz et al. (2002); Daszynska-Daszkiewicz et al. (2007) and Townsend (2003a) included the effects of rotation when calculating mode visibilities. They showed that in contrast to the non-rotating case,

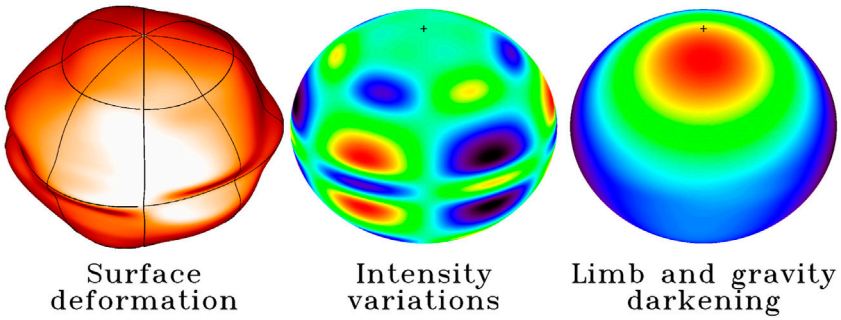

FIGURE 10
Plots showing the different terms that intervene in mode visibility calculations. The surface deformation is greatly exaggerated to make it easier to see.

amplitude ratios and phase differences depend both on the azimuthal order and the inclination. This complicates mode identification as there are more cases to investigate, but may also help to place tighter constraints on mode identification. However, the effects of rotation on the pulsation modes in the above works where approximated using either a perturbative approach or the traditional approximation. In contrast, Lignières et al. (2006); Lignières and Georgeot, (2009) fully included the effects of rotation in the pulsation calculations thanks to a 2D numerical approach but approximated the mode visibility calculations by only including the terms related to the temperature variations. They showed that chaotic acoustic modes have visibilities which are higher than that of their non-rotating counterparts, i.e., modes with intermediate $\ell - |m|$ values. Accordingly, they may be visible alongside acoustic island modes thus complicating the interpretation of pulsation spectra. Finally, Reese et al. (2013) calculated mode visibilities including all of the terms for full 2D mode calculations. However, these calculations were done with the adiabatic approximation. Later on, Reese et al. (2017b) approximated non-adiabatic effects by deriving the effective temperature variations from the radial displacement using an ad-hoc function calibrated on 1D non-adiabatic pulsation calculations by the MAD code (Dupret, 2001). They also tested a mode identification strategy which consists in grouping together modes with similar amplitude ratios. This allowed them to group island modes with similar quantum numbers together but required having a large number of observed pulsation modes.

4.3 Line profile variations

Another observable associated with pulsation modes is line profile variations (LPVs). LPVs typically take on the form of bumps that move over time within a spectroscopic line profile and are mainly caused by the Doppler shifts induced by the oscillatory motions from the pulsations. Accordingly, they can also be used to constrain mode geometry and hence identification. A more detailed description of LPVs in the case of rapid rotation is provided in the review by Mirouh (this volume).

5 Interpreting pulsation spectra of rapid rotators

The various attempts that have been made to interpret pulsation spectra in rapidly rotating stars fit into two broad categories: ensemble seismology and seismology "a la carte". The first category applies to whole groups of stars whereas the second concerns detailed seismic investigations of individual targets. In what follows, we will especially focus on the second type of approach by providing a non-exhaustive list of examples. As pointed out above, one of the main obstacles to carrying out a detailed seismic interpretation is the lack of a reliable mode identification. Hence, all of the examples below include some sort of strategy for identifying modes, either based on frequency patterns or on amplitude ratios and phase differences. Finally, apart from μ Eridani, the examples below focus on acoustic modes. An extensive literature also exists on interpreting gravity modes in rapidly rotating stars such as γ Dor and SPB stars (e.g., Van Reeth et al., 2016; Ouazzani et al., 2019). Mirouh (this volume) provides a detailed review of these works.

5.1 Frequency patterns in δ Scuti stars

Recently, Bedding et al. (2020) worked on the seismic interpretation of 60 young δ Scuti stars, most of which were observed by TESS (Ricker et al., 2015). Assmuing the dominant observed modes are axisymmetric, they matched $\ell = 0$ and 1

frequencies from non-rotating models to the observed pulsation spectra with the help of echelle diagrams. Figure 11 shows echelle diagrams for two of the more rapidly rotating stras in the sample along with the expected positions of the $\ell = 0$ and 1 ridges or theoretical frequencies from non-rotating models. They justified this approach by noting that these modes, once normalised by the large separation, remain relatively invariant, even in models rotating at roughly 50% of the critical rotation rate, as shown by full 2D calculations using models based on the SCF method. Although the methodology may differ, this work follows a number of previous efforts using both seismology "a la carte" and ensemble seismology (e.g., García Hernández et al., 2009; Paparó et al., 2016; Michel et al., 2017; Bowman and Kurtz, 2018) to identify frequency patterns and large separations in δ Scuti stars.

5.2 μ Eridani

μ Eridani is an SPB star of spectral type B5 IV. With a projected equatorial velocity $v \sin i = 130$ km s^{-1}, it is rotating at least at 30% of the critical rotation velocity. This star was observed using the Strömgren *uvy* filters in 2012–2013 thus leading to a number of modes detected in all three photometric bands. Daszyńska-Daszkiewicz et al. (2015) therefore devised and applied a multicolour mode identification technique which consisted in carrying out a χ^2 minimisation of the differences between observed amplitude ratios and phase differences, and the corresponding theoretical predictions. This required the use of non-adiabatic pulsation calculations in the presence of rapid rotation, which they carried out using the traditional approximation (thus neglecting the centrifugal deformation). They only included excited modes in their comparisons. Although several possible sets of mode identifications were found, their results point to an equatorial velocity v between 135 and 140 km s^{-1} and hence an inclination not too far from equator-on ($i \gtrsim 70^{\circ}$). They also concluded that modes with $\ell \leq 2$ were not sufficient to carry out the identification and went up to $\ell = 6$.

5.3 β Pictoris

The star β Pictoris has attracted considerable interest since the direct imaging of an exoplanet orbiting around it thanks to adaptive optics (Lagrange et al., 2009; Lagrange et al., 2010). Furthermore, it is a bright star of spectral type A6 V, located at 19.76 pc from us (as based on Gaia DR2 parallax, Gaia Collaboration et al., 2018). It has a disk orbiting around it and rotates with a projected equatorial velocity of $v \sin i = 124 \pm 3$ km s^{-1}, thus making it a moderately fast rotator (Koen et al., 2003). Various instruments observed β Pictoris in 2017–2018 in an attempt to detect the transit of the planet's Hill sphere in front of the star. In addition, β Pic was observed by the BRITE-Constellation (Weiss et al., 2014). This resulted in multiple light curves in separate photometric bands that could be used for the purposes of asteroseismology.

Zwintz et al. (2019) carried out a seismic analysis of this star using rapidly rotating models based on the SCF method. Given that it was observed in multiple photometric bands, it was an ideal target to carry out mode identification based on amplitude ratios. Furthermore, the constraints provided by the orbital

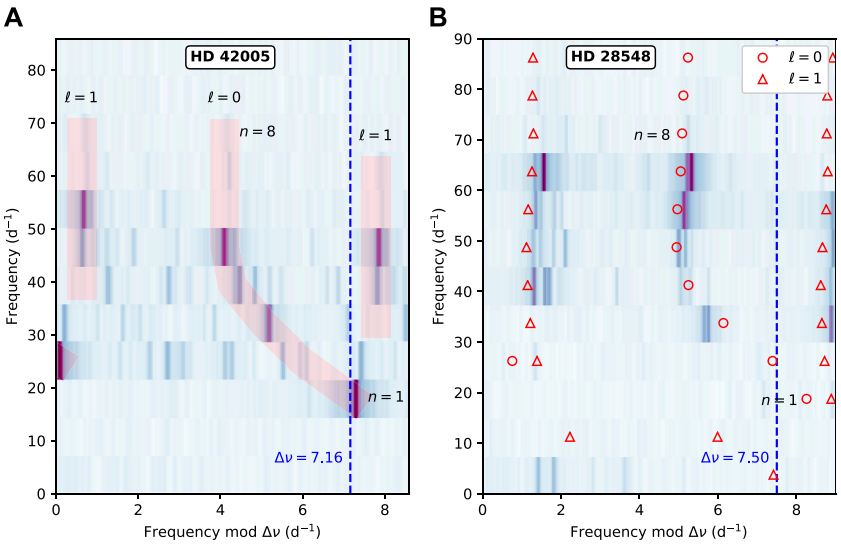

FIGURE 11
Echelle diagrams for HD 42005 **(A)** and HD 28548 **(B)**, with projected equatorial velocities of 130 ± 30 km s^{-1} and 200 ± 50 km s^{-1}, respectively. The stripes in the left correspond to what may be $\ell = 0$ and 1 sequences. The symbols in the right panel are frequencies from non-rotating models that roughly match the observations (Material from: Bedding et al., Nature 581, 7807, 147-151 (2020), Springer Nature Limited).

dynamics of the exoplanet as well as interferometric observations lead to fairly accurate estimates of the mass and radius, thus narrowing down the set of possible solutions. An MCMC search was carried out to find best matching solutions and corresponding stellar parameters. Figure 12 compares the frequencies and amplitude ratios from two of the solutions with the observational constraints. As can be seen, it turned out to be difficult to find models that simultaneously reproduce the observed amplitude ratios and frequencies. In particular, some of the amplitude ratios were reproduced by none of the theoretical modes, regardless of inclination and rotation rate. The causes behind these discrepancies may be shortcomings in the models thus leading to inaccuracies in the frequencies, approximations in the mode visibility calculations such as an ad-hoc modelling of non-adiabatic effects, and/or the fact that not all of the light curves were obtained at the same epoch, which could lead to erroneous amplitude ratios if the mode amplitudes vary over time. As was shown in Bowman et al. (2016), amplitude modulation is common in δ Scuti stars. Nonetheless, among the best solutions obtained by the MCMC procedure were near

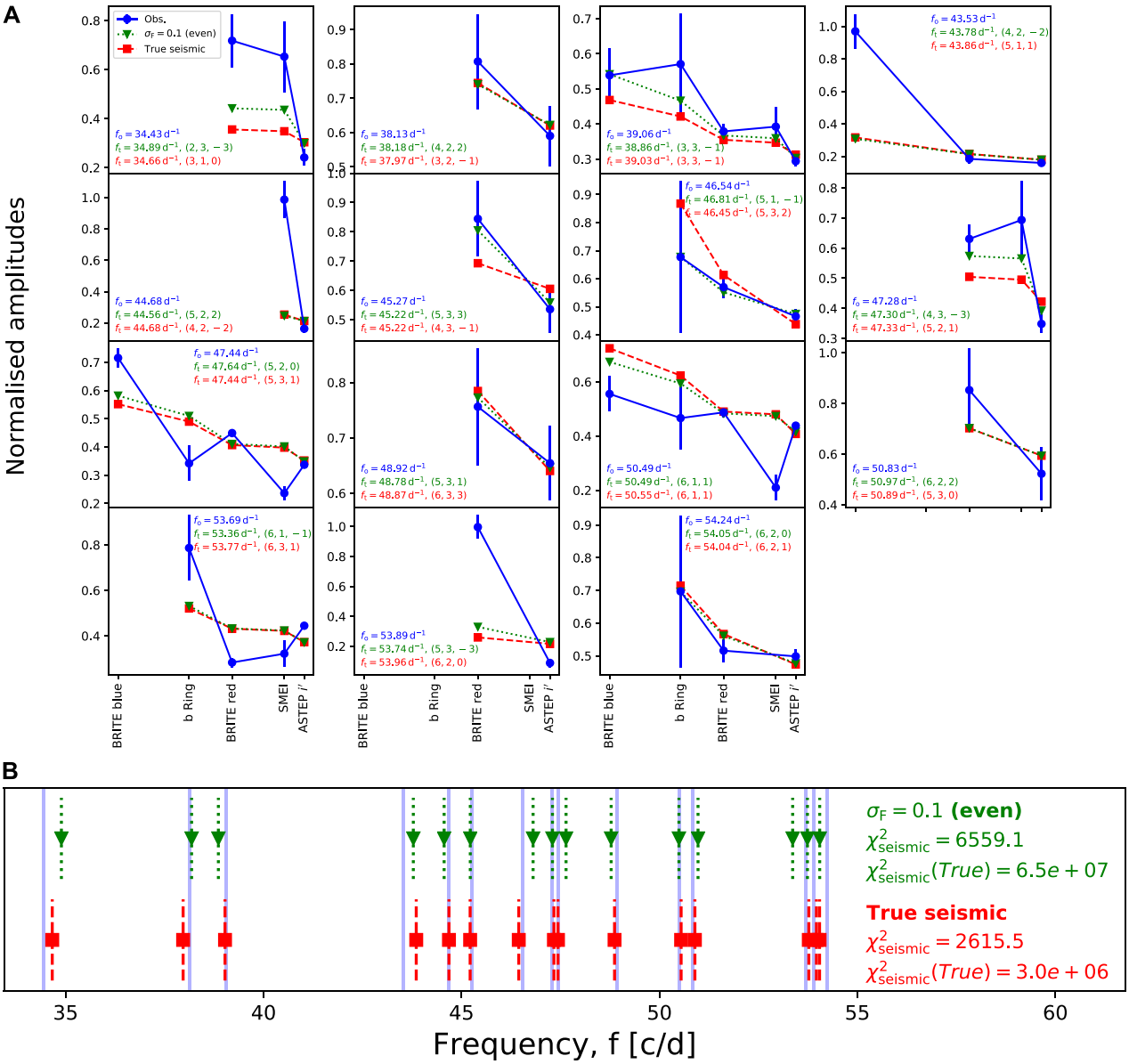

FIGURE 12
Amplitude ratios **(A)** and corresponding pulsation spectra **(B)** coming from best-fitting solutions for β Pictoris. The dark and light blue lines in both panels correspond to the observed amplitude ratios and frequencies. The green and red lines and symbols correspond to two solutions obtained with different error bars on the frequencies (Credit: Zwintz et al. (2019), reproduced with permission © ESO).

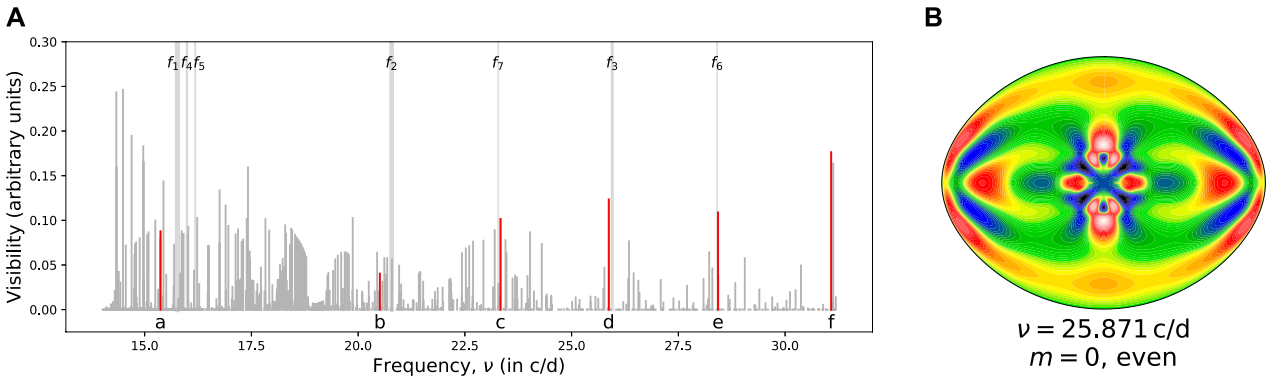

FIGURE 13
(A) Observed and theoretical pulsation spectra for Altair. The observed frequencies are shown by the vertical light grey lines that span the plot and are indicated by the labels f_1 to f_7. The thickness of the lines correspond to the observed amplitudes. The darker grey lines correspond to theoretical pulsation modes. Their height corresponds to mode visibilities. The red lines with the labels "a" to "f" correspond to island modes or mixed gravito-island modes selected to match the observed pulsations. **(B)** Meridional cross-section of mode "d". The colours indicate Lagrangian pressure perturbations on a pseudo-logarithmic scale (Credit: Bouchaud et al. (2020), reproduced with permission © ESO).

equator-on solutions with an inclination around 89° and a rotation rate of 27% of the Keplerian break-up velocity. This would agree with the inclination of the planet's orbit as well as that of the disk.

5.4 Altair

Altair, also known as α Aquilae, is one of the three stars in the summer triangle. It has been a prime target for interferometry due to its proximity (5.13 pc from the Sun) and its rapid rotation. Indeed, both its centrifugal deformation and gravity darkening may be observed (van Belle et al., 2001; Ohishi et al., 2004; Domiciano de Souza et al., 2005; Peterson et al., 2006; Monnier et al., 2007). Various spectroscopic studies have found $v \sin i$ values ranging from 190 km s^{-1} (Carpenter et al., 1984) to 250 km s^{-1} (Stoeckley, 1968). Furthermore, as shown in Buzasi et al. (2005), it is a δ Scuti pulsator, with low-frequency acoustic modes, and possibly some gravito-inertial modes.

Suárez et al. (2005) therefore carried out a seismic study of Altair. They used models produced by the 1D stellar evolution code CESAM (Morel, 1997; Morel and Lebreton, 2008) and calculated pulsation modes using the Filou pulsation code, which applies a second order perturbative method to model the effects of rotation (Tran Minh and Léon, 1995; Suárez et al., 2002). Their study favoured models in a 1.70–1.76 $M_\odot$ mass range with an age between 225 and 775 Myrs. However, given the rapid rotation rate, it proved to be necessary to use full 2D calculations to interpret the pulsations in this star (Reese et al., 2006).

Accordingly, Bouchaud et al. (2020) carried out an extensive study using interferometric, spectroscopic, and seismic data. Given the diversity of observational constraints, a multi-step optimisation procedure was carried out. Using an MCMC approach, models were first selected based on interferometric and spectroscopic constraints before being fine-tuned using the seismic constraints. The four higher frequency modes (starting from 20.785 c/d) were assumed to be $l = 0$ and 1, m = 0 modes (i.e., $\tilde{\ell} = 0$ island modes), thus leading to alternating high and low mode visibilities in qualitative agreement with the observed amplitudes. Interestingly, this is the same type of mode identification as that used in Bedding et al. (2020). By adjusting the model to reproduce the frequencies, it was possible to obtain a model which roughly reproduces all of the constraints. Figure 13 shows a comparison between the observed and theoretical pulsation spectra for Altair along with the meridional cross-section of one of the modes selected to match the observed pulsations. The mass of this model is 1.863 $M_\odot$, its rotation rate 0.744 Ω_K thus leading to $v \sin i$ = 243 km s^{-1}, and its central hydrogen content $X_c = 0.71$ (to be compared with a surface composition of $X_s = 0.739$). This leads to a rough estimate of 100 Myrs for the star's age when compared with 1D stellar evolution models from CESAM. Such an age is lower than the estimate by Suárez et al. (2005) and considerably lower than some of the estimates based on isochrone fitting which exceed 1 Gyr (e.g., Lachaume et al., 1999; Domiciano de Souza et al., 2005). It may thus provide a natural explanation for why the rotation rate is still high.

6 Conclusion

In this review, we have described 2D modelling of pulsations in rapidly rotating stars. Compared to the 1D spherically symmetric case, calculating pulsation modes in rapidly

rotating stars is a formidable problem. As a result, various approximate methods, namely perturbative approaches of various orders and methods based on the traditional approximation, have been devised. These have lead to a number of results and insights in the effects of rotation on stellar pulsations, such as rotational multiplets or a modified period spacing pattern for gravity modes. Then, with the advent of more powerful computers, efficient full 2D numerical approaches were implemented. This has lead to a wealth of theoretical results, thus considerably extending our understanding of pulsations in rapidly rotating stars as well as their structure, and has helped to show some of the limitations of previous methods. As is briefly addressed here, new mode geometries and pulsation frequency patterns emerge at rapid rotation, thus leading to pulsation spectra that are considerably more complicated than that of non-rotating stars.

Given the increased complexity of pulsation spectra in such stars, it is much more difficult to correctly match observed pulsations with those that are calculated in stellar models. Accordingly, it is necessary to extend mode identification techniques to these stars, namely those based on multicolour photometry and line profile variations. However, as described in this review, this first requires generalising all of the relevant formulae to a centrifugally distorted stellar geometry thus increasing their complexity. This then allows us to theoretically predict amplitude ratios and phase differences between different photometric bands, which unlike in the non-rotating case, depend both on the azimuthal order of the mode and the inclination of the star. Comparing such predictions with observations can then be used to constrain the geometry of the observed pulsation modes and hence their identification.

Armed with these new theoretical developments, several authors have looked into interpreting the pulsation spectra of various rapidly rotating stars. They have been able to make headway into identifying the observed pulsations and have started to characterise these stars, including the rotation rate, inclination, mass, and age. Some of these results have brought out some of the limitations in our understanding of the physical phenomena that take place in these stars, and are in sharp contrast with previous results based on 1D numerical approaches, thus highlighting the importance of using full 2D approaches. Much effort is still needed to generalise the use of such methods to large numbers of stars and to interpret the wealth of pulsation data currently available, particularly those coming from recent space missions.

In the future, 3D pulsation calculations may become important for certain types of stars that are not symmetric around the rotation axis due to supplementary physical phenomena. For instance, rapidly oscillating Ap (roAp) stars have a strong magnetic field which is inclined with respect to the rotation axis, and close binaries undergo tidal deformation that can only be described in a 3D context. Pulsation calculations in such stars would probably use a similar approach as the one described here except that summations over multiple azimuthal orders rather than a single m value would intervene in the pulsation modes and equations, and the ϕ component of coupling integrals (Eq. 17) would not separate out. Accordingly, this would require heavy computational resources, particularly to store the discretised system in memory and to speed up calculations through parallelisation. However, it may provide further insights into the pulsation physics and underlying stellar structure as did 2D calculations for rotating stars, and provide answers to long-standing questions such as the orientation of the pulsation modes with respect to the rotation and magnetic axes in roAp stars (e.g., Kurtz, 1990; Bigot and Dziembowski, 2002). From an observational point of view, one might expect highly complicated pulsation spectra with frequency multiplets being further subdivided, thus leading to $(2\ell + 1)^2$ rather than $(2\ell + 1)$ components per multiplet (e.g., Gough and Thompson, 1990).

Author contributions

The author confirms being the sole contributor of this work and has approved it for publication.

Funding

Funds for this publication came from the Agence Nationale de la Recherche (ANR) *via* the MASSIF project under grant ANR-21-CE31-0018-01, which is gratefully acknowledged.

Acknowledgments

DRR thanks the various researchers with whom he has had the privilege to work with on this fascinating topic: François Lignières, Michel Rieutord, Jérôme Ballot, Kévin Bouchaud, Giovanni Mirouh, Rhita-Maria Ouazzani, Marc-Antoine Dupret, Keith MacGregor, MarieJo Goupil, Armando Domiciano de Souza, Antonio García Hernández, Juan-Carlos Suárez, Frédéric Royer, Tim Bedding, Simon Murphy, Konstanze Zwintz, and many others. DR thanks both referees, Catherine Lovekin and Dominic Bowman, for helpful comments that have improved the manuscript.

Conflict of interest

The author declares that the research was conducted in the absence of any commercial or financial relationships that could be construed as a potential conflict of interest.

Publisher's note

References

Ballot, J., Lignières, F., Prat, V., Reese, D. R., and Rieutord, M. (2012). "2D computations of g-modes in fast rotating stars,"*Progress in solar/stellar physics with helio- and asteroseismology*. Editors H. Shibahashi, M. Takata, and A. E. Lynas-Gray (Astronomical Society of the Pacific Conference Series), 389.

Ballot, J., Lignières, F., and Reese, D. R. (2013). Numerical exploration of oscillation modes in rapidly rotating stars. *Lect. Notes Phys.* 865, 91. doi:10.1007/978-3-642-33380-4_5

Ballot, J., Lignières, F., Reese, D. R., and Rieutord, M. (2010). Gravity modes in rapidly rotating stars. Limits of perturbative methods. *Astron. Astrophys.* 518, A30. doi:10.1051/0004-6361/201014426

Balona, L. A. (2000). "Understanding pulsations in OB stars," in *ASP conf. Ser. 203: IAU colloq. 176: The impact of large-scale surveys on pulsating star research*. Editors L. Szabados and D. Kurtz, 401–407.

Baruteau, C., and Rieutord, M. (2013). Inertial waves in a differentially rotating spherical shell. *J. Fluid Mech.* 719, 47–81. doi:10.1017/jfm.2012.605

Bedding, T. R., Murphy, S. J., Hey, D. R., Huber, D., Li, T., Smalley, B., et al. (2020). Very regular high-frequency pulsation modes in young intermediate-mass stars. *Nature* 581, 147–151. doi:10.1038/s41586-020-2226-8

Berthomieu, G., Gonczi, G., Graff, P., Provost, J., and Rocca, A. (1978). Low-frequency gravity modes of a rotating star. *A&A* 70, 597–606.

Bigot, L., and Dziembowski, W. A. (2002). The oblique pulsator model revisited. *Astron. Astrophys.* 391, 235–245. doi:10.1051/0004-6361:20020824

Bildsten, L., Ushomirsky, G., and Cutler, C. (1996). Ocean g-modes on rotating neutron stars. *Astrophys. J.* 460, 827. doi:10.1086/177012

Bouabid, M.-P., Dupret, M.-A., Salmon, S., Montalbán, J., Miglio, A., Noels, A., et al. (2013). Effects of the Coriolis force on high-order g modes in γ Doradus stars. *Mon. Not. R. Astron. Soc.* 429, 2500–2514. doi:10.1093/mnras/sts517

Bouchaud, K., Domiciano de Souza, A., Rieutord, M., Reese, D. R., and Kervella, P. (2020). A realistic two-dimensional model of Altair. *Astron. Astrophys.* 633, A78. doi:10.1051/0004-6361/201936830

Bowman, D. M., Kurtz, D. W., Breger, M., Murphy, S. J., and Holdsworth, D. L. (2016). Amplitude modulation in δ sct stars: Statistics from an ensemble study of kepler targets. *Mon. Not. R. Astron. Soc.* 460, 1970–1989. doi:10.1093/mnras/stw1153

Bowman, D. M., and Kurtz, D. W. (2018). Characterizing the observational properties of δ Sct stars in the era of space photometry from the Kepler mission. *Mon. Notices R. Astronomical Soc.* 476, 3169–3184. doi:10.1093/mnras/sty449

Gaia CollaborationBrown, A. G. A., Vallenari, A., Prusti, T., de Bruijne, J. H. J., and Babusiaux, C. (2018). Gaia Data Release 2. Summary of the contents and survey properties. *Astron. Astrophys.* 616, A1. doi:10.1051/0004-6361/201833051

Burke, K. D., Reese, D. R., and Thompson, M. J. (2011). On the effects of rotation on acoustic stellar pulsations: Validity domains of perturbative methods and close frequency pairs. *Mon. Not. R. Astron. Soc.* 414, 1119–1126. doi:10.1111/j.1365-2966.2011.18453.x

Buzasi, D. L., Bruntt, H., Bedding, T. R., Retter, A., Kjeldsen, H., Preston, H. L., et al. (2005). Altair: The brightest δ Scuti star. *Astrophys. J.* 619, 1072–1076. doi:10.1086/426704

Carpenter, K. G., Slettebak, A., and Sonneborn, G. (1984). Rotational velocities of later B type and A type stars as determined from ultraviolet versus visual line profiles. *Astrophys. J.* 286, 741. doi:10.1086/162650

Christensen-Dalsgaard, J. (2008). ASTEC—The aarhus STellar evolution code. *Astrophys. Space Sci.* 316, 13–24. doi:10.1007/s10509-007-9675-5

Christensen-Dalsgaard, J., and Mullan, D. J. (1994). Accurate frequencies of polytropic models. *Mon. Not. R. Astron. Soc.* 270, 921–935. doi:10.1093/mnras/270.4.921

Christensen-Dalsgaard, J. (1982). On solar models and their periods of oscillation. *Mon. Not. R. Astron. Soc.* 199, 735–761. doi:10.1093/mnras/199.3.735

Christensen-Dalsgaard, J., Schou, J., and Thompson, M. J. (1990). A comparison of methods for inverting helioseismic data. *Mon. Not. R. Astron. Soc.* 242, 353–369. doi:10.1093/mnras/242.3.353

Clement, M. J. (1981). Normal modes of oscillation for rotating stars. I - the effect of rigid rotation on four low-order pulsations. *Astrophys. J.* 249, 746. doi:10.1086/159335

Clement, M. J. (1984). Normal modes of oscillation for rotating stars. II Variational solutions. *Astrophys. J.* 276, 724. doi:10.1086/161658

Clement, M. J. (1986). Normal modes of oscillation for rotating stars. III - variational calculations with an improved set of basis vectors. *Astrophys. J.* 301, 185. doi:10.1086/163886

Clement, M. J. (1989). Normal modes of oscillation for rotating stars. IV. Nonaxisymmetricvariational solutions for 15 M_{odot} models. *Astrophys. J.* 339, 1022. doi:10.1086/167356

Clement, M. J. (1998). Normal modes of oscillation for rotating stars. V. A new numerical method for computing nonradial eigenfunctions. *Astrophys. J. Suppl. Ser.* 116, 57–74. doi:10.1086/313097

Cowling, T. G. (1941). The non-radial oscillations of polytropic stars. *Mon. Not. R. Astron. Soc.* 101, 367–375. doi:10.1093/mnras/101.8.367

Daszyńska-Daszkiewicz, J., Dziembowski, W. A., Jerzykiewicz, M., and Handler, G. (2015). Oscillation modes in the rapidly rotating slowly pulsating B-type star μ Eridani. *Mon. Not. R. Astron. Soc.* 446, 1438–1448. doi:10.1093/mnras/stu2216

Daszyńska-Daszkiewicz, J., Dziembowski, W. A., Pamyatnykh, A. A., and Goupil, M.-J. (2002). Photometric amplitudes and phases of nonradial oscillation in rotating stars. *Astron. Astrophys.* 392, 151–159. doi:10.1051/0004-6361:20020911

Daszynska-Daszkiewicz, J., Dziembowski, W. A., and Pamyatnykh, A. A. (2007). On the prospects for detection and identification of low-frequency oscillation modes in rotating B type stars. *Acta Astron.* 57, 11–32.

Deupree, R. G. (1995). Stella evolution with arbitrary rotation laws. 2: Massive star evolution to core hydrogen exhaustion. *Astrophys. J.* 439, 357. doi:10.1086/175179

Deupree, R. G. (1990). Stellar evolution with arbitrary rotation laws. I - mathematical techniques and test cases. *Astrophys. J.* 357, 175. doi:10.1086/168903

Deupree, R. G. (2011). Theoretical p-mode oscillation frequencies for the rapidly rotating δ Scuti star α ophiuchi. *Astrophys. J.* 742, 9. doi:10.1088/0004-637x/742/1/9

Dintrans, B., and Rieutord, M. (2000). Oscillations of a rotating star: A non-perturbative theory. *A&A* 354, 86–98.

Dintrans, B., Rieutord, M., and Valdettaro, L. (1999). Gravito-inertial waves in a rotating stratified sphere or spherical shell. *J. Fluid Mech.* 398, 271–297. doi:10.1017/s0022112099006308

Domiciano de Souza, A., Kervella, P., Jankov, S., Abe, L., Vakili, F., di Folco, E., et al. (2003). The spinning-top Be star Achernar from VLTI-VINCI. *Astron. Astrophys.* 407, L47–L50. doi:10.1051/0004-6361:20030786

Domiciano de Souza, A., Kervella, P., Jankov, S., Vakili, F., Ohishi, N., Nordgren, T. E., et al. (2005). Gravitational-darkening of Altair from interferometry. *A&A.* 442, 567–578. doi:10.1051/0004-6361:20042476

Dupret, M.-A., De Ridder, J., De Cat, P., Aerts, C., Scuflaire, R., Noels, A., et al. (2003). A photometric mode identification method, including an improved non-adiabatic treatment of the atmosphere. *Astron. Astrophys.* 398, 677–685. doi:10.1051/0004-6361:20021679

Dupret, M. A. (2001). Nonradial nonadiabatic stellar pulsations: A numerical method and its application to a beta cephei model. *Astron. Astrophys.* 366, 166–173. doi:10.1051/0004-6361:20000219

Dupret, M., De Ridder, J., Neuforge, C., Aerts, C., and Scuflaire, R. (2002). Influence of non-adiabatic temperature variations on line profile variations of slowly rotating beta Cep stars and SPBs. I. Non-adiabatic eigenfunctions in the atmosphere of a pulsating star. *Astron. Astrophys.* 385, 563–571. doi:10.1051/0004-6361:20020193

Dziembowski, W., Krolikowska, M., and Kosovichev, A. (1988). Nonlinear mode coupling in oscillating stars. III. Amplitude limiting effect of the rotation in the Delta Scuti stars. *Acta Astron* 38, 61–75.

Dziembowski, W., and Krolikowska, M. (1985). Nonlinear mode coupling in oscillating stars. II - limiting amplitude effect of the parametric resonance in main sequence stars. *Acta Astron* 35, 5–28.

Dziembowski, W. (1977). Light and radial velocity variations in a nonradially oscillating star. *Acta Astron.* 27, 203–211.

Dziembowski, W. (1982). Nonlinear mode coupling in oscillating stars. I - second order theory of the coherent mode coupling. *Acta Astron* 32, 147–171.

Espinosa, F., Pérez Hernández, F., and Roca Cortés, T. (2004). Oscillation modes in axially symmetric stars. *ESA SP-559 SOHO 14 Helio- Asteroseismol. Towards a Gold. Future* 559, 424–427.

Espinosa Lara, F., and Rieutord, M. (2013). Self-consistent 2D models of fast-rotating early-type stars. *Astron. Astrophys.* 552, A35. doi:10.1051/0004-6361/201220844

Ferrari, V. (2005). Imprint of the equation of state of dense matter on gravitational waves emitted by oscillating neutron stars. *J. Phys. Conf. Ser.* 8, 58–70. doi:10.1088/1742-6596/8/1/008

García Hernández, A., Martín-Ruiz, S., Monteiro, M. J. P. F. G., Suárez, J. C., Reese, D. R., Pascual-Granado, J., et al. (2015). Observational dν-ρ relation for δ sct stars using eclipsing. *Bin. Space Photometry* 811, L29.

García Hernández, A., Moya, A., Michel, E., Garrido, R., Suárez, J. C., Rodríguez, E., et al. (2009). Asteroseismic analysis of the CoRoT δ Scuti star HD 174936. *Astron. Astrophys.* 506, 79–83. doi:10.1051/0004-6361/200911932

Garrido, R., Garcia-Lobo, E., and Rodriguez, E. (1990). Modal distribution of pulsating stars by using Stroemgren photometry. *A&A* 234, 262.

Gastine, T., and Dintrans, B. (2008). Direct numerical simulations of the κ-mechanism. II. Nonlinear saturation and the Hertzsprung progression. *Astron. Astrophys.* 490, 743–752. doi:10.1051/0004-6361:200809891

Goode, P. R., and Thompson, M. J. (1992). The effect of an inclined magnetic field on solar oscillation frequencies. *Astrophys. J.* 395, 307. doi:10.1086/171653

Gough, D. O. (1981). A new measure of the solar rotation. *Mon. Not. R. Astron. Soc.* 196, 731–745. doi:10.1093/mnras/196.3.731

Gough, D. O., and Thompson, M. J. (1990). The effect of rotation and a buried magnetic field on stellar oscillations. *Mon. Not. R. Astron. Soc.* 242, 25–55. doi:10.1093/mnras/242.1.25

Goupil, M. J., and Talon, S. (2002). "Seismology of δ Scuti stars: Problems and prospects (invited paper)," in *ASP conf. Ser. 259: IAU colloq. 185: Radial and nonradial pulsationsn as probes of stellar physics*. Editors C. Aerts, T. R. Bedding, and J. Christensen-Dalsgaard, 306.

Hatta, Y., Sekii, T., Takata, M., and Kurtz, D. W. (2019). The two-dimensional internal rotation of KIC 11145123. *Astrophys. J.* 871, 135. doi:10.3847/1538-4357/aaf881

Heynderickx, D., Waelkens, C., and Smeyers, P. (1994). A photometric study of β Cephei stars. II. Determination of the degrees L of pulsation modes. *A&A Supp.* 105, 447–480.

Ipser, J. R., and Lindblom, L. (1991). The oscillations of rapidly rotating Newtonian stellar models. II - dissipative effects. *Astrophys. J.* 373, 213. doi:10.1086/170039

Jackson, S., MacGregor, K. B., and Skumanich, A. (2005). On the use of the self-consistent-field method in the construction of models for rapidly rotating main-sequence stars. *Astrophys. J. Suppl. Ser.* 156, 245–264. doi:10.1086/426587

Karami, K. (2008). Third order effect of rotation on stellar oscillations of a B star. *Chin. J. Astron. Astrophys.* 8, 285–308. doi:10.1088/1009-9271/8/3/06

Koen, C., Balona, L. A., Khadaroo, K., Lane, I., Prinsloo, A., Smith, B., et al. (2003). Pulsations in β Pictoris. *Mon. Not. R. Astron. Soc.* 344, 1250–1256. doi:10.1046/j.1365-8711.2003.06912.x

Kurtz, D. W. (1990). Rapidly oscillating AP stars. *Annu. Rev. Astron. Astrophys.* 28, 607–655. doi:10.1146/annurev.aa.28.090190.003135

Lachaume, R., Dominik, C., Lanz, T., and Habing, H. J. (1999). Age determinations of main-sequence stars: Combining different methods. *A&A* 348, 897–909.

Lagrange, A. M., Bonnefoy, M., Chauvin, G., Apai, D., Ehrenreich, D., Boccaletti, A., et al. (2010). A giant planet imaged in the disk of the young star β Pictoris. *Science* 329, 57–59. doi:10.1126/science.1187187

Lagrange, A. M., Gratadour, D., Chauvin, G., Fusco, T., Ehrenreich, D., Mouillet, D., et al. (2009). A probable giant planet imaged in the β Pictoris disk. VLT/NaCo deep L'-band imaging. *Astron. Astrophys.* 493, L21–L25. doi:10.1051/0004-6361:200811325

Ledoux, P. (1951). The nonradial oscillations of gaseous stars and the problem of beta Canis majoris. *Astrophys. J.* 114, 373. doi:10.1086/145477

Lee, U., and Baraffe, I. (1995). Pulsational stability of rotating main sequence stars: The second order effects of rotation on the nonadiabatic oscillations. *A and A* 301, 419.

Lee, U. (2006). r modes of slowly pulsating B stars. *Mon. Not. R. Astron. Soc.* 365, 677–687. doi:10.1111/j.1365-2966.2005.09751.x

Lee, U. (2008). Pulsation in rapidly rotating stars. *Commun. Asteroseismol.* 157, 203–208.

Lee, U. (2001). Pulsational stability of g-modes in slowly pulsating B stars. *Astrophys. J.* 557, 311–319. doi:10.1086/321554

Lee, U., and Saio, H. (1987). Low-frequency oscillations of uniformly rotating stars. *Mon. Not. R. Astron. Soc.* 224, 513–526. doi:10.1093/mnras/224.3.513

Lignières, F., and Georgeot, B. (2009). Asymptotic analysis of high-frequency acoustic modes in rapidly rotating stars. *Astron. Astrophys.* 500, 1173–1192. doi:10.1051/0004-6361/200811165

Lignières, F., and Georgeot, B. (2008). Wave chaos in rapidly rotating stars. *Phys. Rev. E* 78, 016215. doi:10.1103/physreve.78.016215

Lignières, F., Rieutord, M., and Reese, D. (2006). Acoustic oscillations of rapidly rotating polytropic stars. *Astron. Astrophys.* 455, 607–620. doi:10.1051/0004-6361:20065015

Lignières, F., Rieutord, M., and Valdettaro, L. (2001). "Acoustic modes in spheroidal cavities," in *SF2A-2001: Semaine de l'Astrophysique Francaise*. Editors F. Combes, D. Barret, and F. Thévenin, 127.

Lovekin, C. C., Deupree, R. G., and Clement, M. J. (2009). Effects of uniform and differential rotation on stellar pulsations. *Astrophys. J.* 693, 677–690. doi:10.1088/0004-637x/693/1/677

Lovekin, C. C., and Deupree, R. G. (2008). Radial and nonradial oscillation modes in rapidly rotating stars. *Astrophys. J.* 679, 1499–1508. doi:10.1086/587615

Lynden-Bell, D., and Ostriker, J. P. (1967). On the stability of differentially rotating bodies. *Mon. Not. R. Astron. Soc.* 136, 293–310. doi:10.1093/mnras/136.3.293

MacGregor, K. B., Jackson, S., Skumanich, A., and Metcalfe, T. S. (2007). On the structure and properties of differentially rotating, main-sequence stars in the 1-2 m_{solar} range. *Astrophys. J.* 663, 560–572. doi:10.1086/518303

Maeder, A. (2009). Physics, Formation and Evolution of rotating stars. *Astronomy and astrophysics library*. Berlin, Heidelberg: Springer-Verlag.

Manchon, L. (2021). *On the transport of angular momentum in stellar radiative zones in 2D*. Ph.D. thesis. Saclay: Université de Paris.

Marques, J. P., Goupil, M. J., Lebreton, Y., Talon, S., Palacios, A., Belkacem, K., et al. (2013). Seismic diagnostics for transport of angular momentum in stars. I. Rotational splittings from the pre-main sequence to the red-giant branch. *Astron. Astrophys.* 549, A74. doi:10.1051/0004-6361/201220211

Meynet, G., and Maeder, A. (2000). Stellar evolution with rotation. V. Changes in all the outputs of massive star models. *A&A* 361, 101–120.

Michel, E., Dupret, M.-A., Reese, D., Ouazzani, R.-M., Debosscher, J., Hernández, A. G., et al. (2017). What CoRoT tells us about δ Scuti stars. Existence of a regular pattern and seismic indices to characterize stars. *Eur. Phys. J. Web Conf.* 160, 03001.

Mirouh, G. M., Angelou, G. C., Reese, D. R., and Costa, G. (2019). Mode classification in fast-rotating stars using a convolutional neural network: Model-based regular patterns in δ Scuti stars. *Mon. Notices R. Astronomical Soc. Lett.* 483, L28–L32. doi:10.1093/mnrasl/sly212

Mirouh, G. M., Baruteau, C., Rieutord, M., and Ballot, J. (2016). Gravito-inertial waves in a differentially rotating spherical shell. *J. Fluid Mech.* 800, 213–247. doi:10.1017/jfm.2016.382

Monnier, J. D., Zhao, M., Pedretti, E., Thureau, N., Ireland, M., Muirhead, P., et al. (2007). Imaging the surface of Altair. *Science* 317, 342–345. doi:10.1126/science.1143205

Morel, P. (1997). Cesam: A code for stellar evolution calculations. *Astron. Astrophys. Suppl. Ser.* 124, 597–614. doi:10.1051/aas:1997209

Morel, P., and Lebreton, Y. (2008). Cesam: A free code for stellar evolution calculations. *Astrophys. Space Sci.* 316, 61–73. doi:10.1007/s10509-007-9663-9

Ogilvie, G. I. (2009). Tidal dissipation in rotating fluid bodies: A simplified model. *Mon. Not. R. Astron. Soc.* 396, 794–806. doi:10.1111/j.1365-2966.2009.14814.x

Ohishi, N., Nordgren, T. E., and Hutter, D. J. (2004). Asymmetric surface brightness distribution of Altair observed with the navy prototype optical interferometer. *Astrophys. J.* 612, 463–471. doi:10.1086/422422

Ouazzani, R.-M., Roxburgh, I. W., and Dupret, M.-A. (2015). Pulsations of rapidly rotating stars. II. Realistic modelling for intermediate-mass stars. *Astron. Astrophys.* 579, A116. doi:10.1051/0004-6361/201525734

Ouazzani, R.-M., Salmon, S. J. A. J., Antoci, V., Bedding, T. R., Murphy, S. J., Roxburgh, I. W., et al. (2017). A new asteroseismic diagnostic for internal rotation in γ Doradus stars. *Mon. Not. R. Astron. Soc.* 465, 2294–2309. doi:10.1093/mnras/stw2717

Ouazzani, R. M., Dupret, M. A., and Reese, D. R. (2012). Pulsations of rapidly rotating stars. I. The ACOR numerical code. *Astron. Astrophys.* 547, A75. doi:10.1051/0004-6361/201219548

Ouazzani, R. M., Lignières, F., Dupret, M. A., Salmon, S. J. A. J., Ballot, J., Christophe, S., et al. (2020). First evidence of inertial modes in γ Doradus stars: The core rotation revealed. *Astron. Astrophys.* 640, A49. doi:10.1051/0004-6361/201936653

Ouazzani, R. M., Marques, J. P., Goupil, M. J., Christophe, S., Antoci, V., Salmon, S. J. A. J., et al. (2019). γ Doradus stars as a test of angular momentum transport models. *Astron. Astrophys.* 626, A121. doi:10.1051/0004-6361/201832607

Palacios, A., Talon, S., Charbonnel, C., and Forestini, M. (2003). Rotational mixing in low-mass stars. *Astron. Astrophys.* 399, 603–616. doi:10.1051/0004-6361:20021759

Papaloizou, J., and Pringle, J. E. (1978). Non-radial oscillations of rotating stars and their relevance to the short-period oscillations of cataclysmic variables. *Mon. Not. R. Astron. Soc.* 182, 423–442. doi:10.1093/mnras/182.3.423

Paparó, M., Benkő, J. M., Hareter, M., and Guzik, J. A. (2016). Unexpected series of regular frequency spacing of δ Scuti stars in the non-asymptotic regime. II. Sample-echelle diagrams and rotation. *Astrophys. J. Suppl. Ser.* 224, 41. doi:10.3847/0067-0049/224/2/41

Peterson, D. M., Hummel, C. A., Pauls, T. A., Armstrong, J. T., Benson, J. A., Gilbreath, G. C., et al. (2006). Resolving the effects of rotation in Altair with long-baseline interferometry. *Astrophys. J.* 636, 1087–1097. doi:10.1086/497981

Reese, D. (2006). *La modélisation des oscillations d'étoiles en rotation rapide*. Ph.D. thesis. Paul Sabatier: Université Toulouse III -.

Reese, D., Lignières, F., and Rieutord, M. (2006). Acoustic oscillations of rapidly rotating polytropic stars. II. Effects of the Coriolis and centrifugal accelerations. *Astron. Astrophys.* 455, 621–637. doi:10.1051/0004-6361:20065269

Reese, D., Lignières, F., and Rieutord, M. (2008). Regular patterns in the acoustic spectrum of rapidly rotating stars. *Astron. Astrophys.* 481, 449–452. doi:10.1051/0004-6361:20078075

Reese, D. R., Dupret, M.-A., and Rieutord, M. (2017a). Non-adiabatic pulsations in ESTER models. *Eur. Phys. J. Web Conf.* 160, 02007. doi:10.1051/epjconf/201716002007

Reese, D. R., Lignières, F., Ballot, J., Dupret, M.-A., Barban, C., van't Veer-Menneret, C., et al. (2017b). Frequency regularities of acoustic modes and multi-colour mode identification in rapidly rotating stars. *Astron. Astrophys.* 601, A130. doi:10.1051/0004-6361/201321264

Reese, D. R., MacGregor, K. B., Jackson, S., Skumanich, A., and Metcalfe, T. S. (2009). Pulsation modes in rapidly rotating stellar models based on the self-consistent field method. *Astron. Astrophys.* 506, 189–201. doi:10.1051/0004-6361/200811510

Reese, D. R., Mirouh, G. M., Espinosa Lara, F., Rieutord, M., and Putigny, B. (2021). Oscillations of 2D ESTER models. I. The adiabatic case. *Astron. Astrophys.* 645, A46. doi:10.1051/0004-6361/201935538

Reese, D. R., Prat, V., Barban, C., van 't Veer-Menneret, C., and MacGregor, K. B. (2013). Mode visibilities in rapidly rotating stars. *Astron. Astrophys.* 550, A77. doi:10.1051/0004-6361/201220506

Reese, D. R. (2013). Stable higher order finite-difference schemes for stellar pulsation calculations. *Astron. Astrophys.* 555, A148. doi:10.1051/0004-6361/201321725

Ricker, G. R., Winn, J. N., Vanderspek, R., Latham, D. W., Bakos, G. Á., Bean, J. L., et al. (2015). Transiting exoplanet survey satellite (TESS). *J. Astronomical Telesc. Instrum. Syst.* 1, 014003.

Rieutord, M. (2001). Ekman layers and the damping of inertial R-modes in a spherical shell: Application to neutron stars. *Astrophys. J.* 550, 493. doi:10.1086/321676

Rieutord, M., Espinosa Lara, F., and Putigny, B. (2016). An algorithm for computing the 2D structure of fast rotating stars. *J. Comput. Phys.* 318, 277–304. doi:10.1016/j.jcp.2016.05.011

Rieutord, M., and Valdettaro, L. (1997). Inertial waves in a rotating spherical shell. *J. Fluid Mech.* 341, 77–99. doi:10.1017/s0022112097005491

Rieutord, M., and Valdettaro, L. (2010). Viscous dissipation by tidally forced inertial modes in a rotating spherical shell. *J. Fluid Mech.* 643, 363–394. doi:10.1017/S002211200999214X

Roxburgh, I. W. (2006). 2-dimensional models of rapidly rotating stars. II. Hydrostatic and acoustic models with $\Omega = \Omega(r, \theta)$. *Astron. Astrophys.* 454, 883–888. doi:10.1051/0004-6361:20065109

Royer, F. (2009). "On the rotation of A-type stars," in *The rotation of Sun and stars* (Berlin Springer Verlag), 207–230.

Saio, H. (1982). R-mode oscillations in uniformly rotating stars. *Astrophys. J.* 256, 717. doi:10.1086/159945

Saio, H. (1981). Rotational and tidal perturbations of nonradial oscillations in a polytropic star. *Astrophys. J.* 244, 299. doi:10.1086/158708

Saio, H., Takata, M., Lee, U., Li, G., and Van Reeth, T. (2021). Rotation of the convective core in γ Dor stars measured by dips in period spacings of g modes coupled with inertial modes. *Mon. Not. R. Astron. Soc.* 502, 5856–5874. doi:10.1093/mnras/stab482

Savonije, G. J. (2007). Non-radial oscillations of the rapidly rotating Be star HD 163868. *Astron. Astrophys.* 469, 1057–1062. doi:10.1051/0004-6361:20077377

Savonije, G. J., Papaloizou, J. C. B., and Alberts, F. (1995). Nonadiabatic tidal forcing of a massive uniformly rotating star. *Mon. Not. R. Astron. Soc.* 277, 471–496. doi:10.1093/mnras/277.2.471

Schou, J., Antia, H. M., Basu, S., Bogart, R. S., Bush, R. I., Chitre, S. M., et al. (1998). Helioseismic studies of differential rotation in the solar envelope by the solar oscillations investigation using the michelson Doppler imager. *Astrophys. J.* 505, 390–417. doi:10.1086/306146

Schou, J., Christensen-Dalsgaard, J., and Thompson, M. J. (1994). On comparing helioseismic two-dimensional inversion methods. *Astrophys. J.* 433, 389. doi:10.1086/174653

Scuflaire, R., Montalbán, J., Théado, S., Bourge, P. O., Miglio, A., Godart, M., et al. (2008). The liège oscillation code. *Astrophys. Space Sci.* 316, 149–154. doi:10.1007/s10509-007-9577-6

Soufi, F., Goupil, M.-J., and Dziembowski, W. A. (1998). Effects of moderate rotation on stellar pulsation. I. Third order perturbation formalism. *A&A* 334, 911–924.

Stergioulas, N., Apostolatos, T. A., and Font, J. A. (2004). Non-linear pulsations in differentially rotating neutron stars: Mass-shedding-induced damping and splitting of the fundamental mode. *Mon. Not. R. Astron. Soc.* 352, 1089–1101. doi:10.1111/j.1365-2966.2004.07973.x

Stoeckley, T. R. (1968). Determination of aspect and degree of differential rotation, from line profiles in rapidly rotating stars. *Mon. Not. R. Astron. Soc.* 140, 121–139. doi:10.1093/mnras/140.2.121

Suárez, J.-C., Michel, E., Pérez Hernández, F., Lebreton, Y., Li, Z. P., Fox Machado, L., et al. (2002). A study of correlation between the oscillation amplitude and stellar parameters of δ Scuti stars in open clusters. *Astron. Astrophys.* 390, 523–531. doi:10.1051/0004-6361:20020565

Suárez, J. C., Bruntt, H., and Buzasi, D. (2005). Modelling of the fast rotating δ Scuti star Altair. *Astron. Astrophys.* 438, 633–641. doi:10.1051/0004-6361:20042410

Suárez, J. C., Goupil, M. J., Reese, D. R., Samadi, R., Lignières, F., Rieutord, M., et al. (2010). On the interpretation of echelle diagrams for solar-like oscillations effect of centrifugal distortion. *Astrophys. J.* 721, 537–546. doi:10.1088/0004-637X/721/1/537

Thompson, M. J., Christensen-Dalsgaard, J., Miesch, M. S., and Toomre, J. (2003). The internal rotation of the Sun. *Annu. Rev. Astron. Astrophys.* 41, 599–643. doi:10.1146/annurev.astro.41.011802.094848

Townsend, R. H. D. (2003a). A semi-analytical formula for the light variations due to low-frequency g modes in rotating stars. *Mon. Not. R. Astron. Soc.* 343, 125–136. doi:10.1046/j.1365-8711.2003.06640.x

Townsend, R. H. D. (2003b). Asymptotic expressions for the angular dependence of low-frequency pulsation modes in rotating stars. *Mon. Not. R. Astron. Soc.* 340, 1020–1030. doi:10.1046/j.1365-8711.2003.06379.x

Townsend, R. H. D. (2005). Influence of the Coriolis force on the instability of slowly pulsating B stars. *Mon. Not. R. Astron. Soc.* 360, 465–476. doi:10.1111/j.1365-2966.2005.09002.x

Townsend, R. H. D. (1997). Spectroscopic modelling of non-radial pulsation in rotating early-type stars. *Mon. Not. R. Astron. Soc.* 284, 839–858. doi:10.1093/mnras/284.4.839

Tran Minh, F., and Léon, L. (1995). Numerical solution of stellar nonradial oscillations: The galerkin and B-splines method. *Part. Phys. Astrophysics* 458, 219. doi:10.1007/BFb0118720

van Belle, G. T., Ciardi, D. R., Thompson, R. R., Akeson, R. L., and Lada, E. A. (2001). Altair's oblateness and rotation velocity from long-baseline interferometry. *Astrophys. J.* 559, 1155–1164. doi:10.1086/322340

Van Reeth, T., Tkachenko, A., and Aerts, C. (2016). Interior rotation of a sample of γ Doradus stars from ensemble modelling of their gravity-mode period spacings. *Astron. Astrophys.* 593, A120. doi:10.1051/0004-6361/201628616

Watson, R. D. (1988). Contributing factors to flux changes in nonradial stellar pulsations. *Astrophys. Space Sci.* 140, 255–290. doi:10.1007/BF00638984

Weiss, W. W., Rucinski, S. M., Moffat, A. F. J., Schwarzenberg-Czerny, A., Koudelka, O. F., Grant, C. C., et al. (2014). BRITE-Constellation: Nanosatellites for precision photometry of bright stars. *Publ. Astron. Soc. Pac.* 126, 573–585. doi:10.1086/677236

Yoshida, S., and Eriguchi, Y. (1999). A numerical study of normal modes of rotating neutron star models by the cowling approximation. *Astrophys. J.* 515, 414–422. doi:10.1086/307012

Yoshida, S., and Eriguchi, Y. (1995). Gravitational radiation driven secular instability of rotating polytropes. *Astrophys. J.* 438, 830. doi:10.1086/175126

Zahn, J.-P. (1992). Circulation and turbulence in rotating stars. *A&A* 265, 115–132.

Zwintz, K., Reese, D. R., Neiner, C., Pigulski, A., Kuschnig, R., Müllner, M., et al. (2019). Revisiting the pulsational characteristics of the exoplanet host star β Pictoris. *Astron. Astrophys.* 627, A28. doi:10.1051/0004-6361/201834744

frontiers | Frontiers in Astronomy and Space Sciences

TYPE Review
PUBLISHED 07 October 2022
DOI 10.3389/fspas.2022.952296

OPEN ACCESS

EDITED BY
Javier Pascual Granado,
Spanish National Research Council (CSIC), Spain

REVIEWED BY
Masao Takata,
The University of Tokyo, Japan
Timothy Van Reeth,
KU Leuven, Belgium

*CORRESPONDENCE
Giovanni M. Mirouh,
gmm@ugr.es

SPECIALTY SECTION
This article was submitted to Stellar and Solar Physics, a section of the journal Frontiers in Astronomy and Space Sciences

RECEIVED 24 May 2022
ACCEPTED 16 September 2022
PUBLISHED 07 October 2022

CITATION
Mirouh GM (2022), Forward modelling and the quest for mode identification in rapidly rotating stars.
Front. Astron. Space Sci. 9:952296.
doi: 10.3389/fspas.2022.952296

Forward modelling and the quest for mode identification in rapidly rotating stars

Giovanni M. Mirouh*

Física Teórica y del Cosmos Department, Universidad de Granada, Granada, Spain

Asteroseismology has opened a window on the internal physics of thousands of stars, by relating oscillation spectra properties to the internal physics of stars. Mode identification, namely the process of associating a measured oscillation frequency to the corresponding mode geometry and properties, is the cornerstone of this analysis of seismic spectra. In rapidly rotating stars this identification is a challenging task that remains incomplete, as modes assume complex geometries and regular patterns in frequencies get scrambled under the influence of the Coriolis force and centrifugal flattening. In this article, I will first discuss the various classes of mode geometries that emerge in rapidly rotating stars and the related frequency and period patterns, as predicted by ray dynamics, complete (non-)adiabatic calculations, or using the traditional approximation of rotation. These patterns scale with structural quantities and help us derive crucial constraints on the structure and evolution of these stars. I will summarize the amazing progress accomplished over the last few years for the deciphering of gravity-mode pulsator oscillation spectra, and recent developments based on machine-learning classification techniques to distinguish oscillation modes and pattern analysis strategies that let us access the underlying physics of pressure-mode pulsators. These approaches pave the way to ensemble asteroseismology of classical pulsators. Finally, I will highlight how these recent progress can be combined to improve forward seismic modelling. I will focus on the example of Rasalhague, a well-known rapid rotator, to illustrate the process and the needed advances to obtain à-la-carte modelling of such stars.

KEYWORDS

stars: oscillations, stars:rotation, stars:interiors, stars:individual α Ophiuchi, stars: evolution

1 Introduction

Over the last few decades, helio- and asteroseismology have started a golden age for stellar physics. The advent of space-based photometry missions (such as CoRoT, Baglin et al., 2009, Gilliland et al., 2010, TESS, Ricker 2014, and BRITE, Weiss et al., 2014) has led to the detection of variability in numerous stars, the measurement of oscillation frequencies and their regular spacings, and the identification of the mode geometries.

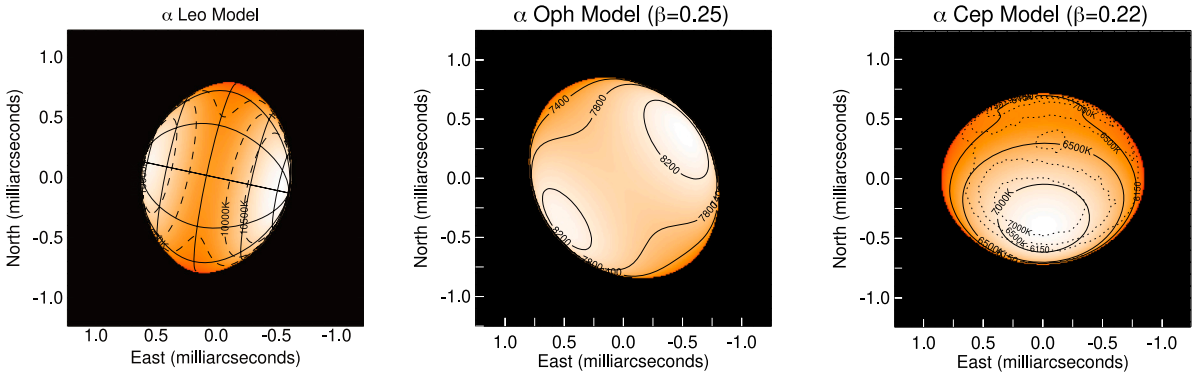

FIGURE 1
Interferometric observations of rapidly rotating stars, showing the centrifugal distortion and gravity darkening phenomena. Left to right: Regulus (α Leo, Che et al., 2011), Rasalhague (α Oph, Zhao et al., 2009), Alderamin (α Cep, Zhao et al., 2009).

This has triggered a cascade of new theoretical developments for stellar models, oscillation codes and inversion techniques.

However, these developments were long limited to slowly rotating solar-like and red giant stars. Upper main-sequence pulsators present a rapid rotation (Royer, 2009) that affects both their structure and their oscillations. A rotating star is centrifugally distorted (Potter, 2012), which induces a meridional circulation (Zahn, 1992; Rieutord, 2006) and latitudinal surface temperature gradients (von Zeipel, 1924; Espinosa Lara and Rieutord, 2011). Figure 1 presents three examples of interferometric measurements of the surface shape and temperatures for three close pulsating A stars.

Pulsations can be either pressure or gravito-inertial modes. Pressure modes (or acoustic modes) are restored by pressure forces and tend to propagate at high frequencies. Gravity modes are restored by buoyancy and exist at low frequencies. Mixed modes can appear when a pressure and a gravity mode propagating in two separate cavities inside the star at the same frequency couple. In the presence of rotation, the Coriolis force can act as a restoring force to create the so-called inertial modes, or combine with buoyancy to create gravito-inertial modes. At high rotation rates, the Coriolis force is the dominating effect of rotation on gravity modes while pressure modes are mostly affected by the centrifugal distortion, both effects modify the oscillation frequencies and obfuscate regular patterns in the spectra. This creates new complex mode geometries (Reese et al., 2008; Lignières and Georgeot, 2009; Ballot et al., 2013) that render mode identification challenging. Taking these effects fully into account requires dedicated two-dimensional models (Espinosa Lara and Rieutord, 2013; Rieutord et al., 2016) and oscillation calculations (Reese et al., 2009a, 2021; Ouazzani et al., 2012). The mathematical details of these tools are provided in Reese (this volume).

In this review, I consider pulsating stars on the upper main sequence, that can be split into four classes: in increasing order of mass, these are the γ Doradus (F-late A), δ Scuti (A-F), slowly-pulsating B (SPB, B3-B9) and β Cephei (B0-B2) stars (Aerts et al., 2010). γDor stars harbour low-frequency gravito-inertial and inertial modes excited through a combination of convective flux blocking at the base of the surface convection zone (Pesnell, 1987; Guzik et al., 2000; Dupret et al., 2004a; 2005) in colder γDor stars and κ mechanism in their warmer counterparts (Xiong et al., 2016). δSct stars pulsate at higher frequencies because of acoustic modes excited by the κ mechanism (Zhevakin, 1963; Dupret et al., 2004a). These two classes of modes have more massive counterparts: SPBs pulsate with low-frequency (gravito-) inertial modes and βCep stars harbour acoustic and low-order gravity modes, that are explained in both cases by the κ mechanism activated by the metal opacity bump (Cox et al., 1992; Dziembowski et al., 1993).

Due to their overlapping instability ranges, many γDor/δSct hybrids (e.g. Handler et al., 2002; Grigahcène et al., 2010; Balona et al., 2015) and SPB/βCep hybrids (e.g. Handler et al., 2004; De Cat et al., 2007; Handler, 2009; Burssens et al., 2020) have been detected. A series of works by Osaki (1974); Lee and Saio (2020); Lee (2022) also proposes resonant coupling with overstable convection in the core as a possible excitation mechanism for gravity modes in the envelope of early-type stars, with frequencies close to the core rotation rate. This may account for rotational-modulation-like signals observed in SPB stars and hybrid pulsators.

The individual identification of modes in rapidly rotating stars is hampered by a limited knowledge of the mode selection mechanisms, the impact of rotation on both their structure and

oscillations, the sheer number of possible oscillation modes theoretically predicted by high-resolution calculations and our impossibility to predict mode amplitudes. Patterns in frequency or period have opened a window on the internal physics of solar-like and red-giant stars, after being described theoretically (e.g. Shibahashi, 1979; Tassoul, 1980; Miglio et al., 2008) and identified in observations (as in Mosser et al., 2013; Vrard et al., 2016). Such patterns, albeit far more elusive, exist in rapidly rotating stars and have been investigated by theoretical works for both p-mode (e.g. Lignières and Georgeot, 2009; Suárez et al., 2014; Mirouh et al., 2019) and g-mode spectra (e.g. Bouabid et al., 2013; Ouazzani et al., 2017, 2020; Dhouib et al., 2021; Tokuno and Takata, 2022). Detections in both p-mode (e.g. García Hernández et al., 2015; Paparó et al., 2016a,b; García Hernández et al., 2017; Bedding et al., 2020) and g-mode pulsators (e.g Van Reeth et al., 2015; Li et al., 2020b; Pedersen et al., 2021; Garcia et al., 2022) yield estimates of the fundamental parameters and the internal physics of an ever-increasing number of stars.

Relating frequency and period spacings to structure quantities thus offers crucial statistical information and precious constraints for forward modelling and paves the way to ensemble seismology for classical pulsators (Michel et al., 2017; Bowman and Kurtz, 2018).

Tools and strategies that are well established for slow rotators have been redeveloped to take into account rotational effects. One such tool is line-profile variations, which can yield oscillation frequencies and a partial identification (see Lee and Saio, 1990; Telting and Schrijvers, 1997; Zima, 2006) for both pressure and gravito-inertial nonradial modes from time series of spectroscopic measurements (e.g. Aerts et al., 1992; Zima et al., 2006; Shutt et al., 2021). Reese et al. (2017a) offers a first adaptation of the technique to complete calculations of pressure modes in rapid rotators.

In this review I will first describe the impact of the Coriolis force and the centrifugal flattening of rotating stars on acoustic, inertial and gravito-inertial mode geometries (Section 2). Comparing with non-rotating stars, I will discuss the intricate frequency and period patterns that rapid-rotator oscillation spectra describe, and the strategies to extract them from space-based photometry data (Section 3). I will then explain how spectroscopic line-profile variations can be evaluated to derive frequencies of rapid rotators (Section 4), and describe the example of the forward modelling of Rasalhague (Section 5).

As I focus on rotation and complete two-dimensional calculations of models and oscillation modes, I will leave out magnetic fields and their impact on oscillations. I refer the reader to the literature regarding detections of magnetic fields in A stars, theoretical study of magneto-acoustic oscillations and extensive results for rapidly-oscillating Ap (roAp) stars (Mathis et al., 2021; Holdsworth, 2021, and references therein). Interactions between magnetic fields and low-frequency oscillations have been the focus of a lot of recent work, regarding internal gravity waves (Rogers and MacGregor, 2010, 2011; Lecoanet et al., 2017, 2022, e.g.), coherent gravito-inertial modes (e.g. Loi, 2020; Prat et al., 2020; Dhouib et al., 2021) and mixed modes (Loi and Papaloizou, 2018; Bugnet et al., 2021) such as depressed dipole modes in red giants (e.g. García et al., 2014; Stello et al., 2016).

2 Mode geometries in rapidly rotating stars

Contrary to the non-rotating case, oscillations in rapidly rotating stars cannot be described using simple spherical harmonics. Perturbative approaches quickly show their limits, and strategies that include rotation from the start (even under some approximations) are necessary to compute models and oscillations. Several approaches have been implemented, with various levels of accuracy and complexity.

2.1 Including rotation to compute oscillations

The simplest way of including the effects of rotation is to treat its effects as corrections to non-rotating solutions of pulsations. These corrections are described, for both the centrifugal flattening and the Coriolis acceleration, as successive powers of the rotation rate Ω, which is supposed to be small (e.g. Ledoux, 1951; Gough and Thompson, 1990; Lee and Baraffe, 1995; Soufi et al., 1998). For high enough rotation rates, even the highest-order perturbative calculations misestimate frequencies and describe the mode geometries poorly: Ballot et al. (2013) and Reese (2006) have evaluated the range of applicability of perturbative treatments for gravito-inertial and pressure modes, respectively.

The traditional approximation (Eckart, 1960; Berthomieu et al., 1978) consists in neglecting the latitudinal component of the rotation vector $\mathbf{\Omega}$ in the Coriolis acceleration, assuming $\mathbf{\Omega} = \Omega \cos\theta \boldsymbol{e}_r$. If the centrifugal distortion of the star and the perturbation to the gravitational potential are neglected as well, the system ruling adiabatic oscillations becomes separable in radius r and colatitude θ, effectively preventing coupling between modes described by different spherical harmonics (Bildsten et al., 1996). This makes the equations much more tractable with the added benefit that the horizontal component of the oscillations can be described mathematically by means of the known Hough functions (Lee and Saio, 1987). Recent developments by Henneco et al. (2021); Dhouib et al. (2021) generalise the traditional approximation to include the effects of the centrifugal distortion and a differential rotation and predict detectable impacts on both low- and high-order gravito-inertial modes. However, and contrary to the other techniques presented here, the traditional approximation is a

non-perturbative approach only applicable to high-order g modes (such as those detected in γDor and SPB stars).

Ray theory relies on the short-wavelength approximation (Gough, 1993; Lignières and Georgeot, 2009). In this approximation, it is possible to combine the oscillation equations into only one eikonal equation that relates the wavenumber and the location of a ray in the star (Ott, 1993). This is akin to deriving geometric optics from wave optics. We can thus compute rays, that are the paths waves are expected to follow inside the star. While this calculation does not immediately provide the modes' energy distribution, it provides insights on mode propagation domains, geometries and identification.

Finally, the most accurate approach consists in the computation of fully two-dimensional models and the linear calculation of their adiabatic and/or non-adiabatic oscillations. This approach provides exact mode geometries and frequencies, allowing us to search for frequency and period patterns, compute visibilities and attempt mode-by-mode identification. However, linear mode calculations cannot yield mode amplitudes, so assumptions (such as the equirepartition of energy, or the same amplitude for all modes) are necessary to discuss mode detectability meaningfully. The tools for these calculations are complex, and were the focus of numerous efforts summarized in Reese (this volume). The analysis of the results they yield is challenging as there is no mathematical function to describe the geometries obtained with this method and that are presented in the rest of this section.

2.2 Complete calculations

The oscillation equations are derived from perturbing the continuity, Euler's and Poisson's equations (with additional closure equations such as the equations of state). These equations are presented in detail in the review by Reese (this volume). Choosing the geometrical description and discretization carefully, the perturbed equations form an eigenvalue problem in which each eigenvalue is an oscillation angular frequency ω, which is related to the frequency ν through $\omega = 2\pi\nu$, with the associated eigenvector describing the mode geometry. In the non-rotating case, the radial component of the modes is characterised by its radial order n—n being a relative integer, the sum of the numbers of p-mode nodes counted as positive and g-mode nodes counted as negative—and the horizontal component is described using a single spherical harmonic Y_ℓ^m—where ℓ is its degree and m is the azimuthal order. Without rotation, all modes at a given n and ℓ but different m have the same frequency.

The equations change when including rotation. In all three of them, the eigenvalue is shifted in the co-rotating frame, so that the inertial angular frequency ω is replaced by the co-rotating value $\omega + m\Omega$. The definition of a co-rotating frame here is improper but used for simplicity, as it implies that the rotation is solid: the discussion in this article includes differential rotation. Non-radial modes thus split into multiplets as m values can go from $-\ell$ to ℓ, $m < 0$ and $m > 0$ being prograde and retrograde modes, respectively.

The Euler equation becomes significantly more complex, as to include the Coriolis acceleration, centripetal entrainment and the baroclinicity terms. These rotational terms create a coupling between successive spherical harmonic coordinates, so that each mode can no longer be described as a single spherical harmonic but a (finite) series of them. No simple closure relation limits the number of spherical harmonics to use, and convergence of the solutions requires special care.

Finally, the boundary conditions also change to accomodate the centrifugal distortion of the stellar surface. As the star remains axisymmetric, the solutions do not depend on the azimuth and m remains separable. The detailed derivation of the equations can be found, for instance, in Reese et al. (2008, 2021).

These equations will yield various mode geometries. I present here the various subclasses of modes and their properties, as derived from using the traditional approximation (for g modes), ray dynamics, and/or complete calculations.

2.3 Acoustic modes

Pressure (acoustic) modes propagate at high frequencies and usually probe the outer layers of the stars. They are restored by pressure forces, their propagation properties are impacted not only by the Coriolis force but also by the centrifugal distortion. They are divided into four geometries derived from ray theory, first put forward by Lignières and Georgeot (2009): 2-period island, 6-period island, whispering gallery and chaotic modes. Figure 2 shows examples for the three most-studied classes of acoustic modes.

2-period island modes are the rapidly rotating counterpart to modes with a low ($\ell - |m|$) value—that is, few latitudinal nodal lines. At rotation rates higher than ~40% of the critical rotation, they propagate in a torus located around the stellar equator, which corresponds to a short, stable trajectory in the ray dynamics. This torus and the associated ray trajectory are smaller and closer to the equator for higher rotation rates. It is possible to define new quantum numbers along the ray trajectory, by defining $\tilde{n}$ and $\tilde{\ell}$ as the number of nodes along and perpendicular to the ray trajectory (Reese et al., 2009a, and left panel of Figure 2). These quantum numbers can be related to their non-rotating counterparts through

$$\tilde{n} = 2n + \epsilon \quad \text{and} \quad \tilde{\ell} = \frac{\ell - |m| - \epsilon}{2}, \quad \text{with} \quad \epsilon = \ell + m \bmod 2. \tag{1}$$

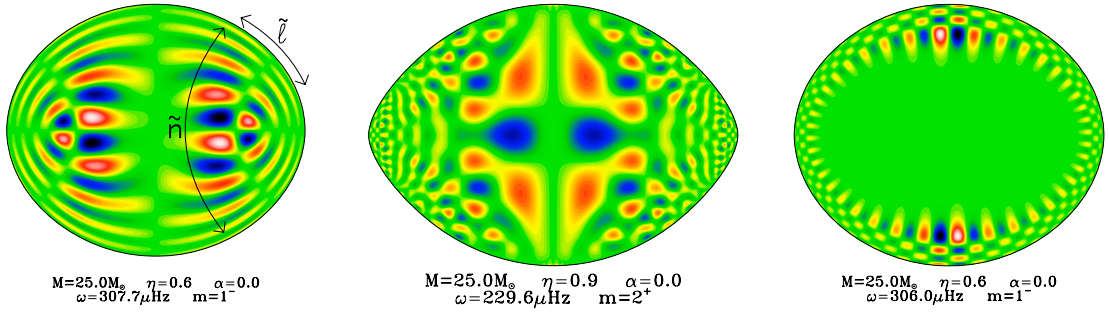

FIGURE 2
Different classes of acoustic modes. Left to right: a 2-period island mode, a chaotic mode, a whispering gallery mode. The shown quantity is the Lagrangian pressure perturbation rescaled by the square root of the stellar density, $\delta P/\sqrt{\bar{\rho}}$. Figure taken from Reese et al. (2009a).

This mathematical description of the modes is essential to investigate regular patterns in oscillation spectra, as highlighted in Section 3. Because they have large lengthscales, 2-period island modes induce significant surface signatures, are expected to be the most visible (Reese et al., 2013; 2017b), and have been studied extensively (e.g. Reese et al., 2009a; Pasek et al., 2011; Ouazzani et al., 2015; Mirouh et al., 2019; Reese et al., 2021).

6-period island modes are relatively rare and have low visibility. Their geometry is somewhat similar to that of the more common and visible chaotic modes, described below. Because of this, they are often left out of analyses (so much so that 2-period island modes are often simply dubbed "island modes"). They are the rapidly rotating counterpart of modes with medium ($\ell - |m|$) values.

Chaotic modes emerge from the constructive interference of rays that present a chaotic trajectory. They also are related to modes with medium ($\ell - |m|$) values. Evano et al. (2019) offers the only extensive study of this class of modes. They characterize their geometry by its complexity and apparent ramdomness. Chaotic modes present irregular nodal lines, except near the stellar surface where nodal lines tend to become radial. They are particularly interesting as they are the only p-mode class to propagate in the entire stellar interior, probing deep layers while reaching the surface.

Finally, whispering gallery modes propagate close to the surface without probing deep layers at any point. While their geometry is somewhat affected by the rotational distortion of the star, they keep lengthscales and a global structure similar to those of their non-rotating counterparts, high-($\ell - |m|$) modes. As such, the geometry of these modes can be described with the number of nodal lines crossed at a given depth d (that is, at a radius $r = R_s(\theta) - d$ where $R_s(\theta)$ is the surface radius, where d is chosen so that r passes in between the mode's nodal lines) and perpendicularly to that radius (equivalent to $\tilde{n}$ and $\tilde{\ell}$, respectively).

2.4 Gravito-inertial modes

Gravito-inertial modes, just like non-rotating gravity modes, are in the low-frequency part of the oscillation spectra and propagate in stellar radiative zones. In early-type stars, they are likely to be excited in γDor and SPB stars, in which they can provide insight on the conditions near the stellar core. Their restoring force is buoyancy, that combines with the Coriolis acceleration. As the Coriolis acceleration scales with $2\Omega/\omega$, its effect is more important for low-frequency modes in the co-rotating frame. Gravito-inertial modes are usually divided in three geometries, depending on their frequencies and presented in Figure 3. We distinguish sub-inertial modes which propagate at angular frequencies $\omega < 2\Omega$ and super-inertial modes at $\omega > 2\Omega$.

The effect of rotation on sub-inertial modes is the appearance of a forbidden region in which oscillations cannot propagate. Ballot et al. (2010) describes this region in the case where the stratification dominates over rotation ($N \ll \Omega$) as a cone that extends at an angle $\theta \sim \arccos(\omega/2\Omega)$ from the rotation axis. This confirms the equatorial confinement of the modes in rotating stars predicted by Matsuno (2008); Lee and Saio (1990). The precise shape of the boundary of forbidden regions for the propagation of sub-inertial modes has been refined to include stratification (Dintrans et al., 1999) and differential rotation (Mirouh et al., 2016).

Most super-inertial modes are marginally affected by rotation, as their geometry stays close to their non-rotating equivalent, resembling simple spherical harmonics with radial and horizontal scales of the same order of magnitude at all rotation rates.

The most striking exception is rosette modes, that are super-inertial modes whose geometry is significantly different from any spherical harmonic. They were described for the first time by Ballot et al. (2012). These modes emerge from a close degeneracy

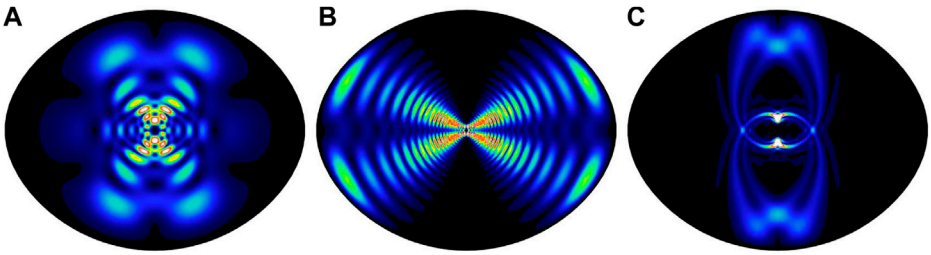

FIGURE 3
Different classes of gravito-inertial modes. **(A–C)**: an unperturbed super-inertial mode, a sub-inertial mode and a rosette super-inertial mode. The shown quantity is the mode kinetic energy. Figure taken from Ballot et al. (2013).

between modes whose frequencies would be near-identical in the absence of rotation. Takata and Saio (2013) show that such degeneracies appear for rotation rates as low as 10% of the critical rotation rate and lead to numerous families of rosette modes. This suggests that rosette modes are not a rare occurrence in moderate rotators, even though their distribution in extreme rotators is still unknown. It appears that retrograde non-axisymmetric rosette modes tend to form preferentially over their prograde counterparts (Saio and Takata, 2014). It is also worth noting that because they originate from coupling between different non-rotating modes, rosette modes cannot be found under the traditional approximation.

These modes are spatially concentrated on very thin layers around the stellar core and describe a rosette pattern aligned with the rotation axis. Ray tracing shows that their energy focuses on short closed loops (Ballot et al., 2012; Prat et al., 2016), and that the period and orientation of these closed loops can be related to the original family of modes (whose identification is otherwise lost, Takata, 2014). The surface signature of rosette modes is still to be derived precisely and be identified with observed modes, in which case they could provide useful constraints on a star's deep layers.

2.5 Other modes

Finally, other classes of modes can exist in rapidly rotating stars. Rossby modes are, among inertial oscillations, the ones that attracted most interest from the astrophysical community. Theoretical studies, notably by Papaloizou and Pringle (1978); Saio (1982); Saio et al. (2018), show they are large-scale toroidal modes that induce significant flows at the stellar surface that are less affected by equatorial confinement at high rotation rates compared to gravito-inertial modes.

Inertial modes can propagate in convective zones, restored by only Coriolis forces. They propagate in the core of intermediate-mass stars in a frequency domain that overlaps with gravito-inertial waves propagating elsewhere in the star (Rieutord et al., 2001; Baruteau and Rieutord, 2013). The signature of such modes in the core of γDor stars can be detected through their coupling with gravito-inertial modes reaching the stellar surface (Ouazzani et al., 2020; Saio et al., 2021). Similarly, so-called overstable convective modes resonances have been suggested as an excitation mechanism in rotating stars from $2M_{\odot}$ upwards. These modes are core inertial modes, that couple with gravito-inertial modes in the envelope at frequencies close to core rotation rate multiples (Osaki, 1974; Lee and Saio, 2020; Lee, 2021, 2022).

Mixed modes also exist in rapidly rotating intermediate-mass stars, as rapid rotation extends the gravito-inertial domain to higher frequencies, making coupling with pressure modes more likely (Osaki, 1974). These modes are very interesting as they probe both the deep layers of the star and carry a surface signature, but their geometries and frequencies are affected in a complex way by the coupling. Such modes are detected in δSct stars such as Rasalhague (Monnier et al., 2010) or HD174966 (García Hernández, private comm.), and become more likely with increasing age as the Brunt-Väisälä frequency in the star increases and allows for higher-frequency gravito-inertial modes (Aerts et al., 2010). They have also been computed in two-dimensional models by, e.g., Mirouh et al. (2017).

3 Regular patterns in oscillation spectra

Now that the mode geometries in rapidly rotating stars have been introduced, I will discuss the regular patterns these modes are expected to follow according to theoretical calculations, and how the wealth of space-based measurements and innovative pattern-recognition techniques have permitted their detection.

3.1 Regular patterns in slow rotators

Before delving into the frequency patterns of rapidly rotating star spectra, it is useful to remind the reader here of the regular

patterns that can be found in slowly rotating stars with solar-like oscillations. I refer the reader to the review of Jackiewicz (2021) for more details.

Helioseismology has established that solar oscillation frequencies are distributed on a regular comb. Once modes are identified univocally using the quantum numbers (n, ℓ, m), we find that high radial order modes present a regular spacing in frequency ν for acoustic modes and in period Π for gravity modes. We define the p-mode large separation (Tassoul, 1980) as

$$\Delta\nu = \nu_{n+1,\ell} - \nu_{n,\ell} = \left(2\int_0^R \frac{\mathrm{d}r}{c_\mathrm{s}}\right)^{-1}, \tag{2}$$

where c_s is the speed of sound. The g-mode period spacing Shibahashi (1979) is defined as

$$\Delta\Pi_\ell = \Pi_{n+1,\ell} - \Pi_{n,\ell} = \frac{2\pi^2}{\sqrt{\ell(\ell+1)}}\left(\int_{\mathrm{g\,cavity}} N\frac{\mathrm{d}r}{r}\right)^{-1} \tag{3}$$

where N is the Brunt-Väisälä frequency that quantifies stratification. In solar-like pulsators, in which mode excitation is due to convection and stochastic, it is possible to define another seismic observable, ν_max, the frequency at which the p-mode spectrum envelope reaches its maximum amplitude. The readily-available quantities $\Delta\nu$ and ν_max can then be linked to the stellar mass and radius *via* scaling laws (Brown et al., 1991; Kallinger et al., 2010; Mosser et al., 2010). Improving these relations has been a significant part of the recent effort for those stars, to refine the derived masses and radii, include new parameters or automate the process.

When the star rotates, the degeneracy in m is lifted and non-radial modes spawn multiplets as m ranges from $-\ell$ to ℓ. With the introduction of rotational splittings, the frequencies of non-axisymmetric modes relate to their axisymmetric counterparts through

$$\nu_{n,\ell,m} = \nu_{n,\ell} - \frac{m\Omega}{2\pi}(1 - \mathcal{C}_{n,\ell}). \tag{4}$$

$\mathcal{C}_{n,\ell}$ is the Ledoux constant, that tends asymptotically to $1/(\ell(\ell+1))$ for gravito-inertial modes and to 0 for pressure modes (Ledoux, 1951). More recently, rotational splittings have been shown to be slightly different depending on the nature and propagation domain of the underlying mode, thus allowing for the derivation of rotation profiles using mixed modes (e.g. Beck et al., 2012; Deheuvels et al., 2014; Triana et al., 2017; Di Mauro et al., 2018; Ahlborn et al., 2020). Automating this analysis led to the development of inversion techniques, such as RLS (Regularized Least Squares, Christensen-Dalsgaard et al., 1990) or SOLA (Subtractive Optimally Localised Averages, Pijpers and Thompson, 1994). The ultimate aim is a characterisation of the stellar rotation or structure throughout the star, as was done for the Sun (Korzennik and Eff-Darwich, 2011).

As mentioned, the exploitation of regular spacings requires univocal mode identification, which presents several challenges in rapidly rotating intermediate-mass pulsators. First, because of Coriolis forces and centrifugal distortion, frequencies are significantly shifted and both gravito-inertial and pressure modes assume complex geometries. Because of the complexity of the excitation mechanisms, there is no reliable way of predicting mode amplitudes theoretically and the mode selection effects are not fully understood.

3.2 Acoustic modes

The ray dynamics analysis of Lignières and Georgeot (2009) identified regular patterns for several subclasses of acoustic modes. There are four geometry classes for p modes: 2- and 6-period island, whispering gallery, and chaotic modes. Modes in each of these classes follow different patterns, as illustrated by the schematic subspectra presented in Figure 4.

2-period island modes are the ones for which the most progress has been achieved. They are expected to follow a linear distribution of the kind

$$\nu_{\tilde{n},\tilde{\ell},m} = \tilde{n}\,\widetilde{\Delta\nu} + \tilde{\ell}\widetilde{\delta\nu} - ms_m(\Omega) + \tilde{\alpha}, \tag{5}$$

where $\widetilde{\Delta\nu}$ is the island-mode large separation (and is expected to be commensurate to half the non-rotating large separation $\Delta\nu$), s_m is the rotational splitting which depends on the rotation rate in the propagation domain, and $\tilde{\alpha}$ is fixed so that the formula is exact at a reference frequency. This asymptotic relation has been studied extensively both from ray theory (Lignières and Georgeot, 2008, 2009; Pasek et al., 2011, 2012) and complete calculations of the oscillations (Reese et al., 2008; Mirouh et al., 2019; Reese et al., 2021).

Owing to the precision of asteroseismic measurements and the development of dedicated techniques, such a regular frequency distribution has been detected in observed spectra. García Hernández et al. (2015) identified regular patterns in acoustic spectra for a sample of eclipsing binaries and extracted a large separation that they attributed to the likely visible 2-period island modes. Using eclipses and the binary orbits, they were able to link the large separation with the mean stellar density through a scaling law. Their scaling relations were later confirmed from fully-2D models and oscillations by Mirouh et al. (2019): in this work, the synthetic 2-period island modes were sorted out by means of a convolutional neural network for a range of models at various rotation rates and ages. It confirmed "the scaling between mean density and large separation, and that this relation does not depend explicitly on the rotation rate. This scaling has also been recovered for low-mass δSct stars using grids of 1D models with enhanced mixing by Rodríguez-Martín et al. (2020) and on the larger samples of Paparó et al. (2016b); García Hernández et al. (2017); Bedding et al. (2020). A further confirmation of the 2-

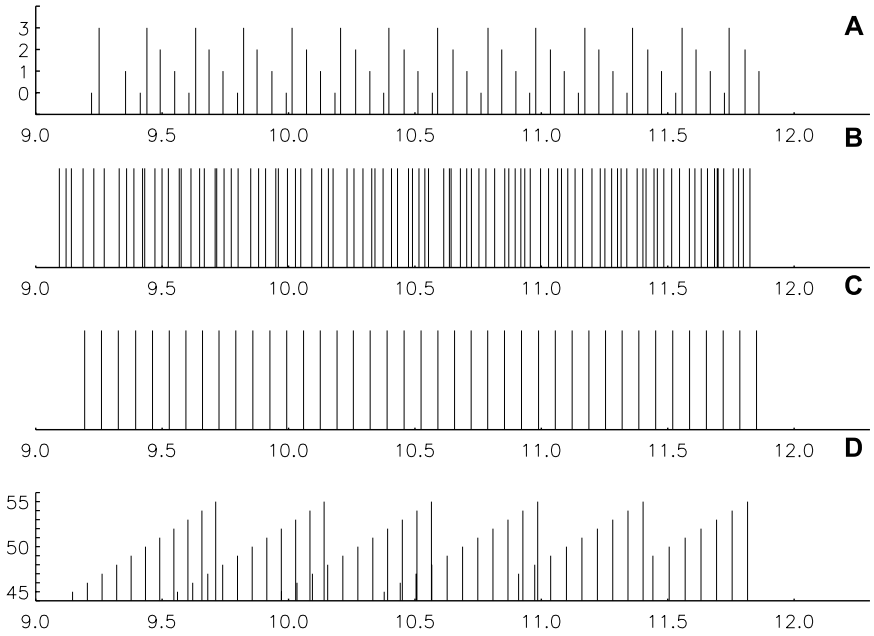

FIGURE 4
Frequency sub-spectra for the four classes of axisymmetric acoustic modes. **(A)** 2-period island modes, **(B)** chaotic modes, **(C)** 6-period island modes, **(D)** whispering gallery modes. The horizontal axis is the mode frequency in units of ω_p—computed from the keplerian velocity computed using the polar radius –, and the vertical axis represents the second quantum number—the rapid rotator equivalent to the degree ℓ—when defined. Figure taken from Lignières and Georgeot (2009).

period island nature of the observed modes lies in the detection of half the large separation in the pattern detection (García Hernández et al., 2009; Ramón-Ballesta et al., 2021), which is an exclusive feature of island modes (Evano et al., 2019). It is also worth noting that the modes detected in δSct stars are most often not in the asymptotic regime, so that the measured large separations are about 15% below their asymptotic values (García Hernández et al., 2009; Mirouh et al., 2019).

Rotational splittings have also been found in the 2-period island mode spectra of δSct stars (e.g. Paparó et al., 2016b; Ramón-Ballesta et al., 2021). While rotational splittings in slow rotators are symmetrical (that is, $\nu_{n,\ell,-m} - \nu_{n,\ell,0} = \nu_{n,\ell,0} - \nu_{n,\ell,m}$), splittings in rapidly rotating stars lose this property. They also are often so large that asymmetric multiplets blend in the spectrum, making them harder to identify and exploit. Modelling these splittings can rely on perturbative treatments to the first-order (e.g. Schou et al., 1998; Deheuvels et al., 2014), second-order (e.g. Saio, 1981; Suárez, 2009) and third-order (Soufi et al., 1998; Ouazzani and Goupil, 2012) that model the asymmetry of the splittings. A complete calculation that applies to all rotation rates provides the generalised rotational splittings, that is $\nu_{n,\ell,-m} - \nu_{n,\ell,m}$, through an integral of the rotation rate over the modes' propagation domain and the definition of rotational kernels (Reese et al., 2009b, 2021), thus paving the way to inversion methods for rapid rotators. Since the discovery of island-mode regular patterns by García Hernández et al. (2015), several strategies have been developed to extract large separations from observed spectra. Investigating the distribution of frequency differences, computing Fourier transforms of the spectrum itself, spectrum autocorrelation functions have all proved efficient to derive both the large separation and rotational splittings (Mantegazza et al., 2012; Reese et al., 2017b; Ramón-Ballesta et al., 2021). A brand new approach based on the entropy content of observed oscillation spectra offers another promising way of extracting regular separations (Suárez, this volume).

To complement the regular patterns discovered for 2-period island modes and their link with the stellar density, Barceló Forteza et al. (2018, 2020) have investigated the envelope of the oscillation spectra of δSct stars in search of another asteroseismic indicator. They found that the peak frequency of this asymmetric envelope, ν_{max}, can be related to the effective temperature and surface gravity of the star. Assessing these two quantities for stars featuring gravity darkening can yield an estimate of the stellar inclination, and in turn a model-dependent estimate of the stellar

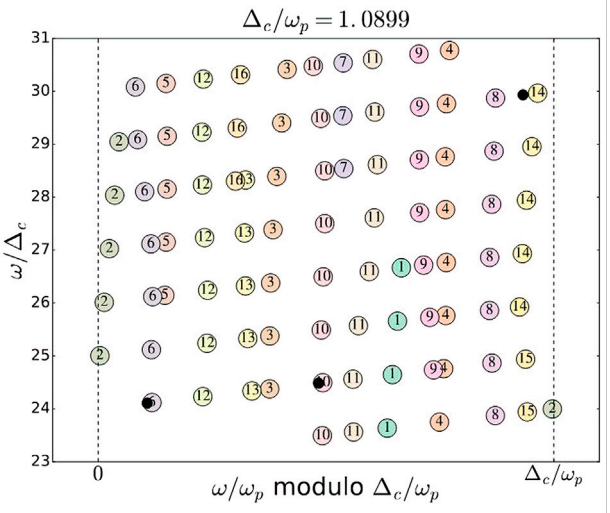

FIGURE 5
Échelle diagram showing all chaotic modes in a polytrope in the high-frequency range—the frequency unit ω_p is computed from the keplerian velocity computed using the polar radius –. Series of similar modes are labelled 1 to 16, while black dots are modes that do not belong to any series. Figure taken from Evano et al. (2019).

mass and radii in a way that is reminiscent of the approach used for solar-like stars.

Recently, Salmon et al. (2022) has developed a forward-modelling framework for β Cep stars, that relies on low-order pressure modes along with gravity and mixed modes, to infer fundamental parameters. Their hare-and-hounds exercise, which relies on 1D Geneva models (Eggenberger et al., 2008), yields accurate parameters starting from only ~ 5 identified oscillation frequencies. Such a framework could serve as an example for the exploitation of island modes computed from 2D models, using the associated theoretical tools discussed above (see also Section 5).

Frequency subspectra of chaotic modes are dense, and were originally thought not to have structure (Lignières and Georgeot, 2009). Evano et al. (2019) computed the autocorrelation of these subspectra and found evidence of a regular spacing. They show that while chaotic modes do not tend to an exact asymptotic distribution of oscillation frequencies, they exhibit a pseudo-large separation $\Delta_c\nu$ for all their models at all rotation rates. They relate $\Delta_c\nu$ with the average acoustic time over the meridional plane T_0 through $\Delta_c\nu \sim 2\pi/T_0$. Chaotic modes thus form series of modes that present a very similar geometry. Figure 5 presents an échelle diagram—that is a frequency spectrum folded every $\Delta_c\nu$ to bring out patterns—for chaotic modes in a polytrope. Well-defined ridges follow the series, but some of them are interrupted at high frequencies, and are replaced in the spectrum by another or by a series of high-frequency island modes. The pseudo-large separation of chaotic modes is very close to that of island modes (within 1%). However, the detected patterns are not expected to come from this spacing, as the half-large separation detection is not expected from chaotic modes.

Island modes of period 6 were identified as one of the four classes of acoustic modes emerging from ray theory by Lignières and Georgeot (2009). They propose a simple asymptotic relation for these modes:

$$\nu_{n',\ell',m} = n'\Delta'\nu + ms'_m + \alpha' \tag{6}$$

where the various terms match are similar to those of Eq. 5. The details of this asymptotic relation, and the link between the separation $\Delta'\nu$ and stellar structure quantities are still to be investigated.

Finally, whispering gallery modes also seem to follow regular patterns. However, while it is straightforward to define suitable quantum numbers from the energy distribution of whispering gallery modes, Lignières and Georgeot (2009) did not find a satisfactory fit of their frequencies to a linear law in the form of Eq. 5 or (6). More studies are required to understand the nature of the patterns these modes follow.

3.3 Gravito-inertial modes

In the absence of rotation, the spectrum of high-order gravity modes is understood as a set of modes regularly spaced in period, which can be represented by a flat line in a $P - \Delta P$ diagram. The value of the period separation provides an estimate of the stellar age, as it decreases as a peak in the Brunt-Väisälä builds up at the core-envelope interface. The deviation from this flat distribution, in the form of with regular dips, is an indicator of a chemical gradient at the core-envelope interface whose depth can be related with mixing efficiency (Miglio et al., 2008). The pattern described by these dips informs us about the location of the chemical gradient.

When the star rotates, the general trend in the $P - \Delta P$ plane is not necessarily flat but varies monotonically (Bouabid et al., 2013; Van Reeth et al., 2015). Using the traditional approximation, Ouazzani et al. (2017) thus defines the slope of this trend as a new observable that is directly linked to the rotation rate near the stellar core modulated by the azimuthal order m. These ridges were observed in many γDor (e.g. Bedding et al., 2015; Guo and Li, 2019; Li et al., 2020a,b; Garcia et al., 2022) and SPB stars (Pápics et al., 2017; Pedersen et al., 2021; Szewczuk et al., 2021, 2022, e.g), with a variety of behaviors related to mixing and rotation.

Forward modelling has driven a lot of the progress on g-mode asteroseismology of slowly to moderately rotating stars in the recent years. Through the definition of rigorous frameworks (Aerts et al., 2018; Johnston et al., 2019), state-of-the-art 1D models and modes computed assuming the traditional approximation, partial mode identification has been obtained for

numerous individual stars (e.g. Szewczuk and Daszyńska-Daszkiewicz, 2018; Zhang et al., 2018). This process yields not only stellar fundamental parameters such as mass and age, but also constraints on core-interface mixing (Wu et al., 2020; Pedersen et al., 2021, e.g.) or binary interactions (Sekaran et al., 2021; Guo et al., 2022).

Recent works relying on the traditional approximation also provide model-independent approaches. For instance, Van Reeth et al. (2016); Li et al. (2020b); Takata et al. (2020a,b) use the rotation frequency and the buoyancy radius as free input parameters. Christophe et al. (2018) suggests a clever rescaling of the period spectra to extract signatures of differential rotation and buoyancy glitches from the gravito-inertial mode spectrum. Christophe et al. (2018) also emphasizes the well-known limits of the traditional approximation of rotation: attempts at extending it to include radially differential rotation (Mathis, 2009) or centrifugal distortion (Dhouib et al., 2021) may provide extra insights on the physics of g-mode pulsators. However, these approaches require a prescription for a differential rotation profile (which is prone to a lot of degeneracy) and are computationally expensive.

While the traditional approximation has led to a significant breakthrough in the analysis of g-mode pulsators, permitting ensemble seismology and forward seismic modelling for this class of stars, performing the full calculation of gravito-inertial modes is the logical next step to include differential rotation and enable the search for rosette modes in observations.

3.4 Rossby modes

Rossby modes have long been theorized, and were first detected in rapid rotators by Van Reeth et al. (2016). They have since been detected in a variety of g-mode pulsators (both γDor and SPB stars, e.g. Saio et al., 2018; Li et al., 2019; Takata et al., 2020b). Their ubiquitous nature suggests an easy excitation mechanism, and stellar activity or tidal forcing have been proposed. Rossby modes present spacings that appear in the $P - \Delta P$ plane, like gravito-inertial modes. They present small period spacings, that increase rapidly with the period (leading to a characteristic upward slope, Van Reeth et al., 2016). Saio et al. (2018) suggests that the "hump-and-spike" stars discovered by Balona (2017) are spotted stars in which the "hump" is the Rossby-mode spectrum and the "spike" a harmonic of the stellar rotation rate. The calculations underlying this description are made within the traditional approximation framework, and have no equivalent based on complete two-dimensional calculations.

4 Line-profile variations

Modes that propagate in the outer layers of the star induce a small distortion of the stellar surface along with temperature variations. In rotating stars, these oscillatory motions leave a Doppler signature in the spectral line profile that can be tracked in time through a series of spectroscopic observations. Such line-profile variations (LPVs) are not simple to analyse as they depend on the geometry of each oscillation mode present at the surface, but their analysis can offer a partial mode identification. Once a specific line profile is selected or an averaged one is computed, a spectral analysis of its time variations yields oscillation frequencies and azimuthal orders.

A lot of work has been done on the theoretical description of LPVs induced by both pressure modes and gravito-inertial modes. For instance, the modelling efforts for p-mode LPVs (Balona, 1987; Cugier, 1993; Zima, 2006) permitted the interpretation of spectroscopic measurements in δSct and βCep stars (e.g. Aerts et al., 1992; Zima et al., 2006). Theoretical developments based on the perturbative approach (e.g. Shutt et al., 2021) or the traditional approximation of rotation (such as Lee and Saio, 1990; Townsend, 1997) yielded similar results to interpret γDor pulsators.

Some of these methods have been implemented in widespread software packages. For instance, the BRUCE and KYLIE packages (Townsend, 1997) rely on the traditional approximation for the calculation of theoretical LPVs of gravito-inertial modes in moderate rotators (as demonstrated in Bowman et al., 2022). Another widespread implementation is that of the Fourier Parameter Fitting method (FPF) of Zima (2006). The FAMIAS code (Zima, 2008) does not rely on the traditional approximation but on a first-order perturbative calculation, which enables the analysis of LPVs due to both gravito-inertial and pressure modes, but restricts it to slow rotators.

LPVs have also been detected in several rapidly rotating stars (e.g. Telting and Schrijvers, 1998; Balona and Lawson, 2001; Poretti et al., 2009) and require special care. While the theoretical developments of Lee and Saio (1990); Townsend (1997) are used for gravito-inertial modes in rapid rotators, pressure-mode LPVs have benefitted from two-dimensional codes, starting with Clement (1994). The work of Reese et al. (2017a) is the most up-to-date such effort: it relies on non-adiabatic modes computed with the high-resolution oscillation code TOP (Reese et al., 2009a, 2021) paired with the self-consistent, two-dimensional ESTER models (Rieutord and Espinosa Lara, 2013; Rieutord et al., 2016).

Reese et al. (2017a) shows that p-mode LPV signatures are maximal in the wings of the line profile, contrary to what is expected in slow rotators (Lee and Saio, 1990). This can be explained by the complex geometries of modes in rapidly rotating stars, making LPVs equally more complex to decipher. The centrifugal flattening and gravity darkening make the amplitude of the signatures dependent on the stellar inclination, and different modes affect different spectral lines in various ways, depending on the range of temperature at the stellar surface (see, e.g. Takeda et al., 2008, for the rapid rotator Vega).

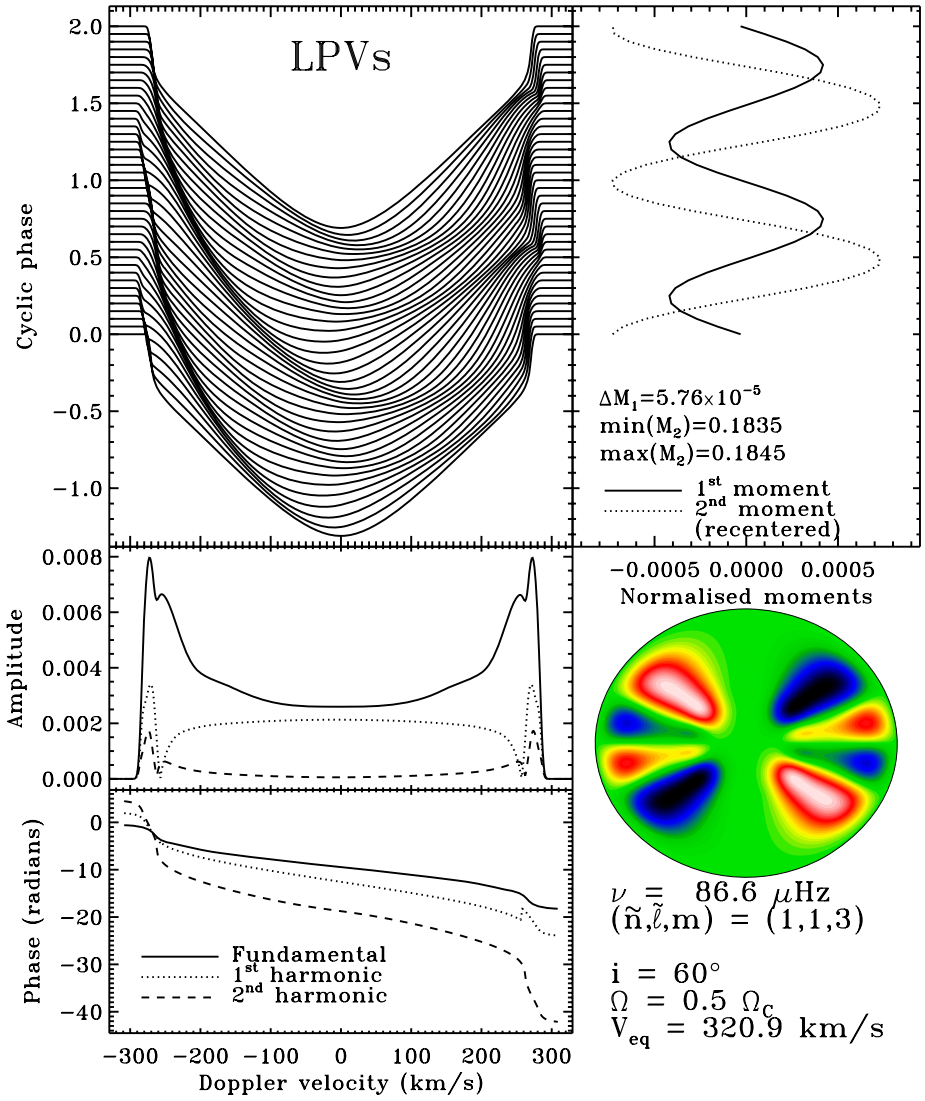

FIGURE 6
Line-profile variations in a 9$M_\odot$ ESTER model at 50% of its breakup velocity. Left, top to bottom: stacked line profiles, amplitudes and phases of the first three harmonics. Right, top to bottom: first and second moments of the LPVs, meridional cut of the oscillation mode, and model properties. Figure taken from Reese et al. (2017b).

Figure 6 presents the result of such calculations for a 2-period island mode 9$M_\odot$ ESTER model at 50% of its breakup velocity, This calculation relies on a few simplifying assumptions such as Gaussian equilibrium line profiles and rather crude limb- and gravity-darkening prescriptions. These assumptions will have to be relaxed to properly interpret time series of high-resolution spectra, and will surely be the topic of upcoming work.

Eventually, adapting widespread automated procedures such as the FPF method (Zima, 2006) to two-dimensional models will enable a simpler detection of identified modes that will serve as anchors for both pattern recognition and forward modelling.

5 Forward seismic modelling of fast rotators: The example of Rasalhague

Forward - or direct - modelling is a method of obtaining accurate properties of stars by directly modifying its input

parameters and computing associated observables until a satisfactory match with measurements is found. This strategy is adapted for rapidly rotating stars, especially when the number of oscillation modes detected in them is relatively small and the regular patterns in the spectra are difficult to disentangle.

The necessary steps for forward asteroseismic modelling are:

1) Compute an appropriate model for a reasonable set of input parameters, for rotating stars this shall include centrifugal flattening and gravity darkening,
2) Establish criteria—e.g. on mode visibility or excitation—to select the most observable oscillation modes from the synthetic spectrum,
3) Identify the selected modes thus found with the observed ones,
4) Repeat the process by varying the initial model parameters until a good match is obtained.

This strategy was successfully applied to slowly rotating classical pulsators, such as HD 129929 (Aerts et al., 2003) for which 6 gravity-mode frequencies were detected. By means of non-adiabatic oscillations, Aerts et al. (2004); Dupret et al. (2004b) not only obtained a stellar mass and age with uncertainties of a few percent, but also constrained envelope convective penetration and differential rotation. Some other successes of the forward-modelling approach for g-mode pulsators are given in Section 3.3.

I present here an application of the forward modelling approach to the rapidly rotating δ Scuti star Rasalhague (α Ophiuchi A, HD159561). It is a rapidly rotating pressure-mode pulsator, in which the centrifugal distortion is expected to significantly impact oscillation frequencies and geometries.

CHARA interferometry reveals that this A5 star is seen equator-on ($v \sin i = 239 \pm 12$ km s^{-1} and $i = 87.5 \pm 0.6^{\circ}$, Zhao et al., 2009). It also has a known K6 companion (Cowley et al., 1969; Hinkley et al., 2011), spectroscopic measurements that provide chemical information (Erspamer and North, 2003) and 57 oscillations frequencies measured with MOST (Monnier et al., 2010, including mostly pressure modes and a few gravito-inertial or mixed modes). These numerous observations make Rasalhague an optimal example for forward modelling.

Until recently, the masses derived from fitting the binary orbit of this system ($2.40^{+0.23}_{-0.37}$ M$_{\odot}$, Hinkley et al., 2011) and fitting the stellar flux with Yonsei-Yale models (2.18 ± 0.02 M$_{\odot}$, Monnier et al., 2010) covered a wide range. The precision of the binary orbit fit was significantly improved by observations near periastron passage, yielding a mass of 2.20 ± 0.06M$_{\odot}$, matching estimates from interferometry and models closely (Gardner et al., 2021). The oscillation spectrum contains 57 frequencies ranging from 1.7 to 48.5 cycles per day—20–560 μHz. It contains both gravity and pressure modes over the same frequency range, making it a δ Scuti/γ Doradus hybrid pulsator. The overlap is undeniably due to the star's rapid rotation and its impact on mode frequencies, as slowly rotating hybrid pulsators usually present a clearer frequency separation between the p- and g-mode subspectra.

The first attempt at modelling Rasalhague was by Deupree (2011), using the 2D ROTORC code (Deupree, 1990, 1995). He uses nine solid-body rotating and one slightly differentially-rotating models, and computes adiabatic oscillations with $-4 \leq m \leq 4$, using six or eight spherical harmonics for each mode. He then identifies oscillation modes by matching MOST frequencies to their closest synthetic counterpart within one stardard deviation. Figure 7 presents the match between synthetic frequencies for different azimuthal orders and the observed ones. The échelle diagram is folded with a $\Delta\nu = 47.6\,\mu$Hz that emerges from the models, but does not match the estimate of García Hernández et al. (2015).

While an interesting first attempt, this study has clear limitations already mentioned in the original paper. First, the synthetic spectrum computed by Deupree (2011) is so dense that several synthetic frequencies lie within the observational uncertainties for numerous modes, which makes the differentiation between models difficult. More importantly, increasing the number of spherical harmonics to describe each mode from six to eight leads to a drastic change in the mode geometry. This shows that 6- and 8-harmonic calculations are underresolved, which undermines the whole analysis. The MOST dataset has been studied by García Hernández et al. (2015, 2017) who found regular patterns in the oscillation spectrum. For frequencies above 116 μHz they found a large separation of $38 \pm 1\,\mu$Hz that corresponds to a mean density of $0.123 \pm 0.021\rho_{\odot}$. The 116 μHz frequency is that of the lowest-order radial pressure mode, while the $38 \pm 1\,\mu$Hz pattern is due to 2-period island modes. These seismic parameters and partial mode identification have guided the new modelling effort I describe here.

This new calculation relies on the ESTER and TOP codes and is presented in Mirouh et al. (2013); Mirouh et al. (2017). The ESTER code computes the structure of a rotating star in two dimensions, including centrifugal distortion, gravity darkening and meridional circulation, but treats mixing in a very simplified manner that does not track core recession and cannot include a surface convection zone. It is paired with the TOP code, a high-resolution spectral code to compute the adiabatic and non-adiabatic oscillations of rotating models. For this work, we compute a 2.22M$_{\odot}$ model whose surface temperature, radii and rotation match the interferometric measurements. We compute adiabatic modes with $-4 \leq m \leq 4$, this time using twenty spherical harmonics for each mode. To select the best candidates for identification, we compute mode visibilities (that is, the induced surface signature Reese et al., 2013; 2017b) and the growth or damping rate (that is, the rate at which the mode is excited or damped in the star). Growth and damping rates are directly obtained through solving the non-adiabatic oscillation equations or from work integrals computed in the adiabatic approximation, that is, assuming that non-adiabatic effects do not impact the mode geometry (Unno et al., 1989; Mirouh et al., 2013).

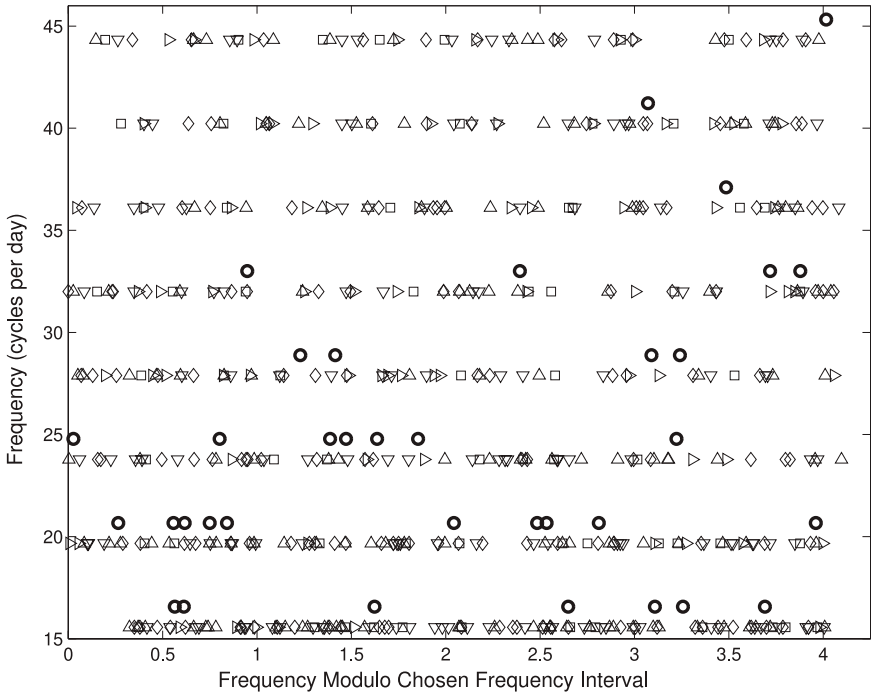

FIGURE 7
Echelle diagram comparing synthetic modes at different azimuthal orders m (squares: $|m| = 0$, diamonds $|m| = 1$, inverted triangles $|m| = 2$, triangles $|m| = 3$ and right-facing triangles $|m| = 4$) with observed frequencies (thick circles artifically offset). Figure taken from Deupree (2011).

The aim is to select the most visible excited modes that match the measured frequencies. The top panel of Figure 8 shows the visibility of each mode, and visual inspection brings out two overlapping populations. Pressure modes are the most visible and cover the whole frequency range, while gravito-inertial modes exist at low frequency ($\omega < \sqrt{N^2 + 4\Omega^2}$) and have lower visibilities. This difference comes from the energy distribution in the star, as gravito-inertial modes are focused around the stellar core and seldom reach the stellar surface and acoustic modes propagate up to the surface.

Computing growth and damping rates using work integrals in the quasi-adiabatic approximation yields only linearly-stable modes, with acoustic modes being more damped than gravito-inertial modes. This can be attributed to a poor description of the modes at the stellar surface and prevents any identification of the observed modes (Mirouh et al., 2013).

Non-adiabatic calculations reveal the presence of linearly-unstable modes (Mirouh et al., 2017), as shown in the bottom plot of Figure 8. However, those modes do not seem to match the expected distribution: most unstable modes are gravito-inertial modes that describe a somewhat regular spacing which does not match the large separation of García Hernández et al. (2015, 2017), while the most visible modes are damped. The origin of unstable (super-inertial) gravito-inertial modes in ESTER models of Rasalhague comes as a surprise: as the models do not feature a convective envelope, they cannot include the convective blocking excitation mechanism. If the computed modes are to explain the gravity modes observed by Monnier et al. (2010), their excitation must be provided by another mechanism. Candidates include the κ mechanism for gravity modes, as proposed by Xiong et al. (2016), the overstable convective modes suggested notably in Lee (2021), or the elusive differential rotation mechanism suggested by Mirouh et al. (2016).

At this point it is thus impossible to identify modes. This may be due to the non-adiabatic calculations whose stability must be ensured, and ESTER models' inclusion of surface effects. A better understanding of the intertwined regular patterns in the spectra (described in Section 3) can also be obtained by the systematic application of classification algorithms such as that of Mirouh et al. (2019). This algorithm is a supervised machine learning approach, that relies on a bank of well-identified pressure perturbation profiles to separate rapidly a set of computed modes into the various geometries presented in section 2. Mirouh et al. (2019) focused on extracting patterns for island modes, and their algorithm can be extended to study other pressure and gravito-inertial modes. Other machine learning approaches, both supervised and unsupervised, applied to individual modes or entire observed spectra, will undoubtedly be the next step towards mode identification in rapid rotators such as Rasalhague. Rasalhague also seems to be a good candidate for line-profile variation detections (described in Section 4), as it is seen equator-on which would maximize the signature of island modes.

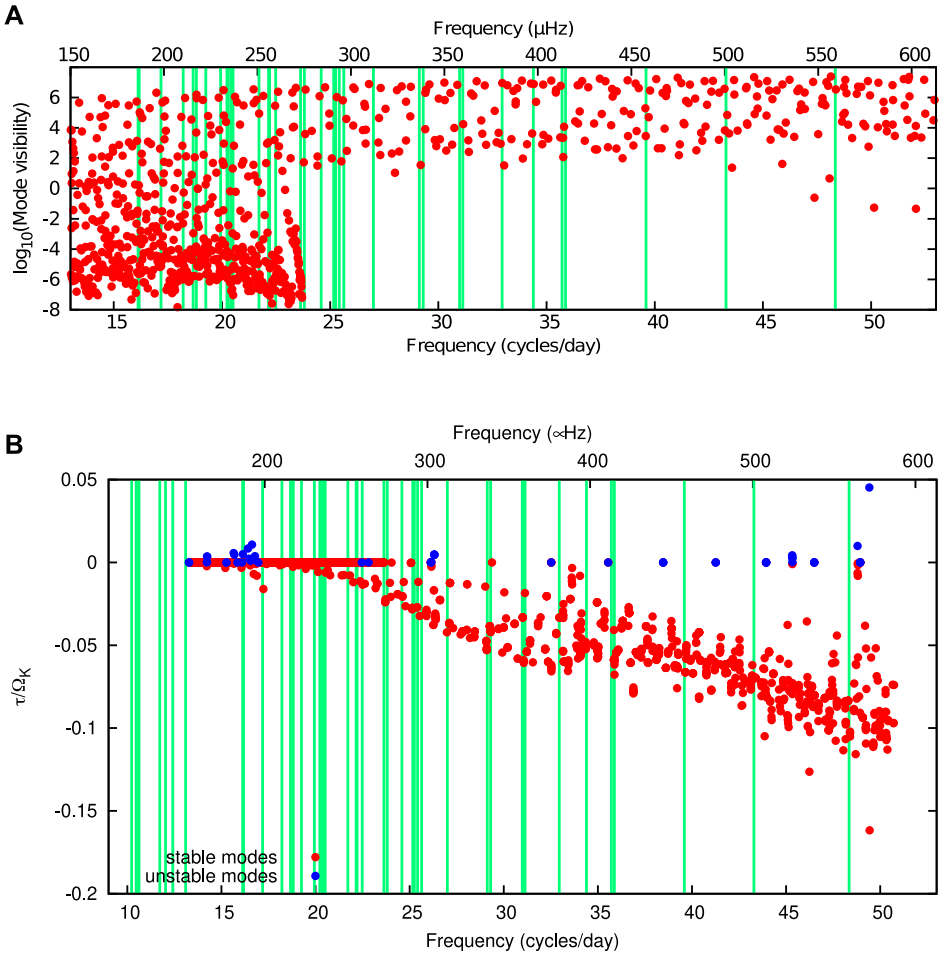

FIGURE 8
Properties of axisymmetric (m = 0) modes. **(A)**: mode visibilities. **(B)**: mode damping (red) or growth (blue) rates obtained from non-adiabatic calculations. Green lines denote frequencies from Monnier et al. (2010). Figure taken from Mirouh et al. (2017).

These improvements will be necessary to obtain a satisfactory two-dimensional seismic model of Rasalhague and open the way to the study of other rapidly rotating pulsators observed through interferometry, such as Alderamin, Regulus or Achernar. Another very interesting star is the rapid rotator Altair whose realistic modelling, albeit not seismic, was achieved by Bouchaud et al. (2020) and which features 15 oscillation frequencies (Le Dizès et al., 2021).

6 Summary

Rapid rotation makes early-type main-sequence pulsators a much more complex object of study compared to slowly rotating late-type counterparts. While our understanding of these stars has been lagging behind that of solar-like pulsators for years, the gap is closing at an increasing speed. The application of the traditional approximation for gravito-inertial modes in moderate rotators, and the development of two-dimensional models and oscillation codes for both pressure and gravito-inertial modes at all rotation rates, have unveiled the complex geometries and patterns the modes assume. Pattern analysis in high-quality oscillation spectra reveal an increasing amount of information on rotating stars. I presented the topology of both gravito-inertial and acoustic modes under the combined effect of the Coriolis force and centrifugal distortion.

Kepler and TESS revealed numerous regularities in the low-frequency spectra of γ Doradus and SPB stars, that were matched by gravito-inertial and Rossby modes computed with the traditional approximation. This opened a window on differential rotation and mixing inside those stars, and statistics are now building up to reach a better understanding of the structure and evolution of these stars. Pressure-mode pulsators such as δ Scuti benefitted from recent progress in two-dimensional models and oscillation codes. Theoretical patterns are identified and linked to structure quantities, and an entire toolkit is now available to compute

these modes, their visibilities and damping rates. I described in this article two developments that may be the final pieces of the puzzle. One of them is the development of classification algorithms to automate mode identification and derive patterns for each subclass of acoustic modes, and the other is line-profile variations adapted to rapidly rotating stars to provide solid anchor points to forward seismic modelling approaches.

Just like Kepler and TESS have allowed unprecedented progress in the deciphering of classical pulsator oscillation spectra, the future PLATO mission holds the promise of yet another revolution. The sheer amount of stars for which lightcurves will eventually be available will be a stepping stone towards a full understanding of rotation, angular momentum mixing and their impact on intermediate- and high-mass stellar evolution.

Author contributions

GMM has written this entire article and is accountable for its content.

Funding

GMM ackowledges support by "Contribution of the UGR to the PLATO2.0 space mission. Phases C/D-1", funded by MCNI/AEI/PID 2019-107061GB-C64.

Acknowledgments

The author thanks Daniel R. Reese, Antonio García Hernández and Juan Carlos Suárez for insightful discussions that helped define and improve this review, along with both anonymous referees whose detailed comments led to significant improvements to this article. Special acknowledgements also go to the PIMMS workshop attendees for the interesting discussions that took place there.

Conflict of interest

The author declares that the research was conducted in the absence of any commercial or financial relationships that could be construed as a potential conflict of interest.

Publisher's note

All claims expressed in this article are solely those of the authors and do not necessarily represent those of their affiliated organizations, or those of the publisher, the editors and the reviewers. Any product that may be evaluated in this article, or claim that may be made by its manufacturer, is not guaranteed or endorsed by the publisher.

References

Aerts, C., Christensen-Dalsgaard, J., and Kurtz, D. W. (2010). *Asteroseismology*. Springer.

Aerts, C., de Pauw, M., and Waelkens, C. (1992). Mode identification of pulsating stars from line profile variations with the moment method. An example : The beta Cephei star delta ceti. *A&A* 266, 294.

Aerts, C., Molenberghs, G., Michielsen, M., Pedersen, M. G., Björklund, R., Johnston, C., et al. (2018). Forward asteroseismic modeling of stars with a convective core from gravity-mode oscillations: Parameter estimation and stellar model selection. *Astrophys. J. Suppl. Ser.* 237, 15. doi:10.3847/1538-4365/aaccfb

Aerts, C., Thoul, A., Daszyńska, J., Scuflaire, R., Waelkens, C., Dupret, M. A., et al. (2003). Asteroseismology of HD 129929: Core overshooting and nonrigid rotation. *Science* 300, 1926–1928. doi:10.1126/science.1084993

Aerts, C., Waelkens, C., Daszyńska-Daszkiewicz, J., Dupret, M.-A., Thoul, A., Scuflaire, R., et al. (2004). Asteroseismology of the β Cep star HD 129929. I. Observations, oscillation frequencies and stellar parameters. *Astron. Astrophys.* 415, 241–249. doi:10.1051/0004-6361:20034142

Ahlborn, F., Bellinger, E. P., Hekker, S., Basu, S., and Angelou, G. C. (2020). Asteroseismic sensitivity to internal rotation along the red-giant branch. *Astron. Astrophys.* 639, A98. doi:10.1051/0004-6361/201936947

Baglin, A., Auvergne, M., Barge, P., Deleuil, M., Michel, E., and CoRoT Exoplanet Science Team (2009). "CoRoT: Description of the mission and early results," in *Transiting planets*. Editors F. Pont, D. Sasselov, and M. J. Holman, 253, 71.

Ballot, J., Lignières, F., Prat, V., Reese, D. R., and Rieutord, M. (2012). "2D computations of g-modes in fast rotating stars," in *Progress in solar/stellar physics with helio- and asteroseismology*. Editors H. Shibahashi, M. Takata, and A. E. Lynas-Gray (Hakone, Japan: Astronomical Society of the Pacific Conference Series), 462, 389.

Ballot, J., Lignières, F., and Reese, D. R. (2013). "Numerical exploration of oscillation modes in rapidly rotating stars," in *Lecture notes in physics, berlin springer verlag*. Editors M. Goupil, K. Belkacem, C. Neiner, and F. Lignières (Paris, France: J. J. Green), 865, 91.

Ballot, J., Lignières, F., Reese, D. R., and Rieutord, M. (2010). Gravity modes in rapidly rotating stars. Limits of perturbative methods. *Astron. Astrophys.* 518, A30. doi:10.1051/0004-6361/201014426

Balona, L. A., Daszyńska-Daszkiewicz, J., and Pamyatnykh, A. A. (2015). Pulsation frequency distribution in δ Scuti stars. *Mon. Not. R. Astron. Soc.* 452, 3073–3084. doi:10.1093/mnras/stv1513

Balona, L. A., and Lawson, W. A. (2001). Short-period line profile variations in the Be star ϵ Cap. *Mon. Not. R. Astron. Soc.* 321, 131–142. doi:10.1046/j.1365-8711.2001.03994.x

Balona, L. A. (1987). Mode identification from line profile variations - III. Temperature variation and toroidal modes. *Mon. Not. R. Astron. Soc.* 224, 41–52. doi:10.1093/mnras/224.1.41

Balona, L. A. (2017). Starspots on A stars. *Mon. Not. R. Astron. Soc.* 467, 1830–1837. doi:10.1093/mnras/stx265

Barceló Forteza, S., Moya, A., Barrado, D., Solano, E., Martín-Ruiz, S., Suárez, J. C., et al. (2020). Unveiling the power spectra of δ Scuti stars with TESS. The temperature, gravity, and frequency scaling relation. *Astron. Astrophys.* 638, A59. doi:10.1051/0004-6361/201937262

Barceló Forteza, S., Roca Cortés, T., and García, R. A. (2018). The envelope of the power spectra of over a thousand δ Scuti stars. The $T_{\rm eff}$ - $\nu_{\rm max}$ scaling relation. *Astron. Astrophys.* 614, A46. doi:10.1051/0004-6361/201731803

Baruteau, C., and Rieutord, M. (2013). Inertial waves in a differentially rotating spherical shell. *J. Fluid Mech.* 719, 47–81. doi:10.1017/jfm.2012.605

Beck, P. G., Montalban, J., Kallinger, T., De Ridder, J., Aerts, C., García, R. A., et al. (2012). Fast core rotation in red-giant stars as revealed by gravity-dominated mixed modes. *Nature* 481, 55–57. doi:10.1038/nature10612

Bedding, T. R., Murphy, S. J., Colman, I. L., and Kurtz, D. W. (2015). "Échelle diagrams and period spacings of g modes in γ Doradus stars from four years of Kepler observations," in *European physical journal web of conferences*, 10, 01005. doi:10.1051/epjconf/201510101005

Bedding, T. R., Murphy, S. J., Hey, D. R., Huber, D., Li, T., Smalley, B., et al. (2020). Very regular high-frequency pulsation modes in young intermediate-mass stars. *Nature* 581, 147–151. doi:10.1038/s41586-020-2226-8

Berthomieu, G., Gonczi, G., Graff, P., Provost, J., and Rocca, A. (1978). Low-frequency gravity modes of a rotating star. *A&A* 70, 597.

Bildsten, L., Ushomirsky, G., and Cutler, C. (1996). Ocean g-modes on rotating neutron stars. *Astrophys. J.* 460, 827. doi:10.1086/177012

Bouabid, M.-P., Dupret, M.-A., Salmon, S., Montalbán, J., Miglio, A., and Noels, A. (2013). Effects of the Coriolis force on high-order g modes in γ Doradus stars. *Mon. Not. R. Astron. Soc.* 429, 2500–2514. doi:10.1093/mnras/sts517

Bouchaud, K., Domiciano de Souza, A., Rieutord, M., Reese, D. R., and Kervella, P. (2020). A realistic two-dimensional model of Altair. *Astron. Astrophys.* 633, A78. doi:10.1051/0004-6361/201936830

Bowman, D. M., and Kurtz, D. W. (2018). Characterizing the observational properties of δ Sct stars in the era of space photometry from the Kepler mission. *Mon. Not. R. Astron. Soc.* 476, 3169–3184. doi:10.1093/mnras/sty449

Bowman, D. M., Vandenbussche, B., Sana, H., Tkachenko, A., Raskin, G., Delabie, T., et al. (2022). The CubeSpec space mission. I. Asteroseismology of massive stars from time-series optical spectroscopy: Science requirements and target list prioritisation. *Astron. Astrophys.* 658, A96. doi:10.1051/0004-6361/202142375

Brown, T. M., Gilliland, R. L., Noyes, R. W., and Ramsey, L. W. (1991). Detection of possible p-mode oscillations on Procyon. *Astrophys. J.* 368, 599. doi:10.1086/169725

Bugnet, L., Prat, V., Mathis, S., Astoul, A., Augustson, K., García, R. A., et al. (2021). Magnetic signatures on mixed-mode frequencies. I. An axisymmetric fossil field inside the core of red giants. *Astron. Astrophys.* 650, A53. doi:10.1051/0004-6361/202039159

Burssens, S., Simón-Díaz, S., Bowman, D. M., Holgado, G., Michielsen, M., de Burgos, A., et al. (2020). Variability of OB stars from TESS southern Sectors 1-13 and high-resolution IACOB and OWN spectroscopy. *Astron. Astrophys.* 639, A81. doi:10.1051/0004-6361/202037700

Che, X., Monnier, J. D., Zhao, M., Pedretti, E., Thureau, N., Mérand, A., et al. (2011). Colder and hotter: Interferometric imaging of β cassiopeiae and α leonis. *Astrophys. J.* 732, 68. doi:10.1088/0004-637x/732/2/68

Christensen-Dalsgaard, J., Schou, J., and Thompson, M. J. (1990). A comparison of methods for inverting helioseismic data. *Mon. Not. R. Astron. Soc.* 242, 353–369. doi:10.1093/mnras/242.3.353

Christophe, S., Ballot, J., Ouazzani, R. M., Antoci, V., and Salmon, S. J. A. J. (2018). Deciphering the oscillation spectrum of γ Doradus and SPB stars. *Astron. Astrophys.* 618, A47. doi:10.1051/0004-6361/201832782

Clement, M. J. (1994). "Pulsation in rapidly rotating stars," in *Pulsation; rotation; and mass loss in early-type stars*. Editors L. A. Balona, H. F. Henrichs, and J. M. Le Contel, 162, 117.

Cowley, A., Cowley, C., Jaschek, M., and Jaschek, C. (1969). A study of the bright stars. I. A catalogue of spectral classifications. *Astron. J.* 74, 375–406. doi:10.1086/110819

Cox, A. N., Morgan, S. M., Rogers, F. J., and Iglesias, C. A. (1992). An opacity mechanism for the pulsations of OB stars. *Astrophys. J.* 393, 272. doi:10.1086/171504

Cugier, H. (1993). Modeling line profiles in beta Cephei stars including temperature and pressure effects. *Acta Astron.* 43, 27.

De Cat, P., Briquet, M., Aerts, C., Goossens, K., Saesen, S., Cuypers, J., et al. (2007). Long term photometric monitoring with the mercator telescope*** - frequencies and mode identification of variable o-b stars. *Astron. Astrophys.* 463, 243–249. doi:10.1051/0004-6361:20066202

Deheuvels, S., Doğan, G., Goupil, M. J., Appourchaux, T., Benomar, O., Brunt, H., et al. (2014). Seismic constraints on the radial dependence of the internal rotation profiles of six Kepler subgiants and young red giants. *Astron. Astrophys.* 564, A27. doi:10.1051/0004-6361/201322779

Deupree, R. G. (1995). Stella evolution with arbitrary rotation laws. 2: Massive star evolution to core hydrogen exhaustion. *Astrophys. J.* 439, 357–364. doi:10.1086/175179

Deupree, R. G. (1990). Stellar evolution with arbitrary rotation laws. I - mathematical techniques and test cases. *Astrophys. J.* 357, 175–187. doi:10.1086/168903

Deupree, R. G. (2011). Theoretical p-mode oscillation frequencies for the rapidly rotating δ Scuti star α Ophiuchi. *Astrophys. J.* 742, 9. doi:10.1088/0004-637x/742/1/9

Dhouib, H., Prat, V., Van Reeth, T., and Mathis, S. (2021). The traditional approximation of rotation for rapidly rotating stars and planets. II. Deformation and differential rotation. *Astron. Astrophys.* 656, A122. doi:10.1051/0004-6361/202141152

Di Mauro, M. P., Ventura, R., Corsaro, E., and Lustosa De Moura, B. (2018). The rotational shear layer inside the early red-giant star KIC 4448777. *Astrophys. J.* 862, 9. doi:10.3847/1538-4357/aac7c4

Dintrans, B., Rieutord, M., and Valdettaro, L. (1999). Gravito-inertial waves in a rotating stratified sphere or spherical shell. *J. Fluid Mech.* 398, 271–297. doi:10.1017/s0022112099006308

Dupret, M.-A., Grigahcène, A., Garrido, R., Gabriel, M., and Scuflaire, R. (2005). Convection-pulsation coupling. II. Excitation and stabilization mechanisms in δ Sct and γ Dor stars. *Astron. Astrophys.* 435, 927–939. doi:10.1051/0004-6361:20041817

Dupret, M.-A., Thoul, A., Scuflaire, R., Daszyńska-Daszkiewicz, J., Aerts, C., Bourge, P.-O., et al. (2004b). Asteroseismology of the β Cep star HD 129929. II. Seismic constraints on core overshooting, internal rotation and stellar parameters. *Astron. Astrophys.* 415, 251–257. doi:10.1051/0004-6361:20034143

Dupret, M. A., Grigahcène, A., Garrido, R., Gabriel, M., and Scuflaire, R. (2004a). Theoretical instability strips for δ Scuti and γ Doradus stars. *Astron. Astrophys.* 414, L17–L20. doi:10.1051/0004-6361:20031740

Dziembowski, W. A., Moskalik, P., and Pamyatnykh, A. A. (1993). The opacity mechanism in B-type stars - II. Excitation of high-order g-modes in main-sequence stars. *Mon. Not. R. Astron. Soc.* 265, 588–600. doi:10.1093/mnras/265.3.588

Eckart, C. (1960). Variation principles of hydrodynamics. *Phys. Fluids (1994).* 3, 421–427. doi:10.1063/1.1706053

Eggenberger, P., Meynet, G., Maeder, A., Hirschi, R., Charbonnel, C., Talon, S., et al. (2008). The Geneva stellar evolution code. *Astrophys. Space Sci.* 316, 43–54. doi:10.1007/s10509-007-9511-y

Erspamer, D., and North, P. (2003). Automated spectroscopic abundances of A and F-type stars using echelle spectrographs. *Astron. Astrophys.* 398, 1121–1135. doi:10.1051/0004-6361:20021711

Espinosa Lara, F., and Rieutord, M. (2011). Gravity darkening in rotating stars. *Astron. Astrophys.* 533, A43. doi:10.1051/0004-6361/201117252

Espinosa Lara, F., and Rieutord, M. (2013). Self-consistent 2D models of fast rotating early-type stars. *Astron. Astrophys.* 552, A35. doi:10.1051/0004-6361/201220844

Evano, B., Lignières, F., and Georgeot, B. (2019). Regularities in the spectrum of chaotic p-modes in rapidly rotating stars. *Astron. Astrophys.* 631, A140. doi:10.1051/0004-6361/201936459

García Hernández, A., Martín-Ruiz, S., Monteiro, M. J. P. F. G., Suárez, J. C., Reese, D. R., Pascual-Granado, J., et al. (2015). Observational $\Delta\nu$- relation for δ Sct stars using eclipsing binaries and space photometry. *Astrophys. J.* 811, L29. doi:10.1088/2041-8205/811/2/l29

García Hernández, A., Moya, A., Michel, E., Garrido, R., Suárez, J. C., Rodríguez, E., et al. (2009). Asteroseismic analysis of the CoRoT δ Scuti star HD 174936**. *Astron. Astrophys.* 506, 79–83. doi:10.1051/0004-6361/200911932

García Hernández, A., Suárez, J. C., Moya, A., Monteiro, M. J. P. F. G., Guo, Z., Reese, D. R., et al. (2017). Precise surface gravities of δ Scuti stars from asteroseismology. *MNRAS* 471, L140–L144. doi:10.1093/mnrasl/slx117

García, R. A., Pérez Hernández, F., Benomar, O., Silva Aguirre, V., Ballot, J., Davies, G. R., et al. (2014). Study of KIC 8561221 observed by kepler: An early red giant showing depressed dipolar modes. *Astron. Astrophys.* 563, A84. doi:10.1051/0004-6361/201322823

Garcia, S., Van Reeth, T., De Ridder, J., Tkachenko, A., Ijspeert, L., and Aerts, C. (2022). Detection of period-spacing patterns due to the gravity modes of rotating dwarfs in the TESS southern continuous viewing zone. *Astron. Astrophys.* 662, A82. doi:10.1051/0004-6361/202141926

Gardner, T., Monnier, J. D., Fekel, F. C., Williamson, M., Baron, F., Hinkley, S., et al. (2021). Establishing α oph as a prototype rotator: Precision orbit with new keck, CHARA, and RV observations. *Astrophys. J.* 921, 41. doi:10.3847/1538-4357/ac1172

Gilliland, R. L., Brown, T. M., Christensen-Dalsgaard, J., Kjeldsen, H., Aerts, C., Appourchaux, T., et al. (2010). Kepler asteroseismology program: Introduction and first results. *Pub. Astron. Soc. Pac.* 122, 131–143. doi:10.1086/650399

Gough, D. O. (1993). "Linear adiabatic stellar pulsation," in *Astrophysical fluid dynamics, les houches 1987*. Editors J.-P. Zahn and J. Zinn-Justin (Elsevier), 399

Gough, D. O., and Thompson, M. J. (1990). The effect of rotation and a buried magnetic field on stellar oscillations. *Mon. Not. R. Astron. Soc.* 242, 25–55. doi:10.1093/mnras/242.1.25

Grigahcène, A., Antoci, V., Balona, L., Catanzaro, G., Daszyńska-Daszkiewicz, J., Guzik, J. A., et al. (2010). Hybrid γ doradus-δ Scuti pulsators: New insights into the physics of the oscillations from kepler observations. *Astrophys. J.* 713, L192–L197. doi:10.1088/2041-8205/713/2/L192

Guo, Z., and Li, G. (2019). A mass-accreting gamma doradus pulsator with a synchronized core in kepler eclipsing binary KIC 7385478. *Astrophys. J.* 882, L5. doi:10.3847/2041-8213/ab3a53

Guo, Z., Ogilvie, G. I., Li, G., Townsend, R. H. D., and Sun, M. (2022). A new window to tidal asteroseismology: Non-linearly excited stellar eigenmodes and the period spacing pattern in KOI-54. *mnras. arXiv e-prints*arXiv:2202.06101. doi:10.1093/mnras/stac2611

Guzik, J. A., Kaye, A., Bradley, P., Cox, A., and Neuforge, C. (2000). Driving the gravity mode pulsations in γ doradus variables. *Preprint* 1, 593.

Handler, G., Balona, L. A., Shobbrook, R. R., Koen, C., Bruch, A., Romero-Colmenero, E., et al. (2002). Discovery and analysis of p-mode and g-mode oscillations in the A-type primary of the eccentric binary HD 209295. *Mon. Not. R. Astron. Soc.* 333, 262–278. doi:10.1046/j.1365-8711.2002.05295.x

Handler, G. (2009). Confirmation of simultaneous p and g mode excitation in HD 8801 and γ Peg from time-resolved multicolour photometry of six candidate 'hybrid' pulsators. *Mon. Not. R. Astron. Soc.* 398, 1339–1351. doi:10.1111/j.1365-2966.2009.15005.x

Handler, G., Shobbrook, R. R., Jerzykiewicz, M., Krisciunas, K., Tshenye, T., Rodríguez, E., et al. (2004). Asteroseismology of the β Cephei star ν Eridani - I. Photometric observations and pulsational frequency analysis. *Mon. Not. R. Astron. Soc.* 347, 454–462. doi:10.1111/j.1365-2966.2004.07214.x

Henneco, J., Van Reeth, T., Prat, V., Mathis, S., Mombarg, J. S. G., and Aerts, C. (2021). The effect of the centrifugal acceleration on period spacings of gravito-inertial modes in intermediate-mass stars. *Astron. Astrophys.* 648, A97. doi:10.1051/0004-6361/202039464

Hinkley, S., Monnier, J. D., Oppenheimer, B. R., Roberts, L. C., Jr., Ireland, M., Zimmerman, N., et al. (2011). Establishing α oph as a prototype rotator: Improved astrometric orbit. *Astrophys. J.* 726, 104. doi:10.1088/0004-637x/726/2/104

Holdsworth, D. L. (2021). The roAp stars observed by the Kepler Space Telescope. *Front. Astron. Space Sci.* 8, 31. doi:10.3389/fspas.2021.626398

Jackiewicz, J. (2021). Solar-like oscillators in the kepler era: A review. *Front. Astron. Space Sci.* 7, 595017. doi:10.3389/fspas.2020.595017

Johnston, C., Tkachenko, A., Aerts, C., Molenberghs, G., Bowman, D. M., Pedersen, M. G., et al. (2019). Binary asteroseismic modelling: Isochrone-cloud methodology and application to kepler gravity mode pulsators. *Mon. Not. R. Astron. Soc.* 482, 1231–1246. doi:10.1093/mnras/sty2671

Kallinger, T., Weiss, W. W., Barban, C., Baudin, F., Cameron, C., Carrier, F., et al. (2010). Oscillating red giants in the CoRoT exofield: Asteroseismic mass and radius determination. *Astron. Astrophys.* 509, A77. doi:10.1051/0004-6361/200811437

Korzennik, S. G., and Eff-Darwich, A. (2011). The rotation rate and its evolution derived from improved mode fitting and inversion methodology. *J. Phys. Conf. Ser.* 271, 012067.

Le Dizès, C., Rieutord, M., and Charpinet, S. (2021). *Seismology of Altair with MOST*. Astronomy and Astrophysics, 653, A26. doi:10.1051/0004-6361/202141291

Lecoanet, D., Bowman, D. M., and Van Reeth, T. (2022). Asteroseismic inference of the near-core magnetic field strength in the main-sequence B star HD 43317. *MNRAS* 512, L16–L20. doi:10.1093/mnrasl/slac013

Lecoanet, D., Vasil, G. M., Fuller, J., Cantiello, M., and Burns, K. J. (2017). Conversion of internal gravity waves into magnetic waves. *Mon. Not. R. Astron. Soc.* 466, 2181–2193. doi:10.1093/mnras/stw3273

Ledoux, P. (1951). The nonradial oscillations of gaseous stars and the problem of beta Canis majoris. *Astrophys. J.* 114, 373. doi:10.1086/145477

Lee, U., and Baraffe, I. (1995). Pulsational stability of rotating main sequence stars: The second order effects of rotation on the nonadiabatic oscillations. *Astron. Astrophys.* 301, 419.

Lee, U. (2022). Non-linear excitation of low-frequency modes by overstable convective modes in rotating stars. *Mon. Not. R. Astron. Soc.* 513, 2522–2534. doi:10.1093/mnras/stac1021

Lee, U. (2021). Overstable convective modes in rotating early-type stars. *Mon. Not. R. Astron. Soc.* 505, 1495–1508. doi:10.1093/mnras/stab1433

Lee, U., and Saio, H. (1990). Line profile variations caused by low-frequency nonradial pulsations of rapidly rotating stars. *Astrophys. J.* 349, 570. doi:10.1086/168344

Lee, U., and Saio, H. (1987). Low-frequency oscillations of uniformly rotating stars. *Mon. Not. R. Astron. Soc.* 224, 513–526. doi:10.1093/mnras/224.3.513

Lee, U., and Saio, H. (2020). Rotating convective core excites non-radial pulsations to cause rotational modulations in early-type stars. *Mon. Not. R. Astron. Soc.* 497, 4117–4127. doi:10.1093/mnras/staa2250

Li, G., Guo, Z., Fuller, J., Bedding, T. R., Murphy, S. J., Colman, I. L., et al. (2020a). The effect of tides on near-core rotation: Analysis of 35 kepler γ doradus stars in eclipsing and spectroscopic binaries. *Mon. Not. R. Astron. Soc.* 497, 4363–4375. doi:10.1093/mnras/staa2266

Li, G., Van Reeth, T., Bedding, T. R., Murphy, S. J., Antoci, V., Ouazzani, R.-M., et al. (2020b). Gravity-mode period spacings and near-core rotation rates of 611 γ Doradus stars with Kepler. *Mon. Not. R. Astron. Soc.* 491, 3586–3605. doi:10.1093/mnras/stz2906

Li, G., Van Reeth, T., Bedding, T. R., Murphy, S. J., and Antoci, V. (2019). Period spacings of γ Doradus pulsators in the Kepler field: Rossby and gravity modes in 82 stars. *Mon. Not. R. Astron. Soc.* 487, 782–800. doi:10.1093/mnras/stz1171

Lignières, F., and Georgeot, B. (2009). Asymptotic analysis of high-frequency acoustic modes in rapidly rotating stars. *Astron. Astrophys.* 500, 1173–1192. doi:10.1051/0004-6361/200811165

Lignières, F., and Georgeot, B. (2008). Wave chaos in rapidly rotating stars. *Phys. Rev. E* 78, 016215. doi:10.1103/PhysRevE.78.016215

Loi, S. T. (2020). Effect of a strong magnetic field on gravity-mode period spacings in red giant stars. *Mon. Not. R. Astron. Soc.* 496, 3829–3840. doi:10.1093/mnras/staa1823

Loi, S. T., and Papaloizou, J. C. B. (2018). Effects of a strong magnetic field on internal gravity waves: Trapping, phase mixing, reflection, and dynamical chaos. *Mon. Not. R. Astron. Soc.* 477, 5338–5357. doi:10.1093/mnras/sty917

Mantegazza, L., Poretti, E., Michel, E., Rainer, M., Baudin, F., García Hernández, A., et al. (2012). Pulsation spectrum of δ Scuti stars: The binary HD 50870 as seen with CoRoT and HARPS. *Astron. Astrophys.* 542, A24. doi:10.1051/0004-6361/201118682

Mathis, S., Bugnet, L., Prat, V., Augustson, K., Mathur, S., and García, R. (2021). Probing the internal magnetism of stars using asymptotic magneto-asteroseismology. *Astron. Astrophys.* 647, A122. doi:10.1051/0004-6361/202039180

Mathis, S. (2009). Transport by gravito-inertial waves in differentially rotating stellar radiation zones. I - theoretical formulation. *Astron. Astrophys.* 506, 811–828. doi:10.1051/0004-6361/200810544

Matsuno, T. (2008). Quasi-geostrophic motions in the equatorial area. *J. Meteorological Soc. Jpn.* 44, 25–43. doi:10.2151/jmsj1965.44.1_25

Michel, E., Dupret, M.-A., Reese, D., Ouazzani, R.-M., Debosscher, J., Hernández, A. G., et al. (2017). What CoRoT tells us about δ Scuti stars. Existence of a regular pattern and seismic indices to characterize stars. *Eur. Phys. J. Web Conf.*, 160, 03001. doi:10.1051/epjconf/201716003001

Miglio, A., Montalbán, J., Noels, A., and Eggenberger, P. (2008). Probing the properties of convective cores through g modes: High-order g modes in SPB and γ doradus stars. *Mon. Not. R. Astron. Soc.* 386, 1487–1502. doi:10.1111/j.1365-2966.2008.13112.x

Mirouh, G. M., Angelou, G. C., Reese, D. R., and Costa, G. (2019). Mode classification in fast-rotating stars using a convolutional neural network: Model-based regular patterns in δ Scuti stars. *MNRAS* 483, L28–L32. doi:10.1093/mnrasl/sly212

Mirouh, G. M., Baruteau, C., Rieutord, M., and Ballot, J. (2016). Gravito-inertial waves in a differentially rotating spherical shell. *J. Fluid Mech.* 800, 213–247. doi:10.1017/jfm.2016.382

Mirouh, G. M., Reese, D. R., Rieutord, M., and Ballot, J. (2017). "Non-adiabatic oscillations of fast-rotating stars: The example of Rasalhague," in *SF2A-2017: Proceedings of the annual meeting of the French society of Astronomy and Astrophysics*, Paris, France. Editors C. Reylé, P. Di Matteo, F. Herpin, E. Lagadec, A. Lançon, Z. Meliani, et al. sf2a, Société Française d'Astronomie et d'Astrophysique.

Mirouh, G., Reese, D., Espinosa Lara, F., Ballot, J., and Rieutord, M. (2013). "Asteroseismology of fast-rotating stars: The example of α ophuichi," in *Precision asteroseismology*. Editors W. Chaplin, J. Guzik, G. Handler, and A. Pigulski, 865. *IAU Symposium 301*, 1, astro–ph/.

Monnier, J. D., Townsend, R. H. D., Che, X., Zhao, M., Kallinger, T., Matthews, J., et al. (2010). Rotationally modulated g-modes in the rapidly rotating δ Scuti star Rasalhague (α Ophiuchi). *Astrophys. J.* 725, 1192–1201. doi:10.1088/0004-637x/725/1/1192

Mosser, B., Belkacem, K., Goupil, M.-J., Miglio, A., Morel, T., Barban, C., et al. (2010). Red-giant seismic properties analyzed with CoRoT. *Astron. Astrophys.* 517, A22. doi:10.1051/0004-6361/201014036

Mosser, B., Michel, E., Belkacem, K., Goupil, M. J., Baglin, A., Barban, C., et al. (2013). Asymptotic and measured large frequency separations. *Astron. Astrophys.* 550, A126. doi:10.1051/0004-6361/201220435

Osaki, Y. (1974). An excitation mechanism for pulsations in beta CEP stars. *Astrophys. J.* 189, 469–477. doi:10.1086/152825

Ott, E. (1993). *Chaos in dynamical systems*. Cambridge University Press.

Ouazzani, R.-M., Dupret, M.-A., and Reese, D. R. (2012). Pulsations of rapidly rotating stars. I. The ACOR numerical code. *Astron. Astrophys.* 547, A75. doi:10.1051/0004-6361/201219548

Ouazzani, R.-M., Roxburgh, I. W., and Dupret, M.-A. (2015). Pulsations of rapidly rotating stars. II. Realistic modelling for intermediate-mass stars. *Astron. Astrophys.* 579, A116. doi:10.1051/0004-6361/201525734

Ouazzani, R.-M., Salmon, S. J. A. J., Antoci, V., Bedding, T. R., Murphy, S. J., and Roxburgh, I. W. (2017). A new asteroseismic diagnostic for internal rotation in γ Doradus stars. *Mon. Not. R. Astron. Soc.* 465, 2294–2309. doi:10.1093/mnras/stw2717

Ouazzani, R. M., and Goupil, M. J. (2012). Rotational splittings for slow to moderate rotators. *Astron. Astrophys.* 542, A99. doi:10.1051/0004-6361/201117151

Ouazzani, R. M., Lignières, F., Dupret, M. A., Salmon, S. J. A. J., Ballot, J., Christophe, S., et al. (2020). First evidence of inertial modes in γ Doradus stars: The core rotation revealed. *Astron. Astrophys.* 640, A49. doi:10.1051/0004-6361/201936653

Papaloizou, J., and Pringle, J. E. (1978). Gravitational radiation and the stability of rotating stars. *Mon. Not. R. Astron. Soc.* 184, 501–508. doi:10.1093/mnras/184.3.501

Paparó, M., Benkő, J. M., Hareter, M., and Guzik, J. A. (2016b). Unexpected series of regular frequency spacing of δ Scuti stars in the non-asymptotic regime. II. Sample-echelle diagrams and rotation. *Astrophys. J. Suppl. Ser.* 224, 41. doi:10.3847/0067-0049/224/2/41

Paparó, M., Benkő, J. M., Hareter, M., and Guzik, J. A. (2016a). Unexpected series of regular frequency spacing of δ Scuti stars in the non-asymptotic regime. I. The methodology. *Astrophys. J.* 822, 100. doi:10.3847/0004-637X/822/2/100

Pápics, P. I., Tkachenko, A., Van Reeth, T., Aerts, C., Moravveji, E., Van de Sande, M., et al. (2017). Signatures of internal rotation discovered in the Kepler data of five slowly pulsating B stars. *Astron. Astrophys.* 598, A74. doi:10.1051/0004-6361/201629814

Pasek, M., Georgeot, B., Lignières, F., and Reese, D. R. (2011). Regular modes in rotating stars. *Phys. Rev. Lett.* 107, 121101. doi:10.1103/PhysRevLett.107.121101

Pasek, M., Lignières, F., Georgeot, B., and Reese, D. R. (2012). Regular oscillation sub-spectrum of rapidly rotating stars. *Astron. Astrophys.* 546, A11. doi:10.1051/0004-6361/201219716

Pedersen, M. G., Aerts, C., Pápics, P. I., Michielsen, M., Gebruers, S., Rogers, T. M., et al. (2021). Internal mixing of rotating stars inferred from dipole gravity modes. *Nat. Astron.* 5, 715–722. doi:10.1038/s41550-021-01351-x

Pesnell, W. D. (1987). A new driving mechanism for stellar pulsations. *Astrophys. J.* 314, 598–604. doi:10.1086/165089

Pijpers, F. P., and Thompson, M. J. (1994). The SOLA method for helioseismic inversion. *Astron. Astrophys.* 281, 231.

Poretti, E., Michel, E., Garrido, R., Lefèvre, L., Mantegazza, L., Rainer, M., et al. (2009). HD 50844: A new look at δ Scuti stars from CoRoT space photometry. *Astron. Astrophys.* 506, 85–93. doi:10.1051/0004-6361/200912039

Potter, A. T. (2012). *Rotation and magnetism in massive stars*. Ph.D. thesis, University of Cambridge.

Prat, V., Lignières, F., and Ballot, J. (2016). Asymptotic theory of gravity modes in rotating stars. I. Ray dynamics. *Astron. Astrophys.* 587, A110. doi:10.1051/0004-6361/201527737

Prat, V., Mathis, S., Neiner, C., Van Beeck, J., Bowman, D. M., and Aerts, C. (2020). Period spacings of gravity modes in rapidly rotating magnetic stars. II. The case of an oblique dipolar fossil magnetic field. *Astron. Astrophys.* 636, A100. doi:10.1051/0004-6361/201937398

Ramón-Ballesta, A., García Hernández, A., Suárez, J. C., Rodón, J. R., Pascual-Granado, J., and Garrido, R. (2021). Study of rotational splittings in δ Scuti stars using pattern finding techniques. *Mon. Not. R. Astron. Soc.* 505, 6217–6224. doi:10.1093/mnras/stab1719

Reese, D. (2006). *La modélisation des oscillations d'étoiles en rotation rapide*. Toulouse (France): Université Toulouse III - Paul Sabatier. Ph.D. thesis.

Reese, D., Lignières, F., and Rieutord, M. (2008). Regular patterns in the acoustic spectrum of rapidly rotating stars. *Astron. Astrophys.* 481, 449–452. doi:10.1051/0004-6361:20078075

Reese, D. R., Dupret, M.-A., and Rieutord, M. (2017a). Non-adiabatic pulsations in ESTER models." in European Physical Journal Web of Conferences, Angra do Heroismo, Portugal, 160, 02007. doi:10.1051/epjconf/201716002007

Reese, D. R., Lignières, F., Ballot, J., Dupret, M. A., Barban, C., van't Veer-Menneret, C., et al. (2017b). Frequency regularities of acoustic modes and multi-colour mode identification in rapidly rotating stars. *Astron. Astrophys.* 601, A130. doi:10.1051/0004-6361/201321264

Reese, D. R., MacGregor, K. B., Jackson, S., Skumanich, A., and Metcalfe, T. S. (2009a). Pulsation modes in rapidly rotating stellar models based on the self-consistent field method. *Astron. Astrophys.* 506, 189–201. doi:10.1051/0004-6361/200811510

Reese, D. R., Mirouh, G. M., Espinosa Lara, F., Rieutord, M., and Putigny, B. (2021). Oscillations of 2D ESTER models. I. The adiabatic case. *Astron. Astrophys.* 645, A46. doi:10.1051/0004-6361/201935538

Reese, D. R., Prat, V., Barban, C., van 't Veer-Menneret, C., and MacGregor, K. B. (2013). Mode visibilities in rapidly rotating stars. *Astron. Astrophys.* 550, A77. doi:10.1051/0004-6361/201220506

Reese, D. R., Thompson, M. J., MacGregor, K. B., Jackson, S., Skumanich, A., and Metcalfe, T. S. (2009b). Mode identification in rapidly rotating stars. *Astron. Astrophys.* 506, 183–188. doi:10.1051/0004-6361/200911914

Ricker, G. R. (2014). The transiting exoplanet survey satellite mission. *J. Am. Assoc. Var. Star Observers (JAAVSO)* 42, 234.

Rieutord, M., and Espinosa Lara, F. (2013). "*Ab initio* modelling of steady rotating stars," in *Studying stellar rotation and convection*. Editors M. Goupil, K. Belkacem, C. Neiner, F. Lignières, and J. J. Green (Roscoff, France: Lecture Notes in Physics, Berlin Springer Verlag).

Rieutord, M., Espinosa Lara, F., and Putigny, B. (2016). An algorithm for computing the 2D structure of fast rotating stars. *J. Comput. Phys.* 318, 277–304. doi:10.1016/j.jcp.2016.05.011

Rieutord, M., Georgeot, B., and Valdettaro, L. (2001). Inertial waves in a rotating spherical shell: Attractors and asymptotic spectrum. *J. Fluid Mech.* 435, 103–144. doi:10.1017/s0022112001003718

Rieutord, M. (2006). The dynamics of the radiative envelope of rapidly rotating stars. i. a spherical boussinesq model. *Astron. Astrophys.* 451, 1025–1036. doi:10.1051/0004-6361:20054433

Rodríguez-Martín, J. E., García Hernández, A., Suárez, J. C., and Rodón, J. R. (2020). Study of the low-order $\Delta\nu$-ρ^{-} relation for moderately rotating δ Scuti stars and its impact on their characterization. *Mon. Not. R. Astron. Soc.* 498, 1700–1709. doi:10.1093/mnras/staa2378

Rogers, T. M., and MacGregor, K. B. (2011). On the interaction of internal gravity waves with a magnetic field - II. Convective forcing. *Mon. Not. R. Astron. Soc.* 410, 946–962. doi:10.1111/j.1365-2966.2010.17493.x

Rogers, T. M., and MacGregor, K. B. (2010). On the interaction of internal gravity waves with a magnetic field â " I. Artificial wave forcing. *Mon. Not. R. Astron. Soc.* 401, 191–196. doi:10.1111/j.1365-2966.2009.15618.x

Royer, F. (2009). "On the rotation of A-type stars," in *The rotation of Sun and stars*. Editors J.-P. Rozelot and C. Neiner (Lecture Notes in PhysicsBerlin Springer Verlag), 765, 207.

Saio, H., Kurtz, D. W., Murphy, S. J., Antoci, V. L., and Lee, U. (2018). Theory and evidence of global Rossby waves in upper main-sequence stars: r-Mode oscillations in many kepler stars. *Mon. Not. R. Astron. Soc.* 474, 2774–2786. doi:10.1093/mnras/stx2962

Saio, H. (1982). R-mode oscillations in uniformly rotating stars. *Astrophys. J.* 256, 717–735. doi:10.1086/159945

Saio, H. (1981). Rotational and tidal perturbations of nonradial oscillations in a polytropic star. *Astrophys. J.* 244, 299–315. doi:10.1086/158708

Saio, H., Takata, M., Lee, U., Li, G., and Van Reeth, T. (2021). Rotation of the convective core in γ Dor stars measured by dips in period spacings of g modes coupled with inertial modes. *Mon. Not. R. Astron. Soc.* 502, 5856–5874. doi:10.1093/mnras/stab482

Saio, H., and Takata, M. (2014). Rosette modes of oscillations of rotating stars caused by close degeneracies. II. Nonaxisymmetric modes. *Publ. Astron. Soc. Jpn. Nihon. Tenmon. Gakkai.* 66, 58. doi:10.1093/pasj/psu027

Salmon, S. J. A. J., Eggenberger, P., Montalbán, J., Miglio, A., Noels, A., Buldgen, G., et al. (2022). Asteroseismology of β Cephei stars: The stellar inferences tested in hare and hound exercises. *Astron. Astrophys.* 659, A142. doi:10.1051/0004-6361/202142483

Schou, J., Antia, H. M., Basu, S., Bogart, R. S., Bush, R. I., Chitre, S. M., et al. (1998). Helioseismic studies of differential rotation in the solar envelope by the solar oscillations investigation using the michelson Doppler imager. *Astrophys. J.* 505, 390–417. doi:10.1086/306146

Sekaran, S., Tkachenko, A., Johnston, C., and Aerts, C. (2021). A comparison of the dynamical and model-derived parameters of the pulsating eclipsing binary KIC 9850387. *Astron. Astrophys.* 648, A91. doi:10.1051/0004-6361/202040154

Shibahashi, H. (1979). Modal analysis of stellar nonradial oscillations by an asymptotic method. *Pub. Astron. Soc. Jap.* 31, 87.

Shutt, T. R., Brunsden, E., and Pollard, K. R. (2021). Spectroscopic frequency and mode identification of γ Doradus stars HD 109799 and HD 103257. *Mon. Not. R. Astron. Soc.* 507, 1149–1156. doi:10.1093/mnras/stab1972

Soufi, F., Goupil, M. J., and Dziembowski, W. A. (1998). Effects of moderate rotation on stellar pulsation. I. Third order perturbation formalism. *Astron. Astrophys.* 334, 911.

Stello, D., Cantiello, M., Fuller, J., Garcia, R. A., and Huber, D. (2016). Suppression of quadrupole and octupole modes in red giants observed by kepler. *Publ. Astron. Soc. Aust.* 33, e011. doi:10.1017/pasa.2016.9

Suárez, J. C. (2009). "Analysis of the internal rotation profile of stars using rotational mode splitting asymmetries," in *Stellar pulsation: Challenges for theory and observation*. Editors J. A. Guzik and P. A. Bradley (Santa Fe NM, USA: American Institute of Physics Conference Series), 1170, 370–372. doi:10.1063/1.3246515

Suárez, J. C., García Hernández, A., Moya, A., Rodrigo, C., Solano, E., Garrido, R., et al. (2014). Measuring mean densities of δ Scuti stars with asteroseismology. Theoretical properties of large separations using TOUCAN. *Astron. Astrophys.* 563, A7. doi:10.1051/0004-6361/201322270

Szewczuk, W., and Daszyńska-Daszkiewicz, J. (2018). KIC 3240411 - the hottest known SPB star with the asymptotic g-mode period spacing. *Mon. Not. R. Astron. Soc.* 478, 2243–2256. doi:10.1093/mnras/sty1126

Szewczuk, W., Walczak, P., Daszyńska-Daszkiewicz, J., and Moździerski, D. (2022). Seismic modelling of a very young SPB star - KIC 8264293. *Mon. Not. R. Astron. Soc.* 511, 1529–1543. doi:10.1093/mnras/stac168

Szewczuk, W., Walczak, P., and Daszyńska-Daszkiewicz, J. (2021). Variability of newly identified B-type stars observed by Kepler. *Mon. Not. R. Astron. Soc.* 503, 5894–5928. doi:10.1093/mnras/stab683

Takata, M., Ouazzani, R. M., Saio, H., Christophe, S., Ballot, J., Antoci, V., et al. (2020a). A diagnostic diagram for γ Doradus variables and slowly pulsating B-type stars. *Astron. Astrophys.* 635, A106. doi:10.1051/0004-6361/201936297

Takata, M., Ouazzani, R. M., Saio, H., Christophe, S., Ballot, J., Antoci, V., et al. (2020b). Inferring the internal structure of γ Doradus variables from Rossby modes. Extension of the ν - diagram. *Astron. Astrophys.* 644, A138. doi:10.1051/0004-6361/202038098

Takata, M. (2014). Rosette modes of oscillations of rotating stars caused by close degeneracies. III. JWKB analysis. *Publ. Astron. Soc. Jpn. Nihon. Tenmon. Gakkai.* 66, 80. doi:10.1093/pasj/psu055

Takata, M., and Saio, H. (2013). Rosette modes of oscillations of rotating stars caused by close degeneracies. I. Axisymmetric modes. *Publ. Astron. Soc. Jpn. Nihon. Tenmon. Gakkai.* 65, 68. doi:10.1093/pasj/65.3.68

Takeda, Y., Kawanomoto, S., and Ohishi, N. (2008). Rotational feature of Vega revealed from spectral line profiles. *Astrophys. J.* 678, 446–462. doi:10.1086/528949

Tassoul, M. (1980). Asymptotic approximations for stellar nonradial pulsations. *Astrophys. J. Suppl. Ser.* 43, 469–490. doi:10.1086/190678

Telting, J. H., and Schrijvers, C. (1998). A new bright beta Cephei star: Line-profile variability in omega1˙ SCO. *Astron. Astrophys.* 339, 150.

Telting, J. H., and Schrijvers, C. (1997). Line-profile variations of non-radial adiabatic pulsations of rotating stars. II. The diagnostic value of amplitude and phase diagrams derived from time series of spectra. *Astron. Astrophys.* 317, 723.

Tokuno, T., and Takata, M. (2022). Asteroseismology of the dip structure in period-spacings of rapidly rotating γ Doradus stars caused by the coupling between core and envelope oscillations. *Mon. Not. R. Astron. Soc.* 514, 4140–4159. doi:10.1093/mnras/stac1492

Townsend, R. H. D. (1997). Spectroscopic modelling of non-radial pulsation in rotating early-type stars. *Mon. Not. R. Astron. Soc.* 284, 839–858. doi:10.1093/mnras/284.4.839

Triana, S. A., Corsaro, E., De Ridder, J., Bonanno, A., Pérez Hernández, F., and García, R. A. (2017). Internal rotation of 13 low-mass low-luminosity red giants in the Kepler field. *Astron. Astrophys.* 602, A62. doi:10.1051/0004-6361/201629186

Unno, W., Osaki, Y., Ando, H., Saio, H., and Shibahashi, H. (1989). *Nonradial oscillations of stars*. University of Tokyo Press.

Van Reeth, T., Tkachenko, A., and Aerts, C. (2016). Interior rotation of a sample of γ Doradus stars from ensemble modelling of their gravity-mode period spacings. *Astron. Astrophys.* 593, A120. doi:10.1051/0004-6361/201628616

Van Reeth, T., Tkachenko, A., Aerts, C., Pápics, P. I., Triana, S. A., Zwintz, K., et al. (2015). Gravity-mode period spacings as a seismic diagnostic for a sample of γ doradus stars from kepler space photometry and high-resolution ground-based spectroscopy. *Astrophys. J. Suppl. Ser.* 218, 27. doi:10.1088/0067-0049/218/2/27

von Zeipel, H. (1924). The radiative equilibrium of a rotating system of gaseous masses. *Mon. Not. R. Astron. Soc.* 84, 665–684. doi:10.1093/mnras/84.9.665

Vrard, M., Mosser, B., and Samadi, R. (2016). Period spacings in red giants. *Astron. Astrophys.* 588, A87. doi:10.1051/0004-6361/201527259

Weiss, W. W., Rucinski, S. M., Moffat, A. F. J., Schwarzenberg-Czerny, A., Koudelka, O. F., Grant, C. C., et al. (2014). BRITE-Constellation: Nanosatellites for precision photometry of bright stars. *Publ. Astron. Soc. Pac.* 126, 573–585. doi:10.1086/677236

Wu, T., Li, Y., Deng, Z.-m., Lin, G.-f., Song, H.-f., and Jiang, C. (2020). Asteroseismic analyses of slowly pulsating B star KIC 8324482: Ultraweak element mixing beyond the central convective core. *Astrophys. J.* 899, 38. doi:10.3847/1538-4357/aba430

Xiong, D. R., Deng, L., Zhang, C., and Wang, K. (2016). Turbulent convection and pulsation stability of stars - II. Theoretical instability strip for δ Scuti and γ Doradus stars. *Mon. Not. R. Astron. Soc.* 457, 3163–3177. doi:10.1093/mnras/stw047

Zahn, J.-P. (1992). Circulation and turbulence in rotating stars. *Astron. Astrophys.* 265, 115.

Zhang, X. B., Fu, J. N., Luo, C. Q., Ren, A. B., and Yan, Z. Z. (2018). Seismic study of the γ doradus-type pulsations in the eclipsing binary KIC 10486425. *Astrophys. J.* 865, 115. doi:10.3847/1538-4357/aadd9a

Zhao, M., Monnier, J. D., Pedretti, E., Thureau, N., Mérand, A., ten Brummelaar, T., et al. (2009). Imaging and modeling rapidly rotating stars: α Cephei and α Ophiuchi. *Astrophys. J.* 701, 209–224. doi:10.1088/0004-637x/701/1/209

Zhevakin, S. A. (1963). Physical basis of the pulsation theory of variable stars. *Annu. Rev. Astron. Astrophys.* 1, 367–400. doi:10.1146/annurev.aa.01.090163.002055

Zima, W. (2006). A new method for the spectroscopic identification of stellar non-radial pulsation modes I. The method and numerical tests. *Astron. Astrophys.* 455, 227–234. doi:10.1051/0004-6361:20064876

Zima, W. (2008). FAMIAS user manual. *Commun. Asteroseismol.* 155, 17–121. doi:10.1553/cia155s17

Zima, W., Wright, D., Bentley, J., Cottrell, P. L., Heiter, U., Mathias, P., et al. (2006). A new method for the spectroscopic identification of stellar non-radial pulsation modes. II. Mode identification of the δ Scuti star FG Virginis. *Astron. Astrophys.* 455, 235–246. doi:10.1051/0004-6361:20064877

frontiers | Frontiers in Astronomy and Space Sciences

TYPE Original Research
PUBLISHED 07 November 2022
DOI 10.3389/fspas.2022.932499

OPEN ACCESS

EDITED BY
Antonio García Hernández,
University of Granada, Spain

REVIEWED BY
Ernst Paunzen,
Masaryk University, Czechia
Patricia Jeanne Lampens,
Royal Observatory of Belgium, Belgium

*CORRESPONDENCE
Mariel Lares-Martiz,
martiz_mariel@hotmail.com

SPECIALTY SECTION
This article was submitted to Stellar and Solar Physics,
a section of the journal Frontiers in Astronomy and Space Sciences

RECEIVED 29 April 2022
ACCEPTED 27 September 2022
PUBLISHED 07 November 2022

CITATION
Lares-Martiz M (2022), Asteroseismic inferences from the study of non-linearities in δ Sct stars.
Front. Astron. Space Sci. 9:932499.
doi: 10.3389/fspas.2022.932499

Asteroseismic inferences from the study of non-linearities in δ Sct stars

Mariel Lares-Martiz*

Stellar Variability Group, Institute of Astrophysics of Andalusia, Department of Stellar Physics, IAA-CSIC, Granada, Spain

Many pulsating star light curves must be interpreted strictly within the framework of a non-linear theory. The detection of non-linear interactions between pulsation modes has increased due to the ultra-precise photometric data provided by space missions. For this reason, it is now possible and essential to continue the effort of building data-driven non-linear pulsation models. The analysis of non-linear stellar light curves has become a fundamental challenge in asteroseismology in the era of space missions. In this article, a diagnostic method is presented. It is based on an observational characterization of the non-linear behavior of high-amplitude delta Scuti (HADS) stars. It diagnoses the nature of non-linear pulsations in δ Sct stars of lower amplitudes. It potentially provides an extra hint for identifying a radial mode and determine its radial order n. Additionally, it could show signatures of moderate to rapid rotation in these stars. Overall, this article shows the capabilities for making asteroseismic inferences from studying combination frequencies in δ Sct stars.

KEYWORDS

variable stars, asteroseismology, non-linear pulsations, non-linearities, combination frequencies, HADS stars, Delta Scuti stars, Gamma Doradus stars

1 Introduction

The linear pulsation theory cannot explain the special features of some pulsating star light curves. This is the case of the so-called *bump* in Cepheid light curves (Christy, 1964), the sharp ascents and slow descents of luminosity in RR Lyrae (Christy, 1966), δ Sct (Stellingwerf, 1980; Buchler et al., 1997), and white dwarf light curves (Brickhill, 1992; Brassard et al., 1995; Goupil et al., 1998; Wu, 2001; Montgomery, 2005), as well as the upward and downward symmetry in SPB and γ Dor light curves (Kurtz et al., 2015), among other examples. These distortions of the sinusoidal shape of the light curve are effects, in the time domain, of non-linear mechanisms happening within the star. In the frequency domain (e.g., in a power spectrum), the effects or signature of the non-linearities within the star appear as excess power at combination frequencies of the independent pulsation modes. These independent modes are often called parent frequencies, and their interaction generates combination frequencies, often called children frequencies.

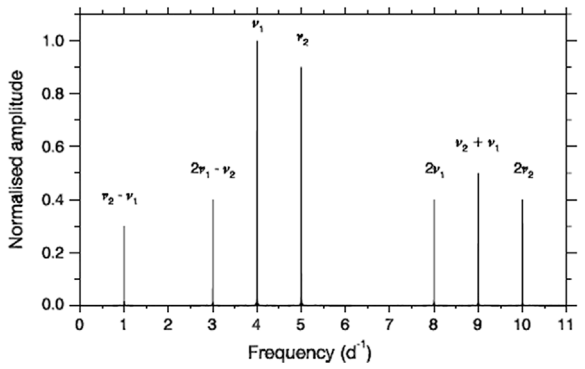

FIGURE 1
Example of fine structure of combination frequencies resembling a rotational splitting. Figure taken from Bowman (2017). Figure inspired by Breger and Kolenberg (2006, Figure 1).

Recently, the subject of non-linear pulsations has attracted new reconsideration and has become a fundamental challenge for asteroseismology. Proper mode identification is critical to model variable stars. It is troublesome even considering only linear modes (Mirouh, this volume). The presence of non-linearities is an additional obstacle to take into account. It is not straightforward to identify combination frequencies from independent modes either. An independent mode of pulsation could be located at the frequency value of a combination by chance. For example, the regularities of the frequency spectrum could be wrongly interpreted as signatures of stellar rotation (Breger and Kolenberg, 2006; Bowman, 2017, see **Figure 1** for a schematic example). This is particularly relevant in δ Sct stars, which often show puzzling power spectra that make it complex to perform mode identification. Fortunately, the ultra-precise photometric data available from space missions allow the detection of more combination frequencies, enabling additional in-depth study of the non-linear behavior exhibited by pulsating stars through observations (Balona, 2012; Kurtz et al., 2015; Bowman et al., 2016; Zong et al., 2018; Van Beeck et al., 2021).

A recurrent issue when studying the non-linear behavior of a pulsating star is the need to unambiguously identify the nature of the combination frequencies. Two distinct physical origins of non-linearities have been widely discussed (Breger and Lenz, 2008; Degroote et al., 2009; Breger and Montgomery, 2014; Balona, 2016; Zong et al., 2016; Bowman, 2017). On the one hand, resonant mode coupling, in which a stable mode becomes unstable (ω_3) if any resonance condition involving an interaction between the parent frequencies (ω_1, ω_2) is met (e.g., $\omega_3 \approx \omega_1 + \omega_2$, $\omega_3 \approx 2\omega_1$, $2\omega_0 \approx \omega_+ + \omega_-$). This is for rotationally induced resonance, where ω_0 is the central frequency of a dipole splitting m = 0, and ω_+ and ω_- corresponds to the m = +1 and m = −1, respectively. For non-radial parent modes, resonance can be helpful for mode identification (Buchler et al., 1997; Goupil et al., 1998).

On the other hand, the stellar medium can behave non-linearly when interacting with pulsation modes, causing short-term retention of the stellar flux and then its release over a longer time. Physically, the non-linear processes/mechanisms involved in observing such asymmetric (or non-sinusoidal) light curves could involve the interaction between the oscillation and the variation of the depth of the convective zone in the outer layer of a pulsating star (Brickhill, 1992; Wu, 2001), the non-linear flux response of the stellar medium induced by surface geometrical and temperature distortions (Brassard et al., 1995), or stellar atmospheric shock waves (Gillet and Fokin, 2014). Most of these theories were developed for white dwarfs and extrapolated to other pulsating stars, where a convective envelope is believed to be present. Combination frequencies resulting from the non-linear response of the stellar medium to pulsation do not have any asteroseismic use for δ Sct stars (Balona, 2012). They are considered spurious frequencies because they are not a solution to the perturbed stellar structure equations, and until now, their main interest has been to identify and remove them from the power spectra.

Distinguishing whether non-linearity is due to mode coupling or to non-linear response surpasses the goal of mode identification. The study of these is also relevant for shedding light on the mode selection processes in these stars, which is still a significant lack in the current theory of δ Sct stars. The excitation and damping mechanisms operating in these stars need to be revised (Balona and Dziembowski, 2011; Balona et al., 2015; Balona, 2018), or other mechanisms that cause amplitude enhancements or decreases in the power spectra that current models are unable to reproduce need to be introduced. In consequence, developing an understanding of non-linearities using high-quality photometry will put a good part of asteroseismic inferences into question.

A special subgroup among the δ Sct variables is the HADS stars. McNamara (2000) characterized this subgroup by defining their peak-to-peak light variation to be $\Delta m \geq 0.3$ mag. This range corresponds to the highest observed amplitudes in δ Sct stars, which vary from thousandths up to tenths of a magnitude (Aerts et al., 2010). This difference suggests that an amplitude-limiting mechanism must operate in δ Sct stars but not in HADS stars (Breger and Montgomery, 2000). Dziembowski and Krolikowska (1985) showed that parametric resonance is the most likely amplitude-limiting mechanism at work in δ Sct stars. Bowman et al. (2016) also argued that the lack of amplitude modulation in HADS stars, which is sometimes a signature of resonant mode coupling, supports the hypothesis that resonance does not function in HADS stars. Furthermore, HADS stars are typically slow rotators and normally pulsate in radial modes (McNamara, 2000; Rodríguez et al., 2000). While some studies have claimed to find non-radial modes present in

HADS (Garrido and Rodriguez, 1996; Pigulski et al., 2006), the resonance of non-radial modes is facilitated by a high rotational velocity (Baade, 1984; Saio et al., 2018), with velocities that are not expected for HADS stars. Consequently, HADS stars might be appropriate objects for studying the stellar envelope's non-linear response. This suggests that they might be resonance-free pulsators, such that the combination frequencies in these stars would be caused only by the non-linear response processes in the stellar envelope. However, it is not a proven fact that HADS are resonance-free pulsators (resonance can also yield constant amplitudes, e.g., bump Cepheids or double-mode Cepheids).

Here a new diagnostic method is presented to make asteroseismic inferences from the study of non-linearities. From an empirical characterization of the non-linear behavior of HADS stars, the method can identify the physical origin of non-linearities in δ Sct stars of lower amplitudes. This method can potentially identify whether the parent frequencies are radial, thus providing an extra hint for mode identification. It might also show signatures of moderate to fast rotation in HADS stars. The article is organized as follows: **Section 2** describes the method to identify non-linearities in the power spectra and the mathematical framework to study them. In addition, a characterization is presented of non-linear behavior in a set of HADS stars, along with the explanation of the diagnostic method. The results of the application of the method to a sample of δ Sct stars are given in **Section 3**, along with the asteroseismic inferences that can be made. Finally, **Section 4** summarizes the conclusions drawn from this study, open issues, and future work.

2 Data and analysis methods

In signal processing theory, the Volterra expansion describes the output signal of a non-linear system. Garrido and Rodriguez (1996) were the first to propose it as a general framework suitable to describe non-linear light curves. In this framework, the non-linear light curve is described as a sum of sinusoids whose frequencies are independent modes of pulsations and combination frequencies (harmonic, sum and subtraction combinations). Each sinusoid composing an output signal also depends on a set of unknown complex functions called the generalized transfer functions (Γ_O). For example, when the input to a non-linear system is composed of two real-valued sine waves at frequencies ω_0 and ω_1, the output $Y(t)$ can be expressed (see p. 30 in Priestley, 1988) by

$$\begin{aligned} Y(t) = {} & A_0 \cdot \Gamma_1(\omega_0) \cdot e^{i\cdot\omega_0\cdot t+\phi_0} + A_1 \cdot \Gamma_1(\omega_1) \cdot e^{i\cdot\omega_1\cdot t+\phi_1} \\ & + A_0^2 \cdot \Gamma_2(\omega_0,\omega_0) \cdot e^{2\cdot i\cdot\omega_0\cdot t+2\cdot\phi_0} \\ & + A_1^2 \cdot \Gamma_2(\omega_1,\omega_1) \cdot e^{2\cdot i\cdot\omega_1\cdot t+2\cdot\phi_1} \\ & + A_0 \cdot A_1 \cdot \Gamma_2(\omega_0,\pm\omega_1) \cdot e^{i\cdot(\omega_0\pm\omega_1)\cdot t+(\phi_0\pm\phi_1)} \\ & + A_1 \cdot A_0 \cdot \Gamma_2(\omega_1,\pm\omega_0) \cdot e^{i\cdot(\omega_1\pm\omega_0)\cdot t+(\phi_1\pm\phi_0)} + \cdots \end{aligned} \tag{1}$$

The system is entirely determined when the Γ_O functions are fully known. They characterize the non-linear system, and so it is important to properly represent them. Their representation is implemented by relating the Γ_O functions to the Fourier parameters (frequencies, amplitudes, and phases). The following section explains these relations and a method of determining the Fourier parameters.

2.1 The best parent method and the Γ_O functions

In the Volterra expansion framework, explained in detail in Lares-Martiz et al. (2020), it is possible to derive a general expression for the Fourier parameters of the terms composing the light curve of a non-linear system (in our case, a pulsating star). For the frequencies, amplitudes and phases, the general form would be

$$\omega_c = \pm n\omega_i \pm m\omega_j \ldots, \tag{2}$$

$$A_c = |\Gamma_O| \cdot A_i^n \cdot A_j^m, \tag{3}$$

$$\varphi_c = \arg\{\Gamma_O\} + \left(\pm n\varphi_i \pm m\varphi_j\right), \tag{4}$$

where $\omega_{i,j}$, $A_{i,j}$, and $\varphi_{i,j}$ are the frequencies, amplitudes, and phases of the parent modes. Likewise, n and m are integer numbers. Ω_c is a combination frequency, with A_c and φ_c as its corresponding amplitude and phase. $\arg\{\Gamma_O\}$ and $|\Gamma_O|$ are the argument and modulus of the complex generalized transfer functions (Γ_O) characterizing the non-linear system.

2.1.1 The best parent method

The best parent method (BPM) identifies the family of combination frequencies in the power spectrum that follows **Eq. 2**. It guarantees that this family yields the residual light curve with minimum variance. The parents that generate this family are found by building a grid of possible parent modes around a first guess. The initial guesses are selected from peaks where there is excess power matching any of the known period-ratio relations (Suárez and Garrido, 2006, for the fundamental mode P_0 and first overtone P_1: P_0/P_1, and Stellingwerf, 1979, for the fundamental mode and second overtone P_2: P_0/P_2 and for the fundamental mode and third overtone P_3: P_0/P_3). The two most dominant frequencies are chosen if no frequency obeys these period ratios. The advantage of the BPM over other algorithms (e.g., COMBINE; Reegen, 2011) is that the parent search is conducted exhaustively and automatically, achieving great precision in terms of frequency. The details of this method, its performance, and other more advantages are described in Lares-Martiz et al. (2020) and Lares-Martiz (2021).

Eq. 2 is restricted to a two-term expression when computing the BPM. This will avoid fits by chance, as almost any number

can be written as a linear combination of the form of Eq. 2 if this expression has many terms. The integer numbers n and m are chosen so ω_c is never above the Nyquist frequency. The output of the BPM algorithm is a list of statistically significant combination frequencies along with their amplitudes and phases (A_c and Φ_c, respectively). In this study, the statistical significance of each frequency is confirmed with a Student's t-test at a confidence level of 99.9%.

2.1.2 The Γ_O functions

The Volterra expansion depends on the set of complex functions called generalized transfer functions, or Γ_O functions (Eq. (1)). Index O denotes the order of non-linear interactions defined as $O = |n| + |m|$, i.e., Γ_1 represents the system response for each independent frequency, Γ_2 represents the system response for second-order interactions, and so on. The complex generalized transfer functions contain the non-linear physics involved in the star. Therefore, it is of great interest to somehow characterize them. The Γ_O functions must be fully known to obtain a physical model that explains non-linear effects.

From the Volterra expansion (Eqs. 2, 3, 4), the modulus and the argument of the Γ_O functions are

$$A_r = |\Gamma_O| = \frac{A_c}{(A_i)^n (A_j)^m}, \tag{5}$$

$$\Delta\phi = \arg\{\Gamma_O\} = \varphi_c - (\pm n\varphi_i \pm m\varphi_j), \tag{6}$$

where A_r and $\Delta\phi$ are the amplitude ratio and relative phase, respectively, using Simon and Lee (1981) nomenclature.

2.2 The Γ_O functions of HADS stars: The non-linear response Template

The Γ_O functions of 17 HADS stars are studied in this section. Figure 2 shows the modulus and the argument of the Γ_O functions of all statistically significant harmonic, sum, and subtraction combination frequencies detected by BPM in the spectra of the 17 HADS stars. The subtraction combinations (symbols with red circles) seemed to be more scattered in their relative phases or amplitude ratio patterns. A few plausible explanations are provided in Section 4.1.1.3. Regardless of the subtraction problem, we continued to analyze the harmonics and sum combinations, considering the interesting patterns obtained. In Figure 3 we show only the relative phases and amplitude ratios involving harmonic and sum combination frequencies. The y-axis in this figure represents the difference between the observed phase for a combination frequency and the phase that a combination of two signals predicts (Eq. 6). This axis is cyclic (from 0 to 2π rad), and we represent one cycle of the relative phases for simplicity. This means that only combinations up to the order $O = 9$ are represented. The x-axis represents the

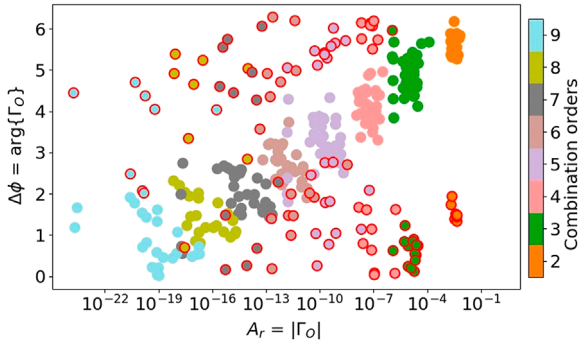

FIGURE 2
Raw template of combination frequencies (harmonics, sums, and subtractions) from the non-linear response. Concretely, up to $O = 9$ of the relative phases and amplitudes ratios for the 17 HADS stars listed in Table 1. Symbols with red circles are the subtraction combinations.

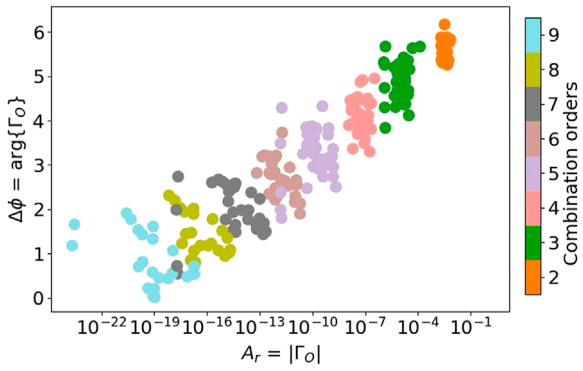

FIGURE 3
Same as Figure 2 but without the subtraction combinations.

amplitude ratios (Eq. 5). Figure 3 therefore shows that the Γ_O functions seem to follow a similar pattern in every HADS star, characterizing their non-linear behavior.

The general pattern seems distorted for 6 of the 17 analyzed HADS stars: the combination frequency orders overlap. From the 6 HADS showing distorted patterns, four of them are mono-periodic, and two are double-mode HADS stars. Although HADS stars are typically slow rotators ($v \sin i \lesssim 30$ km s^{-1}; Rodríguez et al., 2000; McNamara, 2000; Balona, 2016), one of the four mono-periodic stars have moderate rotational velocities range (TIC 126659093: $v \sin i = 35$ km s^{-1}. Value source: Antoci et al., 2019, Table A1). This might distort the relative phases plot (see Figure 4, left plot), allowing us to infer moderate to high rotational velocities in other stars with similar deviations in their relative phases plot (e.g., TIC 261089835 and TIC 431589510, for which no rotation values are available) (see Figure 4, right plot).

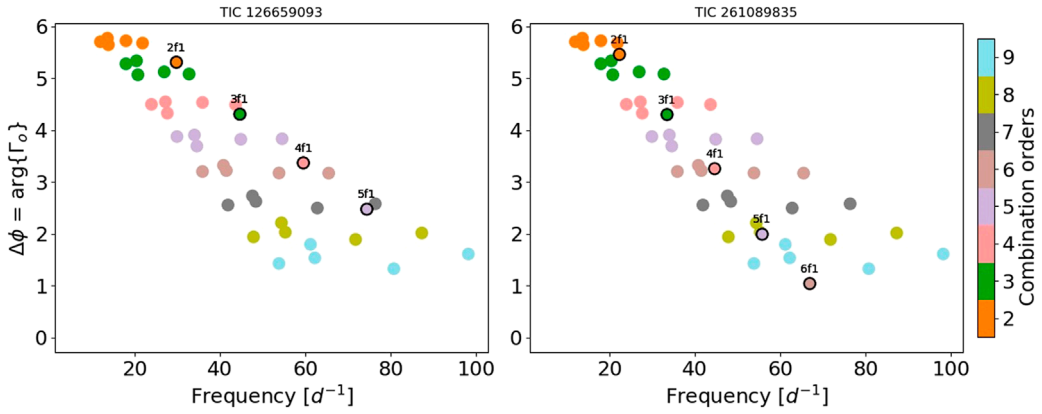

FIGURE 4
Two examples of a distorted relative phases pattern where combination frequency orders seem to overlap. TIC 126659093 has a known moderate rotational velocity ($v \sin i$ = 35 km s^{-1}, Antoci et al., 2019). For TIC 261089835, no rotation velocity is available, but it is an example of inferred moderate or high rotational speed because of similar deviations in their relative phases. Symbols with black circles: relative phases of the HADS star identified in the title of each panel. Symbols without black circles: relative phases of the HADS stars of the Template. For clarity, in the Template of this figure only the mono-periodic HADS stars (without a distorted pattern) are represented.

The two double-mode HADS stars that are showing a distorted pattern (TIC 260654654 and KIC 9408694) have period ratios for their fundamental and first overtone, different from the aforementioned (see **Section 2.1.1**) period-relation typical for δ Sct stars. It is widely known that near-degeneracy of the frequencies becomes very important for rotational velocities larger than about 15–20 km s^{-1} (Suárez et al., 2007). Therefore, it is possible to infer rotational velocities in this range or above for these stars. In fact, KIC 9408694 is a well-known fast rotator ($v \sin i \approx$ 100 km s^{-1} Balona et al., 2012). A sample of the 17 HADS stars is listed in **Table 1**. The HADS stars showing a distorted pattern are marked with a "d" in column 1.

Being able to infer rotational velocities through the study of non-linearities happening in the stellar envelope is a promising conjecture that is worth exploring in future research. However, the case of TIC 9632550, which shows a slightly distorted pattern, is still open for discussion. In Antoci et al. (2019, Table A1), there is a reference to a projected rotational value of $v \sin i$ = 23 km s^{-1}; however, it is also stated that it is a SB2 binary. Therefore, the distortion in the relative phases and amplitude ratio plots may also have an origin in binary interaction, which would be interesting to examine in future research.

Figure 5 shows the relative phases and amplitude ratios of all statistically significant harmonics and sum combination frequencies of the 11 HADS stars that do not show a distorted pattern. As noted in **Section 2.1.2**, the Γ_O functions characterize and represent the non-linear physics that may be involved in the non-linear system, in our case, a pulsating star. Therefore, the akin representation of the Γ_O functions for each HADS star indicates that they all share the same non-linear physical origin. As noted in 1, resonance might not be operating in HADS stars

TABLE 1 Time series information of the HADS stars used in this work.

Star name	Modes	T [d]	δ_t [s]	Obs. Sequence
KIC 5950759	Dm	31.04	58.85	Quarter 4
GSC 00144–03031	Dm	76.67	31.99	Run LRa04
TIC 51991595	Mp	13.04	120.00	Sector 2
TIC 139845816	Mp	13.23	120.00	Sector 1
TIC 144309524	Mp	13.04	120.00	Sector 2
TIC 183532876	Mp	13.04	120.00	Sector 2
TIC 224285325	Dm	13.04	120.00	Sector 2
TIC 231632224	Mp	13.23	120.00	Sector 1
TIC 355547586	Dm	13.23	120.00	Sector 1
TIC 355687188	Dm	13.04	120.00	Sector 2
TIC 358502706	Dm	13.23	119.99	Sector 1
d TIC 9632550	Mp	13.04	120.00	Sector 2
d TIC 126659093	Mp	13.23	120.00	Sector 1
d TIC 260654645	Dm	13.04	120.00	Sector 2
d TIC 261089835	Mp	13.23	120.00	Sector 1
d TIC 431589510	Mp	13.04	120.00	Sector 2
d KIC 9408694	Dm	27.07	58.85	Quarter 6a

T is the length of the observation in days and δ_t is the cadence or sampling rate in seconds. For the TESS and Kepler light curves, we used the instrumental effects free light curve resulting from the Pre-Search data Conditioning (PDC) pipeline, accessible in the Mikulski Archive for Space Telescopes (MAST: https://archive.stsci.edu/). Stars with a distorted relative phase pattern are marked with the letter d ahead of the name. Modes column tells if the star is mono-periodic (Mp) or a double-mode pulsator (Dm).

Bowman et al. (2016), so, under this reasonable assumptions, it is possible to associate the pattern shown in **Figure 5** to non-linearities from the response of the stellar medium to pulsation, meaning that the common physical origin can be associated to non-linear processes happening in the stellar envelope. The form of the Γ_O functions in a pure resonance situation is investigated to prove this. Γ_O functions are expected to show different behavior

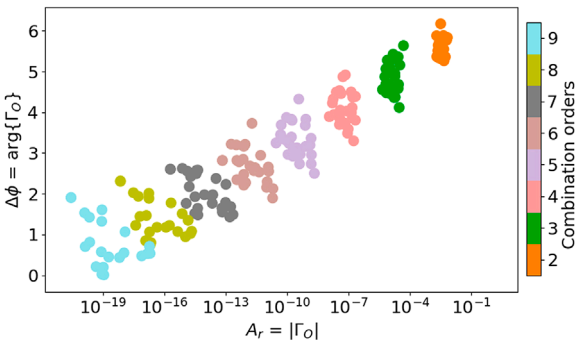

FIGURE 5
Non-linear response Template. Same as **Figure 3**, without the HADS stars showing a distorted pattern which are identified with a 'd' ahead of the identifier in column 1 of **Table 1** (5 mono-periodic and 6 double-mode).

for a different non-linear nature, such as resonance, which it does. This is shown in **Section 3.1.2**.

Additionally, as HADS stars tend to pulsate in radial modes, it is possible to empirically associate the general pattern with the non-linearities of radial pulsations. Indeed, the Volterra expansion does not add any restriction to the type of pulsation mode (in terms of radial or non-radial pulsations). Nonetheless, in this set of 11 HADS stars, the fundamental mode and first overtone period ratio correspond to the expected period ratio for δ Sct stars. Consequently, the affirmation that the regularities in the pattern allude to combination frequencies of radial modes is realistic. Note, however, that this does not mean it cannot indicate to combination frequencies of non-radial modes. In this way, the Γ_O functions in **Figure 5** might imply non-linearities of finite-amplitude radial pulsations. Hereafter, **Figure 5** is referred to as the non-linear response template (the Template).

2.3 The diagnostic plots

The Template can be used to tackle the problem of identifying the physical origin of a combination frequency. As discussed in **Section 1**, in δ Sct stars, this identification is very complex and sometimes cannot be done at all. The possibility of diagnosing a combination frequency nature by plotting the argument and modulus of the Γ_O function over the Template is explored in this study. Such plots are called *Diagnostic plots*, as they test that the argument and modulus of the Γ_O function match the ones from a non-linear response. This empirical methodology was tested in a sample of 117 A-F stars observed by the TESS space satellite.

The BPM was computed for each star of the 117 A-F set using the first two highest amplitude frequencies or, when possible, a pair of frequencies that follow any of the period relations mentioned in **Section 2.1.1**. This ensures that the combination frequencies have independent eigenmodes as parents and not in combinations. In the set of 117 A-F stars, 74 were identified in Antoci et al. (2019) as δ Sct stars or hybrids. By only considering two frequencies as parents, the study will exclude combinations from other parents.

3 Results

3.1 Diagnostic plots for δ Sct stars

Supplementary Table S1 (located in the Supplementary Material section of this article) shows the results of computing the BPM for 74 δ Sct stars (or hybrids). The best possible parents, the combination frequencies detected, and the status of each combination regarding its match or lack of match with respect to the Template are also listed.

Before discussing the diagnostic plots, it is essential to note that combination frequencies can reach amplitudes higher than their parent modes Kurtz et al. (2015). When dealing with radial modes, as in HADS stars, the amplitude ratio pattern characterizes the amplitudes of combination frequencies from the non-linear response mechanism. However, when analyzing δ Sct stars of lower amplitudes, the highest-amplitude peaks (taken as parent frequencies) can be non-radial. Cancellation effects affecting non-radial modes could distort the observed amplitude ratios, causing incorrect discarding of combination frequencies that do not follow the amplitude ratio trend of the Template. For this reason, amplitude ratio patterns are useful to support identification but not to establish the nature of non-linearities.

3.1.1 Matching cases

At least 10 δ Sct stars from the sample of 74 δ Sct stars (or hybrids) matched the Template (**Figure 6**). From the arguments given in **Section 2.2**, we interpret those combination frequencies to be caused by the non-linear response of the stellar medium to pulsation **Figure 7**.

3.1.1.1 Application of the matching cases: Mode identification

Agreement with the Template allows us to identify a combination frequency from the non-linear response. Additionally, it is possible to argue that the parents of such combination frequencies are radial modes. This is supported by the fact that the Template represents the non-linear interaction of independent modes in HADS stars, mainly radial modes (**Section 2.2**). In this way, analyzing combination frequencies might give an extra hint for mode identification. An example of this is TIC 150394126. The identification of f_1+f_2 as being due to the non-linear response nature (because it matches the relative phases for a second order combination frequency of the Template), (see **Figure 7**) could imply that f_1 and f_2 are radial modes. Taking into

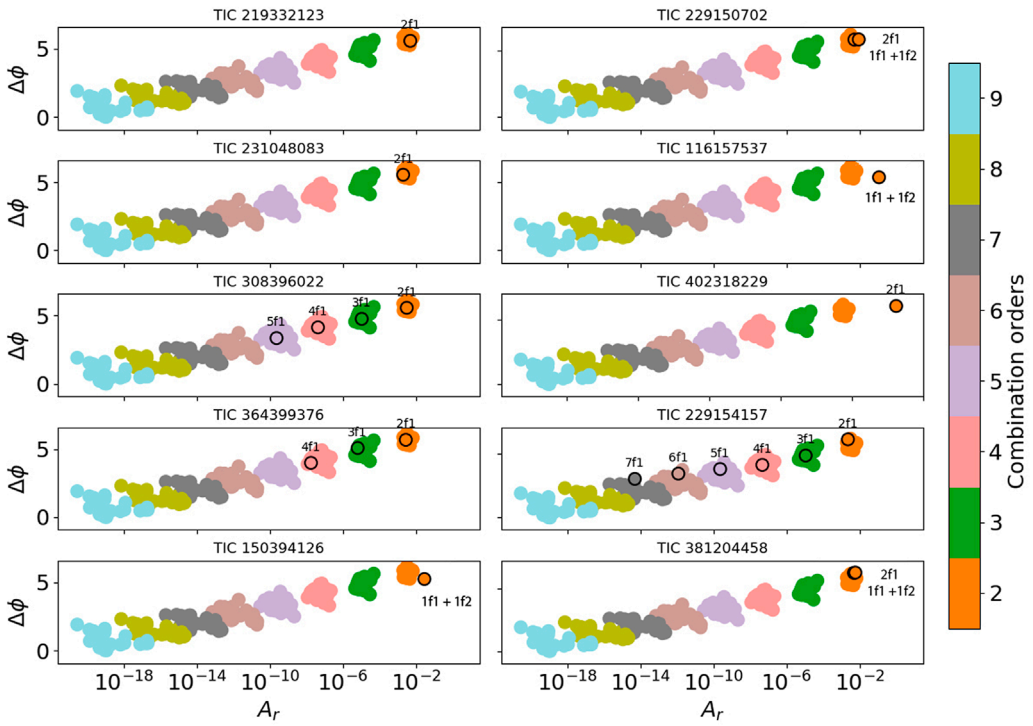

FIGURE 6
Diagnostic plots of combination frequencies matching the non-linear response Template. Matching criterion: the agreement should be in the relative phase (see **Section 3.1**). Symbols with black circles: relative phases and amplitude ratios of the HADS star identified in the title of each panel. Symbols without black circles: relative phases and amplitude ratios of the HADS stars of the Template.

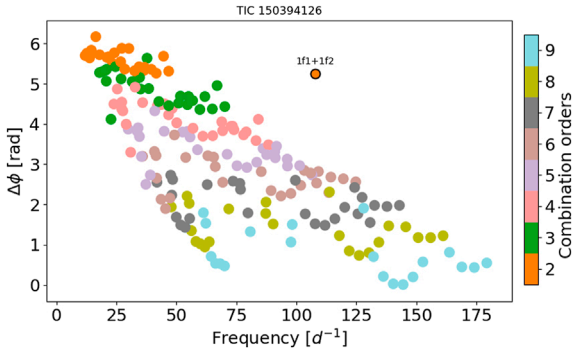

FIGURE 7
Relative phase diagnostic plot for the statistically significant combination frequency $f_1 + f_2$ found in TIC 150394126 (symbol with black circles). Symbols without black circles: relative phases and amplitude ratios of the HADS stars of the Template.

account the period relations of Suárez and Garrido (2006) and Stellingwerf (1979) and that for δ Sct stars, modes of consecutive radial order (at least for radial orders in the range of n = [2–8]) are equally separated by the *large separation* ($\Delta\nu$, similar to the solar-like stars large separation) (García Hernández et al., 2009; Suárez et al., 2014), is possible to estimate the radial orders of f_1 and f_2.

Assuming that $f_1 = \nu_n = 49.08808\ \mathrm{d}^{-1}$ and $f_2 = \nu_{n+1} = 58.58333\ \mathrm{d}^{-1}$ and the combination frequency $f_1 + f_2 = 107.67141\ \mathrm{d}^{-1}$, then

$$\Delta\nu = 9.49525\ \mathrm{d}^{-1}, \tag{7}$$

$$\frac{\nu_n}{\nu_{n+1}} = 0.838, \tag{8}$$

and from Suárez and Garrido (2006)and Stellingwerf (1979) period relations, it is possible to calculate

$$0.818 \leq \frac{\nu_2}{\nu_3} \leq 0.831. \tag{9}$$

Although it is at the limit of the $\frac{\nu_2}{\nu_3}$ range, accounting for the errors suggests f_1 to be a radial mode of radial order $n = 2$ and f_2 to be a radial mode of radial order $n = 3$.

Note that non-linearities are not exclusively linked to radial modes. Because the pattern is built from radial parent modes, it can be said that it works for radial parent modes. Now, does it have the same behavior for non-radial parents? Can partial cancellation mess up with the amplitude ratios? Is the flux

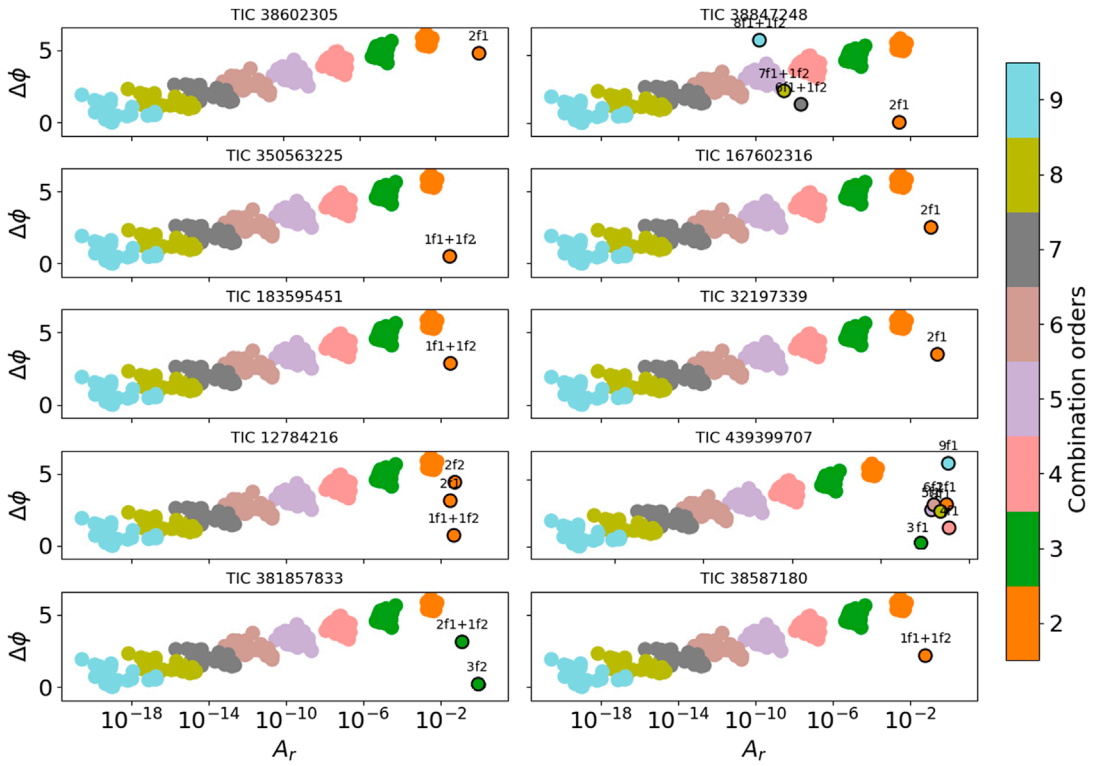

FIGURE 8
Diagnostic plots of combination frequencies not matching the non-linear response Template. Matching criterion: the agreement should be in the relative phase (see **Section 3.1**). Symbols with black circles: relative phases and amplitude ratios of the HADS star identified in the title of each panel. Symbols without black circles: relative phases and amplitude ratios of the HADS stars of the Template.

retained and then released by the same amount in the surface convective layers of the star when this outer stellar medium interacts with non-radial modes? The answer is: possibly—a test to prove it is provided in **Section 3.2**. Here, we offer an example of obtaining an extra hint for mode identification through non-linearities studies if such a pattern is only related to non-linearities of radial parent modes.

3.1.2 No-matching cases

What about the combination frequencies that do not match the non-linear response Template? Such cases are shown in **Figure 8**. Sustained by the arguments given in **Section 2.3**, the interpretations of relative phases disagreeing with the Template could indicate one of these situations:

1. An effect of the non-linear response of the stellar medium to non-radial pulsations (the template for this is still unknown; while it might be the same as the Template, as HADS stars can also pulsate in non-radial modes. This is not proven.).
2. A resonantly excited or coupled mode.
3. An independent mode.

Therefore, not matching the Template would imply that those combination frequencies do not form part of a non-linear response of the stellar medium to radial pulsation modes. Random diagnostic plots refer to the 3^{rd} point. The first and second points are the ones to be differentiated and tested here.

3.1.2.1 Application of the no-matching cases: mode coupling vs non-linear response

As noted in **Section 1**, differentiating whether a combination frequency is due to resonantly excited modes or to a non-linear response could shed some light on the mechanisms of mode selection operating in δ Sct stars. Several studies have discussed the nature of combination frequencies in δ Sct stars to support the mode-coupling theory (Handler et al., 2000; Nowakowski, 2005; Breger and Lenz, 2008; Balona et al., 2012; Breger et al., 2012; Bowman and Kurtz, 2014; Breger and Montgomery, 2014; Barceló Forteza et al., 2015; Bowman et al., 2016). In this section, we focus on the Breger and Montgomery (2014) method, which identifies which frequencies are parents and combinations in addition to discriminating whether a combination frequency

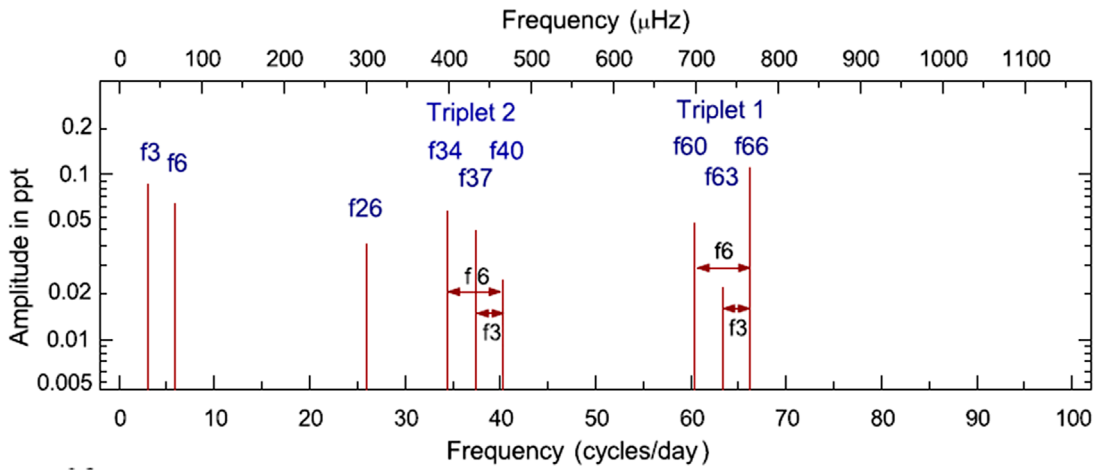

FIGURE 9
Nine most dominant frequencies of the T family. Figure taken from Breger and Montgomery (2014).

is a resonantly excited mode or only an effect from the non-linear response. Their method is based on the assumption that amplitudes of the members of a resonantly coupled family are similar; therefore, larger values of what is called the *coupling factor* ($\mu_c = \frac{A_3}{A_1 A_2}$, where A_3 is the amplitude of the combination and A_1 and A_2 are the amplitude of the parent modes) are expected, in comparison to the expected small value of μ_c if the parents have very different amplitudes (the case for non-linear response family). However, it is important to note that to test their models, the modes must show large-scale amplitude modulation; therefore, the application of their method can be cumbersome since variation in time between all the modes has to be studied to check the expected interchange of energy. By applying this technique, the fast-rotating δ Sct star KIC 8054146 was analyzed by Breger and Montgomery (2014). Their models for the amplitude of the coupled child match observations very precisely. One of their conclusions was that the f_{26} frequency and Triplet 1 contain the parent modes, whereas the Triplet 2 contains the resonantly excited modes (see **Figure 9** for a representation of the frequency distribution.)

In **Figure 10** we represent the diagnostic plot for the f_{40} frequency, the higher frequency component of Triplet 2. Its diagnostic plot was expected not to match the Template as Breger and Montgomery (2014) thorough study concludes (in **Figure 10**, the resonance at $f_{40} = f_{66} - f_{26}$ is marked using the Breger and Montgomery (2014) nomenclature). The relative phase of f_{40} does not match the relative phase for combinations of order 2 when the non-linearity is due to the response nature, supporting Breger and Montgomery's (2014) conclusion.

In **Figure 9**, f_3 represents in reality two very close frequencies ($f_{3a} = 2.9301$ d^{-1} and $f_{3b} = 2.9340$ d^{-1}). Breger and Montgomery (2014) discussed the possibility of f_6 component being a linear combination of the form $2f_{3a}$ or $f_{3a} + f_{3b}$. In

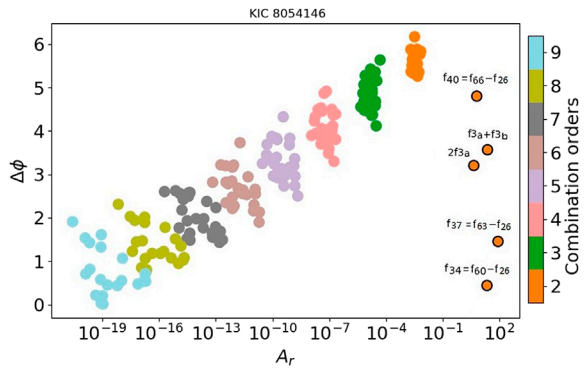

FIGURE 10
Diagnostic plot for combination frequencies in KIC 8054146 between Triplet two and f_{26} (in Breger and Montgomery, 2014, nomenclature) (see **Section 3.1.2** and **Figure 9**). f_{40},f_{34} and f_{37} composing the Triplet one do not follow the Template, supporting Breger and Montgomery (2014)'s conclusion of them being resonantly excited. Same for $f_{3a} + f_{3b}$ and $2f_{3a}$. Symbols with black circles: relative phases and amplitude ratios of KIC 8054146. Symbols without black circles: relative phases and amplitude ratios of the HADS stars of the Template.

Figure 10, we diagnose these components. The relative phase for f_6 is not agreeing with the combination order two zone of the Template, even if this frequency is considered to be $2f_{3a}$ or $f_{3a} + f_{3b}$. In this way, f_6 is not due to the non-linear nature. This is in line with Breger and Montgomery's (2014) conclusion regarding how these low frequencies are resonantly excited.

Relative phases in **Figure 10** are very similar to those in **Figure 8** (e.g., TIC 381857833, TIC 38587180, TIC 32197339, and TIC 183595451, and TIC 350563225). Not matching the Template might be a signature of non-linearities resulting from

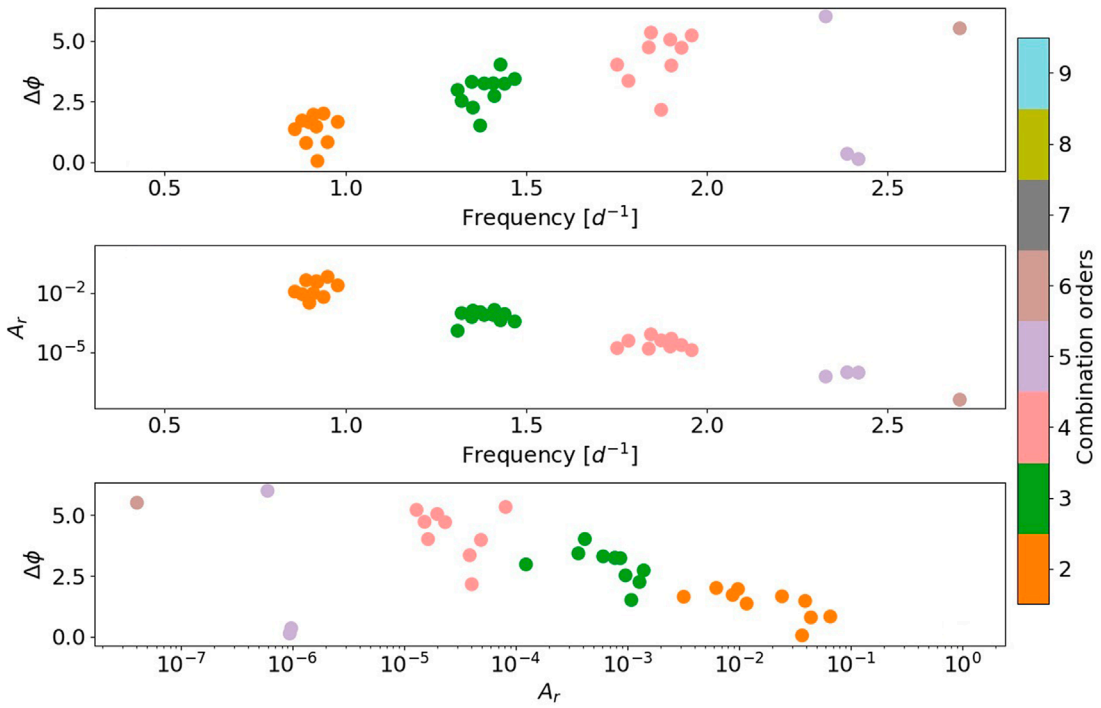

FIGURE 11
Relative phase (upper panel) and amplitude ratio (mid panel) of combination frequencies for KIC 8113425. Relative phase as a function of the amplitude ratio (bottom panel).

resonant mode coupling. Nevertheless, a second possibility can cause a combination frequency not to match the Template. It is still possible that the relative phases and amplitude ratios found in **Figure 8** do match a pattern of non-linear response nature but from non-radial parent modes. This is considered in the next section, where the Γ_O functions of combination frequencies from non-radial parents are studied. The non-radial p-modes identification in δ Sct stars is not clear. To ensure or increase the chances of choosing non-radial modes as parent frequencies (or at least combination frequencies of non-radial parents), we study stars pulsating in the g-mode regime, such as γ Dor stars. As with δ Sct stars, many γ Dor stars show hybrid phenomena, but in the next section, we focus on the g-mode frequency regime to augment the possibilities of choosing non-radial parents.

3.2 The Γ_O functions of γ Dor stars

This section presents the arguments and moduli of the Γ_O functions for three previously studied γ Dor stars. The three γ Dor stars analyzed are KIC 8113425 (Kurtz et al., 2015), KIC 5608334 (Saio et al., 2018), and TIC 30531417 (Antoci et al., 2019). The first and the last ones are chosen since they have strong non-linear light curves; therefore, many non-linearities are expected to be detected. The second one is chosen because previous studies have argued that it meets resonance conditions, so it would be interesting to check their Γ_O functions patterns. Combination frequencies have been detected in their power spectra through BPM analysis.

3.2.1 KIC 8113425

This γ Dor has a strong non-linear light curve whose power spectrum shows the typical frequency groups for these variables (Kurtz et al., 2015). The first four highest peaks of its power spectrum and the two-termed combination frequencies together account for 58.04% of all variability in light. Matching a structure of many combination frequencies by chance or resonant mode coupling is highly improbable. Therefore, this star is a promising target for analyzing the relative phases and amplitude ratios.

The relative phases of the statistically significant combination frequencies for KIC 8113425 are shown in the upper panel of **Figure 11**. Although they take very different values, the arguments of the Γ_O functions follow an increasing trend with the order of the combinations and with the frequency. This is because relative phases increase with the frequency in g-mode pulsators, contrary to the p-mode case, which shows a decrease in frequency. Interestingly, this agrees with the asteroseismic fact that frequency increases with the radial order n in p-modes, whereas the frequency decreases in g-modes. The reader

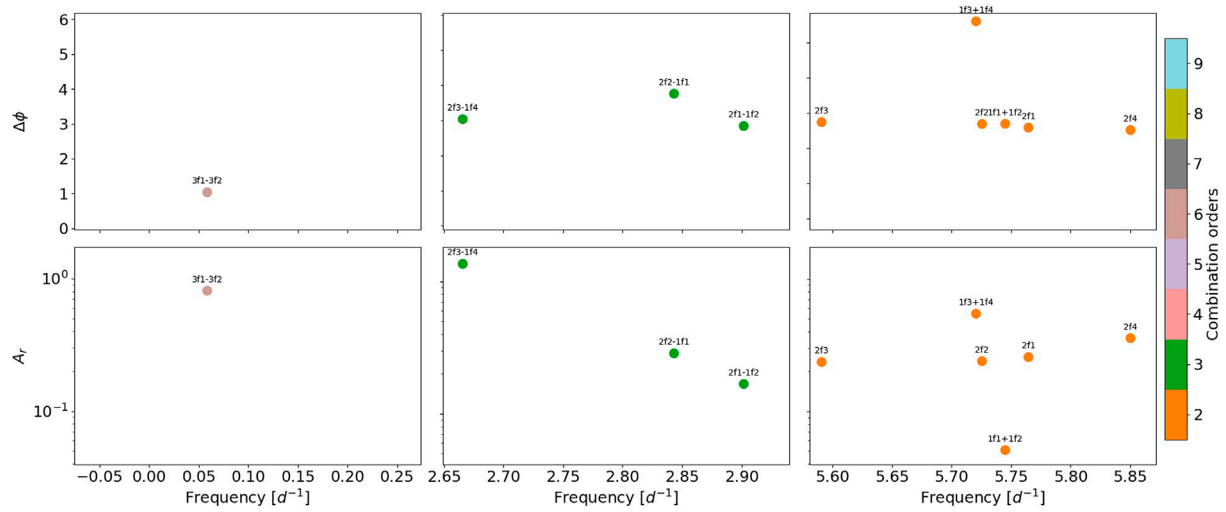

FIGURE 12
Relative phase (upper panels) and amplitude ratio (bottom panels) of harmonics, sums, and subtraction combination frequencies of KIC 5608334.

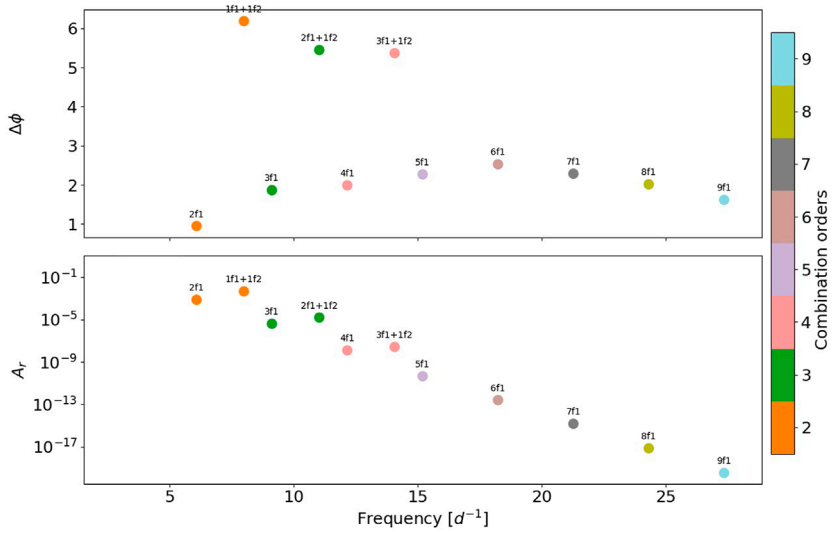

FIGURE 13
Relative phase (upper panel) and amplitude ratio (bottom panel) for sums and harmonics combination frequencies of TIC 30531417.

should recall that the y-axis is cyclic, the statistically significant frequencies of order five do not show a discontinuity.

In γ Dor stars, the non-linearities may come from non-radial parent modes, so cancellation effects could affect the observed amplitudes, enabling the possibility of combination frequencies having higher amplitudes than their parents (Kurtz et al., 2015). However, this does not seem to be happening in this star, as seen in the amplitude ratios (mid panel of **Figure 11**). As in the p-mode case, one can plot relative phases as a function of amplitude ratios (Bottom panel of **Figure 11**). This γ Dor star, we might see proof that it does not matter whether the mode is radial or non-radial, as there is also clustering in terms of the order of the combination. However, the clustering occurs in the opposite direction (increasing order on the y-axis), possibly because the parent is a g-mode. Building these plots to develop a more significant sample would help discern whether the increasing or decreasing order on the y-axis is due to the radial or non-radial nature of the mode or the g-mode or p-mode nature.

3.2.2 KIC 5608334

The relative phases and amplitude ratios for the harmonics, sum and subtraction combination frequencies detected in KIC 5608334 are plotted in **Figure 12**. If the relative phase value does not match the Template, this might suggest that the modes are resonantly excited, as observed in δ Sct stars (see **Section 3.1.2**).

The resonance of non-radial modes is facilitated by a high rotational velocity (Baade, 1984). Saio et al. (2018) studied this star and showed how the detected combination frequencies in this star are the consequences of rotationally induced resonance due to its rapid rotation ($v \sin i \approx 74$–163 km s^{-1}). Therefore, KIC 5608334 is another example of a reported case of pure resonance showing relative phases not matching the Template. This example strengthens the assumption of how relative phases and amplitude ratios behave when the combination frequencies are caused by the resonance mechanism.

3.2.3 TIC 30531417

TIC 30531417 shows a very regular light curve. The principal component of the power spectrum belongs to the g-mode frequency range ($0.3 < \nu < 3$ d^{-1}) but presents an unusually high amplitude for its pulsation variability (0.33 peak-to-peak mag) for a γ Dor star (typically of 0.1 mag Paunzen et al., 2020). For this reason, it was baptized by Antoci et al. (2019) as a high-amplitude γ Dor (HAGD) star. The BPM was computed first for the highest-amplitude peak, extracting almost all the harmonics. A second mode was detected at $\nu_2 = 4.96067$ d^{-1} after inspection of the residual light curve.

The relative phases were expected to follow an increasing pattern, similar to the first γ Dor analyzed in this section (KIC 8113425). Unfortunately, this hypothesis is not supported (see **Figure 13**). The relative phase of the principal component, whose frequency is in the g-mode regime, seems to be increasing with frequency and with the combination order. However, it does not grow at the same rate as KIC 8113425, and from $6f_1$, it starts to decrease. These different growing rates could indicate that it is not the same type of pulsator. Looking at the log(g) value (3.44423), it appeared to be a quite evolved star, and in the SIMBAD Astronomical Database, it is catalogued as an RR-Lyrae. Regarding ν_2, the second-order harmonic seems to follow the non-linear response Template, so ν_2 is possibly a radial p-mode.

4 Discussion

Using the Volterra expansion as a general framework to model the non-linear behavior of pulsating stars has proven efficient. It has served to develop a self-consistent method that determines, with great precision, the combination frequencies composing a light curve (Lares-Martiz et al., 2020). Additionally, studying the Volterra-based phase differences and amplitude ratios allowed us to characterize the non-linear behavior of finite-amplitude pulsations in HADS stars for the first time. The Γ_O functions represent the non-linear physical process involved in the non-linear behavior. They follow a similar pattern for all the HADS stars, implying that their non-linearities have the same physical origin. Furthermore, the patterns for reported resonance cases are very different from the behavior seen in HADS stars. All these findings support the statement of Bowman et al. (2016), that resonances are not present in HADS stars. Therefore, non-linearities in HADS stars can be associated with the non-linear response of the stellar envelope to pulsation.

Under the reasonable assumption that non-linearities in HADS stars are due to the non-linear response processes, in this article, I present a method that diagnoses the nature of a combination frequency in lower-amplitude δ Sct stars. Whether they match or do not match the heuristic Template for non-linearities in HADS stars, we can distinguish combination frequencies from the non-linear response from other non-linear processes (such as resonance) or independent modes of pulsation. Results of the application of this innovative method hold promising implications for non-linear asteroseismology. For example, there are more combination frequencies in the small sample of 17 HADS stars than in the 74 δ Sct stars sample. This fact supports the generally accepted explanation for the high amplitudes observed in HADS stars, which is the lack of an amplitude-limiting mechanism (Breger and Montgomery, 2000). Also, it supports the Dziembowski and Krolikowska (1985) claim of parametric resonance as the most likely amplitude-limiting mechanism operating in δ Sct stars of lower amplitudes.

Diagnostic charts provide intriguing conjectures, suggesting that the non-linearities are more useful for asteroseismic inferences than previously thought. However, we acknowledge that many questions arise as to the interpretations of the diagnostic plots. For example, is the Template for combination frequencies of radial parent modes only? Indeed, the Template was found in HADS stars, mainly radial pulsators. Because of this argument, it is possible to conjecture that combination frequency matching the Template gives an extra hint for mode identification, supposing that its parents are radial. Nonetheless, HADS stars also pulsate in non-radial modes, and the Volterra expansion does not limit the possibility of the Template showing the same regularities in the case of combination frequencies with non-radial parents. Despite previous efforts (see **Section 3.2**), whether the pattern remains the same for non-radial modes remains an open question.

The non-matching cases also raised interpretations that could be convenient when making asteroseismic inferences. An example of not-matching the general Template occurs when the pattern is distorted, meaning that the combination overlaps across different orders of the Template. It is possible to associate this signature with moderate to high rotational velocities (see **Section 2.2** and **Figure 4**). Still, this needs to be

proven to a larger sample to remove the label of speculation. Suppose the pattern does not match the Template at all. In that case, this indicates other possibilities of reproducing non-linear signatures: resonantly excited modes, independent modes whose frequency lies close to a combination value by chance, or the possibility of non-linearities of non-radial parents. Comparing the results of the disagreeing diagnostic plots for the sample of 74 δ Sct stars with reported cases of resonant mode coupling, it was found that the patterns are broadly comparable. The Breger and Montgomery (2014) method to distinguish the nature of a combination frequency requires significant amplitude modulation in three modes with similar amplitudes. Finding such cases is not easy because the time variability of each combination member and the variations between all the signal components must be tracked. In this sense, the diagnostic plots provide a way to establish the non-linear response nature of the combination frequency, and if it does not match the Template, then recur to a more in-depth study such as Breger and Montgomery's.

More questions arise regarding the subtraction combinations and the Fourier parameters time modulation. Therefore, the following subsections will discuss apparent limitations or open issues for establishing diagnostic plots as a completely reliable method.

4.1 Open issues and future work

4.1.1 Open issues

4.1.1.1 Amplitude and phase time modulation

So far, the amplitude and phases of each combination frequency are calculated for the entire light curve as if they were constant. The time variability of the Fourier parameters could affect the relevance of the diagnostic method. Mainly, we discuss the possibility of the relative phases being jeopardized by the time variability of any of the parameters. We leave out the amplitude ratios from the discussion as we already acknowledge that this plot may be compromised by other mechanisms (e.g., partial cancellation of the parent modes).

A phase variation as a function of time is introduced in a one-component signal $Y(t)$ in the following way:

$$Y(t) = A\cos\left(\omega t + \phi(t)\right), \tag{10}$$

and the phase function of time can be represented by a Taylor series

$$\phi(t) \approx \phi_0 + \phi'(t)\,t + \cdots, \tag{11}$$

where $\phi'(t) \equiv \tilde{\omega}$, then

$$Y(t) = A\cos\left(\omega t + \phi_0 + \phi'(t) + \cdots\right) \approx A\cos\left((\omega + \tilde{\omega})\,t + \phi_0\right). \tag{12}$$

If the phase variation is small, it translates into a slight frequency shift. Moreover, the observed phase (ϕ_0) is the same as if there were no phase variation. Consequently, the patterns of the relative phase plots are not compromised by the phase modulation.

4.1.1.2 Non-radial modes

The Template is true for radial parent modes, and because of this was possible to conjecture that it might give an extra hint for mode identification. Nonetheless, the Volterra expansion does not limit the possibility of the Template showing the same regularities in the case of combination frequencies with non-radial parents. Therefore, we attempted to show how the relative phases and amplitude ratios plot looks for combination frequencies of non-radial parents in γ Dor stars, where the chance of choosing non-radial parent modes is higher (or at least combinations of non-radial parents).

The characterization of non-linearities observed in g-mode pulsators, particularly for γ Dor stars, is far from complete. Under the theoretical formulations presented in this work and the three stars analyzed, finding a pattern that would unite them all was impossible. However, examination of it yielded relevant results. In KIC 5608334, a γ Dor star previously known to show a rotationally induced resonant mode coupling (see **Section 3.2.2**), the relative phases have values around 0, π, and 2π. The patterns differed from the resonant mode coupling case in the other two γ Dor stars. The pattern seemed clustered and clear, increasing in relative phases with the order of combination (although at different rates depending on the star). G-modes interacting with the stellar envelope might show different non-linear responses. This might be possible due to an unknown dependence on the frequency of the Γ_O functions. If this is true, one can distinguish g-modes from p-modes. An example can be seen in **Figure 13**, where $f1$ is probably a g-mode, where its relative phases increase with the frequency up to a point where the response change and start to decrease. Moreover, it is possible to argue that $f2$ is a radial p-mode because the combinations involving $f2$ show a similar response as for HADS stars radial p-modes, but not the same because the g-mode $f1$ is also involved.

The generalized transfer functions of A/F-type hybrid pulsators are not yet well-characterized. Carrying out the relative phases and amplitude ratios study to a larger sample of γ Dor stars and δ Sct stars with non-radial modes will investigate to what extent the generalized Γ_O functions can be helpful to characterize the non-linear behavior in these stars.

4.1.1.3 Subtraction combinations

Difference combinations in HADS stars showed scattered relative phases and amplitudes ratio plots (see symbols with red circles in **Figure 2**). When fitting the Fourier parameters, errors of the parameters corresponding to subtraction combinations were higher. The low-amplitude δ Sct stars showed very

scattered values of relative phases and amplitude ratios for the subtractions, even for the stars showing agreement with the Template. This might have an explanation in the fact that their amplitudes may be smaller than the detection threshold, so the fitted frequencies are other independent modes in the low-frequency regime (e.g., rotation signatures or g-modes in the case of a hybrid star). It could also be due to an unknown dependence of the Γ_O functions on the frequency. Another possible explanation is that subtraction does not hold the commutative property (see **Eq. 6**). As a result, the phase would be different regarding the order of the factors in the subtraction, implying that somehow the Γ_O functions may not be symmetric, meaning that

$$arg\{\Gamma_2(\omega_0, \pm\omega_1)\} = \tilde{\phi_{obs}} - (\phi_0 \pm \phi_1), \tag{13}$$

is different from

$$arg\{\Gamma_2(\omega_1, \pm\omega_0)\} = \tilde{\phi_{obs}} - (\phi_1 \pm \phi_0). \tag{14}$$

4.1.2 Future work

Ultimately, the broad implication of the present research is that to confirm the conclusions obtained in this work, it would be necessary to carry out a systematic and as complete as possible comparative study of the phenomenon of non-linearities in a sample of different pulsating stars. The sample should cover various masses, evolutionary stages, metallicities, and rotational velocities. It is worthwhile to continue the work of Garrido and Rodriguez (1996) and Lares-Martiz et al. (2020), who provided a promising method to model non-linear behavior in δ Sct stars. Studying the Γ_O functions is a convenient and feasible way to build data-driven non-linear asteroseismic models. Thanks to the legacy data from CoRoT, Kepler, and TESS, we have hundreds to thousands of high-accuracy light curves of pulsating stars at our disposal to perform a complete statistical study. Such a study will significantly impact the understanding of the phenomenon of non-linearities and how pulsation spectra of any star are determined. This might mean a complete revision of the asteroseismological results carried out to date and thus of the data analysis pipelines of current and future missions such as PLATO.

Data availability statement

Publicly available datasets were analyzed in this study. These data can be found at: https://tasoc.dk/search_data/, https://archive.stsci.edu/.

Author contributions

The author MM contributed to the conception and design of the study, organized the data, performed the analysis, and wrote the sections of the manuscript.

Funding

The author MM acknowledges funding support from Spanish public funds for research under project ESP 2017-87676-C5-5-R. Author acknowledge financial support from the State Agency for Research of the Spanish MCIU through the "Center of Excellence Severo Ochoa" award to the Instituto de Astrofísica de Andalucía (SEV-2017-0709).

Acknowledgments

MM acknowledges financial support from the State Agency for Research of the Spanish MCIU through the "Center of Excellence Severo Ochoa" award to the Instituto de Astrofísica de Andalucía (SEV-2017-0709). The author wants to thank the IP and colleagues of the GVE team in IAA for all the comments and feedback while conducting this research. The author also wants to thank GM Mirouh, for his tips and comments during the writing of this article.

Conflict of interest

The author declares that the research was conducted in the absence of any commercial or financial relationships that could be construed as a potential conflict of interest.

Publisher's note

Supplementary material

The Supplementary Material for this article can be found online at: https://www.frontiersin.org/articles/10.3389/fspas.2022.932499/full#supplementary-material

References

Aerts, C., Christensen-Dalsgaard, J., and Kurtz, D. W. (2010). *Asteroseismology*. Dordrecht: Springer.

Antoci, V., Cunha, M. S., Bowman, D. M., Murphy, S. J., Kurtz, D. W., Bedding, T. R., et al. (2019). The first view of δ Scuti and γ Doradus stars with the TESS mission. *Mon. Not. R. Astron. Soc.* 490, 4040–4059. doi:10.1093/mnras/stz2787

Baade, D. (1984). Discovery and preliminary identification of two retrograde nonradial pulsation modes in the Be star MU Centauri. *Astronomy Astrophysics* 135, 101

Balona, L. A. (2016). Combination frequencies in high-amplitude δ Scuti stars. *Mon. Not. R. Astron. Soc.* 459, 1097–1103. doi:10.1093/mnras/stw671

Balona, L. A. (2012). Combination frequencies in δ Scuti stars. *Mon. Not. R. Astron. Soc.* 422, 1092–1097. doi:10.1111/j.1365-2966.2012.20682.x

Balona, L. A., Daszyńska-Daszkiewicz, J., and Pamyatnykh, A. A. (2015). Pulsation frequency distribution in δ Scuti stars. *Mon. Not. R. Astron. Soc.* 452, 3073–3084. doi:10.1093/mnras/stv1513

Balona, L. A., and Dziembowski, W. A. (2011). Kepler observations of δ Scuti stars. *Mon. Not. R. Astron. Soc.* 417, 591–601. doi:10.1111/j.1365-2966.2011.19301.x

Balona, L. A. (2018). Gaia luminosities of pulsating A-F stars in the Kepler field. *Mon. Not. R. Astron. Soc.* 479, 183–191. doi:10.1093/mnras/sty1511

Balona, L. A., Lenz, P., Antoci, V., Bernabei, S., Catanzaro, G., Daszyńska-Daszkiewicz, J., et al. (2012). Kepler observations of the high-amplitude δ Scuti star V2367 Cyg. *Mon. Not. R. Astron. Soc.* 419, 3028–3038. doi:10.1111/j.1365-2966.2011.19939.x

Barceló Forteza, S., Michel, E., Roca Cortés, T., and García, R. A. (2015). Evidence of amplitude modulation due to resonant mode coupling in the δ Scuti star KIC 5892969. A particular or a general case? *Astron. Astrophys.* 579, A133. doi:10.1051/0004-6361/201425507

Bowman, D. M. (2017). *Amplitude modulation of pulsation modes in delta Scuti stars*. Leuven: Springer Cham. doi:10.1007/978-3-319-66649-5

Bowman, D. M., Kurtz, D. W., Breger, M., Murphy, S. J., and Holdsworth, D. L. (2016). Amplitude modulation in δ Sct stars: Statistics from an ensemble study of Kepler targets. *Mon. Not. R. Astron. Soc.* 460, 1970–1989. doi:10.1093/mnras/stw1153

Bowman, D. M., and Kurtz, D. W. (2014). Pulsational frequency and amplitude modulation in the δ Sct star KIC 7106205. *Mon. Not. R. Astron. Soc.* 444, 1909–1918. doi:10.1093/mnras/stu1583

Brassard, P., Fontaine, G., and Wesemael, F. (1995). The modeling of energy distributions and light curves of ZZ Ceti stars. 1: Basic theory and semianalytic expressions for the emergent flux. *Astrophys. J. Suppl. Ser.* 96, 545–580. doi:10.1086/192128

Breger, M., Fossati, L., Balona, L., Kurtz, D. W., Robertson, P., Bohlender, D., et al. (2012). Relationship between low and high frequencies in δ Scuti stars: Photometric kepler and spectroscopic analyses of the rapid rotator KIC 8054146. *Astrophys. J.* 759, 62. doi:10.1088/0004-637X/759/1/62

Breger, M., and Kolenberg, K. (2006). Equidistant frequency triplets in pulsating stars: The combination mode hypothesis. *Astron. Astrophys.* 460, 167–172. doi:10.1051/0004-6361:20065808

Breger, M., and Lenz, P. (2008). Amplitude variability and multiple frequencies in 44 tauri: 2000-2006. *Astron. Astrophys.* 488, 643–651. doi:10.1051/0004-6361:200810187

Breger, M., and Montgomery, M. (2000). Delta Scuti and related stars." in Astronomical Society of the Pacific Conference Series. 210

Breger, M., and Montgomery, M. H. (2014). Evidence of resonant mode coupling and the relationship between low and high frequencies in a rapidly rotating a star. *Astrophys. J.* 783, 89. doi:10.1088/0004-637X/783/2/89

Brickhill, A. J. (1992). The pulsations of ZZ Ceti stars - V. The light curves. *Mon. Notices R. Astronomical Soc.* 259, 519–528. doi:10.1093/mnras/259.3.519

Buchler, J. R., Goupil, M. J., and Hansen, C. J. (1997). On the role of resonances in nonradial pulsators. *Astronomy Astrophysics* 321, 159

Christy, R. F. (1966). A study of pulsation in RR Lyrae models. *Astrophys. J.* 144, 108. doi:10.1086/148593

Christy, R. F. (1964). The calculation of stellar pulsation. *Rev. Mod. Phys.* 36, 555–571. doi:10.1103/RevModPhys.36.555

Degroote, P., Aerts, C., Ollivier, M., Miglio, A., Debosscher, J., Cuypers, J., et al. (2009). CoRoT's view of newly discovered B-star pulsators: Results for 358 candidate B pulsators from the initial run's exoplanet field data. *Astron. Astrophys.* 506, 471–489. doi:10.1051/0004-6361/200911884

Dziembowski, W., and Krolikowska, M. (1985). Nonlinear mode coupling in oscillating stars. II - limiting amplitude effect of the parametric resonance in main sequence stars. *Acta Astron.* 35, 5

García Hernández, A., Moya, A., Michel, E., Garrido, R., Suárez, J. C., Rodríguez, E., et al. (2009). Asteroseismic analysis of the CoRoT δ Scuti star HD 174936. *Astron. Astrophys.* 506, 79–83. doi:10.1051/0004-6361/200911932

Garrido, R., and Rodriguez, E. (1996). Microvariability in high-amplitude delta Scuti radially pulsating stars. *Mon. Notices R. Astronomical Soc.* 281, 696–702. doi:10.1093/mnras/281.2.696

Gillet, D., and Fokin, A. B. (2014). Emission lines and shock waves in RR Lyrae stars. *Astron. Astrophys.* 565, A73. doi:10.1051/0004-6361/201322938

Goupil, M. J., Dziembowski, W. A., and Fontaine, G. (1998). On some observational consequences of nonlinearities in stellar pulsations. *Balt. Astron.* 7, 21–41. doi:10.1515/astro-1998-0108

Handler, G., Arentoft, T., Shobbrook, R. R., Wood, M. A., Crause, L. A., Crake, P., et al. (2000). Delta Scuti network observations of XX pyx: Detection of 22 pulsation modes and of short-term amplitude and frequency variations. *Mon. Notices R. Astronomical Soc.* 318, 511–525. doi:10.1046/j.1365-8711.2000.03817.x

Kurtz, D. W., Shibahashi, H., Murphy, S. J., Bedding, T. R., and Bowman, D. M. (2015). A unifying explanation of complex frequency spectra of γ dor, SPB and Be stars: Combination frequencies and highly non-sinusoidal light curves. *Mon. Not. R. Astron. Soc.* 450, 3015–3029. doi:10.1093/mnras/stv868

Lares-Martiz, M., Garrido, R., and Pascual-Granado, J. (2020). Self-consistent method to extract non-linearities from pulsating star light curves - I. Combination frequencies. *Mon. Not. R. Astron. Soc.* 498, 1194–1204. doi:10.1093/mnras/staa2256

Lares-Martiz, M. (2021). *Non-linear terms in Delta Scuti stars power spectra (PhD thesis*. Granada: Universidad de Granada.

McNamara, D. H. (2000). The identification of pulsation modes of high-amplitude δ Scuti stars in ω centauri and the carina galaxy. *Publ. Astronomical Soc. Pac.* 112, 1096–1102. doi:10.1086/316605

Montgomery, M. H. (2005). A new technique for probing convection in pulsating white dwarf stars. *Astrophys. J.* 633, 1142–1149. doi:10.1086/466511

Nowakowski, R. M. (2005). Multimode resonant coupling in pulsating stars. *Acta Astron.* 55, 1. doi:10.48550/arXiv.astro-ph/0501510

Paunzen, E., Bernhard, K., Hümmerich, S., Hambsch, F.-J., Lloyd, C., and Otero, S. (2020). High-amplitude γ Doradus variables. *Mon. Not. R. Astron. Soc.* 499, 3976–3991. doi:10.1093/mnras/staa2905

Pigulski, A., Kołaczkowski, Z., Ramza, T., and Narwid, A. (2006). High-amplitude delta Scuti stars in the galactic bulge from the OGLE-II and MACHO data. *Mem. Soc. Astron. Ital.* 77, 223. doi:10.48550/arXiv.astro-ph/0509523

Priestley, M. B. (1988). *Non-linear and non-stationary time series analysis*. Academic Press.

Reegen, P. (2011). SigSpec user's manual. *cia.* 163, 3–98. doi:10.1553/cia163s3

Rodríguez, E., López-González, M. J., and López de Coca, P. (2000). A revised catalogue of delta Sct stars. *Astron. Astrophys. Suppl. Ser.* 144, 469–474. doi:10.1051/aas:2000221

Saio, H., Bedding, T. R., Kurtz, D. W., Murphy, S. J., Antoci, V., Shibahashi, H., et al. (2018). An astrophysical interpretation of the remarkable g-mode frequency groups of the rapidly rotating γ Dor star, KIC 5608334. *Mon. Not. R. Astron. Soc.* 477, 2183–2195. doi:10.1093/mnras/sty784

Simon, N. R., and Lee, A. S. (1981). The structural properties of Cepheid light curves. *Astrophys. J.* 248, 291–297. doi:10.1086/159153

Stellingwerf, R. F. (1980). *Nonlinear delta Scuti models - the main sequence catastrophe*. New Brunswick: Springer Berlin Heidelberg, 125, 50. doi:10.1007/3-540-09994-8_5

Stellingwerf, R. F. (1979). Pulsation in the lower Cepheid strip. I. Linear survey. *Astrophys. J.* 227, 935–942. doi:10.1086/156802

Suárez, J. C., Garrido, R., and Moya, A. (2007). The role of rotation on Petersen diagrams. II. The influence of near-degeneracy. *Astron. Astrophys.* 474, 961–967. doi:10.1051/0004-6361:20077647

Suárez, J. C., and Garrido, R. (2006). The effect of rotation on Petersen Diagrams. *Mem. Soc. Astron. Ital.* 77, 502.

Suárez, J. C., Hernández, A. G., Moya, A., Rodrigo, C., Solano, E., Garrido, R., et al. (2014). "Theoretical properties of regularities in the oscillation spectra of A-F main-sequence stars," in *Precision asteroseismology*. Editors J. A. Guzik, W. J. Chaplin, and G. Handler, 301, 89–92. doi:10.1017/S1743921313014142

Van Beeck, J., Bowman, D. M., Pedersen, M. G., Van Reeth, T., Van Hoolst, T., and Aerts, C. (2021). Detection of non-linear resonances among gravity modes of slowly pulsating B stars: Results from five iterative pre-whitening strategies. *Astron. Astrophys.* 655, A59. doi:10.1051/0004-6361/202141572

Wu, Y. (2001). Combination frequencies in the Fourier spectra of white dwarfs. *Mon. Notices R. Astronomical Soc.* 323, 248–256. doi:10.1046/j.1365-8711.2001.04224.x

Zong, W., Charpinet, S., Fu, J.-N., Vauclair, G., Niu, J.-S., and Su, J. (2018). Oscillation mode variability in evolved compact pulsators from kepler photometry. I. The hot B subdwarf star KIC 3527751. *Astrophys. J.* 853, 98. doi:10.3847/1538-4357/aaa548

Zong, W., Charpinet, S., and Vauclair, G. (2016). Signatures of nonlinear mode interactions in the pulsating hot B subdwarf star KIC 10139564. *Astron. Astrophys.* 594, A46. doi:10.1051/0004-6361/201629132

Frontiers in
Astronomy and Space Sciences

Explores planetary science and extragalactic astronomy in all wavelengths

Advances the understanding of our universe - from planetary science to extragalactic astronomy, to high-energy and astroparticle physics.

Discover the latest Research Topics

See more →

Frontiers

Avenue du Tribunal-Fédéral 34
1005 Lausanne, Switzerland
frontiersin.org

Contact us

+41 (0)21 510 17 00
frontiersin.org/about/contact